RADIOLOGY AND ONCOLOGY

vol.58 no.3
september 2024

RADIOLOGY AND ONCOLOGY

September 2024
Vol. 58 No. 3
Pages 313-458
ISSN 1318-2099
UDC 616-006
CODEN: RONCEM
eISSN: 1581-3207

Publisher
Association of Radiology and Oncology

Aims and Scope
Radiology and Oncology (ISSN 1318-2099) is a multidisciplinary journal devoted to the publishing original and high-quality scientific papers and review articles, pertinent to oncologic imaging, interventional radiology, nuclear medicine, radiotherapy, clinical and experimental oncology, radiobiology, medical physics, and radiation protection. Papers on more general aspects of interest to the radiologists and oncologists are also published (no case reports).

Editorial office

Radiology and Oncology
Zaloška cesta 2
P. O. Box 2217
SI-1000 Ljubljana
Slovenia
Phone: +386 1 5879 369
Phone/Fax: +386 1 5879 434
E-mail: gsersa@onko-i.si

Reader for English
Vida Kološa

Secretary
Mira Klemenčič, Zvezdana Vukmirović, Vijoleta Kaluža, Uroš Kuhar

Design
Monika Fink-Serša, Samo Rovan, Ivana Ljubanović

Layout
Matjaž Lužar

Printed by
Tiskarna Ozimek, Slovenia

Published quarterly in 300 copies

Beneficiary name: DRUŠTVO RADIOLOGIJE IN ONKOLOGIJE
Zaloška cesta 2
1000 Ljubljana
Slovenia

Beneficiary bank account number: SI56 02010-0090006751
IBAN: SI56 0201 0009 0006 751
Our bank name: Nova Ljubljanska banka, d.d.,
Ljubljana, Trg republike 2,
1520 Ljubljana; Slovenia

SWIFT: LJBASI2X

Subscription fee for institutions EUR 100, individuals EUR 50

The publication of this journal is subsidized by the Slovenian Research Agency.

Indexed and abstracted by:

- *Baidu Scholar*
- *Case*
- *Chemical Abstracts Service (CAS) - CAplus*
- *Chemical Abstracts Service (CAS) - SciFinder*
- *CNKI Scholar (China National Knowledge Infrastructure)*
- *CNPIEC - cnpLINKer*
- *Dimensions*
- *DOAJ (Directory of Open Access Journals)*
- *EBSCO (relevant databases)*
- *EBSCO Discovery Service*
- *Embase*
- *Genamics JournalSeek*
- *Google Scholar*
- *Japan Science and Technology Agency (JST)*
- *J-Gate*
- *Journal Citation Reports/Science Edition*
- *JournalGuide*
- *JournalTOCs*
- *KESLI-NDSL (Korean National Discovery for Science Leaders)*
- *Medline*
- *Meta*
- *Microsoft Academic*
- *Naviga (Softweco)*
- *Primo Central (ExLibris)*
- *ProQuest (relevant databases)*
- *Publons*
- *PubMed*
- *PubMed Central*
- *PubsHub*
- *QOAM (Quality Open Access Market)*
- *ReadCube*
- *Reaxys*
- *SCImago (SJR)*
- *SCOPUS*
- *Sherpa/RoMEO*
- *Summon (Serials Solutions/ProQuest)*
- *TDNet*
- *Ulrich's Periodicals Directory/ulrichsweb*
- *WanFang Data*
- *Web of Science - Current Contents/Clinical Medicine*
- *Web of Science - Science Citation Index Expanded*
- *WorldCat (OCLC)*

This journal is printed on acid- free paper

On the web: ISSN 1581-3207
https://content.sciendo.com/raon
http://www.radioloncol.com

contents

review

Subdiaphragmatic activity-related artifacts in myocardial perfusion scintigraphy

Anja Strok[1], Barbara Guzic Salobir[1], Monika Stalc[1,2], Katja Zaletel[1,2]

[1] Division of Nuclear Medicine, University Medical Centre Ljubljana, Ljubljana, Slovenia
[2] Faculty of Medicine, University of Ljubljana, Ljubljana, Slovenia

Radiol Oncol 2024; 58(3): 313-319.

Received 8 June 2024
Accepted 21 June 2024

Correspondence to: Assist. Prof. Monika Štalc, M.D., Ph.D., Division of Nuclear Medicine, University Medical Centre Ljubljana, Zaloška cesta 7, SI-1000, Slovenia. E-mail: monika.stalc@kclj.si

Disclosure: No potential conflicts of interest were disclosed.

Background. Myocardial perfusion imaging (MPI) with single photon emission computed tomography is an established non-invasive technique for assessing myocardial ischemia. This method involves the intravenous administration of a radiopharmaceutical that accumulates in the heart muscle proportional to regional blood flow. However, image quality and diagnostic accuracy can be compromised by various technical and patient-related factors, including high non-specific radiopharmaceutical uptake in abdominal organs such as the stomach, intestines, liver, and gallbladder, leading to subdiaphragmatic artifacts. These artifacts are particularly problematic for evaluating inferior wall perfusion and often necessitate repeated imaging, which decreases gamma camera availability and prolongs imaging times.

Conclusions. Despite numerous investigated techniques to reduce interfering gastrointestinal activity, results have been inconsistent, and current MPI guidelines provide scant information on effective procedures to mitigate this issue. Based on our experience, some possible approaches to reducing artifacts include choosing stress testing with an exercise stress test, when possible, late imaging, fluid intake, and consuming carbonated water immediately before imaging.

Key words: myocardial perfusion imaging; artifacts, subdiaphragmatic activity; single photon emission computed tomography; intervention

Introduction

Myocardial perfusion imaging (MPI) with single photon emission computer tomography (SPECT) is an established non-invasive imaging modality for evaluating myocardial ischemia. It is based on the intravenous application of a radiopharmaceutical that accumulates in the heart muscle in proportion to the regional blood flow.[1,2]

The radioactive isotope emits energy in the form of gamma rays (photons), which are detected by a tomography gamma camera approximately one hour after the application of the radiopharmaceutical. The data on the intensity of the accumulation of the radiopharmaceutical in the heart muscle is converted into images by the computer. Thus, scintigrams are generated to assess blood flow to the heart muscle during stress (exercise or pharmacological) and at rest.[1,2]

The quality of the visual and quantitative analysis of MPI images is influenced by many technical and patient-related factors.[3,4] Some limitations arise directly from the characteristics of the radiopharmaceuticals. They exhibit high unspecific uptake in the abdominal organs (stomach, intestines, liver, and gallbladder), which can create artifacts.[1-3] Subdiaphragmatic activity is one of the most prevalent artifacts in SPECT imaging[3,4], often interfering with the evaluation of inferior wall perfusion in approximately 10–50% of cases.[5]

Artifacts in the inferior myocardial wall caused by subdiaphragmatic activity present a significant challenge by diminishing image quality and the diagnostic accuracy of the study. This can lead to suboptimal or even inadequate patient management.[3] In daily practice, abdominal activity interference often necessitates repeated imaging for some patients, which limits gamma camera availability, prolongs imaging times, and increases radiation exposure for both personnel and patients in the waiting room.

Currently, there is no standard approach to determine which technique(s) are most effective in reducing interfering subdiaphragmatic activity. Multiple techniques have been investigated to reduce interfering gastrointestinal activity while waiting for imaging, but results have been inconsistent. In MPI guidelines, information about procedures to reduce intestinal and liver activity is scarce.

In this review, we describe the effect of different interventions on subdiaphragmatic activity in MPI.

Subdiaphragmatic artifacts on myocardial perfusion imaging

The radiopharmaceutical used for MPI consists of a radioactive isotope of tehnecium-99m (99mTc) bound to a tetrofosmin or sestamibi molecule, which binds irreversibly to viable myocytes. In addition to the heart, radiopharmaceuticals used for MPI also accumulate in other organs and tissues. Initially, they localize in the liver due to their high lipophilicity and are then excreted via the hepatobiliary system into the duodenum. From there, tracer activity will move distally in the small bowel, or it may reflux into the stomach. Radiotracer can also accumulate in the gastric mucosa by active transport and retention in mitochondria or as a result of the dissociation of a tracer molecule and uptake of free 99mTc-pertechnetate.[3,6,7] This subdiaphragmatic radioactivity accumulation in the immediate vicinity of the heart causes artifacts, which interfere with the correct assessment of perfusion in the heart muscle, most often in the inferior wall of the left ventricle. In rare cases, such as with a hiatal hernia, the lateral wall can also be affected.[3]

Artifacts can cause either apparent increased or decreased activity in the adjacent inferior wall of the left ventricle, leading to false-negative or false-positive inferior wall perfusion defects, thereby mimicking ischemia, or concealing true perfusion defects.[3,4,8]

Scatter radiation from the radiotracer, combined with the effect of volume averaging, can create the appearance of increased perfusion in the inferior myocardial wall, which might mask a true perfusion defect in this region. On the other hand, scattering or superimposition of subdiaphragmatic activity on the inferior myocardial wall may cause normalization problems throughout the remainder of the left ventricle, resulting in the appearance of relatively low activity and simulating an extensive perfusion defect.[3,4]

In clinical practice, the most common way of evaluating interfering extracardiac artifacts is visually on reconstructed SPECT images (Figure 1).

When the interfering activity could result in either a significant overestimation or underestimation of uptake in the myocardium, scans are normally repeated after 0.5–1 hour.

For study purposes, the intensity of interfering artifacts can be visually scored using a grading scale, similar to the one used previously by Albuitahi *et al*.[9] and Bresser *et al*.[8]. The grading scale ranges from 0 to 3: 0 for absent subdiaphragmatic activity, 1 for mild subdiaphragmatic activity with no impact on visual interpretation, 2 for moderate subdiaphragmatic activity with a significant effect on interpretation, and 3 for severe subdiaphragmatic activity leading to a substantial impact on interpretation. Moderate and severe subdiaphragmatic tracer activity is considered relevant for the interpretation of MPI scans.

Artifacts can also be analyzed semi quantitatively on raw planar scintigrams by calculating the ratio between the myocardial and extracardiac activity (MYO:EXT ratio), a metric that has been well-studied and validated in multiple previous investigations.[8,10-14] The MYO:EXT ratio compares the inferior wall of the left ventricle myocardium to the infra-cardiac region[10,11] and correlates strongly with the level of activity interfering with image interpretation or, as mentioned before, visual grading.[10] Because this method is time-consuming, it is mainly used for academic purposes and not in routine clinical practice. The method of obtaining this ratio is shown in Figure 2.

Type of stress testing and subdiaphragmatic artefacts

The frequency and intensity of the interfering extracardiac activity are affected by the patient's

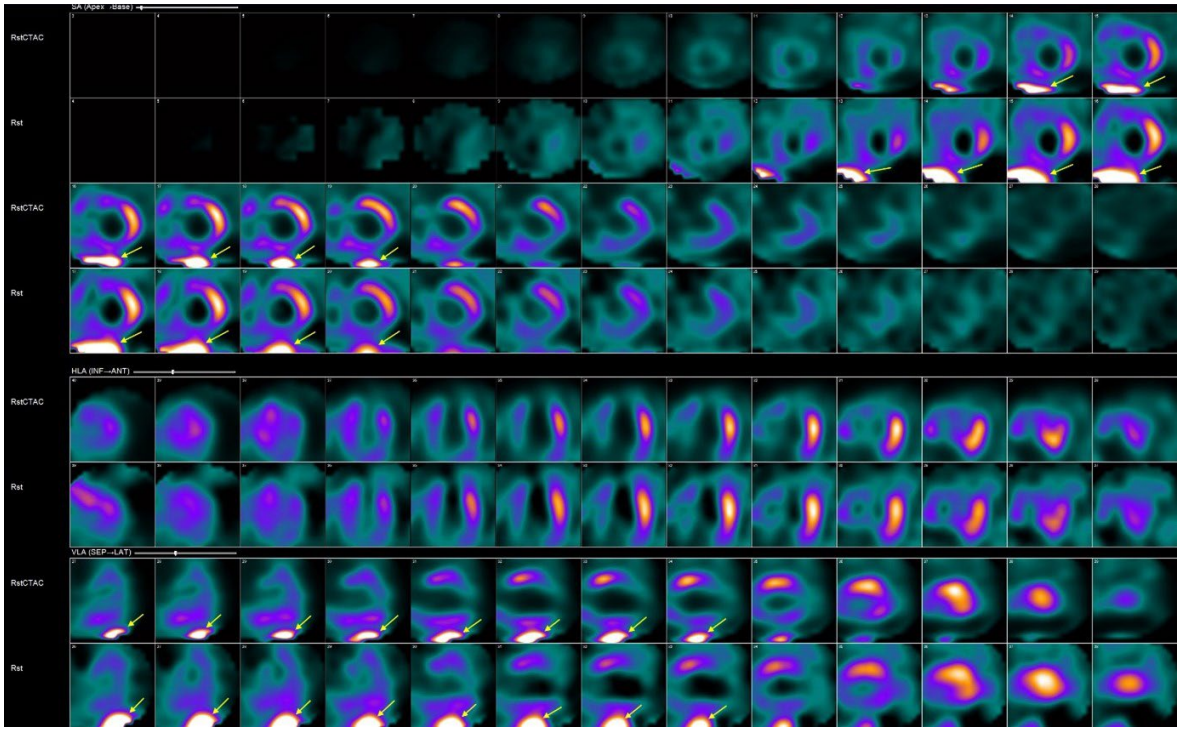

FIGURE 1. Interfering subdiaphragmatic activity (yellow arrow) on short and vertical long axis images of the left ventricle with (upper raw) and without attenuation correction (lower raw).

physiological characteristics as well as the type of test performed. It is well-known that subdiaphragmatic activity is higher after vasodilator stress testing compared to exercise stress due to increased hepatic and gastrointestinal blood flow.[1,7,10]

Therefore, whenever the patient can achieve a sufficient level of exercise and has no contraindications, a stress study on the bicycle or treadmill is a preferred method. In patients who are unable to exercise or achieve sufficient exercise workload, or who have complete left bundle branch block or a predominantly electro systolic rhythm with a pacemaker implanted, pharmacological stress with vasodilators is used. Regadenosone is the most commonly used pharmacologic agent for stress testing in many centres, while dipyridamole and adenosine are less common.[1,2]

Vasodilators induce myocardial hyperaemia interacting with adenosine receptors. Regadenosone is a highly specific adenosine A2A receptor agonist that induces coronary vasodilation. Adenosine and dipyridamole are less specific agents and they also stimulate the A1, A2B, and A3 adenosine receptors.[1,4] For that reason and because only about 5% of the cardiac output goes into the myocardial vasculature and the majority of the radiopharmaceutical distributes into other organs and tissues[7], vasodilators provoke known and unwanted adverse effects[1], such as depressed activity and conduction of the sinoatrial and atrioventricular nodes and possible atrioventricular heart block (receptor A1), peripheral vasodilation and hypotension (receptor A2B), and bronchoconstriction which can lead to severe and life-threatening events (receptor A3).[2,4] By promoting peripheral vasodilatation and dilatation of the splanchnic vasculature, pharmacological stress test leads to more pronounced accumulation of radiopharmaceuticals in the abdominal organs compared to exercise stress.[1,3,4,10]

Due to established facts, the addition of low-level exercise along with the vasodilator stress is recommended practice in guidelines. It minimizes artifacts by increasing skeletal muscle blood flow and reducing splanchnic blood flow to the viscera.[1,2,4,15,16] Combining the two methods results in improved image quality.[2] Additionally, the combination of a vasodilator with a low-level exercise protocol tailored to the abilities of the individual patient helps significantly reduce vasodilator-induced side effects (flushing, dizziness, nausea, headache, hypotension).[1]

Based on our experience (unpublished data), approximately 60% of the patients require a pharmacological stress test, and even 80% of the sub-

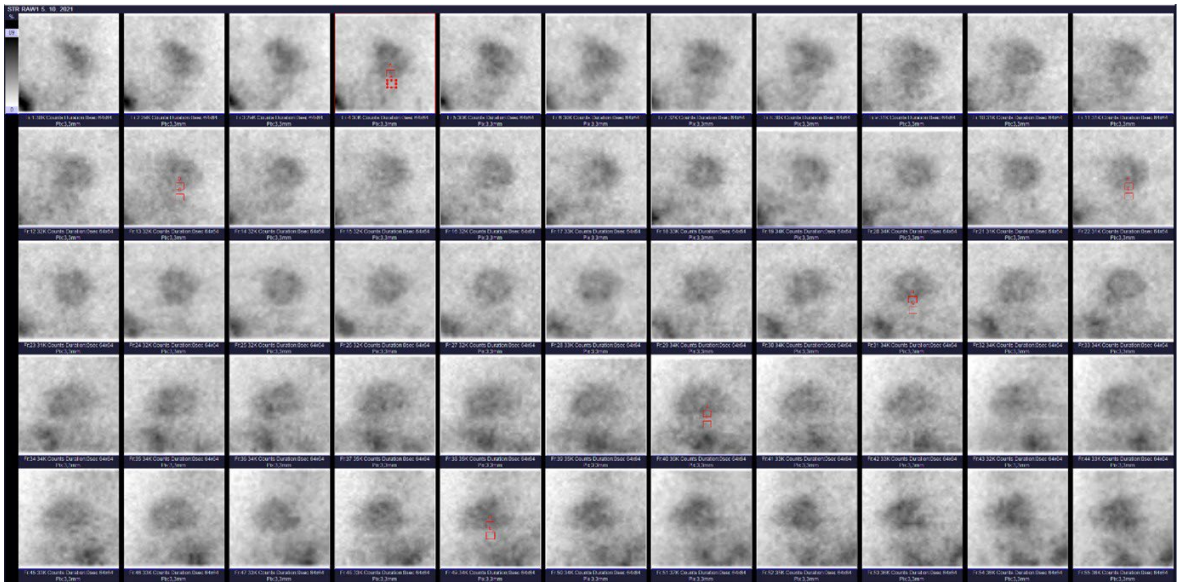

FIGURE 2. An example of manually drawn regions of interests (ROIs) over the midportion of the inferior wall of the myocardium and the adjacent underlying abdominal regions on multiple projections on raw planar images of the stress study. After pixel counts were obtained for every ROI, the mean myocardial and extracardiac counts were used to calculate the ratio of myocardial to extracardiac activity (MYO:EXT ratio).

jects during the COVID-19 epidemic in the years 2020–2022.

The use of pharmacologic stress testing has increased due to factors such as poor physical performance, general frailty and musculoskeletal conditions that hinder walking.[17] Furthermore, in response to the COVID-19 pandemic, the American Society of Nuclear Cardiology and the Society of Nuclear Medicine and Molecular Imaging issued recommendations aimed at reducing viral exposure risk for healthcare workers and patients. These guidelines highlight the importance of minimizing interaction time and maximizing physical distancing. To reduce droplet exposure to exercise staff and limit close contact, pharmacological stress protocols using vasodilator agents have been preferred.[18]

Technical aspects of minimizing subdiaphragmatic artifacts

Subdiaphragmatic artifacts can be reduced to some extent by the usage of iterative reconstruction methods during processing or attenuation correction.[1,19]

Attenuation correction methods can be based on traditional line-source transmission or CT-based with attenuation maps in novel SPECT/CT systems and are most useful for correcting artifacts due to soft tissue attenuation (originating from the breast or left hemidiaphragm). While a substantial number of artifacts can be corrected with these methods, but a few may also arise with their use.[4] Scatter effects may be more pronounced on attenuation-corrected images.[19]

The use of iterative reconstruction methods has been recommended to minimize artifacts related to extracardiac activity. The iterative process is well suitable to include physical effects, such as photon attenuation and contributions from photons scattered in the patient. Because iterative techniques have been demonstrated to produce superior image reconstructions, they are preferred over traditional filtered-back projections (FBP).[1] Prominent infracardiac activity can result in apparent decreased activity in the adjacent myocardium due to the reconstruction algorithm used in FBP. This is because relatively large streaks of negative numbers due to the ramp filter pass through the heart region and thus reduce the counts.[1,3] This leads to artefactual decreased activity adjacent to hot objects. The phenomenon worsens with greater the subdiaphragmatic activity.[3]

Cardiac perfusion images are usually obtained with the patient in the supine position. Studies have demonstrated that in the presence of an inferior wall artifact in the stress supine MPI, a posi-

tional change (prone imaging) can be an effective technique to eliminate common artifacts. Altering the standard patient position can help overcome not only attenuation artifacts but also interfering with external activity by lowering of the diaphragm and displacing abdominal organs away from the inferior myocardial wall.[1,4,20]

In a few patients, duodenogastric reflux is observed, which can affect the quality of the scans. To alleviate the refluxed activity, some suggest positioning the patients lying on their right-hand side for 20 minutes.[10]

Impact of food and liquid intake

The most common techniques used to reduce interfering activity involve the administration of food or liquids between injection and imaging. This is done to either stimulate hepatobiliary clearance of tracer or to distend the stomach and push the bowel loops inferiorly, further from the myocardium (volume effect). Techniques such as consuming a fatty meal, solid food, milk, lemon juice, carbonated beverages, plain water, or combined interventions have been explored with variable results[6,8,10-14,19,21,22], and currently, there is no standard approach to determining which technique is most effective in reducing the artifacts.[1]

A recently published randomized study did not confirm the significant effectiveness of concomitant drinking of lemonade and carbonated mineral water in reducing subdiaphragmatic activity.[8] On contrary, one of the previous studies showed a significant reduction in subdiaphragmatic activity by using smaller amounts of carbonated beverages. The study protocol was advantageous for patients with heart or renal failure in whom the intake of water may be a problem. Because it is desirable for these patients to drink as little water as possible and given that small volumes of soda water induce a greater volume expansion of the stomach compared to normal water, the use of carbonated beverages is the preferred method.[11] Also, Hussain *et al*. demonstrated that ingestion of carbonated water significantly improved an interfering gut artifact in the majority of their patients.[14] An example of the effect of carbonated water is shown on Figure 3.

Peace and colleagues found no significant effect of drinking water and fat milk[10], while others observed a reduced accumulation of radiopharmaceuticals in the gastrointestinal tract when combined with drinking milk and water. They

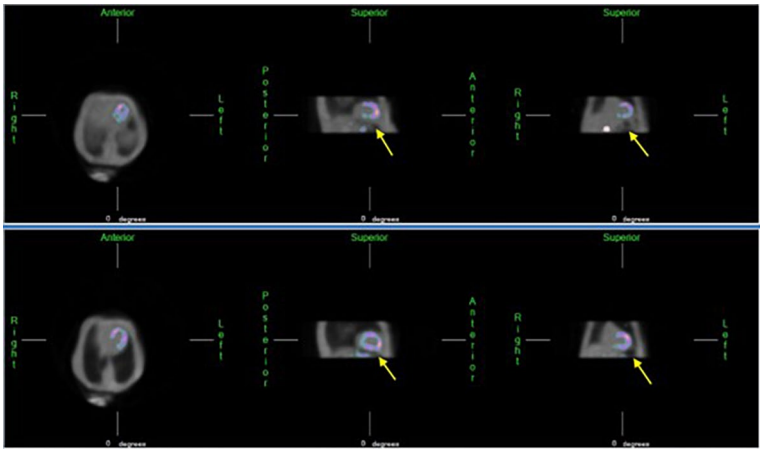

FIGURE 3. By administering carbonated water before imaging, carbon dioxide gas may additionally expand the stomach. The upper part of the stomach adjacent to the inferior wall of the heart is mainly filled with gas instead of water. By distending the stomach, we increase the distance between the gut and the heart, thereby reducing imaging artifacts (yellow arrow).

hypothesized that milk stimulates liver clearance and peristaltic movement, while water reduces activity in the stomach and accelerates the transition of biliary-excreted activity along the bowel tract.[19]

Similarly, in a study examining the impact of multiple techniques (drinking lemon juice, water, milk or a combination of measures), milk intake proved to be an important factor in reducing subdiaphragmatic activity, likely due in part to faster gallbladder drainage after ingesting a fatty meal.[6] They also found that the quality of scintigrams improved when drinking fluids and eating food simultaneously.[21] This is in agreement with the results of an earlier study by Boz *et al*., where the volume effect after consuming water and a sandwich was investigated, and the usefulness of stomach fullness on extracardiac activity was demonstrated by comparing patients in fasting and non-fasting states. They increased the volume of the stomach with a combination of fluids and solid food to push the intestine caudally and thus remove intestinal artifacts further away from the myocardium.[12]

Impact of drugs

The use of drugs that stimulate hepatobiliary clearance or gastric motility, such as erythromycin and metoclopramide, has been reviewed with varying results.[7,10] Metoclopramide, used for treating and preventing nausea and vomiting, is known for accelerating intestinal transit but had no effect on

abdominal activity in MPI and was consequently not recommended for routine practice.[7,23]

Drugs like the antibiotic erythromycin, which mimics motilin and leads to faster gastric emptying, have yielded favourable results but have been studied only in small groups.[7]

Some have hypothesized that iodinated oral contrast could be used to absorb gamma rays emitted from bowel activity but came to conclusion that some reduction in infracardiac activity was probably due to the volume effect.[10,24]

It was reported that proton-pump inhibitors, used to reduce stomach acid production, increase the accumulation of radiopharmaceutical in the stomach wall and can jeopardize the quality of MPI scans.[7]

None of these interventions and data seem to have become an integral part of the imaging protocol, and more recent and comprehensive studies with a larger number of patients are needed.

The impact of fasting

Gastrointestinal activity and related artifacts were less pronounced in patients who were fasting or had only eaten a light meal prior to examination.[3]

The role of late scanning

One of the most important approaches to minimize interfering subdiaphragmatic activity is to wait an adequate amount of time between radiopharmaceutical administration and imaging.[3]

Because MPI radiopharmaceuticals are cleared from the liver at a greater rate than from the heart, delaying the imaging allows physiologic clearance of the tracer from regions adjacent to the heart and has the benefit of reducing interfering hepatic activity.[1,2,4,9,10,21]

The recommended time interval between injection and acquisition for Tc99m- tetrofosmin by the manufacturer to yield the best image quality in relation to subdiaphragmatic activity is as soon as 15 minutes. However, MPI guidelines advise later post-injection acquisitions. Minimum delays of approximately 15 minutes for exercise, 30 to 45 minutes for rest, and 45 to 60 minutes for pharmacologic stress studies are optimal. Longer delays for repeated studies (up to 2 hours) can be used when needed.[1,2]

The prolongation of the time between radiopharmaceutical application and imaging improves the quality of scintigrams[4,8,10], but some authors, on the other hand, warn that it can potentially lead to reconstruction artifacts due to the increase in activity in the bowel loops[8,10] and consequently advise early acquisition over late scanning.

The impact of physical activity

To our knowledge, no studies have examined the role of controlled physical activity while waiting for MPI imaging, and the value of this intervention is uncertain.

Previous research has indicated that walking exercise can significantly influence gastrointestinal motility. For example, Noh *et al*. and colleagues found that intensive walking (exceeding 3000 steps) during bowel preparation before a colonoscopy led to notably higher bowel cleansing scores.[25] Others have shown that physical activity accelerates colonic transit times.[26-28] For patients with gynaecological cancer, engaging in pre-operative walking was connected to a more rapid recovery of bowel function post-surgery.[29] The literature also indicates that aerobic exercise can enhance intestinal motility, especially when practiced consistently over several weeks.[30] However, the mechanisms by which walking stimulates intestinal motility remain unclear.

Consistent with previous literature findings, we assume that adopting a similar approach might reduce artifacts by accelerating gastrointestinal peristalsis after a pharmacological stress test. This could result in a faster clearance of radiopharmaceuticals from the gastrointestinal tract, potentially improving the diagnostic accuracy of the study.

Our recent unpublished data from a randomized study show that the use of electronic pedometer watches encouraged patients to walk while waiting for imaging. However, the number of steps did not affect the occurrence or intensity of gastrointestinal activity-related artifacts, nor did it impact the acceptance rate of scans after pharmacological stress, compared to self-paced walking.

Conclusions

The problem of subdiaphragmatic activity in MPI is significant, and various approaches have been tested to reduce artifacts, but none have proven effective enough to be included in the guidelines. Based on our experience, some possible approaches to reducing artifacts include choosing stress

testing with an exercise stress test, when possible, late imaging, fluid intake, and consuming carbonated water immediately before imaging.

References

1. Verberner HJ, Acampa W, Anagnostopoulos C, Ballinger J, Bengel F, De Bondt P, et al. EANM procedural guidelines for radionuclide myocardial perfusion imaging with SPECT and SPECT/CT: 2015 revision. *Eur J Nucl Med Mol Imaging* 2015; **42:** 1929-40. doi: 10.1007/s00259-015-3139-x
2. Henzlova MJ, Duvall WL, Einstein AJ, Travin MI, Veberne HJ. ASNC imaging guidelines for SPECT nuclear cardiology procedures: Stress, protocols and tracers. *J Nucl Cardiol* 2016; **23:** 606-39. doi: 10.1007/s12350-015-0387-x
3. Burrel S, MacDonald A. Artifacts and pitfalls in myocardial perfusion imaging. *J Nucl Med Techol 2006*; **32:** 193-211. PMID: 17146108
4. Dvorak RA, Brown RKJ, Corbet JR. Interpretation of SPECT/CT myocardial perfusion images: common artifacts and quality control techniques. *Radiographics* 2011; **31:** 2041-57. doi: 10.1148/rg.317115090
5. Cherng SC, Chen YH, Lee MS, Yang SP, Huang WS, Cheng CY. Acceleration of hepatobiliary excretion by lemon juice on 99m-Tc-tetrofosmin cardiac SPECT. *Nucl Med Commun* 2006; **27:** 859-64. doi: 10.1097/01.mnm.0000243377.57001.33
6. Malek H, Hedayati R, Yaghoobi N, Bitarafan-Rajabi A, Firoozabadi SH, Rastgou F. The effect of milk, water and lemon juice on various subdiaphragmatic activity-related artifacts in myocardial perfusion imaging. *Res Cardiovasc Med* 2015; **4:** e29235. doi: 10.5812/cardiovascmed.29235
7. Molavipordajani S, Abedi SM, Hosseinimehr SJ, Fatahian A, Mardanshahi A. The effects of pharmacological interventions, exercise, and dietary supplements on extra-cardiac radioactivity in myocardial perfusion single-photon emission computed tomography imaging. *Nucl Med Comm* 2020; **41:** 841-7. doi: 10.1097/MNM.0000000000001226
8. Bresser PL, Sathekge MM, Makanjee CR, Wyk DV, Vorster M. A randomized-controlled study of a modified technique to reduce extracardiac activity in myocardial perfusion imaging. *Nucl Med Commun* 2017; **38:** 21-8. doi: 10.1097/MNM.0000000000000600
9. Albutaihi I, van der Veen L, Scholte A, Stokkel MP. The effects of early and late scanning on image quality and functional parameters in myocardial perfusion imaging. *Clin Nucl Med* 2010; **35:** 764-9. doi: 10.1097/RLU.0b013e3181ef0963
10. Peace RA, Lloyd JJ. The effect of imaging time, radiopharmaceutical, full fat milk and water on interfering extra-cardiac activity in myocardial perfusion single photon emission computed tomography. *Nucl Med Commun* 2005; **26:** 17-24. doi: 10.1097/00006231-200501000-00004
11. Hara M, Monzen H, Futai R, Inagaki K, Shimoyama H, Morikawa M, et al. Reduction of infracardiac intestinal activity by a small amount of soda water in tehnecium-99m tetrofosmin myocardial perfusion scintigraphy with adenosine stress. *J Nucl Card* 2008; **15:** 241-5. doi: 10.1016/j.nuclcard.2007.09.029
12. Boz A, Yildiz A, Gungor F, Karayalc¸ in B, Erkilic M. The volume effect of the stomach on intestinal activity on same-day exercise–rest Tc-99m tetrofosmin myocardial imaging. *Clin Nucl Med* 2001; **26:** 622-5. doi: 10.1097/00003072-200107000-00010
13. Vermeltfoort IA, van Dijk AB, de Jong JA, Teule GJ, Gevers M, Verhoeven B, et al. A randomized study of the effect of carbonated water prior to myocardial SPECT. *Ann Nucl Med* 2014; **28:** 669-73. doi: 10.1007/s12149-014-0863-4
14. Hussain S, Sultan FAT. Role of carbonated water technique to enhance Tc-99m tetrofosmin myocardial perfusion imaging by reducing subdiaphragmatic artefacts. *Ann Nucl Med* 2020; **34:** 787-92. doi: 10.1007/s12149-020-01504-4
15. Ceyrat Q, Mesguich C, Janvier L, Douard H, Bordenave L, Pinaquy JB. The impact of combination of regadenoson and isometric exercise on image quality of myocardial perfusion scintigraphy. *J Nucl Cardiol* 2016; **24:** 993-7. doi: 10.1007/s12350-016-0711-0
16. Thomas GS, Prill NV, Majmundar H, Fabrizi RR, Thomas JJ, Hayashida C, et al. Treadmill exercise during adenosine infusion is safe, results in fewer adverse reactions, and improves myocardial perfusion image quality. *J Nucl Cardiol* 2000; **7:** 439-46. doi: 10.1067/mnc.2000.108030
17. Argulian E, Po JRF, Uretsky S, Kommaraju KK, Patel S, Agarwal V, et al. Comparison of the current reasons for undergoing pharmacologic stress during echocardiographic and radionucliude stress testing. *J Nucl Cardiol* 2017; **24:** 546-54. doi: 10.1007/s12350-016-0398-2
18. Skali H, Murthy VL, Al-Mallah MH, Bateman TM, Beanlands R, Better N, et al. Guidance and best practices for nuclear cardiology laboratories during the coronavirus disease 2019 (COVID-19) pandemic: an information statement from ASNC and SNMMI. *J Nucl Cardiol* 2020; **27:** 1022-9. doi: 10.1007/s12350-020-02123-2
19. Dongen AJ, Rijk PP. Minimizing liver, bowel and gastric activity in myocardial perfusion SPECT. *J Nucl Med* 2000; **41:** 1315-7. PMID: 10945520
20. Stathaki M, Koukouraki S, Papadaki E, Tsaroucha A, Karkavitsas N. The benefits of prone SPECT myocardial perfusion imaging in reducing both artifact defects and patient radiation exposure. *Arq Bras Cardiol* 2015; **105:** 345-52. doi: 10.5935/abc.20150122
21. Lyngholm AM, Pedersen BH, Petersen LJ. Randomized, single-blind, factorial design study of interaction of food and time on intestinal activity in 99mTc-tetrofosmin stress myocardial perfusion scintigraphy. *Nucl Med Commun* 2008; **29:** 759-63. doi: 10.1097/MNM.0b013e3283031af8
22. Malhotra G, Upadhye TS, Nabar A, Asopa RV, Nayak UN, Rajan MG. Can carbonated lime drink intake prior to myocardial perfusion imaging with Tc-99m MIBI reduce the extracardiac activity that degrades the image quality and leads to fallacies in interpretation? *Clin Nucl Med* 2010; **35:** 160-4. doi: 10.1097/RLU.0b013e3181cc63a1
23. Weinmann P, Moretti JL. Metoclopramide has no effect on abdominal activity of sestamibi in myocardial SPECT. *Nucl Med Commun* 1999; **20:** 6235. doi: 10.1097/00006231-199907000-00005
24. Iqbal SM, Khalil ME, Lone BA, Gorski R, Blum S, Heller EN. Simple techniques to reduce bowel activity in cardiac SPECT imaging. *Nucl Med Commun* 2004; **25:** 355-9. doi: 10.1097/00006231-200404000-00007
25. Noh CK, Kim IS, Lee GH, Park JW, Lee E, Park B, et al. Comparison of effectiveness between abdominal vibration stimulation and walking exercise for bowel cleansing before therapeutic colonoscopy. *Gut Liver* 2020; **14:** 468-76. doi: 10.5009/gnl19999
26. De Schryver AM, Keulemans YC, Peters HP, Akkermans LM, Smout AJ, De Vries WR et al. Effects of regular physical activity on defecation pattern in middle-aged patients complaining of chronic constipation. *Scand J Gastroenterolo* 2005; **40:** 422-9. doi: 10.1080/00365520510011641
27. Cheskin LJ, Kamla N, Crowell MD, Schuster MM, Whitehead WE. Mechanisms of constipation in older persons and effects of fiber compared with placebo. *J Am Geriatr Soc* 1995; **43:** 666-9. doi: 10.1111/j.1532-5415.1995.tb07203.x
28. Rao SS, Beaty J, Chamberlain M Lambert PG, Gisolfi C. Effects of acute graded exercise on human colonic motility. *Am J Physiol* 1999; **276:** G1221-6. doi: 10.1152/ajpgi.1999.276.5.G1221
29. Özdemir İA, Comba C, Demirayak G, Gülseren V, Erdogan SV, Aslanova F, et al. Impact of pre-operative walking on post-operative bowel function in patients with gynecologic cancer. *Int J Gynecol Cancer* 2019; **29:** 1311-6. doi: 10.1136/ijgc-2019-000633
30. Kim YS, Song BK, Oh JS, Woo SS. Aerobic exercise improves gastrointestinal motility in psychiatric inpatients. *World J Gastroenterol* 2014; **20:** 10577-84. doi: 10.3748/wjg.v20.i30.10577

review

Anastomosing hemangioma of the ovary – a comprehensive review of this rare ovarian entity

Sebastjan Merlo[1,2,3], Gregor Vivod[1,2], Barbara Gazic[4], Nina Kovacevic[1,2,3]

[1] Department of Gynecological Oncology, Institute of Oncology Ljubljana, Ljubljana, Slovenia
[2] Faculty of Medicine, University of Ljubljana, Ljubljana, Slovenia
[3] Faculty of Health Care Angele Boskin, Jesenice, Slovenia
[4] Department of Pathology, Institute of Oncology Ljubljana, Ljubljana, Slovenia

Radiol Oncol 2024; 58(3): 320-325.

Received 9 April 2024
Accepted 14 August 2024

Correspondance to: Assist. Prof. Nina Kovačević M.D., Ph.D., Department of Gynecological Oncology, Institute of Oncology Ljubljana, Zaloška cesta 2, SI-1000 Ljubljana, Slovenia. E-mail: nkovacevic@onko-i.si

Disclosure: No potential conflicts of interest were disclosed.

Background. Anastomosing hemangioma of the ovary is a rare vascular tumor that predominantly affects middle-aged women. Despite its benign nature, its histological appearance can mimic aggressive vascular lesions, posing diagnostic challenges. This review aims to provide an overview of this uncommon entity.

Methods. The PubMed and Scopus databases were searched for relevant articles published in English. Information on all retrieved cases was extracted and reviewed in detail.

Results. We found 33 cases with relevant details of anastomosing heamangioma of the ovary. Despite the small number of cases we found, our study demonstrated the importance of an accurate hystopathological evaluation.

Conclusions. Although the preliminary imaging and initial microscopic features may appear alarming, careful microscopic examination reveals benign behavior. There is a need to raise awareness of this unusual and rare entity to improve morphologic recognition and avoid misdiagnosis that could lead to unnecessary treatment or patient anxiety.

Key words: anastomosing hemangioma; ovary; ovarian hemangioma; urogenital tract

Introduction

Anastomosing hemangioma is a rare benign vascular tumor reported to occur in the kidney, testis, paravertebral soft tissue, gastrointestinal tract, liver, and in rare instances, in the ovary.[1-4] It was first described in 2009 by Montgomery and Epstein.[5] Since then, only a limited number of cases have been reported in the literature, contributing to its diagnostic uncertainty. Most cases of anastomosing hemangioma of the ovary presents as a solitary, well-circumscribed mass or is incidental findings.[1] Occasionally, ovarian anastomosing hemangiomas have been associated with ascites and elevated serum CA 125 levels raising concern for an epithelial malignancy. Ovarian hemangiomas can be mistaken for malignant ovarian tumors due to their appearance on imaging studies. Appropriate preoperative diagnostics, including ultrasound, MRI, and sometimes CT scans, are essential to differentiate hemangiomas from more serious conditions such as ovarian cancer, which would require a different surgical approach and postoperative management.[6,7]

Histologically, anastomosing hemangioma is characterized by anastomosing sinusoidal capillary sized blood vessels lined by bland endothelial cells with hobnail appearance, in a hyalinized and edematous stroma. The cells may show minimal atypia, which can be mistaken for low-grade an-

giosarcoma.[7] Immunohistochemical staining may reveal positivity for endothelial markers such as CD31 and CD34, aiding in its diagnosis.[8]

We reviewed the current and relevant literature on anastomosing hemangiomas of the ovary to increase awareness of this rare entity. Prior to our review, only 33 cases of anastomosing hemangioma of the ovary have been reported in the English-language literature.[1,3,6-15] Most of reviews are presented as case reports or small case series, and the largest series includes 12 cases of anastomosing hemangioma of the ovary.[9] To add to the literature, we present and describe our case of anastomosing hemangioma of the ovary.

Materials and methods

Search strategy

The PubMed database was searched for relevant articles published in English between January 1990 and December 2023. The search strategy included the following terms: (Hemangioma[mesh] OR Hemangioma*[tiab]) AND (anastomosing Hemangioma*[tiab] OR anastomosing[tiab] OR anastomos*[tiab]) AND (Ovary[mesh] OR Ovary[tiab] OR ovaries[tiab] OR ovarina[tiab] OR Ovarian Neoplasms[mesh] OR Ovarian Neoplasms[tiab] OR Cancer of Ovary[tiab] OR Cancer of the Ovary[tiab] OR Ovarian Cancer*[tiab] OR Ovary Cancer*[tiab] OR Ovary Neoplasms[tiab] OR ovarian malignancy[tiab] OR ovarian tumor*[tiab] OR Ovarian Carcinoma[tiab]) AND 1990/01/01:2024/01/01[Date - Publication]. The Scopus database was also searched. The references of all relevant reviews found were also examined to avoid omitting qualified studies. In addition, references to related articles were searched to identify studies that might meet the criteria. Evaluation of each article was conducted independently by three reviewers (S.M., G.V. and N.K.).

Inclusion criteria

The inclusion criteria were as follows: Women with a histopathological diagnosis of anastomosing hemangioma of the ovary; all published retrospective small studies and case reports containing patient-relevant information; clinical presentation, size of the hemangioma; stromal lutenization. In the case of duplicates in the literature, the most recent and comprehensive articles were selected. We also included the case report by Metodiev *et al*. in which the abstract was written in English.[12]

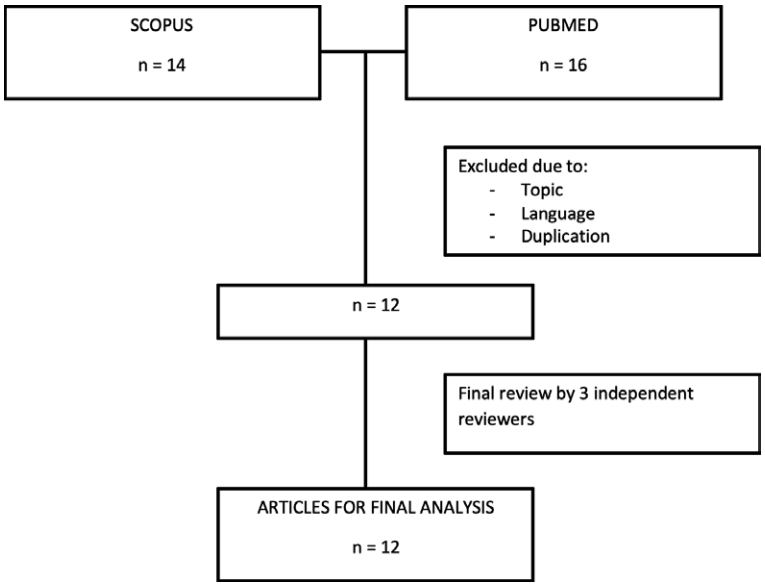

FIGURE 1. Literature review flowchart.

Exclusion criteria

The articles were excluded for one of the following reasons: Articles not specifying the type of ovarian tumor and articles not in English language.

Data extraction

Study information that were extract and reviewed in detail: Patient age at diagnosis, tumor size and location, histopathological type, clinical presentation, and presence of stromal luteinization.

Results

A new case

A 60 years old woman was sent to Department of Gynecological Oncology, Institute of Oncology Ljubljana with a suspected left-sided ovarian mass. Vaginal ultrasound showed a mixed cystic and solid appearance. The largest diameter of the mass was 50 millimeters. Family history was negative for malignancy. Her medical history was unremarkable. The tumor markers CA 125, CEA, HE4, CA 19-9, CA 72-4 and CA 15-3 were all negative. She underwent laparoscopic bilateral salpingo-oophorectomy. Left ovary was partly fragmented. In one of the fragments, there was a well circumscribed lesion, measuring 25 mm in diameter, with yellow-brown, spongy appearance was present. Microscopic examination of H&E-stained

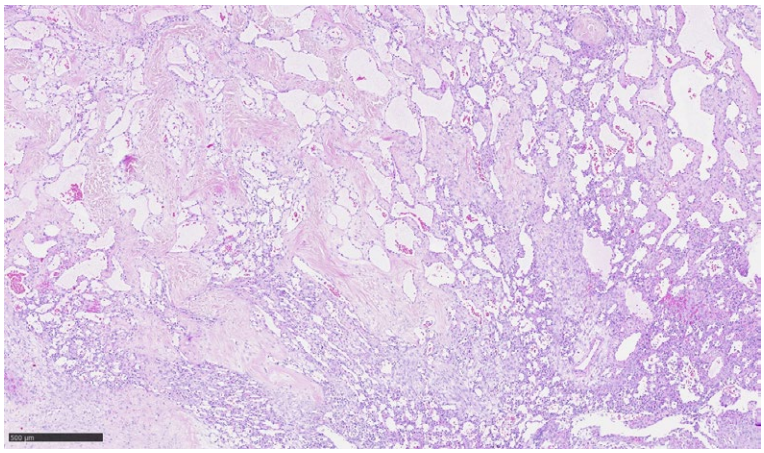

FIGURE 2. HE: Anastomosing sinusoidal-like vessels lined by endothelial cells without cytologic atypia.

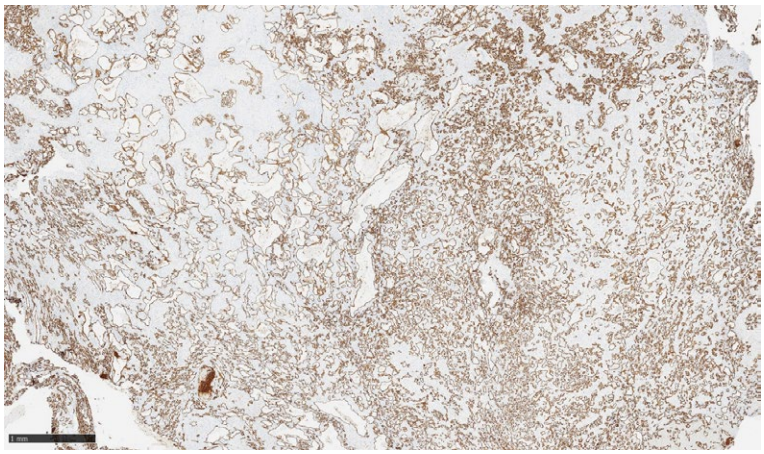

FIGURE 3. CD 31 highlights endothelial cells lining numerous vessels.

slides revealed well-demarcated vascular proliferation, composed mostly of capillary-sized blood vessels with an anastomosing growth pattern and some larger vessels of medium size. Vessels lining was composed of a single layer of endothelial cells without cytologic atypia or mitotic figures (Figure 2). The lesion was surrounded by luteinized ovarian stroma. Immunohistochemically the tumor cells were positive for CD31, CD34 and ERG (Figure 3).

Review of literature

A flowchart showing the phases of the search strategy is shown in Figure 1. Our search in the Scopus and PubMed databases initially returned 30 results. After the initial screening, 18 articles were excluded due to duplicates and non-English language. Of the remaining 12 articles, the titles and abstracts were screened by reviewers and were classified as relevant and were subjected to a full text and literature review. For the final analysis all 12 papers with relevant details were selected.

The mean age of the 32 women diagnosed with anastomosing hemangioma of the ovary was 59.2 years. In 18 women tumor was incidental finding, three women presented with elevated CA 125 serum level and ascites. Only ascites was present in one patient and five women have ultrasound detected ovarian mass. The mean maximum diameter of tumor was 20.6 mm. The detailed data of the patients and the tumor characteristics are listed in Table 1.

Discussion

The definition of anastomosing hemangioma was established in 2009.[5] The most likely theory that explaining the pathogenesis of this phenomenom characterizes anastomosing hemangioma of ovary as behaving like enlarging follicles that cause pressure on the neighboring tissue and lead to the development of luteinized stromal cells.[6]

In our review of literature, we found 33 cases of anastomosing hemangiomas of the ovary reported in the English literature. In our case the patient was 60 years old, while the mean age in the previous literature was 52.9 years (range from 26 to 81) (Table 1). The tumor size ranged from 1 millimeter to 100 millimeters, with the mean size being 20.6 millimeters. In our case tumor size was 50 millimeters.

Anastomosing hemangioma of the ovary typically affects women in their middle age, although cases have been reported across a wide age range.[6] Clinically, patients may present with nonspecific symptoms such as abdominal pain, discomfort, or palpable pelvic mass. However, due to its rarity and lack of specific clinical features, anastomosing hemangioma is often an incidental finding on imaging studies or during surgical exploration for unrelated conditions. The absence of pathognomonic symptoms underscores the importance of histopathological evaluation for definitive diagnosis.[16] Radiological imaging, including ultrasound and MRI, may demonstrate a hypervascular mass, although definitive diagnosis often relies on histological examination following surgical excision.[10] In our case, too, the ovarian mass was an incidental finding with no specific clinical signs. Tumor markers were all negative and the ultrasound re-

TABLE 1. Published cases of anastomosing hemangiomas of the ovary in the English literature

No	Author	Age	Clinical presentation	Size (mm)	Stromal luteinization
1	Metodiew *et al.*[12]	70	NA	7	Yes
2	Kryvenko *et al.*[3]	70	Incidental	2	No
3	Kryvenko *et al.*[3]	49	Incidental	1	No
4	Kryvenko *et al.*[3]	77	Incidental	11	Yes
5	O'Neill *et al.*[10]	NA	NA	NA	NA
6	O'Neill *et al.*[10]	NA	NA	NA	NA
7	O'Neill *et al.*[10]	NA	NA	NA	NA
8	O'Neill *et al.*[10]	NA	NA	NA	NA
9	Dundr *et al.*[6]	66	Incidental	5	Yes
10	Dundr *et al.*[6]	43	Incidental	13	Yes
11	Dundr *et al.*[6]	69	Incidental	15	Yes
12	Dundr *et al.*[6]	81	Incidental	35	Yes
13	Dundr *et al.*[6]	68	Ascites, elevated CA 125	35	Yes
14	Dundr *et al.*[6]	69	Mass	12	Yes
15	Gunduz *et al.*[8]	62	Incidental	90	Yes
16	Subbarayan *et al.*[7]	50	Ascites	30	Yes
17	Rezk *et al.*[1]	60	Ascites, elevated CA 125	65	Yes
18	Stewart and Salfinger[11]	48	Incidental	8	Yes
19	McHenry and Buza[9]	55	Mass	12	Yes
20	McHenry and Buza[9]	62	Mass	10	Yes
21	McHenry and Buza[9]	67	Incidental	5	Yes
22	McHenry and Buza[9]	76	Incidental	7	Yes
23	McHenry and Buza[9]	58	Incidental	8	Yes
24	McHenry and Buza[9]	53	Mass	6	Yes
25	McHenry and Buza[9]	73	Incidental	4	Yes
26	McHenry and Buza[9]	65	Incidental	10	Yes
27	McHenry and Buza[9]	50	Incidental	9	Yes
28	McHenry and Buza[9]	69	Incidental	6	No
29	McHenry and Buza[9]	63	Incidental	3	No
30	McHenry and Buza[9]	55	Incidental	2	No
31	Wang *et al.*[13]	28	Mass	40	No
32	Wu *et al.*[14]	26	Mass, ascites, elevated CA 125	46	NA
33	Jha *et al.*[15]	35	Mass	100	Yes

NA = not available

sults were non-specific. The final histologic findings were decisive for the final diagnosis.

Stromal luteinization as a unique feature of ovarian anastomosing hemangiomas was reported in 22 of 28 cases (78.6%), and in 5 cases this data was not available (Table 1). Some of the prior cases presented association between anastomosing hemangioma of ovary with ascites and elevated serum CA 125, mimicking an epithelial ovarian malignancy.[1,6,7] These findings were not observed in our experience.

Particular histologic characteristics are described as non-lobular proliferation of anastomosing capillary sized vessels with sinusoidal-like ar-

rangements resembling the red pulp of the spleen, with vessels lined by bland endothelial cells.[6] The lack of atypical endothelial cells and mitotic figures helps to differentiate anastomosing hemangiomas from its malignant counterpart, angiosarcoma.[17] Evaluation of the entire anastomosing hemangioma lesion, when possible, reveals that its growth is limited, lacking a broadly infiltrative pattern. The differential diagnosis of anastomosing hemangioma also includes capillary hemangioma, cavernous hemangioma, hemangioendothelioma, epithelioid hemangioma, and non-neoplastic vascular proliferations.[9]

Surgical excision remains the cornerstone of management for anastomosing hemangioma of the ovary. Complete resection is curative in the majority of cases, with favorable long-term outcomes. Management decisions should be individualized based on factors such as tumor size, location, and patient preferences, with a focus on preserving ovarian function and fertility when feasible. Overall, the prognosis of anastomosing hemangioma of the ovary is excellent following complete surgical resection. Recurrence rates are low, particularly with adequate surgical margins. However, cases of recurrence have been reported, highlighting the importance of vigilant long-term surveillance.[18,19]

Continued collaboration among multidisciplinary teams is essential to advance our understanding and improve outcomes for patients with this rare ovarian tumor. Although the preliminary imaging and initial microscopic features may appear alarming, careful microscopic examination reveals benign behaviour.[10] There is a need to raise awareness of this unusual and rare entity to improve morphologic recognition and avoid misdiagnosis that could lead to unnecessary treatment or patient anxiety.

Conclusions

In conclusion, anastomosing hemangioma of the ovary is a rare vascular tumor that poses diagnostic challenges due to its histological resemblance to more aggressive lesions. Despite its benign nature, accurate diagnosis is essential to avoid unnecessary interventions and ensure appropriate management. Long-term follow-up is crucial due to reported cases of recurrence following incomplete resection. Further research is needed to better understand the pathogenesis of this rare ovarian tumor and to optimize diagnostic and therapeutic approaches. Increased awareness among clinicians and pathologists is essential for timely recognition and management of anastomosing hemangioma of the ovary, ultimately improving patient outcomes.

References

1. Rezk A, Richards S, Patricia Castillo R, Schlumbrecht M. Anastomosing hemangioma of the ovary mimics metastatic ovarian cancer. *Gynecol Oncol Rep* 2020; **34:** 100647. doi: 10.1016/j.gore.2020.100647
2. John I, Folpe AL. Anastomosing hemangiomas arising in unusual locations: a clinicopathologic study of 17 soft tissue cases showing a predilection for the paraspinal region. *Am J Surg Pathol* 2016; **40:** 1084-9. doi: 10.1097/PAS.0000000000000627
3. Kryvenko ON, Gupta NS, Meier FA, Lee MW, Epstein JI. Anastomosing hemangioma of the genitourinary system: eight cases in the kidney and ovary with immunohistochemical and ultrastructural analysis. *Am J Clin Pathol* 2011; **136:** 450-7. doi: 10.1309/AJCPJPW34QCQYTMT
4. Sun K, Wei JF, Zhao M, Teng XD. Anastomosing hemangioma of the liver containing eosinophilic hyaline globules. *Int J Clin Exp Med* 2017; **10:** 7291-5.
5. Montgomery E, Epstein JI. Anastomosing hemangioma of the genitourinary tract: a lesion mimicking angiosarcoma. *Am J Surg Pathol* 2009; **33:** 1364-9. doi: 10.1097/PAS.0b013e3181ad30a7
6. Dundr P, Němejcová K, Laco J, Skálová H, BauerováL, Matěj R, et al. Anastomosing hemangioma of the ovary: a clinicopathological study of six cases with stromal luteinization. *Pathol Oncol Res* 2017; **23:** 717-22. doi: 10.1007/s12253-016-0186-y
7. Subbarayan D, Devaraji A, Senthilnayagam B, Ramanujam S, Nandagopalradha R. Anastomosing hemangioma of the ovary clinically masquerading as epithelial malignancy: a rare case report. *J Midlife Health* 2019; **10:** 48-50. doi:10.4103/jmh.JMH_121_18
8. Gunduz M, Hurdogan O, Onder S, Yavuz E. Cystic anastomosing hemangioma of the ovary: a case report with immunohistochemical and ultrastructural analysis. *Int J Surg Pathol* 2019; **27:** 437-40. doi:10.1177/1066896918817148
9. McHenry A, Buza N. Anastomosing hemangioma of the ovary with Leydig cell hyperplasia: a clinicopathologic study of 12 cases. *Int J Gynecol Pathol* 2023; **42:** 167-75. doi: 10.1097/PGP.0000000000000887
10. O'Neill AC, Craig JW, Silverman SG, Alencar RO. Anastomosing hemangiomas: locations of occurrence, imaging features, and diagnosis with percutaneous biopsy. *Abdom Radiol (NY)* 2016; **41:** 1325-32. doi: 10.1007/s00261-016-0690-2
11. Stewart CJR, Salfinger SG. Anastomosing haemangioma of the ovary with hilus cell hyperplasia. *Pathology* 2020; **52:** 392-394. doi: 10.1016/j.pathol.2019.11.010
12. Metodiev D, Ivanova V, Omainikova B, Boshnakova T. [Ovarian anastomosing hemangioma with stromal luteinization: a case report]. [Bulgarian]. *Akush Ginekol (Sofiia)* 2015; **54:** 58-61. PMID: 26863799
13. Wang Z, Hu J. A case report of anastomosing hemangioma of the ovary. *Medicine (Baltimore)* 2023;**102:** e33801. doi: 10.1097/MD.0000000000033801
14. Wu Q, Luo H. Anastomosing hemangioma of the ovary: a rare benign tumor. *Arch Gynecol Obstet* 2024; **309:** 2909-10. doi:10.1007/s00404-023-07301-4
15. Jha S, Jain P, Dixit S, Sharma S. Anastomosing hemangioma of ovary with stromal luteinization masquerading as sex cord-stromal tumor on intraoperative consultation. *J Microsc Ultrastruct* 2022; **10:** 208. doi:10.4103/jmau.jmau_92_21
16. Gehrig PA, Fowler WC, Lininger RA. Ovarian capillary hemangioma presenting as an adnexal mass with massive ascites and elevated CA-125. *Gynecol Oncol* 2000; **76:** 130-2. doi: 10.1006/gyno.1999.5648
17. Bösmüller H, Gruber C, Haitchi-Petnehazy S, Wagner D, Webersinke G, Hauptmann S. Primary angiosarcoma of the ovary with prominent fibrosis of the ovarian stroma. Case report of an 81-year old patient. *Diagn Pathol* 2011; **6:** 65. doi:10.1186/1746-1596-6-65

18. Heidegger I, Pichler R, Schäfer G, Bernhard Zelger, Bettina Zelger, Friedrich Aigner, et al. Long-term follow up of renal anastomosing hemangioma mimicking renal angiosarcoma. *Int J Urol* 2014; **21:** 836-838. doi: 10.1111/iju.12433

19. Burton KR, Jakate K, Pace KT, Vlachou PA. A case of recurrent, multifocal anastomosing haemangiomas. *BMJ Case Rep* 2017; **2017:** bcr2017220076. doi: 10.1136/bcr-2017-220076

review

Laser speckle contrast imaging of perfusion in oncological clinical applications: a literature review

Rok Hren[1,2,3], Simona Kranjc Brezar[4], Urban Marhl[2], Gregor Sersa[4]

[1] Faculty of Mathematics and Physics, Ljubljana, Slovenia
[2] Institute of Mathematics, Physics, and Mechanics, Ljubljana, Slovenia
[3] Syreon Research Institute, Budapest, Hungary
[4] Institute of Oncology Ljubljana, Ljubljana, Slovenia

Radiol Oncol 2024; 58(3): 326-334.

Received 16 July 2024
Accepted 26 July 2024

Correspondence to: Rok Hren, Ph.D., Faculty of Mathematics and Physics, University of Ljubljana, Jadranska ulica 19, SI-1000 Ljubljana, Slovenia. E-mail: rok.hren@fmf.uni-lj.si

Disclosure: No potential conflicts of interest were disclosed.

Background. Laser speckle coherence imaging (LSCI) is an emerging imaging modality that enables noninvasive visualization and assessment of tissue perfusion and microcirculation. In this article, we evaluated LSCI in imaging perfusion in clinical oncology through a systematic review of the literature.

Methods. The inclusion criterion for the literature search in PubMed, Web of Science and Scopus electronic databases was the use of LSCI in clinical oncology, meaning that all animal, phantom, *ex vivo*, experimental, research and development, and purely methodological studies were excluded.

Results. Thirty-six articles met the inclusion criteria. The anatomic locations of the neoplasms in the selected articles were brain (5 articles), breasts (2 articles), endocrine glands (4 articles), skin (12 articles), and the gastrointestinal tract (13 articles).

Conclusions. While LSCI is emerging as an appealing imaging modality, it is crucial for more clinical sites to initiate clinical trials. A lack of standardized protocols and interpretation guidelines are posing the most significant challenge.

Key words: laser speckle contrast imaging (LSCI); oncology; perfusion; blood flow

Introduction

In the cancer research and treatment, the assessment of tissue perfusion and microcirculation plays a pivotal role in understanding tumor physiology, monitoring treatment responses, and determining surgical outcomes. Among the advanced visualization systems, fluorescence angiography utilizing indocyanine green (FA-ICG) has emerged as an objective tool for evaluating intraoperative perfusion.[1-3] Despite its versatility, FA-ICG imaging has limitations: for example, it requires external dye injection, is constrained by pharmacokinetic factors in repeat assessments, and may potentially lead to allergic reactions to the dye.[2] To overcome these shortcomings, novel imaging techniques have been explored for microvascular imaging.

One such modality is laser speckle contrast imaging (LSCI), a non-invasive optical imaging technique based on the unique properties of laser light to visualize blood flow and tissue perfusion in real-time.[4,5] At the core of LSCI lies the phenomenon of capturing the dynamic interference pattern, known as speckle, created when coherent laser light interacts with moving particles such as red blood cells, generating a real-time 2D color

heatmap of blood flow (Figure 1).[6] By analyzing the temporal fluctuations in the speckle pattern, LSCI can quantitatively assess blood flow velocity, perfusion dynamics, and tissue microcirculation with high spatial and temporal resolution.

LSCI is a versatile modality with its applicability ranging from material science[7] to notable applications in medical therapeutic segments.[8] LSCI has aided, among others, in studying retinal blood flow[9], cardiovascular diseases[10,11] and organ perfusion[6,12], while demonstrating potential as a valuable tool for assessing burns[13-15] and wound healing processes[16-18], and monitoring perfusion during reconstructive surgery[19] and neurosurgery.[20-26] The value of LSCI in quantifying blood flow dynamics within clinical oncology remains unclear, and to that end, we systematically reviewed the literature with a specific focus on studies in which LSCI was conducted on patients in a clinical oncology setting.

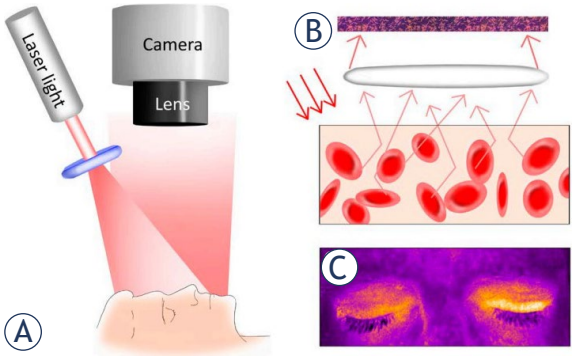

FIGURE 1. Schematic representation of the laser speckle contrast imaging (LSCI) method. **(A)** The technique relies on the interference of light backscattered from moving particles, creating distinct dark and bright areas (speckle pattern) captured by a camera. **(B)** Variations in the speckle pattern are predominantly driven by the movement of red blood cells, enabling interpretation as perfusion. **(C)** Analysis of speckle-pattern variations yields an image displayed on the monitor, where white and yellow depict areas with high perfusion, contrasting with darker areas indicating lower perfusion areas. Taken from Berggren *et al.* [19] and reprinted with permission from the publisher.

Methods

Authors conducted jointly—to minimize potential bias—a comprehensive literature search on April 16, 2024, through PubMed, Web of Science and Scopus electronic databases using the following search terms: "laser speckle coherence imaging tumors", "laser speckle coherence imaging cancer", "laser speckle coherence imaging carcinoma", "laser speckle coherence imaging anastomosis", and "laser speckle coherence imaging thyroid". No restrictions on publication date or language were imposed. The inclusion criterion was the application of LSCI in a clinical oncological setting, meaning that all animal and phantom, *ex vivo*, experimental, research and development, and purely methodological studies were excluded. Special care was taken to remove duplicates across databases and studies; for example, if the study was first published in proceedings and later in a journal, the proceedings article was considered a non-primary publication and therefore excluded. Studies were categorized with respect to the anatomical location of the tumors.

Results

In total, 309 articles were found to be of interest in the PubMed, Web of Science and Scopus databases. After excluding duplicates and applying the exclusion criteria, first considering the title and abstract and then, if necessary, reading the entire article, 36 articles were identified for further analysis. The anatomical locations of tumors in the selected articles were as follows: brain (5 articles), breasts (2 articles), endocrine glands (4 articles), skin (12 articles), and the gastrointestinal (GI) tract (13 articles).

Brain

Parthasarathy *et al.*[21] made a pioneering effort in the evaluation of perfusion in clinical oncology using LSCI. Their pilot study focused on imaging cerebral blood flow either before (1 patient) or after (2 patients) tumor resections, across various cortical regions. The same group continued research on larger patient groups (10 and 8, respectively), demonstrating the feasibility of using LSCI to monitor blood flow during neurosurgery.[22,27] Despite these promising outcomes, their research output ceased after 2017.

Another research group[25] highlighted the potential of LSCI for functional brain mapping during awake craniotomy for tumor removal. They observed a strong correlation between cortical microvascular blood flow, as determined by LSCI, and electrocortical stimulation mapping. Additionally, Ideguchi *et al.*[28] emphasized the capability of LSCI for noninvasive and rapid intraoperative real-time recognition of mass lesion-related

TABLE 1. Included articles reporting the use of laser speckle contrast imaging (LSCI) to quantify perfusion in clinical applications in oncology

Reference	Year of publication	Number of patients	Oncologic setting
Brain			
Parthasarathy *et al.*[21]	2010	3	Tumor resection
Richards *et al.*[22]	2014	10	Tumor resection
Richards *et al.*[27]	2017	8	Tumor resection
Klijn *et al.*[25]	2013	8	Tumor resection
Ideguchi *et al.*[28]	2017	12	Tumor resection
Breasts			
Tesselaar *et al.*[29]	2017	15	Adjuvant radiotherapy for stage I-II breast cancer
Zötterman *et al.*[30]	2020	23	Deep inferior epigastric artery perforator (DIEP) flap surgery
Endocrine glands			
de Paula *et al.*[31]	2021	42	Non-functioning adrenal incidentaloma
Mannoh *et al.*[32]	2017	28	Thyroidectomy/parathyroidectomy
Mannoh *et al.*[33]	2021	72	Thyroidectomy
Mannoh *et al.*[34]	2023	21	Thyroidectomy/parathyroidectomy
Skin			
Tchvialeva *et al.*[35]	2012	214 lesions	Malignant melanoma, squamous cell carcinoma, basal cell carcinoma, melanocytic nevus, seborrheic keratosis
Reyal *et al.*[36]	2012	12	Basal cell carcinoma
Zhang *et al.*[37]	2019	12 (total 143)	Facial nerve palsy due to nerve tumor (also including other etiology)
Zieger *et al.*[38]	2021	9	Basal cell carcinoma
Tenland *et al.*[39]	2019	13	Oculoplastic reconstructive surgery (tarsoconjunctival flaps)
Berggren *et al.*[40]	2019	9	Oculoplastic reconstructive surgery (tarsoconjunctival flaps)
Tenland *et al.*[41]	2021	12	Oculoplastic reconstructive surgery after squamous cell carcinoma, basal cell carcinoma, and intradermal nevus
Berggren *et al.*[42]	2021	7	Oculoplastic reconstructive surgery after squamous cell carcinoma and basal cell carcinoma
Berggren *et al.*[43]	2021	7	Oculoplastic reconstructive surgery after squamous cell carcinoma and basal cell carcinoma
Berggren *et al.*[44]	2021	1	Oculoplastic reconstructive surgery
Berggren *et al.*[45]	2022	7	Oculoplastic reconstructive surgery after squamous cell carcinoma and basal cell carcinoma
Stridh *et al.*[46]	2024	1	Cutaneous angio-sarcoma
Gastrointestinal tract (open surgical setting)			
Eriksson *et al.*[47]	2014	10	Liver resection
Milstein *et al.*[48]	2016	11	Esophagectomy
Ambrus *et al.*[49]	2017	45	Esophagectomy
Ambrus *et al.* [50]	2017	25	Ivor-Lewis esophagectomy
Di Maria *et al.*[51]	2017	2	Colorectal resection
Jansen *et al.*[52]	2018	26	Esophagectomy
Kojima *et al.*[53]	2019	8	Colorectal resection
Kaneko *et al.*[54]	2020	36	Colorectal resection (34 due to colorectal carcinoma)
Gastrointestinal tract (laparoscopic/ thoracoscopic setting)			
Heeman *et al.*[55]	2019	10	Colorectal resection
Kojima *et al.*[56]	2020	27	Colorectal resection
Slooter *et al.*[57]	2020	24	Esophagectomy
Heeman *et al.*[58]	2023	67	Hemicolectomy and sigmoid resection
Nwaiwu *et al.*[59]	2023	40	Colectomy, also non-oncological interventions (Roux-en-Y gastric bypass and sleeve gastrectomy)

vasculature, which could be crucial in mitigating ischemic complications and complementing neurophysiological monitoring.

Breasts

Tesselaar *et al.*[29] conducted a study exploring the relationship between radiation exposure and changes in microvascular perfusion in 15 women undergoing adjuvant radiation therapy for stage I-II breast cancer. Their findings suggested that LSCI holds promise as a useful tool for objectively assessing radiation-induced microvascular changes in the skin, even before visible changes occur, thereby aiding in the earlier prediction of potential severe reactions.

In another prospective clinical pilot study conducted across two centers[30], LSCI was employed in 23 women undergoing primary, secondary, or tertiary deep inferior epigastric artery perforator (DIEP) procedures, either unilateral or bilateral. Researchers used laser speckle patterns to calculate perfusion values in arbitrary units (PU), reflecting the concentration and mean velocity of red blood cells. Categorizing patients into high (> 30) and low (< 30) PU, they found that all flaps with perfusion < 30 PU immediately after surgery had postoperative complications, necessitating revision in 4 women. These results suggest potential utility of LSCI for early detection of flap necrosis, aiding surgeons in identifying viable parts of the flaps. Traditionally, assessment of flap viability relies on subjective methods like skin color, flap temperature, capillary refill time, and dermal edge bleeding.

Endocrine glands

Endothelial reactivity[60,61] was evaluated by LSCI in patients with mostly benign non-functioning adrenal incidentaloma.[31]. Mannoh *et al.*[32] used LSCI to assess parathyroid viability post-thyroidectomy in 20 patients, achieving an accuracy of 91.5% in distinguishing between well vascularized (n = 32) and compromised (n = 27) parathyroid glands compared to visual assessment by an experienced surgeon. Ability to detect vascular compromise with LSCI was further validated in parathyroidectomies in 8 patients, showing that this technique could identify parathyroid gland devascularization before it became visually apparent to the surgeon. LSCI demonstrated promise as a real-time, contrast-free, objective method to mitigate hypoparathyroidism after thyroid surgery.

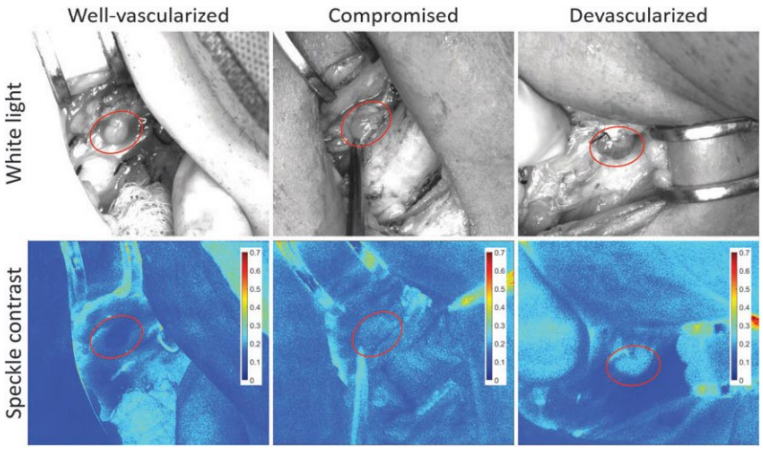

FIGURE 2. Speckle contrast demonstrates lower values for well-vascularized parathyroid glands. Lower speckle contrast values indicate greater blood flow due to more blurring of the speckle pattern, while higher contrast values indicate less blood flow. The top row displays representative white light images, and the bottom row shows speckle contrast images of a well-vascularized (left), a compromised (middle), and a devascularized (right) parathyroid gland, with parathyroid glands marked with ellipses. The corresponding speckle contrast values were 0.11, 0.18, and 0.21, respectively. Taken from Mannoh *et al.* [33] and reprinted with permission from the publisher.

Subsequently, Mannoh *et al.*[33] expanded their research, enrolling 72 patients who underwent thyroidectomy. They established an intraoperative speckle contrast threshold of 0.186 to distinguish between normoparathyroid and hypoparathyroid groups with 87.5% sensitivity and 84.4% specificity. This threshold served as an indicator of adequate parathyroid vascularization, with glands below the value of 0.186 considered adequately perfused (Figure 2).

Additionally, Mannoh *et al.*[34] combined LSCI with ICG angiography in 21 patients undergoing thyroidectomy or parathyroidectomy. While both modalities offered similar information on parathyroid gland blood flow, they suggested advantages of LSCI, including lower costs, non-invasiveness, absence of contraindications, and compatibility with near-infrared autofluorescence (NIRAF) detection, which has recently emerged as a reliable technique for intraoperative parathyroid gland localization or confirmation.[62-64]

Skin

Tchvialeva *et al.*[35] applied LSCI to differentiate among 214 skin lesions, encompassing the three major types of skin cancers (malignant melanoma, squamous cell carcinomas, and basal cell carcinomas – BCCs), and two benign conditions (melanocytic nevus and seborrheic keratoses). In another

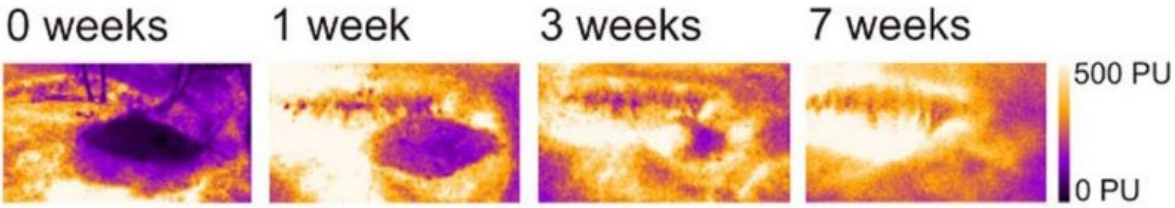

FIGURE 3. Representative examples of laser speckle contrast images, showing the blood perfusion in the free skin grafts, immediately postoperatively (0 weeks), and at follow-up after 1, 3, and 7 weeks. It can be seen that reperfusion occurred simultaneously in the center and periphery of the graft, and that complete reperfusion was achieved after 7 weeks. Taken from Berggren *et al.* [43] and reprinted with permission from the publisher.

early clinical study, LSCI was used to demonstrate that post-occlusive reactive hyperemia could occur in BCC as well.[36] Zhang *et al.*[37] explored differences in facial microvascular perfusion between ipsilateral and contralateral sides in patients with facial nerve palsy (FNP), observing significant decreases on the ipsilateral side, which improved after treatment. In their feasibility study, Zieger *et al.*[38] introduced a compact handheld LSCI device, affirming its reliability in assessing BCC.

In oculoplastics, Tenland *et al.*[39] and Berggren *et al.*[40] conducted studies using LSCI to monitor perfusion in patients with lower eyelid defects after post-tumor surgery large enough to require a tarsoconjunctival graft. Building on their initial work, the group continued research of employing LSCI in various oculoplastic reconstructive surgery procedures. First, Tenland *et al.*[41] monitored perfusion using LSCI in a study in which free bilamellar eyelid grafts appeared to be an excellent alternative to the tarsoconjunctival flap procedure in the reconstruction of both upper and lower eyelid defects. Next, Berggren *et al.*[42] noted rapid revascularization of H-plasty procedure flaps within a week postoperatively, attributing it to the pre-existing vascular network of the flap pedicle, rather than significant angiogenesis. In another study, Berggren *et al.*[43] demonstrated complete reperfusion of skin grafts in the periorbital area after 7 weeks (Figure 3). Berggren *et al.*[44] also presented a case illustrating nearly complete restoration of reperfusion in a rotational full-thickness lower eyelid flap within 5 weeks. Finally, they assessed blood perfusion in glabellar flaps, finding rapid reperfusion.[45] These convincing findings suggest that perioperative LSCI monitoring of perfusion in human periocular flaps and during oculoplastic reconstructive surgery offers an attractive imaging modality for routine clinical use. Not surprisingly, Stridh *et al.*[46] recently conducted a pilot study comprehensively combining LSCI with two other emerging non-invasive medical imaging modalities, hyperspectral imaging [65-67] and photoacoustic imaging[68] to monitor not only blood perfusion but also oxygen saturation and the molecular composition of the tissue.

Gastrointestinal tract (open surgical setting)

The majority of clinical oncology studies with intraoperative LSCI were conducted in an open surgical setting, which we will review first. In an initial pilot clinical study, Eriksson *et al.*[47] assessed liver blood perfusion by occluding the portal vein and hepatic artery in ten consecutive patients undergoing liver resection for colorectal liver metastases. This early effort was followed by Milstein *et al.*[48], who evaluated microvascular blood flow during esophagectomy, affirming that intraoperative LSCI offered a non-contact, non-invasive approach for real-time analysis of potential anastomotic leakage without requiring a contrast medium. This finding was subsequently corroborated by Ambrus *et al.* who first performed gastric microvascular perfusion measurements during esophagectomy in 45 patients[49] and later used LSCI in Ivor-Lewis esophagectomy in 25 patients.[50]

Di Maria *et al.*[51] explored the feasibility of LSCI in 2 patients undergoing colorectal surgery, while Jansen *et al.*[52] investigated the impact of thoracic epidural anesthesia during esophagectomy, once again demonstrating that LSCI could detect subtle changes in gastric microvascular perfusion in real-time. Another group conducted an additional feasibility study of intraoperative LSCI in 8 patients undergoing colorectal surgery.[53] Kaneko *et al.*[54] further expanded on these feasibility studies by enrolling 36 patients undergoing colorectal resection, 34 of whom had colorectal carcinoma, aiming to compare demarcation lines determined by LSCI with transection lines where marginal vessels

were divided. They found that 58.3% (21/36) of demarcation lines matched transection lines, with a median distance of 0.0 mm (0.0–12.1 mm) between the demarcation line determined by LSCI and the transection line.

Gastrointestinal tract (laparoscopic/ thoracoscopic setting)

Heeman *et al.*[55] reported the first intraabdominal application combining a standard laparoscopic surgical setup with LSCI in 10 patients, enabling imaging of intestinal blood flow during a vascular occlusion test. Their findings were corroborated by Kojima *et al.*[56] in a study involving 27 patients (Figure 4). Slooter *et al.*[57] systematically compared four different emerging optical modalities, highlighting the clinical utility of FA-ICG as the most promising. Recently, Heeman *et al.*[58] tested a commercial LSCI system in the oncological clinical setting, noting that the system was "non-disruptive of the surgical procedure with an average added surgical time of only 2.5 min and no change in surgical equipment". They also observed a potential clinical benefit of the LSCI system, with 17% of operating surgeons altering anastomosis locations based on perfusion assessments. Nwaiwu *et al.*[58] evaluated another commercial intraoperative system combining LSCI and FA-ICG in mostly non-oncological patients, demonstrating that LSCI identified the same perfusion boundaries as FA-ICG, with anastomoses and gastric remnants appearing well perfused.

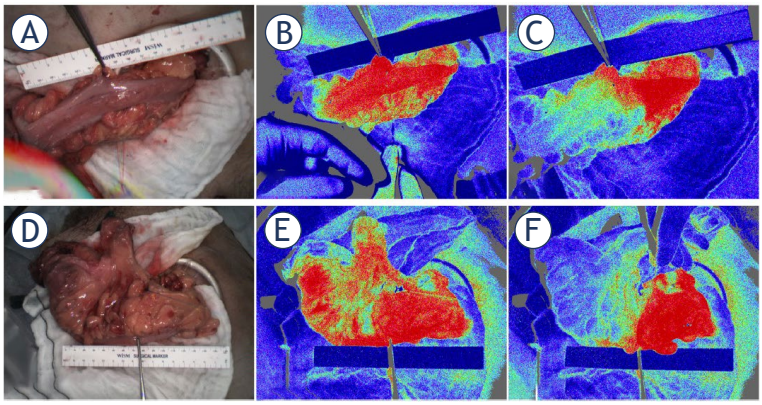

FIGURE 4. Typical laser speckle images in two patients. High-resolution laser speckle contrast imaging (LSCI) can indicate the bowel demarcation line at the point of ligation of the marginal vessels. **(A)** Normal color image before ligating the marginal vessels. **(B)** LSCI image before ligating the marginal vessels. **(C)** LSCI image after ligating the marginal vessels. Taken from Kojima *et al.*[56] and reprinted with permission from the publisher.

Discussion

Based on this literature review, several advantages of LSCI emerge, including its non-invasive and non-contact nature, short acquisition time, high spatial and temporal resolution, low cost of equipment, and simplicity of operation. In the oncological clinical setting, LSCI holds particular promise for assessing skin flap perfusion post-oculoplastic reconstructive surgery and anastomotic perfusion during gastrointestinal reconstruction. While LSCI offers numerous advantages in imaging blood flow dynamics, it is essential to recognize its limitations.

Limited penetration depth

One of the obvious limitations of LSCI in clinical oncology and medical applications, in general, is its restricted penetration depth. LSCI relies on detecting motion contrast generated by moving red blood cells, limiting its applicability to superficial structures. Tumors and lesions located in deeper anatomical locations, such as within organs or soft tissues, may not be adequately visualized due to this limitation, hindering comprehensive evaluation and monitoring of oncological conditions. However, studies like that of Stridh *et al.*[46] demonstrate that PAI as a complementary imaging technique can overcome this limitation. Another possibility to potentially consider is the use of optical clearance techniques[69] to enhance tissue transparency and improve light penetration depth.

Motion artifacts

LSCI is susceptible to motion artifacts, which can arise from either involuntary movement of the subject or vibrations in the imaging setup. These artifacts can lead to image distortions and reduced image quality, compromising the accuracy and reliability of LSCI in clinical oncology. To address this, advanced post-processing algorithms are necessary to improve image quality. Since motion artifacts are well-known sources of artifacts in LSCI, they have been extensively researched. One possibility is to implement motion compensation techniques, such as image stabilization algorithms[70] or gating strategies[71], which can mitigate the effects of motion artifacts in LSCI. By minimizing motion-induced distortions in the speckle pattern, these

techniques improve the accuracy and reliability of blood flow measurements.

Inherent speckle noise

The presence of inherent speckle noise in LSCI images can compromise the accuracy and reliability of blood flow measurements, particularly in low-flow regions or under conditions of low contrast. Speckle noise can obscure subtle flow changes and restrict the sensitivity of LSCI in detecting small-scale perfusion variations. Advanced noise reduction algorithms[72] offer a solution by effectively suppressing speckle noise and enhancing the signal-to-noise ratio. These algorithms filter out unwanted noise components while retaining relevant flow information, thereby improving the sensitivity and specificity of LSCI in detecting perfusion changes, even in challenging imaging conditions.

Lack of standardized protocols and interpretation

A significant limitation of LSCI in clinical oncology is the lack of standardized protocols and interpretation guidelines. Varying acquisition settings, image processing algorithms, or interpretation methodologies across different centers can yield inconsistent and non-comparable results. Establishing standardized protocols and guidelines tailored to oncology applications would enhance the accuracy and reproducibility of LSCI findings.

Despite its potential, the clinical integration of LSCI faces obstacles, including the standardization of imaging protocols, validation of its utility in large-scale clinical trials, and integration into existing surgical workflows. Addressing these limitations requires advancements in technology, algorithm refinement, and increased participation of clinical sites in conducting trials. Overcoming these challenges is essential for realizing the full potential of LSCI in clinical oncology; it is worth noting that other biomedical optical imaging techniques [65-67,73-80] are likely to encounter similar challenges in the future.

Acknowledgment

Authors wish to thank Matija Milanič for careful reading of the manuscript and his help with literature search.

This work was financially supported by the state budget by the Slovenian Research Agency, research grant no. J3-3083 and research programs no. P3-0003, P3-0307, P1-0389, P2-0348, and N1-0283.

References

1. Li H, Xie X, Du F, Zhu X, RenH, Ye C, et al. A narrative review of intraoperative use of indocyanine green fluorescence imaging in gastrointestinal cancer: situation and future directions. *J Gastrointest Oncol* 2023; **14:** 1095-113. doi: 10.21037/jgo-23-230
2. Uppal JS, Meng E, Caycedo-Marulanda A. Current applications of indocyanine green fluorescence in colorectal surgery: a narrative review. *Ann Laparosc Endosc Surg* 2023; **8:** 18-18. doi: 10.21037/ales-22-84
3. Iwamoto M, Ueda K, Kawamura J. A narrative review of the usefulness of indocyanine green fluorescence angiography for perfusion assessment in colorectal surgery. *Cancers* 2022; **14:** 5623. doi: 10.3390/cancers14225623
4. Briers D, Duncan DD, Hirst E, Kirkpatric SJ, Larsson M, Steenberg W, et al. Laser speckle contrast imaging: theoretical and practical limitations. *J Biomed Opt* 2013; **18:** 066018. doi: 10.1117/1.JBO.18.6.066018
5. Briers JD, Richards G, He XW. Capillary blood flow monitoring using laser speckle contrast analysis (LASCA). *J Biomed Opt* 1999; **4:** 164. doi: 10.1117/1.429903
6. Draijer M, Hondebrink E, Van Leeuwen T, Steenbergen W. Review of laser speckle contrast techniques for visualizing tissue perfusion. *Lasers Med Sci* 2009; **24:** 639-51. doi: 10.1007/s10103-008-0626-3
7. Hamed AM, El-Ghandoor H, El-Diasty F, Saudy M. Analysis of speckle images to assess surface roughness. *Optics & Laser Technology* 2004; **36:** 249-53. doi: 10.1016/j.optlastec.2003.09.005
8. Heeman W, Steenbergen W, Van Dam GM, Boerma EC. Clinical applications of laser speckle contrast imaging: a review. *J Biomed Opt* 2019; **24:** 1. doi: 10.1117/1.JBO.24.8.080901
9. Cheng H, Yan Y, Duong TQ. Temporal statistical analysis of laser speckle images and its application to retinal blood-flow imaging. *Opt Express* 2008; **16:** 10214. doi: 10.1364/OE.16.010214
10. Hellmann M, Roustit M, Cracowski JL. Skin microvascular endothelial function as a biomarker in cardiovascular diseases? *Pharmacol Rep* 2015; **67:** 803-10. doi: 10.1016/j.pharep.2015.05.008
11. Margouta A, Anyfanti P, Lazaridis A, Nikolaidou B, Mastrogiannis K, Malliora A, et al. Blunted microvascular reactivity in psoriasis patients in the absence of cardiovascular disease, as assessed by laser speckle contrast imaging. *Life* 2022; **12:** 1796. doi: 10.3390/life12111796
12. Gopal JP, Vaz O, Varley R, Spiers H, Goldsworthy MA, Siddagangaiah V, et al. Using laser speckle contrast imaging to quantify perfusion quality in kidney and pancreas grafts on vascular reperfusion: a proof-of-principle study. *Transplant Direct* 2023; **9:** e1472. doi: 10.1097/TXD.0000000000001472
13. Mirdell R, Farnebo S, Sjöberg F, Tesselaar E. Accuracy of laser speckle contrast imaging in the assessment of pediatric scald wounds. *Burns* 2018; **44:** 90-8. doi: 10.1016/j.burns.2017.06.010
14. Mirdell R, Farnebo S, Sjöberg F, Tesselaar E. Interobserver reliability of laser speckle contrast imaging in the assessment of burns. *Burns* 2019; **45:** 1325-35. doi: 10.1016/j.burns.2019.01.011
15. Mirdell R, Farnebo S, Sjöberg F, Tesselaar E. Using blood flow pulsatility to improve the accuracy of laser speckle contrast imaging in the assessment of burns. *Burns* 2020; **46:** 1398-406. doi: 10.1016/j.burns.2020.03.008
16. Rege A, Thakor NV, Rhie K, Pathak AP. In vivo laser speckle imaging reveals microvascular remodeling and hemodynamic changes during wound healing angiogenesis. *Angiogenesis* 2012; **15:** 87-98. doi: 10.1007/s10456-011-9245-x
17. Zheng KJ, Middelkoop E, Stoop M, Van Zuijlen PPM, Pijpe A. Validity of laser speckle contrast imaging for the prediction of burn wound healing potential. *Burns* 2022; **48:** 319-27. doi: 10.1016/j.burns.2021.04.028
18. Mirdell R, Iredahl F, Sjöberg F, Farnebo S, Tesselaar E. Microvascular blood flow in scalds in children and its relation to duration of wound healing: a study using laser speckle contrast imaging. *Burns* 2016; **42:** 648-54. doi: 10.1016/j.burns.2015.12.005
19. Berggren JV, Stridh M, Malmsjö M. Perfusion monitoring during oculoplastic reconstructive surgery: a comprehensive review. *Ophthalmic Plast Reconstr Surg* 2022; **38:** 522-34. doi: 10.1097/IOP.0000000000002114

20. Hecht N, Woitzik J, König S, Horn P, Vajkoczy P. Laser speckle imaging allows real-time intraoperative blood flow assessment during neurosurgical procedures. *J Cereb Blood Flow Metab* 2013; **33:** 1000-7. doi: 10.1038/jcbfm.2013.42

21. Parthasarathy AB, Weber EL, Richards LM, Fox DJ, Dunn AK. Laser speckle contrast imaging of cerebral blood flow in humans during neurosurgery: a pilot clinical study. *J Biomed Opt* 2010; **15:** 066030. doi: 10.1117/1.3526368

22. Richards LM, Towle EL, Fox DJ, Dunn AK. Intraoperative laser speckle contrast imaging with retrospective motion correction for quantitative assessment of cerebral blood flow. *Neurophoton* 2014; **1:** 1. doi: 10.1117/1.NPh.1.1.015006

23. Woitzik J, Hecht N, Pinczolits A, Sandow N, Major S, Winkler MKL, et al. Propagation of cortical spreading depolarization in the human cortex after malignant stroke. *Neurology* 2013; **80:** 1095-102. doi: 10.1212/WNL.0b013e3182886932

24. Hecht N, Müller MM, Sandow N, Pinczolits A, Vajkoczy P, Woitzik J. Infarct prediction by intraoperative laser speckle imaging in patients with malignant hemispheric stroke. *J Cereb Blood Flow Metab* 2016; **36:** 1022-32. doi: 10.1177/0271678X15612487

25. Klijn E, Hulscher HC, Balvers RK, Holland WPJ, Bakker J, Vincent ALPE, et al. Laser speckle imaging identification of increases in cortical microcirculatory blood flow induced by motor activity during awake craniotomy: clinical article. *J Neurosurg* 2013; **118:** 280-86. doi: 10.3171/2012.10.JNS1219

26. Konovalov A, Gadzhiagaev V, Grebenev F, Stavtsev D, Piavchenko G, Gerasimenko A, et al. Laser speckle contrast imaging in neurosurgery: a systematic review. *World Neurosurg* 2023; **171:** 35-40. doi: 10.1016/j.wneu.2022.12.048

27. Richards LM, Kazmi SS, Olin KE, Waldron JS, Fox DJ, Dunn AK. Intraoperative multi-exposure speckle imaging of cerebral blood flow. *J Cereb Blood Flow Metab* 2017; **37:** 3097-109. doi: 10.1177/0271678X16686987

28. Ideguchi M, Kajiwara K, Yoshikawa K, Goto H, Sugimoto K, Inoue T, et al. Avoidance of ischemic complications after resection of a brain lesion based on intraoperative real-time recognition of the vasculature using laser speckle flow imaging. *J Neurosurg* 2017; **126:** 274-80. doi: 10.3171/2016.1.JNS152067

29. Tesselaar E, Flejmer AM, Farnebo S, Dasu A. Changes in skin microcirculation during radiation therapy for breast cancer. *Acta Oncol* 2017; **56:** 1072-80. doi: 10.1080/0284186X.2017.1299220

30. Zötterman J, Opsomer D, Farnebo S, Blondeel P, Monstrey S, Tesselaar E. Intraoperative laser speckle contrast imaging in DIEP breast reconstruction: a prospective case series study. *Plast Reconstr Surg Glob Open* 2020; **8:** e2529. doi: 10.1097/GOX.0000000000002529

31. De Paula MP, Moraes AB, De Souza MDGC, Cavalari EMR, Campbell RC, da Silva Fernandes G, et al. Cortisol level after dexamethasone suppression test in patients with non-functioning adrenal incidentaloma is positively associated with the duration of reactive hyperemia response on microvascular bed. *J Endocrinol Invest* 2021; **44:** 609-19. doi: 10.1007/s40618-020-01360-z

32. Mannoh EA, Thomas G, Solórzano CC, Mahadevan-Jansen A. Intraoperative assessment of parathyroid viability using laser speckle contrast imaging. *Sci Rep* 2017; **7:** 14798. doi: 10.1038/s41598-017-14941-5

33. Mannoh EA, Thomas G, Baregamian N, Rohde SL, Solórzano CC, Mahadevan-Jansen A. Assessing intraoperative laser speckle contrast imaging of parathyroid glands in relation to total thyroidectomy patient outcomes. *Thyroid* 2021: **31:** 1558-65. doi: 10.1089/thy.2021.0093

34. Mannoh EA, Baregamian N, Thomas G, Solórzano CC, Mahadevan-Jansen A. Comparing laser speckle contrast imaging and indocyanine green angiography for assessment of parathyroid perfusion. *Sci Rep* 2023; **13:** 17270. doi: 10.1038/s41598-023-42649-2

35. Tchvialeva L, Dhadwal G, Lui H, Kalia S, Zeng H, McLean DI, et al. Polarization speckle imaging as a potential technique for *in vivo* skin cancer detection. *J Biomed Opt* 2012; **18:** 061211. doi: 10.1117/1.JBO.18.6.061211

36. Reyal J, Lebas N, Fourme E, Guihard T, Vilmer C, Masurier PL. Post-occlusive reactive hyperemia in basal cell carcinoma and its potential application to improve the efficacy of solid tumor therapies. *Tohoku J Exp Med* 2012; **227:** 139-47. doi: 10.1620/tjem.227.139

37. Zhang Y, Zhao L, Li J, Wang J, Yu H. Microcirculation evaluation of facial nerve palsy using laser speckle contrast imaging: a prospective study. *Eur Arch Otorhinolaryngol* 2019; **276:** 685-92. doi: 10.1007/s00405-019-05281-3

38. Zieger M, Kaatz M, Springer S, Riesenberg R, Wuttig A, Kanka M, et al. Multi-wavelength, handheld laser speckle imaging for skin evaluation. *Skin Res Technol* 2021; **27:** 486-93. doi: 10.1111/srt.12959

39. Tenland K, Memarzadeh K, Berggren J, Nguyen CD, Dahlstrand U, Hult J, et al. Perfusion monitoring shows minimal blood flow from the flap pedicle to the tarsoconjunctival flap. *Ophthalmic Plast Reconstr Surg* 2019; **35:** 346-9. doi: 10.1097/IOP.0000000000001250

40. Berggren J, Tenland K, Ansson CD, Dahlstrand U, Sheikh R, Hult J, et al. Revascularization of free skin grafts overlying modified hughes tarsoconjunctival flaps monitored using laser-based techniques. *Ophthalmic Plast Reconstr Surg* 2019; **35:** 378-82. doi: 10.1097/IOP.0000000000001286

41. Tenland K, Berggren J, Engelsberg K, Bohman E, Dahlstrand U, Castelo N, et al. Successful free bilamellar eyelid grafts for the repair of upper and lower eyelid defects in patients and laser speckle contrast imaging of revascularization. *Ophthalmic Plast Reconstr Surg* 2021; **37:** 168-72. doi: 10.1097/IOP.0000000000001724

42. Berggren J, Castelo N, Tenland K, Engelsberg K, Dahlstand U, Albinsson J, et al. Revascularization after H-plasty reconstructive surgery in the periorbital region monitored with laser speckle contrast imaging. *Ophthalmic Plast Reconstr Surg* 2021; **37:** 269-73. doi: 10.1097/IOP.0000000000001799

43. Berggren J, Castelo N, Tenland K, Dahlstrand, Engelsberg K, Lindstedt S, et al. Reperfusion of free full-thickness skin grafts in periocular reconstructive surgery monitored using laser speckle contrast imaging. *Ophthalmic Plast Reconstr Surg* 2021; **37:** 324-8. doi: 10.1097/IOP.0000000000001851

44. Berggren JV, Sheikh R, Hult J, Engelsberg K, Malmsjö M. Laser speckle contrast imaging of a rotational full-thickness lower eyelid flap shows satisfactory blood perfusion. *Ophthalmic Plast Reconstr Surg* 2021; **37:** e139-e141. doi: 10.1097/IOP.0000000000001921

45. Berggren JV, Tenland K, Sheikh R, Hult J, Engelsberg K, Lindstedt S, et al. Laser speckle contrast imaging of the blood perfusion in glabellar flaps used to repair medial canthal defects. *Ophthalmic Plast Reconstr Surg* 2022; **38:** 274-9. doi: 10.1097/IOP.0000000000002082

46. Stridh M, Dahlstrand U, Naumovska M, Engelsberg K, Gesslein B, Sheikh R, et al. Functional and molecular 3D mapping of angiosarcoma tumor using non-invasive laser speckle, hyperspectral, and photoacoustic imaging. *Orbit* 2024; **9:** 1-11. doi: 10.1080/01676830.2024.2331718

47. Eriksson S, Jan N, Gert L, Sturesson C. Laser speckle contrast imaging for intraoperative assessment of liver microcirculation: a clinical pilot study. *Med Devices* 2014; 25: 257-61. doi: 10.2147/MDER.S63393

48. Milstein DMJ, Ince C, Gisbertz SS, Boateng KB, Geerts BF, Hollmann MW, et al. Laser speckle contrast imaging identifies ischemic areas on gastric tube reconstructions following esophagectomy. *Medicine* 2016; **95:** e3875. doi: 10.1097/MD.0000000000003875

49. Ambrus R, Achiam MP, Secher NH, Svendsen MB, Runitz K, Siemsen M, et al. Evaluation of gastric microcirculation by laser speckle contrast imaging during esophagectomy. *J Am Col Surg* 2017; **225:** 395-402. doi: 10.1016/j.jamcollsurg.2017.06.003

50. Ambrus R, Svendsen LB, Secher NH, Runitz K, Fredriksen HJ, Svendsen MBS, et al. A reduced gastric corpus microvascular blood flow during Ivor-Lewis esophagectomy detected by laser speckle contrast imaging technique. *Scand J Gastroenterol* 2017; **52:** 455-61. doi: 10.1080/00365521.2016.1265664

51. Di Maria C, Hainsworth PJ, Allen J. Intraoperative thermal and laser speckle contrast imaging assessment of bowel perfusion in two cases of colorectal resection surgery. In: Ng EY, Etehadtavakol M, editors. *Application of infrared to biomedical sciences*. Series in BioEngineering. Singapore: Springer; 2017. p. 437-49. doi: 10.1007/978-981-10-3147-2_25

52. Jansen SM, De Bruin DM, Van Berge Henegouwen MI, Bloemen PR, Strackee SD, Veelo DP, et al. Effect of ephedrine on gastric conduit perfusion measured by laser speckle contrast imaging after esophagectomy: a prospective in vivo cohort study. *Dis Esophagus* 2018; **1:** 31. doi: 10.1093/dote/doy031

53. Kojima S, Sakamoto T, Nagai Y, Matsui Y, Nambu K, Masamune K. Laser speckle contrast imaging for intraoperative quantitative assessment of intestinal blood perfusion during colorectal surgery: a prospective pilot study. *Surg Innov* 2019; **26:** 293-301. doi: 10.1177/1553350618823426

54. Kaneko T, Funahashi K, Ushigome M, Kagami S, Yoshida K, Koda T, et al. Noninvasive assessment of bowel blood perfusion using intraoperative laser speckle flowgraphy. *Langenbecks Arch Surg* 2020; **405:** 817-26. doi: 10.1007/s00423-020-01933-9

55. Heeman W, Dijkstra K, Hoff C, Koopal S, Pierie JP, Bouma H, et al. Application of laser speckle contrast imaging in laparoscopic surgery. *Biomed Opt Express* 2019; **10:** 2010-9. doi: 10.1364/BOE.10.002010

56. Kojima S, Sakamoto T, Matsui Y, Nambu K, Masamune K. Clinical efficacy of bowel perfusion assessment during laparoscopic colorectal resection using laser speckle contrast imaging: a matched case-control study. *Asian J Endoscop Surgery* 2020; **13:** 329-35. doi: 10.1111/ases.12759

57. Slooter MD, Jansen SMA, Bloemen PR, van den Elzen RM, Wilk LS, van Leeuwen TG, et al. Comparison of optical imaging techniques to quantitatively assess the perfusion of the gastric conduit during oesophagectomy. *Applied Sciences* 2020; **10:** 5522. doi: 10.3390/app10165522

58. Heeman W, Calon J, Van Der Bilt A, Pierie JPEN, Pereboom I, van Dam GM, et al. Dye-free visualisation of intestinal perfusion using laser speckle contrast imaging in laparoscopic surgery: a prospective, observational multi-centre study. *Surg Endosc* 2023; **37:** 9139-46. doi: 10.1007/s00464-023-10493-0

59. Nwaiwu CA, McCulloh CJ, Skinner G, Shah SK, Kim PC, Schwaitzberg SD, et al. Real-time first-in-human comparison of laser speckle contrast imaging and ICG in minimally invasive colorectal & bariatric surgery. *J Gastrointest Surgery* 2023; **27:** 3083-5. doi: 10.1007/s11605-023-05855-x

60. Yataco AR, Corretti MC, Gardner AW, Womack CJ, Katzel LI. Endothelial reactivity and cardiac risk factors in older patients with peripheral arterial disease. *Am J Cardiol* 1999; **83:** 754-8. doi: 10.1016/S0002-9149(98)00984-9

61. Souza EG, De Lorenzo A, Huguenin G, Oliveira GMM, Tibiriçá E. Impairment of systemic microvascular endothelial and smooth muscle function in individuals with early-onset coronary artery disease: studies with laser speckle contrast imaging. *Coron Artery Dis* 2014; **25:** 23-28. doi: 10.1097/MCA.0000000000000055

62. Paras C, Keller M, White L, Phay J, Mahadevan-Jansen A. Near-infrared autofluorescence for the detection of parathyroid glands. *J Biomed Opt* 2011; **16:** 067012. doi: 10.1117/1.3583571

63. Benmiloud F, Godiris-Petit G, Gras R, Gillot JC, Turrin N, Penarada G, et al. Association of autofluorescence-based detection of the parathyroid glands during total thyroidectomy with postoperative hypocalcemia risk: results of the PARAFLUO multicenter randomized clinical trial. *JAMA Surg* 2020; **155:** 106. doi: 10.1001/jamasurg.2019.4613

64. Dip F, Falco J, Verna S, Prunello M, Loccisano M, Quadri P, et al. Randomized controlled trial comparing white light with near-infrared autofluorescence for parathyroid gland identification during total thyroidectomy. *J Am Coll Surg* 2019; **228:** 744-51. doi: 10.1016/j.jamcollsurg.2018.12.044

65. Stergar J, Hren R, Milanič M. Design and validation of a custom-made laboratory hyperspectral imaging system for biomedical applications using a broadband LED light source. *Sensors* 2022; **22:** 6274. doi: 10.3390/s22166274

66. Hren R, Sersa G, Simoncic U, Milanic M. Imaging perfusion changes in oncological clinical applications by hyperspectral imaging: a literature review. *Radiol Oncol* 2022; **56:** 420-9. doi: 10.2478/raon-2022-0051

67. Hren R, Stergar J, Simončič U, Serša G, Milanič M. Assessing perfusion changes in clinical oncology applications using hyperspectral imaging. In: Jarm T, Šmerc R, Mahnič-Kalamiza S, editors. *9th European Medical and Biological Engineering Conference*. Portorož, Slovenia; 2024 Jun 9-13. Vol 112. IFMBE Proceedings. Switzerland: Springer Nature; 2024. p. 122-9. doi: 10.1007/978-3-031-61625-9_14

68. Lin L, Wang LV. The emerging role of photoacoustic imaging in clinical oncology. *Nat Rev Clin Oncol* 2022; **19:** 365-84. doi: 10.1038/s41571-022-00615-3

69. Xia Q, Li D, Yu T, Zhu J, Zhu D. In vivo skin optical clearing for improving imaging and light-induced therapy: a review. *J Biomed Opt* 2023; **28:** 060901. doi: 10.1117/1.JBO.28.6.060901

70. Heeman W, Maassen H, Dijkstra K, Calon J, van Goor H, Leuvenik H, et al. Real-time, multi-spectral motion artefact correction and compensation for laser speckle contrast imaging. *Sci Rep* 2022; **12:** 21718. doi: 10.1038/s41598-022-26154-6

71. Gnyawali SC, Blum K, Pal D, Ghatak S, Khanna S, Roy S, et al. Retooling laser speckle contrast analysis algorithm to enhance non-invasive high resolution laser speckle functional imaging of cutaneous microcirculation. *Sci Rep* 2017; **7:** 41048. doi: 10.1038/srep41048

72. Han G, Li D, Wang J, Guo Q, Yuan J, Chen R, et al. Adaptive window space direction laser speckle contrast imaging to improve vascular visualization. *Biomed Opt Express* 2023; **14:** 3086. doi: 10.1364/BOE.488054

73. Hren R, Sersa G, Simoncic U, Milanic M. Imaging microvascular changes in nonocular oncological clinical applications by optical coherence tomography angiography: a literature review. *Radiol Oncol* 2023; **57:** 411-8. doi: 10.2478/raon-2023-0057

74. Stergar J, Hren R, Milanič M. Design and validation of a custom-made hyperspectral microscope imaging system for biomedical applications. *Sensors* 2023; **23:** 2374. doi: 10.3390/s23052374

75. Marin A, Hren R, Milanič M. Pulsed photothermal radiometric depth profiling of bruises by 532 nm and 1064 nm lasers. *Sensors* 2023; **23:** 2196. doi: 10.3390/s23042196

76. Rogelj L, Dolenec R, Tomšič MV, Laister E, Simončič U, Milanič M, et al. Anatomically accurate, high-resolution modeling of the human index finger using in vivo magnetic resonance imaging. *Tomography* 2022; **8:** 2347-59. doi: 10.3390/tomography8050196

77. Milanic M, Hren R, Stergar J, Simoncic U. Monitoring of caffeine consumption effect on skin blood properties by diffuse reflectance spectroscopy. *Physiol Res* 2024; **73:** 47-56. doi: 10.33549/physiolres.935138

78. Marin A, Verdel N, Milanič M, Majaron B. Noninvasive monitoring of dynamical processes in bruised human skin using diffuse reflectance spectroscopy and pulsed photothermal radiometry. *Sensors* 2021; **21:** 302. doi: 10.3390/s21010302

79. Milanic M, Marin A, Stergar J, Verdel N, Majaron B. Monitoring of caffeine consumption effect on skin blood properties by diffuse reflectance spectroscopy. In: Dehghani H, Wabnitz H, editors. *Diffuse optical spectroscopy and imaging VI*. SPIE Proceedings; European Conference on Biomedical Optics 2017. Munich Germany; 25-29 Jun 2017. Paper 1041215. doi: 10.1117/12.2286140

80. Verdel N, Marin A, Milanič M, Majaron B. Physiological and structural characterization of human skin in vivo using combined photothermal radiometry and diffuse reflectance spectroscopy. *Biomed Opt Express* 2019; **10:** 944. doi: 10.1364/BOE.10.000944

research article

Role of quantitative imaging biomarkers in an early FDG-PET/CT for detection of immune-related adverse events in melanoma patients: a prospective study

Nezka Hribernik[1,2], Katja Strasek[3], Daniel T Huff[4,5], Andrej Studen[3,6], Katarina Zevnik[7], Katja Skalic[7], Robert Jeraj[3,4,5,6], Martina Rebersek[1,2]

[1] Department of Medical Oncology, Institute of Oncology Ljubljana, Ljubljana, Slovenia
[2] Faculty of Medicine, University of Ljubljana, Ljubljana, Slovenia
[3] Faculty of Mathematics and Physics, University of Ljubljana, Ljubljana, Slovenia
[4] University of Wisconsin Carbone Cancer Centre, Madison, WI, USA
[5] Department of Medical Physics, University of Wisconsin-Madison, Madison, WI, USA
[6] Experimental Particle Physics Department, Jožef Stefan Institute, Ljubljana, Slovenia
[7] Department of Nuclear Medicine, Institute of Oncology Ljubljana, Ljubljana, Slovenia

Radiol Oncol 2024; 58(3): 335-347.

Received 13 June 2024
Accepted 14 July 2024

Correspondence to: Assist. Prof. Martina Reberšek, M.D., Ph.D., Department of Medical Oncology, Institute of Oncology Ljubljana, Zaloška 2, SI-1000 Ljubljana, Slovenia. E-mail: mrebersek@onko-i.si

Disclosure: Robert Jeraj is a co-founder and CSO of AIQ Solutions, Madison, WI, USA. No potential conflicts of interest were disclosed for other co-authors.

Background. To evaluate the role of the novel quantitative imaging biomarker (QIB) $SUV_{X\%}$ of ^{18}F-FDG uptake extracted from early ^{18}F-FDG -PET/CT scan at 4 weeks for the detection of immune-related adverse events (rAE) in a cohort of patients with metastatic melanoma (mM) patients receiving immune-checkpoint inhibitors (ICI).

Patients and methods. In this prospective non-interventional, one-centre clinical study, patients with mM, receiving ICI treatment, were regularly followed by ^{18}F-FDG PET/CT. Patients were scanned at baseline, early point at week four (W4), week sixteen (W16) and week thirty-two (W32) after ICI initiation. A convolutional neural network (CNN) was used to segment three organs: lung, bowel, thyroid. QIB of irAE - $SUV_{X\%}$ - was analyzed within the target organs and correlated with the clinical irAE status. Area under the receiver-operating characteristic curve (AUROC) was used to quantify irAE detection performance.

Results. A total of 242 ^{18}F-FDG PET/CT images of 71 mM patients were prospectively collected and analysed. The early W4 scan showed improved detection only for the thyroid gland compared to W32 scan (p=0.047). The AUROC for detection of irAE in the three target organs was highest when $SUV_{X\%}$ was extracted from W16 scan and was 0.76 for lung, 0.53 for bowel and 0.81 for thyroid. $SUV_{X\%}$ extracted from W4 scan did not improve detection of irAE compared to W16 scan (lung: p = 0.54, bowel: p = 0.75, thyroid: p = 0.3, DeLong test), as well as compared to W32 scan in lungs (p = 0.32) and bowel (p = 0.3).

Conclusions. Early time point ^{18}F-FDG PET/CT at W4 did not lead to statistically significant earlier detection of irAE. However, organ^{18}F-FDG uptake as quantified by $SUV_{X\%}$ proved to be a consistent QIB of irAE. To better assess the role of ^{18}F-FDG PET/CT in irAE detection, the time evolution of ^{18}F-FDG PET/CT quantifiable inflammation would be of essence, only achievable in multi centric studies.

Key words: ^{18}F-FDG PET/CT; immune-checkpoint inhibitors; immune-related adverse effects; quantitative imaging biomarkers; SUV percentiles

Introduction

Immunotherapy with immune checkpoint inhibitors (ICI) is considered the standard of care for the treatment of unresectable stage III and IV metastatic melanoma (mM). It leads to high response rates and improvement of survival in this group of cancer patients.[1-4] ICI treatments can cause different immune-related adverse events (irAE), where an immune response is generated against healthy tissue.[5-7] Nearly one quarter of ICI treated patients experience higher grades of irAE that require hospitalization, 26% due to immune-related pneumonitis (irPneumonitis) and 17% due to immune-related colitis (irColitis).[8] Consequently, prolonged immune suppressive treatment is needed, which can significantly endanger patient health and reduce the efficacy of ICI treatment.

The immense progress of ICI has brought different challenges, one of them being assessment of treatment efficacy and management of variety of irAE. Positron emission tomography/computed tomography with [^{18}F]fluoro-2-deoxy-D-glucose (^{18}F-FDG PET/CT) is a non-invasive method, commonly used in diagnosis, staging, and treatment response monitoring in mM. Its role in the treatment process is being recognized through different guidelines and emerging evidence.[9,10]

In addition to monitoring response, ^{18}F-FDG PET/CT can detect certain irAE, some even before they clinically or biochemically manifest.[11-13] Early detection or even prediction of irAE is of great interest, as this could contribute to better treatment.[11,14] To date, no study has been published investigating whether a systematic search for irAE with ^{18}F-FDG PET/CT imaging as early as four weeks after the start of ICI treatment would help in early detection of irAE. However, several studies investigated utility of different ^{18}F-FDG PET/CT timing. A small prospective study with 20 mM patients evaluated if ^{18}F-FDG PET/CT at days 21-28 would help predicting response to ICI in mM patients. It showed that increased ^{18}F-FDG uptake early during ICI treatment may be associated with immune activation and favourable outcome.[15] No analysis of irAE was reported. A similar study investigated prognostic value of ^{18}F-FDG PET/CT after two cycles of ICI administration.[16] They looked also for patterns of ^{18}F-FDG uptake suggestive of irAE and found that the emergence of PET signs of irAE was not associated with patient survival. Another recent study analysed the usefulness of ^{18}F-FDG PET/CT performed even earlier, one week after starting the treatment with pembrolizumab of mM patients. The study was aimed to evaluate metabolic changes in melanoma metastases one week after treatment start in order to predict the response to treatment. No evaluation of organs for irAE was reported.[17]

The segmentation of metastatic lesions and organs on ^{18}F-FDG PET/CT with deep learning-based convolutional neural network (CNN) has recently been developed.[18,19] In a previous work by our group of 58 mM patients receiving ICI, a novel quantitative imaging biomarker (QIB) of irAE development was proposed – percentiles of SUV distribution ($SUV_{X\%}$) of ^{18}F-FDG uptake within the target organs.[11] Three target organs were considered for identification of irAE: lung, bowel and thyroid. These target organs were segmented using a CNN, and $SUV_{X\%}$ of ^{18}F-FDG uptake within the target organs were correlated with the clinical irAE status. It was shown that increased ^{18}F-FDG uptake within irAE-affected organs provides predictive information about the development of irAE and represents a potential QIB for irAE. Some irAE were detected on ^{18}F-FDG PET/CT before clinical symptoms appeared.[11]

The aim of this prospective study was to evaluate the role of the QIB $SUV_{X\%}$ of ^{18}F-FDG uptake extracted from early ^{18}F-FDG PET/CT scans for the detection of irAE in a cohort of patients with mM, treated with ICI. ^{18}F-FDG PET/CT imaging was performed at an early timepoint at week 4 (W4) and two consecutive scans at week 16 (W16) and week 32 (W23) after ICI initiation. We hypothesized that quantitative analysis of three organs of interest (lung, bowel and thyroid) on week 4 ^{18}F-FDG PET/CT would give information about irAE detection that precede clinical diagnosis and outperform later scans.

Patients and methods

Patient population and study protocol

We have been conducting a noninterventional, prospective study with primary endpoint of quantitative analysis of ^{18}F-FDG PET/CT scans in metastatic melanoma patients for detection of irAE. The patients were treated per standard of care with ICI with anti-cytotoxic T-lymphocyte-associated antigen 4 (anti-CTLA-4) and/or anti programmed death-1 (anti-PD-1) treatment in first and second line of systemic treatment at the Institute of Oncology Ljubljana (OIL), Slovenia. Eligible patients were older than 18 years and had a stage III.D unresectable melanoma or a stage IV mela-

noma. All patients had an Eastern Cooperative Oncology Group (ECOG) performance status score of 0 or 1. Patients were eligible if they had the baseline ^{18}F-FDG PET/CT performed within four weeks prior to ICI treatment initiation. Key exclusion criteria included symptomatic brain metastases and malignant diseases other than melanoma. Written consent was received from all participants.

Patients were monitored with regular ^{18}F-FDG PET/CT. A baseline scan was performed within four week prior toICI initiation. After treatment initiation, ^{18}F-FDG PET/CT was performed at W4 (+/- 5 days), W16 (+/- 7 days), W32 (+/- 7 days) and every 16 weeks after. Because the W4 ^{18}F-FDG PET/CT was performed for investigational purposes, the scan data was not necessarily used to guide treatment decisions. In case of clear progression such as hyperprogression[20], systemic treatment was allowed to be switched based on the decision of the medical oncologists leading the treatment. Clinical data and images included in this analysis were data obtained from disease diagnosis up to the W32 scan plus an additional 4 weeks, allowing for clinical detection of up to W32 clinically unobserved irAE in monitored organs, or 252 day after treatment start in cases where the patient did not have a W32 scan.

All ^{18}F-FDG PET/CT data acquired before and during ICI treatment and all clinical data was collected for review. Grading of irAE was assigned prospectively following Common Terminology Criteria for Adverse Events (CTCAE, v.5.0).[21] Imaging and clinical data were stored in a secure LabKey database server.[22]

The clinical protocol was approved by the Ethics Committee ERIDEK-0034/2020 and the Clinical Trials Protocol Review Committee ERID-KSOPKR-0032/2020 at the Institute of Oncology Ljubljana, and by Commission of the Republic of Slovenia for Medical Ethics (approval number: 0120-256/2020-14, September 15th 2020). It was conducted following the ethical standards defined by the Declaration of Helsinki and the International Conference on Harmonisation Guidelines for Good Clinical Practice. The study was registered with the ClinicalTrials.gov under the registration number NCT06207747.

The study was conducted with acknowledgement and consent of the subjects. All patients have signed informed consent for treatment and consent allowing the usage of their data for scientific purposes. For publication of images in Figure 6 and 7, research participants provided informed consent.

^{18}F-FDG PET/CT image acquisition

^{18}F-FDG PET/CT scans were primarily performed for immunotherapy treatment response evaluation in melanoma patients. All ^{18}F-FDG PET/CT scans were obtained on Biograph mCT PET/CT (Siemens, Knoxville, TN); one scan was obtained at University Clinical Centre Maribor (UKC MB), two at University Clinical Centre Ljubljana (UKC LJ) and the rest were acquired at the Institute of Oncology Ljubljana (OIL) following institutional protocols. Imaging protocol required patients to fast for 6 hours prior to injection of the radiotracer and have a blood glucose level below 10 mmol/L at the time of the scan. Patients were required to hold all diabetic medication, including metformin, for 6 hours prior to radiotracer injection. All scans were acquired per Standard of Care (SOC). CT that meets RECIST analysis needs was acquired according to adjusted protocol including SAFIR reconstruction to minimize dose. Following reconstruction, PET images were normalized by patient weight and injected dose to compute Standardized Uptake Values (SUV). More information on scanning parameters for each scanner can be found in Supplementary Table 1.

^{18}F-FDG PET/CT image analysis

Before image analysis, images were resampled to a cubic 2-mm grid (2mm x 2mm x 2mm) using linear resampling and normalized to have a mean of 0 and variance of 1 within patient to match DeepMedic model developed for Hribernik *et al*.[11]

To quantify organ uptake, a 3D CNN was used to segment three target organs: lung, bowel and thyroid. The architecture used was nnUNet.[23] The network was trained to perform inference on CT component from the ^{18}F-FDG-PET/CT scans to produce contours of all three organs and was trained on same data as DeepMedic network, used in our previous pilot study.[11]

The organ contours, produced by nnUNet were applied to PET component of the ^{18}F-FDG-PET/CT image to quantify ^{18}F-FDG uptake in organs of interest. Percentiles X% of the organ SUV distribution ($SUV_{X\%}$) were extracted, as they were found to be potential biomarkers of irAE in retrospective study of mM patients and were found to be more reliable than $SUV_{max.}$[11,14,24] To quantify organ uptake, only the percentile, that was found to be optimal irAE biomarker in our pilot study in each organ was used: $SUV_{95\%}$ for lung and bowel, $SUV_{75\%}$ for thyroid.[11]

TABLE 1. Patient characteristics

	Characteristics	Count (proportion %)
Number of patients	Total	71 (100)
Age; mean (+/-sd) (yr)		62 (12)
Gender	Male	43 (61)
	Female	28 (39)
ECOG performance status	0	30 (42)
	1	41 (58)
AJCC	III.D	1 (1)
	M1a	16 (23)
	M1b	10 (14)
	M1c	32 (45)
	M1d	12 (17)
Anatomic site of primary	Cutaneous	58 (82)
	Ocular	4 (6)
	Mucosal	3 (4)
	Unknown primary	6 (8)
Prior radical treatment	Surgical resection	38 (54)
	Surgical resection + adjuvant RT	7 (10)
	Surgical resection + adjuvant RT + adjuvant ICI	4 (6)
	Surgical resection + adjuvant RT + adjuvant TKI	2 (3)
	Surgical resection + adjuvant TKI	2 (3)
	Surgical resection + adjuvant interferon alpha	2 (3)
	None	16 (23)
Line of systemic treatment for metastatic disease	1st line	63 (89)
	2nd line	8 (11)
Baseline LDH	Elevated	22 (31)
	Normal	49 (69)
Actionable mutation	*BRAF* wild type	21 (30)
	BRAF V600E	28 (39)
	BRAF V600K	10 (14)
	BRAF V600 - others	1 (1)
	NRAS	11 (16)
Type of systemic treatment	PD-1 inhibitors	47 (66)
	Combination of PD-1 and CTLA-4 inhibitors	24 (34)

AJCC = American Joint Classification of Cancer; BRAF = V-Raf Murine Sarcoma viral oncogene homolog B; CTLA-4 = Cytotoxic T-lymphocyte-associated antigen 4; ECOG = Eastern Cooperative Oncology Group; ICI = Immune checkpoint inhibitors; No = number of patients; NRAS = Neuroblastoma RAS viral homolog; PD-1 = Programmed death-1; SD = standard deviation; RT = radiotherapy; TKI = Tyrosine kinase inhibitors

Statistical analysis

Patients were divided into two groups for each analysed target organ (lung, bowel, thyroid): patients, who experienced irAE from time on ICI start up until the cut-off and patients who did not experience irAE during this period. All timing was calculated in days relative to start of treatment with ICI. In the group of patients experiencing irAE, statistics for all irAE events were calculated per type of irAE and per grade (any grade and high grade: grade 3-5 per CTCAE, v.5.0).[21]

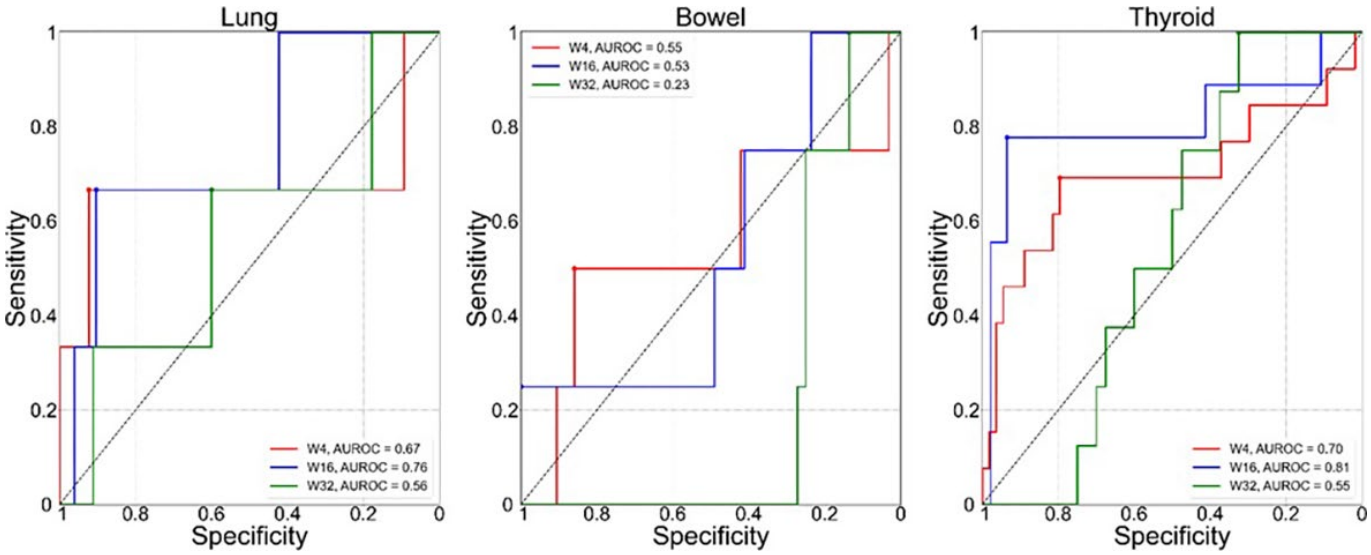

FIGURE 1. ROC curves for the optimal SUV percentile ($SUV_{X\%}$) for predicting irAE status in the three target organs:lung (left), bowel (middle), thyroid (right). Each plot shows comparison of ROC based on the value of $SUV_{X\%}$ extracted from W4 (red), W16 (blue) and W32 (green) ^{18}F-FDG PET/CT. Values of corresponding area under the ROC curve (AUROC) are shown in the legends.

From all clinically detected irAE observed in our follow-up period, the following were included in the analysis: immune-related pneumonitis (irPneumonitis), immune-related colitis (irColitis) and immune-related thyroiditis (irThyroiditis). Receiver Operating Characteristic (ROC) analysis was performed to determine the ability of extracted $SUV_{X\%}$ in each organ to detect observed irAE on scans at W4, W16 and W32 individually. This was done by comparing the $SUV_{X\%}$ extracted from each timepoint scan with the clinical irAE status of the patient up until cut-off for all three analysed organs. Additionally, the maximum organ $SUV_{X\%}$ value, extracted from all available images (including baseline) up until W32, was investigated as a predictor of irAE. This ROC analysis was compared to ROC curves previously obtained in[11] using the same methodology. Area under the ROC curve (AUROC) was calculated. The performance of different models was compared using DeLong test.

In the following part of the analysis, the threshold to differentiate between patients without irAE and those experiencing irAE based on $SUV_{X\%}$ and the normal $SUV_{X\%}$ range from analysis in pilot study were used.[11] In that work, normal ranges of $SUV_{X\%}$ were for lung [0.7, 1.5] g/mL, bowel [1.8, 2.9] g/mL, and thyroid [0.9, 2.0] g/mL. Optimal thresholds used were: $SUV_{95\%}$ = 1.7 g/mL in lung, $SUV_{95\%}$ = 2.7 g/mL in bowel and $SUV_{75\%}$ = 2.1 g/mL in thyroid.

Target organ ^{18}F-FDG uptake was assessed in those patients without clinically diagnosed irAE which had $SUV_{X\%}$ above threshold at any imaging timepoint. Medical oncologist and nuclear medicine specialist identified causes of higher uptake of ^{18}F-FDG in the organ of interest in these patients using patient chart review. $SUV_{X\%}$ values in each organ of interest were compared between causes using Mann-Whitney U test.

Statistical comparison of irAE detection using $SUV_{X\%}$ and clinical detection was done. As a measure of instance when irAE was detected by ^{18}F-FDG-PET/CT, we identified the first scan on which the $SUV_{X\%}$ in the organ of interest was above the mentioned threshold. We compared this instance to the timing of clinical diagnosis of irAE using Wilcoxon signed-rank test.

Image analysis and statistical testing was done using Python programming language version 3.7.16 (Python Software Foundation, https://www.python.org/). Statistically significant differences were observed when p value was below 0.05.

Results

Patient characteristics

Prospective study started with patient inclusion in September 2020. While the study is still ongoing, patient inclusion stopped in September 2022. The inclusion period of the study was initially planned

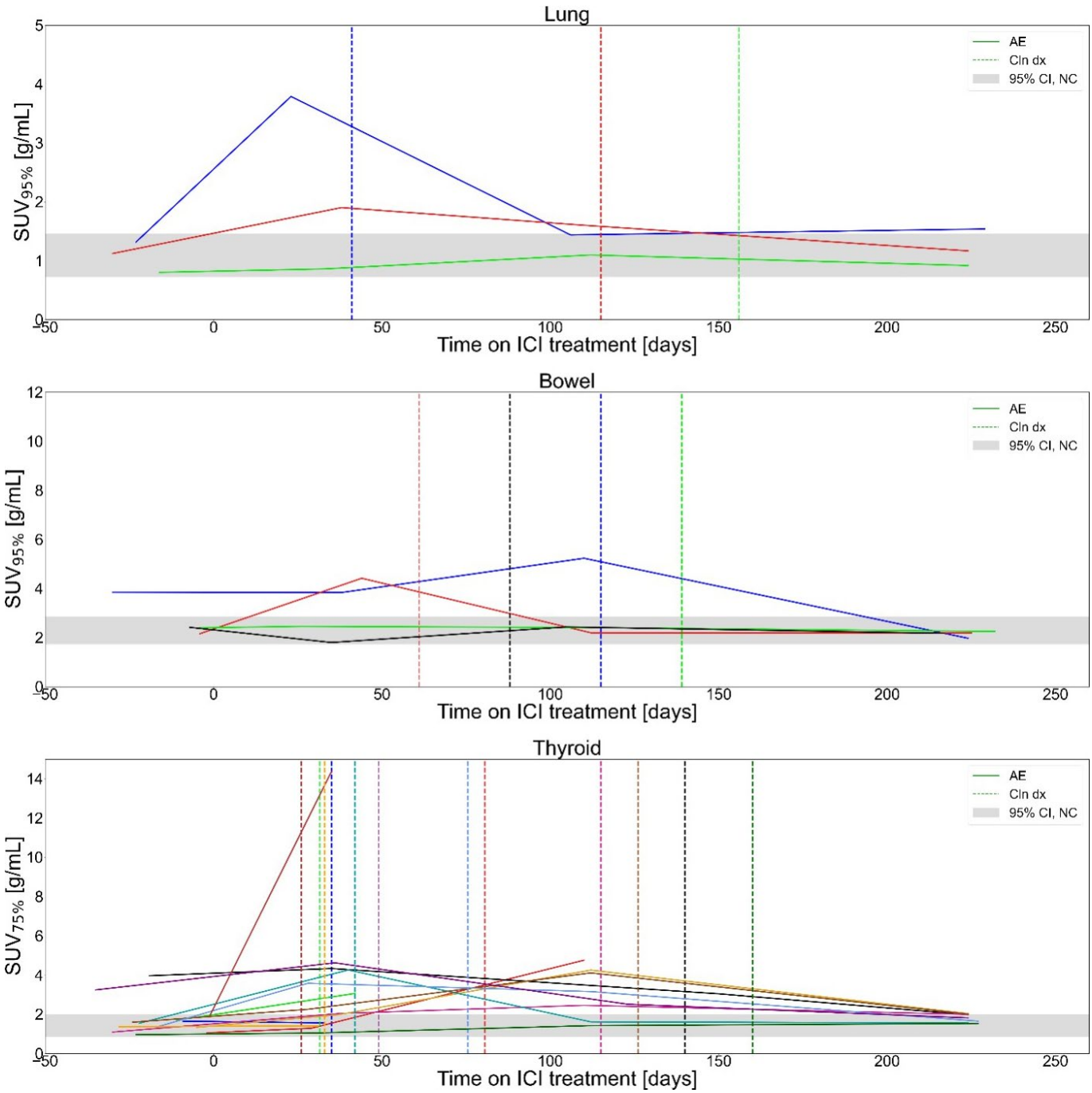

FIGURE 2. Longitudinal optimal SUV percentile ($SUV_{X\%}$) for patients with clinically detected immune-related adverse events (irAE) in bowel, lung and thyroid, included in study. The grey band indicates the 95% confidence interval for organ $SUV_{X\%}$ of patients who did not experience irAE in[11]. Colours were randomly selected for participants in each plot, vertical dashed lines of matching colour indicate dates of clinical irAE identification.

ICI = Immune checkpoint inhibitors

to last 18 months but was extended for 6 months due to the COVID-19 pandemic. Altogether, 71 patients were included in the study; patient demographics are summarised in Table 1.

Clinical detection of irAE

Dates and grades of clinically detected irPneumonitis, irColitis and irThyroiditis were systematical-

ly collected. Number of events for all three types of irAE and median time to first clinical diagnosis of all irAE during observational period are given in Table 2.

During our observational period, 10 patients (14%) developed hypothyroidism and 7 (10%) hyperthyroidism. We identified 13 patients (18%) to have developed irThyroiditis based on patterns of thyroid dysfunction.[25]

TABLE 2. Clinical diagnosis of immune-related adverse events

irAE	Any Grade No (%)	Grade 3-5 No (%)	Time to onset of irAE (mean ± SD) [days]
irPneumonitis	3 (4)	0	104 ± 58
irColitis	4 (6)	2 (3)	101 ± 34
Hypothyroidism	10 (14)	0	91 ± 40
Hyperthyroidism	7 (10)	0	51 ± 50

irAE = immune-related adverse events; No = number of patients; SD = standard deviation

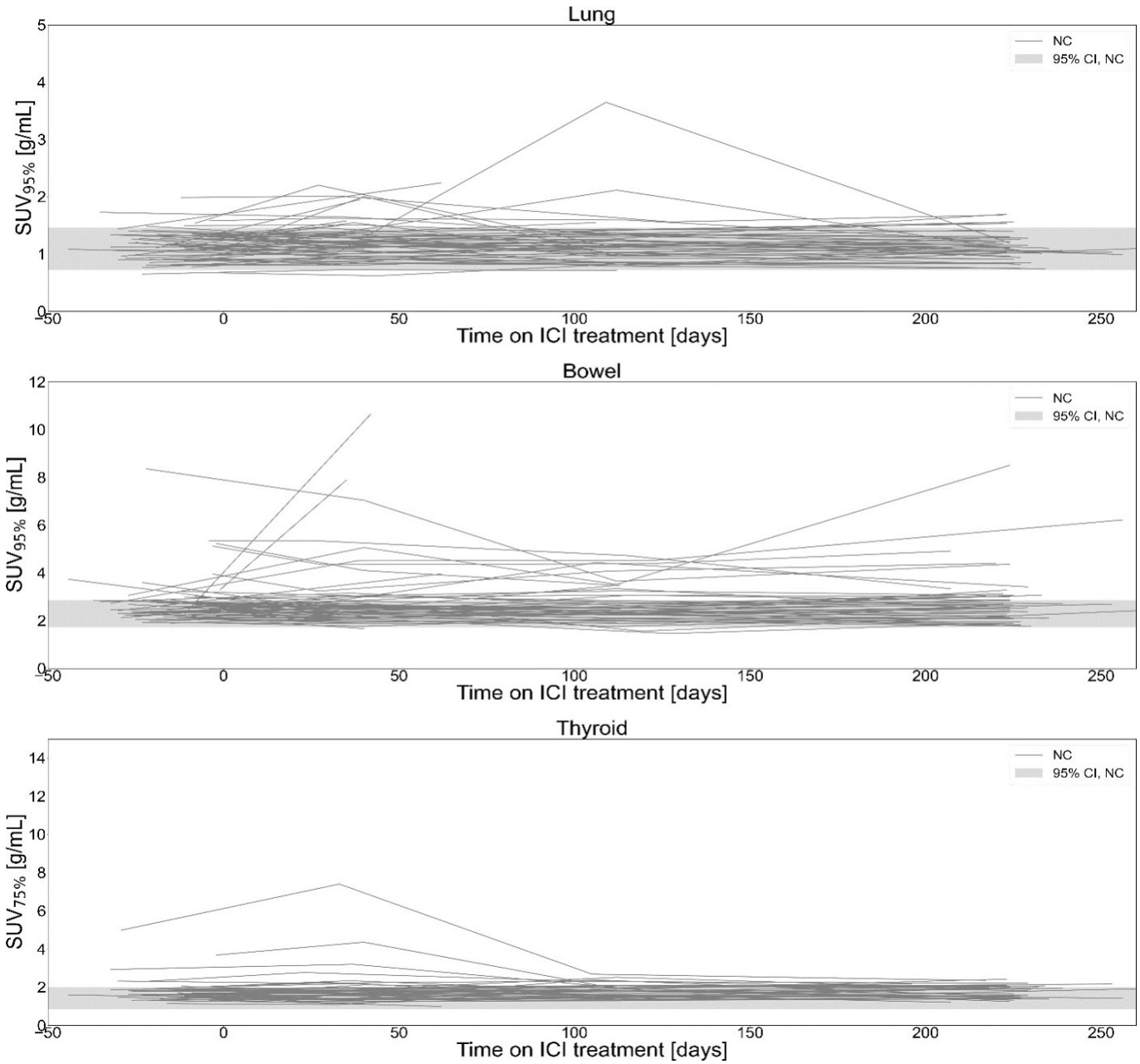

FIGURE 3. Longitudinal optimal SUV percentile ($SUV_{X\%}$) for patients without clinically detected immune-related adverse events (irAE) in bowel, lung and thyroid, included in study. The grey band indicates the 95% confidence interval for organ $SUV_{X\%}$ of patients who did not experience irAE in[11].

ICI = Immune checkpoint inhibitor

TABLE 3. Timing of ^{18}F-FDG PET/CT relative to immune-checkpoint inhibitors (ICI) treatment initiation

	Number of patients	Range (min-max) (days)	Mean (days)	Median (days)	SD (days)
Pre-Treatment	71	[-44, -1]	-16	-16	10
W4 (28 days)	68	[21, 62]	34	34	7
W16 (112 days)	55	[105,150]	115	112	8
W32 (224 days)	48	[196,280]	226	224	12

SD = standard deviation; W = week

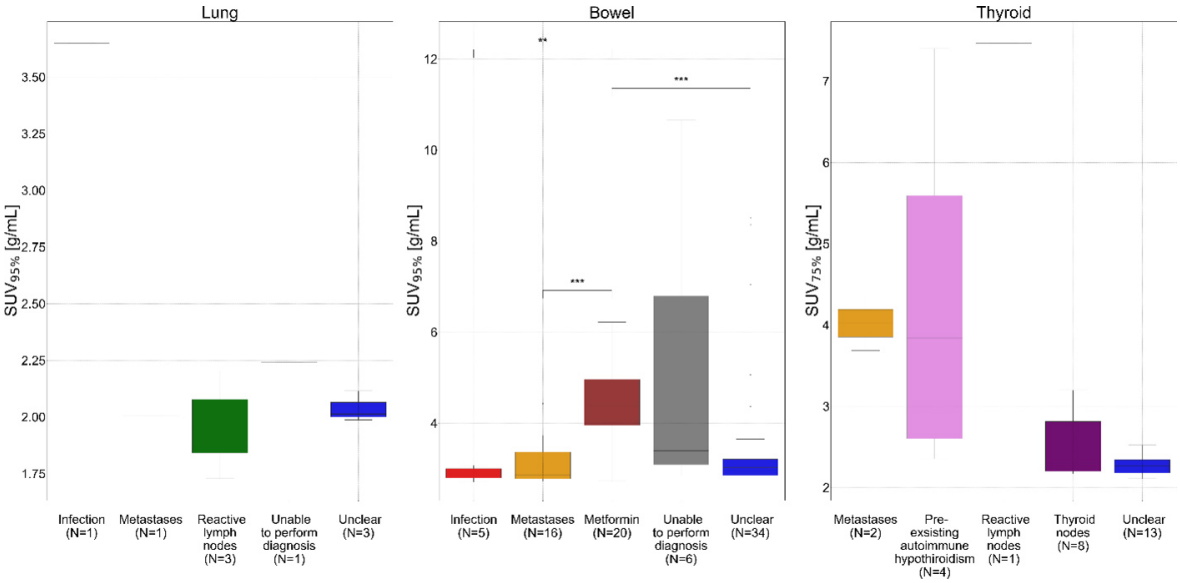

FIGURE 4. Boxplot shows values of optimal SUV percentile ($SUV_{X\%}$) above thresholds for immune-related adverse events (irAE) diagnosis in patients without clinically diagnosed irAE in lung, bowel, and thyroid. Values of $SUV_{X\%}$ are separated based on reason for $SUV_{X\%}$ above threshold, identified from patient's chart. Each image timepoint and $SUV_{X\%}$ extracted from that image is considered as separate instance so multiple points can be contributed by a single patient. p-value was calculated using Mann-Whiteney U test. P-value is shown only for pairings with statistically significant differences

* = shows p-value between 0.05 and 0.01; ** = for p-value between 0.01 and 0.001; *** = for p-value between 0.001 and 0.00001

^{18}F-FDG PET/CT

A total of 242 ^{18}F-FDG PET/CT scans were collected and analyzed. Table 3 shows the number of scans per scan timepoint and timing of the scans. Out of 71 patients, 3 patients had only baseline scan and no further scans due to rapid disease progression and death prior to next imaging appointment. 13 patients had only two scans (baseline and W4); 5 due to disease progression and deterioration of their performance status, 8 due to disease progression and death prior to the next imaging appointment. 7 patients had only three scans (baseline, W4 and W16) due to disease progression and death prior to next imaging appointment. 48 patients had all scans, including W32.

Detection of irAE from ^{18}F-FDG PET/CT scan

To predict irAE status from maximum value of $SUV_{X\%}$ at any of the time points observed, the area under the receiver-operating characteristic curve (AUROC) was 0.57 in bowel, 0.7 in lung, 0.77 in thyroid. Compared to our previous analysis[11], the performance of the model did not change (DeLong test, $p > 0.05$) in all three organs (AUROC: 0.79 in bowel, 0.98 in lung and 0.88 in thyroid in [11]).

To evaluate the role of $SUV_{\%}$ extracted from early ^{18}F-FDG PET/CT scan, the AUROC analysis of all time point scans was done. The AUROC for detection of adverse events in the three target organs was highest when $SUV_{X\%}$ was extracted from

W16 scan and was 0.76 for lung, 0.53 for bowel and 0.81 for thyroid. $SUV_{X\%}$ extracted from W4 scan did not improve detection of irAE compared to W16 scan (lung: p = 0.54, bowel: p = 0.75, thyroid: p = 0.3, DeLong test), as well as compared to W32 scan in lungs (p = 0.32) and bowel (p = 0.3). For thyroid gland, the W4 scan marginally improved detection compared to W32 scan (p = 0.047). Comparison of detection using W16 and W32 scan in thyroid showed, that W16 was more optimal for detection then W32 (p = 0.02), but this was not observed in lungs and bowel (p = 0.09). The ROC curves for selected $SUV_{\%}$ extracted from W4, W16 and W32 scan for lung, bowel and thyroid are shown in Figure 1.

irAE detection by ^{18}F-FDG PET/CT versus clinical detection

Longitudinal time series of $SUV_{X\%}$ for all patients included in the study are shown in Figure 2 and Figure 3. Patients, clinically diagnosed with irPneumonitis, irColitis and irThyroiditis, are shown with patient specific colours (each plot) in Figure 2; dates of clinical diagnosis of irAE for each participant are indicated with dashed vertical lines of the matching color. Longitudinal series of $SUV_{X\%}$ for patients that did not have clinically diagnosed irAE in any of the three organs are shown in Figure 3. The gray band indicated the 95% confidence interval for $SUV_{X\%}$ of patients who did not experience irAE in[11].

We identified false positives cases where $SUV_{X\%}$ was above threshold without clinically confirmed irAE in any of the three organs. Values of $SUV_{X\%}$ above threshold, separated by reason, identified from patient's chart, in lung, bowel and thyroid are shown in boxplot in Figure 4. Of 9 excursions in lung, 3 (33%) remained unclear, 3 (33%) were attributed to reactive lymph nodes and 1 (11%) to infection, metastases in that area, and inability to assess causes of high uptake each. In bowel, 34 excursions of 81 (42%) remained unclear, 20 (25%) were attributed to metformin and 16 (20%), 6 (7%), 5 (6%) to metastases, inability to assess causes of high uptake and infection, respectively. In thyroid, 13 of 28 (46%) excursions were unclear, 8 (29%), 4 (14%), 2 (7%) and 1 (4%) were attributed to thyroid nodes, pre-existing autoimmune thyroiditis, metastases in that area and reactive lymph nodes respectively. Inability to assess causes for $SUV_{X\%}$ above threshold was attributed to cases where poor patient's condition and death prevented clinicians from assessing and confirming irAE. Cases where the cause could not be clarified by analysing patient's charts were assigned to the group unclear.

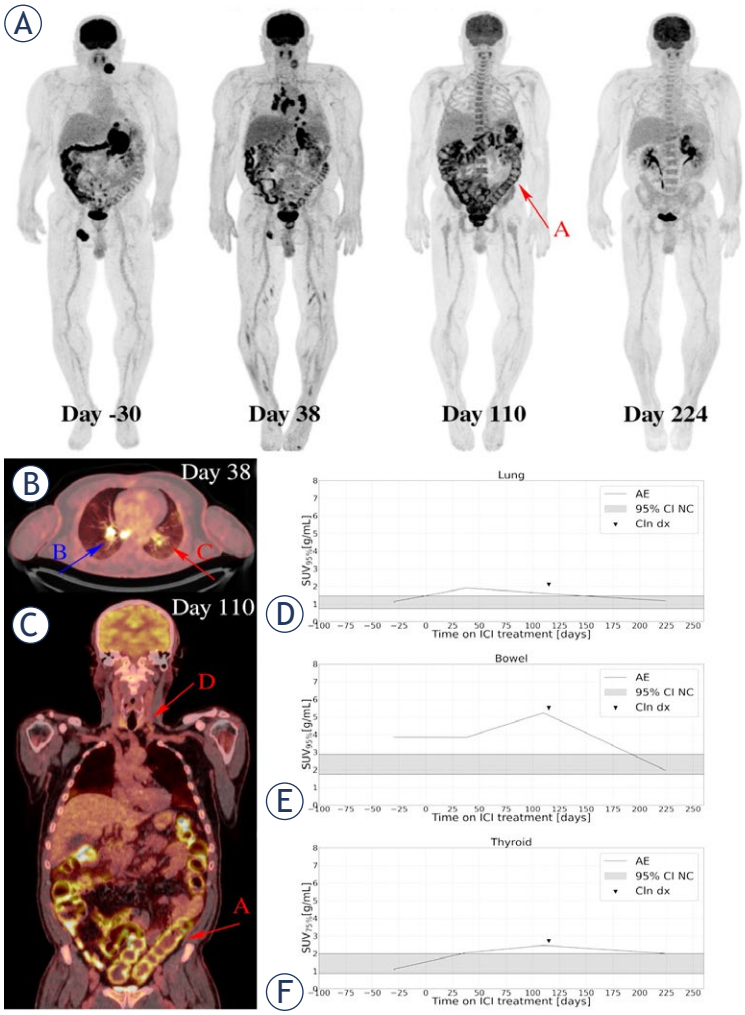

FIGURE 5. A 58-year-old patient, who was diagnosed in April 2022 with *NRAS* mutated melanoma of unknown primary was treated with ipilimumab/nivolumab combination. Serial ^{18}F-FDG PET maximum intensity projections were obtained per study protocol **(A)**. The baseline image (day -30) showed sites of metastases in soft tissue, adrenal gland and spleen. Early time point (W4, day 38) image showed higher metabolic activity in mediastinal lymph nodes typical for granulomatous sarcoid like reaction, which is also seen on axial slices of the day 38 imaging study fused ^{18}F-FDG PET/CT **(B, BLUE ARROW B)**, and diffuse lung opacities with mildly elevated ^{18}F-FDG uptake **(B RED ARROW C)**. Patient reported of having no respiratory symptoms. Partial response in lymph nodes and in the spleen was described, and metabolic progression of the adrenal gland metastasis was observed. Day 110 (W16) image showed elevated ^{18}F-FDG uptake in the thyroid gland **(C RED ARROW D)**, lung, and colon **(C, RED ARROW A)** reflecting multiple irAE. Coronal slices of the day 110 imaging study on fused ^{18}F-FDG PET/CT **(C)**. On day 115 patient reported of having diarrhoea without respiratory or other symptoms, thyroid hormone laboratory test was pathological. Colonoscopy with biopsy was performed and examination by endocrinologist. IrColitis grade 2 and irThyroiditis grade 2 were confirmed. irPneumonitis grade 1 was confirmed based on imaging, no invasive procedure with bronchoscopy was performed for confirmation due to absence of respiratory symptoms and significant irColitis at the same time. After treatment with systemic corticosteroids, diarrhoea resolved. Images on day 224 (W32) were showing resolutions of all irAE and complete metabolic response in all metastatic lesions except progression in adrenal gland. This one metastatic lesion was surgical resected. Due to multiple irAE, the patient then stopped ICI treatment. Quantification of organ ^{18}F-FDG PET uptake demonstrated elevated uptake in lung and preceded clinical symptoms **(D)**, elevated uptake in bowel corresponded with the time of clinical diagnosis of irColitis **(E)** as well as elevated uptake in thyroid corresponded with clinical diagnosis of irThyroiditis **(F)**.

AE = adverse events(irAE

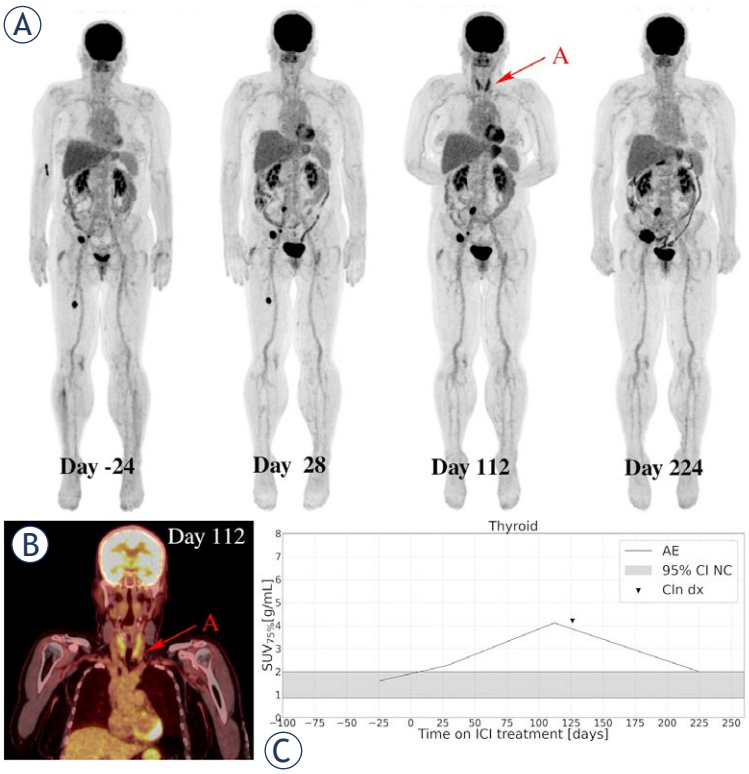

FIGURE 6. A 60-year-old female patient with metastatic *BRAF* V600E-mutated cutaneous melanoma, diagnosed in September 2021, was treated with pembrolizumab in the first-line setting. Serial ^{18}F-FDG PET maximum intensity projections were obtained per protocol **(A)**. The baseline ^{18}F-FDG PET/CT image (day -24) showed metastatic disease present in soft tissue. Day 28 (W4) imaging study showed moderately increased colon uptake and heterogeneous response of all metastatic lesions. Patient had no symptoms of irColitis. Image at day 112 (W16) showed again a heterogeneous response of melanoma metastases and marked increase in ^{18}F-FDG uptake in the thyroid gland **(RED ARROW A)**, which can also be observed on coronal slice of the day 112 imaging study on fused ^{18}F-FDG PET/CT **(B)**. Patient was confirmed to have irThyroiditis on day 126, based on thyroid hormone laboratory test and examination of endocrinologist. Day 224 (W32) image showed decrease in ^{18}F-FDG uptake in the thyroid gland and a clear progression of melanoma metastases. Systemic treatment was changed to targeted treatment with BRAF and MEK inhibitor. Moderate increase in ^{18}F-FDG PET uptake in the thyroid gland was seen already on W4 ^{18}F-FDG PET, 98 days before clinical detected **(C)**.

AE = adverse events(irAE

Statistical analysis showed that patients on metformin had statistically significant higher $SUV_{95\%}$ in bowel compared to those identified with infection or metastases in bowel and unclear reason for higher uptake (Mann-Whitney-U test, $p < 0.05$; Figure 4). There were no statistically significant differences between other reasons and in other organs.

On average, the irAE were identified on ^{18}F-FDG-PET/CT using $SUV_{X\%}$ 38 days prior to clinical diagnosis; 48 days (range: 18, 77) for irPneumonitis, 81 (range: 17, 145) days for irColitis and 27 days (range: -47, 159) for irThyroiditis. Statistical comparison of the timing of clinical irAE diagnosis and timing of first $SUV_{X\%}$ above the threshold for all three observed organs showed that there is no statistically significant difference ($N = 14$, $p = 0.1$, Wilcoxon signed-rank test).

Images of two patients who experienced irPneumonitis, irColitis, and irThyroiditis are highlighted in Figure 5 and Figure 6, respectively.

Discussion

This is the first study that aimed to prospectively evaluate QIB $SUV_{X\%}$ on a W4 ^{18}F-FDG PET/CT scan to detect irAE early during the systemic treatment with ICI. For now, there are only few published studies concerning the value of ^{18}F-FDG PET/CT in detecting irAE, all performed retrospectively and none of them used ^{18}F-FDG PET/CT performed at W4 for early evaluation.[26] Recently published retrospective study determined the organ-specific accuracy of ^{18}F-FDG PET/CT in detecting irAE in melanoma patients in adjuvant setting. They concluded that ^{18}F-FDG PET/CT has a moderate to high sensitivity and specificity for diagnosis of irAE in lung, intestines and thyroid gland.[27] Quantitative approach for the evaluation of ^{18}F-FDG uptake in the target organs was till now used only in our retrospective analysis.[11]

We hypothesized that mM patients who were treated with ICI would demonstrate increased ^{18}F-FDG uptake in the organs of interest before the time of clinical irAE diagnosis, which could be detectable as early as on W4 ^{18}F-FDG PET/CT. We found that $SUV_{X\%}$ had no higher detection performance when extracted from W4 compared to W16 but had improved detection performance power when compared to W32. This might suggest that irAE are not yet visible or cannot be detected on W4 scan, but a later scan, possibly week 8, might be more appropriate for irAE detection. Interestingly enough, this is also the suggested time interval in guidelines for management of mM management.[27,28]

For mM patients receiving ICI, ^{18}F-FDG PET/CT is primarily performed for disease response assessment. Data on optimum time of the first evaluation is scarce. In clinical practice it is usually performed after three to four cycles of ICI but can also be performed earlier of later during the course of the treatment, depending on the decision of medical oncologist and availability of ^{18}F-FDG PET/CT scans.[28] Of the three irAE investigated, the typical

onset times and times to resolution of irThyroiditis fall exactly within W4 to W16, making it highly likely for irThyroiditis to be detected by either of the two early scans.[29] For other two irAE, the onset of irAE can appear at any time during therapy, with a predominant period of 2-16 weeks from the commencement, depending on the type of ICI administered.[6,7,30] It is hence unlikely to capture and detect irAE at its worse on routine ^{18}F-FDG PET-CT images. Our data however shows that quantitative evidence of irAE can be seen in images as early as 80 days prior to clinical diagnosis of colitis. Due to rareness of occurrence in realistic study cohorts, multi-centre studies would be needed to describe the actual time-development curve of irAE. This could define the optimal timepoint of first on-treatment imaging for early diagnosis of irAE and earlier treatment intervention, which would in turn lower the possibility for detrimental impact of irAE on survival outcomes.[31]

In our study, there was no statistically significant difference in time of clinical diagnosis of irAE compared to its identification via $SUV_{X\%}$ extracted from ^{18}F-FDG PET/CT. However, using $SUV_{X\%}$, irAE were on average identified as early as 81 days for irColitis, 48 days for irPneumonities and 27 days for irThyroditis prior to clinical diagnosis. In case of irThyroiditis, the small difference is primarily due to early clinical detection via regular laboratory control of thyroid hormones performed routinely before each ICI infusion. To a lesser extent, the short median time to onset of thyroid disfunction, usually less than two months.[29] coincides well with W4 scans performed in our study. On the other hand, clinical detection of irColitis and irPneumonitis is driven by symptoms exhibited by the patient. Using $SUV_{X\%}$, irColitis and irPneumonitis could be first observed on ^{18}F-FDG PET/CT while patient is still asymptomatic, which would enable closer monitoring and earlier treatment adjustment. This is illustrated in two cases of patients with $SUV_{X\%}$ in affected organs above threshold before clinical diagnosis of irAE in Figures 5 and 6.

The study also assessed $SUV_{X\%}$ for the detection of irAE, previously described in a pilot study from Hribernik *et al.* in a prospective setting.[11] Comparing AUROC curves of $SUV_{X\%}$ for predicting irAE status in the three target organs showed similar predictive power to that first reported in our past publication ($p > 0.05$). This indicates that $SUV_{X\%}$ is a consistent QIB for irAE detection, as was previously concluded in Huff *et al*.[14]

$SUV_{X\%}$ is not a perfect QIB for identification of irAE, as it captures any $SUV_{X\%}$ above the threshold due to causes other than inflammation. Specifically, in the case of bowel, there are different patterns of physiological ^{18}F-FDG uptake, and many different factors known and yet to be determined that possibly influence the physiological bowel ^{18}F-FDG uptake, such as metformin and other antidiabetic therapy, gut microbiota, and bowel movement.[32-34] Additionally, metastases present in organ of interest also impact ^{18}F-FDG uptake and consequently, $SUV_{X\%.}$ Although $SUV_{X\%}$ were hypothesized to be robust to metastases captured in the volume of interest, a more detailed studies, where segmented lesions would be excluded from organ uptake would help assess the impact of metastases uptake on $SUV_{X\%}$ robustness. Other factors that were found to impact value of $SUV_{X\%}$ and lead to false-positive results were also infections, reactive lymph nodes and overactive thyroid nodes before ICI treatment. Many of these possible false-positive cases were already described by Aide *et al*. in his review article.[12]

There are some limitations in this study. Variation in ^{18}F-FDG PET/CT scan timing was present due to various reasons, mainly radiopharmaceutical outages, special interventions during the COVID-19 pandemic, and patient infections or deterioration of condition as the disease progressed. Also, not all patients were scanned on the same device, limiting quantification consistency across scanners. While potentially challenging, the inconsistencies were deemed acceptable due to comparable scanning protocols, low number of images performed elsewhere and similarity of scanners. For multicentric studies, scanner harmonization was shown to remove potential imaging bias. Another limitation is inconsistency in CNN for organ segmentation between previously published work and the present study. Our studies in consistency of AUROC are a strong indicator of $SUV_{X\%}$ robustness over segmentation methods.[35]

Our future aim is to use prospectively gathered data from this clinical study to analyse the potential role of a W4 ^{18}F-FDG PET/CT for prediction of response to ICI. We will evaluate the prediction of response using lesion by lesion analysis, with the possible use of lesion segmentation with CNN and the analysis of different lesion based QIB.

Conclusions

This is the first study to quantitatively analyse early timepoint ^{18}F-FDG PET/CT using $SUV_{X\%}$ for detection of irAE in mM patients on ICI. While $SUV_{X\%}$

ware found to be a consistent biomarker of irAE, its use on a W4 ^{18}F-FDG PET/CT had no higher performance compared to subsequent imaging. As the level of statistics exceeds a single-center studies, further larger studies are needed to investigate the use QIB of ^{18}F-FDG PET/CT.

Acknowledgement

The research was financially supported by The Slovenian Research Agency (ARIS), grant numbers P3-0321 and P1-0389.

References

1. Carlino MS, Larkin J, Long GV. Immune checkpoint inhibitors in melanoma. *Lancet* 2021; **398:** 1002-14. doi: 10.1016/S0140-6736(21)01206-X
2. Michielin O, van Akkooi ACJ, Ascierto PA, Dummer R, Keilholz U; ESMO Guidelines Committee. Cutaneous melanoma: ESMO Clinical Practice Guidelines for diagnosis, treatment and follow-up. *Ann Oncol* 2019; **30:** 1884-901. doi: 10.1093/annonc/mdz411
3. Hribernik N, Boc M, Ocvirk J, Knez-Arbeiter J, Mesti T, Ignjatovic M, et al. Retrospective analysis of treatment-naive Slovenian patients with metastatic melanoma treated with pembrolizumab - real-world experience. *Radiol Oncol* 2020; **54:** 119-27. doi: 10.2478/raon-2020-0003
4. Wolchok JD, Chiarion-Sileni V, Gonzalez R, Grob JJ, Rutkowski P, Lao CD, et al. Long-term outcomes with nivolumab plus ipilimumab or nivolumab alone versus ipilimumab in patients with advanced melanoma. *J Clin Oncol* 2022; **40:** 127-37. doi: 10.1200/JCO.21.02229
5. Ramos-Casals M, Brahmer JR, Callahan MK, Flores-Chávez A, Keegan N, Khamashta MA, et al. Immune-related adverse events of checkpoint inhibitors. *Nat Rev Dis Primers* 2020; **6:** 38. doi: 10.1038/s41572-020-0160-6
6. Postow MA, Sidlow R, Hellmann MD. Immune-related adverse events associated with immune checkpoint blockade. *N Engl J Med* 2018; **378:** 158-68. doi: 10.1056/NEJMra1703481
7. Haanen J, Obeid M, Spain L, Carbonnel F, Wang Y, Robert C, et al; ESMO Guidelines Committee. Management of toxicities from immunotherapy: ESMO Clinical Practice Guideline for diagnosis, treatment and follow-up. *Ann Oncol* 2022; **33:** 1217-38. doi: 10.1016/j.annonc.2022.10.001
8. Balaji A, Zhang J, Wills B, Marrone KA, Elmariah H, Yarchoan M, et al. Immune-related adverse events requiring hospitalization: Spectrum of toxicity, treatment, and outcomes. *J Oncol Pract* 2019; **15:** e825-e834. doi: 10.1200/JOP.18.00703
9. Lopci E, Hicks RJ, Dimitrakopoulou-Strauss A, Dercle L, Iravani A, Seban RD, et al. Joint EANM/SNMMI/ANZSNM practice guidelines/procedure standards on recommended use of [18F] FDG PET/CT imaging during immunomodulatory treatments in patients with solid tumors version 1.0. *Eur J Nucl Med Mol Imaging* 2022; **49:** 2323-41. doi: 10.1007/s00259-022-05780-2
10. Iravani A, Hicks RJ. Imaging the cancer immune environment and Its response to pharmacologic intervention, Part 1: the role of 18F-FDG PET/CT. *J Nucl Med* 2020; **61:** 943-50. doi: 10.2967/jnumed.119.234278
11. Hribernik N, Huff DT, Studen A, Zevnik K, Klaneček Ž, Emamekhoo H, et al. Quantitative imaging biomarkers of immune-related adverse events in immune-checkpoint blockade-treated metastatic melanoma patients: a pilot study. *Eur J Nucl Med Mol Imaging* 2022; **49:** 1857-69. doi: 10.1007/s00259-021-05650-3
12. Aide N, Iravani A, Prigent K, Kottler D, Alipour R, Hicks RJ. PET/CT variants and pitfalls in malignant melanoma. *Cancer Imaging* 2022; **22:** 3. doi: 10.1186/s40644-021-00440-4
13. Wong A, Callahan J, Keyaerts M, Neyns B, Mangana J, Aberle S, et al. 18F-FDG PET/CT based spleen to liver ratio associates with clinical outcome to ipilimumab in patients with metastatic melanoma. *Cancer Imaging* 2020; **20:** 36. doi: 10.1186/s40644-020-00313-2
14. Huff DT, Ferjancic P, Namías M, Emamekhoo H, Perlman SB, Jeraj R. Image intensity histograms as imaging biomarkers: application to immune-related colitis. *Biomed Phys Eng Express* 2021; **7:** 10.1088/2057-1976/ac27c3. doi: 10.1088/2057-1976/ac27c3
15. Cho SY, Lipson EJ, Im HJ, Rowe SP, Gonzalez EM, Blackford A, et al. Prediction of rresponse to immune checkpoint inhibitor therapy using early-time-point 18F-FDG PET/CT imaging in patients with advanced melanoma. *J Nucl Med* 2017; **58:** 1421-8. doi: 10.2967/jnumed.116.188839
16. Sachpekidis C, Kopp-Schneider A, Pan L, Papamichail D, Haberkorn U, Hassel JC, et al. Interim [18F]FDG PET/CT can predict response to anti-PD-1 treatment in metastatic melanoma. *Eur J Nucl Med Mol Imaging* 2021; **48:** 1932-43. doi: 10.1007/s00259-020-05137-7
17. Anderson TM, Chang BH, Huang AC, Xu X, Yoon D, Shang CG, et al. FDG PET/CT imaging 1 week after a single dose of pembrolizumab predicts treatment response in patients with advanced melanoma. *Clin Cancer Res* 2024; **24:** OF1-OF10. doi: 10.1158/1078-0432.CCR-23-2390
18. Taghanaki SA, Zheng Y, Kevin Zhou S, Georgescu B, Sharma P, Xu D, Comaniciu D, et al. Combo loss: Handling input and output imbalance in multi-organ segmentation. *Comput Med Imaging Graph* 2019; **75:** 24–33. doi: 10.1016/j.compmedimag.2019.04.005
19. Wang H, Zhang N, Huo L, Zhang B. Dual-modality multi-atlas segmentation of torso organs from [18F]FDG-PET/CT images. *Int J Comput Assist Radiol Surg* 2019; **14:** 473–82. doi: 10.1007/s11548-018-1879-3
20. Adashek JJ, Subbiah IM, Matos I, Garralda E, Menta AK, Ganeshan DM, et al. Hyperprogression and immunotherapy: Fact, fiction, or alternative fact? *Trends Cancer* 2020; **6:** 181-91. doi: 10.1016/j.trecan.2020.01.005
21. National Cancer Institute (NCI). NCI Common Terminology Criteria for Adverse Events (CTCAE). Version 5.0.2021. [internet]. [cited 2023 Oct 23]. Available at: https://ctep.cancer.gov/protocoldevelopment/electronic_applications/docs/ctcae_v5_quick_reference_8.5x11.pdf
22. Nelson EK, Piehler B, Eckels J, Rauch A, Bellew M, Hussey P, et al. LabKey Server: an open source platform for scientific data integration, analysis and collaboration. *BMC Bioinformatics* 2011; **12:** 71. doi: 10.1186/1471-2105-12-71
23. Isensee F, Jaeger PF, Kohl SAA, Petersen J, Maier-Hein KH. nnU-Net: a self-configuring method for deep learning-based biomedical image segmentation. *Nat Methods* 2021; **18:** 203-11. doi: 10.1038/s41592-020-01008-z
24. Baiocco S, Matteucci F, Mezzenga E, Caroli P, Di Iorio V, Cittanti C, et al. SUV95th as a reliable alternative to SUVmax for determining renal uptake in [68Ga] PSMA PET/CT. *Mol Imaging Biol* 2020; **22:** 1070-7. doi: 10.1007/s11307-019-01451-1
25. Olsson-Brown A, Lord R, Sacco J, Wagg J, Coles M, Pirmohamed M. Two distinct clinical patterns of checkpoint inhibitor-induced thyroid dysfunction. *Endocr Connect* 2020; **9:** 318-25. doi: 10.1530/EC-19-0473
26. Nadaraja S, Helsing J, Naghavi-Bezhad M, Land LH, Ruhlmann CH, Gerke O, et al. Value of 2-[18F] FDG-PET/CT in identifying immune-related adverse events in patients with melanoma or non-small cell lung cancer: a systematic scoping review. *Clin Transl Imaging* 2024; **12:** 187–95. doi: 10.1007/s40336-024-00618-3
27. Gideonse BM, Birkeland M, Vilstrup MH, Grupe P, Naghavi-Behzad M, Ruhlmann CH, et al. Organ-specific accuracy of [18F] FDG-PET/CT in identifying immune-related adverse events in patients with high-risk melanoma treated with adjuvant immune checkpoint inhibitor. *Jpn J Radiol* 2024; **42:** 753-64. doi: 10.1007/s11604-024-01554-y
28. Lopci E, Hicks RJ, Dimitrakopoulou-Strauss A, Dercle L, Iravani A, Seban RD, et al. Joint EANM/SNMMI/ANZSNM practice guidelines/procedure standards on recommended use of [18F]FDG PET/CT imaging during immunomodulatory treatments in patients with solid tumors version 1.0. *Eur J Nucl Med Mol Imaging* 2022; **49:** 2323-41. doi: 10.1007/s00259-022-05780-2
29. Chieng JHL, Htet ZW, Zhao JJ, Tai ES, Tay SH, Huang Y, et al. Clinical presentation of immune-related endocrine adverse events during immune checkpoint inhibitor treatment. *Cancers* 2022; **29:** 2687. doi: 10.3390/cancers14112687

30. Martins F, Sofiya L, Sykiotis GP, Lamine F, Maillard M, Fraga M, et al. Adverse effects of immune-checkpoint inhibitors: epidemiology, management and surveillance. *Nat Rev Clin Oncol* 2019; **16:** 563-80. doi: 10.1038/s41571-019-0218-0

31. Pan EY, Merl MY, Lin K. The impact of corticosteroid use during anti-PD1 treatment. *J Oncol Pharm Pract* 2020; **26:** 814-22. doi: 10.1177/1078155219872786

32. Hamidizadeh R, Eftekhari A, Wiley EA, Wilson D, Alden T, Bénard F. Metformin discontinuation prior to FDG PET/CT: A randomized controlled study to compare 24- and 48-hour bowel activity. *Radiology* 2018; **289:** 418-25. doi: 10.1148/radiol.2018180078

33. Moasses-Ghafari B, Fallahi B, Esfehani AF, Eftekhari M, Rahmani K, Eftekhari A, et al. Effect of diet on physiologic bowel ^{18}F-FDG uptake. *J Nucl Med Technol* 2021; **49:** 241-5. doi: 10.2967/jnmt.120.257857

34. Kang JY, Kim HN, Chang Y, Yun Y, Ryu S, Shin H, et al. Gut microbiota and physiologic bowel ^{18}F-FDG uptake. *EJNMMI Res* 2017; **7:** 72. doi: 10.1186/s13550-017-0318-8

35. Strašek K, Huff DT, Hribernik H, Santoro Fernandey VMA, Vincent T., Klaneček Ž, et al. Assessing the impact of CNN architectures for whole organ segmentation on predictive models of organ toxicity. [abstract]. APS March Meeting 2024. March 4–8, 2024; Minneapolis & Virtual. *Bulletin of the American Physical Society* 2024. Abstract Z18.00003

research article

Quantitative SSTR-PET/CT: a potential tool for predicting everolimus response in neuroendoctine tumour patients

Homeira Karim[1], Michael Winkelmann[1], Freba Grawe[2], Friederike Völter[2], Christoph Auernhammer[3,4], Johannes Rübenthaler[1,3], Jens Ricke[1,3], Maria Ingenerf[1], Christine Schmid-Tannwald[1,3]

[1] Department of Radiology, University Hospital, LMU Munich, Munich, Germany
[2] Department of Nuclear Medicine, University Hospital, LMU Munich, Munich, Germany
[3] ENETS Centre of Excellence, Interdisciplinary Center of Neuroendocrine Tumours of the GastroEnteroPancreatic System at the University Hospital of Munich (GEPNET-KUM), University Hospital of Munich, Munich, Germany
[4] Department of Internal Medicine 4, University Hospital, LMU Munich, Munich, Germany

Radiol Oncol 2024; 58(3): 348-356.

Received 12 March 2024
Accepted 10 May 2024

Correspondence to: Christine Schmid-Tannwald, P.D., M.D., and Maria Ingenerf, M.D., Department of Radiology, University Hospital, LMU Munich, Germany; E-mail: Christine.schmid-tannwald@med.uni-muenchen.de

Disclosure: No potential conflicts of interest were disclosed.

Background. This study aimed to assess ^{68}Ga-DOTA-TATE (-TOC) PET/CT quantitative parameters in monitoring and predicting everolimus response in neuroendocrine tumor (NET) patients with hepatic metastases (NELM).

Patients and methods. This retrospective analysis included 29 patients with 62 target lesions undergoing everolimus treatment and pre-therapy, and follow-up ^{68}Ga-DOTA-TATE (-TOC) PET/CT scans. Response evaluation utilized progression-free survival (PFS) categorized as responders (R; PFS > 6 months) and non-responders (NR; PFS ≤ 6 months). Lesion size and density, along with maximum and median standardize uptake value (SUV) in target lesions, liver, and spleen were assessed. Tumor-to-spleen (T/S) and tumor-to-liver (T/L) ratios were calculated, including the tumor-to-spleen (T/S) ratio and tumor-to-liver (T/L) ratio (using SUVmax/SUVmax, SUVmax/SUVmean, and SUVmean/SUVmean).

Results. PET/CT scans were acquired 19 days (interquartile range [IQR] 69 days) pre-treatment and 127 days (IQR 74 days) post-starting everolimus. The overall median PFS was 264 days (95% CI: 134–394 days). R exhibited significant decreases in Tmax/Lmax and Tmean/Lmax ratios compared to NR (p = 0.01). In univariate Cox regression, Tmean/Lmax ratio was the sole prognostic parameter associated with PFS (HR 0.5, 95% CI 0.28–0.92, p = 0.03). Percentage changes in T/L and T/S ratios were significant predictors of PFS, with the highest area under curve (AUC) for the percentage change of Tmean/Lmax (AUC = 0.73). An optimal threshold of < 2.5% identified patients with longer PFS (p = 0.003). No other imaging or clinical parameters were predictive of PFS.

Conclusions. This study highlights the potential of quantitative SSTR-PET/CT in predicting and monitoring everolimus response in NET patients. Liver metastasis-to-liver parenchyma ratios outperformed size-based criteria, and Tmean/Lmax ratio may serve as a prognostic marker for PFS, warranting larger cohort investigation.

Key words: neuroendocrine tumors; SSTR-PET/CT; everolimus; response

Introduction

Neuroendocrine tumors (NET) are rare, with an incidence of 0.48 per 100,000 population.[1-3] These tumors are often diagnosed at an advanced stage, frequently with liver metastases, limiting curative surgical options and shifting the focus of treatment towards symptom control and reducing tu-

mor spread. Targeting and inhibiting the mTOR protein, which plays a role in the tumorigenesis of NETs of different origins, has emerged as a promising therapeutic strategy for NETs.[1,4]

Everolimus, an mTOR inhibitor, has shown effectiveness as a second-line therapy in advanced pancreatic NETs, prolonging progression-free survival (PFS) and improving overall survival.[1,5-7] However, objective tumor response rates to are generally low, indicating that tumor growth stabilization rather than shrinkage is the primary outcome.[5,8] Conventional response criteria based on tumor size change appear to be suboptimal for evaluating treatment response to targeted anti-cancer drugs in slow-growing tumors like NETs.[8-10] However, it would be crucial to distinguish responders from non-responders early on in clinical practice and enhance the design of oncological studies by establishing a more precise definition of progression-free survival (PFS). The Choi criteria, which incorporate changes in tumor density on CT in addition to size, have demonstrated a better correlation with overall survival: A study by Solis-Hernandez analysed 107 patients with neuroendocrine tumors treated with sunitinib: They found out that Median progression-free survival (PFS) by RECIST and Choi were 11.42 (95 % confidence interval [CI], 9.7–15.9) and 15.8 months (95% CI, 13.9–25.7). In addition, PFS by Choi exhibited greater correlation with overall survival (OS) than PFS by RECIST and RECIST incorrectly estimated prognosis in 49.6%.[11]

PET/CT with ^{68}Ga-labeled somatostatin analogues (SSA) (^{68}Ga-DOTA-TATE, -DOTA-NOC and -DOTA-TOC) has potential to provide new imaging biomarkers for NETs: The majority of well to moderately differentiated neuroendocrine tumors (NETs) (80–95 %) overexpresses somatostatin receptors (SSTRs) on cell surfaces. PET/CT with ^{68}Ga-labeled somatostatin analogues (SSA) (^{68}Ga-DOTA-TATE, -DOTA-NOC and -DOTA-TOC) enables visualization of SSTRs and correlates with the histopathological expression of SSTRs[12-14] and provides a comprehensive assessment of NETs, including their location, size, and metabolic activity.[15] It is recommended for initial staging and follow-up of gastroenteropancreatic neuroendocrine tumors (GEP-NET) by the European Society for Medical Oncology Guidelines Working Group.[16]

However, there is limited research on functional imaging response criteria in patients receiving everolimus. Therefore, this study aims to assess the diagnostic reliability of ^{68}-Ga-DOTA-TATE PET/CT to monitor and predict therapy response to everolimus in NETs.

Patients and methods

Patients

This retrospective study included consecutive patients with histologically confirmed NETs of different primary tumor sites who received everolimus between August 2011 and October 2020 at our department. Eligible patients had liver metastases only or, if not already resected, the primary tumor and had undergone both baseline and follow-up ^{68}Ga-DOTA-TATE (-TOC) PET/CT scans. The selection for everolimus therapy was based on consensus decisions made in an interdisciplinary tumor conference certified for NETs (ENETS Center of Excellence). The study received approval from the local research ethics committee, and the requirement for written informed patient consent was waived.

PET/CT

Whole-body PET/CT scans were conducted using either a GE Discovery 690 (GE Healthcare, Little Chalfont, United Kingdom) or a Biograph 64 TruePoint PET/CT scanner (Siemens Healthcare, Erlangen, Germany). Approximately 60 minutes after intravenous injection of around 220 MBq of ^{68}Ga-DOTA-TATE (-TOC), emission data were acquired. When feasible, 20mg of furosemide were administered. The emission data underwent reconstruction with attenuation correction using concurrent diagnostic CT scans, which covered the neck, thorax, abdomen, and pelvis. The diagnostic CT scan parameters were set at 100–190 mAs, 120 kV, with a collimation of 2 x 5 mm and a pitch of 1.5. Additionally, an iodine-based contrast agent (Ultravist 300TM; Bayer Healthcare, Berlin, Germany; 1.5 mL/kg body weight) was intravenously injected at a rate of 2.5 mL/s, with a 50-second delay to capture the portal venous phase of the liver.

Image analysis

Two board-certified radiologists with experience in nuclear medicine, blinded to the patients' clinical and follow-up data, conducted a consensus review of pre- and post-treatment PET/CT scans. Target lesions, including up to two liver metastases and the pancreatic NET if not resected, were identified based on criteria such as increased tracer uptake exceeding normal physiological activity and a minimum size of 1 cm, detectable on CT scans. In two separate reading sessions, the radiologists measured the maximum lesion size and den-

TABLE 1. Patients demographics

Sex (male)	17 (59%)
Age (mean + SD)	63 ± 13.2
Grading	
G1	7 (24%)
G2	20 (69%)
G3	1 (3%)
n/a	1 (3%)
Ki-67 (mean + SD)	9.1 ± 7.6
Primary tumor site	
Pancreas	11 (38%)
Stomach	1 (3%)
Liver	1 (3%)
Lung	1 (3%)
Small-intestine	11 (38%)
Kidney	1 (3%)
Breast	1 (3%)
Retroperitoneal	1 (3%)
Rectum	1 (3%)
Bilirubin prior to therapy (mg/dl)	0.6 (0.3–1.3)
Bilirubin after therapy (mg/dl)	0.5 (0.2–2.6)
Median CgA prior to therapy (ng/ml) (range)	487 (10–8983)
Median CgA after therapy (ng/ml) (range)	929 (43–23348)

CgA = chromogranin A; SD = standard deviation

sity (in Hounsfield units) of the normal liver and spleen, as well as the liver metastases and NET, on CT scans. The uptake of 68Ga-DOTA-TATE was quantified by obtaining the maximum and mean standardized uptake values (SUVs). Circular volumes of interest (VOIs) were positioned within the predefined target lesion and in the normal liver and spleen parenchyma to calculate tumor-to-organ ratios, including the tumor-to-spleen (T/S) ratio and tumor-to-liver (T/L) ratio (using SUVmax/SUVmax, SUVmax/SUVmean, SUVmean/SUVmax and SUVmean/SUVmean).

Standard of reference and response to treatment

Diagnosis of NET was confirmed by histopathology, and Ki-67 labelling index of the primary tumor was obtained for all included patients. Tumor grading was rated according to 2017 WHO Tumor Classification Guideline (G1: Ki-67 Index was <3%, G2: Ki-67 Index was 3–20%, and G3 NET/NEC: Ki-67 Index was >20%).[17]

Progression-free survival (PFS) was used as a parameter for treatment response, calculated in days/ months from the time of everolimus initiation until progression, as evaluated by the local interdisciplinary tumor board through the assessment of all performed imaging studies (CT, PET/CT, MRI). Responder (R) were defined as patients with PFS > 6 months and non-responders (NR) as patients with PFS ≤ 6 months respectively.

Statistical analysis

Statistical analysis was conducted using commercially available software, including GraphPad Prism Version 6 (San Diego, Calif.), SPSS version 25 (Chicago, IL), and Microsoft Excel v. 16. The level of statistical significance was defined as $p \leq 0.05$. Data were presented as mean with standard deviation (SD) or median values with interquartile range [IQR], as appropriate. Normal distribution of continuous variables was assessed through visual inspection of the frequency distribution (histogram).

Quantitative measurements of the target lesions before and after therapy were compared using a two-tailed, paired t-test, while comparisons of target lesions between different response groups were performed using a two-tailed, unpaired t-test or Wilcoxon rank sum test, depending on the data distribution.

Progression-free survival (PFS) was analyzed using the Kaplan-Meier method, and survival curves were compared using the Log-Rank test. Prognostic parameters for PFS were assessed using Cox proportional hazards regression analysis. In the multivariable model, variables with a p-value ≤ 0.05 in the univariable analysis were included using a stepwise approach.

Results

Patients

A total of 29 patients (12 female, 17 male) with a combined count of 62 target lesions (54 liver metastases, 8 primary tumors) were included in this retrospective study. The baseline PET/CT scans were acquired 19 d (interquartile range (IQR) 69d) before treatment initiation, and the first follow-up PET/CT scans were performed 127 d (IQR 74d) after the start of everolimus treatment. Most of the included patients had G2 tumors (n = 20), followed by G1 tumors (n = 7) and one patient had a high-

grade primary tumor (G3), while grading information was not available for one patient. Detailed patient characteristics are presented in Table 1.

Progression-free survival

At the end of the study, 28/29 patients showed progression on imaging. The overall median PFS was 264 days (95% CI: 134–394 days). The median PFS was 487 days (95% CI: 154–820 days) in the R group (n = 16), and 112 d in the NR group (95% CI: 79–145 days). There was no significant difference in PFS between patients with elevated and non-elevated baseline chromogranin A (CgA) levels (p > 0.7).

Responder *vs.* non-responder

There were no differences in pretherapeutic clinical or imaging parameters between the two response groups. In responders (R), the absolute SUV of the liver metastases (including SUVmax and SUVmean) decreased significantly, while there was no change in non-responders (NR). However, the percentage changes between the response groups were not significantly different. Tmax/Lmax and Tmean/Lmax of liver metastases decreased significantly in responders, while there was no change in non-responders, and the percentage changes were significantly different, with -15.5% in responders compared to 5.5% in non-responders (p = 0.01) (Figures 1 and 2). There were no significant changes in the size of the liver metastases. The density of the liver metastases decreased significantly in responders, while there was no change in non-responders; however, percentual changes were not different between both response groups.

Regarding the primary NET, statistical evaluation was limited due to the small sample size and different primary tumor sites (pancreas: n = 6, duodenum: n = 1, rectum: n = 1), and there were no significant changes in response groups.

SUVmean of the spleen increased significantly in responders (p = 0.02), while it decreased in non-responders (P = 0.04). SUVmax of the liver decreased in both responders and non-responders, while the percentage decrease was slightly higher in non-responders (p = 0.04) (Table 2).

Prognostic and predictive factors

In the univariate Cox regression analysis, the only prognostic parameter associated with PFS was the Tmean/Lmax ratio of the liver metastases

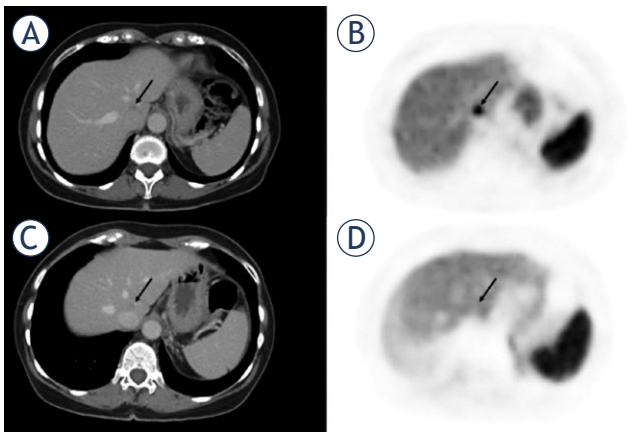

FIGURE 1. 63-year-old female with responding liver metastasis of ileal neuroendocrine tumor. On the pretherapeutic PETCT **(A, B)** there were high tumor-to- liver (T/L) ratio. After three months of treatment with everolimus, the liver metastasis showed no significant shrinkage in size, but a significantly reduced uptake of ^{68}Ga-DOTATATE **(C, D)** compared to pretherapeutic PET/CT (Tmax/Lmax: 0.94 *vs.* 2,09 and Tmean/Lmax 1.54 *vs.* 0.76).

(HR 0.5, 95% CI 0.28–0.92, p = 0.03). Patients with a higher Tmean/Lmax ratio (≥ 2) on baseline imaging showed slightly significantly longer PFS, with a median of 410 days compared to 185 days (p = 0.04). None of the pretherapeutic clinical parameters were associated with PFS.

Among the changes after treatment, the percentage changes of both tumor-to-liver ratios (Tmax/Lmax and Tmean/Lmax) and the Tmax/Smean ratio were significant predictors of PFS. In a secondary analysis, the area under the curve (AUC) was highest for the percentage change of Tmean/Lmax

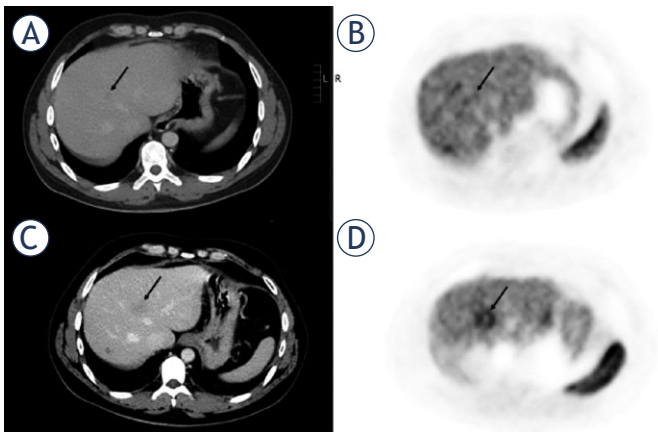

FIGURE 2. 31-year-old male with non-responding liver metastasis of pancreatic neuroendocrine tumor. On the pretherapeutic PET/CT **(A, B)** there were low tumor-to- liver (T/L) ratios. After three months of treatment with everolimus, liver metastasis (arrow) showed an increase in size on CT **(C)**, but also a significantly increased uptake of ^{68}Ga-DOTATATE **(D)** compared to pretherapeutic PET/CT.

TABLE 2. Clinical and imaging parameters at baseline and follow-up with changes

	Responder		Pre- vs. Post-therapy	Non-responder		p-value	R vs. NR Pre-treatment	R vs. NR Post-treatment
	Pre-treatment	Post-treatment	p	Pre-treatment	Post-treatment		p	p
Clinical parameters								
Age	63.5 +- 12.5			62.4 +- 13.4			0.42	
Sex (male)	10 (45%)			7 (37%)			0.2	
Ki-67 %	7.9 (+- 7.8)			10.5 (+-7)			0.28	
Pre Bilirubin	0.6 (0.2)			0.7 (0.3)			0.13	
Pre CgA	551 (77.6–933.5)			422 (47–1414)			0.11	
Imaging parameters								
SUVmax Liver	8 (6–9.3)	9.4 (5–10.9)	0.17	6.9 (4.9–9.2)	6.4 (3.5–10)	0.05	0.6	0.1
SUVmean Spleen	12.3 (9.9–18.6)	16.4 (9.9–20.1)	**0.02**	13.8 (10.1–16.9)	11 (9.8–15.1)	**0.04**	0.3	0.5
SUVmax LM	28.1 (15.1–35.3)	22.2 (14.2–31.7)	**< 0.01**	21.3 (12.7–34.7)	22.5 (9.4–29.6)	0.19	0.3	0.6
SUVmean LM	12.4 (10.5–19.1)	12.9 (9.3–18.9)	**0.03**	14.5 (9.3–18.3)	13.5 (7.8–17.4)	0.13	0.4	0.5
Tmax/Lmax LM	3.0 (2.4–4.3)	2.4 (2–3.3)	**0.02**	2.8 (2.4–3.8)	3 (1.9–4.6)	0.36	0.3	0.8
Tmean/Lmax LM	1.8 (1.4–2.3)	1.6 (1.2–1.9)	**0.02**	1.9 (1.2–2.2)	1.6 (1.4–2.5)	0.26	0.2	0.7
Tmax/Smean LM	1.6 (1.3–2.4)	1.3 (0.9–1.7)	0.25	1.5 (1.2–2.3)	1.5 (0.9–3.0)	0.3	0.4	0.8
Tmean/Smean LM	1.0(0.8–1.1)	0.8 (0.5–1.0)	0.49	0.9 (0.6–1.6)	0.9 (0.5–1.6)	0.46	0.5	1.0
Size LM	21 (17–29)	20 (15–31.2)	0.64	21 (15–32)	21 (15–32)	0.95	0.7	0.5
Density LM (HU)	101.9 (± 19.9)	90.5 (± 20.5)	**0.03**	89.4 (± 22.6)	81.7 (± 22.1)	0.1	0.2	0.3
SUVmax NET	32.8 (6.9–39.8)	30.4 (10.3–31.5)	0.49	36.4 (28.8–47.4)	43.1 (29.7–53.7)	0.97	0.5	0.3
SUVmean NET	16 (4.6–16.9)	13.4 (7.1–14.7)	0.9	17.6 (14–19.4)	22.3 (13.6–28.5)	0.25	0.4	0.3
Size NET	18 (15-36)	25 (11.2–37.3)	0.48	43.5 (24–60.8)	44.5 (25.3–66)	0.37	0.7	0.5
Density NET	83.3 (± 9.1)	81.5 (± 18)	0.9	89.3 (± 17.5)	78.2 (± 11.6)	0.4	0.6	0.8
Change (%) between pre- and post-treatment	**Responder**			**Non-responder**			**R vs. NR p**	
SUVmax Liver	-9.5 (-14–19.9)			-13 (-37.5–8.7)			**0.04**	
SUVmean Spleen	13 (-6.6–29.1)			-10.7 (-26.3–2.6)			**0.01**	
SUVmax LM	-20.4 (-27–6)			-0.9 (-22.8–26.3)			0.21	
SUVmean LM	-10 (-28.5–12.7)			-7 (-23.4–11.1)			0.62	
Tmax/Lmax LM	-15.5 (-47–5.5)			5.5 (-20.4–20.7)			**0.01**	
Tmean/Lmax LM	-16.3 (-37–9)			7 (-22.3–31.1)			**0.03**	
Tmax/Smean LM	-16.6 (-44.2–13.6)			4.5 (-16.8–51.4)			**0.01**	
Tmean/Smean LM	-16.3 (-39.3–8.8)			0.9 (-17.4–50)			**0.04**	
Size LM	-7 (-27.8–6.1)			14.3 (-17.6–28)			0.77	
Density LM	-5.6 (-12.3–0.2)			-7 (-16.5–4.1)			0.8	
SUVmax NET	-7.3 (-16.2–35.5)			-18.1 (-41.6–25.6)			0.77	
SUVmean NET	15.6 (-0.6–48)			18.4 (-7.8–40.5)			0.65	
Size NET	-15.9 (-37.4–11.1)			3.6 (-2.1–13.3)			0.72	
Density NET	-5.2 (-20–14.5)			-18.3 (-22.9– -4.6)			0.69	
Bilirubin	-33 (-61.7–0)			-25 (-66.7–0)			0.43	
CgA	56.4 (17.4–144.9)			32.1 (-2.8–72.8)			0.18	

CgA = chromogranin A; LR = liver metastases; NET = neuroendocrine tumor; NR = non-responder; R = responder; SUV = standardize uptake value; Tmax/Lmax = tumor max to liver max; Tmax/Smean = tumor max to splen max

(AUC = 0.73), followed by the percentage change of Tmax/Lmax (AUC = 0.71). The ROC analysis revealed an optimal threshold for Tmean/Lmax at >2.5 (sensitivity 62%, specificity 80%) and for Tmax/Lmax at >8 (sensitivity 54%, specificity 87%). PFS of patients with any decrease of Tmax/Lmax less than 2.5% was significantly longer with 322 days compared to 142 days (p = 0.003). Also, PFS of patients with an any decrease of Tmax/Lmax less than 8% was significantly longer with 306 days compared to 142 days (p = 0.005) (Figure 3). None of the other imaging parameters, such as density or size, nor any of the clinical parameters, were predictive of PFS.

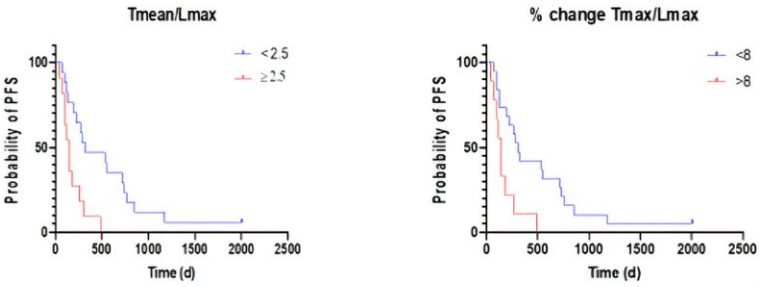

FIGURE 3. Predictive value of %-change of Tmean/Lmax ratio and %-change of Tmax/Lmax ratio.

Discussion

In this study we investigated the utility of clinical, morphological, and SSTR-PET derived functional imaging parameters for evaluating response and predicting outcomes in NET patients treated with everolimus. Our findings suggest that the use of ratios of SUV of the liver metastases (Tmean/Lmax and Tmax/Lmax) could serve as valuable tool for assessing and even predicting therapy response in NET patients receiving everolimus.

We chose progression-free survival (PFS) as the primary endpoint for response evaluation, following the recommendation of the National Cancer Institute Neuroendocrine Tumor Clinical Trials Planning Meeting consensus report. The use of overall survival (OS) for therapy response evaluation in NETs can be challenging due to the long survival times typically associated with these tumors and the range of post-progression salvage therapies available.[18] The overall median PFS in our patient cohort was slightly lower compared to the RADIANT-3 and RADIANT-4 trials, with 8.7 months compared to 11 months, respectively.[5,19] These differences could be attributed to factors such as the small size of our study cohort, the use of everolimus as a late treatment-line at our clinic, and the distribution of tumor grading among patients. In our patient cohort 69% had G2 tumors and 24% had G1 tumors, while in the RADIANT-3 study 82% of the patients had well differentiated tumors and in the RADIANT-4 study 63% had G1 tumors.[5,19]

Conventional response assessment based on percentage changes in the size of target lesions did not show significant differences between the response groups on the first follow-up PET/CT. However, functional imaging parameters, particularly the percentage changes in tumor-to-organ ratios of the liver metastases, were significantly different between response groups, with non-responders showing a median percent increase (median 0.9 to 7%) and responders showing a median percent decrease (median -15.5 to -16.6%). The percentual changes of absolute SUV measurements however, including SUVmax and SUVmean, were not significantly different between response groups.

Tumor-to-organ ratios are affected by the changes in the specific organs, e.g., liver or spleen respectively. Our study revealed a significant increase in spleen SUVmean after treatment in R, while NR showed a decrease in splenic SUVmean. Previous studies have reported a decrease in SSTR uptake in the spleen after long-acting somatostatin analog therapy, accompanied by an increase in tumor uptake.[20,21] Additionally, after splenectomy, higher uptake of ^{68}Ga DOTA-TOC in tumors and some normal tissues has been observed.[22,23] However, these changes' correlation with tumor response has rarely been evaluated.

Quantitative assessment of SSTR PET/CT has its challenges, and relying solely on absolute tumor uptake for response evaluation might lead to erroneous conclusions.[20] In this context, tumor-to-organ ratios offer an advantage, along with the normalization of absolute SUV to obtain scanner-independent parameters. In our study, SUVmax of the liver decreased in both responders and non-responders, with a slightly greater degree of reduction in non-responders (-13% *vs.* -9.5%). This observation could be related to the metabolization of everolimus, which mainly occurs in the liver via the CYP3A4 system. Although serum enzyme elevations may occur in up to 25% of patients, these changes are typically mild and self-limiting.[24,25]

In a secondary analysis, we evaluated the association of different clinical and imaging parameters with PFS using Cox regression analysis.

Among the prognostic factors, the Tmean/Lmax ratio of the liver metastases emerged as the only significant parameter associated with PFS (HR 0.5, 95% CI 0.28–0.92, p = 0.03). Patients with a higher Tmean/Lmax ratio (≥ 2) on baseline imaging exhibited longer PFS, while none of the pretherapeutic clinical parameters showed a significant association with PFS. These findings are consistent with previous studies investigating the prognostic value of SSTR-PET/CT in patients undergoing peptide-receptor-radionuclide therapy (PRRT)[26-28] or lanreotide treatment[29], which also reported that patients with higher baseline tumor-to-liver ratios or SUVmax had a better prognosis or were more likely to respond to therapy. For PRRT, Kratochwil *et al.* proposed a cut-off value of the tumor-to-liver ratio > 2.2 to select patients for treatment by PRRT.[27] The correlation between higher SUV values and the dose delivered by PRRT may explain these findings. However, in the context of a targeted therapy like everolimus, the underlying mechanism remains unclear. One possible explanation is that a target lesion with higher SSR expression might correspond to a more differentiated tumor. Further research is needed to elucidate the precise mechanisms underlying these observations.

In the univariable Cox regression analysis, the percentage change of the tumor-to-organ ratios (Tmax/Lmax and Tmean/Lmax) were found to be significantly associated with PFS. However, none of these parameters remained significant in the multivariable analysis, possibly due to the total study size being a limiting factor for this analysis. ROC analysis was performed on the identified parameters, and the highest AUC was obtained for Tmean/Lmax (AUC = 0.73). Patients with a percentual change of Tmax/Lmax of less than 2.5% showed a significantly longer PFS with 322 days compared to 142 days (p = 0.003). In contrast, none of the other imaging parameters, such as density or size, nor any of the clinical parameters, were predictive of PFS at the first follow-up.

Increasing evidence suggests that conventional response assessment based on tumor size change is limited in evaluating treatment response to antiproliferative or antiangiogenic effects mediated by targeted anti-cancer drugs, particularly in slow-growing tumors such as NETs.[8-10] Low objective response rates in the RADIANT 3 and RADIANT 4 trials, with 5% and 2% in the everolimus group, respectively, further support this observation.[5,19] It suggests that the benefit of everolimus on PFS is mainly attributed to the stabilization of tumor growth or minor tumor shrinkage, without reaching the cutoff for partial response as defined by RECIST.[5,8] Consequently, conventional size-based response criteria in this context may not accurately classify patients as responders *vs*. non-responders, potentially leading to the inappropriate discontinuation of an effective therapy.[21]

For classical FDG PET/CT, numerous studies have demonstrated that a decrease in SUV after therapy can predict survival. For instance, in patients with liver metastasis of pancreatic cancer treated with TARE or in breast cancer patients receiving targeted therapies, a decrease in SUV has been shown to be indicative of improved outcomes.[30,31] However, data regarding SSTR PET/CT is more limited. Some studies have indicated that a decrease in SUV, corrected for spleen or liver uptake, is associated with longer time to progression after PRRT and even correlated with improved clinical symptoms.[32,33] Additionally, in a different study, the change of T/S and T/L ratios on the first follow-up was identified as the best metric to correlate with longer hepatic PFS in NET patients undergoing TARE.[34]

The main limitation of this study was its small sample size, which is related to the low incidence of NETs and everolimus representing a second-line treatment. Additionally, the retrospective analysis represents a limiting factor, as time intervals between PET/CT scans and everolimus treatment were heterogeneous, and prior therapies differed among patients. Another limitation is the use of different scanners. While the use of quantitative SUV is well-established for FDG PET/CT using the PERCIST criteria[35], the interpretation of SUV in SSTR-PET/CT is more complex, as a reduction in uptake could be attributed to tumor regression or dedifferentiation.[26] Therefore, the use of normalized SUV measures by calculating tumor-to-spleen, liver, or blood pool ratios was suggested by various authors.[33,36]

In conclusion, our study highlights the potential value of quantitative SSTR-PET/CT in predicting and monitoring response in patients with NETs receiving everolimus. The use of liver metastasis-to-liver parenchyma ratios (Tmean/Lmax and Tmax/Lmax) showed promise in assessing therapy response, outperforming conventional size-based criteria. The Tmean/Lmax ratio emerged as a promising prognostic marker for progression-free survival (PFS), warranting further investigation in larger cohorts. Despite limitations of retrospective nature and small sample size, functional imaging remains crucial for guiding personalized treatment strategies in NET patients undergoing

targeted therapies like everolimus. Prospective studies with standardized protocols and larger populations are needed to validate these findings' clinical relevance.

References

1. Auernhammer CJ, Spitzweg C, Angele MK, Boeck S, Grossman A, Nölting S, et al. Advanced neuroendocrine tumours of the small intestine and pancreas: clinical developments, controversies, and future strategies. *Lancet Diabetes Endocrinol* 2018; **6:** 404-15. doi: 10.1016/s2213-8587(17)30401-1
2. Dasari A, Shen C, Halperin D, Zhao B, Zhou S, Xu Y, et al. Trends in the incidence, prevalence, and survival outcomes in patients with neuroendocrine tumors in the United States. *JAMA Oncol* 2017; **3:** 1335-42. doi: 10.1001/jamaoncol.2017.0589
3. Klöppel G, Perren A, Heitz PU. The gastroenteropancreatic neuroendocrine cell system and its tumors: the WHO classification. *Ann NY Acad Sci* 2004; **1014:** 13-27. doi: 10.1196/annals.1294.002
4. Briest F, Grabowski P. PI3K-AKT-mTOR-signaling and beyond: the complex network in gastroenteropancreatic neuroendocrine neoplasms. *Theranostics* 2014; **4:** 336-65. doi: 10.7150/thno.7851
5. Yao JC, Shah MH, Ito T, Bohas CL, Wolin EM, Van Cutsem E, et al. Everolimus for advanced pancreatic neuroendocrine tumors. *N Engl J Med* 2011; **364:** 514-23. doi: 10.1056/NEJMoa1009290
6. Lee L, Ito T, Jensen RT. Everolimus in the treatment of neuroendocrine tumors: efficacy, side-effects, resistance, and factors affecting its place in the treatment sequence. *Expert Opin Pharmacother* 2018; **19:** 909-28. doi: 10.1080/14656566.2018.1476492
7. Akirov A, Larouche V, Alshehri S, Asa SL, Ezzat S. Treatment options for pancreatic neuroendocrine tumors. *Cancers* 2019; **11:** 828. doi: 10.3390/cancers11060828
8. Garcia-Carbonero R, Garcia-Figueiras R, Carmona-Bayonas A, Sevilla I, Teule A, Quindos M, et al. Imaging approaches to assess the therapeutic response of gastroenteropancreatic neuroendocrine tumors (GEP-NETs): current perspectives and future trends of an exciting field in development. *Cancer Metastasis Rev* 2015; **34:** 823-42. doi: 10.1007/s10555-015-9598-5
9. Choi JI, Imagawa DK, Bhosale P, Bhargava P, Tirkes T, Seery TE, et al. Magnetic resonance imaging following treatment of advanced hepatocellular carcinoma with sorafenib. *Clin Mol Hepatol* 2014; **20:** 218-22. doi: 10.3350/cmh.2014.20.2.218
10. Krajewski KM, Nishino M, Franchetti Y, Ramaiya NH, Van den Abbeele AD, Choueiri TK. Intraobserver and interobserver variability in computed tomography size and attenuation measurements in patients with renal cell carcinoma receiving antiangiogenic therapy: implications for alternative response criteria. *Cancer* 2014; **120:** 711-21. doi: 10.1002/cncr.28493
11. Solis-Hernandez MP, Fernandez Del Valle A, Carmona-Bayonas A, Garcia-Carbonero R, Custodio A, Benavent M, et al. Evaluating radiological response in pancreatic neuroendocrine tumours treated with sunitinib: comparison of Choi versus RECIST criteria (CRIPNET_ GETNE1504 study). *Br J Cancer* 2019; **121:** 537-44. doi: 10.1038/s41416-019-0558-7
12. Schmid-Tannwald C, Schmid-Tannwald CM, Morelli JN, Neumann R, Haug AR, Jansen N, et al. Comparison of abdominal MRI with diffusion-weighted imaging to 68Ga-DOTATATE PET/CT in detection of neuroendocrine tumors of the pancreas. *Eur J Nucl Med Mol Imaging* 2013; **40**: 897-907. doi: 10.1007/s00259-013-2371-5
13. Papotti M, Bongiovanni M, Volante M, Allìa E, Landolfi S, Helboe L, et al. Expression of somatostatin receptor types 1-5 in 81 cases of gastrointestinal and pancreatic endocrine tumors. A correlative immunohistochemical and reverse-transcriptase polymerase chain reaction analysis. *Virchows Arch* 2002; **440:** 461-75. doi: 10.1007/s00428-002-0609-x
14. Versari A, Camellini L, Carlinfante G, Frasoldati A, Nicoli F, Grassi E, et al. Ga-68 DOTATOC PET, endoscopic ultrasonography, and multidetector CT in the diagnosis of duodenopancreatic neuroendocrine tumors: a single-centre retrospective study. *Clin Nucl Med* 2010; **35**: 321-8. doi: 10.1097/RLU.0b013e3181d6677c
15. Singh S, Poon R, Wong R, Metser U. 68Ga PET Imaging in patients with neuroendocrine tumors: a systematic review and meta-analysis. *Clin Nucl Med* 2018; **43:** 802-10. doi: 10.1097/rlu.0000000000002276
16. Pavel M, Öberg K, Falconi M, Krenning EP, Sundin A, Perren A, et al. Gastroenteropancreatic neuroendocrine neoplasms: ESMO Clinical practice guidelines for diagnosis, treatment and follow-up. *Ann Oncol* 2020; **31:** 844-60. doi: 10.1016/j.annonc.2020.03.304
17. Kim JY, Hong SM, Ro JY. Recent updates on grading and classification of neuroendocrine tumors. *Ann Diagn Pathol* 2017; **29:** 11-6. doi: 10.1016/j.anndiagpath.2017.04.005
18. Yao JC, Pavel M, Lombard-Bohas C, Cutsem EV, Voi M, Brandt U, et al. Everolimus for the treatment of advanced pancreatic neuroendocrine tumors: overall survival and circulating biomarkers from the randomized, Phase III RADIANT-3 study. *J Clin Oncol* 2016; **34:** 3906-13. doi: 10.1200/jco.2016.68.0702
19. Yao JC, Fazio N, Singh S, Buzzoni R, Carnaghi C, Wolin E, et al. Everolimus for the treatment of advanced, non-functional neuroendocrine tumours of the lung or gastrointestinal tract (RADIANT-4): a randomised, placebo-controlled, phase 3 study. *Lancet* 2016; **387:** 968-77. doi: 10.1016/s0140-6736(15)00817-x
20. Cherk MH, Kong G, Hicks RJ, Hofman MS. Changes in biodistribution on (68)Ga-DOTA-Octreotate PET/CT after long acting somatostatin analogue therapy in neuroendocrine tumour patients may result in pseudoprogression. *Cancer Imaging* 2018; **18:** 3. doi: 10.1186/s40644-018-0136-x
21. Weber M, Telli T, Kersting D, Seifert R. Prognostic implications of PET-derived tumor volume and uptake in patients with neuroendocrine tumors. *Cancers* 2023; **15:** 3581. doi: 10.3390/cancers15143581
22. Kratochwil C, Mavriopoulou E, Rath D, Afshar-Oromieh A, Apostolopoulos D, Haufe S, et al. Comparison of 68Ga-DOTATOC biodistribution in patients with and without spleenectomy. *Q J Nucl Med Mol Imaging* 2015; **59:** 116-20. PMID: 24382404
23. Sarikaya I, Sarikaya A, Alnafisi N, Alenezi S. Significance of splenic uptake on somatostatin receptor imaging studies. *Nucl Med Rev Cent East Eur* 2018; **21:** 66-70. doi: 10.5603/NMR.a2018.0012
24. Schieren G, Bölke E, Scherer A, Raffel A, Gerber PA, Kröpil P, et al. Severe everolimus-induced steatohepatis: a case report. *Eur J Med Res* 2013; **18:** 22. doi: 10.1186/2047-783x-18-22
25. Kuhn B, Jacobsen W, Christians U, Benet LZ, Kollman PA. Metabolism of sirolimus and its derivative everolimus by cytochrome P450 3A4: insights from docking, molecular dynamics, and quantum chemical calculations. *J Med Chem* 2001; **44:** 2027-34. doi: 10.1021/jm010079y
26. Öksüz MÖ, Winter L, Pfannenberg C, Reischl G, Müssig K, Bares R, et al. Peptide receptor radionuclide therapy of neuroendocrine tumors with 90Y-DOTATOC: is treatment response predictable by pre-therapeutic uptake of 68Ga-DOTATOC? *Diagn Interven Imaging* 2014; **95:** 289-300. doi: 10.1016/j.diii.2013.07.006
27. Kratochwil C, Stefanova M, Mavriopoulou E, Holland-Letz T, Dimitrakopoulou-Strauss A, Afshar-Oromieh A, et al. SUV of [68Ga]DOTATOC-PET/CT predicts response probability of prrt in neuroendocrine tumors. *Mol Imag Biol:* 2015; **17:** 313-8. doi: 10.1007/s11307-014-0795-3
28. Sharma R, Wang WM, Yusuf S, Evans J, Ramaswami R, Wernig F, et al. (68) Ga-DOTATATE PET/CT parameters predict response to peptide receptor radionuclide therapy in neuroendocrine tumours. *Radiother Oncol* 2019; **141:** 108-115. doi: 10.1016/j.radonc.2019.09.003
29. Kim YI, Yoo C, Oh SJ, Lee SJ, Kang J, Hwang HS, et al. Tumour-to-liver ratio determined by [(68)Ga]Ga-DOTA-TOC PET/CT as a prognostic factor of lanreotide efficacy for patients with well-differentiated gastroenteropancreatic-neuroendocrine tumours. *EJNMMI Res* 2020; **10:** 63. doi: 10.1186/s13550-020-00651-z
30. Sirico M, Bernocchi O, Sobhani N, Giudici F, Corona SP, Vernieri C, et al. Early changes of the standardized uptake values (SUV(max)) predict the efficacy of everolimus-exemestane in patients with hormone receptor-positive metastatic breast cancer. *Cancers* 2020; **12:** 3314 doi: 10.3390/cancers12113314
31. Michl M, Lehner S, Paprottka PM, Ilhan H, Bartenstein P, Heinemann V, et al. Use of PERCIST for prediction of progression-free and overall survival after radioembolization for liver metastases from pancreatic cancer. *J Nucl Med* 2016; **57:** 355-60. doi: 10.2967/jnumed.115.165613

32. Haug AR, Auernhammer CJ, Wangler B, Schmidt GP, Uebleis C, Goke B, et al. 68Ga-DOTATATE PET/CT for the early prediction of response to somatostatin receptor-mediated radionuclide therapy in patients with well-differentiated neuroendocrine tumors. *J Nucl Med* 2010; **51:** 1349-56. doi: 10.2967/jnumed.110.075002

33. Opalińska M, Morawiec-Sławek K, Kania-Kuc A, Al Maraih I, Sowa-Staszczak A, Hubalewska-Dydejczyk A. Potential value of pre- and post-therapy [68Ga] Ga-DOTA-TATE PET/CT in the prognosis of response to PRRT in disseminated neuroendocrine tumors. *Front Endocrinol* 2022; **13:** 929391. doi: 10.3389/fendo.2022.929391

34. Ingenerf M, Kiesl S, Karim S, Beyer L, Ilhan H, Rübenthaler J, et al. (68) Ga-DOTATATE PET/CT and MRI with diffusion-weighted imaging (DWI) in short- and long-term assessment of tumor response of neuroendocrine liver metastases (NELM) following transarterial radioembolization (TARE). *Cancers* 2021; **13:** 4321. doi: 10.3390/cancers13174321

35. O JH, Lodge MA, Wahl RL. Practical PERCIST: a simplified guide to PET response criteria in solid tumors 1.0. *Radiology* 2016; **280:** 576-84. doi: 10.1148/radiol.2016142043

36. Ilan E, Velikyan I, Sandström M, Sundin A, Lubberink M. Tumor-to-blood ratio for assessment of somatostatin receptor density in neuroendocrine tumors using 68Ga-DOTATOC and 68Ga-DOTATATE. *J Nucl Med* 2020; **61:** 217-21. doi: 10.2967/jnumed.119.228072

research article

Introduction of a spectrophotometric method for salivary iodine determination on microplate based on Sandell-Kolthoff reaction

Adrijana Oblak[1,2], Jernej Imperl[3], Mitja Kolar[3], Gregor Marolt[3], Blaz Krhin[1], Katja Zaletel[1,2], Simona Gaberscek[1,2]

[1] Division of Nuclear Medicine, University Medical Centre Ljubljana, Ljubljana, Slovenia
[2] Faculty of Medicine, University of Ljubljana, Ljubljana, Slovenia
[3] Faculty of Chemistry and Chemical Technology, University of Ljubljana, Ljubljana, Slovenia

Radiol Oncol 2024; 58(3): 357-365.

Received 16 April 2024
Accepted 28 May 2024

Correspondence to: Adrijana Oblak, EuSpLM, Division of Nuclear Medicine, University Medical Centre Ljubljana, Ljubljana, Slovenia. E-mail: adrijana.oblak@kclj.si

Disclosure: No potential conflicts of interest were disclosed.

Background. Iodine is an essential element for the synthesis of thyroid hormones. Therefore, a reliable marker of iodine supply is important. Iodine is predominantly excreted via kidneys, but also via salivary glands. Our aim was to introduce a new and simple method for determination of salivary iodine concentration (SLIC).

Materials and methods. Self-prepared chemicals and standards for Sandell-Kolthoff reaction on microplate with ammonium peroxydisulfate (AP) in the range 0−400 µg/L were used. Suitability of water-based standards (WBS) and artificial saliva-based standards (ASS) for standard curve were tested. We followed standards for method validation, defined concentration of used AP and compared our results with Inductively Coupled Plasma Mass Spectrometry (ICP-MS).

Results. WBS gave more reliable results than ASS as an underestimation of iodine concentration was found for ASS. LoB was 6.5 µg/L, LoD 12.0 µg/L, therefore analytical range was 12−400 µg/L. Intra- and inter-assay imprecisions at iodine concentrations, namely 20, 100, 165, and 350 µg/L were 18.4, 5.1, 5.7, and 2.8%, respectively, and 20.7, 6.7, 5.1, and 4.3%, respectively. Suitable molarity of AP was 1.0 mol/L and showed no difference to 1.5 mol/L (P values for samples with concentration 40, 100, and 150 µg/L, were 0.761, 0.085, and 0.275, respectively), whereas there was a significant change using 0.5 mol/L (P<0.001). Saliva samples could be diluted up to 1:8. There was no interference of thiocyanate and caffeine up to 193.5 mg/L. Our original method was comparable to ICP-MS. Spaerman coefficient was 0.989 (95% CI: 0.984−0.993).

Conclusions. The new method for SLIC determination is in excellent agreement with ICP-MS and easy-to-use.

Key words: iodine; salivary iodine concentration; Sandell-Kolthoff reaction; Inductively Coupled Plasma Mass Spectrometry

Introduction

Iodine is an essential trace element for the synthesis of thyroid hormones thyroxine and triiodothyronine, which importantly influence human development and metabolism. The human body contains up to approximately 20 mg of iodine, of which approximately 15 mg is stored in the thyroid gland.[1] Iodine also accumulates in choroid plexus, gastric mucosa, mammary glands during lactation, and in salivary glands.[1,2] With adequate iodine supply, more than 90% of iodine is excreted via urine.[3] Small amounts of iodine are excreted via feces, sweat, and saliva. With iodine deficiency, less iodine is excreted and more is accumulated in the thyroid gland.[4] Iodine supply significantly affects the incidence and severity of thyroid diseases.[5] Therefore, reliable biomarkers are needed for

the assessment of iodine supply. Determination of urinary iodine concentration (UIC) is most widely used. But it has one major drawback: it requires collecting a 24-hour urine sample, as a single spot urine sample is subject to diurnal variations in UIC and is therefore not directly comparable to 24-hour urinary iodine excretion.[6] In salivary glands, iodine is transported from blood to saliva via the Na^+/I^- symporter.[7,8] Thus, salivary iodine could be a biomarker of iodine supply. Saliva samples are easier to obtain and transport than urine samples.

Iodine concentration can be determined using different methods, where Inductively Coupled Plasma with Mass Spectrometry (ICP-MS) is considered a gold standard method. More accessible are spectrophotometric methods with different approaches to remove potential interferences and organic matter in the samples, using different digestion methods followed by manual or automatic Sandell-Kolthoff (S-K) reaction, where catalytic effect of iodide is used to quantify iodine in the sample. Digestion method using chloric(VII) acid has its drawbacks, because it represents a potential hazard, analyses should be performed in fume hoods and HI or I_2 are formed, thereby falsely leading to underestimation of final results. On the other hand, ammonium peroxydisulfate is a non-hazardous, non-explosive oxidizing reagent, that has very good analytical performances, as shown by Pino *et al*.[9]

To our knowledge, salivary iodine concentration (SLIC) was measured for the first time using S-K reaction in 2012 by Gulaboglu *et al*., but the samples were digested with chloric acid.[10] Later, SLIC was only measured by ICP-MS.[11]

ICP-MS is considered the best method for iodine concentration determination, but due to high cost of the instrumentation is not accessible to all laboratories. Our aim was to introduce a simple and low-cost method for determination of SLIC using ammonium peroxydisulfate as an oxidizing reagent followed by S-K reaction on microplate. We have already successfully validated this method for UIC determination.[12] Therefore, we wanted to use this method on a different sample as well, saliva.

Materials and methods

Subjects

Cross-sectional study was conducted at the Division of Nuclear Medicine, University Medical Centre Ljubljana, Slovenia between May 2022 and February 2023. Adult volunteers were invited from local population to participate in the study. Only volunteers without known thyroid diseases were included in the study.

The study was granted by the Republic of Slovenia National Medical Ethics Committee, number 0120-271/2021/3 (valid from 12th of July 2021). Informed consent was obtained from all individuals included in this study.

In all participants, salivary iodine concentration was measured. Saliva was collected into Salivettes® (Sarstedt, Germany) before and 30, 60, and 120 min after any meal during the day. Samples were then centrifuged for 10 min at 1800G at room temperature and frozen at -80°C prior to analysis.

Materials

Chemicals: potassium iodate(V) (KIO_3) (Sigma-Aldrich, Germany), ammonium peroxydisulfate ($(NH_4)_2S_2O_8$) (Sigma-Aldrich, Germany), deionized water (dH_2O) (BRAUN, Aqua B. Braun, Sterile, Ecotainer®, Germany), sodium hydroxide (NaOH) (Merck, Germany), arsenic(III) oxide (As_2O_3) (Sigma-Aldrich, Germany), sodium chloride (NaCl) (Sigma-Aldrich, Germany), concentrated sulfuric(VI) acid (H_2SO_4) (Sigma-Aldrich, Germany), ammonium cerium(IV) sulfate dihydrate ($(NH_4)_4Ce(SO_4)_4x2H_2O$) (Sigma-Aldrich, Germany), 65% nitric(V) acid (HNO_3) (Honeywell, USA).

All laboratory equipment was treated with 65% nitric(V) acid before preparation of reagents to remove any additional iodine from environment. Preparation of reagents as well as digestion processes and analyses took place in a ventilating fume hood. Reagents were prepared in volumetric flasks. Brief summary of preparation: 1 mol/L ammonium peroxydisulfate solution: dissolution of 228.2 g of $(NH_4)_2S_2O_8$ in 1 L of dH_2O, 0.875 mol/L sodium hydroxide solution: dissolution of 8.75 g of NaOH in 0.25 L of dH_2O, 0.05 mol/L arsorous acid (H_3AsO_3) solution: dissolution of 5 g of As_2O_3 in 0.1 L of 0.875 mol/L NaOH on magnetic stirrer. Afterwards, the solution was put in an ice-cold bath and 16 mL of concentrated H_2SO_4 was added while stirring on magnetic stirrer. After cooling, 12.5 g of NaCl was added and diluted with dH_2O up to 0.5 L. Solution was then mixed for 90 min at 60°C. Afterwards the solution was filtrated, 1.75 mol/L sulfuric acid solution: on an ice bath 97 mL of concentrated H_2SO_4 was slowly added to 0.5 L of dH_2O and filled with dH_2O up to 1 L, 0.019 mol/L ammonium cerium(IV) sulfate solution: dissolu-

tion of 6 g of $(NH_4)_4Ce(SO_4)_4x2H_2O$ in 0.5 L of 1.75 mol/L H_2SO_4.

All reagents were stored in amber bottles in the dark at room temperature except for ammonium peroxydisulfate solution, which was stored in the dark at 2–8°C.

We followed all Clinical Laboratory Standard Institute (CLSI) protocols for method establishment, namely EP06, EP07, EP09, EP15-A3, EP17-A2.

Preparation of standards

1.68 g of KIO_3 was dissolved in 1 L of dH_2O. The solution was then used for preparation of intermediate standard with iodine concentration of 1000 μg/L, which was used later for preparation of standards and control samples (CSs).

Standards were prepared with two different matrices, i.e. as artificial saliva to retain properties comparable to real saliva and as a water solution of iodine, which is used in UIC determination, in order to test appropriateness of matrix for standard curve.

Artificial saliva was prepared according to commercially available products that are available for patients after head and neck cancer treatment for moistening mouth and throat. Ingredients used for the preparation of a 100 mL of artificial saliva were 30.45 mg/mL of sorbitol, 10.15 mg/mL of sodium carboxymethylcellulose, 1.218 mg/mL of potassium chloride, 0.856 mg/mL of sodium chloride, 0.348 mg/mL of potassium hydrogen phosphate, 0.148 mg/mL of calcium chloride dihydrate, 0.052 mg/mL of magnesium chloride hexahydrate, and water for injections as solution with pH set at 7.0. Cellulose was added for adjusting viscosity of matrix retaining properties comparable to real saliva.

Both standards and CSs were prepared and stored according to previously published method for UIC determination.[12] Briefly, 6 working standards were prepared at concentrations of iodide: 0, 40, 80, 120, 200, and 400 μg/L. For comparison, both standards were measured on six microplates with S-K reaction. Each standard was measured in 6 replicates on each microplate and the mean concentration was calculated, whereas standards in artificial saliva were also analysed by ICP-MS. CSs were prepared at two different levels: 160 and 280 μg/L.

Preparation of standards

Six pooled saliva samples from different participants were used for testing analytical recovery by adding 10, 20, 40 and 120 μL of intermediate standard with iodine concentration of 1000 μg/L to 500 μL of saliva sample before the digestion step. Samples were measured 8 times and recovery was expressed as the percentage of the measured amount of iodine over the expected amount of iodine.

Three pooled saliva samples from different participants were tested for the potential influence of the molarity of ammonium peroxydisulfate to the final result. For UIC determination, 1 mL of 1.0 mol/L of ammonium peroxydisulfate was used, therefore we tested the same volume of ammonium peroxydisulfate with different concentrations, below and above proposed concentration: 1 mL of 0.5 mol/L, 1.0 mol/L, and 1.5 mol/L.

Linearity of the method was tested using 4 saliva samples, each measured 8 times, in the range up to 165 μg/L. Higher concentrations were not available for linearity testing. Distilled water was used as diluent in ratios of 1:2, 1:4, 1:8, and 1:16. Test was considered as linear, if the recovery was in the range of 80–120%.

The interferences of some potential substances such as thiocyanate and caffeine in the introduced method were tested by adding 19.6, 38.5, 74.1, and 193.5 mg/L of both, potassium thiocyanate and caffeine, to 6 saliva samples. Samples were measured 8 times and results are reported as recoveries expressed as the percentage of the measured over expected amount of iodine. The result was considered as no influences of interferences, if the recovery was in the range of 80–120%.

Limit of blank (LoB) and limit of detection (LoD) of the method were determined. Eighty-eight measurements for LoB from 8 samples on two microplates using two different standard curves were analysed. To test LoB, dH_2O was used. An F-test was used to compare values of measurements between both microplates. For LoD 180 measurements from 12 samples were analysed on five microplates using five different standard curves. LoD samples were in the concentration range between LoB and 4-times LoB value.

For intra- and inter-assay precision, two different types of samples were prepared. Intra-assay precision was assessed on one microplate where 40 replicates were measured, whereas inter-assay precision was measured on 15 microplates, where at least 5 replicates on each microplate were measured. Reproducibility was assessed by using 4 samples, 3 of which were prepared in water solution at concentration levels 20, 100, and 350 μg/L to cover the range of the assay standard curve, and

one was prepared as pooled saliva sample, which was pooled from random saliva samples and final concentration was 165 μg/L. Precisions were measured as coefficients of variation (CV (%)).

Procedure of the method

All reagents reached room temperature and were gently mixed before use. To 250 μL of standards, CSs, and samples, 1 mL of 1 mol/L ammonium peroxydisulfate solution was added. Oxidation of all samples, including standards and CSs, was performed manually in 13 x 100 mm glass tubes. Solution was then mixed and incubated for 1 h on 95°C on dry bath (ScientificTM IsotempTM Digital Dry Bath/Block Heater, Fisher Scientific, UK). After cooling down to room temperature, 50 μL of standards, CSs, and samples were transferred in duplicate to microplate (Nunc Multiwell plate – 96 well solid flat bottom, Merck, Germany). To each well 100 μL of arsorous acid solution was added. Microplate was sealed and incubated for 60 s on a microplate shaker. Afterwards 50 μL of ammonium cerium(IV) sulfate solution was added to each well within 40 s with an 8-channel semi-automatic pipette. Microplate was sealed and put on the microplate shaker for exactly 30 min. Immediately after shaking, an absorbance measurement at 405 nm on a spectrophotometer (SunriseTM, Tecan, Switzerland) was performed. The results were calculated by plotting the linear optical density (OD) data on Y-axis and linear iodide ion concentration on X-axis. Concentration was inversely proportional to absorbance. Standard curves were developed for each microplate separately. A quadratic polynomial was used to calculate concentration from OD.

ICP-MS method

For the validation of the introduced method, SLIC was measured at the Faculty of Chemistry and Chemical Technology of the University of Ljubljana by ICP-MS method. The concentrations of iodine were determined by inductively coupled plasma quadrupole mass spectrometer (ICP-MS 7900ce, Agilent Technologies, USA) with the use of internal standards and optimal instrumental parameters, ensuring the lowest detection limits. A forward RF power of 1.5 kW was used with Ar gas flows: carrier 0.85 L/min, makeup 0.28 L/min, plasma 1.0 L/min, cooling 15 L/min, and sample flow rate 0.2 mL/min. Isotope ^{127}I was measured in 3 replicates with integration/dwell time of 1 s. Saliva samples were diluted 40-times with ultrapure water (resistivity ≥18.2 MΩ · cm, Synergy Water Purification System, Merck Millipore, Merck, Germany). Working standard solutions were prepared by appropriate dilution of iodide stock standard solution (iodide, 1000 mg/L, CGICI1, Inorganic Ventures, USA) with ultrapure water. Calibration curve was based on 7 working standard solutions in the concentration range 0.1–10 μg/L. Intra-assay and inter-assay imprecisions of saliva samples at concentration levels 40 μg/L were 4.0%, and 5.4%, and at 100 μg/L 5.4%, and 5.7%, respectively.

Method comparison

ICP-MS method, considered as a reference method, was used for comparison of the methods. One hundred and ten saliva samples were analysed with ICP-MS as well as with the new S-K method.

Statistical analysis

The Kolmogorov-Smirnov test was used to assess the normality of distribution of analysed data. For comparison of LoB values of measured samples on two different microplates the F-test was used. T-test was used to compare values of different molarity. A $P<0.05$ was considered statistically significant. Data were expressed as means and standard deviations (SD), as means and ranges when reporting results of recoveries, and for method comparison as medians and ranges. The Passing-Bablok regression analysis and Bland-Altman method were used for the method comparison of analysed data, and the Spearman coefficient was determined. Bias was also assessed. Statistical analysis was done using MedCalc Statistical Software version 20.014 (MedCalc Software Ltd, Belgium).

Results

To determine the suitability of artificial saliva standards (ASSs) or water-based standards (WBSs) we have measured both types of samples with S-K reaction. Iodine concentrations in ASS were lower than expected in comparison to WBS, as their OD differed up to 26% at highest concentration level. Therefore, ICP-MS was also used for the analysis of ASS. Comparison of ASS measured by S-K method and ICP-MS is presented in Figure 1. We found a significant difference between the methods as, on the average, 37% lower values were obtained with the use of S-K method in comparison to ICP-MS.

Therefore, ASSs are not appropriate for iodine determination by S-K method. For further SLIC determination by the new S-K method, only WBSs were used.

Assessment of analytical recovery of 6 different saliva samples spiked with different concentrations of iodine showed no differences between measured and expected iodine concentrations. The mean percentage recovery (range) of iodine at each concentration level of addition of 19.6, 38.5, 74.1, and 193.5 μg/L of stock potassium iodate(V) solution to saliva samples with mean iodine concentration (SD) 34.7 (3.1), 72.2 (2.7), 73.7 (1.5), 113.2 (3.5), 136.0 (3.6), and 146.4 μg/L (3.0), respectively, were 103.0% (95.3–111.4%), 99.5% (94.5–102.6%), 99.5% (97.1–102.8%), 95.2% (90.0–96.9%), 95.4% (91.2–95.7%), and 95.0% (88.6–97.8%), respectively.

Three saliva samples at concentration levels of 40, 100, and 150 μg/L were tested with 3 different concentrations of ammonium peroxydisulfate, namely 0.5, 1.0, and 1.5 mol/L, respectively. Results are presented in Figure 2. Based on the results, both, 1.0 mol/L and 1.5 mol/L of ammonium peroxydisulfate solution, could be used as oxygenizing agents before the S-K reaction.

LoD for SLIC was 12.0 μg/L, with less than 5% of both false positives (α) and false negatives (β) less than 5%; based on 268 determinations, with 88 blanks and 180 low-level samples; LoB = 6.5 μg/L. LoB data were non-Gaussian. F-test for comparison of different samples for LoB determination showed no statistical difference between the values on different microplates using different standard curves, P = 0.283, so all data for LoB calculation were used. Finally, analytical range was 12–400 μg/L.

The calculated imprecisions expressed as CV (%) for 3 levels of iodine concentrations, at 20, 100, 300 μg/L, and for pooled sample, are presented in Table 1.

Linearity of the test was assessed on 4 saliva samples. Results are presented in Table 2. The results below the measuring range of the method were omitted from the table.

Recovery tests of 6 different saliva samples spiked with different concentrations of thiocyanate and caffeine showed no significant influence on iodine concentrations. Recoveries are expressed as percentages of observed amount of iodine over expected amount of iodine after potassium thiocyanate or caffeine stock solutions added to samples. The mean percentage recovery (range) of iodine at each concentration level of addition of 19.6, 38.5, 74.1, and 193.5 mg/L of stock solutions of potassium thiocyanate and of caffeine to saliva samples with different iodine concentrations are presented in Table 3.

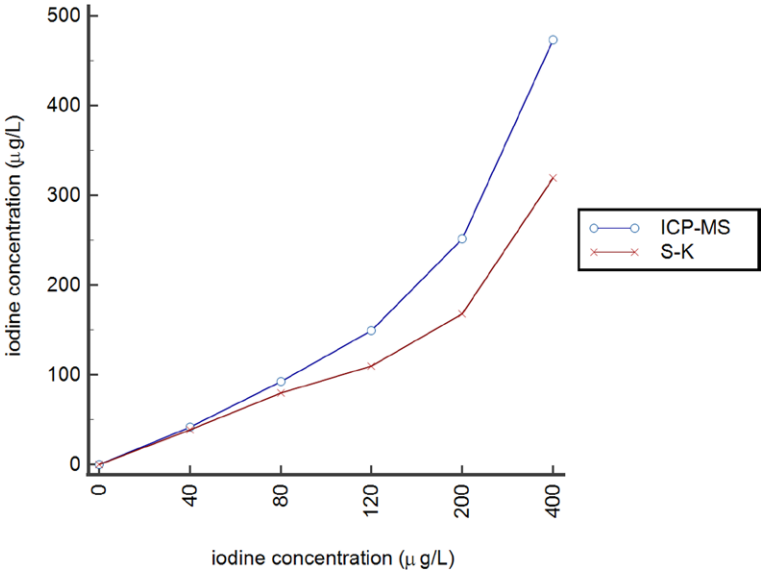

FIGURE 1. Comparison of measurements of artificial saliva standards (ASS) by two different methods, inductively coupled plasma mass spectrometry (ICP-MS) and Sandell-Kolthoff method (S-K) using ammonium peroxydisulfate on microplate.

Comparison of SLIC determination with the S-K method and with the ICP-MS method

The 110 samples covered the whole analytical range. For SLIC the median value (range) using

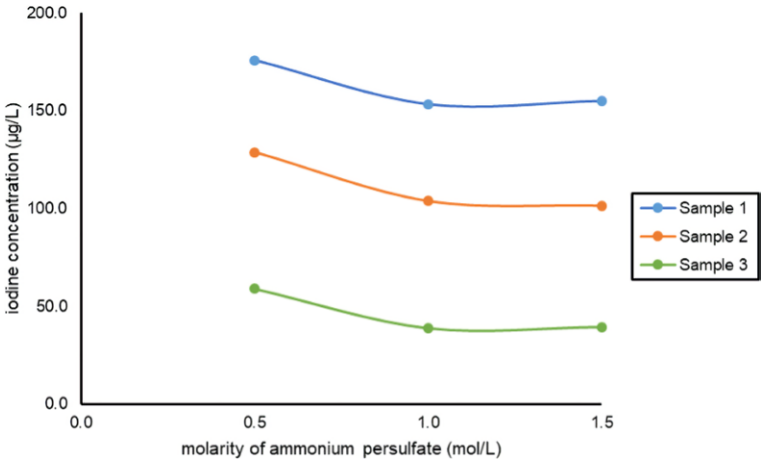

FIGURE 2. Comparison of different ammonium peroxydisulfate concentrations and their influence on the determined salivary iodine concentration. Comparison between 0.5 and 1.5 mol/L, as well as between 0.5 and 1.0 mol/L for all three samples showed significantly different values (P<0.001) for all three samples, whereas P values for samples 1, 2, and 3, showed no difference between 1.0 and 1.5 mol/L. The corresponding P values were 0.275, 0.085, and 0.761, respectively.

TABLE 1. Coefficients of variation (CV [%]) for intra- and inter-assay for 4 different iodine concentrations for salivary iodine concentration (SLIC)

Level	Target value, µg/L	Number of measurements	Intra-assay imprecision, %	Number of measurements	Inter-assay imprecision, %
1	20	40	18.4	198	20.7
2	100	40	5.1	192	6.7
3	350	40	2.8	121	4.3
Pooled sample	165	40	5.7	80	5.1

the S-K method was 124.1 µg/L (25.8–297.3 µg/L), whilst the median value using the ICP-MS method was 129.8 µg/L (22.1–353.5 µg/L). SLIC results of saliva samples obtained by both methods were not normally distributed, Spaerman coefficient was 0.989 (95% CI: 0.984–0.993), and P<0.001. Passing-Bablok regression analysis and Bland-Altman graph are presented in Figure 3 and Figure 4, respectively. The average bias between the methods was 5.9%. We did not observe any bias at concentrations up to 100 µg/L. With higher iodine concentration, the bias between the methods was 8.2%.

Discussion

Determination of UIC is a standard method for iodine supply estimation on the population level. Urine sampling, however, is associated with many problems. Because iodine is also excreted in saliva, which is relatively easy to obtain, we developed a simple, easily implementable and low-cost method for determination of SLIC. Our method is in agreement with the reference ICP-MS method. The method is also suitable for measuring SLIC in saliva samples and UIC in urine samples on the same microplate using the same standard curve as it was already shown in our previous paper.[12]

There is very little published data on the determination of SLIC and none of which is based on the method we describe in this work. The method is based on S-K reaction on microplate using ammonium peroxydisulfate as an oxidizing and digestion reagent, which shows sustainability and good performance characteristics.[12] The main disadvantages are the 'in-house' reagent preparation, potential poisonous arsorous acid, and management of arsenic waste. The main advantages of the method are cost-effectiveness, simplicity, and availability of laboratory equipment.

Water based standards were used for UIC determination. To test the saliva matrix effect, standards using artificial saliva were prepared in the same concentration range as WBS. Using ASSs, iodine

TABLE 2. Dilutions of 4 saliva samples with deionised water. Each sample was measured 8 times and results are presented as mean measured concentration (SD). Recoveries are expressed as the percentages of mean measured amount of iodine over expected amount of iodine after dilution

	Dilution	Measured (M) µg/L (SD)	Expected (E) µg/L	M/E %
Sample 1	Non-diluted	105.7 (1.3)	/	/
	1:2	56.9 (1.3)	52.9	107.7
	1:4	28.8 (2.0)	26.4	109
Sample 2	Non-diluted	35.6 (1.0)	/	/
	1:2	19.2 (1.4)	17.8	108.2
Sample 3	Non-diluted	76.7 (1.3)	/	/
	1:2	40.2 (1.7)	38.4	104.8
	1:4	17.3 (1.2)	19.2	90.3
Pooled sample	Non-diluted	165.1 (5.4)	/	/
	1:2	65.0 (3.6)	61.9	105.0
	1:4	33.8 (1.7)	31.0	109.1
	1:8	17.2 (1.6)	15.5	111.1

concentration was underestimated as compared to using WBSs. The results were also confirmed by ICP-MS. We assume that iodine in ASSs binds to organic molecules in artificial saliva and since only available iodide ions participate in S-K reaction, ASSs are not suitable for the use. To verify whether WBSs are appropriate, we have spiked 6 different saliva samples with different amounts of iodine in concentration range 34.7–146.4 μg/L. The average recoveries were very good, 95.0–103.0%, which was within the desirable range 80–120%. For further analysis only WBSs were used. The analytical range was 12–400 μg/L and could be used for both, UIC and SLIC determination on the same microplate, respectively. Measurement range is wide enough to cover expected values in saliva, and the introduced method is sensitive. Although the ICP-MS method has lower limits of quantification, our new method provides sufficient information for SLIC. The method also shows good intra- and inter-assay imprecision at different levels: low, medium, and high. Linearity of the test showed that saliva samples could be diluted up to 1:8 in the concentration range up to 165 μg/L. Higher dilutions could not be tested, since no samples were available in higher concentrations.

The first step of iodine determination was oxidation of samples to obtain accurate measurements with the elimination of interfering substances that could be present in saliva. This reagent – ammonium peroxydisulfate – was already presented by Pino *et al*.[9] For UIC measurements, 1.0 mol/L of ammonium peroxydisulfate was used. To confirm the suitability of the proposed concentration, we have also tested lower and higher molarities. With 0.5 mol/L of ammonium peroxydisulfate significantly higher iodine concentrations were measured than with 1.0 or 1.5 mol/L (P<0.001 for both). Therefore, 0.5 mol/L proved to be inappropriate. However, no differences were found using either 1.0 or 1.5 mol/L of ammonium peroxydisulfate. In order to be complementary to UIC determination, we continued to use 1.0 mol/L. This way also less ammonium peroxydisulfate is needed, compared to 1.5 mol/L. From the literature it is well known that the disadvantages of the S-K method are the interferences of the substances like iodine, KBr, $CuSO_4$, $MgSO_4$, nitrites, and ascorbic acid[13-15], which may affect the results. However, the results also depend on the use of oxidizing agent. Ascorbic acid does not affect analysis if ammonium peroxydisulfate is used as the oxidizing reagent, however it affects the result if chloric(VII) acid is used.[9,15] No method can guarantee the complete removal of all interfer-

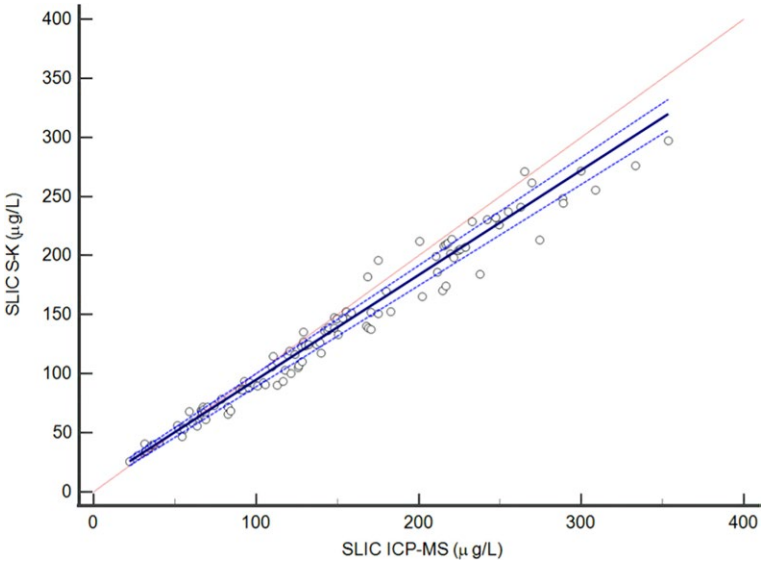

FIGURE 3. Comparison of salivary iodine concentration (SLIC) determined by the Sandell-Kolthoff (S-K) method using ammonium peroxydisulfate on microplate and by the Inductively Coupled Plasma Mass Spectrometry (ICP-MS) using Passing-Bablock regression. The solid line shows the regression line, dashed lines show 95% confidence interval (CI) for the regression line, and dotted line shows the identity line Y = X. The sample size is N = 110. The regression equation is Y = 0.89*X+6.2. The slope is 0.89 (95% CI, 0.86−0.92), and the intercept is 6.2 (95% CI, 3.3−8.6). The Cusum test for linearity showed no significant deviation from linearity (P = 0.89).

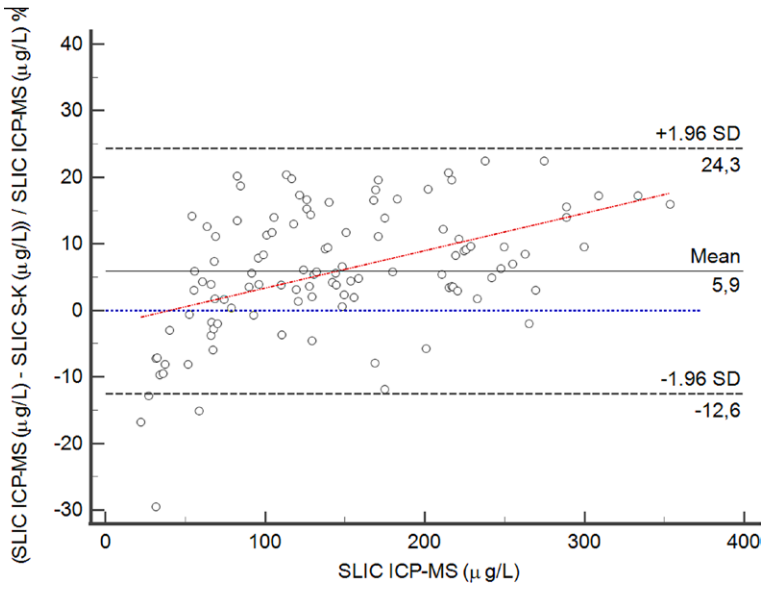

FIGURE 4. Bland-Altman plot of comparison of salivary iodine concentration (SLIC) determined by the Sandell-Kolthoff method (S-K) and by the Inductively Coupled Plasma Mass Spectrometry (ICP-MS). Differences between the methods are plotted against the ICP-MS method, which is a gold standard method. Sample size is N = 110. Horizontal lines represent the mean SLIC by ICP-MS, zero difference, and 95% confidence interval limits of agreement, which are defined as mean difference plus/minus 1.96 times the standard deviation (SD) of the differences. The mean shows a positive bias of 5.9%.

TABLE 3. Recoveries of 6 different saliva samples spiked with 19.6, 38.5, 74.1, and 193.5 mg/L of stock solutions of potassium thiocyanate and of caffeine to saliva samples. Recoveries are expressed as percentages of observed amount of iodine over expected amount of iodine after thiocyanate or caffeine stock solutions added to samples. Each sample was measured 8 times and results are presented as mean salivary iodine concentration (SLIC) (SD) and as the mean percentage recovery (range) of iodine at each concentration level

	Thiocyanate		Caffeine	
	SLIC, µg/L (SD)	Recovery, % (range)	SLIC, µg/L (SD)	Recovery, % (range)
Sample 1	34.7 (3.0)	97.9 (97.3–100.5)	29.1 (1.0)	93.2 (90.7–96.3)
Sample 2	86.0 (7.4)	101.2 (99.0–102.8)	73.0 (1.6)	99.3 (97.0–100.9)
Sample 3	90.7 (3.7)	102.4 (99.0–105.0)	75.2 (1.9)	96.1 (92.0–100.4)
Sample 4	109.0 (3.9)	109.0 (95.9–104.9)	101.3 (3.8)	96.3 (94.1–99.0)
Sample 5	143.0 (2.2)	106.2 (103.8–108.7)	142.1 (2.5)	98.7 (96.1–105.3)
Sample 6	150.6 (3.3)	102.4 (98.2–107.7)	152.8 (3.0)	99.3 (97.3–101.3)

ing substances. Our focus was on possible interferences of thiocyanate, which is found in cigarettes, and caffeine, which is regularly consumed in the form of caffeinated beverages, and are consequently present in saliva. The thiocyanate influence was already tested[9], but we used higher concentrations of thiocyanate comparable to those found in saliva of smokers.[16] The same protocol was followed with caffeine, as higher concentrations than those found in saliva[17] were tested for possible interference with the assay. Neither thiocyanate nor caffeine had any effect on the assay at concentrations up to 193.5 mg/L. However, possible coloration of saliva with thiocyanate or caffeine could affect the end result since the reaction is based on the absorbance measurement. During the process of digestion (i.e. oxidation), the samples were discoloured, which was observed and verified spectrophotometrically and results were negative (not shown in the Results).

Our method for SLIC determination was compared with a reference ICP-MS method to confirm our results. The comparison showed agreement between the evaluated methods as there was no discrepancy between the two up to 100 µg/L. At higher concentrations we found a slight discrepancy, on average 8.2% underestimation of the introduced method. Saliva samples for ICP-MS analysis were diluted 40 times using MQ to overcome matrix effect. With this in mind, it is plausible to assume that the slight discrepancy between the methods could be due to different media used for SLIC determination.

It is also important to emphasize that there is no External quality assurance assessment scheme for measuring SLIC. Therefore, comparison of SLIC determinations between the laboratories cannot be established yet. We believe the best practice for SLIC determination at this moment would be to verify self-laboratory prepared solutions used for reaction through available external program quality assessment for urinary iodine samples. If measurements are within the range, solutions are acceptable, and are also suitable for the use with saliva samples.

In summary, described spectrophotometric method on microplate using S-K reaction with ammonium peroxydisulfate digestion for SLIC determination shows acceptable performance characteristics and agreement with the reference method ICP-MS, which represents the gold standard. Implemented method showed good sensitivity and is suitable for measuring iodine concentration in various biological samples such as SLIC in saliva samples and UIC in urine samples, where microplate and the standard curve can be used. Method also enables different dilution factors for saliva samples, and more importantly, has no interferences to thiocyanate and caffeine, which are quite abundant in saliva samples. It is cost-effective, requires equipment that is usually already available in laboratories and can be therefore performed by almost any laboratory.

Acknowledgments

We extend our gratitude to Darinka Levstek at University Medical Centre Ljubljana, Slovenia, for her technical support and to Prof. Marjan Veber for his assistance that led to collaboration between both working groups. We also appreciate all par-

ticipants for all their effort in collecting biological samples. Research funding: ARIS grant number P1-0153.

References

1. Fisher DA, Oddie TH. Thyroid iodine content and turnover in euthyroid subjects: validity of esti-mation of thyroid iodine accumulation from short-term clearance studies. *J Clin Endocrinol Metab* 1969; **29:** 721-7. doi: 10.1210/jcem-29-5-721
2. Zimmermann MB. Iodine deficiency. *Endocr Rev* 2009; **30:** 376-408. doi: 10.1210/er.2009-0011
3. Nath SK, Moinier B, Thuillier F, Rongier M, Desjeux JF. Urinary excretion of iodide and fluoride from supplemented food grade salt. *Int J Vitam Nutr Res* 1992; **62:** 66-72.
4. DeGroot LJ. Kinetic analysis of iodine metabolism. *J Clin Endocrinol Metab* 1966; **26:** 149-73. doi: 10.1210/jcem-26-2-149
5. Bülow Pedersen I, Knudsen N, Jørgensen T, Perrild H, Ovesen L, Laurberg P. Large differences in incidences of overt hyper- and hypothyroidism associated with a small difference in iodine intake: A prospective comparative register-based population survey. *J Clin Endocrinol Metab* 2002; **87:** 4462-9. doi: 10.1210/jc.2002-020750
6. Iacone R, Idelson PI, Formisano P, Russo O, Lo Noce C, Donfrancesco C, et al. Iodine intake estimated by 24 h urine collection in the Italian adult population: 2008-2012 Survey. *Nutrients* 2021; **13:** 1529. doi: 10.3390/nu13051529
7. Spitzweg C, Joba W, Eisenmenger W, Heufelder AE. Analysis of human sodium iodide symporter gene expression in extrathyroidal tissues and cloning of its complementary deoxyribo-nucleic acids from salivary gland, mammary gland, and gastric mucosa. *J Clin Endocrinol Metab* 1998; **83:** 1746-51. doi: 10.1210/jcem.83.5.4839
8. Jhiang SM, Cho JY, Ryu KY, DeYoung BR, Smanik PA, McGaughy VR, et al. An im-munohistochemical study of Na+/I- symporter in human thyroid tissues and salivary gland tissues. *Endocrinology* 1998; **139:** 4416-9. doi: 10.1210/endo.139.10.6329
9. Pino S, Fang SL, Braverman LE. Ammonium persulfate: a safe alternative oxidizing reagent for measuring urinary iodine. *Clin Chem* 1996; **42:** 239-43.
10. Gulaboglu M, Akgül H, Akgül N, Cetin M. Urine and saliva iodine levels in patients with dental caries and normal healthy volunteers. *Trace Elem Electroly* 2012; **29:** 28-33. doi: 10.5414/tex01186
11. Guo WX, Pan ZY, Zhang Y, Jin Y, Dong SY, Wu W, et al. Saliva iodine concentration in children and its association with iodine status and thyroid function. *J Clin Endocrinol Metab* 2020; **105:** e3451-e9. doi: 10.1210/clinem/dgaa471
12. Oblak A, Arohonka P, Erlund I, Kuzmanovska S, Zaletel K, Gaberšček S. Validation of a spectrophotometric method for urinary iodine determination on microplate based on Sandell-Kolthoff reaction. *Lab Med* 2022; **53:** 376-80. doi: 10.1093/labmed/lmab117
13. Miura Y, Kusakari K. Flow injection analysis of nitrite based on spectrophotometric measurements of iodine formed by oxidation of iodide with nitrite. *Anal Sci* 1999; **15:** 923-6. doi: org/10.2116/analsci.15.923
14. Štolc V. Interference of certain ions with the catalytic action of iodine in the Sandell-Kolthoff reaction. *Fresenius Z Anal Chem* 1961; **183:** 262-7. doi: 10.1007/bf00474698
15. Ford HC, Johnson LA. Ascorbic acid interferes with an automated urinary iodide determi-nation based on the ceric-arsenious acid reaction. *Clin Chem* 1991; **37:** 759. doi: 10.1093/clinchem/37.5.759
16. Flieger J, Kawka J, Tatarczak-Michalewska M. Levels of the thiocyanate in the saliva of tobacco smokers in comparison to e-cigarette smokers and non-smokers measured by HPLC on a phosphatidylcholine column. *Molecules* 2019; **24:** 3790. doi: 10.3390/molecules24203790
17. Zylber-Katz E, Granit L, Levy M. Relationship between caffeine concentrations in plasma and saliva. *Clin Pharmacol Ther* 1984; **36:** 133-7. doi: 10.1038/clpt.1984.151

research article

Predictive potential of dynamic contrast-enhanced MRI and plasma-derived angiogenic factors for response to concurrent chemoradiotherapy in human papillomavirus-negative oropharyngeal cancer

Alja Longo[1,2], Petra Hudler[3], Primoz Strojan[2,4], Gaber Plavc[2,4], Lan Umek[5], Katarina Surlan Popovic[1,2]

[1] Institute of Radiology, University Medical Centre Ljubljana, Ljubljana, Slovenia
[2] Faculty of Medicine, University of Ljubljana, Ljubljana, Slovenia
[3] Institute of Biochemistry and Molecular Genetics, Faculty of Medicine, University of Ljubljana, Ljubljana, Slovenia
[4] Institute of Oncology, Ljubljana, Slovenia
[5] Faculty of Public Administration, University of Ljubljana, Ljubljana, Slovenia

Radiol Oncol 2024; 58(3): 366-375.

Received 24 May 2024
Accepted 22 July 2024

Correspondence to: Alja Longo, M.D., Institute of Radiology, University Medical Centre Ljubljana, Zaloška cesta 2, SI-1000 Ljubljana, Slovenia. E-mail: alja.longo@kclj.si

Disclosure: No potential conflicts of interest were disclosed.

Background. Dynamic contrast-enhanced magnetic resonance imaging (DCE-MRI) can assess tumour vascularity, which depends on the process of angiogenesis and affects tumour response to treatment. Our study explored the associations between DCE-MRI parameters and the expression of plasma angiogenic factors in human papilloma virus (HPV)-negative oropharyngeal cancer, as well as their predictive value for response to concurrent chemoradiotherapy (cCRT).

Patients and methods. Twenty-five patients with locally advanced HPV-negative oropharyngeal carcinoma were prospectively enrolled in the study. DCE-MRI and blood plasma sampling were conducted before cCRT, after receiving a radiation dose of 20 Gy, and after the completion of cCRT. Perfusion parameters k_{trans}, k_{ep}, V_e, initial area under the curve (iAUC) and plasma expression levels of angiogenic factors (vascular endothelial growth factor [VEGF], connective tissue growth factor [CTGF], platelet-derived growth factor [PDGF]-AB, angiogenin [ANG], endostatin [END] and thrombospondin-1 [THBS1]) were measured at each time-point. Patients were stratified into responders and non-responders based on clinical evaluation. Differences and correlations between measures were used to generate prognostic models for response prediction.

Results. Higher perfusion parameter k_{trans} and higher plasma VEGF levels successfully discriminated responders from non-responders across all measured time-points, whereas higher iAUC and higher plasma PDGF-AB levels were also discriminative at selected time points. Using early intra-treatment measurements of k_{trans} and VEGF, a predictive model was created with cut-off values of 0.259 min^{-1} for k_{trans} and 62.5 pg/mL for plasma VEGF.

Conclusions. Early intra-treatment DCE-MRI parameter k_{trans} and plasma VEGF levels may be valuable early predictors of response to cCRT in HPV-negative oropharyngeal cancer.

Key words: DCE-MRI; angiogenesis; VEGF; concurrent chemoradiotherapy; response; head and neck squamous cell carcinoma

Introduction

Head and neck cancers are the seventh most common cancer worldwide, contributing to about 4.5% of global cancer deaths.[1] The most recent (8th) edition of the Union for International Cancer Control (UICC) staging system distinguishes human papilloma virus (HPV) positive and HPV-negative head and neck squamous cell carcinoma (HNSCC) as distinct entities, with the latter typically associated with poorer prognoses.[2] In recent decades, non-surgical treatment strategies for locally advanced HPV-negative HNSCC have remained largely unchanged, relying primarily on concurrent chemoradiotherapy (cCRT). The identification of reliable biomarkers for predicting responses to cCRT could aid in stratifying patients for potential individualised treatment adjustments.

Vascular-rich HNSCCs are thought to be more responsive to treatment and show greater sensitivity to radiation compared to less vascular HNSCCs due to enhanced delivery of chemotherapeutic agents and improved oxygenation status.[3] Vascular characteristics of HNSCC can be investigated using functional MR imaging, specifically dynamic contrast-enhanced MRI (DCE-MRI). In recent years, both pre-treatment and early intra-treatment functional MR imaging have shown promising results in predicting cCRT outcomes for HNSCC.[4,5] Perfusion parameter k_{trans}, a measure of capillary permeability, is particularly promising for its potential clinical application in predicting survival and could be used to guide treatment decisions.[5]

Tumour vascularity depends on angiogenesis, a process regulated by various angiogenic factors and cytokines within the tumour microenvironment. Key players in this regulation include vascular endothelial growth factors (VEGFs), which are potent inducers of angiogenesis and vascular permeability. In addition, several other angiogenic factors have been implicated in promoting angiogenesis in HNSCC, including connective tissue growth factor (CTGF), platelet-derived growth factor (PDGF) and angiogenin (ANG), whereas endostatin (END) and thrombospondin-1 (THBS1) have been investigated as endogenous angiogenesis inhibitors.[6–9]

The objective of this study was to investigate differences in DCE-MRI perfusion parameters and the levels of specific plasma angiogenic factors in HPV-negative oropharyngeal squamous cell carcinoma (OPSCC) patients, distinguishing between responders and non-responders to cCRT. Our goal was to identify measures that could improve patient stratification and enhance the accuracy of outcome prediction.

Patients and methods

This was a single-centre prospective study conducted at the Institute of Radiology, University Medical Centre Ljubljana, in collaboration with the Institute of Oncology Ljubljana and the Institute of Biochemistry and Molecular Genetics, Faculty of Medicine, University of Ljubljana. The study was approved by the National Medical Ethics Committee of the Republic of Slovenia (No. 0120-247/2019/4, 12 June 2019) and the Committee for Medical Ethics of the Institute of Oncology Ljubljana (OI: 28.5.2019, ERIDEK-0064/2019). Written informed consent was obtained from all patients.

Patient selection

We consecutively included patients with previously untreated locally advanced HPV-negative OPSCC who were scheduled for curative cCRT. Patients were treated with the intensity-modulated radiotherapy (RT) technique to a radiation dose of 70 Gy in 35 fractions over 7 weeks. Cisplatin 40 mg/m2/week IV or carboplatin 1.5 AUC/week were administered concurrently with RT. HPV status was determined by p16 immunohistochemistry and *in situ* hybridization studies. Patients with concurrent malignancies and those unable to undergo MRI examination were excluded from the study.

Study design

Patients underwent DCE-MRI before treatment initiation, after receiving 20 Gy of irradiation, and 10–12 weeks after cCRT completion. Peripheral venous blood samples were obtained at each MRI timepoint.

MR imaging

MRI scans were conducted using a 3.0T MAGNETOM Trio, A Tim System scanner (Siemens Healthineers®, Forchheim, Germany), equipped with a head and neck receive coil. The diagnostic imaging protocol included an axial T2-weighted sequence with short tau inversion recovery (STIR) (TR/TE 5010/71 ms, TI 170 ms, matrix size 256 x 256, slice thickness 3 mm, 10% gap,

and field of view (FOV) 18 x 18 cm) and a contrast-enhanced (CE) axial T1-weighted volumetric interpolated breath-hold examination (VIBE) sequence (TR/TE 3.26/1.26 ms, voxel size 1.1 x 0.9 x 1.5 mm, matrix size 288 x 288, and FOV 250 cm²). DCE-MRI was performed using a 3D fast low-angle shot (FLASH) sequence optimized for spatial and temporal resolution (TR/TE 5/1.16 ms, matrix size 220 cm², slice thickness 4 mm, temporal resolution 9 s, total acquisition time 6 min). T1 mapping was utilized to convert signal intensities into gadolinium concentration. The T1 map was derived from two pre-contrast flip angle images (6° and 15°). Baseline images were acquired for 27 seconds. Intravenous administration of the paramagnetic contrast medium gadobutrol (Gadovist®, Bayer HealthCare Pharmaceuticals) was performed at a dose of 0.1 mmol/kg body weight with a flow rate of 3.5 mL/s, followed by a 20 mL saline flush. The diagnostic imaging protocol (axial STIR and CE axial T1 VIBE) was employed for pre-treatment tumour evaluation and radiation treatment planning.

Treatment response

Patients were stratified into two groups based on clinical evaluation. Responders demonstrated complete disappearance of the primary tumour within 10–12 weeks following cCRT. Non-responders encompassed all other patients, including those with partial response, stable disease, or progressive disease.

DCE-MRI perfusion analysis

We conducted the post-processing of DCE 3D datasets using a commercially available Tissue 4D workflow within the syngo.via medical imaging software (Siemens Healthineers, Forchheim, Germany). We utilized a population-based arterial input function with an intermediate pre-set, and motion correction was automatically conducted using the software algorithm.

Regions of interest (ROI) delineation was verified by two experienced head and neck radiologists (A. L., K. Š. P.). ROI were delineated across VIBE multiple images, resulting in the generation of volumes of interest (VOI). VOI delineation was conducted twice for each examination. Initially, the entire tumour volume was delineated, excluding larger vessels and necrotic regions. These were assessed visually based on their appearance and enhancement characteristics, with large necrotic areas showing little to no enhancement. Subsequently, a smaller tumour volume was delineated, characterized by homogeneous or near-homogeneous enhancement, with a substantial margin from surrounding heterogeneities. The Tofts two-compartment pharmacokinetic model was utilised to derive a set of perfusion parameters, which included the volume transfer constant between blood plasma and extracellular extravascular space (k_{trans}), the total extracellular extravascular space (EES) volume fraction (V_e), the reflux constant (k_{ep}) and the initial area under the curve (iAUC) for the selected VOI. The software generated parameter maps depicted as colour-coded images. The mean values of perfusion parameters from the two delineated VOIs were used for analysis.

Biochemical analysis of plasma angiogenic factors

Blood samples underwent processing to yield 0.5 ml plasma samples, which were immediately stored in the Protein LoBind® Tubes (Eppendorf, Hamburg, Germany) at -80°C. Plasma concentrations of VEGF, CTGF, PDGF-AB, ANG, END, and THBS1 were measured at selected time-points using the enzyme-linked immunosorbent assay (ELISA) technique. The following ELISA Kits were used for the analysis: Human VEGF ELISA Kit (KHG0111), Human PDGF-AB ELISA Kit (EHPDGFAB), Human Angiogenin ELISA Kit (EHANG), Human Endostatin ELISA Kit (EHCOL18A1), Human Thrombospondin 1 ELISA Kit (EHTHBS1), all Invitrogen (Life Technologies Corporation, Carlsbad, CA, USA); and Human CTGF Mini ABTS ELISA Development Kit Catalog# 900-M317 Range (PEPROTech, EC Ltd., London, VB, part of Thermo Fisher Scientific Inc., Waltham, MA, USA).

All steps were performed following the manufacturers' protocols, and each assay was conducted in duplicate or triplicate to ensure accuracy and reliability. To determine the levels of ANG, END, PDGF-AB, and THBS1, the plasma samples underwent dilution at ratios of 8000-, 100-, 2-, and 400-fold using 1x Assay Diluent A or D. The absorbance measurements were conducted using Synergy H4 (Biotek) at 450 or 405 nm with wavelength correction at 650 nm. Standard curves were calculated in GraphPad Prism V. 10 for Windows (GraphPad Software, Boston, MA, USA, www.graphpad.com) using curve fitting analyses, followed by the calculation of results for plasma samples. Sample concentrations were expressed in ng/mL or pg/mL.

TABLE 1. Summary of patient, tumour and treatment characteristics

Number of patients	25
Age, median (range)	60 (45–70)
Male gender (%)	25 (100)
Primary location (%)	
Oropharynx	25 (100)
Stage (%)	
III	5 (20)
IVa	8 (32)
IVb	12 (48)
Radiotherapy dose (Gy), median (range)	70 (68–70)
Concomitant chemotherapy, median no. of cycles (range)	6 (1–7)

Statistical methods

Shapiro-Wilk tests were used to assess the normality of data distributions. Depending on the results, either Student's t-tests for independent samples or Mann-Whitney U tests were employed to investigate disparities in DCE-MRI perfusion parameters and plasma levels of angiogenic factors between responders and non-responders. P-value below 0.05 was considered significant, while a p-value between 0.05 and 0.10 was regarded as indicative of a trend. Spearman correlation analysis was performed to analyse correlations between DCE-MRI perfusion parameters and biochemical parameters. Predictive models for treatment outcomes were developed using logistic regression analysis and a classification tree model. These models were validated using the leave-one-out strategy. The data analysis was carried out using Python extension libraries, including Orange[10], Pandas[11], NumPy[11], Matplotlib[12], and Scipy[13].

Results

Clinical characteristics

Twenty-five patients met the inclusion criteria. Initial DCE-MRI was performed on average 11 days (SD 4.2; range 3–18) prior to cCRT initiation, and the intra-treatment DCE-MRI was performed after receiving an average of 21 Gy (SD 2.9; range 18–34) of irradiation. Venous samples were collected an average of 11 days (SD 6.4; range 2–19) prior to cCRT initiation, and the intra-treatment samples were obtained after receiving an average of 23 Gy (SD 5.7; range 18–40) of irradiation. Patient and tumour characteristics are summarised in Table 1.

Data exclusion and missing values in analysis

Significant discrepancies were noted in the DCE-MRI parameter values for one patient, indicating a possible technical issue. As a result, we decided to exclude this patient with stage III OPSCC, leaving us with 24 patients for analysis. Additionally, there was missing data in the biochemical analysis, with two patients failing to attend the follow-up visit at 10–12-week post-cCRT. Furthermore, some data were missing due to values falling below the detection limit, including 8 samples for ANG and 1 sample for THBS1.

Treatment outcome

The median follow-up for 24 patients was 30 months (range 17–53 months). At the last follow-up visit, 17 patients were alive, 3 of them with active malignant disease. 7 patients died, with index cancer and infection being the cause of death in 5 and 2 patients, respectively. The latter 2 patients were free of treated cancer at the time of death. Among the participants, 15 were classified as responders (complete response), whereas 9 were categorised as non-responders (incomplete response). All non-responders experienced disease progression during the follow-up period. Of these, one individual was eligible for salvage surgery and remained recurrence-free throughout the follow-up period, while two others developed distant metastases, involving the lung and skin, respectively. Conversely, among the responders, one patient experienced local recurrence and subsequently underwent surgery, while another developed distant metastasis involving the bone and lung. The remaining 13 responders remained disease-free throughout the follow-up period.

Correlation between perfusion parameters and plasma angiogenic factors

Spearman correlation analysis revealed no strong correlations between DCE-MRI perfusion parameters and biochemical parameters. However, moderate positive correlations were observed between k_{ep} and both VEGF and ANG before treatment, as well as between VEGF and both k_{trans} and iAUC after receiving 20 Gy of RT. On the other hand, moderate negative correlation was observed between k_{trans} and THBS1 and also between iAUC and CTGF after receiving 20 Gy of RT. The remaining param-

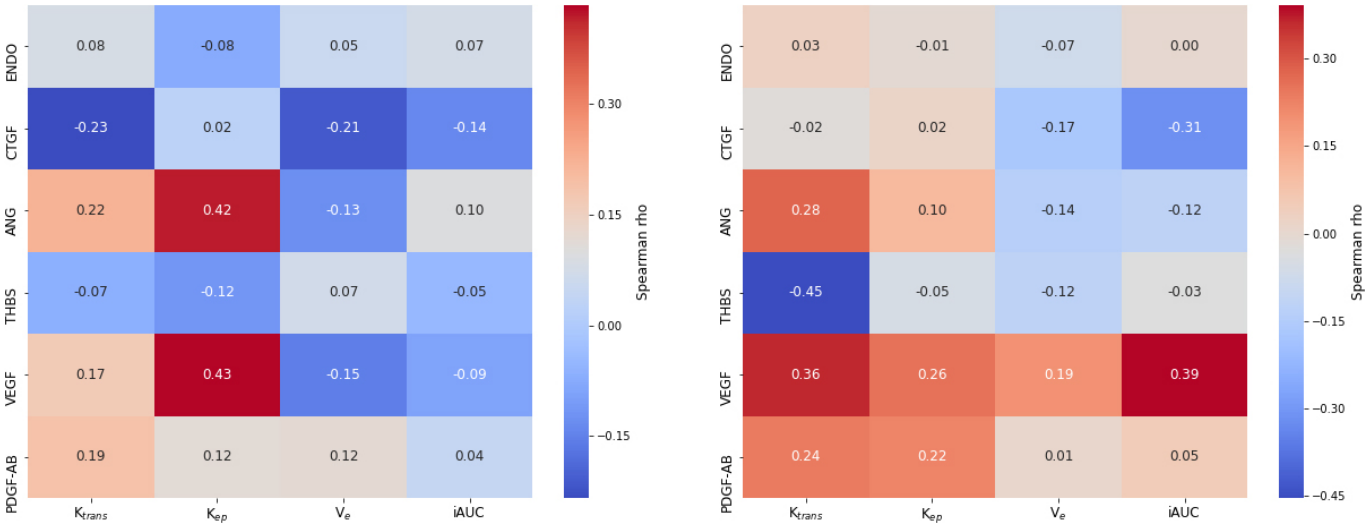

FIGURE 1. A correlation heatmap visualising perfusion parameters alongside plasma concentrations of angiogenic factors before concurrent chemoradiotherapy (cCRT) initiation (left) and after receiving 20 Gy radiotherapy (right).

TABLE 2. Correlations between dynamic contrast-enhanced magnetic resonance imaging (DCE-MRI) perfusion parameters and biochemical parameters, along with their respective Spearman's rho and p-values

Time-point	DCE-MRI parameter	Biochemical parameter	Spearman rho	p
Before treatment	k_{ep}	VEGF	0.433	0.034*
	k_{ep}	ANG	0.420	0.058
After 20 Gy	k_{trans}	THBS1	-0.453	0.026*
	k_{trans}	VEGF	0.362	0.083
	iAUC	VEGF	0.391	0.056
	iAUC	CTFG	-0.315	0.134

ANG = angiogenin; CTGF = connective tissue growth factor; iAUC = initial area under the curve; THBS1 = thrombospondin-1; VEGF = vascular endothelial growth factor

eters exhibited weak correlations, including k_{trans} and VEGF before treatment (Spearman rho = 0,166) (Table 2, Figure 1).

Representative co-registered anatomic MR images and colour-coded pharmacokinetic parametric maps of a responder and a non-responder patient before and after 20 Gy RT are shown in Figures 2 and 3, respectively.

Dynamic contrast-enhanced (DCE) parameters

Compared to non-responders, responders exhibited higher k_{trans} values before treatment (0.270, SD 0.087 min-1 *vs.* 0.169, SD 0.062 min-1, p = 0.006) as well as after receiving 20 Gy of RT (0.289, SD 0.067 min-1 *vs.* 0.215, SD 0.027 min-1, p = 0.007) (Table 3). After receiving 20 Gy of RT, an increase in k_{trans} was observed in both groups. iAUC was larger in responders compared to non-responders before treatment (0.334, SD 0.109 *vs.* 0.220, SD 0.092, p = 0.015) but not after receiving 20 Gy of RT (0.361, SD 0.070 *vs.* 0.336, SD 0.099, p = 0.468). Before treatment, responders exhibited a larger V_e compared to non-responders (0.306, SD 0.082 *vs.* 0.237, SD 0.108, p = 0.092); however, this difference was only observed as a trend. After receiving 20 Gy of RT, there was an increase in V_e in all patients, but the fractional increase in V_e between responders and non-responders was insignificant.

Responders exhibited a trend of higher k_{ep} values compared to non-responders after receiving 20 Gy of RT (0.819, SD 0.229 *vs.* 0.709, SD 0.086, p = 0.065). Before treatment, k_{ep} values did not distinguish between responders and non-responders.

Biochemical analysis

Plasma levels of VEGF were consistently higher in responders compared to non-responders across all three time points – before treatment (p = 0.011), after receiving 20 Gy of RT (p < 0.001) as well as 10–12 weeks following the completion of cCRT (p = 0.010) (Table 4). There were no significant differences observed in the dynamics of plasma VEGF levels between the two groups (p = 0.462).

Plasma levels of PDGF-AB showed a decreasing trend across the three time points for all patients,

with no significant difference observed in the dynamics between responders and non-responders. After receiving 20 Gy of RT, plasma levels of PDGF-AB were higher in responders compared to non-responders (p = 0.021), whereas no significant difference was observed between the two groups before treatment (p = 0.431) and 10–12 weeks after CRT completion (p = 0.919).

Apart from several values falling below the detection limit, there was considerable variation in the measured levels of plasma ANG among all patients. No notable dynamics or significant differences were observed between responders and non-responders. Plasma levels of THBS1 remained stable across the three time points, with no discernible differences observed between responders and non-responders. An insignificant increase in plasma levels of END was observed across the three time points in all patients, with no noticeable differences between responders and non-responders. Plasma levels of CTGF displayed considerable variability, with no notable differences observed between responders and non-responders (Table 4).

Predicting treatment response

Based on Spearman correlation analysis and descriptive statistics for DCE-MRI and biochemical parameters between responders and non-responders, we selected two variables for inclusion in statistical modelling to predict treatment outcomes, namely k_{trans} and VEGF as measured after receiving 20 Gy of RT. The multivariate logistic regression (LR) analysis, which incorporated two predictor variables, k_{trans} and plasma VEGF after receiving 20 Gy of RT, yielded a classification accuracy (CA) of 0.708 and area under the ROC curve (AUC) of 0.859. Notably, the variable VEGF achieved statistical significance (p = 0.033), whereas the variable k_{trans} approached significance (p = 0.056).

A univariate LR analysis utilizing only the variable k_{trans}, measured after receiving 20 Gy of RT, exhibited a higher CA of 0.792, but a significantly lower AUC of 0.625. Notably, the variable k_{trans} demonstrated statistical significance (p = 0.019).

The classification tree model, using the same two variables, achieved CA of 0.833 and AUC of 0.881. The classification tree (Figure 4) structure consists of one terminal node on the first branch and two terminal nodes on the second. Variable k_{trans} was found to be the most influential in determining treatment response with a cut off value of 0.259 min^{-1}, followed by variable VEGF with a cut off value of 62.5 pg/mL.

TABLE 3. A summary of tumour perfusion characteristics for responders and non-responders: mean values, standard deviations (SD), and corresponding p-values

DCE-MRI parameter	Responders (n = 15)	Non-responders (n = 9)	p
k_{trans} (SD)			
Before treatment	0.270 (0.087)	0.169 (0.062)	0.006**
After 20 Gy	0.289 (0.067)	0.215 (0.027)	0.007**
Δ	0.019 (0.060)	0.047 (0.078)	0.326
k_{ep} (SD)			
Before treatment	0.924 (0.231)	0.817 (0.258)	0.144
After 20 Gy	0.819 (0.229)	0.709 (0.086)	0.065
Δ	-0.105 (0.274)	-0.108 (0.245)	0.980
V_e (SD)			
Before treatment	0.306 (0.082)	0.237 (0.108)	0.092
After 20 Gy	0.366 (0.086)	0.347 (0.107)	0.636
Δ	0.059 (0.093)	0.109 (0.196)	0.721
iAUC (SD)			
Before treatment	0.334 (0.109)	0.220 (0.092)	0.015*
After 20 Gy	0.361 (0.070)	0.336 (0.099)	0.468
Δ	0.027 (0.120)	0.116 (0.183)	0.676

iAUC = initial area under the curve

Discussion

In the present study we confirmed the efficacy of DCE-MRI in combination with plasma angiogenic factor analysis before and early during cCRT in predicting response to cCRT in patients with HPV-negative OPSCC.

The key DCE-MRI perfusion parameter k_{trans} reflects microvascular permeability and blood flow within the primary tumour.[10] In our study, we showed that responders to cCRT had significantly higher pre-treatment k_{trans} values compared to non-responders. This finding is in line with several previous reports on HNSCC and other malignancies that linked higher pre-treatment k_{trans} values to longer survival and better local control.[10-16] This supports the premise that higher perfusion within tumours is associated with increased oxygenation levels, which in turn enhances radiosensitivity and improves chemotherapeutic drug delivery.[3] A previous study exploring intra-treatment dynamics of DCE-MRI parameters in HNSCC has shown a larger fractional increase in primary tumour k_{trans} and V_e in responders versus non-responders.[17] Similarly, patients achieving locoregional control

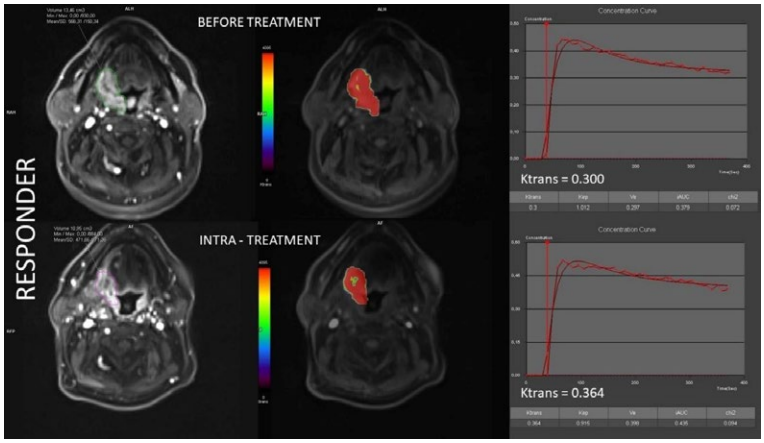

FIGURE 2. Co-registered volumes of interest (VOI) and color-coded k_{trans} maps, together with concentration curves alongside corresponding k_{trans} values before treatment (upper section) and intra-treatment after receiving 20 Gy radiotherapy (bottom section) in a representative responder patient.

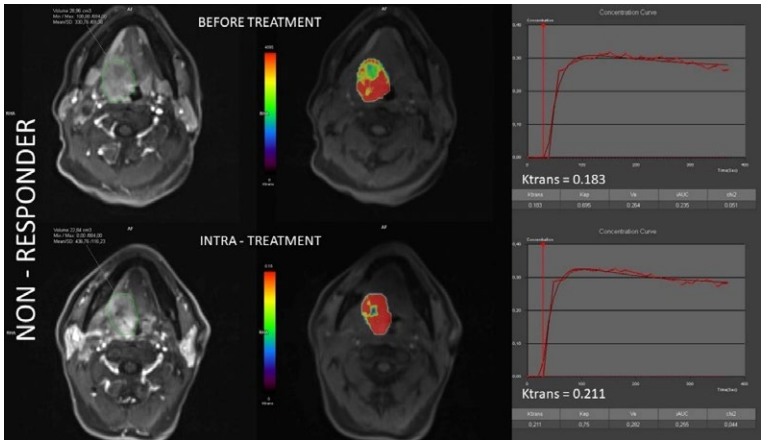

FIGURE 3. Co-registered volumes of interest (VOI) and color-coded k_{trans} maps, together with concentration curves alongside corresponding k_{trans} values before treatment (upper section) and intra-treatment after receiving 20 Gy radiotherapy (bottom section) in a representative non-responder patient.

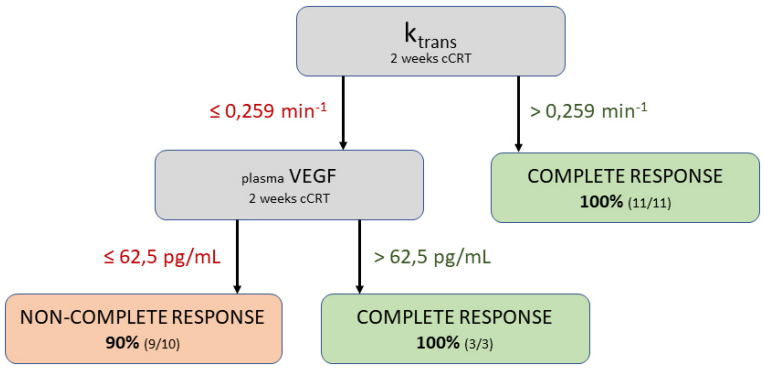

FIGURE 4. Graphical presentation of the classification tree model.

cCRT = concurrent chemoradiotherapy; VEGF = vascular endothelial growth factor

demonstrated persistently elevated or increasing levels of intra-treatment blood flow (BF), volume (BV), and permeability surface (PS), whereas one study reported a decrease in k_{trans} after 2 weeks of cCRT, which was linked to significantly reduced survival.[4,15] Interestingly, we observed an increase in k_{trans} values among both responders and non-responders after receiving 20 Gy RT. This observation aligns with the concept that low-dose radiation induces proangiogenic signalling, promotes angiogenesis, improves tumour perfusion, enhances vascular permeability, reduces hypoxia, and subsequently leads to vascular normalisation.[18] Our results suggest that this effect exists independently of the final treatment outcome. iAUC is influenced by permeability, blood flow, and washout, providing an alternative parameter to k_{trans} in clinical trials.[19,20] Our study showed that pre-treatment iAUC was higher in responders compared to non-responders, mirroring the k_{trans} results. However, unlike k_{trans}, this distinction disappeared after receiving 20 Gy of RT.

In addition to the increase in blood flow and vascular permeability, radiation-induced cellular degradation leads to the expansion of interstitial space.[17] DCE-MRI parameter V_e reflects the EES, which consists of interstitial fluid and connective tissue and differs significantly in neoplastic tissues from most normal tissues.[21] Earlier research has indicated a mostly positive correlation between elevated pre-treatment V_e and favourable outcomes, but these findings were inconsistent.[12-14] One study reported a greater fractional increase in V_e among responders compared to non-responders.[17] Similarly, in the present study we observed a tendency for a larger pre-treatment V_e in responders compared to non-responders. We observed a rise in V_e across all patients after receiving 20 Gy of RT. However, both the fractional increase of V_e and the absolute difference in V_e values after receiving 20 Gy of RT between responders and non-responders were found to be insignificant. We assume that the differences in the EES of tumours that may exist before treatment between responders and non-responders are diminished by the shared effects of radiotherapy.

VEGF is a main driver of angiogenesis, known to be upregulated in the plasma of various cancer patients.[22-24] Several studies have investigated the relationship between VEGF expression in tissue specimens and DCE-MRI parameters, especially k_{trans}, resulting in conflicting findings.[25-28] VEGF has been investigated as a potential biomarker in various cancer types, including HNSCC.[29,30] High

TABLE 4. Expression of plasma angiogenic factors for responders and non-responders: mean values, 95% confidence interval (CI) and corresponding p-values

Plasma Angiogenic Factor	Responders (n = 15)	Non-responders (n = 9)	p
VEGF (95% CI) pg/mL			
Before treatment	66.9 (58.1–75.7)	50.2 (41.8–58.5)	0.011*
After 20 Gy	68.4 (61.0–75.7)	48.0 (40.4–55.5)	0.0006**
10–12 weeks after cCRT completion	74.7 (50.8–98.6)	49.0 (38.5–59.5)	0.010*
PDGF-AB (95% CI) pg/mL			
Before treatment	2826.6 (1909.3–3743.9)	2430.6 (1179.1–3682.1)	0.431
After 20 Gy	2496.0 (2105.8–2886.2)	1799.1 (1319.3–22789)	0.021*
10–12 weeks after cCRT completion	1513.5 (902.7–2124.3)	1468.5 (779.1–2157.9)	0.919
ANG (95% CI) pg/mL			
Before treatment	2140.8 (1588.2–2693.4)	1218.0 (223.0–2213.0)	0.060
After 20 Gy	2124.1 (1653.4–2594.9)	1438.0 (405.6–2470.4)	0.131
10–12 weeks after cCRT completion	1898.1 (1248.7–2547.6)	1384.8 (255.7–2513.9)	0.347
THBS1 (95% CI) ng/mL			
Before treatment	1113.2 (1069.3–1157.2)	1115.6 (1055.8–1175.5)	0.943
After 20 Gy	1112.3 (1051.5–1173.1)	1162.7 (1064.2–1261.2)	0.257
10–12 weeks after cCRT completion	1061.2 (1008.8–1113.8)	1136.8 (1002.9–1270.7)	0.210
END (95% CI) pg/mL			
Before treatment	64792.6 (52731.7–76853.4)	59350.6 (47299.1–71402.1)	0.521
After 20 Gy	71269.2 (55039.7–87498.7)	59636.7 (48124.0–71149.5)	0.283
10–12 weeks after cCRT completion	84744.3 (65061.5–104427.2)	74754.7 (54514.5–94994.9)	0.475
CTGF (95% CI) pg/mL			
Before treatment	32.6 (13.9–51.2)	24.4 (14.4–34.5)	0.976
After 20 Gy	31.2 (24.1–122.8)	23.5 (12.3–34.8)	0.721
10–12 weeks after cCRT completion	26.1 (15.7–36.6)	23.2 (15.1–31.3)	1

ANG = angiogenin; cCRT = concurrent chemoradiotherapy; CTGF = connective tissue growth factor; END = endostatin; PDGF-AB = platelet-derived growth factor AB; THBS1 = thrombospondin-1; VEGF = vascular endothelial growth factor

VEGF expression levels in serum have been linked to increased tumour growth, invasiveness, and a higher risk of metastasis.[31] To our knowledge, no studies to date have explored the combination of DCE-MRI with plasma angiogenic factors as potential prognostic biomarkers. According to literature, the average reported healthy plasma VEGF value is 42 pg/mL (SD 20, range 9–126 pg/mL), whereas in cancer it is 74 pg/mL (SD 116, range 19–730 pg/mL), the latter displaying considerable variability.[23] A pre-therapeutic plasma VEGF threshold below 26 ng/L was reported to correlate with a more favourable outcome in HNSCC.[30] Our results, on the other hand, indicate a different trend - plasma VEGF levels were consistently higher in responders when compared to non-responders across all three time points – before treatment, after receiving 20 Gy of RT, as well as 10–12 weeks following the completion of cCRT. Explaining the rationale behind this observation is challenging, as the factors affecting plasma VEGF levels are highly multifactorial. Compared to the total amount of VEGF in the human body, tumour contributes to a relatively small percentage of VEGF. Besides the tumour, skeletal muscles seem to serve as a significant reservoir for VEGF in the body. Moreover, the renal clearance of VEGF should be considered as a contributing factor to plasma VEGF levels.[23] Although it may be overly ambitious to assume a direct relationship between tumour blood flow, permeability and circulating plasma VEGF levels, the observed higher plasma VEGF levels in responders merit consideration and further investigation. Since lower-doses of radiation induce proangiogenic signalling and

promote angiogenesis, elevated levels of VEGF, as a crucial player in angiogenesis, may manifest in the circulating plasma as a reflection of this process.[18] This could explain why the correlation between VEGF and k_{trans}/iAUC appears only after the start of the treatment. It could also provide insight into why these two parameters performed the best when conducting statistical modelling.

PDGF promotes tumour-associated angiogenesis by up-regulating VEGF production.[31,32] A sole notable distinction between responders and non-responders emerged at the intra-treatment time-point for plasma PDGF-AB, which displayed higher levels among responders. This observation emerged in the same intra-treatment time point where elevated plasma VEGF levels appeared as effective predictors of complete response. This further suggests that physiological processes occurring early during cCRT may be reflected in the plasma levels of these two pro-angiogenic factors. Apart from VEGF and PDGF-AB, none of the analysed angiogenic factors exhibited significant promise for predicting response.

The most effective multivariate predictive models incorporated intra-treatment plasma VEGF and k_{trans} values. Both logistic regression and classification tree models outperformed the univariate models that used only the k_{trans} variable, indicating that plasma VEGF levels provide significant additional predictive value in determining response. Based on our analysis, the classification tree model utilising intra-treatment plasma VEGF and k_{trans} emerged as the best-performing model.

While this study has several limitations, notably its small sample size and the lack of healthy controls for angiogenic factors, our study cohort stands out for its high homogeneity in tumour stage and HPV status, making it unique compared to similar studies. Validating our findings would necessitate a larger study, including healthy controls. Additionally, it is important to note that absolute values of perfusion parameters can vary depending on the post-processing software used for pharmacokinetic modelling in DCE-MRI. Therefore, caution is needed when comparing these values across different studies.

In conclusion, the early intra-treatment DCE-MRI parameter k_{trans} and plasma VEGF levels emerged as the two most robust predictors for treatment response to cCRT in HPV-negative oropharyngeal cancer, yielding effective predictive models with cut-off values of 0.259 min^{-1} for k_{trans} and 62.5 pg/mL for plasma VEGF.

Acknowledgments

This research was funded by the Slovenian Research and Innovation Agency (ARIS), grant number P3-0307.

References

1. Barsouk A, Aluru JS, Rawla P, Saginala K, Barsouk A. Epidemiology, risk factors, and prevention of head and neck squamous cell carcinoma. *Med Sci* 2023; **11:** 42. doi: 10.3390/medsci11020042
2. Shinomiya H, Nibu KI. Etiology, diagnosis, treatment, and prevention of human papilloma virus-associated oropharyngeal squamous cell carcinoma. *Int J Clin Oncol* 2023; **28:** 975-81. doi: 10.1007/s10147-023-02336-8
3. Chen Z, Han F, Du Y, Shi H, Zhou W. Hypoxic microenvironment in cancer: molecular mechanisms and therapeutic interventions. *Signal Transduct Target Ther* 2023; **8:** 70. doi: 10.1038/s41392-023-01332-8
4. Martens RM, Noij DP, Ali M, Koopman T, Marcus JT, Vergeer MR, et al. Functional imaging early during (chemo)radiotherapy for response prediction in head and neck squamous cell carcinoma; a systematic review. *Oral Oncol* 2019; **88:** 75-83. doi: 10.1016/j.oraloncology.2018.11.005
5. Bos P, van der Hulst HJ, van den Brekel MWM, Schats W, Jasperse B, Beets-Tan RGH, et al. Prognostic functional MR imaging parameters in head and neck squamous cell carcinoma: a systematic review. *Eur J Radiol* 2021;**144:** 109952. doi: 10.1016/j.ejrad.2021.109952
6. Kikuchi R, Kikuchi Y, Tsuda H, Maekawa H, Kozaki K, Imoto I, et al. Expression and clinical significance of connective tissue growth factor in advanced head and neck squamous cell cancer. *Hum Cell* 2014; **27:** 121-8. doi: 10.1007/s13577-014-0092-0
7. Bran B, Bran G, Hörmann K, Riedel F. The platelet-derived growth factor receptor as a target for vascular endothelial growth factor-mediated anti-angiogenetic therapy in head and neck cancer. *Int J Oncol* 2009; **34:** 255-61. doi: 10.3892/ijo_00000147
8. Homer JJ, Greenman J, Stafford ND. Circulating angiogenic cytokines as tumour markers and prognostic factors in head and neck squamous cell carcinoma. *Clin Otolaryngol Allied Sci* 2002; **27:** 32-7. doi: 10.1046/j.0307-7772.2001.00519.x
9. Huang C, Zhou X, Li Z, Liu H, He Y, Ye G, et al. Downregulation of thrombospondin-1 by DNA hypermethylation is associated with tumor progression in laryngeal squamous cell carcinoma. *Mol Med Rep* 2016; **14:** 2489-96. doi: 10.3892/mmr.2016.5580
10. Demšar J, Curk T, Erjavec A, Gorup Č, Hočevar T, Milutinovič M et al. Orange: Data Mining Toolbox in Python. *J Mach Learn Res.* 2013; **14**: 2349–2353.
11. McKinney W. Data structures for statistical computing in Python. *Proceedings of the 9th Python in Science Conference,* 2010; 51-56.
12. Hunter J D Matplotlib: A 2D Graphics Environment. *Comput Sci Eng* 2007; **9**(3), 90–95.
13. Virtanen P, Gommers R, Oliphant T E, Haberland M, Reddy T, Cournapeau D, et. al. SciPy 1.0: Fundamental algorithms for scientific computing in Python. *Nature Methods* 2020; **17**(3), 261-272.
14. Bernstein JM, Homer JJ, West CM. Dynamic contrast-enhanced magnetic resonance imaging biomarkers in head and neck cancer: potential to guide treatment? A systematic review. *Oral Oncol* 2014; **50:** 963-70. doi: 10.1016/j.oraloncology.2014.07.011
15. Dijkhoff RAP, Beets-Tan RGH, Lambregts DMJ, Beets GL, Maas M. Value of DCE-MRI for staging and response evaluation in rectal cancer: a systematic review. *Eur J Radiol* 2017; **95:** 155-68. doi: 10.1016/j.ejrad.2017.08.009
16. Ng SH, Liao CT, Lin CY, Chan SC, Lin YC, Yen TC, et al. Dynamic contrast-enhanced MRI, diffusion-weighted MRI and 18F-FDG PET/CT for the prediction of survival in oropharyngeal or hypopharyngeal squamous cell carcinoma treated with chemoradiation. *Eur Radiol* 2016; **26:** 4162-72. doi: 10.1007/s00330-016-4276-8

17. Chan SC, Cheng NM, Hsieh CH, Ng SH, Lin CY, Yen TC, et al. Multiparametric imaging using 18F-FDG PET/CT heterogeneity parameters and functional MRI techniques: prognostic significance in patients with primary advanced oropharyngeal or hypopharyngeal squamous cell carcinoma treated with chemoradiotherapy. *Oncotarget* 2017; **8:** 62606-21. doi: 10.18632/oncotarget.15904

18. Ng SH, Lin CY, Chan SC, Yen TC, Liao CT, Chang JT, et al. Dynamic contrast-enhanced MR imaging predicts local control in oropharyngeal or hypopharyngeal squamous cell carcinoma treated with chemoradiotherapy. *PLoS One* 2013; **8:** e72230. doi: 10.1371/journal.pone.0072230

19. Baer AH, Hoff BA, Srinivasan A, Galbán CJ, Mukherji SK. Feasibility analysis of the parametric response map as an early predictor of treatment efficacy in head and neck cancer. *Am J Neuroradiol* 2015; **36:** 757-62. doi: 10.3174/ajnr.A4296

20. Wong KH, Panek R, Dunlop A, Mcquaid D, Riddell A, Welsh LC, et al. Changes in multimodality functional imaging parameters early during chemoradiation predict treatment response in patients with locally advanced head and neck cancer. *Eur J Nucl Med Mol Imaging* 2018; **45:** 759-67. doi: 10.1007/s00259-017-3890-2

21. Yamazaki T, Young KH. Effects of radiation on tumor vasculature. *Mol Carcinog* 2022; **61:** 165-72. doi: 10.1002/mc.23360

22. Bisdas S, Seitz O, Middendorp M, Chambron-Pinho N, Bisdas T, Vogl TJ, et al. An exploratory pilot study into the association between microcirculatory parameters derived by MRI-based pharmacokinetic analysis and glucose utilization estimated by PET-CT imaging in head and neck cancer. *Eur Radiol* 2010; **20:** 2358-66. doi: 10.1007/s00330-010-1803-x

23. Galbraith SM. MR in oncology drug development. *NMR Biomed* 2006; **19:** 681-9. doi: 10.1002/nbm.1093

24. Lowry M, Zelhof B, Liney GP, Gibbs P, Pickles MD, Turnbull LW. Analysis of prostate DCE-MRI: comparison of fast exchange limit and fast exchange regimen pharmacokinetic models in the discrimination of malignant from normal tissue. *Invest Radiol* 2009; **44:** 577-84. doi: 10.1097/RLI.0b013e3181b4c1fe

25. Hanahan D, Weinberg RA. Hallmarks of cancer: the next generation. *Cell* 2011; **144:** 646-74. doi: 10.1016/j.cell.2011.02.013

26. Kut C, Mac Gabhann F, Popel AS. Where is VEGF in the body? A meta-analysis of VEGF distribution in cancer. *Br J Cancer* 2007; **97:** 978-85. doi: 10.1038/sj.bjc.6603923

27. Macedo F, Ladeira K, Longatto-Filho A, Martins SF. Gastric cancer and angiogenesis: is VEGF a useful biomarker to assess progression and remission? *J Gastric Cancer* 2017; **17:** 1-10. doi: 10.5230/jgc.2017.17.e1

28. Liu B, Gao H, Zhou F, Zhao W, Yang Y. Dynamic contrast-enhanced magnetic resonance imaging in cervical cancer: correlation between quantitative parameters and molecular markers hypoxia-inducible factors-1-alpha, vascular endothelial growth factor, and Ki-67. *Clin Radiol* 2024; **79:** e826-e33. doi: 10.1016/J.CRAD.2024.01.039

29. Di N, Cheng W, Jiang X, Liu X, Zhou J, Xie Q, et al. Can dynamic contrast-enhanced MRI evaluate VEGF expression in brain glioma? An MRI-guided stereotactic biopsy study. *J Neuroradiol* 2019; **46:** 186-92. doi: 10.1016/j.neurad.2018.04.008

30. Lindgren A, Anttila M, Arponen O, Rautiainen S, Könönen M, Vanninen R, et al. Prognostic value of preoperative dynamic contra st-enhanced magnetic resonance imaging in epithelial ovarian cancer. *Eur J Radiol* 2019; **115:** 66-73. doi: 10.1016/j.ejrad.2019.03.023

31. Keil VC, Pintea B, Gielen GH, Hittatiya K, Datsi A, Simon M, et al. Meningioma assessment: kinetic parameters in dynamic contrast-enhanced MRI appear independent from microvascular anatomy and VEGF expression. *J Neuroradiol* 2018; **45:** 242-8. doi: 10.1016/j.neurad.2018.01.050

32. Kulapaditharom B, Boonkitticharoen V, Sritara C. Plasma vascular endothelial growth factor dysregulation in defining aggressiveness of head and neck squamous cell carcinoma. *J Oncol* 2012; **2012:** 687934. doi: 10.1155/2012/687934

33. Siemert J, Wald T, Kolb M, Pettinella I, Böhm U, Pirlich M, et al. Pretherapeutic VEGF level in plasma is a prognostic bio-marker in head and neck squamous cell carcinoma (HNSCC). *Cancers* 2021; **13:** 3781. doi: 10.3390/cancers13153781

34. Dumitru CS, Raica M. Vascular endothelial growth factor family and head and neck squamous cell carcinoma. *Anticancer Res* 2023; **43:** 4315-26. doi: 10.21873/anticanres.16626

35. Laschke MW, Elitzsch A, Vollmar B, Vajkoczy P, Menger MD. Combined inhibition of vascular endothelial growth factor (VEGF), fibroblast growth factor and platelet-derived growth factor, but not inhibition of VEGF alone, effectively suppresses angiogenesis and vessel maturation in endometriotic lesions. *Hum Reprod* 2006; **21:** 262-8. doi: 10.1093/humrep/dei308

research article

Does portal vein anatomy influence intrahepatic distribution of metastases from colorectal cancer?

Anaïs Tribolet[1,2], Maxime Barat[3,4], David Fuks[2,3], Mathilde Aissaoui[3,4], Philippe Soyer[3,4], Ugo Marchese[2,3], Martin Gaillard[2,3], Alexandra Nassar[2,3], Jean Hardwigsen[1], Stylianos Tzedakis[2,3]

[1] Department of Digestive Surgery and Liver Transplantation, La Timone Hospital, AP-HM, University Aix-Marseille, Marseille, France

[2] Department of Hepatobiliary, Digestive and Endocrine Surgery, Cochin Hospital, AP-HP, Paris, France

[3] Université Paris Cité, Faculté de Médecine, Paris, France

[4] Department of Radiology, Cochin Hospital, Paris, France

Radiol Oncol 2024; 58(3): 376-385.

Received 29 March 2024
Accepted 13. June 2024

Correspondence to: Dr Stylianos Tzedakis, Department of Digestive, Pancreatic, Hepato-biliary and Endocrine Surgery, Cochin Hospital, APHP, University of Paris, 27, rue du Faubourg Saint Jacques, 75014, Paris, France. E-mail: stylianos.tzedakis@aphp.fr

Disclosure: No potential conflicts of interest were disclosed.

Background. Other than location of the primary colorectal cancer (CRC), a few factors are known to influence the intrahepatic distribution of colorectal cancer liver metastases (CRLM). We aimed to assess whether the anatomy of the portal vein (PV) could influence the intrahepatic distribution of CRLM.

Patients and methods. Patients with CRLM diagnosed between January 2018 and December 2022 at two tertiary centers were included and imaging was reviewed by two radiologists independently. Intra-operator concordance was assessed according to the intraclass correlation coefficient (ICC). The influence of the diameter, angulation of the PV branches and their variations on the number and distribution of CRLM were compared using Mann-Whitney, Kruskal-Wallis, Pearson's Chi-square and Spearman's correlation tests.

Results. Two hundred patients were included. ICC was high (> 0.90, P < 0.001). Intrahepatic CRLM distribution was right-liver, left-liver unilateral and bilateral in 66 (33%), 24 (12%) and 110 patients (55%), respectively. Median number of CRLM was 3 (1−7). Type 1, 2 and 3 portal vein variations were observed in 156 (78%), 19 (9.5%) and 25 (12%) patients, respectively. CRLM unilateral or bilateral distribution was not influenced by PV anatomical variations (P = 0.13), diameter of the right (P = 0.90) or left (P = 0.50) PV branches, angulation of the right (P = 0.20) or left (P = 0.80) PV branches and was independent from primary tumor localisation (P = 0.60). No correlations were found between CRLM number and diameter (R: 0.093, P = 0.10) or angulation of the PV branches (R: 0.012, P = 0.83).

Conclusions. PV anatomy does not seem to influence the distribution and number of CRLM.

Key words: colorectal liver metastases; portal vein anatomy; liver topography; portal variations; portal flow

Introduction

Colorectal cancer (CRC) is the third most common cancer worldwide, with more than two million affected patients in 2020, and the second most common cause of death, with more than one million deaths per year.[1] The liver is the most common organ of dissemination in patients with CRC. Between 15% and 25% of patients with CRC are diagnosed with synchronous liver metastasis at the time of

diagnosis; while up to 25% patients with non-metastatic CRC will develop liver metastases within five years following initial diagnosis.[2,3] In association with chemotherapy, surgery remains the only curative option for patients with colorectal liver metastases (CRLM).[4] Considerations when assessing resectability of CRLM usually take into account technical aspects such as tumour relationship to vascular inflow, outflow, and biliary drainage but also liver disease burden (i.e. size and number).[5]

The number and size of CRLMs are well-known prognostic markers of disease[5,6], however, little is known about the factors influencing CRLM intrahepatic distribution. Primary colorectal cancer localization has already been described as a factor determining CRLM intrahepatic distribution, although evidence is conflicting. Several authors have hypothesized that the portal vein (PV) 'streamline flow', resulting in cells moving in different layers, may influence CRLM intrahepatic distribution.[7-9] Indeed, since the PV is formed by the confluence of the superior mesenteric and splenic vein, it has been theorized that venous blood flow from mesenteric veins mix incompletely in the PV resulting in a disproportionate lobar distribution within the liver due to superior mesenteric venous drainage preferentially directed towards the right liver.[10]

On the other hand, it has already been shown that right portal vein (RPV) diameter is larger than left portal vein (LPV) diameter (principally related to the higher right liver volume)[11,12] and that PV flow volume tends to change in proportion to changes in PV cross-sectional area[13], thus creating disproportionate flow volume and metastatic potential between the two hemi-livers. Finally, little is known on the influence that PV variations, found in up to 20–35% of individuals, might have in flow volume changes and CRLM distribution.[14,15] The development of CRLM is a multifactorial process and knowledge of potential PV anatomy influence on the CRLM distribution could enable to anticipate and tailor patient management and surveillance. Indeed, a high metastatic burden of the right or left liver related with PV variations could influence the choice of an anatomical liver resection (due to the higher risk of missing lesions) or parenchyma-sparing liver surgery in case of multiple CRLM. Since no study has assessed the influence of PV diameter and consequently flow volume on CRLM intrahepatic distribution so far, the aim of the present study was to evaluate the influence of PV parameters and anatomical variations on intrahepatic distribution of CRLM.

Patients and methods

Study population

Between January 2018 and December 2022, data of all consecutive patients undergoing curative liver resection for CRLMs were retrieved from a prospectively collected database at two tertiary hepatobiliary centres. Histologic confirmation of CRLM was obtained by examination of resected specimens. Patients with previous hepatectomy and those for whom computed tomography (CT) and magnetic resonance imaging (MRI) were not available or uninterpretable were excluded. Previous primary CRC resection was not an exclusion criterion. Patients with histologically proven cirrhosis and those presenting with severe liver dysmorphy or segmental/lobar atrophy were also excluded.[16] This study was approved by the institutional review board (number: AAA-2023-09046).

Patient and tumour characteristics

The collected data included baseline patients' demographic data, primary tumour location, synchronous or metachronous diagnosis of CRLM, resected primary CRC, tumour node metastasis (TNM) classification tumour stage and RAS, BRAF tumour mutational status as well as microsatellite instability (MSI) or stability (MSS) status. Patients with primary CRC located between the cecum and transverse colon were included in the right-sided colon group while patients with CRC located between the splenic flexure and the recto-sigmoid junction were included in the left-sided colon group. Rectal cancer was divided into high rectum group and a low and medium rectum group, related to different venous drainage axes.[17]

Computed tomography imaging and analyses

For this retrospective study, each set of CT and MRI images of individual patients of the two centres were reviewed, in a random manner, following anonymization using a picture archiving and communication system workstation (DirectView, v. 11.3, Carestream Health, Rochester, NY) by two radiologists (with 12 and 10 years of experience in abdominal imaging, respectively).

All abdominal CT and MRI examinations were performed before induction of chemotherapy to decrease missing-metastasis biases using a multidetector CT (64-detector) scanners from different manufacturers. CT acquisitions covered the en-

TABLE 1. Bilateral, right and left unilateral distribution of colorectal liver metastases and vascular anatomy

Characteristics	Overall, N = 200[a]	Bilateral N =110 (55%)[a]	Right unilateral N = 66 (33%)[a]	Left unilateral N = 24 (12%)[a]	P-value[b]
Patient					
Age (years)	64 (57–71)	63 (53–70)	65 (58–74)	67 (63–71)	**0.02**
Gender: female	81 (41)	47 (43)	29 (44)	5 (21)	0.11
BMI (kg/m2)	24 (21.0–27.0)	24 (21.0–27.0)	24 (22.0–26.0)	24 (23.0–27.3)	0.70
Primitive tumor location					0.60
Right colon	34 (17)	16 (15)	12 (18)	6 (25)	
Left colon	112 (57)	60 (56)	38 (58)	14 (58)	
Rectum	52 (26)	32 (30)	16 (24)	4 (17)	
T stage					0.60
0–2	31 (18)	15 (17)	10 (17)	6 (26)	
3–4	139 (82)	74 (83)	48 (83)	17 (74)	
N stage					0.80
0	66 (40)	33 (38)	23 (43)	10 (43)	
1–2	98 (60)	55 (63)	30 (57)	13 (57)	
KRAS mutation	60 (30)	33 (30)	20 (30)	7 (29)	> 0.90
BRAF mutation	6 (3)	4 (3.6)	2 (3)	0 (0)	> 0.90
MSI	4 (2)	2 (1.8)	1 (1.5)	1 (4.2)	0.60
Number of CRLM	3 (1–7)	6 (4–11)	1 (1–3)	1 (1–1)	**< 0.01**
Synchronous CRLM	140 (70)	87 (79)	38 (58)	15 (63)	**0.01**
Vascular					
PV variations					0.13
Type 1	156 (78)	88 (80)	51 (77)	17 (71)	
Type 2	19 (9,5)	13 (12)	3 (4.5)	3 (13)	
Type 3	25 (13)	9 (8.2)	12 (18)	4 (17)	
PV diameter					
Main trunk	13.5 (12.4–15)	13.3 (12.4–15)	13.7 (12.50–15)	13.8 (12.15–14.20	> 0.90
RPV	11.3 (10.0–12.9)	11.4 (10.0–13.0)	11.3 (10.0–12.6)	11.3 (10.3–12.1)	0.90
LPV	10.7 (9.6–12.0)	10.7 (9.6–12.0)	10.5 (9.0–11.9)	10.9 (10.1–12.0)	0.50
Ratio diameter RPV/LPV	1.1 (0.9–1.2)	1.1 (0.9–1.2)	1.1 (1.0–1.3)	1.1 (0.9–1.2)	0.40
PV branches angulation					
RPV	153 (142–163)	151 (140–162)	155 (145–168)	158 (147–164)	0.20
LPV	97 (80–115)	98 (77–113)	97 (81–118)	98 (84–116)	0.80
Predominant PV branch[c]					0.50
RPV	123 (67)	67 (67)	43(70)	13 (57)	
LPV	61 (33)	33 (33)	18(30)	10 (43)	
Arterial variations					
Right hepatic artery	22 (11)	13 (12)	8 (12)	1 (4.2)	0.70
Left hepatic artery	24 (12)	12 (11)	8 (12)	4 (17)	0.70

[a] = n (%), median (interquartile range, IQR); [b] = Fisher's exact test, Kruskal-Wallis; [c] = primitive branch of the portal vein presenting the largest cross-sectional area

BMI = body mass index; CRLM = indicates colorectal cancer liver metastasis; LPV = left portal vein; MSI = microsatellite instability; PV = portal vein; RPV = right portal vein

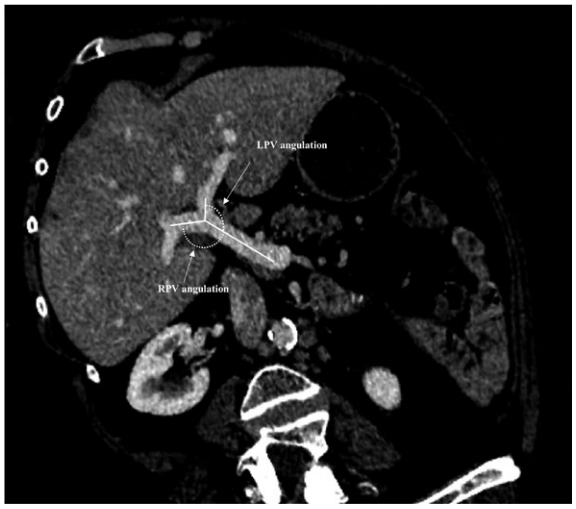

FIGURE 1. Measurements of right portal vein and left portal vein angulation.

RPV = right portal vein, LPV = left portal vein

tire abdomen and pelvis. To examine the anatomy of the PV, all examinations included at least an acquisition during the portal-venous phase performed after a delay of 70 to 80 s after intravenous administration of iodinated contrast material. Portal-venous phase was defined when all portal branches and hepatic veins were fully enhanced. The number of CRLM was assessed using MRI examinations including T2-weighted sequences, diffusion weighted sequences, T1 DIXON weighted sequences and T1 with fat saturation with and without gadolinium-chelate enhanced images. MR images were acquired on a 1.5T Siemens Avanto (centre 1 and 2) and a 3T Siemens Skyra (centre 1) scanner. CT exams were acquired using three dimensional acquisitions, thickness of 0.6mm, automatic z-axis-modulation and optimized noise. Characteristics of the different MRI protocols in the two centres are summarized in Supplementary Table 1.

Portal vein anatomy and CRLM intrahepatic distribution

Common anatomic variations of the PV were identified and recorded as previously described.[5,18] Normal PV anatomy included division of the PV into right and left branches immediately before reaching the liver, with further division of the right portal branch into anterior and posterior sectorial branches (Type 1). Type 2 PV variation included PV trifurcation with left portal branch and both right sectorial portal branches sharing the same origin. Type 3 variation included right anterior sectorial branch arising from the left PV. The following imaging PV parameters were finally recorded: (1) The primitive branch of the PV presenting the largest cross-sectional area was also recorded and defined as the predominant PV branch (right or left). (2) PV diameter of the main PV, the primitive RPV and LPV measured just before and after main PV bifurcation using previously published methods.[19] (3) RPV and LPV angulations were measured as follows: after three-dimensional-reconstruction in the plane of the PV, the angle between the last segment of the PV and the initial segment of RPV and LPV lumens were calculated using previously published methods (Figure 1).[20] For type 2 portal anatomy variations, the diameter of the right and left anterior sectorial branches were summed up and angulations averaged for the right liver. For patients with a type 3 PV variation CRLM localized in the anterior sector (segments 5 and 8) were attributed to the left liver, given the fact that right anterior segmental branch originated from the LPV.

Intrahepatic distribution of CRLM was recorded as follows: the number of CRLM as well as their segmental location were recorded according to the Couinaud segment classification.[21] The left liver was composed of segments 2, 3, 4 while the right liver included segments 5, 6, 7 and 8. Lesions located in segment 1 were considered independently given the specificity of portal vein vascularization.[22]

Statistical analysis

The distribution of quantitative variables was assessed using the Shapiro-Wilk test. Quantitative variables were reported as means ± standard deviations (SD) or medians with 25–75 interquartile range (IQR) depending on their distribution[23] and were compared using the Mann-Whitney, Kruskal-Wallis or Student t-test as appropriate. Categorical variables were expressed as raw numbers, proportions and percentages and were compared using Pearson's Chi-square or Fisher's exact test as appropriate. Intra-class correlation coefficient (ICC) based on a two-way random effects model was used to determine the reliability of the measurements between the two radiologists.[24] ICC between 0.00 and 0.20; 0.21 and 0.40; 0.41 and 0.60; 0.61 and 0.80; and 0.81 and 1.00, indicated slight, fair, moderate, substantial, and almost perfect agreement. Correlations between portal vein diameter, angulation and number of CRLM in the relevant liver

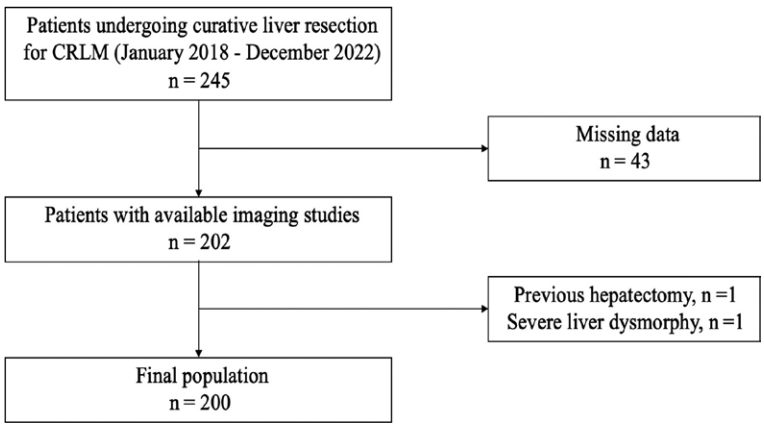

FIGURE 2. Patient flowchart.

CRLM = colorectal liver metastasis

segment were evaluated using Spearman correlation tests. Sensitivity analysis involved subgroup comparison of patients presenting only unilateral (right and left) CRLM and patients presenting a single CRLM to account for early stage of disease. All statistical tests were two-tailed, with $P < 0.05$ considered to indicate statistically significant differences. All analyses were performed using RStudio statistical software (Version 1.4.1103 © 2009-2021 RStudio, Inc).

Results

Study population and baseline characteristics

During the study period, 245 patients were diagnosed with CRLM. Among these patients, 45 (18%) patients were excluded due to missing data (n = 43), previous hepatectomy (n = 1) and presence of liver dysmorphia related to cirrhosis (n = 1). The final population included 200 patients (Figure 2). Median age was 64 years (Q1, Q3: 57, 71) and 41% were females. CRLM were predominant in the right liver with 807 (65%) lesions compared to 436 (35%) lesions in the left liver ($P < 0.01$). The majority of patients (70%) presented with synchronous CRLM and were more often bilateral than unilateral (55% vs. 45%; $P = 0.01$). Among patients with unilateral lesions 24 (12%) were localized only in the left liver and 66 (33%) only in the right liver. Primary tumour location was left-sided in 112 (57%) patients, right-sided in 34 (17%) patients and rectal in 52 (26%) patients. The majority of patients (82%) presented a T3–T4 primary tumour stage. Patient characteristics were similar between unilateral right, left and bilateral CRLM and are detailed in Table 1.

Type 1 portal vein anatomy was most frequently observed with 156 (78%) patients while 19 (9.5%) patients had a type 2 and 25 (12%) patients a type 3 variation. Arterial variations consisted in the presence of an accessory left hepatic artery in 24 (12%) patients and an accessory right hepatic artery in 22 (11%) patients. The median diameter of the main PV was 13.5 mm (Q1, Q3: 12.4, 15), and RPV 11.3 mm (Q1, Q3: 10, 12.9) was significantly larger than the LPV 10.7 mm (Q1, Q3: 9.6, 12) ($P = 0.002$). Overall, 123 (61.5%) patients presented a predominant (branch with the largest cross-sectional area) RPV and 61 patients (30.5%) a predominant LPV, while 16 (8%) patients presented an identical diameter. The median angulation of the RPV and LPV was 153° (Q1, Q3: 142, 163°) and 97° (Q1, Q3: 80, 115°), respectively ($P < 0.001$). Liver vascular anatomy is detailed in Table 1.

Portal vein anatomy and intrahepatic distribution of colorectal cancer liver metastases

ICC between radiologists was excellent in the evaluation of the number and intrahepatic distribution of CRLM (0.99; 95% CI: 0.99–1.00; $P < 0.001$) and PV angulation measurements (0.97; 95% CI: 0.93–0.99; $P < 0.001$) and was very good for PV diameter and variations measurements (0.86; 95% CI: 0.73–0.99; $P < 0.001$).

The median diameter of the main PV in bilateral, unilateral right and left liver CRLM was 13.3 mm (Q1, Q3: 12.4, 15), 13.7 mm (Q1, Q3: 12.5, 15) and 13.8 mm (Q1, Q3: 12.1, 14.2), respectively and no significant differences were found ($P > 0.90$). Accordingly, the median RPV diameter was 11.4 mm (Q1, Q3: 10, 13), 11.3 mm (Q1, Q3: 10, 12.6) and 11.3 mm (Q1, Q3: 10.3, 12.1) ($P = 0.90$) and median LPV diameter was 10.7 mm (Q1, Q3: 9.6, 12), 10.5 mm (9, 11.9) and 10.9 mm (Q1, Q3: 10.1, 12) ($P = 0.50$). Concerning PV branch angulations, the median angulation of the RPV was 151° (Q1, Q3: 140, 162) for the bilateral distribution of CRLM, 155° (Q1, Q3: 145 – 168) for the right unilateral, 158° (Q1, Q3: 147, 164) for the left unilateral ($P = 0.20$) and the median angle of the LPV was 98° (Q1, Q3: 77, 113) for the bilateral distribution of CRLM, 97° (Q1, Q3: 81, 118) for right unilateral and 98° (Q1, Q3: 84, 116) for left unilateral ($P = 0.80$). Finally, unilateral - bilateral CRLM intrahepatic distribution was also independent of PV variations. Type 1 anatomy of the

PV was present in 88 patients (80%) for bilateral, in 51 patients (77%) for unilateral right and in 17 patients (71%) for unilateral left distribution (P = 0.13). Characteristics of the PV anatomy according to bilateral, unilateral right and left CRLM intrahepatic distribution are detailed in Table 1.

In subgroup analysis, considering only patients with unilateral CRLM or patients with a predominant RPV or LPV no significant associations between the intrahepatic distribution of CRLM and PV anatomy were found. Subgroup left unilateral versus right unilateral analysis and RPV versus LPV predominance are detailed in Table 2 and 3, respectively.

Finally, among 56 patients with a single CRLM, 37 patients (66%) presented a single metastasis in the right liver, and 19 patients (34%) presented a single metastasis in the left liver. Right and left intrahepatic distribution was independent of the diameter of the PV (P > 0.90), the RPV (P = 0.60) and LPV (P = 0.50), as well as the RPV (P = 0.50) and LPV (P = 0.50) angulation and PV anatomy variations (P = 0.80).

TABLE 2. Unilateral right and left distribution of colorectal liver metastases and portal anatomy

Characteristics,	Right unilateral, N = 66 (73%)[a]	Left unilateral, N = 24 (27%)[a]	p-value[b]
Number of CRLM	1 (1–3)	1 (1–1)	**0.03**
PV variations			0.50
Type 1	51 (77)	17 (71)	
Type 2	3 (4.5)	3 (13)	
Type 3	12 (18)	4 (17)	
PV diameter			
Main trunk	13.7 (12.5–15.0)	13.8 (12.2–14.2)	0.70
RPV	11.3 (10.0–12.6)	11.3 (10.3–12.1)	0.60
LPV	10.5 (9.0–11.9)	10.9 (10.1–12)	0.20
Ratio diameter RPV/LPV	1.1 (1.0–1.3)	1.1 (0.9–1.2)	0.20
PV branches angulation			
RPV	155 (145–168)	158 (147–164)	> 0.90
LPV	97 (81–118)	98 (84–116)	0.90
Predominant PV[c]			0.30
RPV	43 (70)	13 (57)	
LPV	18 (30)	10 (43)	

[a] = n (%), median (interquartile range, IQR); [b] = Fisher's exact test, Kruskal-Wallis; [c] = primitive branch of the portal vein presenting the largest cross-sectional area

CRLM = colorectal liver metastasis; LPV = left portal vein; PV = portal vein; RPV = right portal vein

Portal vein anatomy variations and number of CRLM

Overall, the median number of CRLM was 3 (Q1, Q3: 1, 7). The median number of CRLM was significantly greater both in the bilateral CRLM group (6; Q1, Q3: 4, 11) by comparison with those in the unilateral group (1; Q1, Q3: 1, 2) (P < 0.01) and the right unilateral group (1; Q1, Q3: 1, 3) when compared to the left unilateral (1; IQR: 1, 1) (P = 0.03). There was no significant correlation between the number of CRLM in the corresponding hemi-liver and the diameter (R: 0.093; 95% CI: 0.08–0.12; P = 0.10) or the angulation of the PV branches (R: 0.012; 95% CI: 0.009–0.02; P = 0.83). Relation between diameter and PV branches angulation and number of CRLM are presented in Figure 3A and 3B, respectively.

The number of CRLM in the right liver (P = 0.40), in the left liver (P = 0.60) and the number of affected segments in the right (P = 0.60) and in the left liver (P = 0.70) did not significantly differ according to the side of the predominant portal branch.

Primitive CRC and CRLM intrahepatic distribution

The intrahepatic distribution of CRLM in right-sided CRC was bilateral in 16 (49%) patients, left unilateral for 6 (18%) patients, right unilateral in 11 (33%) patients, whereas for left-sided CRC, CRLM were bilateral in 79 (56%) patients, right unilateral in 47 (33%) patients, left unilateral in 16 (11%) patients (P = 0.60). No differences in median number of total CRLM were found between right-sided (2; Q1, Q3: 1, 6) and left-sided (3; Q1, Q3: 1, 8) CRC was (P = 0.20). Finally, the ratio of right to left liver CRLM was 1 (Q1, Q3: 1.0, 1.3) for right-sided and 1.1 (Q1, Q3: 1.0, 3.0) for left-sided CRC (P = 0.20) (Table 4).

Discussion

Few factors are known to influence the intrahepatic distribution of CRLM. Primary CRC localization has already been described as a factor determining intrahepatic CRLM distribution, although evidence is conflicting.[8,10,25–27] The aim of this study was to assess whether the anatomy of the portal vein (PV), through variations in blood flow, as well as its anatomical variations could have an influence on the topography of CRLM. No significant difference in the distribution of CRLM in relation

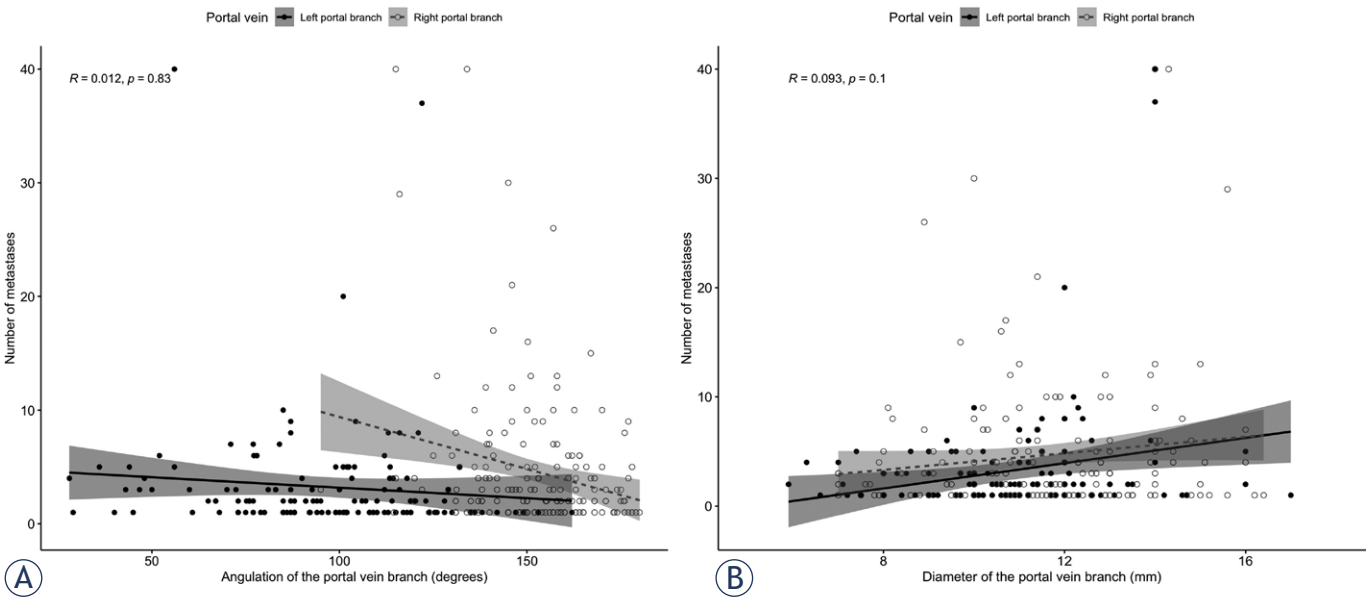

FIGURE 3. Graphs show correlation between portal vein branches' diameter **(A)**, angulation **(B)** and the number of colorectal liver metastases (CRLM).

R = Spearman's correlation coefficient

TABLE 3. Predominance of right portal vein (RPV) or left portal vein (LPV) and intrahepatic distribution of colorectal liver metastasis (CRLM)

Characteristics	Predominant RPV N = 123 (67%)[a,b,c]	Predominant LPV N = 61 (33%)[a,b,c]	p-value[d]
Distribution of CRLM			0.50
Bilateral	67 (54)	33 (54)	
Right unilateral	43 (35)	18 (30)	
Left unilateral	13 (11)	10 (16)	
Number of segments involved (right liver)	2 (1–3)	2 (1–3)	0.60
Number of segments involved (left liver)	1 (0–2)	1 (0–2)	0.70
Total number of CRLM	3 (1–8)	4 (1–5)	0.70
Number of CRLM in the right liver	2 (1–5)	2 (1–4)	0.40
Number of CRLM in the left liver	1 (0–3)	1 (0–2)	0.60
Ratio number of CRLM right/left liver	1 (1.0–3.0)	1 (1.0–2.0)	0.70
Ratio number of CRLM per segment (right liver)	1 (1.0–2.0)	1 (1.0–2.0)	0.60
Ratio number of CRLM per segment (left liver)	1 (1.0–1.8)	1 (1.0–2.0)	> 0.90

[a] = n (%), median (interquartile range, IQR); [b] = primitive branch of the portal vein presenting the largest cross-sectional area; [c] = Sixteen patients presented an identical RPV and LPV diameter and were excluded; [d] = Fisher's exact test, Wilcoxon rank sum test

with the PV anatomy were identified. Indeed, neither the presence of an anatomical variation of the PV, nor a variation in diameter or angulation of the PV and its branches appeared to have any impact on the unilateral – bilateral distribution or in the number of CRLM. Additionally, in this study we did not find any correlation between the primary tumour location and the intrahepatic distribution of CRLM.

Spread of CRC to the liver is mainly hematogenous through the portal circulation.[28] The PV is formed by the confluence of the superior mesenteric and splenic vein and its flow volume tends to change in proportion to changes in PV cross-sectional area thus creating disproportionate flow volume and metastatic potential between the two hemi-livers.[13] Indeed, flow velocity depends on pressure and flow resistance and according to Poiseuille's law, flow resistance depends on the geometry of the tube with the length and radius of the tube. The diameter of the vessel is therefore an important factor, among other parameters, modifying blood flow.[29] It is known that the diameter of the RPV is larger and the angle more open than the diameter and angle of the LPV.[12] Diameter has

been hypothesized to be linked to a higher blood flow and hemi-liver volume.[12] Consequently, we hypothesized that since a larger diameter or a more open angle of a portal branch, could lead to an increase in blood flow, it could potentially increase the metastatic potential in the segments vascularized by these branches. Indeed, in our study, patients' weight, height and gender, known parameters influencing the diameter of PV and its branches[19] were not different and although the total number of CRLM was greater in the right than in the left liver, individual diameter and angulation variations of the PV branches were very small and no direct relation with the number and intrahepatic distribution of CRLM was found. Moreover, anatomical variations of the PV in our population were similar to current literature reports1[4,15] and were also independent of the CRLM intrahepatic distribution.

The results of our study are in line with other studies showing no influence of the primary CRC location on the distribution of CRLM. Several studies have shown an unequal intrahepatic distribution of CRLM depending on the location of the primary CRC and in based on the hypothesis was that CRLM would be distributed differently in the liver due to 'streamline flow' in the PV, linked to the different venous drainage of the right and left colon.[7] Results are not however unequivocal, with some studies reporting an equivalent distribution between right and left liver depending on the location of the primary site[26,27] and others reporting a preferential distribution of right-sided CRC metastases in the right liver.[8,10,25] Other intrinsic tumour characteristics have also been described as potential factors influencing CRLM anatomical distribution. A recent study showed that CRLM distribution may differ between different primary tumours as is the case of breast cancer.[30] In their study, the authors showed that breast cancer most commonly affects the left liver lobe when compared with CRLM and part of the reason seems to be related to its diverse growth cell rate and metastatic potential, tumour size, and histological grade, the knowledge of which can have significant therapeutic implications. Concerning CRLM, although no intrinsic biologic tumour characteristic responsible for the difference in liver metastasis distribution has been clearly identified, gene mutations are known as both prognostic factors for survival and segmental location of the primary CRC[6] and further studies are needed to extrapolate the role of molecular patterns in CRLM anatomical distribution.

TABLE 4. Location of primary colorectal cancer and intrahepatic distribution of colorectal cancer liver metastases

–	Right colon N = 33 (19%)[a]	Left colon N = 142 (81%)[a]	p-value[b]
Distribution of CRLM			0.60
Bilateral	16 (49)	79 (56)	
Right unilateral	11 (33)	47 (33)	
Left unilateral	6 (18)	16 (11)	
Number of CRLM	2 (1–6)	3 (1–8)	0.20
Number of CRLM in the right liver	1 (1–3)	2 (1–5)	0.12
Number of CRLM in the left liver	1 (0–2)	1 (0–3)	0.70
Ratio number of CRLM right/ left liver	1 (1–1)	1 (1–3)	0.20

[a] = n (%), median (interquartile range, IQR); [b] = Fisher's exact test, Wilcoxon rank sum test

CRC = colorectal cancer; CRLM = indicates colorectal liver metastasis

To our knowledge, this is the first study to investigate the effect of different parameters of the portal anatomy over the topography of CRLM. Robustness of our results are supported by independent image analysis by two radiologists with almost perfect inter-operator concordance. Moreover, our sensitivity analyses performed in the subgroup of patients presenting only unilateral and only single CRLM (to compare patients with similar metastatic liver tumour burden) further strengthen our findings.[5] Nevertheless, this study presents some limitations. Patients are not diagnosed at the same time in the course of their disease, and therefore it is unknown if portal blood flow could be related with the intrahepatic distribution of CRLM at different timepoints of disease. Moreover, patients with synchronous and metachronous liver CRLM were included and already known differences in the oncologic behaviour of synchronous CRLM may have influenced our results. Indeed, patients with synchronous CRLM are known to have a higher number of lesions, a billboard distribution at diagnosis and a worse prognosis.[31] Furthermore, the underlying liver parenchyma characteristics (cirrhosis, nodular regenerative hyperplasia and ultimately chemotherapy-induced sinusoidal obstruction syndrome) non-available in this study may have further influenced liver venous flow (notably portal vein diameter and portal venous flow increase as already described[32,33]) and thus CRLM distribution regardless of the PV anatomy, however, this

bias is likely to be limited due to exclusion of all patients with histologically proven liver cirrhosis.

Although negative, this study could have had an impact in tailoring CRLM surgical management if a potential influence of PV anatomy on CRLM intrahepatic distribution had been confirmed. For example, a hypothetical correlation of right-sided CRLM liver distribution and predominant RPV or type 3 PV anatomy in patients with multiple lesions could have influenced the surgeon's choice to perform an anatomical liver resection (i.e. right-hepatectomy) rather than a parenchyma-sparing liver surgery (if lesions were accessible to both treatments) to lower the high risk of missing lesions in the remaining right liver. Nevertheless, since no significant relationship has been demonstrated, parenchymal sparing liver strategies should remain the first objective whenever possible[34] enabling repeated liver resections, when necessary, since surgery remains the best curative treatment in CRLM.

In conclusion, the present study did not find any significant impact of the PV anatomy, nor primary CRC tumour location, on the distribution and number of CRLM. Future studies could focus on liver parenchymal and Doppler PV flow characteristics, not studied here, to further investigate potential predictive factors.

References

1. World Health Organization. Colorectal cancer. [internet]. [cited 2023 Aug 17]. Accessible at: https://Www.Who.Int/News-Room/Fact-Sheets/Detail/Colorectal-Cancer
2. Engstrand J, Nilsson H, Strömberg C, Jonas E, Freedman J. Colorectal cancer liver metastases - a population-based study on incidence, management and survival. *BMC Cancer* 2018; **18:** 78. doi: 10.1186/s12885-017-3925-x
3. Manfredi S, Lepage C, Hatem C, Coatmeur O, Faivre J, Bouvier AM. Epidemiology and management of liver metastases from colorectal cancer. *Ann Surg* 2006; **244:** 254-9. doi: 10.1097/01.sla.0000217629.94941.cf
4. Phelip JM, Tougeron D, Léonard D, Desolneux G, Dupré A, Michel P, et al. Metastatic colorectal cancer (mCRC): French intergroup clinical practice guidelines for diagnosis, treatments and follow-up (SNFGE, FFCD, GERCOR, UNICANCER, SFCD, SFED, SFRO, SFR). *Dig Liver Dis* 2019; **51:** 1357-63. doi: 10.1016/j.dld.2019.05.035
5. Sasaki K, Morioka D, Conci S, Margonis GA, Sawada Y, Ruzzenente A, et al. The tumor burden score: a new "metro-ticket" prognostic tool for colorectal liver metastases based on tumor size and number of tumors. *Ann Surg* 2018; **267:** 132-41. doi: 10.1097/SLA.0000000000002064
6. Gagnière J, Dupré A, Gholami SS, Pezet D, Boerner T, Gönen M, et al. Is hepatectomy justified for braf mutant colorectal liver metastases? A multi-institutional analysis of 1497 patients. *Ann Surg* 2020, **271:** 147-54. doi: 10.1097/SLA.0000000000002968
7. Copher GH, Dick BM. "Stream line" phenomena in the portal vein and the selective distribution of portal blood in the liver. *Arch Surg* 1928; **17:** 408-19.
8. Konopke R, Distler M, Ludwig S, Kersting S. Location of liver metastases reflects the site of the primary colorectal carcinoma. *Scand J Gastroenterol* 2008; **43:** 192-5. doi: 10.1080/00365520701677755
9. Desai AG, Park CH, Schilling JF. "Streaming" in portal vein. its effect on the spread of metastases to the liver. *Clin Nucl Med* 1985; **10:** 556-9.
10. Rhu J, Heo JS, Choi SH, Choi DW, Kim JM, Joh JW, et al. Streamline flow of the portal vein affects the lobar distribution of colorectal liver metastases and has a clinical impact on survival. *Ann Surg Treat Res* 2017; **92:** 348. doi: 10.4174/astr.2017.92.5.348
11. Paturet G. *Traité on human anatomy*, Volume III. [French]. Paris: Masson & C; 1958. p. 856-9.
12. Trigaux JP, Beers B, Melange M, Buysschaert M. Alcoholic liver disease: value of the left-to-right portal vein ratio in its sonographic diagnosis. *Gastrointest Radiol* 1991; **16:** 215-20. doi: 10.1007/BF01887349
13. Arbeille PP, Besnard SS, Kerbeci PP, Mohty DM. Portal vein cross-sectional area and flow and orthostatic tolerance: A 90-day bed rest study. *J Appl Physiol* 2005; **99:** 1853-7. doi: 10.1152/japplphysiol.00331.2005
14. Lee WK, Chang SD, Duddalwar VA, Comin JM, Perera W, Lau WF, et al. Imaging assessment of congenital and acquired abnormalities of the portal venous system. *Radiographics* 2011; **31:** 905-26. doi: 10.1148/rg.314105104
15. Covey AM, Brody LA, Getrajdman GI, Sofocleous CT, Brown KT. Incidence, patterns, and clinical relevance of variant portal vein anatomy. *AJR Am J Roentgenol* 2004; **183:** 1055-64. doi: 10.2214/ajr.183.4.1831055
16. Hadjis NS, Hemingway A, Carr D, Blumgart LH. Liver lobe disparity consequent upon atrophy. *J Hepatol* 1986; **3:** 285-93. doi: 10.1016/s0168-8278(86)80480-9
17. Godlewski G, Prudhomme M. Embryology and anatomy of the anorectum. Basis of surgery. *Surg Clin North Am* 2000; **80:** 319-43. doi: 10.1016/s0039-6109(05)70408-4
18. Carneiro C, Brito J, Bilreiro C, Barros M, Bahia C, Santiago I, et al. All about portal vein: A pictorial display to anatomy, variants and physiopathology. *Insights Imaging* 2019; **10:** 38. doi: 10.1186/s13244-019-0716-8
19. Stamm ER, Meier JM, Pokharel SS, Clark T, Glueck DH, Lind KE, et al. Normal main portal vein diameter measured on CT is larger than the widely referenced upper limit of 13 mm. *Abdom Radiol* 2016; **41:** 1931-6. doi: 10.1007/s00261-016-0785-9
20. Givehchi S, Safari MJ, Tan SK, Shah MNB, Sani FBM, Azman RR, et al. Measurement of coronary bifurcation angle with coronary CT angiography: a phantom study. *Phys Med* 2018; **45:** 198-204. doi: 10.1016/j.ejmp.2017.09.137
21. Soyer P. Segmental anatomy of the liver: utility of a nomenclature accepted worldwide. *AJR Am J Roentgenol* 1993; **161:** 572-3. doi: 10.2214/ajr.161.3.8352107
22. Couinaud, C. Dorsal sector of the liver. *Chirurgie* 1998; **123:** 8-15. doi: 10.1016/s0001-4001(98)80033-0
23. Barat M, Jannot AS, Dohan A, Soyer P. How to report and compare quantitative variables in a radiology article. *Diagn Interv Imaging* 2022; **103:** 571-3. doi: 10.1016/j.diii.2022.09.007
24. Benchoufi M, Matzner-Lober E, Molinari N, Jannot AS, Soyer P. Interobserver agreement issues in radiology. *Diagn Interv Imaging* 2020; **101:** 639-41. doi: 10.1016/j.diii.2020.09.001
25. Shirai Y, Wakai T, Ohtani T, Sakai Y, Tsukada K, Hatakeyama K. Colorectal carcinoma metastases to the liver. does primary tumor location affect its lobar distribution? *Cancer* 1996; **77:** 2213-6. doi: 10.1002/(SICI)1097-0142(19960601)77:11<2213: AID-CNCR5>3.0.CO;2-Q
26. Wigmore SJ, Madhavan K, Redhead DN, Currie EJ, Garden OJ. Distribution of colorectal liver metastases in patients referred for hepatic resection. *Cancer* 2000; **89:** 285-7. doi: 10.1002/1097-0142(20000715)89:2<285::aid-cncr12>3.0.co;2-#
27. Çoruh AG, Uzun Ç, Bozca E, Bozca B, Demir IB, Atasever HG, et al. Is it possible to predict the side of hepatic metastases according to the primary location of colorectal cancer? *Pol J Radiol* 2020; **85:** e595-e9. doi: 10.5114/pjr.2020.99848
28. Shin AE, Giancotti FG, Rustgi AK. Metastatic colorectal cancer: mechanisms and emerging therapeutics. *Trends Pharmacol Sci* 2023; **44:** 222-36. doi: 10.1016/j.tips.2023.01.003

29. Nader E, Skinner S, Romana M, Fort R, Lemonne N, Guillot N, et al. Blood rheology: key parameters, impact on blood flow, role in sickle cell disease and effects of exercise. *Front Physiol* 2019; **10:** 1329. doi: 10.3389/fphys.2019.01329

30. Khan D, Khan AK, Khan SD, Aman M, Amin A, Wassem M, et al. The tendency of segmental distribution of hepatic metastasis according to couinaud classification: a comparison of portal versus systemic route of metastasis due to primary colorectal and breast tumors. *Ann Med Surg* 2023; **85:** 4806-10. doi: 10.1097/MS9.0000000000001241

31. Tsai MS, Su YH, Ho MC, Liang JT, Chen TP, Lai HS, et al. Clinicopathological features and prognosis in resectable synchronous and metachronous colorectal liver metastasis. *Ann Surg Oncol* 2007; **14:** 786-94. doi: 10.1245/s10434-006-9215-5

32. Yao H, Wang Y. Relationship between hemodynamic parameters and portal venous pressure in cirrhosis patients with portal hypertension. *Open Life Sci* 2020; **15**: 981-7. doi: 10.1515/biol-2020-0101.

33. Bissonnette J, Généreux A, Côté J, Nguyen B, Perreault P, Bouchard L, et al. Hepatic hemodynamics in 24 patients with nodular regenerative hyperplasia and symptomatic portal hypertension. *J Gastroenterol Hepatol* 2012; **27**: 1336-40. doi: 10.1111/j.1440-1746.2012.07168.x.

34. Memeo R, de Blasi V, Adam R, Goéré D, Azoulay D, Ayav A, et al. Parenchymal-sparing hepatectomies (PSH) for bilobar colorectal liver metastases are associated with a lower morbidity and similar oncological results: a propensity score matching analysis. *HPB* 2016; **18:** 781-90. doi: 10.1016/j.hpb.2016.06.004

research article

The superior value of radiomics to sonographic assessment for ultrasound-based evaluation of extrathyroidal extension in papillary thyroid carcinoma: a retrospective study

Hui Zhu[1], Hongxia Luo[1], Yanyan Li[1], Yuhua Zhang[1], Zhijing Wu[2], Yan Yang[1]

[1] Department of Ultrasound, the Second Affiliated Hospital of Wenzhou Medical University, Wenzhou, China
[2] Department of Statistical Science, University College London, London, United Kingdom

Radiol Oncol 2024; 58(3): 386-396.

Received 4 April 2024
Accepted 1 July 2024

Correspondence to: Yan Yang, M.D., Department of Ultrasound, the Second Affiliated Hospital of Wenzhou Medical University, China.
E-mail: Yangyan@wmu.edu.cn.

Disclosure: No potential conflicts of interest were disclosed.

Background. Extrathyroidal extension was related with worse survival for patients with papillary thyroid carcinoma. For its preoperative evaluation, we measured and compared the predicting value of sonographic method and ultrasonic radiomics method in nodules of papillary thyroid carcinoma.

Patients and methods. Data from 337 nodules were included and divided into training group and validation group. For ultrasonic radiomics method, a best model was constructed based on clinical characteristics and ultrasonic radiomic features. The predicting value was calculated then. For sonographic method, the results were calculated using all samples.

Results. For ultrasonic radiomics method, we constructed 9 models and selected the extreme gradient boosting model for its highest accuracy (0.77) and area under curve (0.813) in validation group. The accuracy and area under curve of sonographic method was 0.70 and 0.569. Meanwhile. We found that the top-6 important features of xgboost model included no clinical characteristics, all of whom were high-dimensional radiomic features.

Conclusions. The study showed the superior value of ultrasonic radiomics method to sonographic method for preoperative detection of extrathyroidal extension in papillary thyroid carcinoma. Furthermore, high-dimensional radiomic features were more important than clinical characteristics.

Key words: ultrasonic radiomics; extrathyroidal extension; sonography; papillary thyroid carcinoma

Introduction

Thyroid cancer was one of the most pervasive carcinomas in clinic worldwide. From 1990 to 2017, its incident cases and deaths increased by 169% and 87%, respectively. China ranked the top 3 incident cases and South Asia had the largest number of deaths around the world in 2017.[1] Papillary thyroid carcinoma (PTC) was the most common histological type of thyroid malignancy.[2] Although it presented with indolent behavior, some patients still suffered from high risk of recurrence or death.[3,4] Literatures showed that risk factors like male sex, older age, larger tumors size and extrathyroidal extension (ETE) could lead to more advanced disease.[4,5] Besides, patients with ETE were reported

to have worse survival and poorer prognoses than those without, no matter minimal ETE or gross ETE.[5,6] In clinical practice, total/subtotal thyroidectomy was suggested for patients with ETE while hemithyroidectomy was recommended for those without.[7] In order to avoid total/subtotal thyroidectomy in patients without ETE, a noninvasive way to preoperatively evaluate ETE was in urgent need.

ETE was defined as tumor extension of perithyroidal structures, which can be divided into minimal ETE (identified by histological examination) and gross ETE (identified by preoperative or intraoperative evidence) according to American Joint Committee on Cancer (AJCC) tumor-node-metastasis staging system.[8,9] Preoperative ultrasonic (US) examination was the first-line diagnostic tool in detecting PTC.[10] Several studies had revealed the predicting value of sonographic assessment for ETE. The reported sensitivity of sonographic assessment for ETE varied from 65.2% to 85.3%. And its specificity varied from 68.9% to 81.8%.[11-13] Meanwhile, gross ETE (78%, 99.7%) was proven to have higher sensitivity and specificity than minimal ETE (30%, 93%).[10] With such low diagnostic performance, more accurate method was in demand for ETE evaluation.

Radiomics analysis quantitatively extracted high-throughput features from medical images and converted them into mineable data to help diagnosing or predicting diseases in clinical practice.[14,15] It combined radiology and machine learning and had been widely used in diagnosing disease and prognosing outcome.[2,16,17] Recent studies had shown that radiomic features of magnetic resonance imaging (MRI), computer tomography (CT) and US images of PTC had potential predicting value in ETE with high area under the curve (AUC) of 0.812-0.906.[7,8,15,18] However, little was known about the superior predicting value of US radiomics method to sonographic method.

The purpose of this study was to compare the predicting value of sonographic method and radiomics method of ETE based on US radiomic features and clinical characteristics of PTC nodules.

Patients and methods

The study was conducted in accordance with the Declaration of Helsinki (as revised in 2013). The study was approved by institutional ethics board of the Second Affiliated Hospital of Wenzhou Medical University (NO.: 2021-K-20-01) and individual consent for this retrospective analysis was waived.

Patients and clinical characteristics

This study included 460 consecutive patients (575 nodules) who were diagnosed with PTC pathologically from January 2018 to September 2019 in our hospital. The inclusion criteria were as follows: 1) preoperative US examination within two weeks of surgery; 2) initial surgical resection (total thyroidectomy, near total thyroidectomy or hemithyroidectomy) with cervical dissection, and the ETE state was confirmed pathologically and/or by intraoperative evidence. The exclusion criteria were as follows: 1) incomplete clinical characteristics; 2) multifocal lesions in the same lobe of thyroid; 3) radiofrequency ablation before surgery. Finally, 310 patients (337 nodules) with mean age of 45.95 ± 11.69 years (from 12 to 77 years) and male-to-female ratio of 0.40 (89:221) were included in this study. Among them, 27 patients had one lesion on each lobe of the thyroid. According to previous study, minimal ETE was defined as an extension into the sternothyroid muscle or parathyroid soft tissues.[9] And it was confirmed pathologically in this study. Meanwhile, gross ETE was defined as cancer invasion into the subcutaneous soft tissue, trachea, larynx, esophagus or recurrent laryngeal nerve.[9] It was determined during surgery and further confirmed pathologically. Thus, nodules were divided into those with minimal ETE (n = 99), those with gross ETE (n = 4) and those without ETE (n = 234) (ETE negative group). Because of the very small sample of gross ETE, nodules with minimal ETE and gross ETE were categorized as ETE positive group.

Clinical characteristics comprised of age, sex, biochemical results and US findings. Standardized biochemical examination included those concerning preoperative assessment and those concerning thyroid function. Liver function analysis, renal function analysis, differential blood count and routine urianlysis were classified into former ones. Blood calcium ion, thyroid function analysis (free triiodothyronine 3 and 4, total triiodothyronine 3 and 4 and thyroid stimulating hormone) (FT3, FT4, TT3, TT4 and TSH), thyroglobulin (TG), antithyroglobulin antibodies (ANTITGAB) and antithyroid peroxidase antibody (ANTITPOAB) were classified into latter ones. The composition, echogenicity, shape, margin and echogenic foci consisted of the US findings of each nodule. They were measured, scored and classified according to the Thyroid Imaging Reporting and Data System (TI-RADS) criteria of American College of Radiology.[19] A total of 34 clinical characteristics were enrolled. The flowchart of this study was shown in Figure 1.

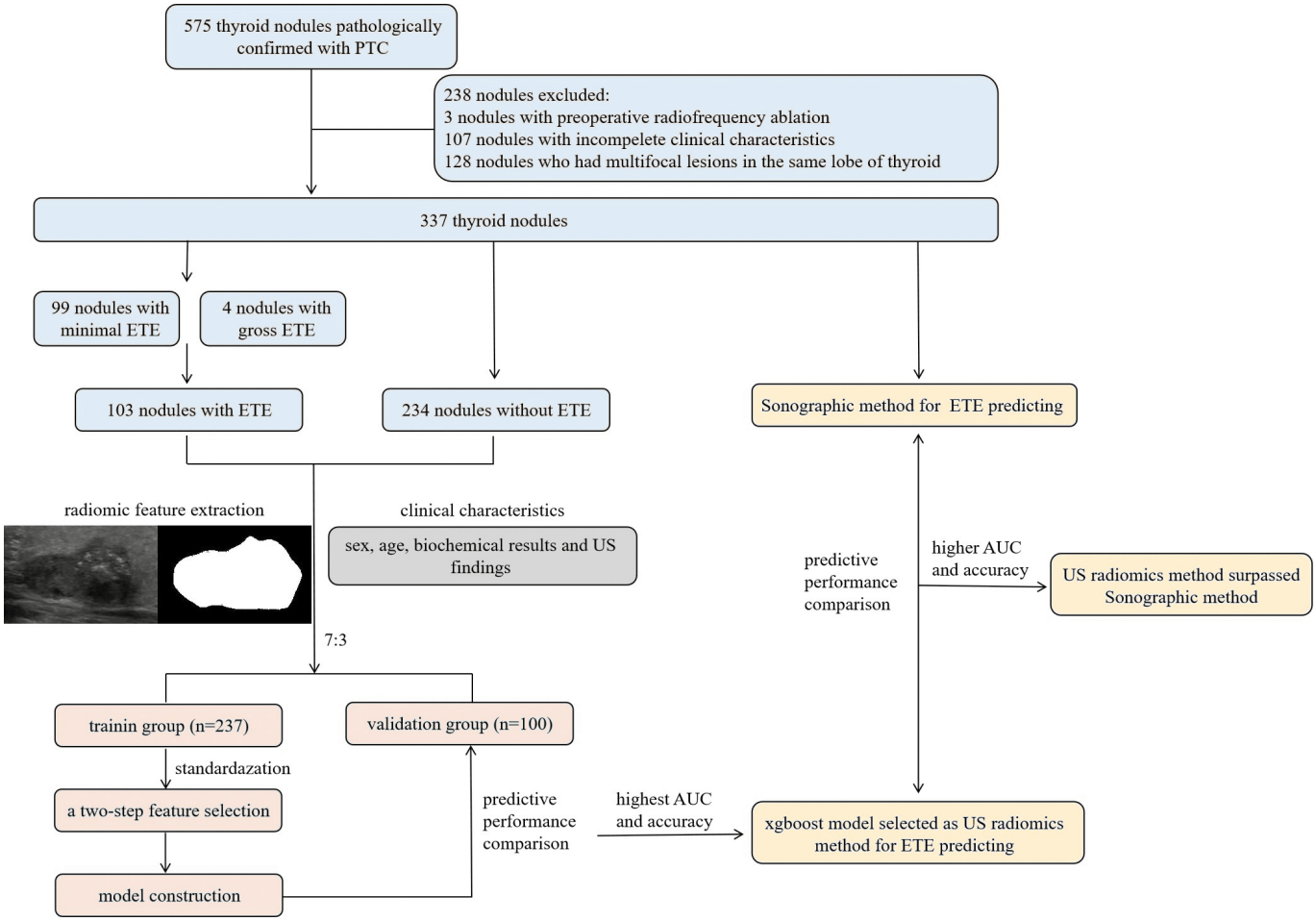

FIGURE 1. The flowchart for this retrospective study.

AUC = area under the curve; ETE = extrathyroidal extension; PTC = papillary thyroid carcinoma; US = ultrasonic; xgboost = the extreme gradient boosting

Sonographic method for extrathyroidal extension predicting

The assessment of ETE was performed by two US experts (YY, HL) who had 24 and 16 years of experience in US thyroid examination. Consensus were made when disagreements appeared and each of them reviewed half of the nodules without knowing the pathological state of ETE. Based on previous studies, sonographic ETE was suspected on US images when a capsular abutment or protrusion presented.[13] Capsular abutment referred to nodules' contact of the thyroid capsule, which could be graded by their perimeter ratio (< 25%, 25-50% or > 50%). While protrusion referred to nodules protruding thyroid capsule and invading the muscles or soft tissue around the thyroid gland, including the trachea, fat space between the trachea, esophagus, esophagus sulcus, cervical sheath vessels, et al.[10,13] The predictive performance of sonographic method was calculated using all nodules and compared by the AUC of the receiver operating characteristic (ROC), sensitivity, specificity, accuracy, positive predictive value (PPV) and negative predictive value (NPV).

US radiomic feature extraction

Different US systems were employed in nodules' examination, including Esaote MyLab Class C (Esaote, Italy), Siemens ACUSON OXANA 2 (Siemens Medical Solutions, USA), GE Volume E8 (GE Medical Systems, USA), Hitachi HI VISION Preirus (Hitachi-Aloka Medical, Japan) and Mindray Resona 7T (Mindray Medical International, China). High-frequency linear probes (5 MHz to 14 MHz) were used depending on US systems. In order to have the best image for

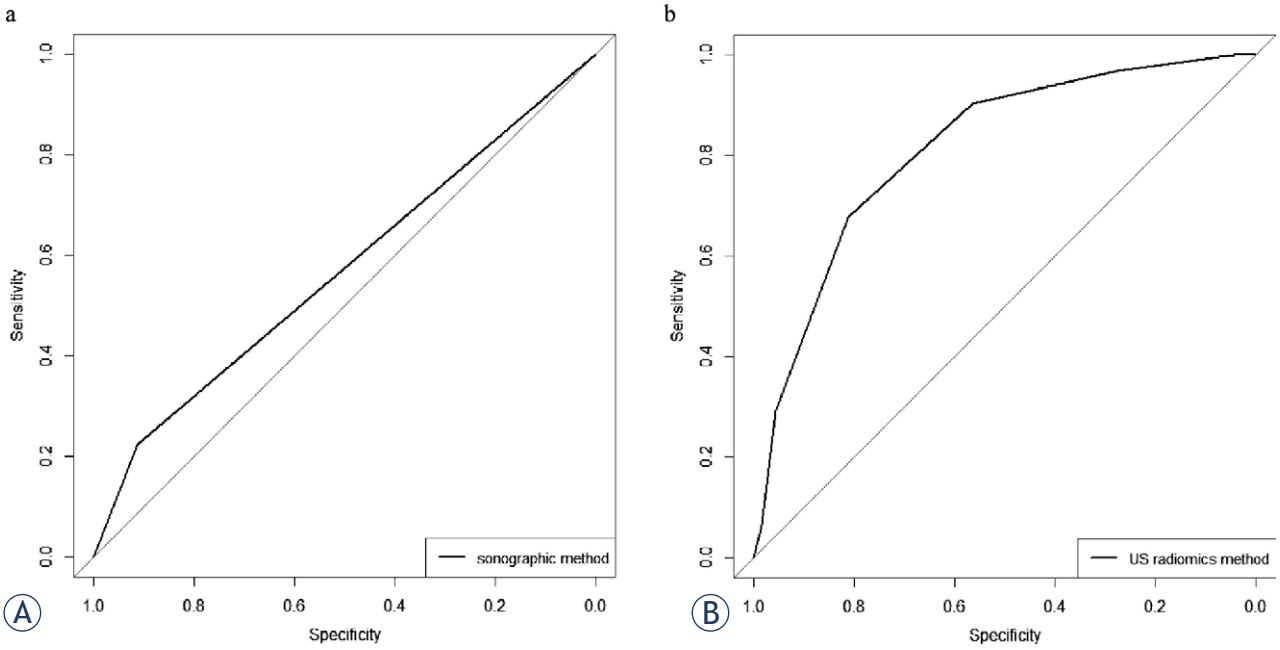

FIGURE 2. The ROC curves of sonographic method and US radiomics method for ETE predicting. **(A)** The ROC curve of sonographic method in all nodules. **(B)** The ROC curve of US radiomics method in validation group.

ETE = extrathyroidal extension; ROC = the receiver operating characteristic; US = ultrasonic

nodule, the depth and width of US systems were adjusted individually. Images of transverse and longitudinal section of nodules were saved as JPG files before the largest cross section of nodules were chosen for feature extraction. The US experts who were blinded to the pathological state of ETE reviewed the images, measured the US findings of nodules and delineated the region of interest (ROI) manually by Paint Win10. Consensus were made when disagreements appeared. Each expert review half of the nodules, respectively.

From those ROIs of US images, a total of 1769 US radiomic features were extracted using PyRadiomics (version 3.7, http://pyradiomics.readthedocs.io/en/latest/index.html). The features included 9 shape features, 360 first-order statistical features and 1400 textural features. Gray-level size-zone matrix (GLSZM), gray-level co-occurrence matrix (GLCM), gray-level dependence matrix (GLDM) and gray-level runlength matrix (GLRLM) consisted of the gray matrices in textural features. What's more, high-dimensional features were acquired by filters including Laplacian of Gaussian (LOG) with different sigma values (1.0 mm-10.0 mm with step 1.0 mm), square root, square, exponential, wavelet with 2D transform (low-pass/high-pass, LH; low-pass/low-pass, LL; high-pass/high-pass, HH; high-pass/low-pass, HL;), gradient and logarithm.

US radiomics method for extrathyroidal extension predicting and comparison with sonographic method

All nodules were randomly assigned to training group (237 nodules) and validation group (100 nodules) by a ratio of 7:3. In order to show the randomness of grouping, the clinical characteristics between training group and validation group were compared. Then all features were enrolled in the following progression, including 1769 US radiomic features and 34 clinical characteristics. To eliminate redundant and irrelevant features as well as reduce variables recruited into model, a two-step features selection method was applied after standardization. Firstly, the minimum redundancy maximum relevance (mRMR) was used to select the most relevant features. Secondly, they were further selected by least absolute shrinkage and selection operator (LASSO) algorithm and candidate features were obtained. Ten-fold cross validation was used to avoid overfitting.[20]

In total, nine predicting models were constructed using these candidate features, including k

TABLE 1. Characteristics of nodules in training and validation groups

Characteristics	Training group (n = 237)	Validation group (n = 100)	*p*-value
Sex			0.708
Male	64 (27.00)	29 (29.00)	
Female	173 (73.00)	71 (71.00)	
Age (years)[a]	45.97 ± 11.92	46.70 ± 11.64	0.606
Size (mm)	9.69 ± 6.08	10.62 ± 7.60	0.550
WBC (×10^9/L)	5.96 ± 1.52	6.12 ± 1.45	0.241
NEUT (×10^9/L)	3.65 ± 1.26	3.75 ± 1.18	0.326
LYM (×10^9/L)	1.89 ± 0.56	1.91 ± 0.62	0.716
HB (g/L)	138.39 ± 16.01	141.70 ± 15.13	0.094
RBC (×10^12/L)	4.69 ± 0.46	4.70 ± 0.45	0.752
PLT (×10^9/L)	252.85 ± 58.65	255.70 ± 64.90	0.656
ALT (U/L)	23.50 ± 19.98	24.15 ± 18.41	0.280
AST (U/L)	21.53 ± 7.86	21.48 ± 7.68	0.696
ALB (g/L)	45.15 ± 3.19	44.93 ± 3.01	0.473
BUN (mmol/L)	4.83 ± 1.27	4.93 ± 1.29	0.391
CREA (umol/L)	58.14 ± 13.36	57.54 ± 12.82	0.489
UA (umol/L)	315.27 ± 82.01	325.80 ± 86.12	0.261
Ca (mmol/L)	2.40 ± 0.11	2.41 ± 0.10	0.460
TT3 (ng/ml)	1.10 ± 0.31	1.09 ± 0.18	0.828
TT4 (μg/dl)	8.32 ± 1.72	8.09 ± 1.62	0.329
FT3 (pg/ml)	3.36 ± 1.16	3.33 ± 0.41	0.346
FT4 (ng/dl)	1.30 ± 0.26	1.29 ± 0.20	0.829
TSH (μIU/ml)	1.66 ± 0.99	1.96 ± 1.38	0.090
ANTITGAB (IU/ml)	122.12 ± 325.06	114.13 ± 349.18	0.335
ANTITPOAB (IU/ml)	41.11 ± 101.64	52.08 ± 124.91	0.912
TG (ng/ml)	36.10 ± 72.10	42.00 ± 84.61	0.886
Urinary leukocyte[b]			0.412
Negative	188 (79.32)	87 (87.00)	
Positive 1+	19 (8.02)	5 (5.00)	
Positive 2+	17 (7.17)	3 (3.00)	
Positive 3+	10 (4.22)	3 (3.00)	
Positive 4+	10 (4.22)	2 (2.00)	
URBC[b]			0.144
Negative	208 (87.76)	89 (89.00)	
Positive 1+	21 (8.86)	6 (6.00)	
Positive 2+	6 (2.53)	1 (1.00)	
Positive 3+	0 (0)	2 (2.00)	
Positive 4+	2 (0.84)	2 (2.00)	
Urinary protein[b]			0.524
Negative	145 (61.18)	64 (64.00)	
Positive 1+	63 (26.58)	28 (28.00)	
Positive 2+	29 (12.24)	8 (8.00)	
Composition[b]			1.000
Predominately cystic	2 (0.84)	0 (0)	
Predominately solid	235 (99.16)	100 (100.00)	
Solid	0 (0)	0 (0)	
Echogenicity[b]			0.966
Hyperechoic or isoechoic	8 (3.38)	3 (3.00)	
Hypoechoic	191 (80.59)	82 (82.00)	
Markedly hypoechoic	38 (16.03)	15 (15.00)	
Shape[b]			0.974
Wider-than-tall	100 (42.19)	42 (42.00)	
Taller-than-wide	137 (57.81)	58 (58.00)	
Margin[b]			0.083
Smooth or ill-defined	143 (60.34)	54 (54.00)	
Lobulated or irregular	70 (29.54)	27 (27.00)	
Extrathyroidal extension	24 (10.13)	19 (19.00)	
Echogenic foci[b]			0.465
No calcification	68 (28.69)	20 (20.00)	
Macrocalcifications	63 (26.58)	23 (23.00)	
Peripheral calcifications	6 (2.53)	2 (2.00)	
Microcalcifications	147 (62.03)	72 (72.00)	
TI-RADS classification[b]			1.000
III	1 (0.42)	0 (0)	
IV	19 (8.02)	8 (8.00)	
V	216 (91.14)	92 (92.00)	
ETE			0.910
Negative	165 (69.62)	69 (69.00)	
Positive	72 (30.38)	31 (31.00)	

Continuous variables were presented with Mean ± SD and were calculated by Mann-Whitney U test. Data marked with [a] were calculated by Student's t-test. Categorical variables were presented with number and percentage (percentage in parentheses) and were calculated by Chi-square analysis. Data marked with [b] were calculated by Fisher exact test.

ALB = albumin; ALT = alamine aminotransferase; ANTITGAB = anti-thyroglobulin antibodies; ANTITPOAB = anti-thyroid peroxidase antibody; AST = asparate aminotransferase; BUN = blood urea nitrogen; Ca = calcium ion; CREA = creatinine; ETE = extrathyroidal extension; FT3 = free triiodothyronine 3; FT4 = free triiodothyronine 4; HB = hemoglobin; LYM = lymphocyte; NEUT = neutrophil; PLT = platelets; RBC = red blood cell; SD = standard deviation; TG = thyroglobulin; TI-RADS = Thyroid Imaging Reporting and Data System; TSH = thyroid stimulating hormone; TT3 = total triiodothyronine 3; TT4 = total triiodothyronine 4; UA = uric acid; URBC = urinary red blood cell; WBC = white blood cell

nearest neighbors (KNN), binary logistics regression (LR), support vector machine (SVM), naive-bayes (NB), randomforest (RF), decision tree (DT), adaptive boosting (adaboost), the extreme gradient boosting (xgboost) and gradient boosting machine (GBM). Their predictive performances were compared by AUC, sensitivity, specificity, accuracy, PPV and NPV. And the model with the highest AUC and accuracy was chosen as US radiomics method. Finally, the predictive performances of US radiomics method and sonographic method were compared. The statistical process was shown in Figure 1.

Statistical analysis

Continuous variables were presented as mean ± standard deviation (SD) and were measured by Mann-Whitney U test or Student's t-test depending on the results of normality analysis. Categorical variables were presented as number (frequency) and Chi-square analysis or Fisher exact test were performed afterwards. SPSS software (version 19.0, IBM) was employed for the calculation mentioned above. The random allocation, standardization, mRMR, LASSO algorithm, KNN, binary LR, SVM, NB, RF, DT, adaboost, xgboost, GBM, DeLong's test and other statistical analysis were carried out with R software (version 4.0.3, MathSoft, http://www.r-project.org). DeLong's test was employed for statistical significance in AUC comparison.[21] A value of $p < 0.05$ was considered statistically significant.

Results

Clinical characteristics of nodules

Clinical characteristics of training group and validation group were summarized in Table 1, including age, sex, biochemical results and US findings. The training group comprised of 237 nodules with a positive ETE rate of 30.38%. And the validation

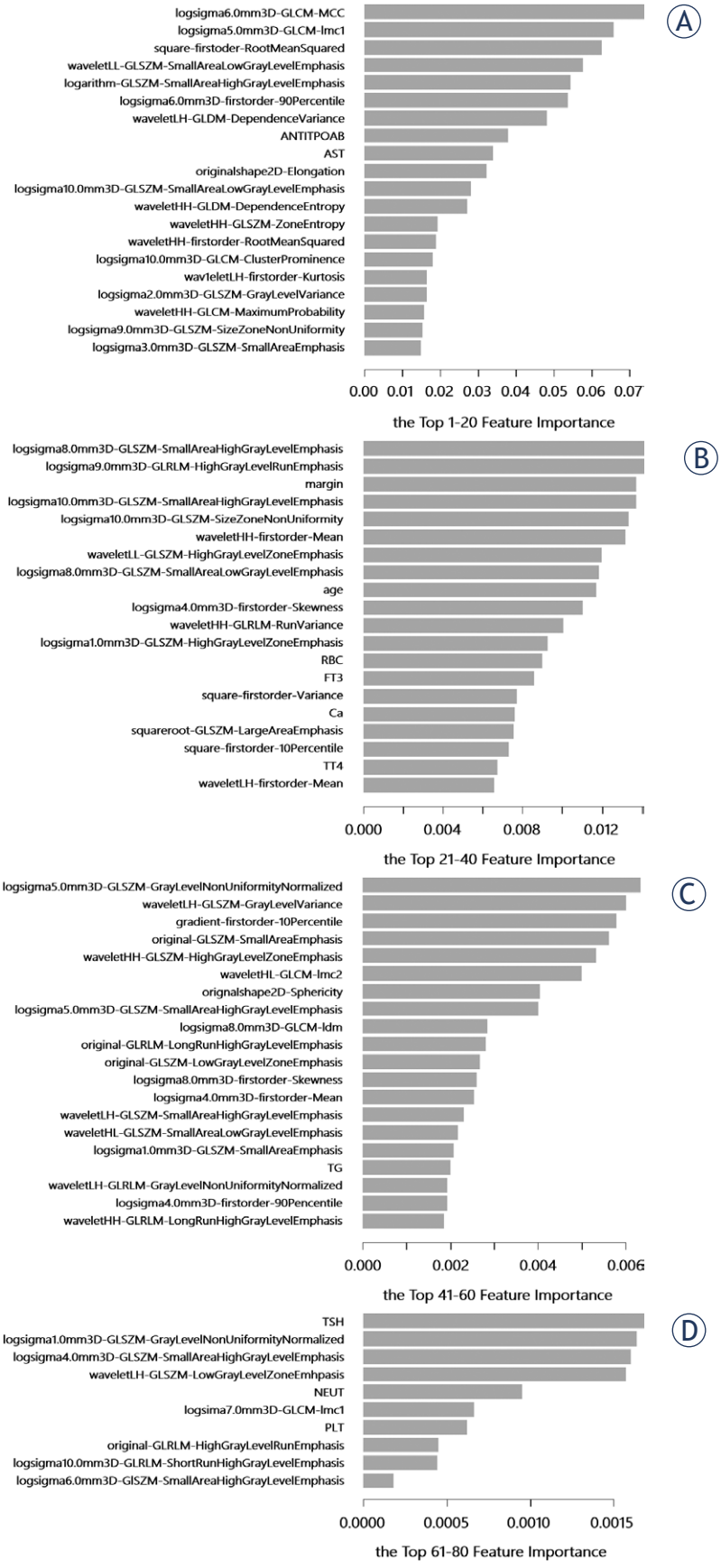

FIGURE 3. The image of feature importance for xgboost model. **(A-D)** the top 1-20, top 21-40, top 41-60 and top 61-80 feature importance of xgboost model.

xgboost=the extreme gradient boosting; GLSZM=Gray-level size-zone matrix; GLCM=gray-level co-occurrence matrix; GLDM=gray-level dependence matrix; GLRLM=gray-level runlength matrix; LH=low-pass/high-pass; LL=low-pass/low-pass; HH=high-pass/high-pass; HL=high-pass/low-pass; ANTITPOAB=anti-thyroid peroxidase antibody; AST=asparate aminotransferase; RBC=red blood cell; FT3=free triiodothyronine 3; Ca=calcium ion; TT4=total triiodothyronine 4; TG=thyroglobulin; TSH=thyroid stimulating hormone; NEUT=neutrophil; PLT=platelets.

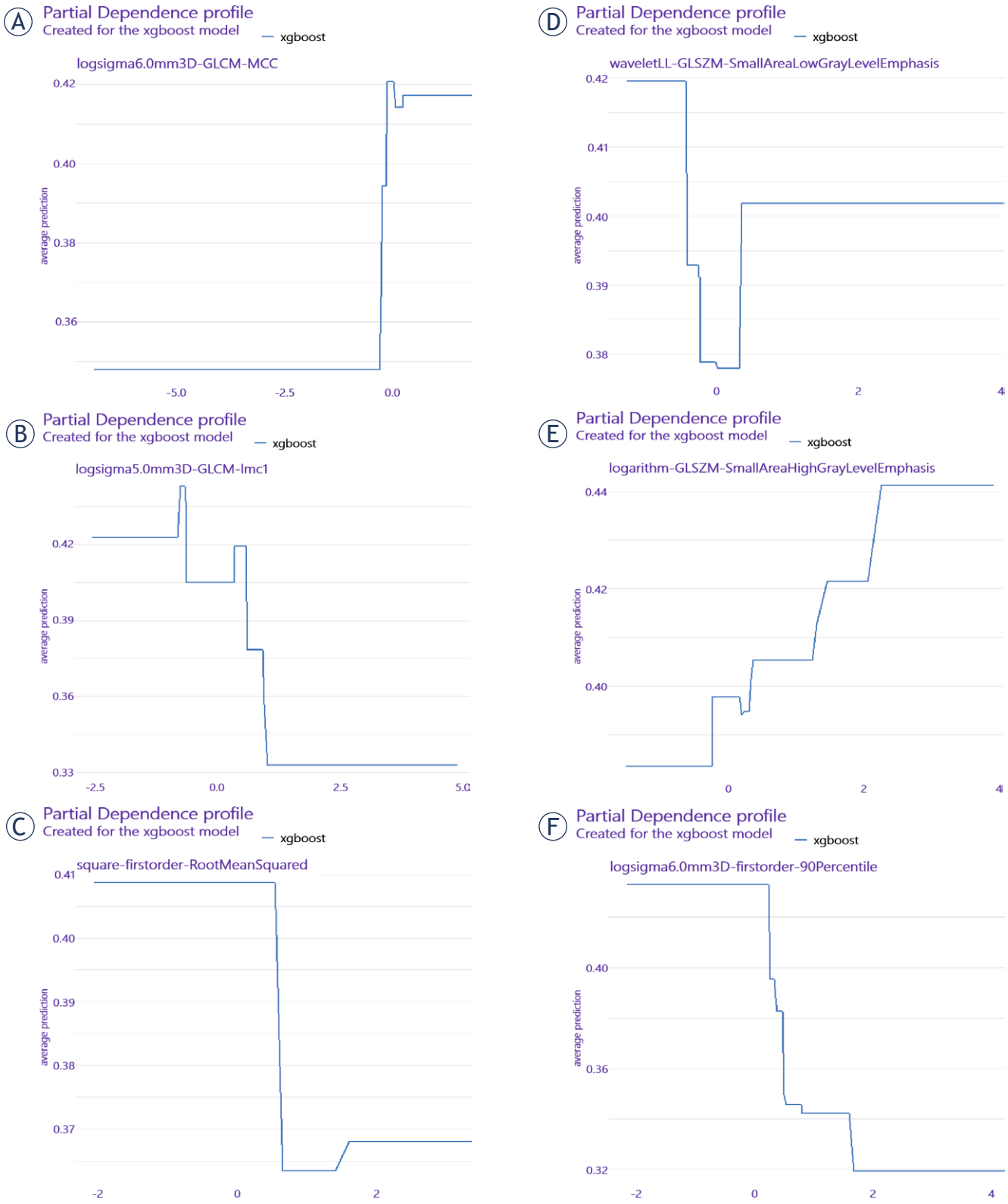

FIGURE 4. Partial dependence profile of the top-6 important features in xgboost model. **(A-F)** Partial dependence profile of logsigma6.0mm3D-GLCM-MCC, logsigma5.0mm3D-GLCM-Imc1, square-firstorder-RootMeanSquared, waveletLL-GLSZM-SmallAreaLowGrayLevelEmphasis, logarithm-GLSZM-SmallAreaHighGrayLevelEmphasis and logsigma6.0mm3D-firstorder-90Percentile in xgboost model in training group. xgboost, the extreme gradient boosting; GLSZM, Gray-level size-zone matrix; GLCM, gray-level co-occurrence matrix; LL, low-pass/low-pass.

TABLE 2. Comparison of predictive performance for models and sonographic method for extrathyroidal extension predicting

Model	Accuracy (95% CI)	Sensitivity	Specificity	PPV	NPV	AUC	*p*-value
xgboost	0.77(0.6751-0.8483)	0.6774	0.8116	0.6176	0.8485	0.813	-
RF	0.73(0.6320-0.8139)	0.3548	0.8986	0.6111	0.7561	0.741	0.000006
GBM	0.75(0.6534-0.8312)	0.5164	0.8551	0.6154	0.7973	0.737	0.000012
binary LR	0.74(0.6427-0.8226)	0.6774	0.7681	0.5676	0.8413	0.730	0.000237
NB	0.55(0.4473-0.6497)	0.9355	0.3768	0.4028	0.9286	0.656	0.000000
DT	0.68(0.5792-0.7698)	0.3871	0.8116	0.4800	0.7467	0.634	0.000000
adaboost	0.71(0.6107-0.7964)	0.3548	0.8696	0.5500	0.7500	0.612	0.000000
SVM	0.70(0.6002-0.7876)	0.2903	0.8841	0.5294	0.7349	0.567	0.000000
KNN	0.69(0.5897-0.7787)	0.1935	0.9130	0.5000	0.7159	0.553	< 2.2x10^-16
Sonographic method	0.70(0.6514-0.7515)	0.5349	0.7279	0.2233	0.9145	0.569	< 2.2x10^-16

adaboost = adaptive boosting; AUC = area under the curve; CI = confidence interval; DT = decision tree; ETE = extrathyroidal extension; GBM = gradient boosting machine; KNN = k nearest neighbour; LR = logistics regression; NB = naivebayes; NPV = negative predictive value; PPV = positive predictive value; RF = randomforest; SVM = support vector machine; xgboost = the extreme gradient boosting

group comprised of 100 nodules with similar positive ETE rate of 31.00%. No significant differences were found in any characteristics between the two groups. Of all the nodules, images acquired by Esaote, Siemens, GE, Hitachi and Mindray systems accounted for 70.33% (237/337), 15.13% (51/337), 8.90% (30/337), 4.15% (14/337) and 1.48% (5/337).

Sonographic method for extrathyroidal extension predicting

The predictive performance for sonographic method was summarized in Table 2. And its ROC was shown in Figure 2A. A relatively high accuracy (0.70), specificity (0.7279) and NPV (0.9145) was found for this method. However, its sensitivity (0.5349), PPV (0.2233) and AUC (0.569) was at a low level.

US radiomics method for extrathyroidal extension predicting

After standardization, the top-99 most relevant features to ETE were retained using mRMR. And 81 candidate features were selected using LASSO algorithm afterwards. Among the nine predicting models, xgboost model had the highest accuracy (0.77) and AUC (0.813) with *p*-value <0.05 compared to other models (Table 2). Meanwhile, with its relatively high specificity (0.8116), and NPV (0.8485), it was chosen as US radiomics method. Then the predictive performance of US radiomics method and sonographic method was compared. And the results showed that the AUC of US radiomics method was significantly higher than that of sonographic method with *p*-value <0.05. Meanwhile, the accuracy, sensitivity, specificity and PPV of US radiomics method was higher than that of sonographic method (Figure 2B, Table 2). Thus, we believe US radiomics method surpassed sonographic method in ETE predicting (Figure 1).

Partial dependence profile of US radiomics method

The image of feature importance for xgboost model was shown in Figure 3. And the top-6 features were chosen at a cut-off of 0.05 (Gain value). The partial dependence profiles of the them were revealed in Figure 4, in which the variation trends between features and ETE states were presented.

Discussion

The association between minimal ETE and poor prognosis of PTC patients had been questioned since 2006.[22] In 2017, the AJCC tumor-node-metastasis staging system changed the stratification criteria and excluded minimal ETE as an isolated risk factor for poor prognosis.[9,22] However, controversial opinions and contradictory results arose consistently. In resent review of SEER database, which contained approximately 10% of differentiated thyroid cancer patients in America, Liu *et al.* found that patients with minimal ETE had signifi-

cantly lower rates of cancer-specific survival and overall survival than those without.[3] Danilovic *et al.* revealed 596 PTC patients and indicated that both minimal ETE and gross ETE were independent risk factors of recurrence, although gross ETE might lead to a worse one.[23] What's more, Almeida *et al*. concluded that minimal ETE was the only aggressive feature for low-risk PTC after analyzing over 1100 PTCs.[22] In clinical practice, the detection of ETE determined the selection of optimal treatment of PTC patients. Usually, total thyroidectomy or subtotal thyroidectomy was suggested for patients with ETE while hemithyroidectomy was recommended for those without. However, surgical procedure of hemithyroidectomy didn't only retain some functionality of the thyroid but also protect parathyroid functions and contralateral laryngeal recurrent nerve.[7] Therefore, an effective way to evaluate ETE preoperatively could help patients in multi-aspect.

In this study, we retrospectively analyzed 337 PTC nodules, which included 4 gross ETE and 99 minimal ETE, and measured the predicting value of sonographic method and US radiomics method. The sensitivity, specificity, PPV, NPV, accuracy and AUC of sonographic method accounted for 53.49%, 72.79%, 22.33%, 91.45%, 70% and 0.569. Those values of US radiomics method accounted for 67.74%, 81.16%, 61.76%, 84.85%, 77% and 0.813. Thus, we concluded that the predicting value of US radiomics method surpassed sonographic method. Meanwhile, we found the top-6 important features selected by xgboost model included two GLCM, two GLSZM and two first-order features, among which four LOG (sigma values: 5.0 mm and 6.0 mm), one wavelet (LL), one square and one logarithm filters were acquired.

In studies of Lamartina, Han, Hu and Lee, the sensitivity, specificity, PPV, NPV, and accuracy of sonographic assessment for minimal ETE or overall ETE varied from 30.0% to 79.7%, from 79.5% to 93%, from 51.0% to 76.1%, from 76.6% to 86.1%, and from 71.7% to 81.9%, respectively.[10,24-26] Consistent to our study, the sensitivities of their results were lower than the specificities. Similar trend was found in PPVs and NPVs. However, Han reported an AUC of 0.746 for ETE predicting, which was higher than our result.[24] That might be explained by the smaller population size (n = 111) acquired in their study.[24] To our knowledge, only one article about US radiomics prediction of ETE was published by Wang in 2021.[7] In their study, they included clinical characteristics like age, sex, size and radiological ETE diagnosis, as well as location, border and vascularization elastic properties classification of tumor. The radiomic features they extracted included first-order features, shape features and texture features. And the texture features covered GLRLM, GLSZM, GLDM, GLCM and neighbourhood grey-tone dependency matrix (NGTDM). A radiomic nomogram model was selected as the best model with an AUC of 0.824 in validation group. It obtained two clinical characteristics (tumor location and radiologist diagnosis of ETE) and one radiomics signature, which was comprised of waveletLL-GLSZM, NGTDM, waveletHH-GLCM, waveletLH-GLCM corr, waveletLH-GLCM clus and waveletLH-GLSZM. Similar to their study, clinical characteristics we acquired were less important than radiomic features, and the majority of selected radiomic features were GLCM and GLSZM features.

First-order features mainly described the distribution of voxel intensities while texture features measured the inter-relationship between voxel distributions.[27] GLCM represented the grey levels of neighbouring pixels with spatial relationship in an image and was commonly applied in studies.[28] The direction independent technique, GLSZM, quantified homogeneous zones for specific grey level in an image.[28] LOG filter was a combination of Laplacian operator and Gaussian filter, which could decrease the noise and the impact of signals in a medical image.[29,30] What's more, it could detect edges and smooth images. With different sigma parameters, a series of textural coarseness were derived for further evaluation.[30] Another widely used filter, wavelet, focused on individual voxels and the relationship between them.[31] It could enhance certain characteristics of images with decomposition of high-pass and low-pass in the x and y directions.[31] In our study, we found that all the important features we selected in xgboost model were high-dimensional features. Besides, we found a higher rate of LOG filtered features than other filters. Taken together with different functions of filters, we concluded that the LOG filter might had better predicting value than others in our study.

Preoperative US examination was the first-line diagnostic tool for PTC patients to detect the presence of lymph node metastasis and ETE.[10] However, it had the disadvantage of subjectivity and reliance on the experience level of operator.[7] US radiomics could solve the problems for it extracted and recognized the voxel intensities and distributions automatically whereas accurately predicted ETE preoperatively. Thus, it could help PTC patients from

avoiding unnecessary operations and reducing the risk of reoperation.[7]

The limitations in our study were summarized as following. First of all, the clinical procedure was not strict due to the retrospective nature. With the lack of clinical information or US images, several cases had to be excluded as a result. Secondly, capture of unrepresentative portion of tumors might happen because of discrete images. And that might increase the variability of US images and influence the repeatability of this study. Thus, we checked and chose images with strict standard to keep the image quality consistent. What's more, the conclusion was derived from relatively small sample in monocentric database. And larger cohorts in multicenter database were required in the future to improve its repeatability.

In conclusion, our study proved the superior value of US radiomics method to sonographic method in preoperatively detecting ETE for PTC patients. Meanwhile, we found high-dimensional radiomic features had better predicting value than clinical characteristics.

Acknowledgments

Funding

This work was supported by project of Wenzhou Science and Technology Bureau [grant number: Y20211029] and the Natural Science Foundation of Zhejiang Province [grant number: LSY19H180008].

Authors' contribution

HZ and YY conception and design of the work; HZ, YL and YY acquired the data and processed it before statistical analyzing; YL and YZ analyzed the data; ZW interpreted the results; all authors drafted the work and revised it.

References

1. Deng Y, Li H, Wang M, Li N, Tian T, Wu Y, et al. Global burden of thyroid cancer from 1990 to 2017. *JAMA Netw Open* 2020; **3:** e208759. doi: 10.1001/jamanetworkopen.2020.8759
2. Liu T, Ge X, Yu J, Guo Y, Wang Y, Wang W, et al. Comparison of the application of B-mode and strain elastography ultrasound in the estimation of lymph node metastasis of papillary thyroid carcinoma based on a radiomics approach. *Int J Comput Assist Radiol Surg* 2018; **13:** 1617-27. doi: 10.1007/s11548-018-1796-5
3. Liu Z, Huang Y, Chen S, Hu D, Wang M, Zhou L, et al. Minimal extrathyroidal extension affects the prognosis of differentiated thyroid cancer: Is there a need for change in the AJCC classification system? *PLoS One* 2019; **14:** e0218171. doi: 10.1371/journal.pone.0218171
4. Radowsky JS, Howard RS, Burch HB, Stojadinovic A. Impact of degree of extrathyroidal extension of disease on papillary thyroid cancer outcome. *Thyroid* 2014; **24:** 241-4. doi: 10.1089/thy.2012.0567
5. Youngwirth LM, Adam MA, Scheri RP, Roman SA, Sosa JA. Extrathyroidal extension is associated with compromised survival in patients with thyroid cancer. *Thyroid* 2017; **27:** 626-31. doi: 10.1089/thy.2016.0132
6. Bortz MD, Kuchta K, Winchester DJ, Prinz RA, Moo-Young TA. Extrathyroidal extension predicts negative clinical outcomes in papillary thyroid cancer. *Surgery* 2021; **169:** 2-6. doi: 10.1016/j.surg.2020.04.003
7. Wang X, Agyekum EA, Ren Y, Zhang J, Zhang Q, Sun H, et al. A radiomic nomogram for the ultrasound-based evaluation of extrathyroidal extension in papillary thyroid carcinoma. *Front Oncol* 2021; **11:** 625646. doi: 10.3389/fonc.2021.625646
8. Chen B, Zhong L, Dong D, Zheng J, Fang M, Yu C, et al. Computed tomography radiomic nomogram for preoperative prediction of extrathyroidal extension in papillary thyroid carcinoma. *Front Oncol* 2019; **9:** 829. doi: 10.3389/fonc.2019.00829
9. Kim M, Kim WG, Oh HS, Park S, Kwon H, Song DE, et al. Comparison of the seventh and eighth editions of the American joint committee on cancer/union for international cancer control tumor-node-metastasis staging system for differentiated thyroid cancer. *Thyroid* 2017; **27:** 1149-55. doi: 10.1089/thy.2017.0050
10. Lamartina L, Bidault S, Hadoux J, Guerlain J, Girard E, Breuskin I, et al. Can preoperative ultrasound predict extrathyroidal extension of differentiated thyroid cancer? *Eur J Endocrinol* 2021; **185:** 13-22. doi: 10.1530/EJE-21-0091
11. Kwak JY, Kim EK, Youk JH, Kim MJ, Son EJ, Choi SH, et al. Extrathyroid extension of well-differentiated papillary thyroid microcarcinoma on US. *Thyroid* 2008; **18:** 6094. doi: 10.1089=thy.2007.0345
12. Park JS, Son KR, Na DG, Kim E, Kim S. Performance of preoperative sonographic staging of papillary thyroid carcinoma based on the sixth edition of the AJCC/UICC TNM classification system. *AJR Am J Roentgenol* 2009; **192:** 66-72. doi: 10.2214/AJR.07.3731
13. Lee CY, Kim SJ, Ko KR, Chung KW, Lee JH. Predictive factors for extrathyroidal extension of papillary thyroid carcinoma based on preoperative sonography. *J Ultrasound Med* 2014; **33:** 231-8. doi: 10.7863/ultra.33.2.231
14. Jiang M, Li C, Tang S, Lv W, Yi A, Wang B, et al. Nomogram based on shear-wave elastography radiomics can improve preoperative cervical lymph node staging for papillary thyroid carcinoma. *Thyroid* 2020; **30:** 885-97. doi: 10.1089/thy.2019.0780
15. He J, Zhang H, Wang X, Sun Z, Ge Y, Wang K, et al. A pilot study of radiomics signature based on biparametric MRI for preoperative prediction of extrathyroidal extension in papillary thyroid carcinoma. *J Xray Sci Technol* 2021; **29:** 171-83. doi: 10.3233/XST-200760
16. Lee H, Lee EJ, Ham S, Lee HB, Lee JS, Kwon SU, et al. Machine learning approach to identify stroke within 4.5 hours. *Stroke* 2020; **51:** 860-6. doi: 10.1161/STROKEAHA.119.027611
17. Wang H, Song B, Ye N, Ren J, Sun X, Dai Z, et al. Machine learning-based multiparametric MRI radiomics for predicting the aggressiveness of papillary thyroid carcinoma. *Eur J Radiol* 2020; **122:** 108755. doi: 10.1016/j.ejrad.2019.108755
18. Kwon MR, Shin JH, Park H, Cho H, Kim E, Hahn SY. Radiomics based on thyroid ultrasound can predict distant metastasis of follicular thyroid carcinoma. *J Clin Med* 2020; **9:** 2156. doi: 10.3390/jcm9072156
19. Haugen BR, Alexander EK, Bible KC, Doherty GM, Mandel SJ, Nikiforov YE, et al. 2015 American thyroid association management guidelines for adult patients with thyroid nodules and differentiated thyroid cancer: The American thyroid association guidelines task force on thyroid nodules and differentiated thyroid cancer. *Thyroid* 2016; **26:** 1-133. doi: 10.1089/thy.2015.0020
20. Hu W, Wang H, Wei R, Wang L, Dai Z, Duan S, et al. MRI-based radiomics analysis to predict preoperative lymph node metastasis in papillary thyroid carcinoma. *Gland Surg* 2020; **9:** 1214-26. doi: 10.21037/gs-20-479
21. DeLong ER, DeLong DM, Clarke-Pearson DL. Comparing the areas under two or more correlated receiver operating characteristic curves: a nonparametric approach. *Biometrics* 1988; **44:** 837-45. doi: 10.2307/2531595
22. Almeida MFO, Couto JS, Ticly ALT, Guardia VC, Marone MMS, Scalissi NM, et al. The impact of minimal extrathyroidal extension in the recurrence of papillary thyroid cancer patients. *Arch Endocrinol Metab* 2020; **64:** 251-6. doi: 10.20945/2359-3997000000245

23. Danilovic DLS, Castroneves LA, Suemoto CK, Elias LO, Soares IC, Camargo RY, et al. Is there a difference between minimal and gross extension into the strap muscles for the risk of recurrence in papillary thyroid carcinomas? *Thyroid* 2020; **30:** 1008-16. doi: 10.1089/thy.2019.0753

24. Han DY, Sohn YM, Seo M, Yun SJ, Park WS, Jeon SH, et al. Shear-wave elastography in thyroid ultrasound: Can be a predictor of extrathyroidal extension and cervical lymph node metastasis in papillary thyroid carcinoma? *Medicine* 2020; **99:** e23654. doi: 10.1097/MD.0000000000023654

25. Lee YC, Jung AR, Sohn YM, Kim EJ, Eun YG. Ultrasonographic features associated with false-negative and false-positive results of extrathyroidal extensions in papillary thyroid microcarcinoma. *Eur Arch Otorhinolaryngol* 2018; **275:** 2817-22. doi: 10.1007/s00405-018-5115-0

26. Hu S, Zhang H, Sun Z, Ge Y, Li J, Yu C, et al. Preoperative assessment of extrathyroidal extension of papillary thyroid carcinomas by ultrasound and magnetic resonance imaging: a comparative study. *Radiol Med* 2020; **125:** 870-6. doi: 10.1007/s11547-020-01184-0

27. Nazari M, Shiri I, Hajianfar G, Oveisi N, Abdollahi H, Deevband MR, et al. Noninvasive Fuhrman grading of clear cell renal cell carcinoma using computed tomography radiomic features and machine learning. *Radiol Med* 2020; **125:** 754-62. doi: 10.1007/s11547-020-01169-z

28. Osapoetra LO, Chan W, Tran W, Kolios MC, Czarnota GJ. Comparison of methods for texture analysis of QUS parametric images in the characterization of breast lesions. *PLoS One* 2020; **15:** e0244965. doi: 10.1371/journal.pone.0244965

29. Dinapoli N, Barbaro B, Gatta R, Chiloiro G, Casa C, Masciocchi C, et al. Magnetic resonance, vendor-independent, intensity histogram analysis predicting pathologic complete response after radiochemotherapy of rectal cancer. *Int J Radiat Oncol Biol Phys* 2018; **102:** 765-74. doi: 10.1016/j.ijrobp.2018.04.065

30. Suo S-T, Zhuang Z-G, Cao M-Q, Qian L-J, Wang X, Gao R-L, et al. Differentiation of pyogenic hepatic abscesses from malignant mimickers using multislice-based texture acquired from contrast-enhanced computed tomography. *Hepatobiliary & Pancreatic Diseases International* 2016; **15:** 391-8. doi: 10.1016/s1499-3872(15)60031-5

31. Vuong D, Tanadini-Lang S, Huellner MW, Veit-Haibach P, Unkelbach J, Andratschke N, et al. Interchangeability of radiomic features between [18F]-FDG PET/CT and [18F]-FDG PET/MR. *Med Phys* 2019; **46:** 1677-85. doi: 10.1002/mp.13422

research article

Emergency and prophylactic uterine artery embolization in gynecology and obstetrics - a retrospective analysis

Polona Vihtelic[1,2], Eva Skuk[2,3], Natasa Kenda Suster[2,3], Marina Jakimovska Stefanovska[2,3], Peter Popovic[1,2]

[1] Clinical Institute of Radiology, University Medical Centre Ljubljana, Ljubljana, Slovenia
[2] Faculty of Medicine, University of Ljubljana, Ljubljana, Slovenia
[3] Division of Obstetrics and Gynecology, University Medical Centre Ljubljana, Ljubljana, Slovenia

Radiol Oncol 2024; 58(3): 397-405.

Received 21 February 2024
Accepted 21 June 2024

Correspondence to: Assoc. Prof. Peter Popovič, M.D., Ph.D., Clinical Institute of Radiology, University Medical Centre Ljubljana, Zaloška cesta 7, SI-1000 Ljubljana, Slovenia. E-mail: peter.popovic@kclj.si

Polona Vihtelič and Eva Skuk contributed equally to this work.

Disclosure: No potential conflicts of interest were disclosed.

Background. This study aimed to evaluate the safety and efficacy of emergency and prophylactic uterine artery embolization (UAE) in our clinical practice, including technical success, clinical success, and associated complications.

Patients and methods. In this retrospective study, we analyzed 64 women who underwent emergency (*n* =18) and prophylactic (*n* = 46) UAE. Indications for emergency UAE included postpartum hemorrhage or severe hemorrhage during pregnancy termination, while prophylactic UAE was performed prior to surgical removal of retained products of conception (RPOC), delivery with abnormal placental implantation, or pregnancy termination (cervical pregnancy or fetal anomalies accompanied by abnormal placental implantation). Technical success of UAE was defined as complete exclusion of the vascular lesion and contrast stasis on the final angiogram, while clinical success was defined as cessation of bleeding after UAE Termination without a hysterectomy.

Results. The overall clinical success of UAE in our study was 97% (62/64). All embolization procedures were technically and clinically successful in the prophylactic group without life-threatening hemorrhages or hysterectomies (100% success rate, 46/46). However, while 100% technical success was similarly attained in the emergency group, bleeding was successfully controlled in 89% of cases (16/18). In two patients with significant blood loss (over 2000 mL), embolization failed to achieve hemostasis, resulting in persistent bleeding and subsequent hysterectomy.

Conclusions. UAE is a safe and effective procedure for managing primary postpartum hemorrhage or severe hemorrhage during pregnancy termination and for decreasing the risk of severe hemorrhage during surgical removal of RPOC, delivery with abnormal placental implantation, or pregnancy

Key words: postpartum hemorrhage; retained products of conception; endovascular treatment; uterine artery embolization; hysterectomy; fertility

Introduction

Complications during pregnancy include severe life-threatening hemorrhage that can occur during vaginal or cesarean delivery, pregnancy termination, or surgical removal of retained products of conception (RPOC).

Primary postpartum hemorrhage (PPH) is a leading cause of obstetric morbidity and mortality globally, accounting for more than 100,000 mater-

nal deaths annually. Pathologic postpartum hemorrhage, which occurs in up to 10% of deliveries, is characterized by excessive blood loss during childbirth, defined as more than 500 mL for vaginal deliveries and more than 1,000 mL for cesarean births. Postpartum hemorrhage is further classified based on the time of its occurrence. Primary postpartum hemorrhage refers to excessive bleeding within 24 hours after delivery, whereas secondary postpartum hemorrhage describes bleeding that occurs anytime within six weeks after birth.[1-4] The most common causes of primary PPH are summarized in the 4 T mnemonics and include uterine **a**tony, **t**rauma (birth canal lacerations), **t**issue (retained/abnormal placenta), and **t**hrombin (coagulopathies). Uterine atony accounts for approximately 70% of cases of PPH and can lead to hemorrhagic shock, which may progress to endothelial damage and disseminated intravascular coagulation (DIC).[1-5] Placental causes, including abruption or placental implantation abnormalities (*placenta previa, accreta, percreta, increta*), are less frequent conditions but can also lead to severe postpartum hemorrhage.[2,3]

Retained products of conception (RPOC) refer to persistent placental and/or fetal tissue that remains in the uterine cavity after a vaginal or cesarean delivery, miscarriage, or pregnancy termination.[6-9] The estimated prevalence of RPOC is approximately 1% in term pregnancies and is more frequent after medical termination of pregnancy or miscarriage.[8] Recent literature reports a newly identified form of RPOC with highly vascularized characteristics on Doppler ultrasound observations. According to the literature, the occurrence rate of this particular entity is estimated to be around 18%.[6] RPOC is associated with long-term complications, such as intrauterine adhesions, menstrual abnormalities, infertility, recurrent pregnancy loss, and placental complications.[3,6-8]

Hemorrhage during pregnancy termination occurs in less than 1% of abortions. Bleeding may result from uterine atony, placental abnormalities spectrum, lacerations, and coagulopathies.[3,9]

Cervical pregnancy is a rare form of ectopic pregnancy, where pregnancy implants in the endocervical canal, and it accounts for less than 1% of all ectopic pregnancies. The incidence is estimated to be 1 in 9,000 pregnancies. The condition requires pregnancy termination, and the main potential complication is a high risk of severe hemorrhage.[10,11]

Selective transcatheter uterine artery embolization was first reported in 1979 as a second-line therapy for severe persistent postpartum hemorrhage.[4] Subsequent publications have further established the efficacy and safety of endovascular methods in controlling uterine bleeding and achieving hemostasis.[1-5] In 2017, the American College of Obstetricians and Gynecologists incorporated transcatheter arterial embolization (TAE) into their recommendations for managing postpartum hemorrhage, emphasizing the importance of preserving the uterus and potentially future fertility. Additionally, the International Federation of Gynecology and Obstetrics recognized the safety and efficacy of TAE in their 2022 PPH management guidelines, stating that this technique is a viable option for patients prioritizing fertility preservation.[4]

Embolic agents include absorbable gelatin sponges, microspheres, liquid agents, and cyanoacrylate glue. The preferred embolic material in our practice is the gelatin sponge, as this is the most frequently studied embolic agent in the treatment of postpartum hemorrhage, which temporarily (3 – 6 weeks) occludes the target vessel. Subsequent recanalization of the arteries has a theoretical advantage for patients desiring future fertility.[1,5]

Imaging findings

PPH and pregnancy termination-related hemorrhage are conditions that require immediate intervention; therefore, imaging is often limited to digital subtraction angiography during an endovascular procedure. Computer tomography angiography (CTA) is routinely not performed in the preprocedural assessment of postpartum hemorrhage due to time delay in the setting of active bleeding and radiation exposure to radiosensitive tissue in a typically young patient. However, CTA can be used when the underlying cause or location of hemorrhage is uncertain or if there is a recurrence of bleeding after an initially successful embolization.[12]

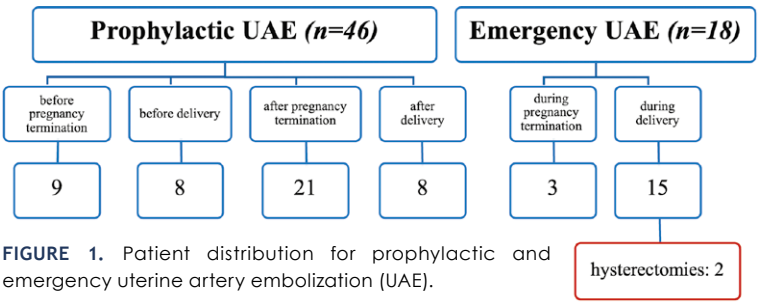

FIGURE 1. Patient distribution for prophylactic and emergency uterine artery embolization (UAE).

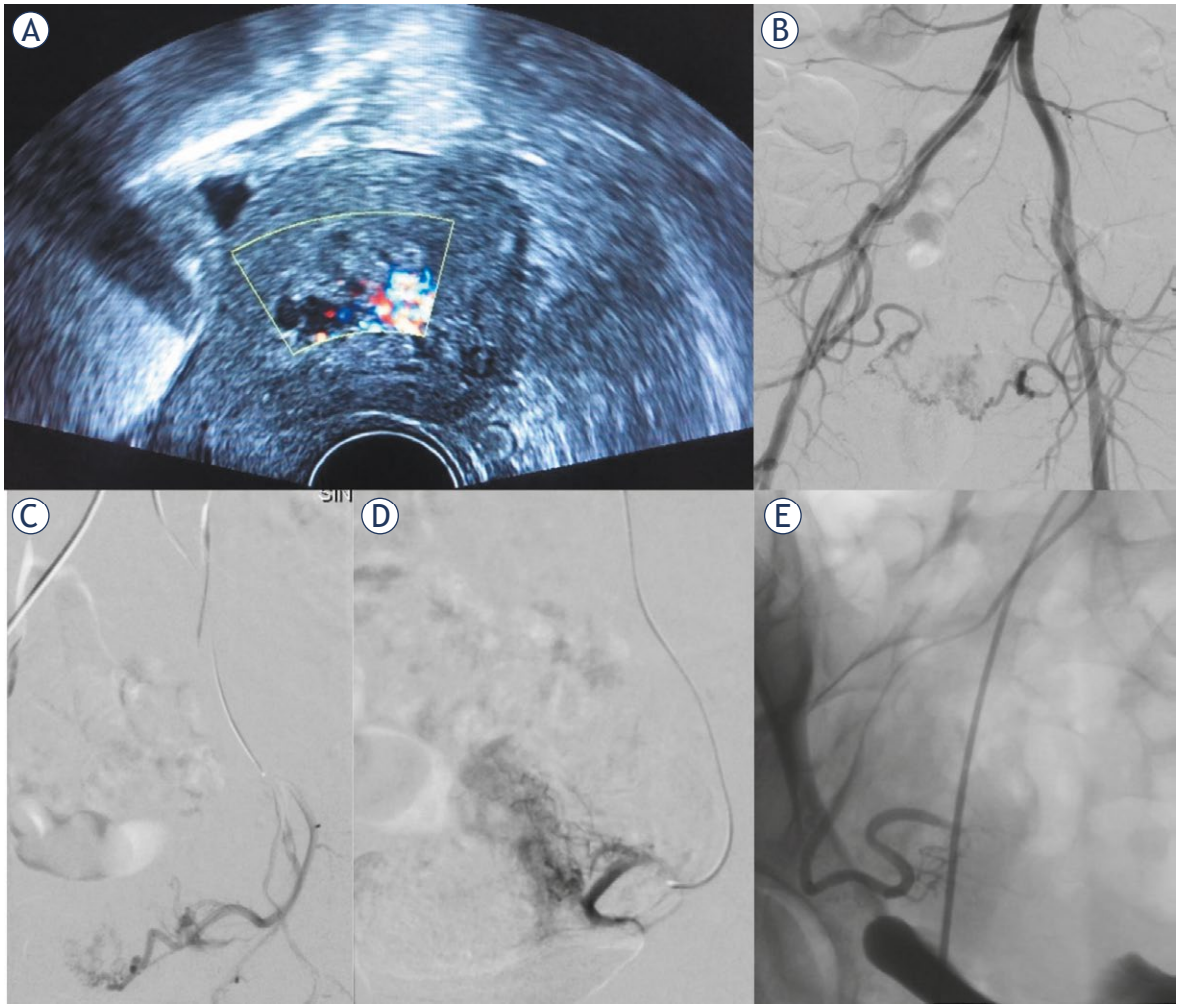

FIGURE 2. (A) Transvaginal ultrasonography in a 34-year-old female with vaginal bleeding after spontaneous termination of pregnancy at 12 weeks of gestation. Color Doppler ultrasound showed a 45 x 30 mm mass in the uterus with increased vascularity suggestive of retained products of conception. **(B)** Pelvic arteriogram demonstrating numerous spiral arteries in the uterus fed by both right and left uterine arteries, confirming the diagnosis of RPOC. **(C)** Left uterine arteriogram in the same patient before prophylactic embolization with absorbable gelatin sponge particles showing numerous spiral arteries. Post-embolization left **(D)** and right **(E)** uterine arteriogram demonstrating successful embolization. Subsequently, surgical resection of retained products of conception was successfully performed.

Doppler ultrasound and magnetic resonance imaging can identify placental irregularities, cervical pregnancy, and vascularization in the case of RPOC. These two imaging techniques are often required in planning delivery and the proper treatment protocol for pregnancy termination or RPOC.[11-13] In the case of RPOC, ultrasound helps us to assess the degree of vascularization. The marked vascularity feature is established in the presence of an exuberant color Doppler signal (Figure 2A).[6-8]

Contrast-enhanced CT has a limited role in the evaluation of hypervascular RPOC due to inaccuracy in soft tissue assessment. RPOC on CT shows an intensely enhanced heterogenous mass in the uterine cavity during the arterial phase or extravasation of intravenous contrast in case of large arterial hemorrhage in the postpartum period.[14-15] Pelvic MRI provides more detailed information if the diagnosis of hypervascularity in RPOC is unclear and there is no urgency.[7,14] Key MRI findings include intracavitary uterine soft-tissue mass with variable T1 and T2 signal intensities, variable amounts of enhancing tissue, and variable degrees of myometrial thinning and obliteration of the junctional zone (Figure 3A).[14,16]

Digital subtraction angiography (DSA) is the gold standard for evaluating blood vessels

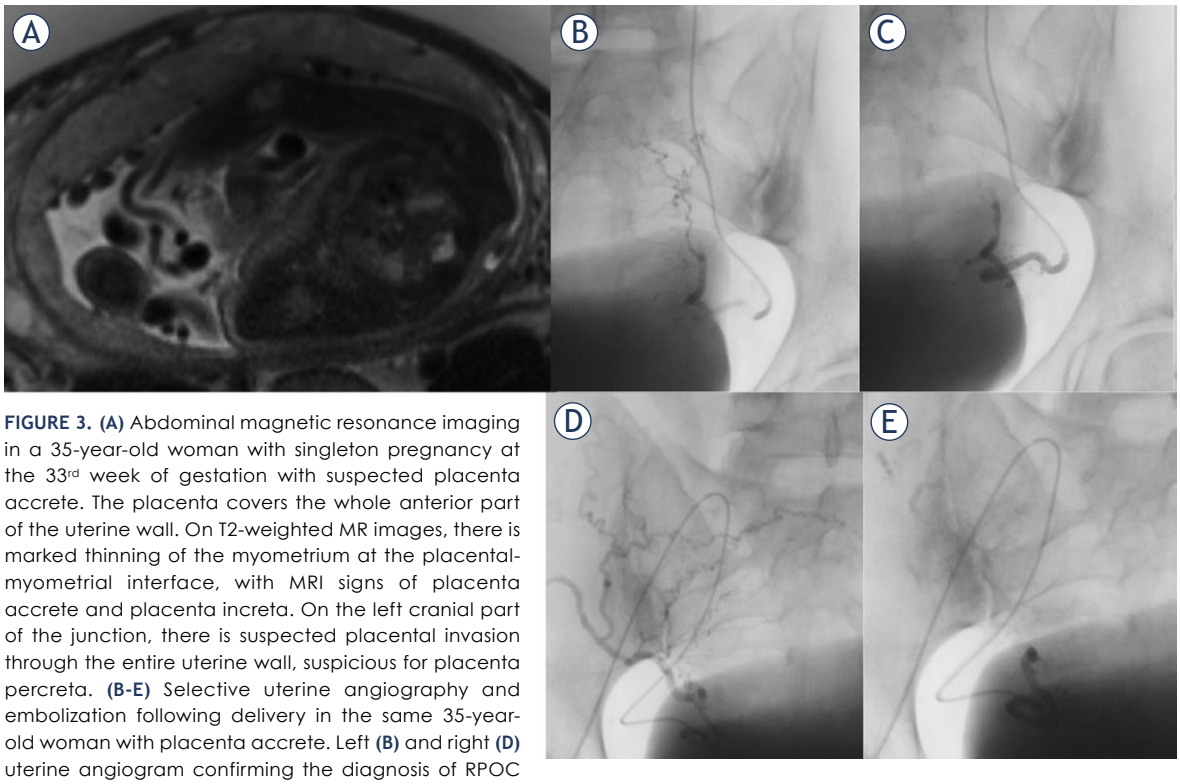

FIGURE 3. (A) Abdominal magnetic resonance imaging in a 35-year-old woman with singleton pregnancy at the 33rd week of gestation with suspected placenta accrete. The placenta covers the whole anterior part of the uterine wall. On T2-weighted MR images, there is marked thinning of the myometrium at the placental-myometrial interface, with MRI signs of placenta accrete and placenta increta. On the left cranial part of the junction, there is suspected placental invasion through the entire uterine wall, suspicious for placenta percreta. **(B-E)** Selective uterine angiography and embolization following delivery in the same 35-year-old woman with placenta accrete. Left **(B)** and right **(D)** uterine angiogram confirming the diagnosis of RPOC with numerous voluminous spiral arteries before prophylactic embolization. Left **(C)** and right **(E)** post-embolization angiogram after successful selective uterine artery embolization with absorbable gelatin sponge particles to reduce vascularity prior to surgical removal. After embolization, the placental tissue was successfully resected, and hysterectomy was prevented.

and confirming intrauterine vascular lesions.[6] Angiographic findings include enlarged and tortuous uterine arteries with well-defined focal masses made up of vascular tangles, a focal blush of contrast, early venous return, extravasation, and pseudoaneurysm (Figures 2B, D; 3B, D).[6,8] However, the presence of active extravasation on DSA is relatively rare in cases of postpartum hemorrhage, particularly in cases of uterine atony. The required rate of bleeding for angiographic detection is typically around 1–2 mL/min, which may be too low to detect in cases of uterine atony.[17]

Treatment options

Severe acute uterine cavity bleeding during vaginal/cesarean delivery, pregnancy termination, and removal of RPOC is initially managed by complete emptying of the contents of the uterine cavity, uterine massage, uterotonics, fluid resuscitation, and tranexamic acid administration. In some patients, further mechanical (intrauterine balloon tamponade) or sometimes surgical (internal iliac artery ligation) interventions are required.[18] Hysterectomy has traditionally been considered the last and definitive treatment option.[4,12,13] To avoid the sterility and significant morbidity associated with emergent hysterectomy, uterine artery embolization has been emphasized as a minimally invasive therapy for rapidly controlling hemorrhage that is refractory to standard gynecological treatment.[5]

In some cases of uterine hemorrhage, immediate hemodynamic instability is not a predominant concern, but according to imaging findings (ultrasound and MRI), a high risk for severe hemorrhage is expected with further gynecological intervention. Such cases may include vaginal/cesarean delivery with abnormal placentation, pregnancy termination with abnormal placentation, termination of cervical pregnancy, and surgical removal of highly vascularized RPOC (Figure 2, 3).[3,6,7,12,13] In these cases, prophylactic uterine artery embolization (UAE) is performed prior to surgical removal of RPOC, delivery, or pregnancy termination to reduce the risk of hemorrhage, offering a safe alternative to hysterectomy and, therefore, preserving fertility.[6-8]

Patients and methods

Study population

This retrospective single-center study was conducted at the University Medical Centre Ljubljana and was approved by the National Medical Ethics Committee of the Republic of Slovenia on December 8, 2021 (ref. no. 0120-285/2021/11). The study analyzed clinical data over a ten-year period (from 2012 to 2022). The data were obtained from the hospital information system of the University Medical Centre Ljubljana, the Perinatal Information system of the Republic of Slovenia, and from the completed patient questionnaires.

A total of 64 patients were included in the analysis and divided into two main categories – women who underwent prophylactic (46 patients) or emergency (18 patients) UAE. Patients in the prophylactic group were treated with UAE with the goal of decreasing the risk of massive bleeding during surgical removal of RPOC, pregnancy termination, or delivery. Patients in the emergency group were treated with UAE to control acute uterine cavity hemorrhage during pregnancy termination or delivery that was refractory to standard gynecological management. In both indications, the ultimate goal was to reduce blood loss and avoid an emergency hysterectomy.

The following data were collected from the medical records: age of patients, gynecological history, gestational week at pregnancy termination or delivery, indication for pregnancy termination, placental abnormalities, cause of PPH, type of UAE (prophylactic/emergency), estimated total blood loss during pregnancy termination, delivery or gynecological procedure and the necessity for hysterectomy.

The clinical diagnoses were made by a complete gynecological examination, followed by a sonographic assessment with a color Doppler ultrasound. Pelvic magnetic resonance imaging (MRI) was performed in indecisive cases and when there was no urgency. All patients underwent a diagnostic uterine digital subtraction angiography to confirm the diagnosis of intrauterine vascular lesion or hemorrhage before embolization. The decision on endovascular treatment was made by a multidisciplinary team, including gynecologists/obstetricians and interventional radiologists.

UAE procedure

Pelvic angiography was performed via a transfemoral approach under local anesthesia, followed by a selective bilateral or unilateral uterine artery angiography (Figure 2, 3). In all cases, a 5-French sheath was inserted into the right common femoral artery, followed by catheterization and angiography of the internal iliac artery to identify the uterine arteries on both sides as well as potential sites of bleeding. Next, selective catheterization of uterine arteries with a microcatheter (Progreat, Terumo) was performed to decrease the risk of inducing vasospasm. Arterial feeder pedicles were embolized by absorbable gelatin sponge particles (Marbagelan), microspheres, and balloon occlusion at the level of the internal iliac artery. The embolization was completed after contrast stasis as determined by fluoroscopy and confirmed by bilateral uterine artery angiography.

Study endpoints and definitions

This study aimed to evaluate the safety and efficacy of UAE in a cohort of 64 patients who underwent the procedure for the management of obstetric or gynecologic hemorrhage. The study focused on analyzing technical success, clinical success, and complications.

Pregnancy termination (also called abortion) was defined as the cessation of pregnancy before the 22nd gestational week or when the fetus weighs less than 500 g. Conversely, the termination of pregnancy beyond the 22nd gestational week was categorized as delivery.

Technical success was defined as the embolization of bilateral or unilateral uterine arteries with complete exclusion of the vascular lesion and contrast stasis on the final angiogram. Clinical success was defined as cessation of bleeding after UAE without a hysterectomy.

Postembolization complications were documented according to the criteria of the Society of Interventional Radiology.[19] To confirm the efficacy of the interventional procedure and uterine surgical treatment, patients were carefully monitored on outpatient follow-up visits with referring obstetricians or gynecologists until confirmation of the absence of any re-bleeding or uterine irregularities.

Results

The age range of the women included in the study was 22 – 45 years (mean 34 ± 6). Among them, 46 patients (72%) were treated with prophylactic UAE and 18 (28%) with emergency UAE.

TABLE 1. Clinical overview of the prophylactic uterine artery embolization (UAE) group

PROPHYLACTIC UAE	Number of cases	Intervention	Blood loss during gynecological procedure	Hysterectomy
BEFORE PREGNANCY TERMINATION				
Fetal anomalies accompanied by placental abnormalities	5	**Embolization** → pregnancy termination	300–400 mL (median 300 mL)	**0**
Cervical pregnancy	4	**Embolization** → pregnancy termination	100–400 mL (median 250 mL)	**0**
BEFORE DELIVERY				
Placental abnormalities with or without fetal anomalies	8	**Embolization** → vaginal/ cesarean delivery	200–1,800 mL (median 400 mL)	**0**
AFTER PREGNANCY TERMINATION				
Retained products of conception (RPOC)	21	**Embolization** → surgical removal of RPOC	100– 400 mL	**0**
AFTER DELIVERY				
Retained products of conception RPOC	8	**Embolization** → surgical removal of RPOC	100– 500 mL	**0**

In the prophylactic UAE group (Table 1), the patients were further subdivided into four subgroups based on both timing and cause of pregnancy termination and cause of RPOC.

We performed UAE prior to pregnancy termination in cases involving fetal anomalies accompanied by placental abnormalities (5 patients) or cervical pregnancy (4 patients). Minimal blood loss was observed during the subsequent gynecological procedure, and no hysterectomies were required in both cases. Additionally, 8 patients underwent embolization prior to delivery due to placental abnormalities with or without accompanied fetal anomalies. No hysterectomies were required despite slightly higher blood loss in this group, including one patient with a blood loss of 1,800 mL. Lastly, we performed embolization due to highly vascularized RPOC in 21 patients after pregnancy termination (Figure 2) and in 8 patients after delivery (Figure 3), followed by safe surgical removal, and hysterectomies were avoided in all cases within these two groups.

In the second study group (18 patients), embolization was performed as an emergency intervention to manage uncontrolled bleeding during pregnancy termination or delivery (Table 2). Among these patients, three required embolization during pregnancy termination due to excessive bleeding

TABLE 2. Clinical overview of the emergency uterine artery embolization (UAE) group

EMERGENCY UAE	Number of cases	Intervention	Blood loss during gynecological procedure	Hysterectomy
DURING PREGNANCY TERMINATION				
Hemorrhage	3	Pregnancy termination → hemorrhage → **embolization**	2x 300 mL 1x 1,000 mL	**0**
DURING DELIVERY				
Uterine atony	10	Hemorrhage after vaginal/Cesarean delivery → intrauterine balloon tamponade → **embolization**	8x < 1,000 mL **1x > 2,000 mL** **1x > 3,000 mL**	**2**
Placental abnormalities	5	Hemorrhage after vaginal/Cesarean delivery → intrauterine balloon tamponade → **embolization**	< 800 mL	**0**

despite standard gynecological treatment. The embolization procedure effectively achieved hemostasis.

Causes of PPH included uterine atony (10 patients) and placental abnormalities (5 patients). Eight patients with uterine atony-related hemorrhage were successfully treated with UAE after standard treatment (including intrauterine balloon insertion in three patients) had failed. However, it is important to note that two cases within this group experienced ineffective hemostasis, leading to a peripartum emergency hysterectomy. The first case involved a patient with a unicornuate uterus with severe hemorrhage due to uterine atony following a cesarean section. Following unsuccessful standard treatment, emergency UAE partially alleviated the bleeding, but additional blood loss ensued, and despite extensive gynecological and endovascular efforts, an emergency hysterectomy was ultimately required as a final intervention. In the second case, the patient experienced uterine atony, rupture, and retroperitoneal hematoma following a cesarean delivery of twins, leading to significant blood loss. Despite conservative and surgical interventions followed by UAE, the bleeding persisted, and the patient progressed to hemorrhagic shock. A hysterectomy was eventually performed to save the patient's life. In the last subgroup (5 patients), we effectively managed hemorrhage related to placental abnormalities during delivery using UAE.

Technical and clinical success

The uterine arteries were embolized bilaterally (60 patients, 94%) or unilaterally in cases involving anatomical variants (agenesis of the uterine artery) (4 patients, 6%). Nevertheless, the technical success rate was 100% as the contrast stasis was successfully achieved in all cases, as confirmed by the final angiogram.

Embolization procedures were primarily performed using absorbable gelatin sponge particles (57 patients, 89%). In a minority of cases, alternative occlusion options were employed, including a combination of gelatin sponge with microspheres (3/64), microspheres (1/64), and temporary balloon occlusion at the level of the internal iliac artery (3/64).

In the prophylactic group, a clinical success rate of 100% was achieved, indicating that all patients experienced successful outcomes. In the emergency group, the clinical success rate was 89%. Overall, hemostasis was effectively achieved in 62 out of 64 patients, resulting in a clinical success rate of 97% across the entire cohort.

In the prophylactic group, an estimated median blood loss of 200 mL was observed during the surgical intervention after embolization, and no hysterectomies were required. The performance of embolization as an emergency procedure was associated with higher blood loss. Two postpartum hysterectomies were necessary for our emergency group due to unsuccessful hemostasis despite gynecological and endovascular interventions.

Complications

During the procedures, a single peri-procedural complication in the form of uterine artery spasm was encountered. This complication was successfully managed by administering a short-acting vasodilator (nitroglycerin), allowing for the safe continuation of the embolization without any further problems.

No major post-procedural complication was recorded in our study. However, five patients (8%) reported moderate pain in the lower abdomen in the immediate post-intervention period, which was effectively managed with oral or parenteral analgesics. Additionally, no procedure-attributable complications were noted during the subsequent outpatient follow-up.

Discussion

The effectiveness of UAE in managing primary and secondary postpartum hemorrhage is high, and recent literature reports 99% technical success, whereas the clinical success rates range from 87% to 95%.[1,17,20,21] In our study, technical success in the prophylactic and emergency group was 100%. Clinical success in the prophylactic and emergency groups was 100% and 89%, respectively (overall clinical success rate of 97%). UAE was unsuccessful in achieving hemostasis in 2 patients with uterine atony following cesarean delivery, resulting in blood loss exceeding 2,000 mL and ultimately requiring a hysterectomy. In cases where embolization was unsuccessful, gelatin sponge and microspheres were used as the embolization materials. Our findings of failed endovascular therapy are consistent with those reported in the literature. Brown *et al.* and Sentilhes *et al.* described predictive factors for the failure of UAE, which include blood loss of more than 1,500 mL, DIC, large volume transfusion (> 5 red blood cell units), and cesarean

delivery.[1,2] Sugai *et al*. suggest that using a gelatin sponge as an embolic agent is associated with failure of the embolization in patients with DIC. The formation of a thrombus around the gelatin sponge depends on the patient's coagulation ability, which is impaired in DIC patients.[22] Furthermore, Lee *et al.* observed a strong association between excessive blood loss (> 1,500 mL) accompanied by hemodynamic shock and instability and poor outcomes of UAE in a cohort of 251 patients. Nevertheless, it is still recommended that UAE should also be considered in hemodynamically unstable patients and patients with coagulopathies, but these patients require close monitoring and care.[21]

Our study suggests that UAE is a safe procedure as no major complications were recorded following the procedure. A recent systematic review of 26 studies by Zhang *et al.* reports a complication rate of 13%.[20] The majority of complications are minor and associated with arterial puncture and angiography.[2,17] Postembolization syndrome, characterized by transient abdominal pain, fever, nausea, and mild leukocytosis, is the most frequently reported complication, and it can be effectively managed using analgesic and anti-inflammatory medications. Other complications, such as neuropathy and organ ischemia/uterine infarction, are rare.[20] The effects of UAE on fertility and subsequent pregnancy outcomes have not been sufficiently studied to date, and most fertility outcomes derive from UAE in the case of uterine fibroma.[4] Existing literature reports no adverse effect on fertility in women who underwent pelvic arterial embolization in the majority of cases (91-100%).[6] Hardeman *et al.* demonstrated no significant difference in fertility outcomes between patients who underwent UAE for severe PPH and those who did not undergo the procedure.[23] However, some authors suggest that there may be associated with a slightly increased recurrence rate of PPH and a higher risk of first-trimester miscarriage in subsequent pregnancies.[4,5] Although endovascular embolization preserves fertility compared to hysterectomy, further research is needed to observe the long-term effect on uterine function and future pregnancy outcomes.[6-8,12]

Conclusions

Our study findings suggest that UAE is a safe and effective procedure for managing severe uterine cavity bleeding in PPH or pregnancy termination hemorrhage, as well as for reducing the risk of hemorrhage during surgical removal of highly vascularized RPOC, placental abnormalities in pregnancy termination /delivery and cervical pregnancy termination. It is a minimally invasive, uterine-sparing alternative to radical surgical treatment with hysterectomy and a promising option for patients desiring future fertility. Early cooperation between gynecologists/obstetricians and interventional radiologists may improve the clinical outcomes of UAE. The shortcoming of this study is the lack of long-term follow up to access the effect of UAE on fertility and subsequent pregnancy outcomes comprehensively.

Acknowledgement

Authorship contribution statement
(Contributor Roles Taxonomy, CRediT)
Polona Vihtelic: Writing – original draft, Writing – review & editing, Investigation. Eva Skuk: Writing – review & editing, Investigation, Project administration. Nataša Kenda Suster: Conceptualization, Resources, Writing – review & editing, Supervision, Validation. Marina Jakimovska Stefanovska: Supervision, Resources. Peter Popovič: Conceptualization, Methodology, Investigation, Writing – review & editing, Supervision.

References

1. Brown M, Hong M Jr, Lindquist J. Uterine artery embolization for primary postpartum hemorrhage. *Tech Vasc Interv Radiol* 2021; **24:** 100727. doi: 10.1016/j.tvir.2021.100727
2. Spreu A, Abgottspon F, Baumann MU, Kettenbach J, Surbek D. Efficacy of pelvic artery embolisation for severe postpartum hemorrhage. *Arch Gynecol Obstet* 2017; **296:** 1117-24. doi: 10.1007/s00404-017-4554-y
3. Jiang J, Wang C, Xue M. High-intensity focused ultrasound versus uterine artery embolization for patients with retained placenta accreta. *Eur J Obstet Gynecol Reprod Biol* 2020; **252:** 82-6. doi: 10.1016/j.ejogrb.2020.06.003
4. Radan AP, Schneider S, Zdanowicz JA, Raio L, Mertineit N, Heverhagen JT, et al. Obstetrical and fertility outcomes following transcatheter pelvic arterial embolization for postpartum hemorrhage: a cohort follow-up study. *Life* 2022; **12:** 892. doi: 10.3390/life12060892
5. Lindquist JD, Vogelzang RL. Pelvic artery embolization for treatment of postpartum hemorrhage. *Semin Intervent Radiol* 2018; **35:** 41-7. doi: 10.1055/s-0038-1636520
6. Bazeries P, Paisant-Thouveny F, Yahya S, Bouvier A, Nedelcu C, Boussion F, et al. Uterine artery embolization for retained products of conception with marked vascularity: a safe and efficient first-line treatment. *Cardiovasc Intervent Radiol* 2017; **40:** 520-9. doi: 10.1007/s00270-016-1543-7
7. Ohmaru-Nakanishi T, Kuramoto K, Maehara M, Takeuchi R, Oishi H, Ueoka Y. Complications and reproductive outcome after uterine artery embolization for retained products of conception. *J Obstet Gynaecol Res* 2019; **45:** 2007-14. doi: 10.1111/jog.14067
8. Kimura Y, Osuga K, Nagai K, Hongyo H, Tanaka K, Ono Y, et al. The efficacy of uterine artery embolization with gelatin sponge for retained products of conception with bleeding and future pregnancy outcomes. *CVIR Endovasc* 2020; **3:** 13. doi: 10.1186/s42155-020-00107-4

9. Kerns J, Steinauer J. Management of postabortion hemorrhage: release date November 2012 SFP Guideline #20131. *Contraception* 2013; **87:** 331-42. doi: 10.1016/j.contraception.2012.10.024

10. Bouyer J, Coste J, Fernandez H, Pouly JL, Job-Spira N. Sites of ectopic pregnancy: a 10 year population-based study of 1800 cases. *Hum Reprod* 2002; **17:** 3224-30. doi: 10.1093/humrep/17.12.3224

11. Vela G, Tulandi T. Cervical pregnancy: the importance of early diagnosis and treatment. *J Minim Invasive Gynecol* 2007; **14:** 481-4. doi: 10.1016/j.jmig.2006.11.012

12. Vitale SG, Parry JP, Carugno J, Cholkeri-Singh A, Della Corte L, Cianci S, et al. Surgical and reproductive outcomes after hysteroscopic removal of retained products of conception: a systematic review and meta-analysis. *J Minim Invasive Gynecol* 2021; **28:** 204-17. doi: 10.1016/j.jmig.2020.10.028

13. Lukinovic N, Malovrh EP, Takac I, Sobocan M, Knez J. Advances in diagnostics and management of gestational trophoblastic disease. *Radiol Oncol* 2022; **56:** 430-9. doi: 10.2478/raon-2022-0038

14. Cerovac A, Ljuca D, Arnautalic L, Habek D, Bogdanovic G, Mustedanagic-Mujanovic J, Grgic G. Efficacy of transvaginal ultrasound versus magnetic resonance imaging for preoperative assessment of myometrial invasion in patients with endometrioid endometrial cancer: a prospective comparative study. *Radiol Oncol* 2022; **56:** 37-45. doi: 10.2478/raon-2022-0005

15. De Winter J, De Raedemaecker H, Muys J, Jacquemyn Y. The value of postpartum ultrasound for the diagnosis of retained products of conception: a systematic review. *Facts Views Vis Obgyn* 2017; **9:** 207-16. PMID: 30250654

16. Noonan JB, Coakley FV, Qayyum A, Yeh BM, Wu L, Chen LM. MR imaging of retained products of conception. *AJR Am J Roentgenol* 2003; **181:** 435-9. doi: 10.2214/ajr.181.2.1810435

17. Rand T, Patel R, Magerle W, Uberoi R. CIRSE standards of practice on gynaecological and obstetric haemorrhage. *CVIR Endovasc* 2020; **3:** 85. doi: 10.1186/s42155-020-00174-7

18. Heaston DK, Mineau DE, Brown BJ, Miller FJ Jr. Transcatheter arterial embolization for control of persistent massive puerperal hemorrhage after bilateral surgical hypogastric artery ligation. *AJR Am J Roentgenol* 1979; **133:** 152-4. doi: 10.2214/ajr

19. Filippiadis DK, Binkert C, Pellerin O, Hoffmann RT, Krajina A, Pereira PL. Cirse quality assurance document and standards for classification of complications: the Cirse Classification System. *Cardiovasc Intervent Radiol* 2017; **40:** 1141-6. doi: 10.1007/s00270-017-1703-4

20. Zhang XQ, Chen XT, Zhang YT, Mai CX. The emergent pelvic artery embolization in the management of postpartum hemorrhage: a systematic review and meta-analysis. *Obstet Gynecol Surv* 2021; **76:** 234-44. doi: 10.1097/OGX.0000000000000887

21. Lee HY, Shin JH, Kim J, Yoon HK, Ko GY, Won HS, et al. Primary postpartum hemorrhage: outcome of pelvic arterial embolization in 251 patients at a single institution. *Radiology* 2012; **264:** 903-9. doi: 10.1148/radiol.12111383

22. Sugai S, Nonaka T, Tamegai K, Sato T, Haino K, Enomoto T, et al. Successful repeated uterine artery embolization in postpartum hemorrhage with disseminated intravascular coagulation: a case report and literature review. *BMC Pregnancy Childbirth* 2021; **21:** 710. doi: 10.1186/s12884-021-04191-9

23. Hardeman S, Decroisette E, Marin B, Vincelot A, Aubard Y, Pouquet M, et al. Fertility after embolization of the uterine arteries to treat obstetrical hemorrhage: a review of 53 cases. *Fertil Steril* 2010; **94:** 2574-9. doi: 10.1016/j.fertnstert.2010.02.052

research article

Analysis of magnetic resonance contrast agent entrapment following reversible electroporation *in vitro*

Marko Strucic[1], Damijan Miklavcic[1], Zala Vidic[1], Maria Scuderi[1], Igor Sersa[2], Matej Kranjc[1]

[1] Faculty of Electrical Engineering, University of Ljubljana, Ljubljana, Slovenia
[2] Jožef Stefan Institute, Ljubljana, Slovenia

Radiol Oncol 2024; 58(3): 406-415.

Received 31 July 2024
Accepted 9 August 2024

Correspondence to: Assist. Prof. Matej Kranjc, Ph.D., University of Ljubljana, Faculty of Electrical Engineering, Tržaška c 25, SI-1000 Ljubljana, Slovenia. E-mail: matej.kranjc@fe.uni-lj.si

Disclosure: No potential conflicts of interest were disclosed.

Background. Administering gadolinium-based contrast agent before electroporation allows the contrast agent to enter the cells and enables MRI assessment of reversibly electroporated regions. The aim of this study was evaluation of contrast agent entrapment in Chinese hamster ovary (CHO) cells and comparison of these results with those determined by standard *in vitro* methods for assessing cell membrane permeability, cell membrane integrity and cell survival following electroporation.

Materials and methods. Cell membrane permeabilization and cell membrane integrity experiments were performed using YO-PRO-1 dye and propidium iodide, respectively. Cell survival experiments were performed by assessing metabolic activity of cells using MTS assay. The entrapment of gadolinium-based contrast agent gadobutrol inside the cells was evaluated using T_1 relaxometry of cell suspensions 25 min and 24 h after electroporation and confirmed by inductively coupled plasma mass spectrometry.

Results. Contrast agent was detected 25 min and 24 h after the delivery of electric pulses in cells that were reversibly electroporated. In addition, contrast agent was present in irreversibly electroporated cells 25 min after the delivery of electric pulses but was no longer detected in irreversibly electroporated cells after 24 h. Inductively coupled plasma mass spectrometry showed a proportional decrease in gadolinium content per cell with shortening of T_1 relaxation time ($R^2 = 0.88$ and $p = 0.0191$).

Conclusions. Our results demonstrate that the contrast agent is entrapped in cells exposed to reversible electroporation but exits from cells exposed to irreversible electroporation within 24 h, thus confirming the hypothesis on which detection experiments *in vivo* were based.

Key words: electroporation; membrane permeabilization; magnetic resonance contrast agent; T_1 relaxometry

Introduction

Exposure of cells to short high-voltage electric pulses, if sufficiently high, can cause an increase of cell membrane permeability. This phenomenon, known as electroporation, allows transport of otherwise impermeable molecules (including hydrophilic molecules, such as chemotherapeutic drugs, and large molecules, such as RNA, DNA, etc.) across the membrane. If the cell membrane reseals after exposure to electric pulses, molecules remain entrapped inside the cell. This phenomenon is termed reversible electroporation, if cells preserve their viability.[1] Cell membrane electroporation can also result in cell death, which is known as irreversible electroporation.[2,3] In medicine, electroporation-based treatments and therapies utilize reversible electroporation in electrochemotherapy and gene elec-

trotransfection treatments, while irreversible electroporation is used as tissue ablation treatment.[4-6]

Electroporation can be considered a threshold phenomenon, i.e. if a specific cell is exposed to an electric field above certain value using set pulse parameters, it will determine both whether electroporation occurs and reversibility of this phenomenon.[7-10] Thresholds are simplified concepts assuming electroporation to be a discrete phenomenon. However, cell membrane permeability changes due to exposure to electric field are continuous and depend on the strength of electric field and exposure time.[11,12] It has also been shown that for different cell types[13,14] tissue type[11,15] and different pulse protocols[16-18] different electric field strengths values are needed, i.e. different threshold apply. Successful outcome of both reversible electroporation[19] and irreversible electroporation[20] is thus not easy to predict.

Electroporation *in vitro* can be determined using various methods, including voltage clamp techniques[21], microscopy[22] and most commonly, by detecting a reporter molecule due to increase of molecular transport across the membrane.[23] Latter detection methods are often based on exogenous reporter molecules (propidium iodide, trypan blue, lucifer yellow) and on functional molecules that can be detected inside the cell (DNA, RNA) or cause cell death (cisplatin, bleomycin).[23] In contrast, determining electroporation *in vivo* has proven to be more challenging, with fewer available methods. Electric field distribution is difficult to predict *in vivo*[24-26] and electroporation treatment outcome becomes evident weeks after the treatment.[27-29] One of potentially interesting approaches proposed is using hydrophilic gadolinium-based contrast agent (CA) to visualize reversible electroporation *in vivo* using MRI.[30,31] When CA is administered prior to electroporation, CA can enter the cell during electroporation and become entrapped once the cell membrane reseals, i.e. in reversibly electroporated cells. After CA is washed from the body a decrease of T_1 relaxation times in areas where CA is entrapped can be visualized using MRI.[30,31] This approach was successfully used on follow up studies to assess reversibly electroporated regions *in vivo*[7,31,32], however, the hypothesis on which this approach is based have not yet been evaluated *in vitro*. Therefore, in our study, we focused on the *in vitro* evaluation of CA entrapment in cells exposed to different amplitudes of electric pulses to achieve either reversible or irreversible electroporation. We compared these results with those obtained using standard *in vitro* methods: YO-PRO-1 dye for assessing cell membrane permeability due to electroporation, propidium iodide fluorescent dye for cell membrane integrity, and the MTS assay for cell survival assessment.

Materials and methods

An overview of the time sequence of different experiments performed in the study is shown in Figure 1. Permeabilization experiments were performed using YO-PRO-1 dye which was added before the delivery of electric pulses and the presence of YO-PRO-1 inside the cells was determined immediately after pulse delivery. Cell survival was determined 24 h after pulse delivery by MTS assay. Gadolinium-based contrast agent (CA) gadobutrol was added before delivery of electric pulses for the rest of the experiments. Cell membrane integrity was assessed 25 min after pulse delivery with propidium iodide. At the same time point, the presence of CA inside of the cells was evaluated using inductively coupled plasma mass spectrometry (ICP-MS). CA detection in cell suspensions using T_1 relaxometry was performed 25 min and 24 h after pulse delivery.

Cell preparation

Chinese hamster ovary (CHO-K1) cell line was obtained from the European Collection of Authenticated Cell Cultures (ECACC, cat. no. 85051005). Cells were grown in F-12 Ham nutrient mixture (cat. no. N6658, Sigma-Aldrich, MO, United States) supplemented with 10% fetal bovine serum (FBS, cat. no. F9665, Sigma-Aldrich), 1 U/ml penicillin/streptomycin (cat. no. P0781, Sigma-Aldrich) and 50 μg/ml gentamycin (cat. no. G1397, Sigma-Aldrich) (i.e. complete growth medium) at 37°C in a humidified, 5% CO_2 atmosphere. For the experiment, cells were detached with trypsin solution 10 × trypsin-EDTA (PAA, Leonding, Austria) and 1:9 diluted in Hank's basal salt solution (StemCell, BC, Canada). After cells were detached, trypsin was inactivated by complete growth medium. Cells were transferred to a 50 ml centrifuge tube and centrifuged 5 min at 200 g at room temperature. The supernatant was aspirated, and cells were resuspended Dulbecco's Modified Eagle Medium (DMEM, cat. no. D5671, Sigma-Aldrich) supplemented with 10% fetal bovine serum (FBS, cat. no. F9665, Sigma-Aldrich), 1 U/ml penicillin/streptomycin (cat. no. P0781, Sigma-Aldrich) and 50 μg/ml gentamycin (cat. no. G1397, Sigma-Aldrich) (i.e.

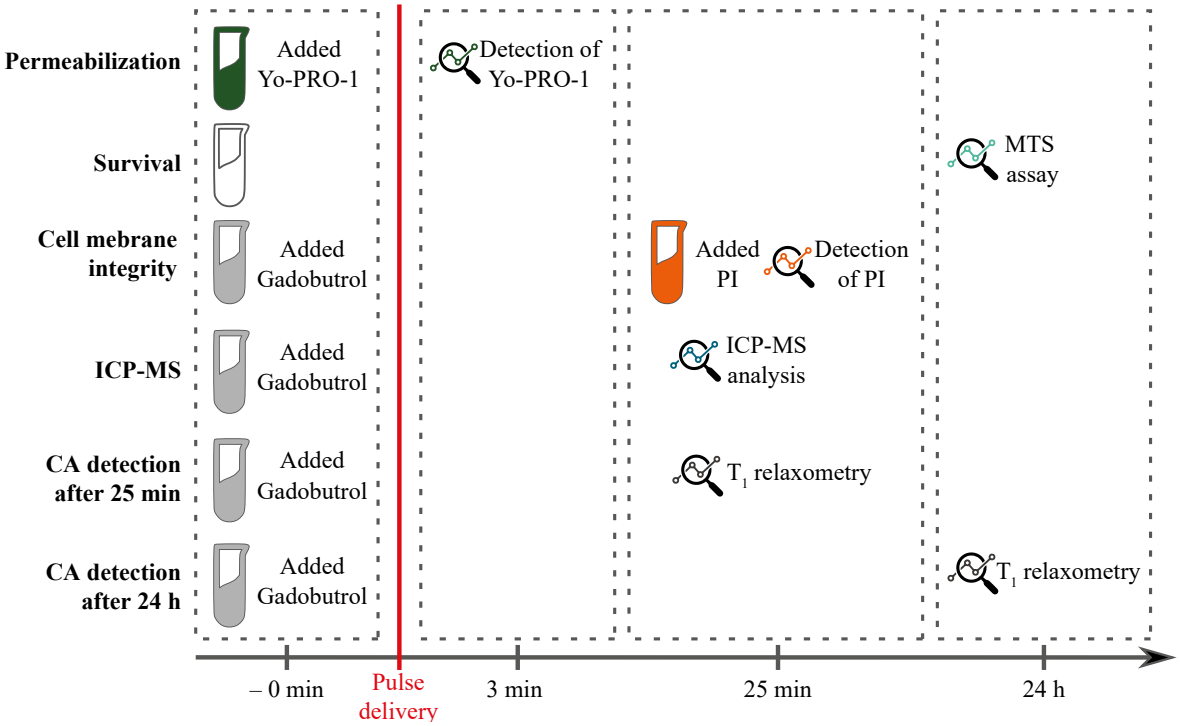

FIGURE 1. An overview of the time sequence of experiments. Red line represents a moment of pulse delivery. For cell membrane integrity, inductively coupled plasma mass spectrometry (ICP-MS), and Gadolinium-based contrast agent (CA) detection experiments gadobutrol was added to cell suspension prior to pulse delivery. Analyses were performed at different time points as indicated in the figure.

PI = Propidium iodide

electroporation medium) as in Vižintin *et al*., 2021.[17] Such medium was used for permeability assay and ICP-MS, while for other assays also 10 mM HEPES buffer (cat. no. H3375, Sigma-Aldrich) was added to electroporation medium. Cell volume fraction of 7% corresponding to the final concentration of 8.9×10^7 cells/ml was used in all experiments.

Delivery of electric pulses

For delivery of electric pulses 150 µl of cell suspension was transferred to cuvette with parallel aluminum plate electrodes (d = 2 mm, VWR, Radnor, PA, USA). Pulse protocol (8 pulses of 100 µs, delivered at a pulse repetition rate of 1 Hz) was delivered with the prototype pulse generator L-POR V0.1 (mPOR, Ljubljana, Slovenia). Delivery of electroporation pulses was monitored using HDO6000 high-definition oscilloscope (Teledyne LeCroy, Chestnut Ridge, NY, USA), a high-voltage differential probe HVD3605A (Teledyne LeCroy) and current probe CP031 (Teledyne LeCroy). Electric field (E) was calculated as E = U/d where d equals distance between aluminum plate electrodes in cuvettes (2 mm) and U equals delivered voltage. Pulse delivery parameters are presented in Table 1.

Permeabilization experiments

Prior to experiments, YO-PRO-1 (cat. no Y3603, Thermo Fisher Scientfic, Waltham, MA, USA) was added to sample to obtain the concentration of 1µM YO-PRO-1. After pulse delivery, 20 µl of the cell suspensions was transferred to a 1.5 ml centrifuge tube and incubated for 3 min at room temperature. After incubation, cells were diluted with 150 µL of fresh electroporation medium, and YO-PRO-1 uptake was detected with a flow cytometer (Attune NxT, Life Technologies, Carlsbad, CA, USA using blue LED laser (wavelength: 488 nm), and a 530/30 nm band-pass filter. The analysis of 10,000 events was performed by the Attune Nxt software. On the dot-plots of forward-scatter and side-scatter, cell debris and (cell) clusters were excluded from the analysis. Fluorescence intensity histograms were used to determine the percentage

of YO-PRO-1 permeabilized cells. Gating was set according to sham control (0 V).

MTS survival assay experiments

For survival experiments 25 min after pulse delivery, 10 µl of cell suspension was diluted in 4 mL Ham-F12 growth medium. After that, 100 µl of sample was transferred to 96-well plate in triplicates. Plates were incubated at 37°C in a humidified, 5% CO_2 atmosphere for 24 h. According to manufacturer's instructions (CellTiter 96 AQueous One Solution Cell Proliferation Assay, Promega, Madison, WI, USA), 20 µL of MTS tetrazolium compound was added to the samples, and after 2 h the absorbance of formazan (reduced MTS tetrazolium compound) was measured with a spectrofluorometer (Tecan Infinite M200, Tecan, Grödig, Austria) at 490 nm. The percentage of viable cells was obtained by the normalization of sample absorbance to the absorbance of the control (0 V).

Cell membrane integrity experiments

Prior to pulse delivery, cells were mixed with gadolinium-based contrast agent gadobutrol (Gadovist® 1.0 mM, Bayer, Leverkusen, Germany) to a final concentration of 22 mM, then 150 µl of sample was transferred to cuvettes. After pulse delivery, cells were incubated at room temperature for 25 min. After incubation, 20 µl of cell suspension was diluted in 150 µl of fresh growth medium. Propidium iodide (PI, cat. no BMS500PI, Thermo Fisher Scientfic) was then added to the sample to the final concentration of 100 µg/ml and cells were incubated at room temperature for another 5 min. This was followed by analysis of PI uptake on flow cytometer using blue LED laser (wavelength: 488 nm) and a 574/26 nm band-pass filter. The analysis of 10,000 events was performed by the Attune Nxt software. On the dot-plots of forward-scatter and side-scatter, cell debris and (cell) clusters were excluded from the analysis. Fluorescence intensity histograms were used to determine the percentage of PI permeabilized cells. Gating was set according to sham control (0 V).

Cell suspension preparation for gadolinium-based contrast agent detection experiments

Prior to pulse delivery, cells were mixed with gadobutrol (Gadovist® 1.0 mM, Bayer, Leverkusen, Germany) to a final concentration of 22 mM, then 150 uL of sample was transferred to cuvettes, 125 µl of the cell suspension was transferred to 5 ml of fresh growth medium 25 min after pulse delivery for the washing steps. Cells were centrifuged for 5 min at 900 g to separate the gadobutrol entrapped in the cells from the medium. Then medium was removed, and cells were resuspended in 2 ml of fresh growth medium, and the centrifugation step was repeated. This washing step was repeated two times. At the end cells were resuspended in 900 µl of fresh growth medium, to achieve 1% cell volume fraction for T_1 relaxometry analysis.

For CA detection experiments at 24 h after pulse delivery, same steps as described above were performed, however, after last centrifugation step cells were seeded in 20 ml of growth medium in T150 cell culture flasks (TPP, Switzerland) for 24 h at 37°C in a humidified 5% CO_2 atmosphere. Afterwards, growth medium from each culture flask was collected in 50 ml centrifuge tube. Cells were then detached with trypsin solution 10 × trypsin-EDTA (PAA) and 1:9 diluted in Hank's basal salt solution (StemCell). Trypsin was inactivated by fresh growth medium. Cells were then harvested and added to previously collected growth medium in a 50 ml centrifuge tube. The centrifugation step was then repeated as in the previous day and the cells were again resuspended in 900 µL of fresh growth medium for T_1 relaxometry analysis.

TABLE 1. Parameters of electric pulses used in experiments

Experiment	U [V]	E [kV/cm]	Single pulse duration [µs]	Pulse repetition rate [1/s]	Number of pulses [/]
Permeabilization	120–400	0.6–2.0	100	1	8
ICP-MS	120–280	0.6–1.4	100	1	8
Cell survival	160–600	0.8–3.0	100	1	8
Cell membrane integrity	160–600	0.8–3.0	100	1	8
CA detection experiments	160–600	0.8–3.0	100	1	8

CA = contrast agent; ICP-MS = inductively coupled plasma mass spectrometry

Gadolinium-based contrast agent detection experiments

Nuclear Magnetic Resonance (NMR) scanner was used for determining T_1 relaxation times of cell suspensions. NMR scanner included a 2.35 T horizontal bore superconducting magnet with resonant proton frequency of 100 MHz

(Oxford Instruments, Abingdon, UK) connected to a Redstone spectrometer (Tecmag, Houston TX, USA) and equipped with microimaging accessories with maximum gradients of 250 mT/m (Bruker, Ettlinger, Germany). T_1 relaxometry was performed using inverse recovery spectroscopic pulse sequence in multiple points along the z axis of the sample with variable repetition rates. Relaxation times were then calculated from the signal intensities in OriginPRO 2024 (OriginLab Corporation, Northampton, MA, USA) using 3 parameter exponential fitting curve using fitting function: $M_z = M_0 - \Delta M e^{-TR/T_1}$, where M_z is measured longitudinal magnetization, M_0 is initial longitudinal magnetization at equilibrium, ΔM is the maximum magnetization difference from equilibrium, TR is repetition time and T_1 is longitudinal relaxation time.

Inductively coupled plasma mass spectrometry experiments

For determination of intracellular concentration of gadolinium (Gd), the cell pellet with 1 x10^7 cells was separated from the supernatant after electroporation and analyzed using inductively coupled plasma mass spectrometry (ICP-MS). To aid sample digestion, 0.1 ml of H_2O_2 and 0.1 ml of HNO_3 (both from Merck, Darmstadt, Germany), were added to the cell pellets. The tubes were then sealed with caps and Teflon tape and left overnight at 80°C. Following digestion, 1.8 ml of Milli-Q water (Direct-Q 5 Ultrapure water system; Merck Millipore, MA, USA) was added. Gadolinium in samples was then measured using ICP-MS (7900 ICP-MS; Agilent Technologies, California, USA) with Gadolinium ICP standard (cat. no. 170318, Merck) used as an internal standard during the measurement. To determine the amount of Gd per cell, the number of cells in the pellet was divided with the measured Gd in the cell pellet of each sample. Control samples (cells which were not electroporated and were not incubated with gadobutrol) were used for blank subtraction for all gadobutrol-treated samples. To reduce cross-contamination of the instrument during the measurement, a mixture containing 1% HNO_3 and 1% HCl (Merck) was used as a rinse between the sample runs.

Statistical analysis

Significant differences were evaluated by the Welch Two Sample t-test at a significance level of 95% ($p < 0.05$). Statistical analysis was performed using MATLAB 2021b (MathWorks, Natick, MA, USA).

Results

In our study we tested the hypothesis that contrast agent (CA) is entrapped inside reversibly electroporated cells. Measurement results of CA by T_1 relaxometry and inductively coupled plasma mass spectrometry (ICP-MS) in cells *in vitro* were compared to results obtained by established methods for assessing cell membrane permeabilization, cell membrane integrity and cell survival. As expected, CA was detected 25 min and 24 h after the delivery of electric pulses in cells that were reversibly electroporated. In addition, CA was present in irreversibly electroporated cells 25 min after the delivery of electric pulses but was no longer detected in irreversibly electroporated cells after 24 h.

Permeabilization and survival

As shown in Figure 2, results of permeabilization experiments using YO-PRO-1 dye show increase in cell membrane permeability with increased pulse amplitude starting between 0.6 and 0.8 kV/cm at which 32.88 ± 3.93% of CHO cells were permeabilized, while at 1.2 kV/cm nearly all cells (96.99 ± 0.45%) in cell suspension were permeabilized. Cell survival, as determined by MTS assay performed at 24 h after the delivery of electric pulses, shows 61.61 ± 12.44% of cells survived when exposed to the electric field of 2.0 kV/cm. Survival at higher pulse amplitudes further decreased. Using these results, the range of electric fields which predominantly cause reversible electroporation was set between 0.8 kV/cm and 2.0 kV/cm (gray shaded area in Figure 2).

Cell membrane integrity

Cell membrane integrity was determined by adding propidium iodide to cell suspensions 25 min after pulse delivery and measuring propidium iodide inside CHO cells by flow cytometry (Figure 3, dotted curve). Propidium iodide uptake into the cells after membrane resealing showed that majority of cells can restore membrane integrity at electric fields lower than 0.8 kV/cm up to which only 1.80 ± 0.26% were stained with propidium iodide. While at electric fields above 2.0 kV/cm cell membrane integrity was no longer restored in 46.34 ± 16.62% of cells (Figure 3, dotted curve). For com-

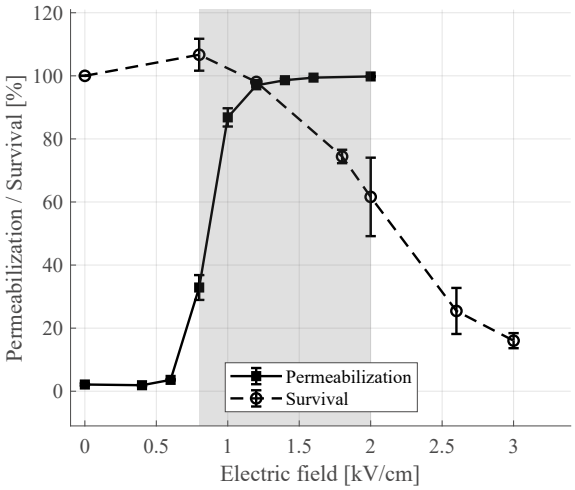

FIGURE 2. Cell membrane permeabilization (solid black line) and cell survival (dashed black line) of Chinese hamster ovary (CHO) cells in relation to applied electric field. Cell membrane permeabilization and cell survival experiments were performed using YO-PRO-1 dye and by assessing metabolic activity of cells using MTS assay, respectively. Each data point presents a mean ± standard deviation (vertical bars) of 3 repetitions. For permeabilization results gating was set according to sham control without applied electric field. Survival results are normalized to the control sample without applied electric field. Area shaded in gray represents range of electric fields which predominantly cause reversible electroporation of cells.

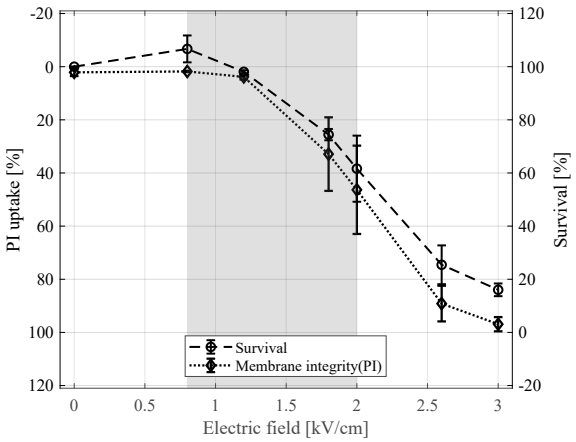

FIGURE 3. Cell membrane integrity experiment determined by adding propidium iodide dye 25 min after pulse delivery and cell survival determined by MTS assay 24 h after pulse delivery in relation to applied electric field. Each data point presents a mean ± standard deviation (vertical bars) of 3 repetitions. For cell membrane integrity results gating was set according to sham control without applied electric field. Survival results are normalized to the control sample without applied electric field and with added 22 μM of gadobutrol. Note the reversed (upside -down) scale of propidium iodide (PI) uptake for easier comparison. Area shaded in gray represents range of electric fields which predominantly cause reversible electroporation of cells.

parison, a cell survival curve obtained by MTS assay at 24 h from Figure 2 is added in Figure 3 (dashed curve).

T_1 relaxation times

T_1 relaxation times of cell suspensions measured 25 mins after the delivery of electric pulses, began to shorten at 0.8 kV/cm compared to the control and continued to decrease until reaching a plateau at electric field of 1.8 kV/cm (Figure. 4 dashed line). T_1 relaxation times of cell suspensions, measured 24 h after the delivery of electric pulses (Figure 4 solid line), showed a similar shortening of T_1 relaxation times as observed when measured 25 min after pulse delivery up to an applied electric field of 1.8 kV/cm. However, from 1.8 kV/cm up to 3 kV/cm, T_1 relaxation times of cells measured 24 h after the delivery of electric pulses started to increase compared to cells measured at 25 min (Figure 4).

Inductively coupled plasma mass spectrometry

To confirm presence of CA (gadobutrol) inside CHO cells after electroporation, inductively cou-

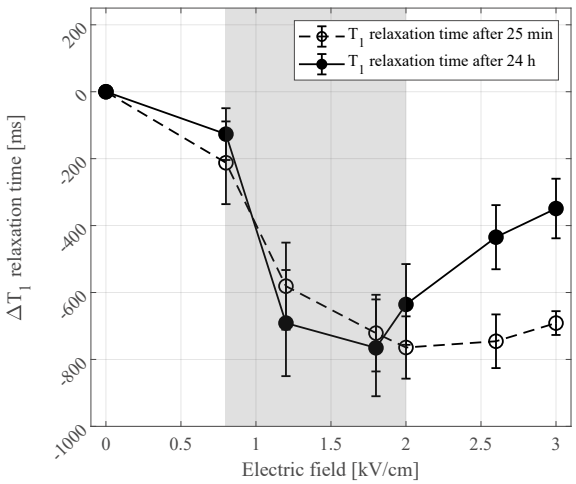

FIGURE 4. Change in T_1 relaxation times obtained from CHO cells 25 mins (dashed line) and 24 h (solid line) after pulse delivery. Each data point presents a mean ± standard deviation (vertical bars) of 3 repetitions. Comparison of T_1 relaxation times obtained 25 mins and 24 h after electroporation (EP) is normalized to control sample,i.e. cell suspension with added 22 μM gadobutrol and without exposure to an electric field. Asterisks (*) indicate statistically significant differences ($p < 0.05$) between T_1 relaxation time curves obtained 25 min and 24 h after pulse delivery. Area shaded in gray represents a range of electric fields which predominantly cause reversible electroporation of cells.

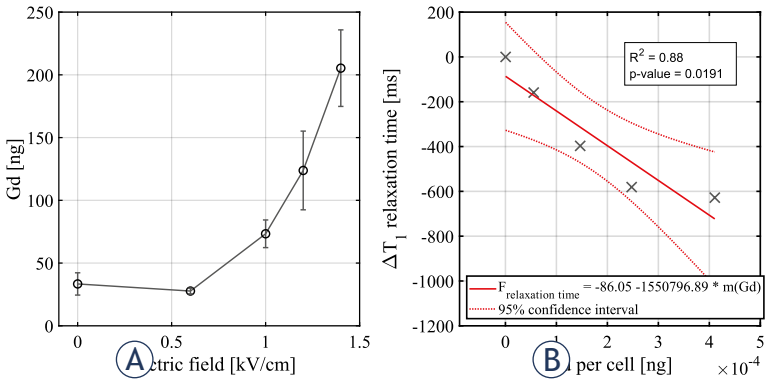

FIGURE 5. Mass of gadolinium per cell in relation to applied electric field 25 min after pulse delivery. Each data point presents a mean ± standard deviation (vertical bars) of 3 repetitions **(A)**. Linear regression fitting of T1 relaxation time in relation to mass of gadolinium per cell. Each symbol represents a point extrapolated from T1 relaxometry results 25 min after pulse delivery **(B)**.

pled plasma mass spectrometry (ICP-MS) analysis was performed 25 min after pulse delivery. Results showed Gd (a paramagnetic core of gadobutrol) was present in increased quantities in cells exposed to electric fields ranging from 0.6 kV/cm to 1.4 kV/cm (Figure 5A). Note that electric field of 1.4 kV/cm, 100% permeabilization was achieved, while cell survival remained unaffected (Figure 2). Based on these results, the gadolinium content per cell was determined by dividing measured gadolinium mass by the number of cells ($1x10^7$) in the pellet. Change in T_1 relaxation times were extrapolated from T_1 relaxometry experiment performed 25 min after pulse delivery. As shown in Figure 5B, linear regression analysis showed a proportional decrease in gadolinium content per cell with shortening of T_1 relaxation time (R^2 = 0.88 and p-value = 0.0191).

Discussion

Gadolinium-based contrast agent gadobutrol (CA) is unable to enter cells under physiological conditions and are rapidly eliminated from the body. The mean elimination half-life of gadobutrol is 1.8 h, which corresponds to the renal elimination rate in healthy individuals. CA are traditionally used in magnetic resonance imaging to increase sensitivity and specificity of diagnostic images enhancing regions with increased perfusion and edema.[33] However, if CA is present in tissue prior to electroporation it can enter cells after pulse delivery and remain entrapped inside reversibly electroporated cells which has been used as threshold determinant in several *in vivo* studies.[30,31,34] Entrapped CA can be detected 24 h – 72 h after injection of CA and electroporation *in vivo*, after remaining CA, i.e. extracellular CA has been eliminated from the body.

In this study, we tested the basic assumption of CA entrapment *in vitro* using CHO cells exposed to different amplitudes of electric pulses. To evaluate CA entrapment in relation to reversible and irreversible electroporation, CA detection by T_1 relaxometry and ICP-MS findings were compared to results obtained from established methods for assessing cell membrane permeabilization, cell membrane integrity and cell survival, i.e. for determining range of reversible electroporation. Thus, determined electric fields for CA uptake detection experiments were ranging from 0.8 kV/cm, where the first significant permeabilization was detected, to 3.0 kV/cm, where cell survival was no longer expected according to cell survival results (Figure 2). The presence of CA in cells was also confirmed by inductively coupled plasma mass spectrometry (ICP-MS) (Figure 5).

Cell membrane permeability determined by the YO-PRO-1 dye reached a plateau within the range of electric fields from 1.0 kV/cm to 1.2 kV (Figure 2). Conversely, results obtained from ICP-MS experiments show increasing amounts of Gd up to an electric field of 1.4 kV/cm (Figure 5A). We therefore extended our investigation by comparing the results of permeabilization and CA detection experiments to higher pulse amplitudes. Comparison showed plateau from T_1 relaxometry results is shifted towards higher electric fields between 1.2 kV/cm and 1.8 kV/cm (Figure 4) compared to permeabilization results. The observed plateau shift could indicate different kinetics of transmembrane transport for different molecules. But it is also important to consider the methodology used in permeabilization experiments. In permeabilization experiments we determined a fraction of permeabilized cells, i.e. YO-PRO-1 positive cells in suspension, whereas in both ICP-MS and T_1 relaxation experiments, the presence of total CA in suspension was determined, allowing accumulation of CA in individual cells at electric fields above those needed for permeabilization of all cells, which can have an additional impact on the T_1 relaxation time shortening.

Interestingly, T_1 relaxation times at 25 min after pulse delivery remained decreased even at higher electric fields than irreversible threshold, e.g. at 2.6 kV/cm and 3.0 kV/cm (Figure 4), suggesting pres-

ence of CA even in cells that are irreversibly electroporated. The MTS survival assay performed 24 h after electroporation showed most cells exposed to electric field between 2.6 kV/cm and 3.0 kV/cm die due to irreversible electroporation (Figure 2). To investigate if the presence of CA in cells exposed to irreversible electroporation is related to transient membrane resealing before eventual cell death, evaluation of cell membrane integrity using propidium iodide was performed 25 min after pulse delivery. The results of cell membrane integrity experiments show good agreement with MTS survival assay (Figure 3) which confirmed lack of cell membrane integrity of cells exposed to irreversible electroporation at 25 min after pulse delivery. Note the cell death can be delayed which is related to varying levels of membrane damage after electroporation.[35] The results of our study with respect to cell membrane integrity are also in agreements with the reported times of 10–15 min for cell membrane resealing for pulse amplitudes in ranges of reversible electroporation.[36-39] Thus, entrapped CA is unable to exit reversibly electroporated cells after 25 min but should be able to exit irreversibly electroporated cells. Since presence of CA in cells exposed to electric fields in range of irreversible electroporation at 25 min cannot be explained by transient resealing (Figure 4, dashed line from 2.6 kV/cm), CA transport kinetics across the membrane could provide an answer.

When comparing transport kinetics of CA across membrane and transport kinetics of fluorescent dyes of similar size such as YO-PRO-1, it is important to consider the importance of size and charge of molecule in question.[40] The transport of neutral CA molecules across the membrane is governed solely by chemical gradients, while the transport of positively charged YO-PRO-1 molecules across the membrane is governed by electrochemical gradient i.e. in addition to the concentration gradient transport is facilitated by the transmembrane voltage. These differences in driving forces of CA and YO-PRO-1 into the cell could also explain for plateau from CA detection experiments being shifted towards higher electric fields compared to plateau obtained from permeabilization experiments. We performed additional T_1 relaxation measurements at 24 h after pulse delivery, i.e. at the same time when survival studies were performed. Results of CA detection after 24 h showed smaller decrease of T_1 relaxation times in range of irreversible electroporation (at 2.6 kV/cm and at 3.0 kV/cm) compared to results at 25 min after pulse delivery. This smaller decrease of T_1 relaxation time indicates that there was less CA present in suspensions that were exposed to higher electric fields 24 h after delivery of electric pulses. To further evaluate kinetics of CA transport across the membrane, average intracellular concentration of CA, at electric fields where plateau is reached (above 1.2 kV/cm), was calculated by combining relaxivity value of CA, T_1 relaxation time of the control, T_1 relaxation time of sample of interest and known cell volume fraction. We determined the average intracellular concentration of CA is approximately 1 μmol/L which is an order of magnitude lower compared to concentration of CA in electroporation medium (22 μmol/L). This can explain that exit of CA from cells is slower compared to its entry into the cell due to lower chemical gradient i.e. smaller difference in CA concentrations. Moreover, since transport of CA across the membrane is governed by chemical gradient only, transport occurs in both directions (i.e. extra- to intracellular during the initial phase immediately after electroporation and intra- to extracellular after CA washing and cell having membrane integrity compromised).

Electroporation outcome can reliably be assessed by evaluating temporary increase in cell membrane permeability using hydrophilic fluorescent dyes such as YO-PRO-1 and propidium iodide.[23,41] However, this method can only be applied *in vivo* through histological analysis of treated tissue after animal euthanasia, making it unfavourable to use for investigations *in vivo*. Also, both YO-PRO-1 and propidium iodide bind to the nucleic acids once inside the cell, preventing them from exiting the cell even if the cell membrane is not resealed. This renders them ineffective in distinguishing between reversible and irreversible electroporation. Furthermore, difficult assessment of electric fields *in situ*[42], is hindering clinical implementation of electroporation-based therapies and treatments despite great efforts and advancements in treatment planning.[43,44] In contrast, the CA entrapment method of electroporation threshold detection employs similar concepts to fluorescent dye use for detecting changes in cell membrane permeability *in vitro* and can be imaged noninvasively using MRI scanner. Given that numerous factors affect cell membrane electroporation, including pulse characteristics and cell types, additional studies involving different cell models and pulse protocols are warranted to validate the universality of the CA entrapment method for electroporation detection. Nevertheless, the applicability of CA entrapment detection in clinical settings in future seems feasible, given the safety of CAs, as

their surrounding chelate cage prevents interaction with biological structures.[45] Nonetheless, further research on the safety of CAs in intracellular environment is needed.

Acknowledgments

This research was funded by Slovenian Research and Innovation Agency (ARIS) research core funding No. P2-0249 and Junior Researcher funding for MS. The work was performed within the network of the research and infrastructural center of the University of Ljubljana, which is financially supported by the Slovenian Research Agency through infrastructural grant I0-0022. This article and research behind it would not be possible without our colleagues Janez Ščančar and Stefan Marković at Jožef Stefan Institute, Department of Environmental Sciences, whose contributions are greatly appreciated. Further, we would like to acknowledge Tamara Polajžer from Faculty of Electrical Engineering, University of Ljubljana for insightful comments.

References

1. Kotnik T, Rems L, Tarek M, Miklavčič D. Membrane electroporation and electropermeabilization: Mechanisms and models. *Annu Rev Biophys* 2019; **48:** 63-91. doi: 10.1146/annurev-biophys-052118-115451
2. Batista Napotnik T, Polajžer T, Miklavčič D. Cell death due to electroporation – a review. *Bioelectrochemistry* 2021; **141:** 107871. doi: 10.1016/j.bioelechem.2021.107871
3. Aycock KN, Davalos RV. Irreversible electroporation: background, theory, and review of recent developments in clinical oncology. *Bioelectricity*. 2019; **1:** 214-34. doi: 10.1089/bioe.2019.0029
4. Yarmush ML, Golberg A, Serša G, Kotnik T, Miklavčič D. Electroporation-based technologies for medicine: principles, applications, and challenges. *Annu Rev Biomed Eng* 2014; **16:** 295-320. doi: 10.1146/annurev-bioeng-071813-104622
5. Verma A, Haines DE, Boersma LV, Sood N, Natale A, Marchlinski FE, et al. Pulsed field ablation for the treatment of atrial fibrillation: PULSED AF pivotal trial. *Circulation* 2023; **147:**1422-32. doi: 10.1161/CIRCULATIONAHA.123.063988
6. Geboers B, Scheffer HJ, Graybill PM, Ruarus AH, Nieuwenhuizen S, Puijk RS, et al. High-voltage electrical pulses in oncology: irreversible electroporation, electrochemotherapy, gene electrotransfer, electrofusion, and electroimmunotherapy. *Radiology* 2020; **295:** 254-72. doi: 10.1148/radiol.2020192190
7. Čorović S, Mir LM, Miklavčič D. In vivo muscle electroporation threshold determination: Realistic numerical models and in vivo experiments. *J Membrane Biol* 2012; **245:** 509-20. doi: 10.1007/s00232-012-9432-8
8. Smerc R, Ramirez DA, Mahnic-Kalamiza S, Dermol-Cerne J, Sigg DC, Mattison LM, et al. A multiscale computational model of skeletal muscle electroporation validated using in situ porcine experiments. *IEEE Trans Biomed Eng* 2023; **70:** 1-12. doi: 10.1109/TBME.2022.3229560
9. Kos B, Mattison L, Ramirez D, Cindrič H, Sigg DC, Iaizzo PA, et al. Determination of lethal electric field threshold for pulsed field ablation in ex vivo perfused porcine and human hearts. *Front Cardiovasc Med* 2023; **10:** 1160231. doi: 10.3389/fcvm.2023.1160231
10. Cindric H, Mariappan P, Beyer L, Wiggermann P, Moche M, Miklavcic D, et al. Retrospective study for validation and improvement of numerical treatment planning of irreversible electroporation ablation for treatment of liver tumors. *IEEE Trans Biomed Eng* 2021; **68:** 3513-24. doi: 10.1109/TBME.2021.3075772
11. Pucihar G, Krmelj J, Reberšek M, Napotnik T, Miklavčič D. Equivalent pulse parameters for electroporation. *IEEE Trans Biomed Eng* 2011; **58:** 3279-88. doi: 10.1109/TBME.2011.2167232
12. Kotnik T, Frey W, Sack M, Haberl Meglič S, Peterka M, Miklavčič D. Electroporation-based applications in biotechnology. *Trends Biotechnol* 2015; **33:** 480-8. doi: 10.1016/j.tibtech.2015.06.002
13. Cemazar M, Jarm T, Miklavcic D, Macek Lebar A, Ihan A, Kopitar AN, et al. Effect of electric-field intensity on electropermeabilization and electrosensitivity of various tumor-cell lines in vitro. *Electro Magnetobiol* 1998; **17:** 263-2.
14. Dermol-Černe J, Miklavčič D, Reberšek M, Mekuč P, Bardet SM, Burke R, et al. Plasma membrane depolarization and permeabilization due to electric pulses in cell lines of different ex-citability. *Bioelectrochemistry* 2018; **122:** 103-14. doi: 10.1016/J.BIOELECHEM.2018.03.011
15. Jacobs IV EJ, Campelo SN, Charlton A, Altreuter S, Davalos R V. Characterizing reversible, irreversible, and calcium electroporation to generate a burst-dependent dynamic conductivity curve. *Bioelectrochemistry* 2024; **155:** 108580. doi: 10.1016/j.bioelechem.2023.108580
16. Vižintin A, Vidmar J, Ščančar J, Miklavčič D. Effect of interphase and inter-pulse delay in high-frequency irreversible electroporation pulses on cell survival, membrane permeabilization and electrode material release. *Bioelectrochemistry* 2020; **134:** 107523. doi: 10.1016/j.bioelechem.2020.107523
17. Vižintin A, Marković S, Ščančar J, Miklavčič D. Electroporation with nanosecond pulses and bleomycin or cisplatin results in efficient cell kill and low metal release from electrodes. *Bioelectrochemistry* 2021; **140:** 107798. doi: 10.1016/j.bioelechem.2021.107798
18. Potočnik T, Sachdev S, Polajžer T, Maček Lebar A, Miklavčič D. Efficient gene transfection by electroporation—In vitro and in silico study of pulse parameters. *Applied Sciences* 2022; **12:** 168237. doi: 10.3390/app12168237.
19. Jordan ET, Collins M, Terefe J, Ugozzoli L, Rubio T. Optimizing electroporation conditions in primary and other difficult-to-transfect cells. *J Biomol Tech* 2008; **19:** 328-34. PMID: 19183796
20. Jiang C, Davalos R V., Bischof JC. A review of basic to clinical studies of irreversible electroporation herapy. *IEEE Trans Biomed Eng* 2015; **62:** 4-20. doi: 10.1109/TBME.2014.2367543
21. Pakhomov AG, Shevin R, White JA, Kolb JF, Pakhomova ON, Joshi RP, et al. Membrane permeabilization and cell damage by ultrashort electric field shocks. *Arch Biochem Biophys* 2007; **465:** 109-18. doi: 10.1016/j.abb.2007.05.003
22. Sengel JT, Wallace MI. Imaging the dynamics of individual electropores. *Proc Natl Acad Sci U S A* 2016; **113:** 5281-6. doi: 10.1073/pnas.1517437113
23. Napotnik TB, Miklavčič D. In vitro electroporation detection methods - an overview. *Bioelectrochemistry* 2017; **120:** 166-82. doi: 10.1016/j.bioelechem.2017.12.005
24. Miklavčič D, Beravs K, Šemrov D, Čemažar M, Demšar F, Serša G. The importance of electric field distribution for effective in vivo electroporation of tissues. *Biophys J* 1998; **74:** 2152-8. doi: 10.1016/S0006-3495(98)77924-X
25. Ivorra A, Rubinsky B. Electric field modulation in tissue electroporation with electrolytic and non-electrolytic additives. *Bioelectrochemistry* 2007; **70:** 551-60. doi: 10.1016/j.bioelechem.2007.02.001
26. Miklavčič D, Šemrov D, Mekid H, Mir LM. A validated model of in vivo electric field distribution in tissues for electrochemotherapy and for DNA electrotransfer for gene therapy. *Biochim Biophys Acta* 2000; **1523:** 73-83. doi: 10.1016/S0304-4165(00)00101-X
27. Boc N, Edhemovic I, Kos B, Music MM, Brecelj E, Trotovsek B, et al. Ultrasonographic changes in the liver tumors as indicators of adequate tumor coverage with electric field for effective electrochemotherapy. *Radiol Oncol* 2018; **52:** 383-91. doi: 10.2478/raon-2018-0041
28. Granata V, Fusco R, Setola SV, Palaia R, Albino V, Piccirillo M, et al. Diffusion kurtosis imaging and conventional diffusion weighted imaging to assess electrochemotherapy response in locally advanced pancreatic cancer. *Radiol Oncol* 2019; **53:** 15-24. doi: 10.2478/raon-2019-0004

29. Zmuc J, Gasljevic G, Sersa G, Edhemovic I, Boc N, Seliskar A, et al. Large liver blood vessels and bile ducts are not damaged by electrochemotherapy with bleomycin in pigs. *Sci Rep* 2019; **9:** 3649. doi: 10.1038/s41598-019-40395-y

30. Paturneau-Jouas M, Parzy E, Vidal G, Carlier PG, Wary C, Vilquin JT, et al. Electrotransfer at MR imaging: tool for optimization of gene transfer protocols-feasibility study in mice. *Radiology* 2003; **228:** 768-75. doi: 10.1148/RADIOL.2283020482

31. Kranjc M, Markelc B, Bajd F, Čemažar M, Serša I, Blagus T, et al. In situ monitoring of electric field dis-tribution in mouse tumor during electroporation. *Radiology* 2015; **274:** 115-23. doi: 10.1148/radiol.14140311

32. Leroy-Willig A, Bureau MF, Scherman D, Carlier PG. In vivo NMR imaging evaluation of efficiency and toxicity of gene electrotransfer in rat muscle. *Gene Ther* 2005; **12:** 1434-43. doi: 10.1038/sj.gt.3302541

33. Scott LJ. Gadobutrol: a review in contrast-enhanced MRI and MRA. *Clin Drug Investig* 2018; **38:** 773-84. doi: 10.1007/s40261-018-0674-9

34. Čorović S, Županič A, Kranjc S, Al Sakere B, Leroy-Willig A, Mir LM, et al. The influence of skeletal muscle anisotropy on electroporation: in vivo study and numerical modeling. *Med Biol Eng Comput* 2010; **48:** 637-48. doi: 10.1007/s11517-010-0614-1

35. Peng W, Polajžer T, Yao C, Miklavčič D. Dynamics of cell death due to electroporation using different pulse parameters as revealed by different vi-ability assays. *Ann Biomed Eng* 2024; **52:** 22-35. doi: 10.1007/s10439-023-03309-8

36. Kandušer M, Šentjurc M, Miklavčič D. Cell membrane fluidity related to electroporation and resealing. *Eur Biophys J* 2006; **35:** 196-204. doi: 10.1007/s00249-005-0021-y

37. Neu WK, Neu JC. Mechanism of irreversible electroporation in cells: Insight from the models. In: Rubinsky B, editor. *Irreversible electroporation. Series in biomedical engineering.* Berlin, Heidelberg: Springer; 2010. p. 85-122.

38. Avazzadeh S, O'Brien B, Coffey K, O'Halloran M, Keane D, Quinlan LR. Establishing irreversible electroporation electric field potential threshold in a suspension in vitro model for cardiac and neuronal cells. *J Clin Med* 2021; **10:** 5443. doi: 10.3390/jcm10225443

39. Saulis G. Pore disappearance in a cell after electroporation: theoretical simulation and comparison with experiments. *Biophys J* 1997; **73:** 1299-309. doi: 10.1016/S0006-3495(97)78163-3

40. Sözer EB, Pocetti CF, Vernier PT. Transport of charged small molecules after electropermeabilization — drift and diffusion. *BMC Biophys* 2018; **11:** 4. doi: 10.1186/s13628-018-0044-2

41. Polajžer T, Miklavčič D. Immunogenic cell death in electroporation-based therapies depends on pulse waveform characteristics. *Vaccines* 2023; **11:** 1036. doi: 10.3390/vaccines11061036

42. Kranjc M, Kranjc S, Bajd F, Serša G, Serša I, Miklavčič D. Predicting irreversible electroporation-induced tissue damage by means of magnetic resonance electrical impedance tomography. *Sci Rep* 2017; **7:** 10323. doi: 10.1038/s41598-017-10846-5

43. Kos B, Voigt P, Miklavcic D, Moche M. Careful treatment planning enables safe ablation of liver tumors adjacent to major blood vessels by percutaneous irreversible electroporation (IRE). *Radiol Oncol* 2015; **49:** 234-41. doi: 10.1515/raon-2015-0031

44. Pavliha D, Kos B, Marčan M, Županič A, Serša G, Miklavčič D. Planning of electroporation-based treatments using web-based treatment-planning software. *J Membr Biol* 2013; **246:** 833-42. doi: 10.1007/s00232-013-9567-2

45. Crich SG, Biancone L, Cantaluppi V, Duò D, Esposito G, Russo S, et al. Improved route for the visualization of stem cells labeled with a Gd-/Eu-Chelate as dual (MRI and fluorescence) agent. *Magn Reson Med* 2004; **51:** 938-44. doi: 10.1002/mrm.20072

research article

Ocular adnexal lymphoma – a retrospective study and review of the literature

Lucka Boltezar[1,2], Danijela Strbac[2,3], Joze Pizem[2,4], Gregor Hawlina[2,5]

[1] Department of Medical Oncology, Institute of Oncology Ljubljana, Ljubljana, Slovenia
[2] Faculty of Medicine, University of Ljubljana, Ljubljana, Slovenia
[3] Department of Radiotherapy, Institute of Oncology Ljubljana, Ljubljana, Slovenia,
[4] Institute of Pathology, Faculty of Medicine, University of Ljubljana, Ljubljana, Slovenia
[5] Eye Hospital, University Medical Centre Ljubljana, Ljubljana, Slovenia

Radiol Oncol 2024; 58(3): 416-424.

Received 30 April 2024
Accepted 12 Avgust 2024

Correspondence to: Assist. Prof. Gregor Hawlina, M.D., Ph.D., Eye Hospital, University Medical Centre Ljubljana, Grablovičeva ul. 46, SI-1000 Ljubljana, Slovenia. E-mail: gregor.hawlina@kclj.si

Disclosure: No potential conflicts of interest were disclosed.

Background. To review the characteristics of all Slovenian patients with ocular adnexal lymphoma (OAL) in the period of 24 years with the aim of evaluating demographic data, lymphoma location and type, disease stage, treatment modality, local control rate and survival rate.

Patients and methods. All patients with histologically diagnosed OAL in the main tertiary centre of Slovenia, Eye Hospital, University Medical Centre Ljubljana, who were treated at Institute of Oncology Ljubljana were included in the study. Patients' data were collected from October 1995 through April 2019.

Results. Seventy-four patients were included in the study having a median age of 68 years at diagnosis. The majority of lymphomas were of B-cell origin (98.6%). The most frequent type was the extranodal marginal zone B-cell lymphoma (MALT) (71.6%). Orbital lymphomas were diagnosed in 56 cases (75.7%) and conjunctival in 18 cases (24.3%). Ocular manifestation was the first sign of the disease in 78.4% of patients and in 67.6% of patients ocular adnexa were the only disease location. Fifty-one patients (68.9%) were treated with radiotherapy, 7 patients (9.4%) with systemic treatment, 5 patients (6.8%) with combined radiotherapy and systemic treatment and in 11 patients, biopsy and active surveillance strategy was applied (14.9%). Local control of the disease was achieved in 96.6% of treated patients. Median overall survival of the whole study group has not been reached yet. Five-year overall survival rate was 80.1% (95% CI 68.1% – 88.5%) and 5-year lymphoma specific survival rate was 87.2% (95% CI 83.2%–91.2%).

Conclusions. OALs comprise a group of heterogeneous diseases with variable outcomes depending predominately on the patient's age and lymphoma type, with low grade lymphomas carrying good prognosis even in elderly patients.

Key words: ocular adnexal lymphoma; orbital lymphoma; conjunctival lymphoma; MALT lymphoma; lymphoma treatment

Introduction

Lymphomas are a heterogeneous group of malignant lymphoid tumors that arise from the clonal proliferation of either B-lymphocytes, T-lymphocytes or, less commonly, of natural killer (NK) cells at different stages of maturation.[1,2] Lymphomas are divided into 2 major categories, namely Hodgkin lymphoma (HL) and non-Hodgkin lymphoma (NHL). The molecular mechanisms include several structural chromosomal abnormalities, for example translocation 14;18 in marginal zone lymphomas, translocation 11;14 in mantle cell lymphomas or bcl-2, bcl-6 and myc translocation

in case of aggressive B-cell lymphomas.[1-5] Ocular adnexal lymphoma (OAL) is defined as lymphoma that occurs in the conjunctiva, lacrimal apparatus, eyelid, or orbit.[3-6] It represents 6–8% of orbital and 10–15% of adnexal tumors.[7] OAL is considered primarily if it involves the ocular adnexa alone and secondarily if it is accompanied by a lymphoma of the identical type at another extraocular site.[6] These tumors may spread locally or disseminate systemically.[8] OAL may present with symptoms of conjunctival salmon patches, ptosis from levator muscle involvement or the insidious and painless development of proptosis with or without diplopia due to an orbital mass.[9] In the orbit, OAL can involve the lacrimal gland, extraocular muscles, or intraconal and extraconal spaces.[9]

Diagnosis based only on clinical and imaging data is inadequate. Consequently, an incisional or excisional biopsy followed by histopathologic, immunophenotypic and molecular genetic studies, either to confirm or to rule out this malignancy, should be performed.[10] Orbital imaging typically shows a poorly defined mass that molds to the shape of surrounding structures without direct invasion or bony erosion.[11,12] In addition to orbital imaging and subsequent biopsy, positron emission tomography alone or combined with computed tomography is often performed for systemic staging of disease and for the assessment of response to therapy.[13] It is important to perform a complete systemic evaluation, both at diagnosis and at regular follow-ups, since more than half of patients will present with systemic lymphoma at the time of ocular diagnosis or will develop a systemic disease later on.[14]

Several successful treatment modalities for OAL have been reported so far, including surgical excision, cryotherapy, external beam radiotherapy for tumors localized to the periocular area or in combination with chemotherapy, immune modulating therapy, or primary antibiotic treatment in case of systemic involvement.[15] Spontaneous remissions of the OAL have been reported in low grade lymphomas but never in high grade subtypes. In general, the outcome of OAL is favourable, however small patient numbers, patient selection criteria, varied histologic subtypes, and the lack of large prospective studies usually make the comparison of the effectiveness of different types of treatment challenging.[16]

The purpose of our study was to review the characteristics of all Slovenian patients with OAL in the period of 24 years with the aim of evaluating demographic data, lymphoma location and type, disease stage, treatment modality, local control rate and survival rate.

Patients and methods

Patients

This retrospective study included all patients with histologically diagnosed OAL in the main tertiary centre of Slovenia Eye Hospital, University Medical Centre Ljubljana, who continued their treatment at the Institute of Oncology Ljubljana. Patients' data were collected from October 1995 through April 2019. The primary end points were lymphoma type, lymphoma location, demographic data and survival rate. Data regarding patient's age, stage of disease, treatment modality, treatment outcome and survival rate were gathered from their electronic records. Survival data were obtained from the Cancer Registry of Republic of Slovenia. Staging was performed according to the guidelines[17] using the Ann Arbor staging system.[18] All patients were treated at Institute of Oncology Ljubljana, the treatment decision for each individual patient was consented at the lymphoma tumor board and patients were treated in accordance with the National lymphoma guidelines[19], which are updated on yearly basis. For low grade lymphomas the active surveillance strategy or radiotherapy treatment was proposed, depending on the comorbidities of each patient and symptoms of the OAL. For high grade lymphomas the treatment strategy was systemic treatment, sometimes combined with radiotherapy in case of high burden of ocular symptoms.

This study was approved by Institutional Review Board and Institutional Ethical Committee (ERIDNPVO-0008/2022, 2.12.2021 and 16.12.2021) and was executed according to the declaration of Helsinki. All patients signed an informed consent form to participate in the study.

Clinical characteristics

Symptoms and signs

Our patients presented with symptoms such as decreased visual acuity, diplopia, tearing or retrobulbar pain and with signs as lid mass, proptosis, ptosis, lacrimal gland mass, chemosis or conjunctival injection, limitation of extraocular movement, enlarged lacrimal sac and globe displacement. After initial full ophthalmological examination, blood tests and orbital imaging including ultrasound

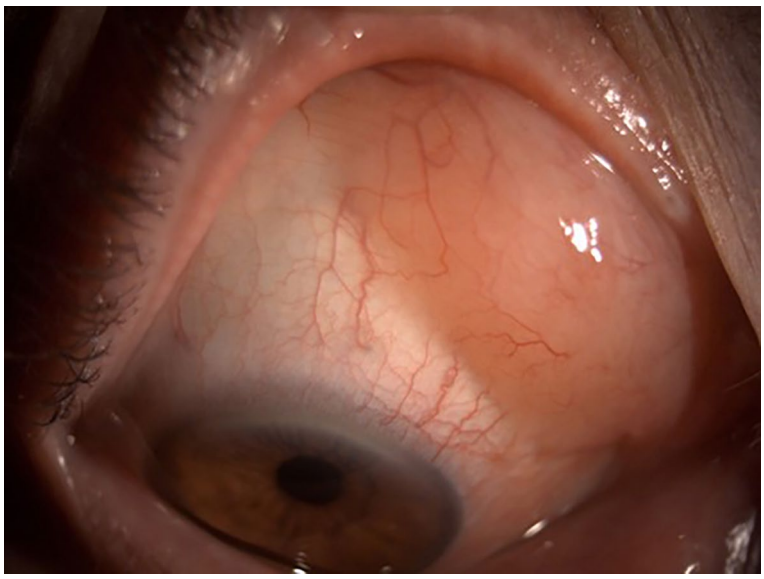

FIGURE 1. Patient with conjunctival lymphoma presents with a characteristic salmon-pink nodular patch in the conjunctiva.

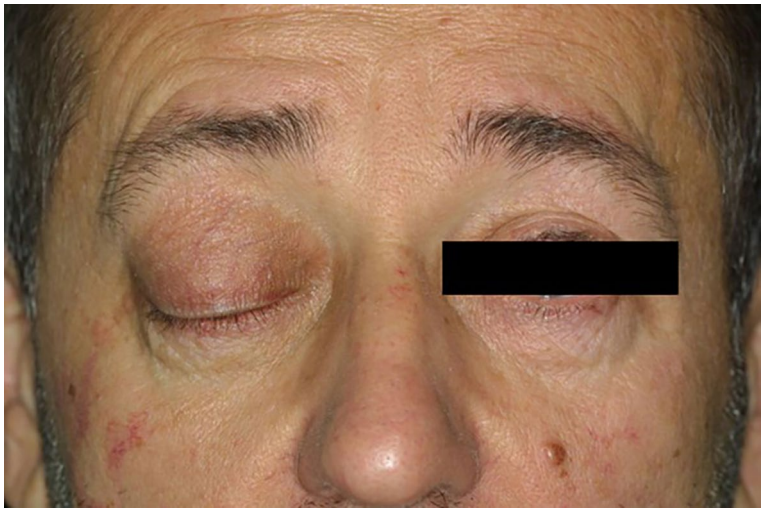

FIGURE 2. Patient with orbital lymphoma presents with a mass lesion within the right eye.

(US), computed tomography (CT) and/or magnetic resonance imaging (MRI) were performed. Subsequently, incisional biopsy was performed in most of the cases while in cases where lesion was small and localized, an excisional biopsy was carried out.

Lymphoma location

Patients with OAL were divided according to the location of lymphoma into orbital and conjunctival lymphoma groups. Conjunctival lymphoma presented as a characteristic salmon-pink nodular patch in the conjunctiva (Figure 1), while orbital lymphoma presented with a mass lesion in eyelids, lacrimal gland, lacrimal sac, extraocular muscle, intraconal or extraconal space (Figure 2).

Locations of the OAL were navigated by patients' physical examination and radiology imaging (CT, MRI and/or US). In conjunctival lymphomas, the biopsy was performed transconjunctivally and specimen included part of the conjunctiva while in orbital lymphoma the biopsy was performed with different anterior orbitotomy approaches. Lymphoma was staged according to the guidelines[17] with a CT of the neck, thorax and abdomen in marginal zone B-cell lymphoma and with positron emission tomography-CT (PET-CT) when other, more aggressive histological subtypes were present.

Histopathologic examination

All biopsy samples were fixed in formalin and embedded in paraffin. In addition to morphological criteria, appropriate immunohistochemical markers were applied for the diagnosis of different types of lymphomas.[20] The following lymphoma types mostly of B-cell origin have been identifed: extranodal marginal zone lymphoma (MALT), follicular lymphoma (FL), mantle cell lymphoma (MCL), chronic lymphocytic leukemia (CLL), diffuse large B-cell lymphoma (DLBCL), together with the peripheral T-cell lymphoma, not otherwise specified.

Statistical analyses

For demographic data, descriptive statistics was used. For numeric variables a non parametric t-test was used (Mann-Whitney). Survival was estimated using the Kaplan-Meier method. Overall survival was defined as time from histological diagnosis until death from any reason or censoring on 14.11.2022. Lymphoma specific survival was defined as time from histological diagnosis until death, caused by or related to lymphoma.

Results

Demographics

A total of 74 patients with a histologically verified lymphoma of the orbit (i.e. eyelid, lacrimal gland, lacrimal sac, and/or rectus muscles) or conjunctiva

TABLE 1. Patients' characteristics

	Males	Females	All
Number of patients	30 (40.5%)	44 (59.5%)	74
Median age, years	72 (range 41 – 89)	67.5 (range 34 – 89)	68
Lymphoma type			
- Marginal zone lymphoma (MALT)	21/30 (70.0%)	32/44 (72.7%)	53/74 (71.6%)
- Mantle cell lymphoma (MCL)	6/30 (20.0%)	3/44 (6.8%)	9/74 (12.2%)
- Follicular lymphoma (FL)	2/30 (6.7%)	4/44 (9.0%)	6/74 (8.1%)
- Diffuse large B-cell lymphoma (DLBCL)	1/30 (3.3%)	3/44 (6.8%)	4/74 (5.4%)
- Chronic lymphocytic leukemia (CLL)	0/30 (0%)	1/44 (2.3%)	1/74 (1.4%)
- Peripheral T-cell lymphoma, not otherwise specified	0/30 (0%)	1/44 (1.4%)	1/74 (1.4%)
Conjunctival lymphoma	7/30 (23.3%)	11/44 (25.0%)	18/74 (24.3%)
Orbital lymphoma	23/30 (76.7%)	33/44 (75.0%)	56/74 (75.7%)

were included. There were 40.5% male and 59.5% female patients. Median age at OAL diagnosis for the whole group was 68 years (range 34 – 89 years). In 58 patients (78.4%), the histological verification was done at the first disease presentation and in 16 patients (21.6%) it was done at recurrent presentation in ocular adnexa. Out of 58 patients with a biopsy at the first disease presentation, 13 patients (22.4%) were subsequently diagnosed with a systemic lymphoma according to radiological staging. Patients' characteristics are presented in Table 1.

Median age did not differ between males and females (p=0.367). There was also no difference in the distribution of conjunctival or orbital lymphomas among males and females (p=0.870). However, all lymphoma types exhibited a female predominance except for MCL, which was more common in males.

Anatomical location

Orbital lymphomas were diagnosed in 56 cases (75.7%) and conjunctival in 18 cases (24.3%). Orbital lymphomas appeared more frequently bilaterally than this was observed with conjunctival lymphoma (p<0.001). All lymphoma subtypes were found in the orbit, with the most frequent types being the MALT and MCL. Specifications of conjunctival and orbital lymphomas are given in Table 2.

Stage

Fifty patients had ocular manifestation as their only lymphoma location at the time of the biopsy (67.6%) while 24 patients (14 females and 10 males) had a systemic lymphoma (32.4%) from the beginning. Of the later, the majority had stage IV disease (87.5%, 21/24 patients), one patient had stage III disease (4.2%, 1/24) and two patients had stage II disease (8.3%, 2/24).

Treatment

Fifty-one patients (68.9%) were treated with radiotherapy, 7 patients (9.4%) with systemic treatment, 5 patients (6.8%) with combined treatment – radiotherapy and systemic treatment and in 11 patients, biopsy and active surveillance strategy was applied (14.9%), usually on account of their advanced age and lack of symptoms. Active surveillance strategy meant that patients were regularly followed by ophtalmologist in four to six monthly periods. Patients diagnosed after 2011 and treated with radiotherapy received 24.05 Gy in 13 daily fractions and patients treated before 2011 received 30,6 Gy in 18 fractions. The techniques applied were either 3D/VMAT, 2D electrons or electron beam planning.

The systemic treatment applied was usually a combination of an anti-CD20 antibody rituximab and an anthracyclin-based regimen and all patients had an advanced stage and an aggressive subtype of lymphoma, except for one patient with an advanced MALT lymphoma. One patient underwent consolidation with autologous stem cell transplant in the first line treatment.

Out of 63 patients, who received upfront treatment with radiotherapy, systemic treatment or a combination of both, in 5 patients the evaluation of treatment was either not possible or was not per-

TABLE 2. Specifications of orbital and conjunctival lymphomas

	Orbital lymphomas	Conjunctival lymphomas	All
Unilateral lymphoma	46/56 (82.1%)	17/18 (94.4%)	63/74 (85.1%)
Bilateral lymphoma	10/56 (17.9%)	1/18 (5.6%)	11/74 (14.9%)
Lymphoma type			
- Marginal zone lymphoma (MALT)	36/56 (64.3%)	17/18 (94.4%)	53/74 (71.6%)
- Mantle cell lymphoma (MCL)	9/56 (16.1%)	0/18 (0%)	9/74 (12.2%)
- Follicular lymphoma (FL)	5/56 (8.9%)	1/18 (5.6%)	6/74 (8.1%)
- Diffuse large B-cell lymphoma (DLBCL)	4/56 (7.1%)	0/18 (0%)	4/74 (5.4%)
- Chronic lymphocytic leukemia (CLL)	1/56 (1.8%)	0/18 (0%)	1/74 (1.4%)
- Peripheral T-cell lymphoma, not otherwise specified	1/56 (1.8%)	0/18 (0%)	1/74 (1.4%)

formed. Treatment outcome for 58 patients with post-treatment evaluation is seen in Table 3.

Recurrence of lymphoma was documented in 25 of 58 patients (43.1%) during follow up (median follow up time being 72 months) while 33 of 58 treated patients remained in a long-term remission and never experienced a recurrence (56.9%). Patients were followed up regularly by the ophtalmologist and oncologist (in case of oncologic treatment) in four to six monthly periods.

Out of 25 patients experiencing a recurrence, only 2 patients had a recurrence in periocular area, that has already been treated previously (3.4%, 2/58) while 23 (92.0%, 23/25) patients had a recurrence outside the previously treated location. The two patients with a recurrence in the already treated eye had been primarily treated with radiotherapy, one with 25 Gray and the other patient with 20 Gy. The local control rate was therefore 96.6%.

For 11 patients on active surveillance strategy, six achieved complete remission of the ocular lesion spontaneously, four had stable disease and one had progression of the lesion. Recurrence of systemic lymphoma later occurred in 5 of these patients (45.5%, 5/11), however, only one patient (20.0%, 1/5) had a recurrence in the eye, which was primarily diagnosed, but not yet treated (that patient had a spontaneous remission of the disease and later on recurrence of the disease).

TABLE 3. Treatment outcome in 58 patients with post-treatment evaluation, post-treatment evaluation being done three to six months after the end of treatment

Treatment outcome	Number of patients
Complete remission	46 (79.3%)
Partial remission	10 (17.2%)
Stable disease	1 (1.7%)
Progressive disease	1 (1.7%)*

* = Patient who progressed during first line treatment had mantle cell lymphoma (MCL)

Survival

Median overall survival of the whole study group has not been reached yet. Twenty-two patients were deceased at the time of the data retrieval (29.7%), however, only 11 (50.0%) of them died due to lymphoma. Median follow up time was 72 months (range 1 – 280 months). Patients, who died due to lymphoma, were: one patient with DLBCL, one patient with FL, five patients with MALT, two patients with MCL, one with CLL and one patient with peripheral T-cell lymphoma, not otherwise specified. Other patients died due to causes unrelated to lymphoma. Patients, who died due to other causes, were significantly older than the rest of the group, p=0.003, while patients, who died due to lymphoma were not older than the rest of the studied group, p=0.453.

Five-year overall survival rate was 80.1% (95% CI 68.1% – 88.5%) and 5-year lymphoma specific survival rate was 87.2% (95% CI 83.2%–91.2%). Figures 3 and 4 show overall survival and lymphoma specific survival, respectively.

Localized lymphoma subgroup

The localized lymphoma subgroup comprised 50 patients in whom no signs of systemic lymphoma could be detected at the time of the biopsy. There were 20 males (40.0%) and 30 females (60.0%).

Their median age was 64 years, range 41–83 years. Conjunctival lymphomas were seen in 17 patients (34.0%) and orbital lymphomas in 33 patients (66.0%). There were 46 (92.0%) patients with MALT lymphomas, two (4.0%) patients with FL and two patients (4.0%) with MCL. All patients who were treated upfront (78.0% (39/50)) were treated with radiotherapy according to the guidelines[17] and for 11 patients (22.0%) the active surveillance strategy was applied. In the active surveillance strategy group one patient had a FL and 10 patients had MALT lymphoma.

Five-year overall survival rate for this subgroup of patients was 91.1% (95% CI 86.9% – 95.3%) and 5-year lymphoma-specific survival was 100%. In 37 patients, the post-treatment evaluation was performed and during follow up 26 patients stayed in long term complete remission (70.3%, 26/37). Nine patients experienced a systemic relapse (24.3%, 9/37) and only two patients had a relapse in the previously treated eye (5.4%, 2/37). All patients with relapses had a MALT lymphoma.

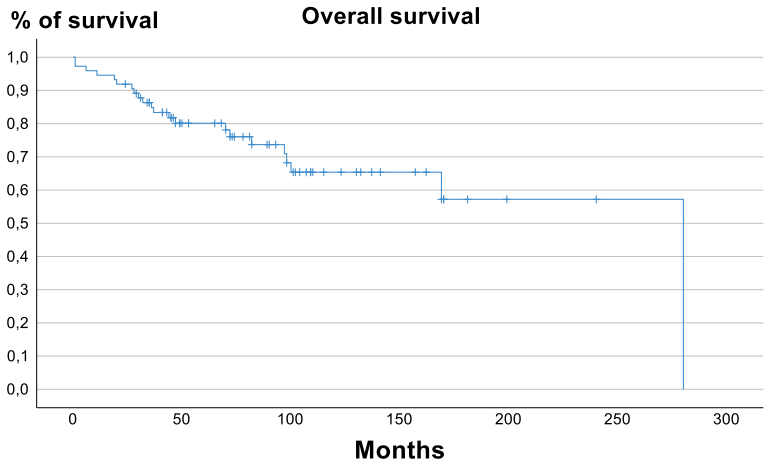

FIGURE 3. Overall survival.

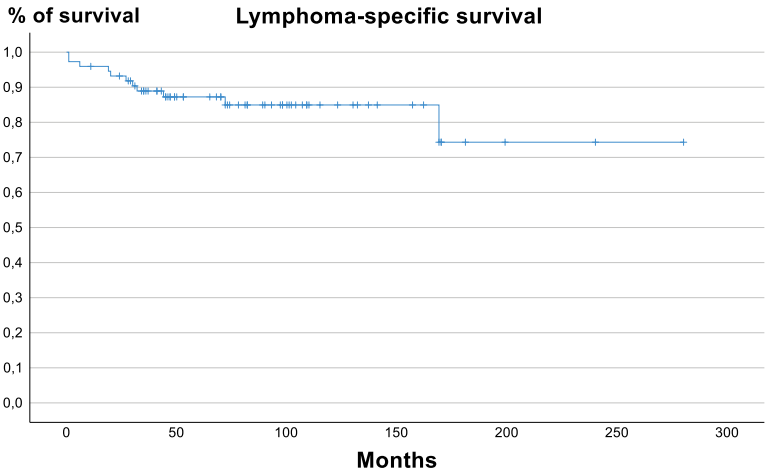

FIGURE 4. Lymphoma specific survival.

Discussion

In our retrospective study we present the characteristics of Slovenian patients with OAL. The study included 74 patients with biopsy-proven OAL between 1995 and 2019 at Eye Hospital, University Medical Centre Ljubljana, Slovenia, and treated at the Institute of Oncology Ljubljana, Slovenia. Compared to median age of OAL presentation of around 60 years reported in previous studies and reviews, we registered a higher median age (68 years) in our group.[16,21-25] In concordance with the previous review where female predominance of 55% was reported, we also registered a higher morbidity in women (59.5%) in our study.[25]

Anatomically, our OAL cases were distributed inside the orbit in 56 cases (75.7%) compared to 18 cases (24.3%) located in conjunctiva. The distribution was similar to the study of Fernandez *et al*. where the orbital fibroadipose tissue was involved in 64% of cases and conjunctiva in 32% of cases.[22] We anatomically divided OAL in the conjunctival lymphoma with characteristic salmon-pink nodular patch and in the orbital lymphoma with a presentation of mass lesion in eyelids, lacrimal gland, lacrimal sac, extraocular muscle, intraconal or extraconal space. In some studies, the eyelids were used as a separate location[16,22] but we included the eyelids' involvement with orbital lymphoma as all our patients with involved eyelids also had an orbital progression of lymphoma. Bilateral involvement of OAL is usually seen in 7%–24% of patients[16], in our series it was in 14.9%. Bilateral involvement was, however, more common in orbital lymphoma (17.9%, 10/56) than in conjunctival lymphoma (5.6%, 1/18). Of note, bilateral OAL was detected only in MALT (4/53, 7.5%), MCL (5/9, 55.6%) and FL (2/6, 33.3%) lymphoma subtypes. According to our results, although the study included a relatively small number of MCL cases, we observed that MCL was more commonly confirmed bilaterally compared to the other types of lymphoma. The study of Rasmussen *et al*. on ocular adnexal MCL showed also a more common bilateral disease. Furthermore, they also reported a more frequent bilateral occurrence of primary than of secondary ocular adnexal MCL.[26] On contrary, all our MCL patients had a secondary lymphoma or a recurrence of systemic lymphoma.

The majority of lymphomas in our study were of B-cell origin (98.6%, 73/74) similarly to the other studies where between 95% and 100% of reported cases corresponded to the B-cell type.[16] Subtypes were MALT (71.6%), which is in agreement with previous studies reporting a 58% occurrence of this type[27], MCL (12.1%), FL (8.1%), DLBCL (5.4%), CLL (1.4%) and peripheral T-cell lymphoma, not otherwise specified (1.4%). All subtypes were found in the orbit, with the most frequent being MALT (64.23%, 35/56) and MCL (16.1%, 9/56), while only MALT (94.4%, 17/18) and FL (5.6%, 1/18) were identified in conjunctiva. Comparably, conjunctival sites were observed in literature in one third of patients and almost always consisted of low-grade NHL (96% of patients).[28] MCL was the only histological subtype which predominated in male patients, which is also consistent with previous studies[8,29-31], all other histological subtypes were predominant in female patients. The only entity that stands out in our study is a relatively high proportion of MCL, 12.2%, since this type is usually diagnosed in only 3–4% of the patients.[22,24] However, all cases of MCL in our series were located in the orbit and represented a primary or secondary manifestation of a systemic lymphoma. Further studies on larger number of patients will be needed to prove this observation.

Half of the treated patients were cured with radiotherapy or, to a minor extent, systemic treatment. Treatment guidelines suggest radiotherapy as the preferred option for localized disease in case of low-grade lymphoma.[17,19] Radiotherapy is a non-invasive treatment with known side effects, the most frequently reported cataract (12.1%) and dry eye (8.5%)[25], that are manageable through time. For example, cataract can be treated with surgery and the more common dry eye disease with artificial tears. The suggested radiotherapy doses range from 24 Gy up to 30 Gy.[17] More than half of our patients were treated with 30 Gy, since the conclusions of a phase III trial of safely lowering the dosage to 24 Gy for indolent lymphoma was released in 2011[32] and our observation and treatment period of included patients began long before that.

Local control rate of 96.6% in our study is in line with Yen's analyses (95.9% for studies of MALT lymphomas and 93.1% for studies that included data on multiple subtypes of lymphoma).[25] Of note, our study included both multiple histologic subtypes of lymphoma and all OAL locations. Five-year overall survival rate in our study was 80.1% similar to Yen's pooled analyses (78.9%).[25] Half of our patients died due to causes unrelated to lymphoma, they were also significantly older than the rest of the study group, which underlines the importance of choosing the proper treatment or even active surveillance strategy with regard to patient's preferences and comorbidities. The higher lymphoma-specific survival compared to the overall survival in our study shows that these patients are elderly, having other comorbidities that are more commonly the cause of death than lymphoma itself. Furthermore, we observed also a relatively high proportion of spontaneous remissions locally (54.5%, 6/11) in the active surveillance strategy group, suggesting that not all patients necessarily need the treatment immediately at presentation.

There is also an option of treating with only 4 Gy in 2 fractions for localized disease as reported by de Castro *et al*.[33] Park *et al*.[34] started a prospective phase II trial of 4 Gy in 2 fractions in stage I patients. Complete remission was observed in 11 lesions and partial remission in 6 of the 17 included lesions, respectively. The lesions with partial response were further treated to 24 Gy. Therefore, the future perspective for localized lesions is to reduce and adapt the radiation treatment if possible while still preserving excellent remissions and reducing the side effects.[34]

In Tanimoto's study with a similar follow up time as in our study[35], 69% of patients with MALT lymphoma did not need any treatment for localized disease. Similar to Tanimoto's study, our active surveillance strategy group was comprised of predominately MALT histology. Even though the active surveillance group was not older than the treated group, we feel obliged to stress the importance of a careful evaluation of treatment strategy, comorbidities and patient's preferences to avoid unnecessary additional complications caused by treatment.

Aggressive lymphomas (DLBCL, MCL, peripheral T-cell lymphoma, not otherwise specified) were treated according to guidelines with systemic treatment resulting in outcomes that are in line with reported histological subtypes.[36,37] Considering the fact that low grade lymphomas are usually incurable and the recurrence of the disease is expected, we need to underline that there were only two cases of recurrence in periocular area, that have been already treated previously. Our 5-year overall survival rate and lymphoma-specific survival rate are high (80.1%; 87.2%), but again, as reported, OALs are known for high survival rates.[16,24,38]

Patients with localized disease (eye only) were in our study analyzed separately. In this group

of patients, a higher 5-year overall (91.1% compared to 80.1%) and lymphoma-specific survival rate (100% compared to 87.2%), as well as a higher number of complete remissions (70.3% compared to 56.9%) and a lower number of systemic recurrences (24.3% compared to 43.1%) were registered. It can be therefore concluded that patients with a localized disease have a better outcome compared to patients with secondary OAL.

Ocular adnexal lymphomas comprise a group of heterogeneous diseases. Their outcomes vary in relation to patient's age and lymphoma type. Individual treatment decisions are mandatory to tailor the treatment suitable for each patient. Radiotherapy has proven to be a highly efficient treatment with an excellent local control rate while systemic treatment should be reserved for disseminated disease.

Acknowledgments

This research was funded by Ministry of Science and Technology, Slovenia, grant number P3-0289.

References

1. Mugnaini EN, Ghosh N. Lymphoma. *Prim Care* 2016; **43:** 661-75. doi: 10.1016/j.pop.2016.07.012
2. Matasar MJ, Zelenetz AD. Overview of lymphoma diagnosis and management. *Radiol Clin North Am* 2008; **46:** 175-98. doi: 10.1016/j.rcl.2008.03.005
3. Bairey O, Kremer I, Rakowsky E, Hadar H, Shaklai M. Orbital and adnexal involvement in systemic non-Hodgkin's lymphoma. *Cancer* 1994; **73:** 2395-99. doi: 10.1002/1097-0142(19940501)73:9<2395::AID-CNCR2820730924>3.0.CO;2-V
4. Ohtsuka K, Hashimoto M, Suzuki Y. A review of 244 orbital tumors in Japanese patients during a 21-year period: origins and locations. *Jpn J Ophthalmol* 2005; **49:** 49-55. doi: 10.1007/s10384-004-0147-y
5. Sjö LD. Ophthalmic lymphoma: epidemiology and pathogenesis. *Acta Ophthalmol* 2009; **87:** 1-20. doi: 10.1111/j.1755-3768.2008.01478.x
6. Coupland SE, White VA, Rootman J, Damato B, Finger PT. A TNM-based clinical staging system of ocular adnexal lymphomas. *Arch Pathol Lab Med* 2009; **133:** 1262-67. doi: 10.5858/133.8.1262
7. Bardenstein DS. Ocular adnexal lymphoma: classification, clinical disease, and molecular biology. *Ophthalmol Clin North Am* 2005; **18:** 187-97. doi: 10.1016/j.ohc.2004.11.001
8. Coupland SE, Krause L, Delecluse HJ, Anagnostopoulos I, Foss HD, Hummel M, et al. Lymphoproliferative lesions of the ocular adnexa: Analysis of 112 cases. *Ophthalmology* 1998; **105:** 1430-41. doi: 10.1016/S0161-6420(98)98024-1
9. McKelvie PA, McNab A, Francis IC, Fox R, O'Day J. Ocular adnexal lymphoproliferative disease: a series of 73 cases. *Clin Exp Ophthalmol* 2001; **29:** 387-93. doi: 10.1046/j.1442-9071.2001.d01-18.x
10. Bernardini FP, Bazzan M. Lymphoproliferative disease of the orbit. *Curr Opin Ophthalmol* 2007; **18:** 398-401. doi:10.1097/ICU.0b013e3282be8fbb
11. Khan SN, Sepahdari AR. Orbital masses: CT and MRI of common vascular lesions, benign tumors, and malignancies. *Saudi J Ophthalmol* 2012; **26:** 373-83. doi: 10.1016/j.sjopt.2012.08.001
12. Sullivan TJ, Valenzuela AA. Imaging features of ocular adnexal lymphoproliferative disease. *Eye* 2006; **20:** 1189-95. doi: 10.1038/sj.eye.6702382
13. Hui K-H, Pfeiffer ML, Esmaeli B. Value of positron emission tomography/computed tomography in diagnosis and staging of primary ocular and orbital tumors. *Saudi J Ophthalmol* 2012; **26:** 365-71. doi: 10.1016/j.sjopt.2012.08.008
14. J R, VA W, JM C, RD G. Lymphoproliferative, leukemic, and histiocytic lesions of the orbit. In: Rootman J, editor. *Diseases of the orbit: a multidisciplinary approach.* 2nd Edition. Philadelphia, USA: Lippincott Williams & Wilkins; 2003; p. 385-416.
15. Cohen V. Treatment options for ocular adnexal lymphoma (OAL). *Clin Ophthalmol* 2009; **3:** 689-92. doi: 10.2147/OPTH.S5828
16. Decaudin D, de Cremoux P, Vincent-Salomon A, Dendale R, Rouic LLL. Ocular adnexal lymphoma: a review of clinicopathologic features and treatment options. *Blood* 2006; **108:** 1451-60. doi:10.1182/blood-2006-02-005017
17. Zucca E, Arcaini L, Buske C, Johnson PW, Ponzoni M, Raderer M, et al. Marginal zone lymphomas: ESMO Clinical Practice Guidelines for diagnosis, treatment and follow-up. *Ann Oncol* 2020; **31:** 17-29. doi: 10.1016/j.annonc.2019.10.010
18. Graue GF, Finger PT, Maher E, Della Rocca D, Della Rocca R, Lelli GJ Jr, et al. Ocular Adnexal lymphoma staging and treatment: American Joint Committee on Cancer versus Ann Arbor. *Eur J Ophthalmol* 2013; **23:** 344-55. doi: 10.5301/ejo.5000224
19. Jezeršek Novaković B. [Recommendations for the management of patients with malignant lymphomas]. [Slovenian]. 2023. Ljubljana: Institute of Oncology Ljubljana. [internet]. [cited 2024 Mar 15]. Available at: https://www.onko-i.si/fileadmin/onko/datoteke/Strokovna_knjiznica/smernice/Priporocila_za_obravnavo_bolnikov_z_malignimi_limfomi_2023.pdf. Published 2023.
20. Swerdlow S, Campo E, Harris N, Jaffe ES, Pileri SA, Stein H, et al., editors. *WHO classification of tumours of haematopoetic and lmyphoid tissues*. 4th edition. Lyon: IARC; 2017.
21. Dalvin LA, Salomão DR, Patel SV. Population-based incidence of conjunctival tumours in Olmsted County, Minnesota. *Br J Ophthalmol* 2018; **102:** 1728-34. doi: 10.1136/bjophthalmol-2017-311530
22. Fernández C, Henry R, Shields C, Bilyk JR, Lally SE, Eagle RC, et al. Ocular adnexal lymphoma: a single-institution retrospective study. *Saudi J Ophthalmol* 2021; **35:** 230-8. doi: 10.4103/1319-4534.343368
23. Ferry JA, Fung CY, Zukerberg L, et al. Lymphoma of the ocular adnexa: a study of 353 cases. *Am J Surg Pathol* 2007; **31:** 170-84. doi: 10.1097/01.pas.0000213350.49767.46
24. Tanenbaum RE, Galor A, Dubovy SR, Karp CL. Classification, diagnosis, and management of conjunctival lymphoma. *Eye Vis* 2019; **6:** 22. doi: 10.1186/s40662-019-0146-1
25. Yen MT, Bilyk JR, Wladis EJ, Bradley EA, Mawn LA. Treatments for ocular adnexal lymphoma. *Ophthalmology* 2018; **125:** 127-36. doi: 10.1016/j.ophtha.2017.05.037
26. Rasmussen P, Sjo LD, Prause JU, Ralfkiaer E, Heegaard S. Mantle cell lymphoma in the orbital and adnexal region. *Br J Ophthalmol* 2009; **93:** 1047-51. doi: 10.1136/bjo.2008.146910
27. Olsen TG, Heegaard S. Orbital lymphoma. *Surv Ophthalmol* 2019; **64:** 45-66. doi: 10.1016/j.survophthal.2018.08.002
28. Meunier J, Rouïc LL-L, Dendale R, Vincent-Salomon A, Asselain B, Arnaud P, et al. Conjunctival low-grade non-Hodgkin's lymphoma: a large single-center study of initial characteristics, natural history and prognostic factors. *Leuk Lymphoma* 2006; **47:** 1295-305. doi: 10.1080/10428190500518966
29. White WL, Ferry JA, Harris NL, Grove AS. Ocular adnexal lymphoma. *Ophthalmology* 1995; **102:** 1994-2006. doi: 10.1016/S0161-6420(95)30764-6
30. Knowles DM, Jakobiec FA, Mcnally L, Burke JS. Lymphoid hyperplasia and malignant lymphoma occurring in the ocular adnexa (orbit, conjunctiva, and eyelids): a prospective multiparametric analysis of 108 cases during 1977 to 1987. *Hum Pathol* 1990; **21:** 959-73. doi: 10.1016/0046-8177(90)90181-4
31. Andrew NH, Coupland SE, Pirbhai A, Selva D. Lymphoid hyperplasia of the orbit and ocular adnexa: a clinical pathologic review. *Surv Ophthalmol* 2016; **61:** 778-90. doi: 10.1016/j.survophthal.2016.04.004

32. Lowry L, Smith P, Qian W, Falk S, Benstead K, Illidge T, et al. Reduced dose radiotherapy for local control in non-Hodgkin lymphoma: a randomised phase III trial. *Radiother Oncol* 2011; **100:** 86-92. doi: 10.1016/j.radonc.2011.05.013

33. De Castro B, Peixeiro RP, Mariz JM, Oliveira Â. Ultra-low dose radiotherapy in the management of low-grade orbital lymphomas. *Reports Pract Oncol Radiother* 2022; **27:** 467-73. doi: 10.5603/RPOR.a2022.0044

34. Park J, Yea JW, Oh SA, Kim MK, Son JH, Park JW. Prospective study of 4 Gy radiotherapy for orbital mucosa-associated lymphoid tissue lymphoma (FORMAL). *Cancers* 2022; **14:** 4274. doi: 10.3390/cancers14174274

35. Tanimoto K, Kaneko A, Suzuki S, Sekiguchi N, Maruyama D, Kim SW, et al. Long-term follow-up results of no initial therapy for ocular adnexal MALT lymphoma. *Ann Oncol* 2006; **17:** 135-40. doi: 10.1093/annonc/mdj025

36. Tilly H, Gomes da Silva M, Vitolo U, Jack A, Meignan M, Lopez-Guillermo A, et al. Diffuse large B-cell lymphoma (DLBCL): ESMO Clinical Practice Guidelines for diagnosis, treatment and follow-up. *Ann Oncol* 2015; **26:** 116-25. doi: 10.1093/annonc/mdv304

37. Dreyling M, Campo E, Hermine O, Jerkeman M, Le Gouill S, Rule S, et al. Newly diagnosed and relapsed mantle cell lymphoma: ESMO Clinical Practice Guidelines for diagnosis, treatment and follow-up. *Ann Oncol* 2017; **28(Suppl 4):** iv62-71. doi: 10.1093/annonc/mdx223

38. Portell CA, Aronow ME, Rybicki LA, Macklis R, Singh AD, Sweetenham JW. Clinical characteristics of 95 patients with ocular adnexal and uveal lymphoma: treatment outcomes in extranodal marginal zone subtype. *Clin Lymphoma Myeloma Leuk* 2014; **14:** 203-10. doi: 10.1016/j.clml.2013.10.011

research article

Vertebral body collapse after spine stereotactic body radiation therapy: a single-center institutional experience

Arsh Issany[1], Austin J Iovoli[2], Richard Wang[3], Rohil Shekher[2], Sung Jun Ma[2], Victor Goulenko[2], Fatemeh Fekrmandi[2], Dheerendra Prasad[2]

[1] Jacobs School of Medicine and Biomedical Sciences, University at Buffalo, New York, USA
[2] Department of Radiation Medicine, Roswell Park Comprehensive Cancer Center, New York, USA
[3] Kirk Kerkorian School of Medicine, University of Nevada, Las Vegas, USA

Radiol Oncol 2024; 58(3): 425-431.

Received 26 December 2023
Accepted 26 April 2024

Correspondence to: Assoc. Prof. Dheerendra Prasad, M.D., Roswell Park Comprehensive Cancer Center, 665 Elm St Buffalo, NY 14203., USA.
E-mail: Dheerendra.Prasad@RoswellPark.org

Disclosure: No potential conflicts of interest were disclosed.

Background. Spine stereotactic body radiation therapy (SBRT) for the treatment of metastatic disease is increasingly utilized owing to improved pain and local control over conventional regimens. Vertebral body collapse (VBC) is an important toxicity following spine SBRT. We investigated our institutional experience with spine SBRT as it relates to VBC and spinal instability neoplastic score (SINS).

Patients and methods. Records of 83 patients with 100 spinal lesions treated with SBRT between 2007 and 2022 were reviewed. Clinical information was abstracted from the medical record. The primary endpoint was post-treatment VBC. Logistic univariate analysis was performed to identify clinical factors associated with VBC.

Results. Median dose and number of fractions used was 24 Gy and 3 fractions, respectively. There were 10 spine segments that developed VBC (10%) after spine SBRT. Median time to VBC was 2.4 months. Of the 11 spine segments that underwent kyphoplasty prior to SBRT, none developed subsequent VBC. No factors were associated with VBC on univariate analysis.

Conclusions. The rate of vertebral body collapse following spine SBRT is low. Prophylactic kyphoplasty may provide protection against VBC and should be considered for patients at high risk for fracture.

Key words: spine metastasis; stereotactic body radiation therapy; vertebral compression fracture; kyphoplasty; spinal instability

Introduction

About a third of cancer patients will develop bone metastases during the course of their disease.[1] The most common site of bone metastasis is the spine, which can often present with back pain, vertebral body collapse (VBC), radiculopathy, and epidural spinal cord compression.[2] Compression of the spinal cord has the potential to cause serious harm with symptoms ranging from pain to paralysis.[2] Optimal management of spine metastases involves multidisciplinary collaboration between surgeons, medical oncologists, pain specialists, and radiation oncology. For patients who are not candidates for immediate neurosurgical intervention, management often involves palliative radiotherapy with the goal of providing symptomatic relief of pain and preventing further progression of disease. With technological advancements in the delivery of radiotherapy, stereotactic body radiation therapy (SBRT) has emerged as an effective technique to safely treat spinal metastases with high doses of

radiation while sparing surrounding healthy tissue.[3]

Delivery of spine SBRT involves precise treatment planning and patient setup utilizing computed topography image verification to ensure the radiation is delivered conformally to the target. The advantages of treating malignant spine metastases with SBRT is controversial. A recent meta-analysis showed the overall pain response may be similar compared to conventional external beam radiotherapy (cEBRT), but more patients had complete pain alleviation with SBRT.[4] Other studies have shown advantages of SBRT compared to cEBRT such as improved local control and pain relief.[5-7] With advances in systemic therapies improving survival for many types of malignancies, local control of all metastatic disease has become increasingly important. Several drawbacks to spine SBRT, however, are increased risks of pain flare and radiation induced VBC. Current literature suggests the rate of VBC is between 4% and 39% for patients with metastatic disease undergoing spine SBRT.[8-13] Chronic pain and kyphotic deformity caused by VBC may lead to depression, impaired mobility, and reduced quality of life.[14] One study also found no clinically relevant differences between conventional radiotherapy and SBRT at 12 weeks for global quality of life, physical functioning, emotional functioning, functional interference, and psychosocial aspects.[15] This necessitates further exploration into the side effects of SBRT.

Multiple risk factors for VBC following spine SBRT have been identified, which include vertebral body involvement, kyphotic/scoliotic spine deformity, lytic tumor, lung and hepatocellular histology, and single-fraction SBRT to a dose of 20 Gy or higher.[9,16] In developing a tool to predict the risk of VBC after spine SBRT, epidural tumor extension, lumbar location, gross tumor volume, and spinal instability neoplastic score (SINS) of more than 6 were associated with increased risk of fracture.[17] While risk factors and predictive models are helpful in identifying patients at high risk of VBC, it remains unclear how to best reduce fracture incidence while also providing effective palliation.

Kyphoplasty is a minimally invasive procedure used in the management of VBC that uses an inflatable balloon to restore bone height then inject bone cement into the vertebral body.[18] This has been shown to be safe and effective for controlling pain in patients with spine metastases.[19,20] Few studies have investigated the effect of prophylactic kyphoplasty prior to spine SBRT on reducing the risk of VBC. The purpose of the present study is to expand on the published experience of spine SBRT and review our single-institution outcomes of spine SBRT with and without prophylactic kyphoplasty as it relates to SINS and VBC.

Patients and methods

Study population

The patient cohort was derived from all patients who received spine SBRT at a single institution between March 2007 and May 2022. Patients with tumors on the spinal cord or dura were excluded. The primary endpoint was development of VBC following completion of spine SBRT, defined as a new VBC or progression of an existing VBC. Data were collected under a protocol (BDR 157322) approved by the Institutional Review Board at Roswell Park Comprehensive Cancer Center. The Strengthening the Reporting of Observational Studies in Epidemiology (STROBE) reporting guideline was followed.

Patient data and treatment

Pertinent clinicopathologic data were abstracted from the electronic medical record for patients treated with spine SBRT. Clinically relevant variables included gender, race, age, Karnofsky Performance Status (KPS), primary malignancy, SINS, kyphoplasty performed, paraspinal extension, treatment dose, and treatment fractionation. SINS was calculated for each vertebral segment treated per published criteria using tumor location, pain, bone lesion type, radiographic spinal alignment, VBC, and posterolateral involvement of spinal elements.[21] Pre-treatment and post-treatment computed tomography (CT) and magnetic resonance imaging (MRI) of the spine was reviewed to obtain pertinent data. Data was collected from the radiation consultation visit prior to the delivery of SBRT and at the time of first imaging follow up after treatment completion. Dose prescribed was at the discretion of the treating radiation oncologist based on pertinent clinicopathologic factors. Institutional protocols outlining dose constraints to surrounding tissue were followed. There was no maximum dose constraint in the target as long as all dose constraints were met. Eclipse (Varian Medical Systems, Palo Alto, CA, USA) was used for the generation and evaluation of radiation treatment plans. We contoured clinical target volume (CTV) and planning target volume (PTV) according to Consensus Contouring Guidelines.[22] SBRT

TABLE 1. Baseline patient characteristics and treatment information

	VBC (N = 10)	%	No VBC (N = 90)	%	Total (N = 100)	%
Median follow up, month (IQR) (n = 100)	10.9	3.9-18.6	12.5	5.1-27.2	12.1	5.0-25.5
Sex (n = 83)*						
Male	5	56%	37	50%	42	51%
Female	4	44%	37	50%	41	49%
Median age, year (IQR) (n = 83)*	67	63-70	69	59-75	68	59–74
Race (n = 83)						
White	8	89%	69	93%	77	93%
Black	2	22%	1	1%	3	4%
Other/unknown	0	0%	3	4%	3	4%
KPS (n = 83)*						
≥ 80	9	90%	70	95%	79	95%
< 80	1	10%	3	4%	4	5%
Primary tumor (n = 100)**						
Lung	4	40%	25	28%	29	29%
Renal	1	10%	23	26%	24	24%
Breast	1	10%	8	9%	9	9%
Prostate	2	20%	10	11%	12	12%
Melanoma	0	0%	2	2%	2	2%
Other	2	20%	22	24%	24	24%
Spine Level (n = 100)**						
Cervical	1	10%	14	16%	15	15%
Thoracic	6	60%	58	64%	64	64%
Lumbosacral	3	30%	18	20%	21	21%
Kyphoplasty pre-SBRT (n = 100)**						
Yes	0	0%	11	12%	11	11%
No	10	100%	79	88%	89	89%
Paraspinal extension (n = 100)**						
Yes	4	40%	36	40%	40	40%
No	6	60%	54	60%	60	60%
Total dose (Gy)/fractions (n = 100)**						
12–17/1	1	10%	12	13%	13	13%
10–24/2	0	0%	2	2%	2	2%
15–30/3	8	80%	61	68%	69	69%
20–30/4-5	1	10%	15	17%	16	16%
Dose (Gy) per fraction (n = 100)**						
< 8	4	40%	31	34%	35	35%
8–12	5	50%	50	56%	55	55%
13–17	1	10%	9	10%	10	10%

IQR = interquartile range; KPS = Karnofsky performance status; SBRT = stereotactic body radiation therapy; VBC = vertebral body collapse

* Categories with designation (n = 100) are lesion-level variables; ** Categories with (n = 83) are patient variables

TABLE 2. Pre-treatment patient spinal instability neoplastic score (SINS) outcomes

	VBC (n=10)	%	No VBC (n = 90)	%	Total (n = 100)	%
Location						
Junctional (O-C2; C7–T2; T11–L1; L5–S1)	3	30%	32	36%	35	35%
Mobile spine (C3–6; L2–4)	3	30%	18	20%	21	21%
Semirigid (T3–10)	4	40%	40	44%	44	44%
Rigid (S2–5)	0	0%	0	0%	0	0%
Mechanical pain						
Yes	5	50%	49	54%	54	54%
No	3	30%	30	33%	33	33%
Pain-free lesion	2	20%	11	12%	13	13%
Bone lesion						
Lytic	8	80%	71	79%	79	79%
Mixed (lytic/blastic)	1	10%	9	10%	10	10%
Blastic	1	10%	10	11%	11	11%
Radiographic spinal alignment						
Subluxation/translation present	0	0%	8	9%	8	8%
Deformity (kyphosis/scoliosis)	2	20%	17	19%	19	19%
Normal	8	80%	65	72%	73	73%
Vertebral body collapse (p = 0.040)						
> 50% collapse	0	0%	9	10%	9	9%
< 50% collapse	1	10%	8	9%	9	9%
No collapse with > 50% body involved	1	10%	38	42%	39	39%
None of the above	8	80%	35	39%	43	43%
Posterolateral involvement						
Bilateral	0	0%	5	6%	5	5%
Unilateral	6	60%	33	37%	39	39%
None of the above	4	40%	52	58%	56	56%
SINS classification						
Stable	4	40%	22	24%	26	26%
Potentially instability	6	60%	63	70%	69	69%
Unstable	0	0%	5	6%	5	5%

VBC = vertebral body collapse

was delivered with a Varian TrueBeam utilizing online cone beam CT imaging, high definition multileaf collimator, and a 6 degrees of freedom couch.

Statistics

Univariate logistic regression using the log-rank method was used to identify factors associated with development of VBC. All p-values were two-sided and variables with $p < 0.05$ were considered statistically significant. Statistical Analysis was conducted using R (version 4.2.0, R Project for Statistical Computing, Vienna, Austria).

Ethical statement

The authors are accountable for all aspects of the work in ensuring that questions related to the accuracy or integrity of any part of the work are appropriately investigated and resolved. The study was conducted in accordance with the Declaration

of Helsinki (as revised in 2013). The study was approved by the institutional review board of Roswell Park Comprehensive Cancer Center (BDR 157322).

Results

A total of 83 patients with 100 treated spine segments were included for analysis. There were 10 patients with simultaneously treated synchronous metastases and 7 patients with metachronous metastases. Baseline patient characteristics and treatment details are described in Table 1. The median age was 68 years (interquartile range [IQR], 59–74) and 51% of patients were male. Median follow up time was 12.1 months (IQR, 5.0–25.5). The most common primary tumor histology treated was lung (29%), followed by renal (24%) and prostate (12%). Median dose and number of fractions used was 24 Gy and 3 fractions, respectively. Categories with (n = 100) are lesion-level variables and categories with (n = 83) are patient variables. The 100 lesions were assumed independent events for patients with multiple lesions. SINS for each spine segment prior to SBRT are summarized in Table 2.

Following SBRT there were 10 spine segments that developed VBC (10%), 9 which were de novo VBC and 1 that was progression of a prior VBC. Median time to VBC was 2.4 months (IQR, 0.9–4.0). Of the 11 spine segments that underwent kyphoplasty prior to SBRT, none developed subsequent VBC. No clinical or SINS factors were associated with VBC upon univariate analysis.

TABLE 3. Logistic univariate analysis of factors associated with vertebral body collapse

	Univariate analysis p-value
Gender	0.60
Age (≥ 68 v.s < 67)	0.89
KPS (≥ 80 vs. < 80)	0.38
Spine level (cervical v.s thoracic)	0.74
Spine Level (cervical vs. lumbosacral)	0.48
Spine Level (thoracic vs. lumbosacral)	0.53
Paraspinal extension	1.00
Dose per fraction (< 9 Gy v.s ≥ 9 Gy)	0.43
Location (rigid/semi-rigid vs mobile/junctional spine)	0.79
Mechanical pain	0.79
Lytic vs non-lytic bone lesion	0.93
Spinal alignment (normal vs. kyphosis/scoliosis)	0.96
Posterolateral involvement	0.29

CI = confidence interval; HR = Hazard ratio; KPS = Karnofsky performance status; SBRT = stereotactic body radiation therapy

Discussion

This study reviewed a large single-institutional experience with spine SBRT through evaluation of VBC and SINS. As implementation of spine SBRT into practice continues to evolve, there is greater need for tools to identify patients at highest risk of adverse events such as VBC. We report the risk of VBC to be 10%, which agrees with other studies that found the risk to range from 4% to 39%.[8-13] The wide range of published VBC rates likely owes to differences in treatment technique and patient selection. Unlike previous reports, our study was unable to identify additional clinical or SINS factors associated with VBC. A systematic review of studies examining risk of VBC post-SBRT and reporting risk factors identified lytic disease, baseline VBC prior to SBRT, higher dose per fraction SBRT, spinal deformity, older age, and more than 40% to 50% of vertebral body involved by tumor to be the most frequent factors associated with VBC on Multivariable analysis.[23]

Management of a radiation induced VBC can be challenging and may require surgical intervention. In a review of patients developing VBC after spine SBRT, they found that 32% of patients needed a salvage spinal reconstruction procedure, consisting primarily of percutaneous cement augmentation procedures in 77% of patients while the remaining patients required open spinal reconstructive surgery.[24] Method of salvage intervention is institutionally dependent and will vary based on resources available, clinical factors, and patient performance status. While spinal instrumentation may provide greater stability than cement augmentation procedures such as kyphoplasty, these are more invasive procedures and typically result in more post-operative pain.

A key finding from our study is no post-treatment VBC occurred in patients that underwent prophylactic kyphoplasty prior to SBRT. While kyphoplasty prior to spine SBRT has previously been shown to be safe and effective in small series, neither reported rates of subsequent VBC.[25,26] In agreement with these findings, another study found the incidence of VBC to be lower in patients that underwent surgical intervention or vertebro-

plasty prior to SBRT.[17] The optimal timing and patient selection for kyphoplasty in those undergoing spine SBRT still remains under investigation. By utilizing previously identified risk factors, patients at high risk of fracture should be considered for kyphoplasty to protect them from complications prior to ablative therapy with SBRT.

Limitations

This study has multiple limitations. As with any retrospective study, there may be loss of data and miscoding during abstraction from the medical record. Additionally, our cohort was limited by the number of patients included. The sample size and low number of VBC events may not have been sufficient to confirm previously identified risk factors for VBC with statistical significance. Another limitation is the heterogeneity of patient clinical factors and years treated, which resulted in variation in how patients were approached with SBRT and different follow-up imaging protocols. Despite these limitations, this study presents valuable data demonstrating low rates of VBC following spine SBRT and the potential protective effects of prophylactic kyphoplasty on further reducing this rate in appropriately selected patients. Furthermore, some patients didn't receive ablative dose to vertebra, only palliative dose was delivered. One patient received only 2x5 Gy and there are few with 5x4 Gy fractionation.

Conclusions

The rate of vertebral body collapse following spine SBRT is low. Prophylactic kyphoplasty may provide protection against VBC and should be considered for patients at high risk for fracture.

Acknowledgements

Funding support

This project is supported in part by funding from the National Cancer Institute of the National Institutes of Health under Award number: R25CA181003. The funding sources had no role in the preparation of this manuscript.

Author contributions

Arsh Issany: Data Curation, Investigation, Formal Analysis, Writing - Original Draft. Austin J. Iovoli: Supervision, Writing – Review & Editing. Richard Wang: Data Curation, Writing – Review & Editing. Rohil Shekher: Methodology, Writing – Review & Editing. Sung Jun Ma: Methodology, Supervision, Writing – Review & Editing. Victor Goulenko: Writing – Review & Editing. Fatemeh Fekrmandi: Writing – Review & Editing. Dheerendra Prasad: Conceptualization, Validation, Supervision, Writing – Review & Editing.

Data sharing

Research data are stored in an institutional repository and will be shared upon request to the corresponding author.

References

1. Abbouchie H, Chao M, Tacey M, Lim Joon D, Ho H, Guerrieri M, et al. Vertebral fractures following stereotactic body radiotherapy for spine metastases. *J Med Imaging Radiat Oncol* 2020; **64:** 293-302. doi: 10.1111/1754-9485.13010
2. Cole JS, Patchell RA. Metastatic epidural spinal cord compression. *Lancet Neurol* 2008; **7:** 459-66. doi: 10.1016/s1474-4422(08)70089-9
3. Wang XS, Rhines LD, Shiu AS, Yang JN, Selek U, Gning I, et al. Stereotactic body radiation therapy for management of spinal metastases in patients without spinal cord compression: a phase 1-2 trial. *Lancet Oncol* 2012; **13:** 395-402. doi: 10.1016/S1470-2045(11)70384-9
4. Bindels BJJ, Hovenier R, Groot OQ, Vincken KL, Rongen JJ, Smits MLJ, et al. Stereotactic body and conventional radiotherapy for painful bone metastases: a systematic review and meta-analysis. *JAMA Network Open* 2024; **7:** e2355409-e2355409. doi: 10.1001/jamanetworkopen.2023.55409
5. Singh R, Lehrer EJ, Dahshan B, Palmer JD, Sahgal A, Gerszten PC, et al. Single fraction radiosurgery, fractionated radiosurgery, and conventional radiotherapy for spinal oligometastasis (SAFFRON): a systematic review and meta-analysis. *Radiother Oncol* 2020; **146:** 76-89. doi: 10.1016/j.radonc.2020.01.030
6. Song X, Wei J, Sun R, Jiang W, Chen Y, Shao Y, et al. Stereotactic body radiation therapy versus conventional radiation therapy in pain relief for bone metastases: a systematic review and meta-analysis. *Int J Radiat Oncol Biol Phys* 2023; **115:** 909-21. doi: 10.1016/j.ijrobp.2022.10.017
7. Zeng KL, Myrehaug S, Soliman H, Husain ZA, Tseng CL, Detsky J, et al. Mature local control and reirradiation rates comparing spine stereotactic body radiation therapy with conventional palliative external beam radiation therapy. *Int J Radiat Oncol Biol Phys* 2022; **114:** 293-300. doi: 10.1016/j.ijrobp.2022.05.043
8. Boehling NS, Grosshans DR, Allen PK, McAleer MF, Burton AW, Azeem S, et al. Vertebral compression fracture risk after stereotactic body radiotherapy for spinal metastases. *J Neurosurg Spine* 2012; **16:** 379-86. doi: 10.3171/2011.11.Spine116
9. Cunha MV, Al-Omair A, Atenafu EG, Masucci GL, Letourneau D, Korol R, et al. Vertebral compression fracture (VCF) after spine stereotactic body radiation therapy (SBRT): analysis of predictive factors. *Int J Radiat Oncol Biol Phys* 2012; **84:** e343-9. doi: 10.1016/j.ijrobp.2012.04.034
10. Ozdemir Y, Torun N, Guler OC, Yildirim BA, Besen AA, Yetisken AG, et al. Local control and vertebral compression fractures following stereotactic body radiotherapy for spine metastases. *J Bone Oncol* 2019; **15:** 100218. doi: 10.1016/j.jbo.2019.100218
11. Sahgal A, Atenafu EG, Chao S, Al-Omair A, Boehling N, Balagamwala EH, et al. Vertebral compression fracture after spine stereotactic body radiotherapy: a multi-institutional analysis with a focus on radiation dose and the spinal instability neoplastic score. *J Clin Oncol* 2013; **31:** 3426-31. doi: 10.1200/jco.2013.50.1411

12. Husain ZA, Sahgal A, De Salles A, Funaro M, Glover J, Hayashi M, et al. Stereotactic body radiotherapy for de novo spinal metastases: systematic review. *J Neurosurg Spine* 2017; **27:** 295-302. doi: 10.3171/2017.1.SPINE16684

13. Rose PS, Laufer I, Boland PJ, Hanover A, Bilsky MH, Yamada J, et al. Risk of fracture after single fraction image-guided intensity-modulated radiation therapy to spinal metastases. *J Clin Oncol* 2009; **27:** 5075-9. doi: 10.1200/jco.2008.19.3508

14. Hulme PA, Krebs J, Ferguson SJ, Berlemann U. Vertebroplasty and kyphoplasty: a systematic review of 69 clinical studies. *Spine* 2006; **31:** 1983-2001. doi: 10.1097/01.brs.0000229254.89952.6b

15. Pielkenrood BJ, Gal R, Kasperts N, Verhoeff JJC, Bartels MMTJ, Seravalli E, et al. Quality of life after stereotactic body radiation therapy versus conventional radiation therapy in patients with bone metastases. *Int J Radiat Oncol Biol Phys* 2022; **112:** 1203-15. doi: 10.1016/j.ijrobp.2021.12.163

16. Mantel F, Sweeney RA, Klement RJ, Hawkins MA, Belderbos J, Ahmed M, et al. Risk factors for vertebral compression fracture after spine stereotactic body radiation therapy: Long-term results of a prospective phase 2 study. *Radiother Oncol* 2019; **141:** 62-6. doi: 10.1016/j.radonc.2019.08.026

17. Kowalchuk RO, Johnson-Tesch BA, Marion JT, Mullikin TC, Harmsen WS, Rose PS, et al. Development and assessment of a predictive score for vertebral compression fracture after stereotactic body radiation therapy for spinal metastases. *JAMA Oncol* 2022; **8:** 412-9. doi: 10.1001/jamaoncol.2021.7008

18. Coumans JV, Reinhardt MK, Lieberman IH. Kyphoplasty for vertebral compression fractures: 1-year clinical outcomes from a prospective study. *J Neurosurg* 2003; **99(1 Suppl):** 44-50. doi: 10.3171/spi.2003.99.1.0044

19. Chi JH, Gokaslan ZL. Vertebroplasty and kyphoplasty for spinal metastases. *Curr Opin Support Palliat Care* 2008; **2:** 9-13. doi: 10.1097/SPC.0b013e3282f5d907

20. Health Quality Ontario. Vertebral augmentation involving vertebroplasty or kyphoplasty for cancer-related vertebral compression fractures: a systematic review. *Ont Health Technol Assess Ser* 2016; **16:** 1-202. PMID: 27298655

21. Fisher CG, DiPaola CP, Ryken TC, Bilsky MH, Shaffrey CI, Berven SH, et al. A novel classification system for spinal instability in neoplastic disease: an evidence-based approach and expert consensus from the Spine Oncology Study Group. *Spine* 2010; **35:** E1221-9. doi: 10.1097/BRS.0b013e3181e16ae2

22. Redmond KJ, Robertson S, Lo SS, Soltys SG, Ryu S, McNutt T, et al. Consensus contouring guidelines for postoperative stereotactic body radiation therapy for metastatic solid tumor malignancies to the spine. *Int J Radiat Oncol Biol Phys* 2017; **97:** 64-74. doi: 10.1016/j.ijrobp.2016.09.014

23. Faruqi S, Tseng CL, Whyne C, Alghamdi M, Wilson J, Myrehaug S, et al. Vertebral compression fracture after spine stereotactic body radiation therapy: A review of the pathophysiology and risk factors. *Neurosurgery* 2018; **83:** 314-22. doi: 10.1093/neuros/nyx493

24. Sahgal A, Whyne CM, Ma L, Larson DA, Fehlings MG. Vertebral compression fracture after stereotactic body radiotherapy for spinal metastases. *Lancet Oncol* 2013; **14**: e310-20. doi: 10.1016/S1470-2045(13)70101-3

25. Barzilai O, DiStefano N, Lis E, Yamada Y, Lovelock DM, Fontanella AN, et al. Safety and utility of kyphoplasty prior to spine stereotactic radiosurgery for metastatic tumors: a clinical and dosimetric analysis. *J Neurosurg Spine* 2018; **28:** 72-8. doi: 10.3171/2017.5.SPINE1746

26. Gerszten PC, Germanwala A, Burton SA, Welch WC, Ozhasoglu C, Vogel WJ. Combination kyphoplasty and spinal radiosurgery: a new treatment paradigm for pathological fractures. *J Neurosurg Spine* 2005; **3:** 296-301. doi: 10.3171/spi.2005.3.4.0296

research article

A retrospective evaluation of therapeutic efficacy and safety of chemoradiotherapy in older patients (aged ≥ 75 years) with limited-disease small cell lung cancer: insights from two institutions and review of the literature

Ayako Shiono[1], Hisao Imai[1,2], Satoshi Endo[2], Kazuki Katayama[1], Hideaki Sato[1], Kosuke Hashimoto[1], Yu Miura[1], Shohei Okazaki[3], Takanori Abe[4], Atsuto Mouri[1], Kyoichi Kaira[1], Ken Masubuchi[2], Kunihiko Kobayashi[1], Koichi Minato[2,5], Shingo Kato[4], Hiroshi Kagamu[1]

[1] Department of Respiratory Medicine, International Medical Center, Saitama Medical University, Saitama, Japan
[2] Division of Respiratory Medicine, Gunma Prefectural Cancer Center, Gunma, Japan
[3] Division of Radiation Oncology, Gunma Prefectural Cancer Center, Gunma, Japan
[4] Department of Radiation Oncology, International Medical Center, Saitama Medical University, Saitama, Japan
[5] Division of Health Evaluation and Promotion, SUBARU Health Insurance Society, Ota Memorial Hospital, Gunma, Japan

Radiol Oncol 2024; 58(3): 432-443.

Received 9 December 2023
Accepted 26 August 2024

Correspondence to: Hisao Imai, M.D., Ph.D., Department of Respiratory Medicine, International Medical Center, Saitama Medical University, 1397-1 Yamane, Hidaka-City, Saitama 350-1298, Japan. E-mail: m06701014@gunma-u.ac.jp

Disclosure: No potential conflicts of interest were disclosed.

Background. The standard treatment for patients in good general condition with limited-disease small cell lung cancer (LD-SCLC) is concurrent platinum/etoposide chemotherapy and thoracic radiotherapy (TRT). However, the efficacy and safety of chemoradiotherapy (CRT) in older patients with LD-SCLC has not been fully explored; moreover, the optimal treatment for this patient group remains unclear. This study aimed to investigate the feasibility and efficacy of CRT in older patients with LD-SCLC.

Patients and methods. From April 2007 to June 2021, consecutive older patients (aged ≥ 75 years) with stage I to III SCLC who received concurrent or sequential CRT at two institutions were retrospectively evaluated for efficacy and toxicity of CRT.

Results. A total of 32 older patients underwent concurrent (n = 19) or sequential (n = 13) CRT for LD-SCLC. The median ages of the patients in the concurrent and sequential CRT groups were 77 (range: 75–81) years and 79 (range: 76–92) years, respectively. The median number of chemotherapeutic treatment cycles was four (range, 1–5), and the response rate was 96.9% in all patients (94.7% in concurrent and 100% in sequential CRT groups). The median progression-free survival (PFS) and median overall survival (OS) for all patients were 11.9 and 21.1 months, respectively. The median PFS was 13.0 and 9.0 months in the concurrent CRT and sequential CRT groups, respectively, with no statistically significant difference ($p = 0.67$). The median OS from the initiation of CRT was 19.2 and 23.5 months in the concurrent and sequential CRT groups, respectively ($p = 0.46$). The frequencies of Grade ≥ 3 hematological adverse events were as follows: decreased white blood cell count, 20/32 (62.5%); decreased neutrophil count, 23/32 (71.9%); anemia, 6/32 (18.8%); decreased platelet count, 7/32 (21.9%); and febrile neutropenia, 3/32 (9.4%). Treatment-related deaths occurred in one patient from each group.

Conclusions. Although hematological toxicities, particularly reduced neutrophil count, were severe, CRT showed favorable efficacy in both concurrent and sequential CRT groups. However, concurrent CRT may not be feasible for all older patients with LD-SCLC; accordingly, sequential CRT may be considered as a treatment of choice for these patients. Further prospective trials are warranted to identify optimal treatment strategies for this patient group.

Key words: chemoradiotherapy; chemotherapy; older patients; efficacy; limited disease; radiotherapy; safety; small cell lung cancer

Introduction

Lung cancer is the leading cause of cancer-related deaths worldwide.[1] Small cell lung cancer (SCLC) accounts for 10–15% of all lung cancers and is an aggressive tumor characterized by early development of extensive metastases and rapid growth.[2,3] Limited-disease SCLC (LD-SCLC) is restricted to one hemithorax and its regional lymph nodes, and it can be treated with a single radiotherapy field. Furthermore, LD-SCLC accounts for one-third of all SCLCs cases at the time of diagnosis.[1] The proportion of older patients with SCLC continues to increase with the growing geriatric population.[4,5] Approximately 30–40% of patients with SCLC are ≥ 70-years-old at their diagnosis[6], and it is becoming increasingly crucial to understand how SCLC therapy should be tailored for older patients.

The standard treatment for patients with LD-SCLC in good general condition is concurrent platinum/etoposide chemotherapy and thoracic radiotherapy (TRT), followed by prophylactic cranial irradiation (PCI) for those who respond to chemoradiotherapy (CRT).[7,8] However, many clinical studies on LD-SCLC have precluded the enrollment of older patients for reasons such as a decline in organ function or comorbidities.[9,10] For example, a previous study demonstrated that a cisplatin plus etoposide combination regimen and concurrent TRT are more effective for the treatment of LD-SCLC than a cisplatin plus etoposide combination and sequential TRT[11]; however, it is noteworthy that patients aged ≥ 75 years were precluded from enrolling in the study.

Retrospective subset studies of patients with LD-SCLC treated with cisplatin, along with etoposide and concurrent early CRT, in randomized phase III studies have demonstrated that severe hematological adverse event, pneumonitis of Grade 4 or more, and treatment-related deaths were observed more frequently in older patients aged ≥ 70 years than their younger counterparts.[12,13] Although the objective response rate and 5-year event-free survival rate were not significantly different between these two subgroups, there was a trend for them to be worse in older patients. Notably, a significant difference in the 5-year overall survival rate was observed in patients < 70 years of age in one trial.[12,13] These results imply that the combination of cisplatin and etoposide is toxic to older patients with LD-SCLC, and that the most suitable treatment remains unclear.

However, the therapeutic efficacy and toxicity of CRT in older patients with LD-SCLC have not yet been fully examined. In particular, as mentioned above, older patients with LD-SCLC aged ≥ 75 years are excluded from clinical trials[11] or studies focusing on patients aged ≥ 75 years are scarce. Thus, the aim of our analysis was to retrospectively evaluate the safety and treatment efficacy of CRT and to explore the most suitable therapy for older patients with LD-SCLC aged ≥ 75 years. We assessed patient backgrounds, treatment compliance, treatment efficacy, and toxicity between patients who underwent concurrent and sequential CRT.

Patients and methods

Patients

We retrospectively analyzed the medical records of consecutive patients with Stage I–III LD-SCLC, aged ≥ 75 years, whose treatment plan involved concurrent or sequential CRT between April 2007 and June 2021 at two Japanese institutions (International Medical Center, Saitama Medical University and Gunma Prefectural Cancer Center). The requirement for written informed consent was waived by the Ethics Committee of Saitama Medical University owing to the retrospective nature of the study. All procedures complied with the tenets of the Declaration of Helsinki. The study design was approved by the Institutional Ethics Committee of the International Medical Center at Saitama Medical University (approval number 2023-033).

The inclusion criteria were as follows: (i) older patients aged ≥ 75 years with cytologically or histologically diagnosed SCLC; (ii) patients with involvement of one hemithorax and its regional lymph nodes that could be treated with a single radiotherapy field; and (iii) patients that underwent first-line CRT (concurrent or sequential). The clinical stage of SCLC was determined based on the Union for International Cancer Control tumor-node-metastasis (TNM) Classification, Seventh Edition.[14] The inclusion criteria for concurrent or sequential CRT at our institutions are as follows: patients with a performance status (PS) of 0–2; neutrophil count, ≥ $1.5 \times 10^3/mm^3$; platelet count, ≥ $1.0 \times 10^5/mm^3$; serum creatinine, ≤ 1.5 mg/dl; total bilirubin, ≤ 2.0 mg/dl; and a transaminase level ≤ 100 U/L.

All patients underwent pretreatment physical examinations, chest radiography, computed tomography (CT) scans of the chest/abdomen, CT or magnetic resonance imaging of the brain,

and bone scintigraphy/^{18}F-fluorodeoxyglucose positron-emission tomography to assess the TNM disease stage. Data of each patient were extracted from the electronic medical records.

Treatment

Chemotherapy

A combination of etoposide (60–100 mg/m^2) on days 1–3 plus cisplatin (60–80 mg/m^2) on day 1 or carboplatin (area under the curve [AUC] 3–5) on day 1 was administered intravenously every 3–4 weeks. The chemotherapeutic agent and its dose were determined by an attending physician. The chemotherapeutic administration cycles were repeated every 3–4 weeks. At our institution, the criteria for initiating subsequent cycles of chemotherapy were the same as the criteria for the inclusion of concurrent or sequential CRT as described in the Patient subsection. If these criteria were not met, subsequent cycles were withheld until the dosing criteria were met. If the dosing criteria were not met seven weeks after the first day of the cycle, chemotherapy was discontinued. Generally, the doses of etoposide and platinum (cisplatin or carboplatin) are reduced or chemotherapeutic regimens are altered in the adverse event of Grade 4 decreased platelet count, prolonged Grade 4 decreased white blood cell count / decreased neutrophil count, or Grade 3 or more severe non-hematological toxicity during the previous chemotherapeutic cycle. For neutropenia, a granulocyte colony-stimulating factor was administered as prophylaxis at the discretion of the attending physician. Treatment was terminated when disease progression was observed, intolerable toxicity occurred, or when the patient withdrew consent for treatment.

Radiotherapy

Generally, TRT is started concurrently in the first cycle of chemotherapy or sequentially after four cycles of chemotherapy in older patients with LD-SCLC. The prescribed dose was 45 Gy in 30 fractions (1.5 Gy twice-daily) for the concurrent case and 60 Gy in 30 fractions (2 Gy daily) for the sequential case. All the patients underwent chest CT to facilitate treatment planning. The primary tumor (gross tumor volume [GTV] primary) was delineated in the pulmonary windows, and nodal involvement (GTV node) was delineated in the mediastinal windows. A clinical target volume (CTV) margin of 5 mm was added to the GTV primary and node. To plan the target volume margin, 5 mm was added to the CTV to ensure that the dose reached the target volume. The initial field in the sequential arm was based on pretreatment tumor volume. Regarding dose constraints, for normal lung volume receiving > 20 Gy (V20), the dose was ≤ 35% of the total lung volume and maximum spinal cord dose was < 45 Gy in a once-daily fraction regimen or < 36 Gy in twice-daily fractions regimen. Additionally, TRT was suspended if the patient experienced a decrease in Grade 4 platelet count, radiation pneumonitis, fever caused by infection, decrease in arterial oxygen pressure exceeding 10 mmHg, or if the patient had difficulty swallowing a liquid diet.

After TRT, PCI was administered to patients with a complete or near-complete response represented by a scar-like shadow on chest CT if the physician in charge judged that the patient would benefit from PCI, which consisted of 25 Gy/10 fractions for the entire brain.

Evaluation of treatment response and adverse events

The best overall response and maximum tumor shrinkage were evaluated as tumor responses. Radiographic tumor responses were classified based on the Response Evaluation Criteria in Solid Tumors (RECIST), version 1.1.[15] Tumor responses were defined as complete response (CR), partial response (PR), stable disease (SD), progressive disease (PD), or not evaluated (NE). If treatment failure occurred, the patients were permitted any subsequent treatment based on their preferences. Treatment CRT-related adverse events were graded according to the Common Terminology Criteria for Adverse Events (version 4.0).

Statistical analysis

Categorical variables were analyzed using Fisher's exact test, and continuous variables were analyzed using Welch's t-test. Progression-free survival (PFS) was calculated from the start of treatment until PD or death from any cause, and overall survival (OS) was calculated from the first day of treatment until death or censored on the date of the last follow-up. Survival curves were calculated using the Kaplan–Meier method and compared between the two groups using the log-rank test. Differences were considered statistically significant at a two-tailed p-value of < 0.05. All statistical analyses were performed using the JMP statistical

software, version 11.0, for Windows (SAS Institute, Cary, NC, USA).

Results

Patient characteristics

The patient selection process is illustrated in Supplementary Figure 1. Thirty-two patients were treated with CRT between April 2007 and June 2021 at both institutions (concurrent CRT group, n = 19; sequential CRT group, n = 13) and were assessed for response, survival, and safety of the treatments. Table 1 shows the patient characteristics in the concurrent/sequential CRT group. Men comprised a majority of the patients (n = 27, 84.3%), and the median age of the entire group was 78 (range, 75–92) years. A total of 96.8% of patients had a PS of 0 or 1, and the remaining patients had a PS of 2. All the patients were smokers, and 71.8% had a disease stage of III. No significant differences were observed in the baseline patient characteristics between the concurrent and sequential CRT groups. The median number of chemotherapeutic treatment cycles was four (range 1–4) in the concurrent CRT group and four (range 2–5) in the sequential CRT group.

Most patients (28, 87.5%) were treated with carboplatin and etoposide in combination with radiotherapy. Supplementary Table 1 lists the treatment delivery. The most frequently administered doses in the concurrent CRT group were AUC 4 for carboplatin and 80 mg/m^2 for etoposide (n = 9 patients, 47.3%), and in the sequential CRT group, they were AUC 5 for carboplatin and 80 mg/m^2 for etoposide (n = 4 patients, 30.7%).

Treatment response and survival

Table 2 shows the results of the treatment response. The response rate was 94.7% in the concurrent CRT group (CR, n = 3; PR, n = 15; SD, n = 0; and PD, n = 0) and 100.0% in the sequential CRT group (CR, n = 0; PR, n = 13; SD, n = 0; and PD, n = 0). No significant differences in treatment response were observed between the concurrent and sequential CRT groups.

Regarding survival, median PFS was 11.9 (95% CI: 8.2–15.2) months (Figure 1A) and median OS was 21.1 (95% CI: 13.0–39.5) months (Figure 1B) for all patients. No significant differences were observed in the PFS or OS between concurrent and sequential CRT groups. Median PFS was 13.0 (95% CI: 7.8–18.2) months in the concurrent group and 9.0 (95% CI: 6.0–not reached) months in the sequential group ($p = 0.67$; Figure 2A). Median OS was 19.2 (95% CI: 11.0–37.1) months in the concurrent CRT group and 23.5 (95% CI: 11.0–not reached) months in the sequential CRT group ($p = 0.46$; Figure 2B).

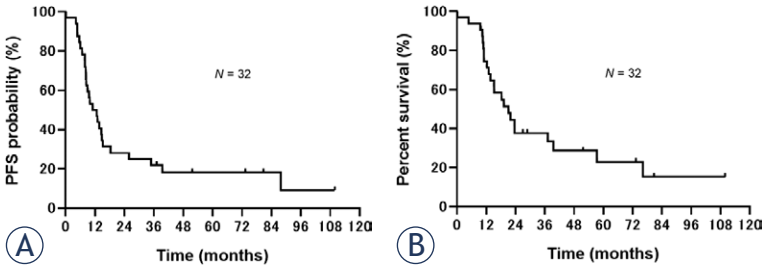

FIGURE 1A. Kaplan-Meier analysis of the progression-free survival of the 32 patients. The median progression-free survival was 11.9 months.

FIGURE 1B. Kaplan-Meier analysis of the overall survival of 32 patients. The median overall survival was 21.1 months.

Toxicity

Treatment-related adverse events of all the patients are presented in Table 3. Toxicity was evaluated in all 32 patients. Myelosuppression was the most frequent treatment-related adverse event—decreased neutrophil counts (Grade 3 or 4) were seen in 71.9% patients and decreased white blood cell counts (Grade 3 or 4) in 62.5% patients. Febrile neutropenia was observed in three patients (9.4%). Grade 3 or 4 anemia occurred in six patients (18.8%), and decreased platelet counts (Grade 3 or 4) in seven patients (21.9%). The incidence of non-hematological toxicities was low, and the most frequent Grade 3 or 4 non-hematologic toxicity was infection (12.5%). Grade 3 or 4 pneumonitis was seen in two patients. Adverse events leading to treatment discontinuation occurred in 6/19 (31.6%) patients in the concurrent CRT group and 1/13 (7.7%) patients

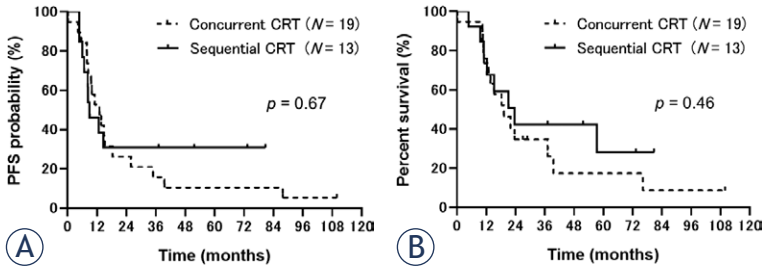

FIGURE 2A. Progression-free survival (PFS) of the concurrent and sequential chemoradiotherapy groups. The median PFS was 13.0 months in the concurrent group and 9.0 months in the sequential group ($p = 0.67$).

FIGURE 2B. The overall survival (OS) of the concurrent and sequential chemoradiotherapy groups. The median OS was 19.2 months in the concurrent group and 23.5 months in the sequential group ($p = 0.46$).

TABLE 1. Baseline patient characteristics

Characteristic	Total (*N* = 32)	Concurrent CRT group (*n* = 19)	Sequential CRT group (*n* = 13)	*p*[a]
Sex				
Male / female	27 / 5	16 / 3	11 / 2	> 0.99
Age (years)				
Median	78	77	79	0.05[b]
Range	75–92	75–81	76–92	
ECOG-PS, *n*				
0 / 1 / 2 / 3 / 4	12 / 19 / 1 / 0 / 0	6 / 12 / 1 / 0 / 0	6 / 7 / 0 / 0 / 0	
Smoking status, *n*				
Yes / no	32 / 0	19 / 0	13 / 0	> 0.99
Histology, *n*				
Small cell carcinoma / combined small cell carcinoma	29 / 3	18 / 1	11 / 2	0.55
Disease stage, *n*				
I / II / III / postoperative recurrence	5 / 4 / 23 / 0	4 / 2 / 13 / 0	1 / 2 / 10 / 0	
History of postoperative adjuvant chemotherapy, *n*				
Yes / no	0 / 32	0 / 19	0 / 13	> 0.99
Number of cycles chemotherapy administered, *n*				
Median	4	4	4	0.19[b]
Range	1–5	1–4	2–5	
Chemotherapy regimen, *n*				
CBDCA+etoposide / CDDP+etoposide	28 / 4	16 / 3	12 /1	0.63
With or without G-CSF prophylaxis, *n*				
Yes / no	27 / 5	17 / 2	10 / 3	0.37
Radiation irradiation method, *n*				
Conventional / accelerated hyperfractionated radiotherapy	26 / 6	14 / 5	12 / 1	0.36
Completion of chemotherapy, *n*				
Yes / no	21 / 11	11 / 8	10 / 3	0.45
Completion of radiotherapy, *n*				
Yes / no	31 / 1	18 / 1	13 / 0	> 0.99
Prophylactic cranial irradiation, *n*				
Yes / no	2 / 30	2 / 17	0 / 13	0.50
Reason for discontinuation of chemotherapy administration[b], *n*				
Progressive disease	1[c]	0	1	
Adverse events	7	6	1	
Others	3	2	1	
Alive at data cutoff, *n*				
Alive / death	8 / 24	4 / 15	4 / 9	0.68

CBDCA = carboplatin; CDDP = cisplatin; CRT = chemoradiotherapy; ECOG-PS = Eastern Cooperative Oncology Group - Performance Status; G-CSF = granulocyte colony-stimulating factor

[a] Comparison between the concurrent and sequential chemoradiotherapy groups

[b] Welch's *t*-test

[c] The clinical progressive disease after two courses of chemotherapy, followed by definitive radiotherapy and partial response (PR)

TABLE 2. Treatment response

Response	Total (*N* = 32)	Concurrent CRT (*n* = 19)	Sequential CRT (*n* = 13)	*p*[a]
Complete response	3	3	0	
Partial response	28	15	13	
Stable disease	0	0	0	
Progressive disease	0	0	0	
Not evaluated	1	1	0	
Response rate (%) (95% CI)	96.9 (82.9–100)	94.7 (73.5–100)	100 (-)	> 0.99
Disease control rate (%) (95% CI)	96.9 (82.9–100)	94.7 (73.5–100)	100 (-)	> 0.99

CRT = chemoradiotherapy; 95% CI = 95% confidence interval

[a] Comparison between the concurrent and sequential chemoradiotherapy groups

in the sequential CRT group and were more frequent in the concurrent CRT group, although the difference was not significant ($p = 0.06$). Treatment-related deaths occurred in two patients, one in each group. One patient suffered from pneumonitis in the sequential group and another patient suffered from acute coronary syndrome in the concurrent group.

Analysis of myelosuppression revealed that hematological toxicities occurring with sequential CRT were milder than those with concurrent CRT (Table 3). The frequencies of Grade 3 or 4 hematologic toxicities in patients receiving sequential CRT versus those receiving concurrent CRT were as follows: white blood cell count decreased by 30.8% versus 84.2%, respectively ($p = 0.004$); neutrophil count decreased by 61.5% versus 78.9%, respectively ($p = 0.43$); anemia decreased by 7.7% versus 26.3%, respectively ($p = 0.36$); and platelet count decreased by 15.4% versus 26.3%, respectively ($p = 0.67$). Febrile neutropenia occurred in 7.7% of patients receiving sequential CRT and in 10.5% of patients receiving concurrent CRT. Other non-hematologic toxicities, such as Grade 3 or higher diarrhea, dermatitis, radiation, infection, pneumothorax, hypotension, generalized muscle weakness, and acute coronary syndrome, were more common in the concurrent CRT group; however, this was not statistically significant.

Subsequent treatment after CRT

Subsequent treatment administered after CRT is presented in Table 4 and recurrence was observed in 27/32 patients. The best supportive care was often the treatment of choice for patients with recurrence after CRT, with a post-relapse chemotherapy conversion rate of 13/27 (48.1%) patients. The most common subsequent chemotherapy was a combination of carboplatin and etoposide, followed by amrubicin monotherapy. Six patients received up to third-line treatment; however, no patients received chemotherapy beyond the fourth-line treatment.

Discussion

This retrospective study assessed the efficacy and safety of CRT in older patients with LD-SCLC. Concurrent and sequential CRT groups demonstrated similar efficacy in the treatment of older patients with LD-SCLC; however, the toxicity profiles tended to be higher in the concurrent CRT group. These safety profiles should be considered when using CRT to treat older patients with LD-SCLC.

Meta-analyses and prospective and retrospective studies specifically focused on older patients with LD-SCLC have shown conflicting results regarding the survival benefits and tolerability of CRT.[16-27] In the CONVERT trial, Christodoulou *et al*. reported the treatment outcomes of a subgroup of patients aged ≥ 70 years with LD-SCLC compared to those of younger patients.[26] Concurrent CRT was found to be feasible in selected, fit older patients with LD-SCLC. Findings of previous studies on CRT in older patients with LD-SCLC are

TABLE 3. Adverse events

Adverse event	All patients (*N* = 32)				Concurrent CRT (*n* = 19)				Sequential CRT (*n* = 13)				
	Any Grade	%	Grade≥3	%	Any Grade	%	Grade≥3	%	Any Grade	%	Grade≥3	%	*p*[a]
Led to discontinuation	7	21.9	6	18.8	6	31.6	6	31.6	1	7.7	0	0.0	0.06
Led to death	-		2	6.3	-	-	1	5.3	-	-	1	7.7	> 0.99
Treatment related[b]													
White blood cell decreased	28	87.5	20	62.5	18	94.7	16	84.2	10	76.9	4	30.8	**0.004**
Neutrophil count decreased	26	81.3	23	71.9	18	94.7	15	78.9	8	61.5	8	61.5	0.43
Anemia	28	87.5	6	18.8	16	84.2	5	26.3	12	92.3	1	7.7	0.36
Platelet count decreased	27	84.4	7	21.9	16	84.2	5	26.3	11	84.6	2	15.4	0.67
Febrile neutropenia	3	9.4	3	9.4	2	10.5	2	10.5	1	7.7	1	7.7	> 0.99
Diarrhea	3	9.4	1	3.1	2	10.5	1	5.3	1	7.7	0	0.0	> 0.99
Constipation	14	43.8	1	3.1	9	47.4	0	0.0	5	38.5	1	7.7	0.41
Dermatitis radiation	8	25.0	1	3.1	2	10.5	1	5.3	6	46.2	0	0.0	> 0.99
Pneumonitis	29	90.6	2	6.3	18	94.7	1	5.3	11	84.6	1	7.7	> 0.99
Infection	7	21.9	4	12.5	4	21.1	3	15.8	3	23.1	1	7.7	0.63
Pneumothorax	2	6.3	2	6.3	2	10.5	2	10.5	0	0.0	0	0.0	0.50
Hypotension	1	3.1	1	3.1	1	5.3	1	5.3	0	0.0	0	0.0	> 0.99
Generalized muscle weakness	1	3.1	1	3.1	1	5.3	1	5.3	0	0.0	0	0.0	> 0.99
Acute coronary syndrome	1	3.1	1	3.1	1	5.3	1	5.3	0	0.0	0	0.0	> 0.99

CRT = chemoradiotherapy. Bold text indicates statistically significant differences.

[a]Comparison between the concurrent cohort and sequential chemoradiotherapy groups of Grade ≥ 3.

[b]Treatment-related adverse events reported as Grade ≥ 3 in ≥ one patient.

summarized in Table 5, along with our findings. Considering the findings of previous prospective trials evaluating CRT in older patients (≥ 70 years) with LD-SCLC, we infer that the response rate, PFS, and OS obtained in our study were satisfactory.[17,23,24,26,27] In meta-analyses and prospective and retrospective studies of older patients with LD-SCLC, the response rates in both the concurrent and sequential CRT groups generally ranged from 70–100%, with PFS ranging from 9–14 months and OS from 17–29 months. Moreover, the therapeutic efficacies were similar, except for those reported by Jeremic *et al*. and Corso *et al.* in which the OS was 15 months and 15.6 months, respectively.

To the best of our knowledge, only a few studies on CRT have been conducted to date in older patients aged ≥ 70 years, and only three studies have been conducted on patients aged ≥ 75 years (two retrospective and one prospective study[18,20,23], both with small numbers of cases; Table 5). A comparison of toxicities between concurrent and sequential CRT groups showed that the frequency of Grade 3 or higher myelosuppression (particularly leukopenia) was higher in the concurrent than in sequential CRT group. However, Kubo *et al*. reported that in the sequential CRT group, Grade 3 or higher neutropenia, thrombocytopenia, febrile neutropenia, and pneumonia were relatively common, which may have been influenced by the chemotherapeutic regimen of cisplatin and topotecan therapy.[23] In general, except in the study by Jeremic *et al*., concurrent CRT was associated with a higher rate of Grade 3 or higher levels of leukopenia, neutropenia, and thrombocytopenia.

TABLE 4. Overview of subsequent chemoradiotherapy treatments

	Second-line	Third-line	≥ Fourth-line
Carboplatin+etoposide	7	0	0
Carboplatin+etoposide+atezolizumab/durvalmab	2	0	0
Carboplatin+irinotecan	0	1	0
Carboplatin+paclitaxel	0	1	0
Amurubicin	4	2	0
Nogitecan	0	0	0
Irinotecan	0	0	0
Others	0	2	0
Best supportive care	14	-	-
No recurrence	5		

In our study, the major adverse events in the concurrent CRT group were hematological toxicities, including decreased white blood cell and neutrophil counts. Gastrointestinal toxicities, including anorexia, nausea, vomiting, and constipation, were relatively mild. However, Grade 3 or higher infection and pneumothorax occurred in three (15.8%) and two (10.5%) patients, respectively. Moreover, there was one treatment-related death. The main adverse events in the sequential CRT group were hematologic toxicities, including decreased white blood cell counts; however, there were significantly fewer cases showing Grade 3 or higher white blood cell decreases, a relatively small proportion of other hematologic and non-hematologic toxicities, including hematocytopenia, and one treatment-related death. In this study, the incidence of Grade 3 or higher adverse events was also higher in the concurrent CRT group than that in the sequential CRT group, except for pneumonitis. Despite prophylactic administration of G-CSF in 27 of 32 patients (84.3%), more than 70% of the total patient, 78.9% of patients in the concurrent CRT group, and 61.5% of patients in the sequential CRT group had Grade 3 or higher neutrophil count decreased. All patients who received G-CSF administered it prophylactically during chemotherapy and not during radiotherapy. Neutrophil count decrease occurred at high rate, but febrile neutropenia occurred in 9.4% of overall patients. Although routine prophylactic administration of G-CSF is not usually recommended, clinical guidelines recommend that patients with risk factors for febrile neutropenia who are treated with chemotherapeutic regimens associated with a ≥ 20% risk of febrile neutropenia should be administered G-CSF as primary prophylaxis.[28,29] Routine prophylactic administration of G-CSF during chemotherapy in CRT in older patients with LD-SCLC is not recommended. However, one report suggests considering primary prophylaxis with G-CSF to prevent febrile neutropenia in male patients with SCLC who are treated with platinum plus etoposide and have a history of radiation therapy, which is a risk factor for febrile neutropenia.[30] Primary prophylaxis with G-CSF may be considered aggressively during chemotherapy in certain situations.

However, it should be noted that when evaluating toxicity, the criteria for determining the Grade of adverse events may not be consistent across different studies. Table 5 shows that treatment discontinuation mainly occurred owing to failure to complete chemotherapy. In studies evaluating concurrent CRT and this study, the proportion of patients who did not complete treatment was > 30%. In this study, of the 19 patients who received concurrent CRT, 6 did not complete a full cycle of chemotherapy owing to toxicity and 1 discontinued TRT. Of the 13 patients who received sequential CRT, one did not complete a full cycle of chemotherapy owing to toxicity. Regarding treatment completion, the concurrent CRT group had a higher rate of toxicity discontinuation than the sequential CRT group in this study. We speculate that patients in good general condition were treated with concurrent CRT and frail patients were treated with sequential CRT. Therefore, as our findings suggest,

TABLE 5. Findings of previous studies on chemoradiotherapy in older patients with limited-disease small cell lung cancer

Report [ref]	Year	Region	Age (years)	Study type	Sample size	PS	Stage	Treatment	Response rate (%) (All, con CRT vs. seq CRT)	PFS (months) (All, con CRT vs. seq CRT)	OS (months) (All, con CRT vs. seq CRT)	Interruption of treatment	Grade 3 or higher[a]
Jeremic et al.[17]	1998	Yugoslavia	≥ 70	Prospective, Phase 2	72	KPS≥60	Limited disease	concurrent CRT (CBDCA+ETP)	75	NR	15	NR	Leukopenia 8.3%, Thrombocytopenia 11%, Infection 4.2%, Pneumonitis 18%
Shimizu et al.[18]	2007	Japan	≥ 75	Retrospective	7	0–1	II–III	concurrent CRT (CBDCA+ETP or CDDP+ETP)	100	NR	24.7	Imcompleted intent cycles of chemotherapy 3/7 (42.8%)	Leukopenia 100%, Neutropenia 100%, Thrombocytopenia 57.1%, FN 42.8%, Pneumonitis 28.5%
Okamoto et al.[19]	2010	Japan	≥ 70	Retrospective	12	0–1	II–III	concurrent CRT (CDDP+ETP)	100	14.2	24.1	Imcompleted intent cycles of chemotherapy 5/12 (41.7%)	Leukopenia 100%, Neutropenia 100%, Thrombocytopenia 33%, FN 67%, Pneumonitis 8%
Shukuya et al.[20]	2013	Japan	≥ 75	Retrospective	20	0–1	II–III	concurrent CRT (CBDCA+ETP or CDDP+ETP); n=5, sequential CRT (CBDCA+ETP or CDDP+ETP); n=15	NR, 100 vs. 80	NR, 208 days vs. 216 days	601 days (seq CRT with CBDCA+ETP)	Con vs. seq CRT; Imcompleted intent cycles of chemotherapy 2/5 (40%) vs., 2/15 (13.3%)	Con vs. seq CRT; Leukopenia 100% vs. 53%, Neutropenia 100% vs. 93%, Thrombocytopenia 20% vs. 27%, FN 60% vs. 13%, Infection 0% vs. 7%, Pneumonitis 0% vs. 27%
Okamoto et al.[21]	2014	Japan	≥ 70	Prospective, Phase 1	12	0–1	Limited disease	concurrent CRT (split CDDP+ETP)	91.6	11.5	17	Imcompleted intent cycles of chemotherapy 5/12 (41.6%)	Leukopenia 100%, Neutropenia 100%, Thrombocytopenia 33%, FN 33%, Pneumonitis 16% (level 2 cohort)
Corso et al.[22]	2015	U.S.A	≥ 70	Retrospective	4362[b]	NR	I–III	concurrent CRT; n=3472, sequential CRT; n=1136	NR	NR	15.6, 17.0 vs. 15.4	NR	NR
Kubo et al.[23]	2016	Japan	≥ 76	Prospective, Phase 2	22	0–2	I–III	sequential CRT (CDDP+TOP)	68	9.1	22.2	Imcompleted intent treatment course of CRT 41%	Neutropenia 96%, Thrombocytopenia 50%, FN 32%, Pneumonitis 18%
Misumi et al.[24]	2017	Japan	≥ 70	Prospective, Phase 1/2	35[c]	0–2	I–III	sequential CRT (CBDCA+CPT11)	88.6	11.2	27.1	Imcompleted intent cycles of chemotherapy 7/35 (20.0%)	Neutrophils 51%, Platelets 11.4%, FN 5.7%, Pneumonitis 5.7%
Stinchcombe et al.[25]	2019	USA	≥ 70	Pooled analysis	254	NR	Limited disease	concurrent CRT (CBDCA+ETP or CDDP+ETP)	NR	10.6	17.8	Imcompleted intent treatment course of CRT 135/250 (54%)	Neutropenia 56%, Pneumonitis 2%
Christodoulou et al.[26]	2019	Europe	≥ 70	Prospective, Phase 3 (subgroup)	67	0–2	I–III	concurrent CRT (CDDP+ETP)	NR	18	29	Imcompleted intent cycles of chemotherapy 25/67 (37.3%)	Neutropenia 84%, Thrombocytopenia 28%, Infection 13%, Pneumonitis 3%
Killingberg et al.[27]	2023	Norway	≥ 70	Prospective, Phase 2 (subgroup)	53	0–2	I–III	concurrent CRT (CBDCA+ETP or CDDP+ETP)	70	12.2	24	Imcompleted TRT as planned 8%, Imcompleted four cycles of chemotherapy 15%	Neutropenia 80%, Thrombocytopenia 30%, Infection 4%, Pneumonitis 4%
Current study		Japan	≥ 75	Retrospective	32	0–2	I–III	concurrent CRT (CBDCA+ETP or CDDP+ETP); n=19, sequential CRT (CBDCA+ETP or CDDP+ETP); n=13	96.9, 94.7 vs. 100	11.8, 13.0 vs. 9.0	21.1, 19.2 vs. 23.5	Con vs. seq CRT; Imcompleted intent cycles of chemotherapy 6/19 (31.6%) vs. 1/13 (7.7%)	Con vs. seq CRT; White blood cell decreased 84.2% vs. 30.8%, Neutrophil count decreased 78.9% vs. 61.5%, Platelet count decreased 26.3% vs. 15.4%, FN 10.5% vs. 7.7%, Infection 15.8% vs. 7.7%, Pneumonitis 5.3% vs. 7.7%

CBDCA = carboplatin; CDDP = cisplatin; con CRT = concurrent chemoradiotherapy; CPT11 = irinotecan; ETP = etoposide; FN = febrile neutropenia; KPS = Karnofsky performance status; NR = not reported; OS = overall survival; PFS = progression-free survival; PS = performance status; seq CRT = sequential chemoradiotherapy

[a] Some studies use different versions of the Common Terminology Criteria for Adverse Events.

[b] Patients receiving CRT with survival of at least 4 months after diagnosis

[c] Phase 2 cohort

it may not be possible to perform concurrent CRT in all older patients (> 75 years) with LD-SCLC. Furthermore, radiation pneumonitis should be considered with caution, as Grade 3 or higher severe pneumonitis occurred in 2/32 patients (6.3%) in our study. To reduce the frequency and severity of radiation pneumonitis, it may be appropriate to set the irradiation field according to the tumor volume after the induction of chemotherapy in the case of sequential CRT.[31]

Older patients with good PS and normal organ function, including those with extensive SCLC, tend to be treated using the same regimens as younger patients undergoing chemotherapy. However, some studies have suggested that these older patients may be at greater risk of severe toxicity as compared to their younger counterparts.[4,32] Regarding whether chemotherapy regimens based on cisplatin or carboplatin, in combination with TRT, are superior, a meta-analysis demonstrated that both cisplatin-based and carboplatin-based chemotherapy regimens are equally effective in SCLC.[33] In addition, the studies shown in Table 5 have shown that carboplatin-based combination regimens are relatively more common in older patients. Thus, non-cisplatin chemotherapeutic regimens such as carboplatin and etoposide have become the favored chemotherapy regimens for older patients with SCLC.[34]

Our study population included patients enrolled from 2007–2021, during which time improvements in supportive care, such as antiemetic drugs, and developments in radiation methods and devices may have affected the efficacy and safety of the treatment. As shown in Table 4, approximately half of the patients who relapsed received subsequent chemotherapy. Kasahara *et al*. reported that treatments administered after first-line CRT might affect OS.[35] In this study, two patients were treated with chemotherapy combined with immune checkpoint inhibitors (ICIs), which may have affected OS. In the future, the use of more active ICIs in older patients with LD-SCLC who relapse after CRT may have a significant impact on the long-term prognosis.

This study had some limitations. First, this study had a retrospective design and a small sample size, thereby limiting the generalizability of the findings. A retrospective study design depends on subjective physician examinations, leading to variabilities in tumor response and PFS data. Second, the intervals between lesion evaluations in this study were not as consistent as those in a prospective trial. Thus, the potential significance of the sources of bias must be considered when interpreting our data. In particular, the severity of non-hematological adverse events may have been underestimated owing to the retrospective nature of this study. Third, patients were treated as inpatients for most of the treatment duration, and data on treatment toxicities were recorded in detail in the patients' medical records. This exploratory analysis could not be considered definitive. Nevertheless, because it is difficult to collect data on a large number of older patients with LD-SCLC who have received CRT, our findings may be helpful for physicians in determining the optimal treatment choice for this patient group.

In summary, although hematological toxicities, particularly decreased neutrophil counts, were severe, CRT showed favorable efficacy not only in the concurrent CRT group, but also in the sequential CRT group. However, concurrent CRT may not be feasible for all older patients with LD-SCLC, and sequential CRT should be considered as a treatment choice for this patient group. Further prospective trials are warranted to develop and evaluate optimal treatment strategies for older patients with LD-SCLC.

Acknowledgements

The authors thank Ms. Kyoko Nakagawa for her assistance in preparing this manuscript. No funding was received for this study.

Author contributions

All the authors have read and approved the final manuscript. Conceptualization and methodology, A.S. and H.I.; Formal analysis and data curation, H.I. and K. Kaira; Project administration, visualization, and writing—original draft preparation, A.S. and H.I.; Supervision, K. Kaira. and H.K.; Investigation and resources, S.E., K. Katayama, H.S., K.H., Y.M., S.O., T.A., A.M., K. Masubuchi, K. Minato, K. Kobayashi, and S.K.; writing, review, and editing, all authors.

Data availability statement

The data that support the findings of this study are available from the corresponding author, HI, upon reasonable request. The data are not publicly available owing to privacy or ethical restrictions.

References

1. Bray F, Ferlay J, Soerjomataram I, Siegel RL, Torre LA, Jemal A. Global cancer statistics 2018: GLOBOCAN estimates of incidence and mortality worldwide for 36 cancers in 185 countries. *CA Cancer J Clin* 2018; **68:** 394-424. doi: 10.3322/caac.21492
2. Govindan R, Page N, Morgensztern D, Read W, Tierney R, Vlahiotis A, et al. Changing epidemiology of small-cell lung cancer in the United States over the last 30 years: analysis of the surveillance, epidemiologic, and end results database. *J Clin Oncol* 2006; **24:** 4539-44. doi: 10.1200/JCO.2005.04.4859
3. Dómine M, Moran T, Isla D, Martí JL, Sullivan I, Provencio M, et al. SEOM clinical guidelines for the treatment of small-cell lung cancer (SCLC) (2019). *Clin Transl Oncol* 2020; **22:** 245-55. doi: 10.1007/s12094-020-02295-w
4. Sekine I, Yamamoto N, Kunitoh H, Ohe Y, Tamura T, Kodama T, Saijo N. Treatment of small cell lung cancer in the elderly based on a critical literature review of clinical trials. *Cancer Treat Rev* 2004; **30:** 359-68. doi: 10.1016/j.ctrv.2003.12.006
5. Morita T. A statistical study of lung cancer in the annual of pathological autopsy cases in Japan, from 1958 to 1997, with reference to time trends of lung cancer in the world. *Jpn J Cancer Res* 2002; **93:** 15-23. doi: 10.1111/j.1349-7006.2002.tb01195.x
6. Pallis AG, Shepherd FA, Lacombe D, Gridelli C. Treatment of small-cell lung cancer in elderly patients. *Cancer* 2010; **116:** 1192-200. doi: 10.1002/cncr.24833
7. National Comprehensive Cancer Network clinical practice guidelines in oncology (NCCN Guidelines®). Small cell lung cancer. [internet]. 2023. [cited 2023 Oct 9]. Available at: https://www.nccn.org/guidelines/guidelines-detail?category=1&id=1462
8. Dingemans AC, Früh M, Ardizzoni A, Besse B, Faivre-Finn C, Hendriks LE, et al. Small-cell lung cancer: ESMO Clinical Practice Guidelines for diagnosis, treatment and follow-up. *Ann Oncol* 2021; **32:** 839-53. doi: 10.1016/j.annonc.2021.03.207
9. Sekine I, Fukuda H, Kunitoh H, Saijo N. Cancer chemotherapy in the elderly. *Jpn J Clin Oncol* 1998; **28:** 463-73. doi: 10.1093/jjco/28.8.463
10. Talarico L, Chen G, Pazdur R. Enrollment of elderly patients in clinical trials for cancer drug registration: a 7-year experience by the US Food and Drug Administration. *J Clin Oncol* 2004; **22:** 4626-31. doi: 10.1200/JCO.2004.02.175
11. Takada M, Fukuoka M, Kawahara M, Sugiura T, Yokoyama A, Yokota S, et al. Phase III study of concurrent *versus* sequential thoracic radiotherapy in combination with cisplatin and etoposide for limited-stage small-cell lung cancer: results of the Japan Clinical Oncology Group Study 9104. *J Clin Oncol* 2002; **20:** 3054-60. doi: 10.1200/JCO.2002.12.071
12. Yuen AR, Zou G, Turrisi AT, Sause W, Komaki R, Wagner H, et al. Similar outcome of elderly patients in intergroup trial 0096. *Cancer* 2000; **89:** 1953-60. doi: 10.1002/1097-0142(20001101)89:9<1953::AID-CNCR11>3.3.CO;2-Y
13. Schild SE, Stella PJ, Brooks BJ, Mandrekar S, Bonner JA, McGinnis WL, et al. Results of combined-modality therapy for limited-stage small cell lung carcinoma in the elderly. *Cancer* 2005; **103:** 2349-54. doi: 10.1002/cncr.21034
14. Goldstraw P, Crowley J, Chansky K, Giroux DJ, Groome PA, Rami-Porta R, et al. The IASLC Lung Cancer Staging Project: proposals for the revision of the TNM stage groupings in the forthcoming (seventh) edition of the TNM Classification of malignant tumours. *J Thorac Oncol* 2007; **2:** 706-14. doi: 10.1097/JTO.0b013e31812f3c1a
15. Eisenhauer EA, Therasse P, Bogaerts J, Schwartz LH, Sargent D, Ford R, et al. New response evaluation criteria in solid tumours: revised RECIST guideline. (version 1.1). *Eur J Cancer* 2009; **45:** 228-47. doi: 10.1016/j.ejca.2008.10.026
16. Gridelli C, Casaluce F, Sgambato A, Monaco F, Guida C. Treatment of limited-stage small cell lung cancer in the elderly, chemotherapy *vs.* sequential chemoradiotherapy *vs.* concurrent chemoradiotherapy: that's the question. *Transl Lung Cancer Res* 2016; **5:** 150-4. doi: 10.21037/tlcr.2016.03.03
17. Jeremic B, Shibamoto Y, Acimovic L, Milisavljevic S. Carboplatin, etoposide, and accelerated hyperfractionated radiotherapy for elderly patients with limited small cell lung carcinoma: a phase II study. *Cancer* 1998; **82:** 836-41. doi: 10.1002/(sici)1097-0142(19980301)82:5<836::aid-cncr6>3.0.co;2-h
18. Shimizu T, Sekine I, Sumi M, Ito Y, Yamada K, Nokihara H, et al. Concurrent chemoradiotherapy for limited-disease small cell lung cancer in elderly patients aged 75 years or older. *Jpn J Clin Oncol* 2007; **37:** 181-5. doi: 10.1093/jjco/hym005
19. Okamoto K, Okamoto I, Takezawa K, Tachibana I, Fukuoka M, Nishimura Y, et al. Cisplatin and etoposide chemotherapy combined with early concurrent twice-daily thoracic radiotherapy for limited-disease small cell lung cancer in elderly patients. *Jpn J Clin Oncol* 2010; **40:** 54-9. doi: 10.1093/jjco/hyp137
20. Shukuya T, Takahashi T, Harada H, Ono A, Akamatsu H, Taira T, et al. Chemoradiotherapy for limited-disease small-cell lung cancer in elderly patients aged 75 years or older. *Jpn J Clin Oncol* 2013; **43:** 176-83. doi: 10.1093/jjco/hys197
21. Okamoto K, Okamoto I, Takeda M, Kobayashi S, Takeda K, Nakamatsu K, et al. A phase I study of split-dose cisplatin and etoposide with concurrent accelerated hyperfractionated thoracic radiotherapy in elderly patients with limited-disease small cell lung cancer. *Jpn J Clin Oncol* 2014; **44:** 743-8. doi: 10.1093/jjco/hyu071
22. Corso CD, Rutter CE, Park HS, Lester-Coll NH, Kim AW, Wilson LD, et al. Role of chemoradiotherapy in elderly patients with limited-stage small-cell lung cancer. *J Clin Oncol* 2015; **33:** 4240-6. doi: 10.1200/JCO.2015.62.4270
23. Kubo T, Fujiwara K, Hotta K, Okada T, Kuyama S, Harita S, et al. A phase II study of topotecan and cisplatin with sequential thoracic radiotherapy in elderly patients with small-cell lung cancer: Okayama Lung Cancer Study Group 0102. *Cancer Chemother Pharmacol* 2016; **78:** 769-74. doi: 10.1007/s00280-016-3135-2
24. Misumi Y, Okamoto H, Sasaki J, Masuda N, Ishii M, Shimokawa T, et al. Phase I/II study of induction chemotherapy using carboplatin plus irinotecan and sequential thoracic radiotherapy (TRT) for elderly patients with limited-disease small-cell lung cancer (LD-SCLC): TORG 0604. *BMC Cancer* 2017; **17:** 377. doi: 10.1186/s12885-017-3353-y
25. Stinchcombe TE, Fan W, Schild SE, Vokes EE, Bogart J, Le QT, et al. A pooled analysis of individual patient data from National Clinical Trials Network clinical trials of concurrent chemoradiotherapy for limited-stage small cell lung cancer in elderly patients *versus* younger patients. *Cancer* 2019; **125:** 382-90. doi: 10.1002/cncr.31813
26. Christodoulou M, Blackhall F, Mistry H, Leylek A, Knegjens J, Remouchamps V, et al. Compliance and outcome of elderly patients treated in the concurrent Once-Daily *versus* Twice-Daily radiotherapy (CONVERT) trial. *J Thorac Oncol* 2019; **14:** 63-71. doi: 10.1016/j.jtho.2018.09.027
27. Killingberg KT, Grønberg BH, Slaaen M, Kirkevold Ø, Halvorsen TO. Treatment outcomes of older participants in a randomized trial comparing two schedules of twice-daily thoracic radiotherapy in limited-stage SCLC. *J Thorac Oncol* 2023; **18:** 803-12. doi: 10.1016/j.jtho.2023.01.012
28. Smith TJ, Bohlke K, Lyman GH, Carson KR, Crawford J, Cross SJ, et al. Recommendations for the use of WBC growth factors: American Society of Clinical Oncology Clinical Practice Guideline Update. *J Clin Oncol* 2015; **33:** 3199-212. doi:10.1200/JCO.2015.62.3488
29. Crawford J, Caserta C, Roila F, Group EGW. Hematopoietic growth factors: ESMO Clinical Practice Guidelines for the applications. *Ann Oncol* 2010; **21(Suppl 5):** v248-51. doi: 10.1093/annonc/mdq195
30. Fujiwara T, Kenmotsu H, Naito T, Kawamura T, Mamesaya N, Kotake M, et al. The incidence and risk factors of febrile neutropenia in chemotherapy-naïve lung cancer patients receiving etoposide plus platinum. *Cancer Chemother Pharmacol* 2017; **79:** 1229-37. doi: 10.1007/s00280-017-3324-7
31. Kies MS, Mira JG, Crowley JJ, Chen TT, Pazdur R, Grozea PN, et al. Multimodal therapy for limited small-cell lung cancer: a randomized study of induction combination chemotherapy with or without thoracic radiation in complete responders; and with wide-field *versus* reduced-field radiation in partial responders: a Southwest Oncology Group Study. *J Clin Oncol* 1987; **5:** 592-600. doi: 10.1200/JCO.1987.5.4.592
32. Oshita F, Kurata T, Kasai T, Fakuda M, Yamamoto N, Ohe Y, et al. Prospective evaluation of the feasibility of cisplatin-based chemotherapy for elderly lung cancer patients with normal organ functions. *Jpn J Cancer Res* 1995; **86:** 1198-202. doi: 10.1111/j.1349-7006.1995.tb03315.x
33. Rossi A, Di Maio M, Chiodini P, Rudd RM, Okamoto H, Skarlos DV, et al. Carboplatin- or cisplatin-based chemotherapy in first-line treatment of small-cell lung cancer: the COCIS meta-analysis of individual patient data. *J Clin Oncol* 2012; **30:** 1692-8. doi: 10.1200/JCO.2011.40.4905

34. Jara C, Gómez-Aldaraví JL, Tirado R, Meseguer VA, Alonso C, Fernández A. Small-cell lung cancer in the elderly--is age of patient a relevant factor? *Acta Oncol* 1999; **38:** 781-6. doi: 10.1080/028418699432941

35. Kasahara N, Imai H, Kaira K, Mori K, Wakuda K, Ono A, et al. Clinical impact of post-progression survival on overall survival in patients with limited-stage disease small cell lung cancer after first-line chemoradiotherapy. *Radiol Oncol* 2015; **49:** 409-15. doi: 10.1515/raon-2015-0037

research article

Long-term results of induction chemotherapy for non-operable esophageal squamous cell carcinoma followed by concurrent chemoradiotherapy: a single-centre experience

Geng Xiang[1], Guangjin Chai[1], Bo Lyu[1], Zhaohui Li[1], Yutian Yin[1], Bin Wang[1], Yanglin Pan[2], Mei Shi[1], Lina Zhao[1]

[1] Department of Radiation Oncology, Xijing Hospital, Air Force Medical University, Xi'an, Shaanxi, China

[2] State Key Laboratory of Cancer Biology, National Clinical Research Center for Digestive Diseases and Xijing Hospital of Digestive Diseases, Xijing Hospital, Air Force Medical University, Xi'an, Shaanxi, China

Radiol Oncol 2024; 58(3): 444-457.

Received 21 February 2024
Accepted 25 June 2024

Correspondence to: DR. Lina Zhao, M.D., Department of Radiation Oncology, Xijing Hospital, The Fourth Military Medical University, Xi'an, Shaanxi, China. E-mail: zhaolina@fmmu.edu.cn; Dr. Mei Shi, M.D., Department of Radiation Oncology, Xijing Hospital, The Fourth Military Medical University, Xi'an, Shaanxi, China. E-mail: mshi82@hotmail.com and Yanglin Pan, State Key Laboratory of Cancer Biology, National Clinical Research Center for Digestive Diseases and Xijing Hospital of Digestive Diseases, Xijing Hospital, Air Force Medical University, Xi'an, Shaanxi, China. E-mail; panyl@fmmu.edu.cn

Disclosure: No potential conflicts of interest were disclosed.

Background. This study aimed to investigate the long-term clinical outcomes and toxicities of induction chemotherapy (IC) followed by concurrent chemoradiotherapy (CCRT) *vs.* CCRT alone in patients with non-operable esophageal squamous cell carcinoma (ESCC).

Patients and methods. Between 2008 and 2022, 271 ESCC patients who received definitive CCRT based on intensity modulated radiation therapy (IMRT)/volumetric modulated arc therapy (VMAT) were enrolled. Through a propensity score-matched (PSM) method, 71 patients receiving IC and CCRT were matched 1:1 to patients who received CCRT alone. The Kaplan-Meier method and Cox proportional hazards model were applied to analyze survival and prognosis.

Results. The IC + CCRT group had no improvement in 5-year overall survival (OS) rate, recurrence-free survival (RFS) rate, and distant metastasis-free survival (DMFS) rate (all $p > 0.05$) compared with the CCRT group. The 5-year OS rate (65.6% *vs.* 17.6% *vs.* 29.3%, $p < 0.001$), RFS rate (65.6% *vs.* 17.6% *vs.* 26.9%, $p < 0.001$), and DMFS rate (62.5% *vs.* 10.3% *vs.* 27.2%, $p < 0.001$) of the IC good responders were significantly higher than that of the IC poor responders and CCRT group. Multivariate analysis revealed that total radiotherapy time (≥ 49 days) and stage III/IV were independent predictive factors of OS, RFS, and DMFS. No significant differences were observed in the rates of grade 3−4 toxicities between both groups.

Conclusions. Our results showed the addition of IC to CCRT was not superior to CCRT in unselected ESCC patients, while IC responders could benefit from this regime without an increase in toxicities.

Key words: esophageal squamous cell carcinoma; induction chemotherapy; concurrent chemoradiotherapy; responder; propensity score matched

Introduction

Esophageal cancer (EC) is the sixth most common cause of cancer death worldwide, with more than 550,000 new cases of esophageal carcinoma diagnosed each year.[1,2] Unlike most Western countries, esophageal squamous cell carcinoma (ESCC) is still the main pathological type in China.[3] Regardless

of its histological type, the overall survival (OS) of patients with EC is still poor.[4] For the management of EC which is deemed a medically unresectable tumor, definitive concurrent chemoradiotherapy (CCRT) is the standard therapy, guaranteeing organ preservation and providing a better quality of life.[5] However, although definitive CCRT results in encouraging short-term outcomes in the majority of patients, the prognosis remains unfavourable , with 5-year overall survival rates of 20%.[6] Especially, the rates of locoregional recurrence (LR) and distant metastasis after definitive CCRT can be as high as 50%.[7,8] Therefore, improvement in treatment intensity is greatly needed.

Induction chemotherapy (IC) is an attractive approach but also controversial. Theoretically, the additional IC followed by concurrent chemoradiotherapy (IC-CCRT) has potential benefits for early eradication of micro-metastases, increased tumor radiosensitivity, prevention of tumor progression, and even prolonged OS.[9] Previous studies have suggested that IC-CCRT has better failure-free survival, overall survival, and distant failure-free survival than CCRT alone in nasopharyngeal cancer, and has been cited by National Comprehensive Cancer Network (NCCN) clinical guidelines.[10] However, the addition of IC to CCRT in the management of ESCC is less reported, and the results of the retrospective studies showed conflicting results.[11-13] A randomized controlled trial showed that compared to CCRT alone, the addition of induction chemotherapy with docetaxel plus cisplatin failed to significantly improve the response rate or survival outcomes in unselected ESCC, which were limited by staging and response evaluation issues.[9] Previous research revealed that IC before CCRT was associated with improvements in pathological complete response (pCR) rate and survival in neoadjuvant therapy settings.[14,15] Therefore, it is important to identify patients who may benefit from IC, especially the patients who are responsive to chemotherapy. Furthermore, the radiotherapy techniques in previous studies were mainly based on 3D-CRT or IMRT.[9,11-13] The true value of IC for ESCC patients remains unclear in the era of modern technique IMRT/volumetric modulated arc therapy (VMAT), which could greatly improve the accuracy of radiotherapy with lower toxicity.[16] To the best of our knowledge, there are no published researches to date that compared IC + CCRT *vs.* CCRT alone for the ESCC patients receiving IMRT/VMAT only.

Therefore, we performed this retrospective study to evaluate the long-term survival outcomes among the ESCC patients who were treated with IC + CCRT to better understand the feasibility, efficacy, and safety of this approach by propensity score matched (PSM) methods. We further performed a stratified analysis to analyze the relationship between tumor response to IC and treatment outcomes.

Patients and methods

Study population

We retrospectively reviewed data derived from patients with diagnosed ESCC between April 2008 and March 2022. All eligible patients met the following criteria: 1) considering non-operable or refusing surgery; 2) histopathological proof of ESCC (T1−4N0−3) without distant metastasis; 3) 18–70 years of age; 4) Eastern Cooperative Oncology Group performance status of 3 or below; 5) receiving either IC + CCRT or CCRT based on IMRT/VMAT; 6) adequate liver and renal functions; 7) either TPF (docetaxel + cisplatin + fluorouracil), PF (cisplatin + fluorouracil), or TP (docetaxel/paclitaxel + cisplatin) as the IC regime. 8) A radiotherapy (RT) dose of more than 50.0 Gy was defined as definitive. Additional information, including gender, pathological diagnosis, tumor location, date of diagnosis, chemotherapy pattern and drugs, radiation technology, and dosage were collected from the hospital outpatient follow-up database. This study was approved by the Ethics Committee of the First Affiliated Hospital of Air Force Medical University (ethical approval number: KY20172035-3).

Treatment

Induction chemotherapy (IC)

For the IC + CCRT group, patients were given one to four cycles of IC based on doctor's choice. IC regimens consisted of TPF (docetaxel 60 mg/m2/day on day 1, cisplatin 50 mg/m2/day on days 1 to 2, and 5-fluorouracil 500 mg/m2/day on days 1 to 3), TP (docetaxel 60 mg/m2/day on day 1 or paclitaxel 150 mg/m2/day on day 1 and day 8, cisplatin 50 mg/m2/day on days 1 to 2), PF (cisplatin 50 mg/m2/day on days 1 to 2 and 5-fluorouracil 500 mg/m2/day on days 1 to 3). The cycles were administered every 3 weeks. Patients were treated with definitive CCRT within 3 to 6 weeks after the end of the last IC cycle.

Concurrent chemoradiotherapy (CCRT)

RT was given using IMRT/VMAT on the first day of chemotherapy in both groups as previously re-

ported.[17] All patients were fixed by thermoplastic body film. Briefly, the gross tumor volume (GTV) was defined as the primary tumor and lymph nodes considered positive by computed tomography (CT) and/or positron emission tomography/computed tomography (PET/CT), and endoscopic findings. The clinical target volume (CTV) was defined as the GTV plus an additional 3 cm craniocaudal expansion along the esophagus, and a 0.5 cm lateral margin. For tumors of the cervical or upper thoracic esophagus, the lymph nodes of the supraclavicular fossa were included in the CTV at the discretion of the physician. The planning target volume (PTV) was defined as the CTV plus an additional margin of 0.5 cm. According to the tumor location and physician discretion, all patients were irradiated in a total dose of more than 50.0 Gy with 1.8–2.2 Gy per fraction and 5 fractions per week. Patients received concurrent chemotherapy (cisplatin or nedaplatin-based regimen) every 3 weeks during radiotherapy for up to five cycles. 4 patients received weekly docetaxel and cisplatin for four or five cycles to alleviate toxic side effects considering the patient's physical condition.

Follow-up

After treatment, all patients received weekly examinations for toxicities during IC or CCRT, such as complete blood count, biochemistry, etc. Patients were re-evaluated for acute side effects such as barium esophagography and complete blood count 1 month after treatment completion, then physical examination, CT scanning of the neck, chest and abdomen, and ultrasound were performed every 3 months during the first 2 years, every 6 months from the second to the fifth year, and annually thereafter. Information about survival status and disease progression was updated until April 2023. The endpoints of the study were OS, recurrence-free survival (RFS), and distant metastasis-free survival (DMFS). OS was calculated from the date of diagnosis to death or last follow-up. RFS was calculated from the date of treatment to locoregional recurrence or death. DMFS was calculated from the date of treatment to distant metastasis or death. Toxicity was assessed according to the National Cancer Institute Common Terminology Criteria for Adverse Events version 4.0 (CTCAE v4.0).

Statistical analysis

The clinical tumor response was assessed 2 weeks after IC by enhanced CT scans and barium swallow according to the Response Evaluation Criteria in Solid Tumor criteria 1.1 (RECIST)[18], which is divided into four grades (complete response [CR], partial response [PR], stable disease [SD], and progressive disease [PD]). Patients were categorized into the following two groups: patients who achieved CR, PR, and SD (IC responders group) and patients who showed PD (IC non-responders group after IC. We also defined CR/PR as "IC good responders" and SD/PD as "IC poor responders".

All statistical tests for data analysis were performed using Statistical Analysis System (SAS) version 9.4. The PSM was performed to reduce the effect of treatment selection bias. A 1:1 matching of CCRT to IC-CCRT patients was generated based on several factors such as age, gender, primary tumor location, T stage, N stage, and initial clinical stage using the nearest neighbour method at a calliper of 0.6. Survival curves were estimated by use of the Kaplan-Meier method and groups were compared for their survival rates by the log-rank test. Both univariate and multivariate analysis were performed by use of Cox regression models to identify significant prognostic factors. Hazard ratios (HRs) and 95% confidence intervals (CIs) were estimated for each prognostic factor. A p-value of < 0.05 was considered to be statistically significant.

Results

Baseline characteristics

In total, the clinical data of 271 newly diagnosed ESCC patients were collected and retrospectively reviewed. From the original data, 71 pairs were selected by the PSM method (Supplementary Figure 1). The baseline characteristics of the patients are summarized in Supplementary Table 1. For the selected subject, the median age was 61.5 years (range 38–74 years), and the study population included 115 (81.0%) males and 27 (19.0%) females. Among the patients, 118 patients (83.1%) had T3 or T4 disease, and 126 (88.7%) had lymph node metastasis. 30 patients (21.2%) had stage I or II disease and 112 (78.9%) had stage III or IV. The median tumor length was 6 cm (range, 2–23 cm). The median total radiation dose was 59.36 Gy (range, 50.4–66.0 Gy). The median follow-up time of the study was 21 months. There were no statistically significant differences in age, gender, zubrod performance status (ZPS) score, tumor length, and stages between the CCRT group and IC + CCRT group.

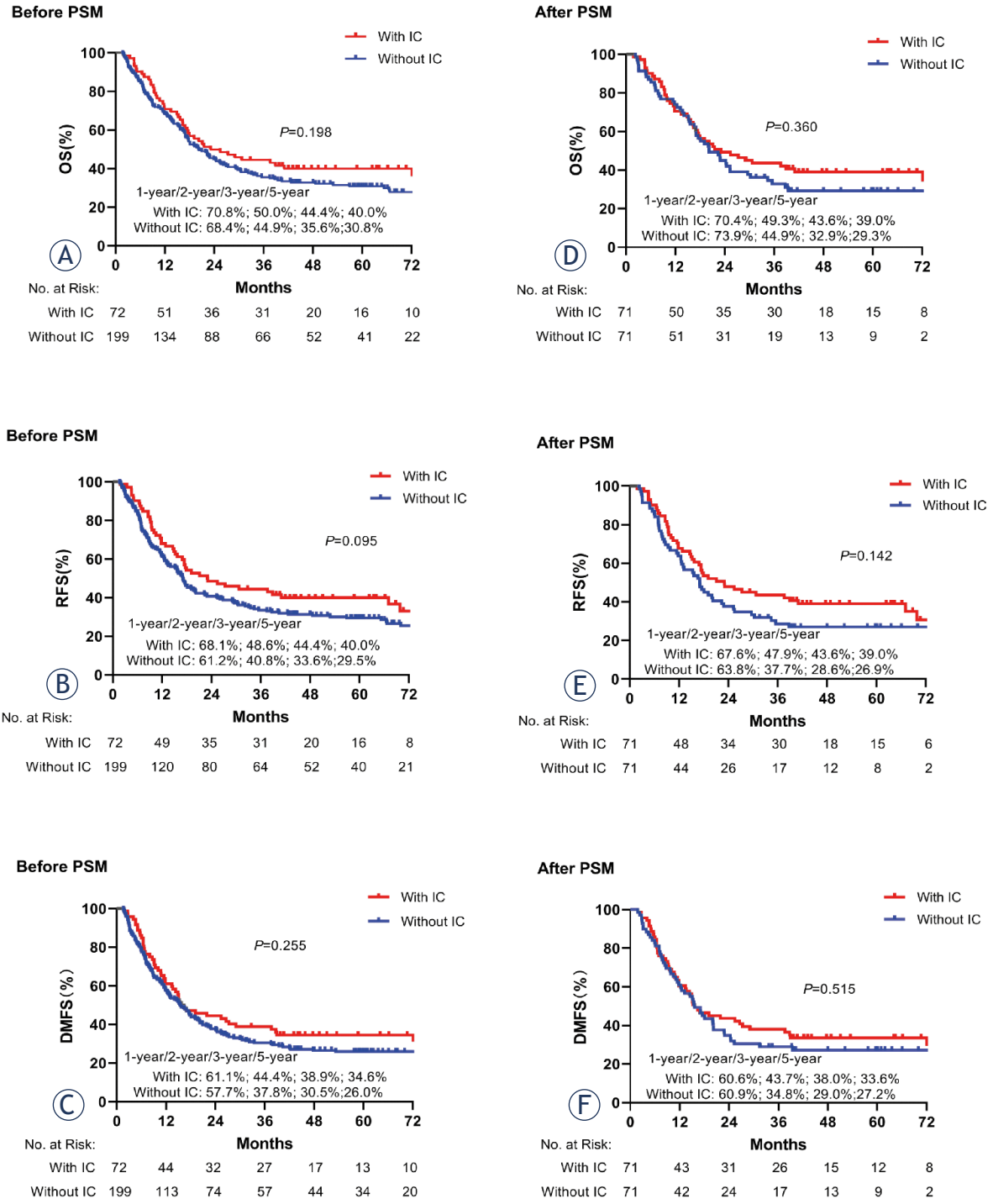

FIGURE 1. Kaplan-Meier survival curves of the induction chemotherapy (IC) + concurrent chemoradiotherapy (CCRT) group and CCRT group in patients before and after matching. **(A, D)** overall survival (OS); **(B, E)** recurrence-free survival (RFS); **(C, F)** distant metastasis-free survival (DMFS).

PSM = propensity score matching

Survival outcomes

In the original data set (n = 271), survival outcomes were similar and non-significant between the CCRT group and IC + CCRT group ($p > 0.05$, Figure 1A–C). In terms of the matched data set, the IC + CCRT group achieved a tendency for improvement in 3-, and 5-year OS rate (43.6%

TABLE 1. Baseline characteristics for patients before and after propensity score matching (PSM) [M (QL, QU)/n(%)]

Variables	Before PSM (n = 271)				After PSM (n = 142)			
	Total	Without IC (n = 199)	With IC (n = 72)	P	Total	Without IC (n = 71)	With IC (n = 71)	P
Age (year)	61.0 (56.0, 65.0)	61.0 (56.0, 66.0)	61.5 (55.0, 65.0)	0.739	61.5 (56.0, 65.0)	61.0 (57.0, 65.0)	62.0 (55.0, 65.0)	0.923
Total radiotherapy time (day)	43.0 (40.0, 47.0)	43.0 (40.0, 48.0)	42.0 (40.0, 45.8)	0.226	43.0 (40.0, 46.3)	43.0 (39.0, 48.0)	42.0 (40.0, 46.0)	0.361
Age (year)				0.820				0.865
< 60	116 (42.8)	86 (43.2)	30 (41.7)		59 (41.5)	30 (42.3)	29 (40.8)	
≥ 60	155 (57.2)	113 (56.8)	42 (58.3)		83 (58.5)	41 (57.7)	42 (59.2)	
Gender				0.073				0.285
Female	62 (22.9)	51 (25.6)	11 (15.3)		27 (19.0)	16 (22.5)	11 (15.5)	
Male	209 (77.1)	148 (74.4)	61 (84.7)		115 (81.0)	55 (77.5)	60 (84.5)	
ECOG PS				<0.001				1.000
0–1	183 (67.5)	148 (74.4)	35 (48.6)		70 (49.3)	35 (49.3)	35 (49.3)	
2–3	88 (32.5)	51 (25.6)	37 (51.4)		72 (50.7)	36 (50.7)	36 (50.7)	
Tumor Length(cm)				0.540				0.851
< 8	203 (74.9)	151 (75.9)	52 (72.2)		103 (72.5)	52 (73.2)	51 (71.8)	
≥ 8	68 (25.1)	48 (24.1)	20 (27.8)		39 (27.5)	19 (26.8)	20 (28.2)	
T stage				0.739				0.179
1–2	37 (13.7)	28 (14.1)	9 (12.5)		24 (16.9)	15 (21.1)	9 (12.7)	
3–4	234 (86.3)	171 (85.9)	63 (87.5)		118 (83.1)	56 (78.9)	62 (87.3)	
N stage				0.181				1.000
0–1	204 (75.3)	154 (77.4)	50 (69.4)		100 (70.4)	50 (70.4)	50 (70.4)	
2–3	67 (24.7)	45 (22.6)	22 (30.6)		42 (29.6)	21 (29.6)	21 (29.6)	
AJCC stage				0.291				0.411
I–II	61 (22.5)	48 (24.1)	13 (18.1)		30 (21.1)	17 (23.9)	13 (18.3)	
III–IV	210 (77.5)	151 (75.9)	59 (81.9)		112 (78.9)	54 (76.1)	58 (81.7)	
IC cycles (times)				<0.001				< 0.001
0	199 (73.4)	199 (100.0)	0 (0)		71 (50.0)	71 (100.0)	0 (0)	
1/2	56 (20.7)	0 (0)	56 (77.8)		56 (39.4)	0 (0)	56 (78.9)	
3/4	16 (5.9)	0 (0)	16 (22.2)		15 (10.6)	0 (0)	15 (21.1)	
Response after IC								
CR	—	—	0 (0)		—	—	0 (0)	
PR	—	—	32 (44.4)		—	—	32 (45.1)	
SD	—	—	33 (45.8)		—	—	32 (45.1)	
PD	—	—	7 (9.7)		—	—	7 (9.9)	

AJCC stage = American Joint Committee on Cancer stage; Adjusted factors = age, gender, ECOG PS, tumor length, T stage, N stage; CR = complete response; ECOG PS = Eastern Cooperative Oncology Group performance status; IC = induction chemotherapy; PD = progressive disease; PR = partial response; PD = stable disease

vs. 32.9%, 39.0% *vs.* 29.3%, p = 0.360; Figure 1D), RFS (43.6% *vs.* 28.6%, 39.0% *vs.* 26.9%, p = 0.142; Figure 1E), and DMFS (38.0% *vs.* 29.0%, 33.6% *vs.* 27.2%, p = 0.515; Figure 1F) compared with the CCRT group, although the difference between the two groups did not reach statistical significance. Details regarding the reasons for death are provided in Supplementary Table1. The most common reasons for death were dysphagia, metastasis or recurrence, and gastrointestinal bleeding (IC + CCRT *vs.* CCRT: 15.5% *vs.* 21.1%, 28.2% *vs.* 29.6%, 11.3% *vs.* 5.6%, respectively), and no statistically signifi-

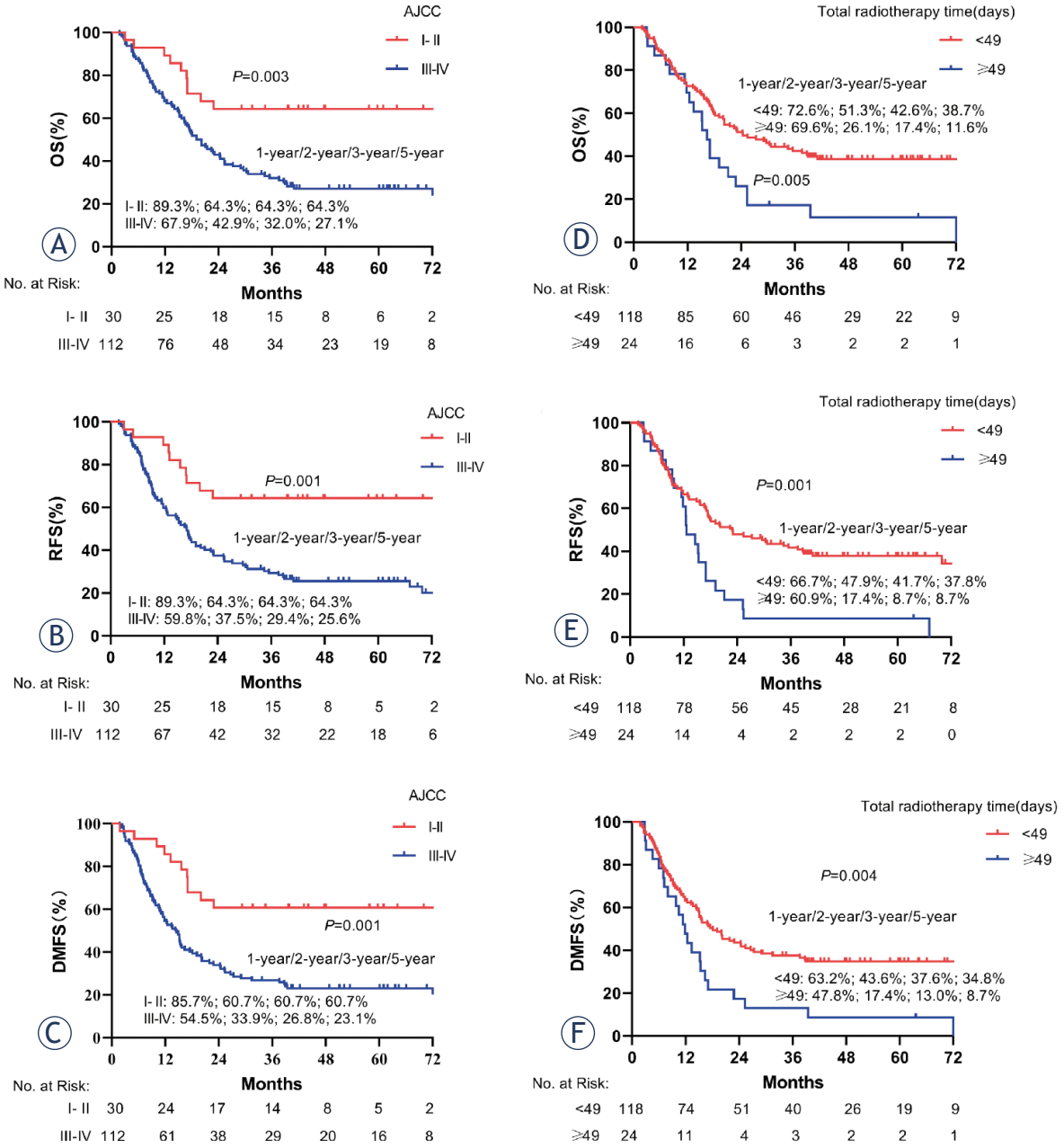

FIGURE 2. Kaplan-Meier survival curves based on the American Joint Committee on Cancer (AJCC) stage and total radiotherapy time for the propensity-matched cohort. **(A, D)** overall survival (OS); **(B, E)** recurrence-free survival (RFS); **(C, F)** distant metastasis-free survival (DMFS).

cant differences were not found between the two groups.

Prognostic factors

We included both demographic and clinicopathologic variables in the univariate analysis (Table 2 and Supplementary Table 2). Total radiotherapy time, age, and the 8th edition of the American Joint Committee on Cancer (AJCC) stage were identified as significant predictive factors of prognosis by multivariate analysis (Table 3 and Supplementary Table 3). Briefly, the total radiotherapy time ≥ 49 days and AJCC stage III/IV were independently associated with worse OS (p = 0.025, HR = 1.762, 95% CI = 1.074–2.891; p = 0.006, HR = 2.533, 95% CI = 1.305–4.916), RFS (p = 0.009, HR = 1.920, 95% CI = 1.178–3.131; p = 0.003, HR = 2.738, 95% CI =

TABLE 2. Univariate Cox analysis of overall survival (OS), recurrence-free survival (RFS), and distant metastasis-free survival (DMFS) after propensity score matching (PSM)

Variables	OS		RFS		DMFS	
	HR (95% CI)	P	HR (95% CI)	P	HR (95% CI)	P
Age (year)	0.986 (0.958–1.014)	0.324	0.985 (0.957–1.014)	0.306	0.981 (0.954–1.008)	0.161
Total radiotherapy time (day)	1.018(1.001–1.034)	0.032	1.015(1.000–1.031)	0.051	1.016(1.001–1.031)	0.039
Age (year)						
< 60	1.000		1.000		1.000	
≥ 60	0.749 (0.498–1.128)	0.167	0.794 (0.530–1.191)	0.265	0.682 (0.459–1.015)	0.059
Gender						
Female	1.000		1.000		1.000	
Male	1.566 (0.886–2.766)	0.122	1.511 (0.870–2.624)	0.143	1.808 (1.026–3.186)	0.040
ECOG PS						
0–1	1.000		1.000		1.000	
2–3	1.058 (0.701–1.596)	0.788	1.121 (0.747–1.682)	0.580	1.125 (0.755–1.675)	0.564
Tumor Length(cm)						
< 8	1.000		1.000		1.000	
≥ 8	1.481 (0.954–2.301)	0.080	1.651 (1.068–2.553)	0.024	1.510 (0.985–2.314)	0.059
Total radiotherapy time (day)						
< 49	1.000		1.000		1.000	
≥ 49	2.018 (1.234–3.300)	0.005	2.203 (1.354–3.583)	0.001	2.016 (1.249–3.255)	0.004
T stage						
1–2	1.000		1.000		1.000	
3–4	2.938 (1.421–6.075)	0.004	3.162 (1.530–6.536)	0.002	2.984 (1.501–5.932)	0.002
N stage						
0–1	1.000		1.000		1.000	
2–3	1.150 (0.744–1.779)	0.529	1.227 (0.798–1.886)	0.352	1.262 (0.827–1.926)	0.280
AJCC stage						
I–II	1.000		1.000		1.000	
III–IV	2.751 (1.426–5.307)	0.003	2.983 (1.548–5.752)	0.001	2.940 (1.568–5.511)	0.001
IC cycles (times)						
0	1.000		1.000		1.000	
1/2	0.935 (0.609–1.435)	0.759	0.835 (0.546–1.275)	0.403	0.921 (0.606–1.399)	0.699
3/4	0.509 (0.230–1.127)	0.096	0.458 (0.207–1.012)	0.054	0.725 (0.356–1.475)	0.374

Hazard ratios and 95% confidence intervals were calculated by a stratified Cox proportional hazards model.

AJCC stage = American Joint Committee on Cancer stage; ECOG PS = Eastern Cooperative Oncology Group performance status; IC = induction chemotherapy

1.413–5.305) and DMFS (p = 0.014, HR = 1.827, 95% CI = 1.127–2.961; p = 0.001, HR = 2.951, 95% CI = 1.560–5.582). Besides, age ≥ 60 (p = 0.011; HR, 0.592; 95% CI, 0.396–0.886) was independently associated with better DMFS (Supplementary Figure 2). As shown in Figure 2, there was a significant difference in OS, RFS, and DMFS in total radiotherapy time and AJCC stage.

Subgroup analysis

Tumor responses after IC are listed in Table 1. After IC, CR was obtained in 0 patients (0%), PR in 32 (45.1%), SD in 32 (45.1%), and PD in 7 patients (9.9%), respectively. For 71 patients with IC, the overall response rate (CR + PR + SD), and good response rate (CR + PR) were 90.1%, and 45.1%, re-

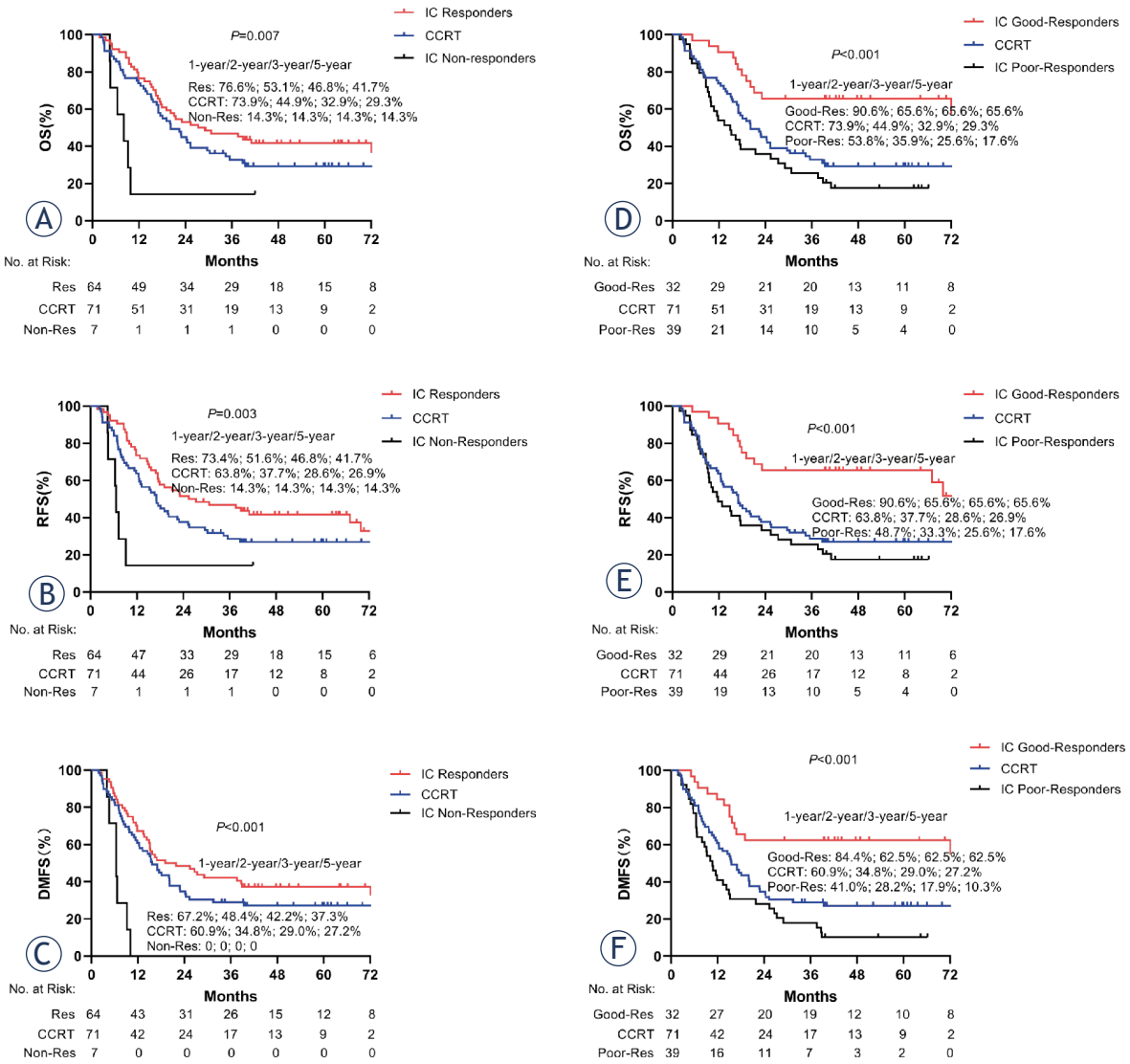

FIGURE 3. Kaplan-Meier estimates of survival curves based on the clinical response to induction chemotherapy. **(A–C)** Induction chemotherapy (IC) non-responders group *vs.* the IC responders group *vs.* the concurrent chemoradiotherapy (CCRT) group. **(D–F)** IC good-responders group *vs.* the IC poor-responders group versus the CCRT group.

spectively. The potential effect of tumor response to IC on survival outcomes was also analysed as a predictive factor. As shown in Figure 3, the responders to IC had significantly more favourable survival compared with non-responders, or with patients in the CCRT group, with corresponding 5-year OS rates of 41.7%, 14.36%, and 29.3%, 5-year RFS rates of 41.7%, 14.3%, and 26.9%, and 5-year DMFS rates of 37.3%, 0%, and 27.2%, respectively ($p < 0.001$ for OS, RFS and DMFS, Figure 3A–C). Likewise, the 5-year OS rates (65.6% *vs.* 17.6% *vs.* 29.3%, $p < 0.001$; Figure 3D), RFS rates (65.6% *vs.* 17.6% *vs.* 26.9%, $p < 0.001$; Figure 3E), and DMFS rates (62.5% *vs.* 10.3% *vs.* 27.2%, $p < 0.001$; Figure 3F) of the IC good responders were significantly higher than that of the IC poor responders and CCRT group. We also studied the survival outcomes and response to IC for different IC regimens. The results showed that there was no significant statistical difference between different IC regimens and OS, RFS, and DMFS ($p > 0.05$) (Supplementary Figure 3). No significant differences were found between different IC regimens and good responders (Supplementary Table 4).

To further distinguish the survival difference in patients on different risk stratification, a subgroup analysis was performed according to the T stage. In the subgroup of patients with T3–4 ESCC

TABLE 3. Cox multivariate analysis of overall survival (OS), recurrence-free survival (RFS), and distant metastasis-free survival (DMFS) after propensity score matching (PSM)

Variables	OS		RFS		DMFS	
	HR (95% CI)	P	HR (95% CI)	P	HR (95% CI)	P
Total radiotherapy time (day)						
< 49	1.000		1.000		1.000	
≥ 49	1.762 (1.074–2.891)	0.025	1.920 (1.178–3.131)	0.009	1.827 (1.127–2.961)	0.014
AJCC stage						
I–II	1.000		1.000		1.000	
III–IV	2.533 (1.305–4.916)	0.006	2.738 (1.413–5.305)	0.003	2.951 (1.560–5.582)	0.001
Age (year)						
< 60					1.000	
≥ 60					0.592 (0.396–0.886)	0.011

Hazard ratios and 95% confidence intervals were calculated by a stratified Cox proportional hazards model.

AJCC stage = American Joint Committee on Cancer stage

disease, 62 and 55 cases receiving IC + CCRT and CCRT, respectively, were selected for subgroup analysis. Compared with the CCRT group, the IC + CCRT group achieved better 5-year OS (33.7% *vs.* 22.5%, p = 0.319; Figure 4D), RFS (33.7% *vs.* 19.6%, p = 0.084; Figure 4E), and DMFS (29.0% *vs.* 19.6%, p = 0.308; Figure 4F), however, there was no significant difference. In addition, IC + CCRT showed a similar tendency for 5-year OS (76.2% *vs.* 57.1%, p = 0.310; Figure 4A), RFS (76.2% *vs.* 57.1%, p = 0.310; Figure 4B), and DMFS (64.8% *vs.* 57.1%, p = 0.642; Figure 4C) versus CCRT in the T1–2 subgroup.

Failure mode

Patterns of treatment failure in ESCC patients are listed in Table 4. In terms of the matched data set, locoregional failure occurred in 12 patients (16.9%) and 11 patients (15.5%) in the IC + CCRT group and CCRT group, respectively. In the IC + CCRT group, 22 patients (31%) experienced distant failure, and in the CCRT group 19 patients experienced distant failure.

Toxicities

During induction chemotherapy, leucopenia was the most common adverse event (Supplementary Table 5), which was observed in 32 patients (45.1%). Patients developed grade 3 or 4 hematologic toxicity including neutropenia (n = 9, 12.7%), leucopenia (n = 9, 12.7%), febrile neutropenia (n = 1, 1.4%), and anemia (n = 1, 1.4%).

Over the entire treatment phase, grade 3–4 radiation esophagitis (RE) was identified in 2.8% (2/71) of the IC + CCRT group and 4.2% (3/71) of the CCRT group (p = 0.678). Hematologic toxicity grade 3-4 was observed in 19 (26.8%) and 20 (28.2%) patients who received IC + CCRT and CCRT alone, respectively (p = 0.944). Although 43.7% of patients (31/71) developed esophageal stricture in the IC + CCRT group, the incidence of grade 3-4 adverse events was only 4.2% (3/71), which was not serious. No significant differences were observed in the rates of other grades 3-4 toxicities between both groups (Table 5).

Discussion

The efficacy of IC has not been well documented previously for ESCC patients receiving IMRT/VMAT-based CCRT. In the present study, we performed a PSM analysis of patients treated with or without IC before standard CCRT to better understand the efficacy and toxicities of IC. We found that IC + CCRT was not superior to CCRT in terms of 5-year OS, RFS, and DMFS regarding original or well-matched data. The stratified analysis further demonstrated IC + CCRT improved the 5-year OS, RFS, and DMFS for the patients with response (responders or good responders) to IC, whereas it might not have a positive impact for non-responding or poorly responding patients and seemed to have limited benefits in long-term survival. Nearly all of the patients who are alive in our study have

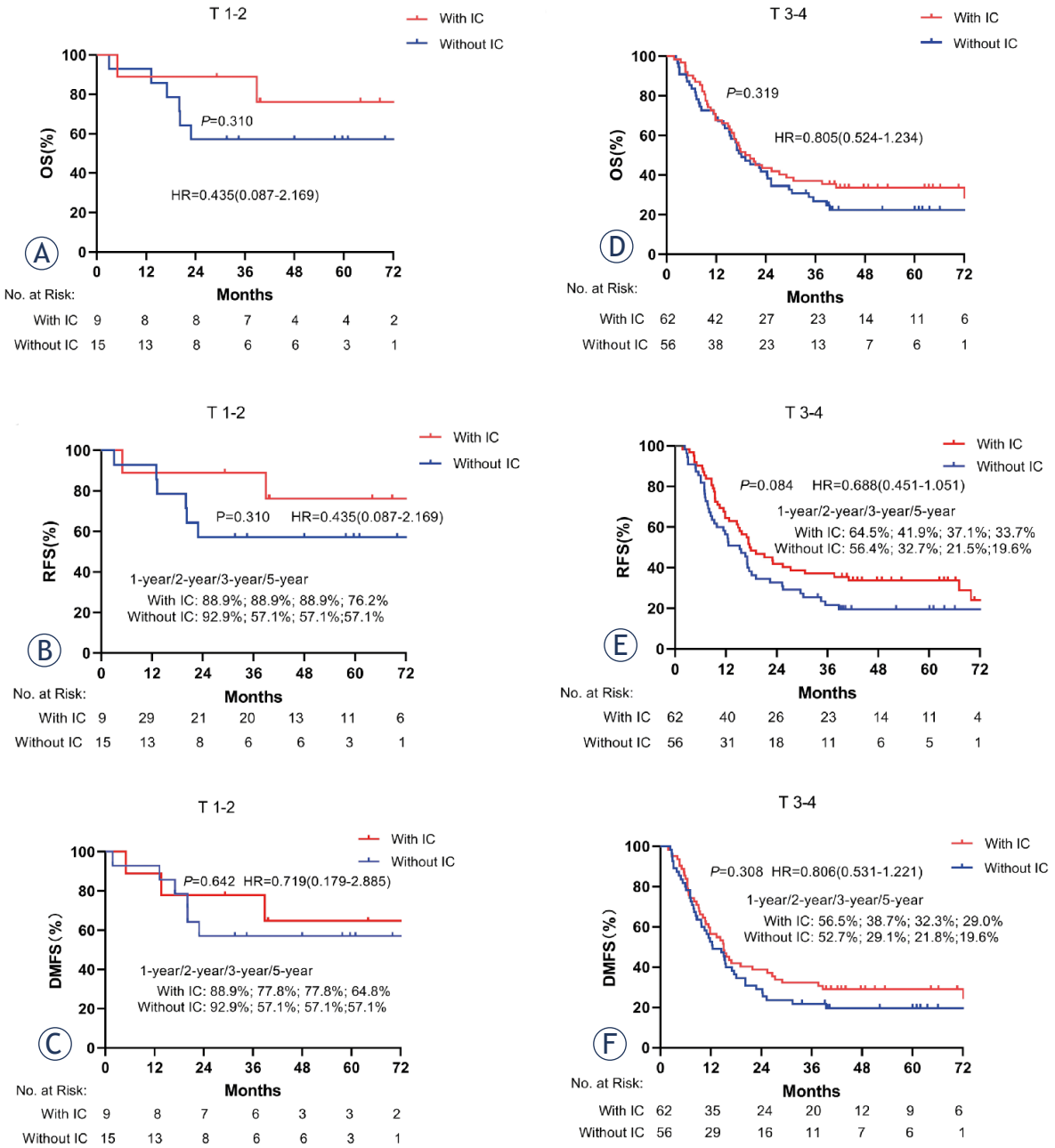

FIGURE 4. Kaplan-Meier estimates of survival curves based on the T stage. **(A–C)** overall survival (OS), recurrence-free survival (RFS), and distant metastasis-free survival (DMFS) of patients with T1–2; **(D–F)** OS, RFS, and DMFS of patients with T3–4.

IC = induction chemotherapy

completed valid follow-up for 2 years (except for individual deleted data), and the longest follow-up period was over 7 years. Concerning toxicity, there was no significant difference in toxicity between patients who had IC and those who did not. According to our knowledge, this is the first study to compare the survival benefits of the addition of IC to CCRT and IMRT/VMAT only in ESCC patients. The main strength of our study is that the application of the PSM method balances the baseline characteristics of the included population to reduce potential confounders, thus mimicking the matching observed in randomized controlled trials (RCTs).

Since the Radiation Therapy Oncology Group (RTOG) 85–01 trial indicated that the outcome

TABLE 4. Failure pattern [n (%)]

Variables	Before PSM			After PSM		
	Without IC (n=199)	With IC (n=72)	p	Without IC (n=71)	With IC (n=71)	p
Local and/or regional						
Local only	26 (13.1)	10 (13.9)	0.860	12 (16.9)	10 (14.1)	0.643
Local and regional	2 (1.0)	1 (1.4)	1.000	0 (0)	1 (1.4)	1.000
Regional only	0 (0)	0 (0)	—	0 (0)	0 (0)	—
Total locoregional failure	28 (14.1)	11 (15.3)	0.802	12 (16.9)	11 (15.5)	0.820
Distant						
Bone only	3 (1.5)	1 (1.4)	1.000	1 (1.4)	1 (1.4)	1.000
Liver only	7 (3.5)	3 (4.2)	1.000	4 (5.6)	3 (4.2)	1.000
Lung only	17 (8.5)	5 (6.9)	0.670	6 (8.5)	5 (7.0)	0.754
Brain only	1 (0.5)	1 (1.4)	1.000	0 (0)	1 (1.4)	1.000
Multiple location [a]	10 (5.0)	6 (8.3)	0.466	4 (5.6)	7 (9.9)	0.346
Other location [b]	19 (9.5)	6 (8.3)	0.760	4 (5.6)	5 (7.0)	1.000
Total distant failure	57 (28.6)	22 (30.6)	0.760	19 (26.8)	22 (31.0)	0.579

[a] Combinations of bone, brain, liver, lung, and lymph nodes; [b] including pleural and lymph nodes

IC = induction chemotherapy; PSM = propensity score matching

TABLE 5. Acute and late toxicities during treatment before and after propensity score matching (PSM) [n (%)]

Toxicities	Before PSM				p	After PSM				p
	Without IC (n=199)		With IC (n=72)			Without IC (n=71)		With IC (n=71)		
	Grade1-2	Grade3-4	Grade1-2	Grade3-4		Grade1-2	Grade3-4	Grade1-2	Grade3-4	
Acute adverse events										
Esophagitis	183 (92.0)	6 (3.0)	67 (93.1)	2 (2.8)	0.951	63 (88.7)	3 (4.2)	66 (93.0)	2 (2.8)	0.678
Myelosuppression	109 (54.8)	58 (29.1)	40 (55.6)	19 (26.4)	0.873	37 (52.1)	20 (28.2)	39 (54.9)	19 (26.8)	0.944
Radiation pneumonitis	1 (0.5)	0 (0)	1 (1.4)	0 (0)	1.000	0 (0)	0 (0)	1 (1.4)	0 (0)	1.000
Esophageal fistula	3 (1.5)	0 (0)	0 (0)	0 (0)	0.696	0 (0)	0 (0)	0 (0)	0 (0)	—
Late adverse events										
Esophageal stricture	92 (46.2)	3 (1.5)	29 (40.3)	3 (4.2)	0.364	29 (40.8)	1 (1.4)	28 (39.4)	3 (4.2)	0.584

Acute adverse events: ≤ 3 months after completion of study treatment; Late adverse events: > 3 months after study treatment

IC = induction chemotherapy

of CCRT was significantly better than that of RT alone for ESCC patients, definitive CCRT has been a standard treatment.[5] However, the long-term outcomes remain limited and the failure rate was 50%.[6,7] Updated meta-analyses and systematic reviews of clinical trials have demonstrated that IC + CCRT could prolong short-term survival in unresectable EC patients.[19] Unfortunately, several subsequent similar studies including a prospective randomized clinical trial got negative results.[9, 11-13] In our study, we found that the IC + CCRT group achieved higher 5-year OS (39.0% *vs.* 29.3%, p = 0.360), RFS (39.0% *vs.* 26.9%, p = 0.142), and DMFS (33.6% *vs.* 27.2%, p = 0.515) compared with the CCRT group, although the difference between the two groups did not reach statistical significance. Rational explanations for the discrepancy may include: 1) The enrolled patients in the current study included clinical stages T1–4N0–3, and the patients with early-stage disease (T1–2N0–1) may not benefit from IC. 2) The regimens of IC in the retrospective studies were not uniform, which may provide a slight bias toward a negative result.

It was reported that the late tumor stage was an important risk factor for poor prognosis in ESCC.[20] In this study, multivariate Cox analysis showed

AJCC stage was regarded as an independent predictive factor that affects OS, RFS, and DMFS. Later AJCC stage has inferior OS (p = 0.006; HR, 2.533; 95% CI, 1.305–4.916) and RFS (p = 0.003; HR, 2.738; 95% CI, 1.413–5.305), and DMFS (p = 0.001; HR, 2.951; 95% CI, 1.560–5.582) than early AJCC stage ESCC, which was similar to those in Hsieh's report.[21] We also found radiotherapy treatment time was another independent predictive factor for OS, RFS, and DMFS. In daily clinical practice, unplanned treatment interruptions are inevitable for many reasons. Sher reported that a prolonged total radiotherapy time > 51 days is associated with an inferior overall survival (hazard ratio = 1.63, p = 0.0058). For each additional day required to finish radiotherapy, the hazard rate of death increased by 4.2%.[22] Cannon *et al.* reviewed outcomes of 171 head and neck cancer patients treated with CCRT and found that patients with radiotherapy time ≤ 49 days had a superior 3-year local control rate and OS compared to those with radiotherapy time > 49 days (88% versus 71%, 81% versus 58%, respectively).[23] In our study, the total radiotherapy time ≥ 49 days has the inferior OS (p = 0.025; HR, 1.762; 95% CI, 1.074–2.891), RFS (p = 0.009; HR, 1.920; 95% CI, 1.178–3.131) and DMFS (p = 0.014; HR, 1.827; 95% CI, 1.127–2.961). For patients with total radiotherapy time ≥ 49 days in our study, the vast majority of interruption was due to machine breakdown, machine maintenance, and treatment toxicity (chemoradiotherapy or radiotherapy only). Briefly, 11 patients experienced treatment breaks because of radiation esophagitis. Meanwhile, 6 patients experienced unscheduled interruptions due to chemotherapy toxicities. Therefore, it seems a necessity for radiotherapy without gaps or delays for the sake of improved outcomes and control of disease progression.

So far, there is no evidence to suggest that advanced age is an independent contraindication for CCRT in the retrospective studies.[20, 24] Wu *et al.* reported that there was no statistically significant difference between CCRT and RT alone for patients aged 75 years or older.[20] In the present study, we found that age is not a predictive factor of OS (p = 0.167; HR, 0.749; 95% CI, 0.498–1.128) and RFS (p = 0.265; HR, 0.794; 95% CI, 0.530–1.191) by multivariate analysis. Interestingly, we found that age < 60 was independently associated with worse DMFS in the current study.[25] Similar results have been found in Colzani'study, suggesting that breast cancer patients younger than 50 years at diagnosis had a higher risk of distant metastasis.[26] The possible reason may be that the metastases lose aggressive character or that the host defense is better equipped to deal with them in advancing age.[27]

IC may only benefit a certain subgroup but not unselected patients with ESCC. As is known to all, the T stage was associated with a worse prognosis in esophageal carcinoma.[28] Akinori reported that IC for T4 esophageal cancer offered comparable local control and survival to conventional CCRT, and suggested that the strategy of IC followed by CCRT was efficient for T4M0 esophageal cancer.[13] To identify the subgroups that may benefit from IC, we performed a stratified analysis based on the T stage. Our results indicated that IC + CCRT group achieved better 5-year OS (33.7% *vs.* 22.5%), RFS (33.7% *vs.* 19.6%), and DMFS (29.0% *vs.* 19.6%) compared with the CCRT group, however, there was no significant difference. Moreover, 90% of the symptoms of dysphagia improved significantly after IC, which was consistent with the trial INT 0122.[29] In the study by Luo *et al.*[12], the IC responders (CR or PR) group achieved significantly more favourable OS compared with the IC non-responders (SD or PD) group and the CCRT alone group (p = 0.002). Besides, the post-hoc analysis in prospective research also demonstrated that response to IC was associated with more favourable survival.[9] Consistent with the results of previous studies, our results suggested that the responders (CR, PR, or SD) to IC had significantly more favourable survival compared with non-responders (PD), or with patients in the CCRT group, with corresponding 5-year OS rates of 41.7%, 14.3%, and 29.3%, respectively. In addition, we further analyzed the potentially important role of IC good responders (CR or PR) from the whole IC group. Our data suggested that the IC good responders might have a significantly prolonged OS, improved locoregional control, and reduced distant metastasis, with corresponding 5-year OS rate, RFS rate, and DMFS of 65.6%, 65.6%, and 62.5%, respectively. Considering the poor prognosis of the IC non-responders or IC poor responders, tumor response after IC could be used to guide subsequent treatment decisions, such as switching to alternative agents included targeted therapies, immunotherapies, or radiosensitizers during radiotherapy for non-responders or IC poor responders. Therefore, further studies are needed to overcome this unfavorable biological characteristic.

In our study, the rate of grade ≥ 3 RE in the IC + CCRT group and the CCRT group had no statistical significance (p = 0.678). There was also no statistical difference in the incidence of myelosuppression (p = 0.944). It has been reported that patients with T4 had an incidence of perforation of

14–23% during CCRT, and the addition of IC before CCRT might reduce the risk of perforation by decreasing the tumor volume before encountering severe esophagitis.[30,31] No esophageal fistula or perforation occurred in our study, which is one of the most troublesome complications caused by CCRT. The possible reason was that ESCC patients by using IMRT/VMAT only are superior to the two-dimensional conformal radiation (2D-CRT) or 3D-CRT. IMRT/VMAT improves the treatment ratio due to the highly conformal dose distributions in the tumor target volume and sharp dose gradients at the transition to the adjacent normal structures. The potential benefits of IMRT/VMAT were investigated in a series of studies.[32] Our results are consistent with the outcomes of the studies in the IMRT/VMAT era.

There were several limitations in our study. First, although we used PSM, a method aimed to minimize the impact of observed confounders, the retrospective nature of this study cannot exclude the possibility of bias caused by confounding factors, and adding too many match restrictions would lead to small sample size and might not represent the initial population. Secondly, our study is limited to ESCC patients and could not applied to other types of EC. Finally, due to the retrospective characteristic, IC regimes and concurrence chemotherapy regimens were not uniform. More well-designed prospective, randomized controlled trials are warranted to further confirm the role of IC.

Conclusions

In this study, our results showed the addition of IC to CCRT was not superior to CCRT in unselected ESCC patients, while IC responders might benefit from this regime without an increase in toxicities.

Acknowledgement

This research was funded by the National Natural Science Foundation of China (82102603 and 82272941).

References

1. Siegel RL, Miller KD, Fuchs HE, Jemal A. Cancer statistics 2021. *CA Cancer J Clin* 2021; **71:** 7-33. doi: 10.3322/caac.21654
2. Smyth EC, Lagergren J, Fitzgerald RC, Lordick F, Shah MA, Lagergren P, et al. Oesophageal cancer. *Nat Rev Dis Primers* 2017; **3:** 17048. doi: 10.1038/nrdp.2017.48
3. Arnold M, Soerjomataram I, Ferlay J, Forman D. Global incidence of oesophageal cancer by histological subtype in 2012. *Gut* 2015; **64:** 381-7. doi: 10.1136/gutjnl-2014-308124
4. Lagergren J, Smyth E, Cunningham D, Lagergren P. Oesophageal cancer. *Lancet* 2017; **390:** 2383-96. doi: 10.1016/S0140-6736(17)31462-9
5. Cooper JS, Guo MD, Herskovic A, Macdonald JS, Martenson Jr JA, Al-Sarraf M, et al. Chemoradiotherapy of locally advanced esophageal cancer: long-term follow-up of a prospective randomized trial (RTOG 85-01). Radiation Therapy Oncology Group. *JAMA* 1999; **281:** 1623-7. doi: 10.1001/jama.281.17.1623
6. Gwynne S, Hurt C, Evans M, Holden C, Vout L, Crosby T. Definitive chemoradiation for oesophageal cancer: a standard of care in patients with non-metastatic oesophageal cancer. *Clin Oncol* 2011; **23:** 182-8. doi: 10.1016/j.clon.2010.12.001
7. Xi M, Xu C, Liao ZX, Hofstetter WL, Murphy MB, Maru DM, et al. The impact of histology on recurrence patterns in esophageal cancer treated with definitive chemoradiotherapy. *Radiother Oncol* 2017; **124:** 318-24. doi: 10.1016/j.radonc.2017.06.019
8. Sudo K, Xiao L, Wadhwa R, Shiozaki H, Elimova E, Taketa T, et al. Importance of surveillance and success of salvage strategies after definitive chemoradiation in patients with esophageal cancer. *J Clin Oncol* 2014; **32:** 3400-5. doi: 10.1200/JCO.2014.56.7156
9. Liu SL, Luo LL, Zhao L, Zhu YJ, Liu H, Li QQ, et al. Induction chemotherapy followed by definitive chemoradiotherapy versus chemoradiotherapy alone in esophageal squamous cell carcinoma: a randomized phase II trial. *Nat Commun* 2021; **12:** 4014. doi: 10.1038/s41467-021-24288-1
10. Sun Y, Li WF, Chen NY, Zhang N, Hu GQ, Xie FY, et al. Induction chemotherapy plus concurrent chemoradiotherapy versus concurrent chemoradiotherapy alone in locoregionally advanced nasopharyngeal carcinoma: a phase 3, multicentre, randomized controlled trial. *Lancet Oncol* 2016; **17:** 1509-20. doi: 10.1016/S1470-2045(16)30410-7
11. Chen MQ, Lin QL, Chen YG, Guo JH, Xu BH, Tian Y. Neoadjuvant chemotherapy may not benefit esophageal squamous cell carcinoma patients treated with definitive chemoradiotherapy. *J Chin Med Assoc* 2017; **80:** 636. doi: 10.1016/j.jcma.2017.06.014
12. Luo LL, Xi M, Yang YD, Li QQ, Zhao L, Zhang P, et al. Comparative outcomes of induction chemotherapy followed by definitive chemoradiotherapy versus chemoradiotherapy alone in esophageal squamous cell carcinoma. *J Cancer* 2017; **8:** 3441-7. doi: 10.7150/jca.21131
13. Akinori M, Michitaka H, Yousuke I, Tsuyoshi K, Tairo R, Gencho K, et al. Induction chemotherapy followed by chemoradiotherapy for T4M0 esophageal cancer. *Esophagus* 2011; **8:** 31-7. doi: 10.1007/s10388-011-0255-y
14. Jin J, Liao ZX, Zhang Z, Ajani J, Swisher S, Chang JY, et al. Induction chemotherapy improved outcomes of patients with resectable esophageal cancer who received chemoradiotherapy followed by surgery. *Int J Radiat Oncol Biol Phys* 2004; **60:** 427-36. doi: 10.1016/j.ijrobp.2004.03.033
15. Malaisrie SC, Hofstetter WL, Correa AM, Ajani JA, Komaki RR, Rice DC, et al. The addition of induction chemotherapy to preoperative, concurrent chemoradiotherapy improves tumor response in patients with esophageal adenocarcinoma. *Cancer* 2006; **107:** 967-74. doi: 10.1002/cncr.22077
16. Li C, Wang X, Wang L, Chen JQ, Zhang WC, Pang QS, et al. Clinical practice and outcome of radiotherapy for advanced esophageal squamous cell carcinoma between 2002 and 2018 in China: the multi-center 3JECROG Survey. *Acta Oncologica* 2021; **60:** 627-34. doi: 10.1080/0284186X.2021.1902564
17. Lyu B, Yin YT, Zhao YL, Yang X, Gong J, Zhang M, et al. Long-term clinical outcomes and safety analysis of superficial esophageal cancer patients treated with definitive or adjuvant radiotherapy. *Cancers* 2022; **14:** 3423. doi: 10.3390/cancers14143423
18. Eisenhauer EA, Therasse P, Bogaerts J, Schwartz LH, Sargent D, Ford R, et al. New response evaluation criteria in solid tumors: revised RECIST guideline (version 1.1). *Eur J Cancer* 2009; **45:** 228-47. doi: 10.1016/j.ejca.2008.10.026
19. Wang JN, Xiao LL, Wang S, Pang QS, Wang J. Addition of induction or consolidation chemotherapy in definitive concurrent chemoradiotherapy versus concurrent chemoradiotherapy alone for patients with unresectable esophageal cancer: a systematic review and meta-analysis. *Front Oncol* 2021; **11:** 665231. doi: 10.3389/fonc.2021.665231
20. Wu HS, Yu YL, Zheng QH, Liu TX, Wu YH, Wang ZP, et al. Benefit of chemotherapy based on platinum with definitive radiotherapy in older patients with locally advanced esophageal squamous cell carcinoma. *Radiat Oncol* 2021; **16:** 1-14. doi: 10.1186/s13014-021-01931-1

21. Hsieh JCH, Chiang PC, Hung TM, Chao YK, Kuo YC, Wen CT, et al. Definitive concurrent chemoradiotherapy with paclitaxel plus carboplatin is superior to cisplatin plus 5-fluorouracil in patients with inoperable esophageal squamous cell carcinoma using retrospective, real-world evidence. *Cancer Med* 2021; **10:** 8300-9. doi: 10.1002/cam4.4025

22. Sher DJ, Posner MR, Tishler RB, Sarlis NJ, Haddad RI, Holupka EJ, et al. Relationship between radiation treatment time and overall survival after induction chemotherapy for locally advanced head-and-neck carcinoma: a subset analysis of TAX 324. *Int J Radiat Oncol Biol Phys* 2011; **81:** 813-8. doi: 10.1016/j.ijrobp.2010.12.005

23. Cannon DM, Geye HM, Hartig GK, Traynor AM, Hoang T, McCulloch TM, et al. Increased local failure risk with prolonged radiation treatment time in head and neck cancer treated with concurrent chemotherapy. *Head Neck* 2014; **36:** 1120-5. doi: 10.1002/hed.23419

24. Xu C, Xi M, Moreno A, Shiraishi Y, Hobbs BP, Huang ML, et al. Definitive chemoradiation therapy for esophageal cancer in the elderly: clinical outcomes for patients exceeding 80 years old. *Int J Radiat Oncol Biol Phys* 2017; **98:** 811-9. doi: 10.1016/j.ijrobp.2017.02.097

25. Cai YL, Lin YX, Jiang LS, Ye H, Li FY, Cheng NS. A novel nomogram predicting distant metastasis in T1 and T2 gallbladder cancer: a SEER-based study. *Int J Med Sci* 2020; **17:** 1704-12. doi: 10.7150/ijms.47073

26. Colzani E, Johansson ALV, Liljegren A, Foukakis T, Clements M, Adolfsson J, et al. Time-dependent risk of developing distant metastasis in breast cancer patients according to treatment, age and tumour characteristics. *Br J Cancer* 2014; **110:** 1378-84. doi: 10.1038/bjc.2014.5

27. Hemminki K, Pavlidis N, Tsilidis KK, Sundquist K, Ji J. Age-dependent metastatic spread and survival: Cancer of unknown primary as a model. *Sci Rep* 2016; **6:** 23725. doi: 10.1038/srep23725

28. Kumabe A, Zenda S, Motegi A, Onozawa M, Nakamura N, Kojima T, et al. Long-term clinical results of concurrent chemoradiotherapy for patients with cervical esophageal squamous cell carcinoma. *Anticancer Res* 2017; **37:** 5039-44. doi: 10.21873/anticanres.11919

29. Minsky BD, Neuberg D, Kelsen DP, Pisansky TM, Ginsberg RJ, Pajak T, et al. Final report of Intergroup Trial 0122 (ECOG PE-289, RTOG 90-12): phase II trial of neoadjuvant chemotherapy plus concurrent chemotherapy and high-dose radiation for squamous cell carcinoma of the esophagus. *Int J Radiat Oncol Biol Phys* 1999; **43:** 517-23. doi: 10.1016/s0360-3016(98)00463-5

30. Ohtsu A, Boku N, Muro K, Chin K, Muto M, Yoshida S, et al. Definitive chemoradiotherapy for T4 and/or M1 lymph node squamous cell carcinoma of the esophagus. *J Clin Oncol* 1999; **17:** 2915-21. doi: 10.1200/JCO.1999.17.9.2915

31. Shinoda M, Ando N, Kato K, Ishikura S, Kato H, Tsubosa Y, et al. Randomized study of low-dose versus standard-dose chemoradiotherapy for unresectable esophageal squamous cell carcinoma (JCOG0303). *Cancer Sci* 2015; **106:** 407-12. doi: 10.1111/cas.12622

32. Chan C, Lang S, Rowbottom C, Guckenberger M, Faivre-Finn C. Intensity-modulated radiotherapy for lung cancer: current status and future developments. *J Thorac Oncol* 2014; **9:** 1598-608. doi: 10.1097/JTO.0000000000000346

erratum

The biology and clinical potential of circulating tumor cells

Taja Lozar[1], Klara Gersak[1,2,3], Maja Cemazar[2,4], Cvetka Grasic Kuhar[2], Tanja Jesenko[2]

[1] Faculty of Medicine, University of Ljubljana, Ljubljana, Slovenia
[2] Institute of Oncology Ljubljana, Ljubljana, Slovenia
[3] General Hospital Izola, Izola, Slovenia
[4] Faculty of Health Sciences, University of Primorska, Izola, Slovenia

Radiol Oncol 2019; 53(2): 131-147.

Received 23 March 2019
Accepted 3 May 2019

Correspondence to: Tanja Jesenko, Ph.D., Institute of Oncology Ljubljana, Department of Experimental Oncology, Zaloška 2, SI-1000 Ljubljana, Slovenia. Phone: +386 1 5879 545; E-mail: tjesenko@onko-i.si

Disclosure: No potential conflicts of interest were disclosed.

doi: 10.2478/raon-2019-0024

Affiliations should be:

Taja Lozar[1], Klara Gersak[1,2,3], Maja Cemazar[2,4], Cvetka Grasic Kuhar[2], Tanja Jesenko[1,2]

[1] Faculty of Medicine, University of Ljubljana, Ljubljana, Slovenia
[2] Institute of Oncology Ljubljana, Ljubljana, Slovenia
[3] General Hospital Izola, Izola, Slovenia
[4] Faculty of Health Sciences, University of Primorska, Izola, Slovenia

doi: 10.2478/raon-2024-0055

Radiol Oncol 2024; 58(3): 313-319.
doi: 10.2478/raon-2024-0053

Subdiafragmatična aktivnost in z njo povezani artefakti pri perfuzijski scintigrafiji srca

Štrok A, Gužič Salobir B, Štalc M, Zaletel K

Izhodišča. Perfuzijska scintigrafija srca je neinvazivna diagnostična metoda, ki ima pomembno vlogo v diagnostiki ishemične bolezni srca. Po intravenskem vbrizganju radiofarmaka, se le-ta nakopiči v srčni mišici sorazmerno s področnim krvnim pretokom. Radiofarmak se nespecifično kopiči tudi v trebušnih organih, kar lahko ustvari artefakte. Subdiafragmatična aktivnost predstavlja enega izmed najpogostejših artefaktov in otežuje ocenjevanje perfuzije spodnje stene srčne mišice. V klinični praksi je zaradi trebušne aktivnosti potrebno pogosto ponoviti slikanje na kameri gama. S tem podaljšujemo čas trajanja preiskave in zmanjšujemo razpoložljivost kamere.

Zaključki. Rezultati raziskav, v katerih so preučevali različne tehnike za zmanjšanje subdiafragmatične aktivnosti, so nasprotujoči. Trenutne smernice za perfuzijsko scintigrafijo srca ne določajo standardiziranega pristopa za učinkovito zmanjšanje tega problema. Glede na izkušnje našega terciarnega centra lahko število tovrstnih artefaktov zmanjšamo z več načini. Kadar je le mogoče bolnike obremenimo dinamično, opravimo kasno slikanje, bolnikom svetujemo pitje vode med čakanjem na slikanje in zaužitje gaziranih pijač neposredno pred slikanjem.

Radiol Oncol 2024; 58(3): 320-325.
doi: 10.2478/raon-2024-0050

Anastomozirajoči hemangiom jajčnikov. Pregled literature o redki entiteti

Merlo S, Vivod G, Gazić B, Kovačević N

Izhodišča. Anastomozirajoči hemangiom jajčnikov je redek žilni tumor, ki večinoma prizadene ženske srednjih let. Kljub benigni naravi lahko njegova histološka slika posnema agresivne žilne lezije, kar predstavlja diagnostične izzive. Namen članka je pregled literature o tej redki entiteti.

Metode. V bazi podatkov PubMed in Scopus smo pregledali članke v angleškem jeziku, ki so omenjali anastomozirajoči hemangiom jajčnikov. Podatke o vseh pridobljenih primerih smo nato podrobno proučili.

Rezultati. Našli smo 33 opisanih primerov anastomozirajočega hemangioma jajčnikov. Kljub majhnemu številu primerov smo prikazali pomen natančne histopatološke ocene.

Zaključki. Čeprav sprva glede na slikovno diagnostiko in histološko sliko lahko pomislimo na maligno obolenje, natančna histološka ocena razkrije benigno entiteto. Potrebno je ozaveščati o tej nenavadni in redki entiteti in s tem preprečevati napačne diagnoze, ki lahko privedejo do nepotrebnega zdravljenja ali zaskrbljenosti bolnice.

Radiol Oncol 2024; 58(3): 326-334.
doi: 10.2478/raon-2024-0042

Slikanje mikrovaskularnih sprememb z laserskimi lisami pri onkoloških kliničnih aplikacijah. Pregled literature

Hren R, Kranjc Brezar S, Marhl U, Serša G

Izhodišča. Slikanje z laserskimi lisami *(angl. laser speckle coherence imaging*, LSCI) je nova metoda medicinskega slikanja, ki omogoča neinvazivno vizualizacijo in analizo vaskularnosti tumorja. V pričujočem članku smo ovrednotili LSCI pri ocenjevanju mikrovaskularnih sprememb v klinični onkologiji s sistematičnim pregledom literature.

Metode. Vključitveni kriterij pri iskanju literature v elektronskih bazah podatkov *PubMed, Web of Science* in *Scopus* je bila uporaba LSCI v klinični onkologiji.

Rezultati. Kriteriju za vključitev je ustrezalo 36 člankov. Anatomske lokacije novotvorb v izbranih člankih so bile možgani (5 člankov), dojke (2 članka), endokrine žleze (4 članki), koža (12 člankov) in prebavila (13 člankov).

Zaključki. LSCI je obetajoča nova metoda slikanja, ki pa se sooča z več omejitvami. Največji izziv predstavlja pomanjkanje standardiziranih protokolov in smernic za interpretacijo meritev.

Radiol Oncol 2024; 58(3): 335-347.
doi: 10.2478/raon-2024-0045

Vloga kvantitativnih slikovnih označevalcev v zgodnji preiskavi ^{18}F-FDG PET/CT za odkrivanje imunsko pogojenih neželenih učinkov pri bolnikih z melanomom. Prospektivna raziskava

Hribernik N, Strašek K, Huff DT, Studen A, Zevnik K, Škalič K, Jeraj R, Reberšek M

Izhodišča. Namen raziskave je bil oceniti vlogo novega kvantitativnega slikovnega označevalca $SUV_{X\%}$, privzema ^{18}F-FDG, pridobljenega iz zgodnje preiskave ^{18}F-FDG PET/CT. Preiskavo smo izvajali 4 tedne po začetku zdravljenja, da bi ugotovili imunsko pogojene neželene učinke v kohorti bolnikov z metastatskim melanomom, ki so prejemali zaviralce imunskih nadzornih točk.

Bolniki in metode. V prospektivno neintervencijsko klinično raziskavo smo vključili bolnike z metastatskim melanomom, ki smo jih zdravili z zaviralci imunskih nadzornih točk in smo jih redno spremljani z ^{18}F-FDG PET/CT. Preiskavo smo naredili pred zdravljenjem, v četrtem tednu (T4), šestnajstem tednu (T16) in dvaintridesetem tednu (T32) po začetku zdravljenja. Za segmentacijo treh ciljnih organov (pljuč, črevesja in ščitnice) smo uporabili konvolucijsko nevronsko mrežo. Kvantitativni slikovni označevalec imunsko pogojenih neželenih učinkov, $SUV_{X\%}$, smo ocenjevali znotraj ciljnih organov in ga primerjali s kliničnimi znaki neželenih učinkov. Za količinsko opredelitev učinkovitosti zaznavanja imunsko pogojenih neželenih učinkov smo uporabili površino pod karakteristično krivuljo delovanja sprejemnika (*angl. area under the receiver-operating characteristic curve*, AUROC).

Rezultati. Skupno smo prospektivno zbrali in analizirali 242 slik ^{18}F-FDG PET/CT pri 71 bolnikih z metastatskim melanomom. Zgodnja preiskava ^{18}F-FDG PET/CT po T4 je pokazala izboljšano odkrivanje samo za ščitnico v primerjavi s preiskavo po T32 ($p = 0,047$). AUROC za odkrivanje imunsko pogojeni neželenih učinkov v treh ciljnih organih je bila najvišja, ko je bil $SUV_{X\%}$ ekstrahiran iz ^{18}F-FDG PET/CT po T16 in je bil 0,76 za pljuča, 0,53 za črevesje in 0,81 za ščitnico. $SUV_{X\%}$, ekstrahiran iz ^{18}F-FDG PET/CT po T4, ni izboljšal odkrivanja neželenih učinkov v primerjavi s slikanjem po T16 (pljuča: $p = 0,54$; črevesje: $p = 0,75$; ščitnica: $p = 0,3$; DeLongov test) kot tudi v primerjavi s slikanjem pljuč po T32 ($p = 0,32$) in slikanjem črevesja ($p = 0,3$).

Zaključki. Zgodnja preiskava ^{18}F-FDG PET/CT po T4 ni pokazala statistično značilnega zgodnejšega odkrivanja imunsko pogojenih neželenih učinkov. Vendar pa se je za organ specifičen privzem ^{18}F-FDG, kvantificiran s $SUV_{X\%}$, pokazal kot dosleden kvantitativni slikovni označevalec za imunsko pogojene neželene učinke. Za boljšo oceno vloge ^{18}F-FDG PET/CT pri odkrivanju imunsko pogojenih neželenih učinkov bi bilo potrebno določiti časovni razvoj kvantificiranega vnetja, kar pa bi lahko opredelili v multicentričnih kliničnih raziskavah.

Radiol Oncol 2024; 58(3): 348-356.
doi: 10.2478/raon-2024-0032

Kvantitativni SSTR-PET/CT. Možno orodje za napovedovanje odgovora na zdravljenje z everolimusom pri bolnikih z nevroendokrinim tumorjem

Karim H, Winkelmann M, Grawe F, Völter F, Auernhammer C, Rübenthaler J, Ricke J, Ingenerf M, Smith-Tannwald C

Izhodišča. Namen raziskave je bil oceniti kvantitativne parametre ^{68}Ga-DOTA-TATE (-TOC) PET/CT pri spremljanju bolnikov in napovedovanju odgovora na zdravljenje z everolimusom pri bolnikih z nevroendokrinimi tumorji in metastazami v jetrih.

Bolniki in metode. V retrospektivno analizo smo vključili 29 bolnikov s 62 tarčnimi lezijami, ki smo jih zdravili z everolimusom. PET/CT s 68Ga-DOTA-TATE (-TOC) smo naredili pred začetkom zdravljenja in med spremljanjem bolnikov. Ocena odgovora na zdravljene je vključevala preživetje brez napredovanja bolezni (*angl. progression-free survival*, PFS). Glede na PFS-je so bili bolniki razvrščeni kot odzivni bolniki (PFS ≤ 6 mesecev). Ocenili smo velikost in gostoto lezij, skupaj z največjo in srednjo standardizirano vrednostjo privzema (*angl. standardize uptake value*, SUV) v lezijah v jetrih in vranicah. Izračunana smo razmerja med tumorjem in vranico (*angl. tumor/splen*, T/S) ter tumorjem in jetri (*angl. tumor/liver* T/L) z uporabo SUVmaks/SUVmaks, SUVmaks/SUVsrednji in SUVsrednji/SUVsrednji.

Rezultati. Preiskavo PET/CT smo naredili 19 dni (interkvartilni raspon [*angl. interquartile range*, IQR] 69 dni) pred zdravljenjem in 127 dni (IQR 74 dni) po začetku zdravljenja z everolimusom. Srednja vrednost PFS-ja je bila 264 dni (95 % interval zaupanja [CI] 134–394 dni). Pri odzivnih bolnikih je bilo značilno zmanjšano razmerje Tmaks/Lmaks in Tsrednji/Lmaks v primerjavi z neodzivnimi (p = 0,01). Univariatna Coxova regresija je pokazala, da je razmerje Tsrednji/Lmaks edini napovedni dejavnik, povezan s PFS-jem (razmerje obetov [HR] 0,5; 95 % CI 0,28−0,92; p = 0,03). Spremembe v razmerjih T/L in T/S so imele pomembno napovedno vrednost za PFS, z najvišjo površino pod krivuljo (AUC) za odstotno spremembo Tsrednji/Lmaks (AUC = 0,73). Optimalna pražna vrednost < 2,5 % je opredelila bolnike z daljšim PFS-jem (p = 0,003). Drugi slikovni ali klinični parametri niso imeli napovedne vrednosti za PFS.

Zaključki. Raziskava je pokazala vrednost kvantitativnega SSTR-PET/CT pri napovedovanju in spremljanju odgovora na zdravljenje z everolimusom pri bolnikih z nevroendokrinimi tumorji in metastazami v jetrih. Razmerja med jetrnimi metastazami in jetrnim parenhimom so umela boljšo napovedno vrednost kot same velikosti metastaz. Razmerje Tsrednji/Lmaks bi lahko služilo kot napovedni pokazatelj za PFS, vendar bi bilo potrebno analizirati večje število bolnikov.

Radiol Oncol 2024; 58(3): 357-365.
doi: 10.2478/raon-2024-0035

Uvedba spektrofotometrične metode za določanje joda v slini s pomočjo Sandell-Kolthoffove reakcije na mikrotitrski ploščici

Oblak A, Imperl J, Kolar M, Marolt G, Krhin B, Zaletel K, Gaberšček S

Izhodišča. Jod je nujno potreben element za sintezo ščitničnih hormonov, zato je pomembno najti zanesljiv označevalec vnosa joda. Jod se večinoma izloča skozi ledvice, vendar tudi preko žlez slinavk. Namen našega dela je bila uvedba enostavne metode za določanje joda v slini.

Materiali in metode. Za izvedbo Sandell-Kolthoffove reakcije, na mikrotitrski ploščici z amonijevim peroksidisulfatom smo uporabili standarde in reagente, ki smo jih pripravili v laboratoriju. V območju 0−400 µg/L smo testirali primernost uporabe standardov, pripravljenih na vodni osnovi ter standardov, pripravljenih z umetno slino. Sledili smo vsem priporočilom in standardom za validacijo metode, definirali koncentracijo uporabljenega amonijevega peroksidisulfata in primerjali rezultate z induktivno sklopljeno plazmo z masno spektrometrijo.

Rezultati. Uporaba standardov, pripravljenih na vodni osnovi, se je izkazala za primernejšo in zanesljivejšo od standardov, pripravljenih z umetno slino, saj z uporabo slednjih podcenimo koncentracijo joda v vzorcu. Spodnja meja detekcije je znašala 6,5 µg/L, spodnja meja linearnosti pa 12,0 µg/L. Analitično območje je tako bilo od 12 do 400 µg/L. Ponovljivost in obnovljivost pri koncentracijah joda v slini 20, 100, 165 in 350 µg/L sta znašali 18,4, 5,1, 5,7 in 2,8 % ter 20,7, 6,7, 5,1 in 4,3 %. Primerna molarnost amonijevega peroksidisulfata za analizo je bila 1,0 mol/L. Med uporabo 1,0 in 1,5 mol/L amonijevega peroksidisulfata ni bilo razlik (P vrednosti za vzorce pri koncentracijah joda v slini 40, 100 in 150 µg/L so bile 0,761, 0,085 in 0,275), medtem ko smo ob uporabi 0,5 mol/L amonijevega peroksidisulfata opazili značilno razliko pri merjenju koncentracije joda v slini (P < 0,001). Vzorce sline je bilo možno redčiti do osemkrat. Interferenci tiocianata in kofeina nista motili analize do koncentracije 193,5 mg/L. Metoda je bila primerljiva z rezultati, pridobljenimi z metodo induktivno sklopljene plazme z masno spektrometrijo. Spaermanov koeficient je bil 0,989 (95 % IZ: 0,984−0,993).

Zaključki. Nova metoda za določanje joda v slini se ujema z metodo induktivno sklopljene plazme z masno spektrometrijo in je enostavna za uporabo.

Radiol Oncol 2024; 58(3): 366-375.
doi: 10.2478/raon-2024-0044

S kontrastom ojačano dinamično magnetnoresonančno slikanje in plazemski angiogeni dejavniki pri napovedi odgovora na sočasno radiokemoterapijo pri humanem papilomskem virus negativnem karcinomu žrela

Longo A, Hudler P, Strojan P, Plavc G, Umek L, Šurlan Popović K

Izhodišča. S kontrastom ojačano dinamično magnetnoresonančno slikanje (*ang. dynamic contrast-enhanced magnetic resonance imaging*, DCE-MRI) je metoda, s katero lahko ocenimo vaskularnost tumorjev. Ta je odvisna od procesov angiogeneze in (vaskularnost) vpliva na odgovor tumorjev na zdravljenje. Raziskali smo povezave med merami DCE-MRI in izražanjem plazemskih angiogenih dejavnikov pri humanem papilomskem virus negativnem (HPV-negativnem) karcinomu žrela in njihovo napovedno vrednost pri odgovoru na sočasno radiokemoterapijo (*ang. concurrent chemoradiotherapy*, cCRT).

Bolniki in metode. Prospektivno smo vključili 25 bolnikov z napredovalim HPV-negativnim karcinomom ustnega žrela. Opravili smo DCE-MRI in odvzeme vzorcev plazme pred cCRT, po prejetih 20 Gy obsevanja in 10–12 tednov po zaključenem zdravljenju. Izmerili smo perfuzijske parametre k_{trans}, k_{ep}, V_e in začetno površino pod krivuljo (*angl. initial area under the curve*, iAUC) ter določili izražanje plazemskih angiogenih dejavnikov (žilnega endotelijskega rastnega dejavnika *[angl. vascular endothelial growth factor*, VEGF], rastnega dejavnika vezivnega tkiva [*angl. connective tissue growth factor*, CTGF], rastnega dejavnika iz trombocitov AB [*angl. platelet-derived growth factor*, PDGF-AB], angiogenina [ANG], endostatina [END] in trombospondina-1 [*angl. thrombospondin-1*, THBS1]). Bolnike smo na podlagi klinične ocene odgovora na zdravljenje razdelili na skupini s popolnim in nepopolnim odgovorom. Na podlagi razlik med skupinama in medsebojnih povezav med merami smo pripravili statistične modele za napoved odgovora na zdravljenje.

Rezultati. Bolniki s popolnim odgovorom za zdravljenje so v primerjavi z bolniki z nepopolnim odgovorom izkazali višje vrednosti k_{trans} in VEGF v vseh merjenih časovnih točkah. Bolniki s popolnim odgovorom so izkazali višje vrednosti iAUC pred cCRT ter višje vrednosti PDGF-AB med cCRT. Na podlagi vrednosti k_{trans} in VEGF v zgodnjem obdobju med cCRT smo pripravili uspešen model za napoved odgovora na zdravljenje z mejno vrednostjo 0,259 min^{-1} za k_{trans} in 62,5 pg/ml za plazemski VEGF.

Zaključki. Vrednosti parametra DCE-MRI k_{trans} in izražanje plazemskega VEGF po prejetih 20 Gy obsevanja bi lahko bila uporabna za napoved odgovora na zdravljenje pri HPV-negativnem karcinomu ustnega žrela.

Radiol Oncol 2024; 58(3): 376-385.
doi: 10.2478/raon-2024-0039

Ali anatomija portalne vene vpliva na intrahepatično porazdelitev metastaz kolorektalnega raka?

Tribolet A, Barat M, Fuks D, Aissaoui M, Soyer P, Marchese U, Gaillard M, Nassar A, Hardwigsen J, Tzedakis S

Izhodišča. Ob lokaciji primarnega kolorektalnega raka je znanih še nekaj dejavnikov, ki vplivajo na intrahepatično porazdelitev jetrnih metastaz kolorektalnega raka. Namen raziskave je bil oceniti, ali lahko tudi anatomija portalne vene vpliva na intrahepatično porazdelitev jetrnih metastaz kolorektalnega raka.

Bolniki in metode. V raziskavo smo vključili bolnike z jetrnimi metastazami kolorektalnega raka, ki smo jih diagnosticirali med januarjem 2018 in decembrom 2022 v dveh terciarnih centrih. Slikanje sta neodvisno pregledala dva radiologa. Ujemanje med operaterji smo ocenjevali glede na korelacijski koeficient znotraj razreda (*angl. intraclass correlation coefficient*, ICC). Vpliv premera, kota vej portalne vene in njihovih variacij na število in porazdelitev jetrnih metastaz smo primerjali z uporabo Mann-Whitneyjevega, Kruskal-Wallisovega, Pearsonovega hi-kvadrata in Spearmanovega korelacijskega testa.

Rezultati. Vključili smo 200 bolnikov. ICC je bil visok (> 0,90; P< 0,001). Intrahepatična porazdelitev jetrnih metastaz je bila enostranska v desnih jetrih pri 66 bolnikih (33 %), v levih jetrih pri 24 (12 %) in obojestranska pri 110 bolnikih (55 %). Srednje število jetrnih metastaz je bilo 3 (1−7). Variacije portalne vene tipa 1, 2 in 3 so opazili pri 156 (78 %), 19 (9,5 %) in 25 (12 %) bolnikih. Na enostransko ali obojestransko porazdelitev jetrnih metastaz niso vplivale anatomske variacije portalne vene (P = 0,13), premer njene desne (P = 0,90) ali leve (P = 0,50) veje, naklon desne (P = 0,20) ali leve (P =0,80) veje. Prav tako je bila enostranska ali obojestranska porazdelitev jetrnih metastaz neodvisna od primarne lokalizacije tumorja (P = 0,60). Tudi med številom jetrnih metastaz in premerom (R: 0,093, P = 0,10) ali kotom vej portalne vene (R: 0,012, P = 0,83) nismo ugotovili korelacije.

Zaključki. V pričujoči raziskavi anatomija portalne veje ni vplivala na porazdelitev in število jetrnih metastaz kolorektalnega raka.

Radiol Oncol 2024; 58(3): 386-396.
doi: 10.2478/raon-2024-0040

Večja vrednost radiomike v primerjavi s sonografsko oceno pri ultrazvočni opredelitvi ekstratiroidalne razširitve papilarnega karcinoma ščitnice. Retrospektivna raziskava

Zhu H, Luo H, Li Y, Zhang Y, Wu Z, Yang Y

Izhodišča. Ekstratiroidalna tumorska razširitev je povezana s slabšim preživetjem bolnikov s papilarnim karcinomom ščitnice. Za predoperativno oceno smo izmerili in primerjali napovedno vrednost sonografske metode in ultrazvočne radiomične metode pri bolnikih z noduli papilarnega karcinoma ščitnice.

Bolniki in metode. Vključili smo podatke bolnikov s 337 nodusi, ki smo jih razdelili v učno in validacijsko skupino. Za metodo ultrazvočne radiomike smo na podlagi kliničnih značilnosti in ultrazvočnih radiomskih značilnosti izdelali in validirali najboljši model. Nato smo izračunali napovedno vrednost. Pri sonografski metodi smo rezultate izračunali na podlagi vseh vzorcev.

Rezultati. Za metodo ultrazvočne radiomike smo sestavili 9 modelov in izbrali kot najustreznejši model ekstremno povečanega gradienta (*angl. extreme gradient boosting*, xgboost) zaradi njegove največje natančnosti (0,77) in površine pod krivuljo (0,813) v validacijski skupini. Natančnost in površina pod krivuljo sonografske metode sta bili 0,70 in 0,569. Ugotovili smo, da prvih šest najpomembnejših značilnosti v izbranem modelu ni bilo kliničnih, pač pa so bile značilnosti visokodimenzionalne radiomske.

Zaključki. V raziskavi se je ultrazvočna radiomska metoda pokazala boljša od sonografske metode za predoperativno odkrivanje ekstratiroidalne razširitve papilarnega karcinoma ščitnice. Visokodimenzionalne radiomske značilnosti pa so bile pomembnejše od kliničnih značilnosti.

Radiol Oncol 2024; 58(3): 397-405.
doi: 10.2478/raon-2024-0037

Nujna in preventivna embolizacija maternične arterije v ginekologiji in porodništvu. Retrospektivna analiza

Vihtelič P, Skuk E, Kenda Šuster N, Jakimovska Stefanovska M, Popovič P

Izhodišča. Namen raziskave je bil oceniti varnost in učinkovitost nujne in preventivne embolizacije materničnih arterij v klinični praksi, vključno s tehničnim in kliničnim uspehom ter povezanimi zapleti.

Bolniki in metode. V retrospektivni raziskavi smo analizirali 64 žensk, ki smo jih zdravili z nujno (n = 18) in preventivno (n = 46) embolizacijo materničnih arterij. Indikacije za nujno embolizacijo so vključevale poporodno krvavitev ali hudo krvavitev med prekinitvijo nosečnosti, medtem ko je bila preventivna embolizacija izvedena pred kirurškim odstranjevanjem rezidualnega tkiva po splavu ali porodu (*angl. retained products of conception, RPOC*), pred porodom z nenormalno vraslo posteljico ali prekinitvijo nosečnosti (cervikalna nosečnost ali fetalne nepravilnosti z nenormalno vraslo posteljico). Tehnični uspeh embolizacije je bil opredeljen kot popolna zapora tarčne žile in zastoj kontrasta na končnem angiogramu. Klinični uspeh je bil opredeljen kot ustavitev krvavitve po embolizaciji brez histerektomije.

Rezultati. Skupni klinični uspeh embolizacij materničnih arterij je bil 97 % (62/64). V preventivni skupini so bili vsi postopki embolizacije tehnično in klinično uspešni, brez življenjsko ogrožajočih krvavitev ali histerektomij (100 % uspešnost, 46/46). Tehnični uspeh posegov v nujni skupini je bil 100 %, krvavitev pa je bila uspešno nadzorovana v 89 % primerov (16/18). Pri dveh bolnicah z večjo izgubo krvi (nad 2000 ml) z embolizacijo nismo dosegli hemostaze, zaradi vztrajajoče krvavitve pa je bila potrebna histerektomija.

Zaključki. Embolizacija materničnih arterij je varen in učinkovit poseg za obladovanje primarne poporodne krvavitve ali hude krvavitve med prekinitvijo nosečnosti ter za zmanjšanje tveganja za hude krvavitve med kirurškim odstranjevanjem rezidualnega tkiva, porodom z nenormalno vraslo posteljico ali prekinitvijo nosečnosti.

Radiol Oncol 2024; 58(3): 406-415.
doi: 10.2478/raon-2024-0047

Analiza ujetja magnetnoresonančnega kontrastnega sredstva v celicah po reverzibilni elektroporaciji *in vitro*

Stručić M, Miklavčič D, Vidic Z, Scuderi M, Serša I, Kranjc M

Izhodišča. Vnos kontrastnega sredstva na osnovi gadolinija v organizem pred elektroporacijo omogoči kontrastnemu sredstvu vstop v celice in evalvacijo reverzibilno elektroporiranih regij z uporabo magnetne resonance. Namen te raziskave je bil ovrednotenje ujetja kontrastnega sredstva v ovarijske celice kitajskega hrčka (CHO) in primerjava rezultatov s standardnimi *in vitro* metodami za oceno prepustnosti celične membrane, integritete celične membrane in preživetja celic po elektroporaciji.

Materiali in metode. Evalvacijo permeabilizacije celične membrane in integritete celične membrane smo izvedli z uporabo barvila YO-PRO-1 in propidijevega jodida. Preživetje celic smo ovrednotili s poskusi, ki so temeljili na presnovni aktivnosti celic z uporabo metabolnega testa MTS. Za evalvacijo ujetega kontrastnega sredstva gadobutrol v reverzibilno elektroporiranih celicah pa smo uporabili T_1 relaksometrijo celičnih suspenzij 25 minut in 24 ur po elektroporaciji in potrdili z masno spektrometrijo z induktivno skopljeno plazmo.

Rezultati. Kontrastno sredstvo smo zaznali v celicah 25 minut in 24 ur po aplikaciji električnih pulzov, ki so bile reverzibilno elektroporirane. Poleg tega je bilo kontrastno sredstvo prisotno v ireverzibilno elektroporiranih celicah 25 minut po aplikaciji električnih pulzov, vendar ga nismo več zaznali v ireverzibilno elektroporiranih celicah po 24 urah. Induktivno sklopljena plazma in masna spektrometrija je pokazala sorazmerno zmanjšanje vsebnosti gadolinija na celico s skrajšanjem relaksacijskega časa T_1 (R^2 = 0,88 in p = 0,0191).

Zaključki. Rezultati raziskave dokazujejo, da je kontrastno sredstvo ujeto v celicah, izpostavljenih reverzibilni elektroporaciji, vendar izstopi iz celic, izpostavljenih ireverzibilni elektroporaciji v 24 urah, kar potrjuje hipotezo, na kateri so temeljili poskusi določanja območij reverzibilne elektroporacije *in vivo*.

Radiol Oncol 2024; 58(3): 416-424.
doi: 10.2478/raon-2024-0048

Limfom očesnih adneksov. Retrospektivna raziskava slovenske populacije ter primerjava z literaturo

Boltežar L, Štrbac D, Pižem J, Hawlina G

Izhodišča. Namen raziskave je bil preučiti značilnosti vseh slovenskih bolnikov z limfomom očesnih adneksov v obdobju 24 let, ovrednotiti demografske podatke, lokalizacijo, vrsto limfoma, stadij bolezni, način zdravljenja, stopnjo lokalnega nadzora bolezni in stopnjo preživetja.

Bolniki in metode. V retrospektivno raziskavo smo vključili vse bolnike s histološko potrjenim limfomom očesnih adneksov, ki smo jih diagnosticirali v terciarnem centru Slovenije, Očesni kliniki Univerzitetnega Kliničnega Centra Ljubljana in nato zdravili na Onkološkem inštitutu Ljubljana. Podatke o bolnikih smo zbrali od oktobra 1995 do aprila 2019.

Rezultati. V raziskavo smo vključili 74 bolnikov, njihova mediana starost ob diagnozi je bila 68 let. Večina limfomov je bila B-celičnega izvora (98,6 %). Najpogostejša podvrsta je bila ekstranodalni B-celični limfom marginalne cone (*angl. mucosa-associated lymphoid tissue*, MALT) (71,6 %). 56 bolnikov je imelo orbitalni limfom (75,5 %), 18 bolnikov pa limfom veznice (24,3 %). Očesna manifestacija je bila prvi znak bolezni pri 78,4 % bolnikov, pri 67,6 % bolnikov so bili očesni adneksi tudi edina lokacija bolezni. 68,9 % bolnikov smo zdravili z radioterapijo, 9,4 % s sistemskim zdravljenjem, 6,8 % s kombinirano radioterapijo in sistemskim zdravljenjem, 11 bolnikov pa smo le opazovali in aktivno sledili, brez specifičnega zdravljenja. Lokalni nadzor bolezni smo dosegli pri 96,6 % zdravljenih bolnikov. Srednje celokupno preživetje vseh bolnikov še ni bilo doseženo. 5-letno celokupno preživetje je bilo 80,1 % (95 % interval zaupanja [IZ] 68,1 % − 88,5 %), 5-letno za limfom specifično preživetje pa 87,2 % (95 % IZ 83,2 % − 91,2 %).

Zaključki. Limfom očesnih adneksov obsega skupino heterogenih bolezni s spremenljivimi izidi, ki so odvisni predvsem od bolnikove starosti in vrste limfoma. Limfomi nizkega gradusa imajo dobro napoved poteka bolezni tudi pri starejših bolnikih.

Radiol Oncol 2024; 58(3): 425-431.
doi: 10.2478/raon-2024-0033

Kompresijski zlom vretenca po stereotaktičnem obsevanju hrbtenice. Izkušnje posamičnega centra

Issany A, Iovoli AJ, Wang R, Shekher R, Ma SJ, Goulenko V, Fekrmandi F, Prasad D

Izhodišča. Za zdravljenje razsejane maligne bolezni vse pogosteje uporabljamo Stereotaktično obsevanje hrbtenice (*angl. stereotactic body radiation therapy*, SBRT). V primerjavi s konvencionalnimi režimi obsevanja dosežemo večje lajšanje bolečine in boljše lokalne kontrole zasevkov. Kompresijski zlom vretenca predstavlja pomemben možen neželen učinek po SBRT hrbtenice. Pregledali smo, kakšne izkušnje imamo v naši ustanovi s SBRT hrbtenice in kompresijskimi zlomi vretenca ter nestabilnostjo hrbtenice (*angl. spinal instability neoplastic score*, SINS).

Bolniki in metode. V retrospektivno analizo smo vključili 83 bolnikov s skupno 100 lezijami hrbtenice, ki smo jih zdravili s SBRT med leti 2007 in 2022. Klinične podatke smo povzeli iz medicinske dokumentacije. Primarni cilj raziskave je bil opredeliti, kakšen je delež kompresijskih zlomov vretenca po zdravljenju. Klinične dejavnike, povezane s kompresijskim zlomom vretenca, smo ugotavljali z logistično univariatno analizo.

Rezultati. Srednja doza obsevanja je bila 24 Gy, srednje število frakcij pa 3. Kompresijski zlom vretenca se je razvil v 10 segmentih hrbtenice, zdravljenih s SBRT (10 %). Srednji čas do zloma vretenca je bil 2,4 meseca. Pri 11 segmentih hrbtenice, pri katerih smo pred SBRT opravili kifoplastiko, se kompresijski zlom vretenca ni razvil. Univariatna analiza ni pokazala dejavnikov, ki bi bili povezani s kompresijskim zlomom vretenca.

Zaključki. Delež kompresijskega zloma vretenca po SBRT hrbtenice je nizek. Pri bolnikih z visokim tveganjem za zlom lahko profilaktična kifoplastika predstavlja zaščito pred kompresijskim zlomom.

Radiol Oncol 2024; 58(3): 432-443.
doi: 10.2478/raon-2024-0054

Retrospektivna ocena terapevtske učinkovitosti in varnosti kemoradioterapije pri starejših bolnikih (starih ≥ 75 let) z omejeno boleznijo drobnoceličnega pljučnega raka. Ugotovitve dveh terciarnih ustanov in pregled literature

Shiono A, Imai H, Endo S, Katayama K, Sato H, Hashimoto K, Miura Y, Okazaki S, Abe T, Mouri A, Kaira K, Masubuchi K, Kobayashi K, Minato K, Kato S, Kagamu H

Izhodišča. Standardno zdravljenje bolnikov z drobnoceličnim rakom pljuč in omejeno boleznijo, v dobrem splošnem stanju je sočasna kemoterapija s platino/etopozidom in radioterapija. Učinkovitost in varnost kemoradioterapije pri starejših bolnikih z drobnoceličnim rakom pljuč in omejeno boleznijo pa nista v celoti raziskani. Optimalno zdravljenje ostaja nejasno. Namen raziskave je bil proučiti izvedljivost in učinkovitost kemoradioterapije pri starejših bolnikih s to boleznijo.

Bolniki in metode. Analizirali smo zaporedne bolnike (stare ≥ 75 let) s stadiji I do III drobnoceličnega raka pljuč, ki so od aprila 2007 do junija 2021 v dveh terciarnih ustanovah prejemali sočasno ali zaporedno kemoradioterapijo. Retrospektivno smo ocenili učinkovitost in toksičnosti zdravljenja.

Rezultati. S sočasno (n = 19) ali zaporedno (n = 13) kemoradioterapije smo zdravili 32 bolnikov. Srednja starost vseh bolnikov je bila 77 (razpon: 75–81) oziroma 79 (razpon: 76–92) let. Srednje število prejetih krogov kemoradioterapije je bilo pri vseh bolnikih 4 (razpon: 1–5), stopnja odgovorov na zdravljenje pa 96,9 % (94, % v skupini s sočasno in 100 % v skupini z zaporedno kemoradioterapijo). Srednje preživetje brez napredovanja bolezni in srednje celokupno preživetje za vse bolnike je bilo 11,9 in 21,1 meseca. Srednje preživetje brez napredovanja bolezni je bilo 13,0 in 9,0 meseca v skupinah s sočasno in zaporedno kemoradioterapijo. Razlika ni bila statistično pomembna (p = 0,67). Srednje celokupno preživetje od začetka kemoradioterapije je bilo 19,2 in 23,5 meseca v skupinah s sočasno in zaporedno kemoradioterapijo (p = 0,46). Pogostost hematoloških neželenih dogodkov stopnje ≥ 3 je bila naslednja: levkopenija 20/32 (62,5 %), nevtropenija 23/32 (71,9 %), anemija 6/32 (18,8 %), trombocitopenija 7/32 (21,9 %) in febrilna nevtropenija 3/32 (9,4 %). Smrt, povezana z zdravljenjem, je nastopila pri enem bolniku iz vsake skupine.

Zaključki. Čeprav je bila hematološka toksičnost, zlasti nevtropenija, huda, smo s kemoradioterapijo dosegli ugodno učinkovitost v obeh skupinah, tako skupini s sočasno kot v skupini z zaporedno kemoradioterapijo. Sočasna kemoradioterapija verjetno ne bo izvedljiva za vse starejše bolnike z omejeno obliko drobnoceličnega raka pljuč, zato je lahko zaporedna kemoradioterapija pri teh bolnikih zdravljenje izbire. Za opredelitev optimalnih strategij bodo potrebne nadaljnje prospektivne raziskave.

Radiol Oncol 2024; 58(3): 444-457.
doi: 10.2478/raon-2024-0038

Dolgoročni rezultati zdravljenja z indukcijsko kemoterapijo pri neoperabilnem ploščatoceličnem karcinomu požiralnika, ki ji je sledila sočasna kemoradioterapija. Izkušnje posamičnega centra

Xiang G, Chai G, Lyu B, Li Z, Yin Y, Wang B, Pan Y, Shi M, Zhao L

Izhodišča. Namen raziskave je bil proučiti dolgoročne klinične rezultate in toksičnost indukcijske kemoterapije, ki ji je sledila sočasna kemoradioterapija, v primerjavi s samo sočasna kemoradioterapijo pri bolnikih z neoperabilnim ploščatoceličnim karcinomom požiralnika.

Bolniki in metode. Med letoma 2008 in 2022 smo v raziskavo vključili 271 bolnikov z neoperabilnim ploščatoceličnim karcinomom požiralnika, ki so prejeli radikalno sočasna kemoradioterapijo. Uporabili smo tehniko radioterapije z modulirano intenzivnostjo (*angl. intensity modulated radiation therapy*, IMRT) ali pa volumetrično modulirano obločno terapijo (*angl. volumetric modulated arc therapy*, VMAT). Z metodo primerjanja rezultatov nagnjenosti (*angl. propensity score-matched*, PSM) smo v razmerju 1:1 primerjali 71 bolnikov, ki so prejemali indukcijsko kemoterapijo in sočasno kemoradioterapijo z bolniki, ki so prejemali samo sočasno kemoradioterapijo. Analizo preživetja in napoved poteka bolezni smo izračunali s Kaplan-Meierjevo metodo in Coxovim modelom sorazmernih tveganj.

Rezultati. Pri skupini bolnikov, ki smo jih zdravili z indukcijsko kemoterapijo in sočasno kemoradioterapijo se 5-letno celokupno preživetje, preživetje brez ponovitve bolezni in preživetje brez oddaljenih metastaz ni izboljšalo (vse $p > 0,05$) v primerjavi s skupino s samo sočasno kemoradioterapijo. Petletno celokupno preživetje (65,6 % proti 17,6 % proti 29,3 %; $p < 0,001$), preživetje brez ponovitve bolezni (65,6 % proti 17,6 % proti 26,9 %; $p < 0,001$) in preživetje brez oddaljenih metastaz (62,5 % proti 10,3 % proti 27,2 %, $p < 0,001$) je bilo v skupini bolnikov z dobrim odzivom na indukcijsko kemoterapijo bistveno višje kot v skupini s slabim odzivom na indukcijsko kemoterapijo in skupini s samo sočasno kemoradioterapijo. Multivariatna analiza je pokazala, da so bili skupni čas radioterapije (≥ 49 dni) in stadij III/IV neodvisni napovedni dejavniki za vse tri oblike preživetja. Med obema skupinama ni bilo opaziti pomembnih razlik v stopnji toksičnosti 3.–4. stopnje.

Zaključki. Rezultati raziskave so pokazali, da dodajanje indukcijske kemoterapije k sočasni kemoradioterapiji ni bilo boljše od same sočasne kemoradioterapije pri neselekcioniranih bolnikih z neoperabilnim ploščatoceličnim karcinomom požiralnika. Odzivniki na indukcijsko kemoterapijo pa so lahko imeli koristi od takšnega načina zdravljenja in nismo zabeležili povečane toksičnosti.

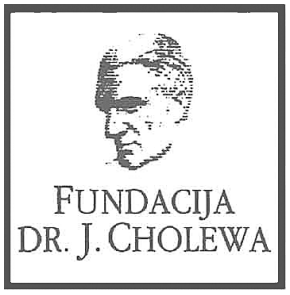

Fundacija ''Docent dr. J. Cholewa''
je neprofitno, neinstitucionalno in nestrankarsko
združenje posameznikov, ustanov in organizacij, ki želijo
materialno spodbujati in poglabljati raziskovalno
dejavnost v onkologiji.

Dunajska 106
1000 Ljubljana
IBAN: SI56 0203 3001 7879 431

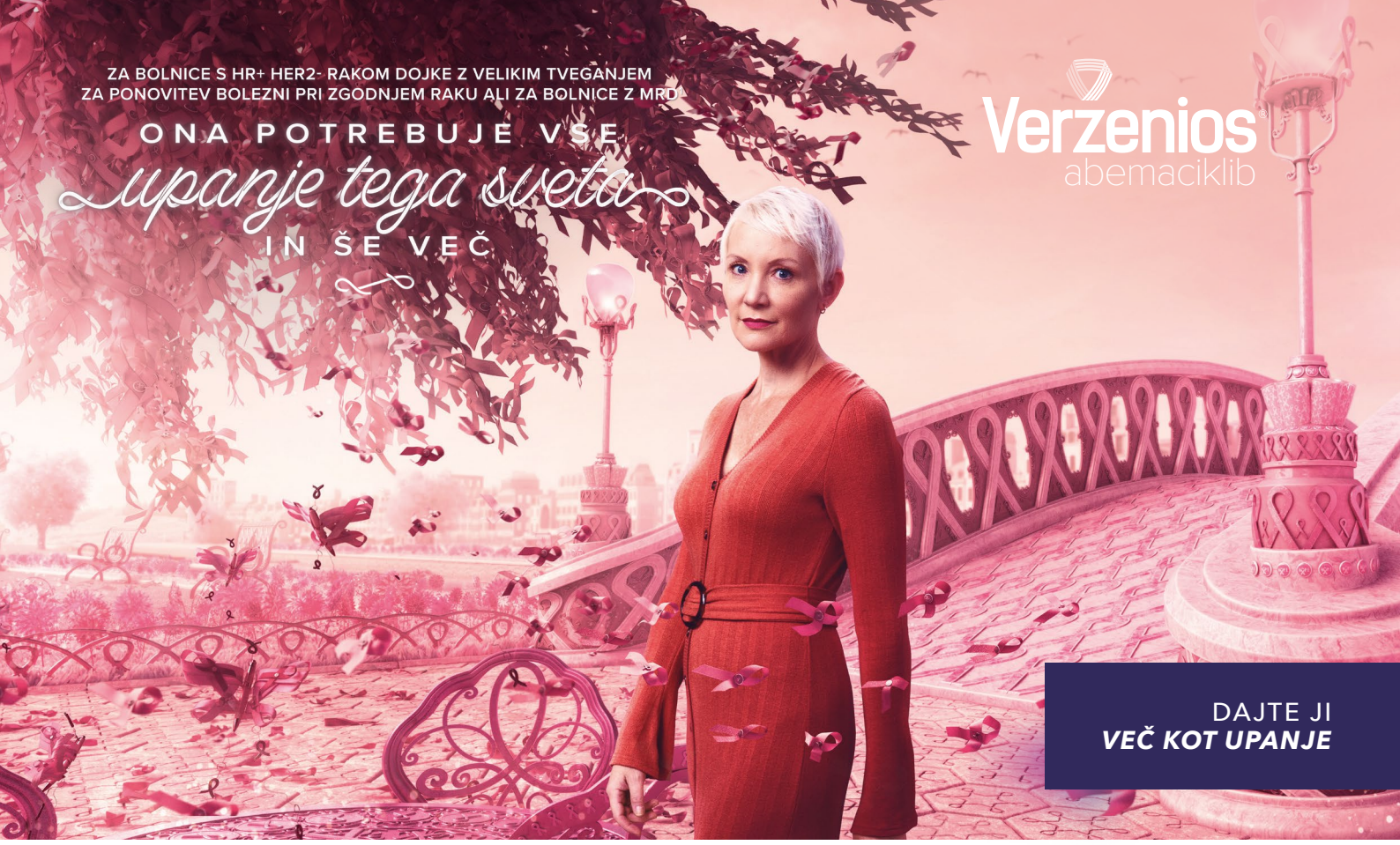

SKRAJŠAN POVZETEK GLAVNIH ZNAČILNOSTI ZDRAVILA

IME ZDRAVILA: Verzenios 50 mg/100 mg/150 mg filmsko obložene tablete **KAKOVOSTNA IN KOLIČINSKA SESTAVA:** Ena filmsko obložena tableta vsebuje 50 mg/100 mg/150 mg abemaciklib. Ena filmsko obložena tableta vsebuje 14 mg/28 mg/42 mg laktoze (v obliki monohidrata). **Terapevtske indikacije**: Zgodnji rak dojk: Zdravilo Verzenios je v kombinaciji z endokrinim zdravljenjem indicirano za adjuvantno zdravljenje odraslih bolnikov z na hormonske receptorje (HR) pozitivnim, na receptorje humanega epidermalnega rastnega faktorja 2 (HER2) negativnim zgodnjim rakom dojk s pozitivnimi bezgavkami, pri katerih obstaja veliko tveganje za ponovitev. Pri ženskah v pred- ali perimenopavzi je treba endokrino zdravljenje z zaviralcem aromataze kombinirati z agonistom gonadoliberina LHRH – luteinizing hormone-releasing hormone). Napredovali ali metastatski rak dojk: Zdravilo Verzenios je indicirano za zdravljenje žensk z lokalno napredovalim ali metastatskim, na hormonske receptorje (HR) pozitivnim in na receptorje humanega epidermalnega rastnega faktorja 2 (HER2) negativnim rakom dojk v kombinaciji z zaviralcem aromataze ali s fulvestrantom kot začetnim endokrinim zdravljenjem ali pri ženskah, ki so prejele predhodno endokrino zdravljenje. Pri ženskah v pred- ali perimenopavzi je treba endokrino zdravljenje kombinirati z agonistom LHRH. **Odmerjanje in način uporabe**: Zdravljenje z zdravilom Verzenios mora uvesti in nadzorovati zdravnik, ki ima izkušnje z uporabo zdravil za zdravljenje rakavih bolezni. Priporočeni odmerek abemaciklib je 150 mg dvakrat na dan, kadar se uporablja v kombinaciji z endokrinim zdravljenjem. *Zgodnji rak dojk:* Zdravilo Verzenios je treba jemati neprekinjeno dve leti, ali do ponovitve bolezni ali pojava nesprejemljive toksičnosti. *Napredovali ali metastatski rak dojk:* Zdravilo Verzenios je treba jemati, dokler ima bolnica od zdravljenja klinično korist ali do pojava nesprejemljive toksičnosti. Če bolnica bruha ali izpusti odmerek zdravila Verzenios, ji je treba naročiti, da naj naslednji odmerek vzame ob predvidenem času; dodatnega odmerka ne sme vzeti. Obvladovanje nekaterih neželenih učinkov lahko zahteva prekinitev in/ali zmanjšanje odmerka. Zdravljenje z abemaciklibom prekinite v primeru povišanja vrednosti AST in/ali ALT >3 x ZMN SKUPAJ s celokupnim bilirubinom > 2,0 x ZMN v odsotnosti holestaze ter pri bolnicah z intersticijsko pljučno boleznijo (ILD)/pnevmonitis stopnje 3 ali 4. Sočasni uporabi močnih zaviralcev CYP3A4 se je treba izogibati. Če se uporabi močnih zaviralcev CYP3A4 ni mogoče izogniti, je treba odmerek abemaciklib znižati na 100 mg dvakrat na dan. Pri bolnicah, pri katerih je bil odmerek znižan na 100 mg abemaciklib dvakrat na dan in pri katerih se sočasnemu dajanju močnega zaviralca CYP3A4 ni mogoče izogniti, je treba odmerek abemaciklib dodatno znižati na 50 mg dvakrat na dan. Pri bolnicah, pri katerih je bil odmerek znižan na 50 mg abemaciklib dvakrat na dan in pri katerih se sočasnemu dajanju močnega zaviralca CYP3A4 ni mogoče izogniti, je mogoče z odmerkom abemaciklib nadaljevati ob natančnem spremljanju znakov toksičnosti. Alternativno je mogoče odmerek abemaciklib znižati na 50 mg enkrat na dan ali prekiniti dajanje abemaciklib. Če je uporaba zaviralca CYP3A4 prekinjena, je treba odmerek abemaciklib povečati na odmerek, kakršen je bil pred uvedbo zaviralca CYP3A4 (po 3-5 razpolovnih časih zaviralca CYP3A4). Prilagajanje odmerka glede na starost in pri bolnicah z blago ali zmerno ledvično okvaro ter z blago (Child Pugh A) ali zmerno (Child Pugh B) jetrno okvaro ni potrebno. Pri dajanju abemaciklib bolnicam s hudo ledvično okvaro sta potrebna previdnost in skrbno spremljanje glede znakov toksičnosti. Način uporabe: Zdravilo Verzenios je namenjeno za peroralno uporabo. Odmerek se lahko vzame s hrano ali brez nje. Zdravila se ne sme jemati z grenivko ali grenivkinim sokom. Bolnice naj odmerke vzamejo vsak dan ob približno istem času. Tableto je treba pogoltniti celo (bolnice tablet pred zaužitjem ne smejo gristi, drobiti ali deliti). **Kontraindikacije**: Preobčutljivost na učinkovino ali katero koli pomožno snov. **Posebna opozorila in previdnostni ukrepi**: Pri bolnicah, ki so prejemale abemaciklib, so poročali o nevtropeniji, o večji pogostnosti okužb kot pri bolnicah, zdravljenih s placebom in endokrinim zdravljenjem, o povečanih vrednostih ALT in AST. Pri bolnicah, pri katerih se pojavi nevtropenija stopnje 3 ali 4, je priporočljivo prilagoditi odmerek. Do primerov nevtropenične sepse s smrtnim izidom je prišlo pri < 1 % bolnic z metastatskim rakom dojk. Bolnicam je treba naročiti, naj o vsaki epizodi povišane telesne temperature poročajo zdravstvenemu delavcu. Bolnice je treba spremljati za znake in simptome globoke venske tromboze (VTE) in pljučne embolije ter jih zdraviti, kot je medicinsko utemeljeno. Glede na stopnjo VTE bo morda treba spremeniti odmerek abemaciklib. Pri bolnikih, pri katerih se pojavi resni arterijski trombembolični dogodek (ATE), je treba oceniti koristi in tveganja nadaljnjega zdravljenja z abemaciklibom. Glede na povečanje vrednosti ALT ali AST je mogoče potrebna prilagoditev odmerka. Driska je najpogostejši neželeni učinek. Bolnice je treba ob prvem znaku tekočega blata začeti zdraviti z antidiaroiki, kot je loperamid, povečati vnos peroralnih tekočin in obvestiti zdravnika. Sočasni uporabi induktorjev CYP3A4 se je treba izogibati zaradi tveganja za zmanjšano učinkovitost abemaciklib. Bolnice z redkimi dednimi motnjami, kot so intoleranca za galaktozo, popolno pomanjkanje laktaze ali malapsorpcija glukoze/galaktoze, tega zdravila ne smejo jemati. Bolnice je treba spremljati glede pljučnih simptomov, ki kažejo na ILD/pnevmonitis, in jih ustrezno zdraviti. Glede na stopnjo ILD/pnevmonitisa je morda potrebno prilagajanje odmerka abemaciklib. **Medsebojno delovanje z drugimi zdravili in druge oblike interakcij**: Abemaciklib se primarno presnavlja s CYP3A4. Sočasna uporaba abemaciklib in zaviralcev CYP3A4 lahko poveča plazemsko koncentracijo abemaciklib. Uporabi močnih zaviralcev CYP3A4 sočasno z abemaciklibom se je treba izogibati. Če je močne zaviralce CYP3A4 treba dajati sočasno, je treba odmerek abemaciklib zmanjšati, nato pa bolnico skrbno spremljati glede toksičnosti. Pri bolnicah, zdravljenih z zmernimi ali šibkimi zaviralci CYP3A4, ni potrebno prilagajanje odmerka, vendar jih je treba skrbno spremljati za znake toksičnosti. Sočasni uporabi močnih induktorjev CYP3A4 (vključno, vendar ne omejeno na: karbamazepin, fenitoin, rifampicin in šentjanževko) se je treba izogibati zaradi tveganja za zmanjšano učinkovitost abemaciklib. Abemaciklib in njegovi glavni aktivni presnovki zavirajo prenašalce v ledvicah, in sicer kationski organski prenašalec 2 (OCT2) ter prenašalca MATE1. *In vivo* lahko pride do medsebojnega delovanja abemaciklib in klinično pomembnih substratov teh prenašalcev, kot je dofelitid ali kreatinin. Trenutno ni znano, ali lahko abemaciklib zmanjša učinkovitost sistemskih hormonskih kontraceptivov, zato se ženskam, ki uporabljajo sistemske hormonske kontraceptive, svetuje, da hkrati uporabljajo tudi mehansko metodo. **Neželeni učinki**: Najpogostejši neželeni učinki so driska, okužbe, nevtropenija, levkopenija, anemija, utrujenost, navzea, bruhanje in zmanjšanje apetita. *Zelo pogosti:* okužbe, nevtropenija, levkopenija, anemija, trombocitopenija, limfopenija, zmanjšanje apetita, glavobol, disgevzija, omotica, driska, bruhanje, navzea, stomatitis, alopecija, pruritus, izpuščaj, pireksija, utrujenost, povečana vrednost alanin-aminotransferaze, povečana vrednost aspartat-aminotransferaze *Pogosti:* povečano solzenje, venska trombembolija, ILD/pnevmonitis, dispepsija, spremembe na nohtih, suha koža, mišična šibkost *Občasni:* febrilna nevtropenija, fotopsija **Rok uporabnosti**: 3 leta **Posebna navodila za shranjevanje** Za shranjevanje zdravila niso potrebna posebna navodila. **Imetnik dovoljenja za promet z zdravilom**: Eli Lilly Nederland B.V., Papendorpseweg 83, 3528BJ, Utrecht, Nizozemska. Datum prve odobritve dovoljenja za promet: 27. september 2018. Datum zadnjega podaljšanja: 23. junij 2023. **Datum zadnje revizije besedila**: 17.06.2024 **Režim izdaje:** Rp/Spec - Predpisovanje in izdaja zdravila je le na recept zdravnika specialista ustreznega področja medicine ali od njega pooblaščenega zdravnika.

Reference: 1. Povzetek glavnih značilnosti zdravila Verzenios, zadnja odobrena verzija.

Pomembno: Predpisovanje in izdaja zdravila je le na recept zdravnika specialista ustreznega področja medicine ali od njega pooblaščenega zdravnika. Pred predpisovanjem zdravila Verzenios si preberite zadnji veljavni Povzetek glavnih značilnosti zdravil. Podrobne informacije o zdravilu so objavljene na spletni strani Evropske agencije za zdravila http://www.ema.europa.eu

Eli Lilly farmacevtska družba, d.o.o., Dunajska cesta 167, 1000 Ljubljana, telefon 01 / 580 00 10, faks 01 / 569 17 05

PP-AL-SI-0302, 20.8.2024, Samo za strokovno javnost.

PR/BSI/BEN/2024/008

TANTUM VERDE®

benzidaminijev klorid

Za lajšanje bolečine in oteklin v ustni in žrelu, ki so posledica radiomukozitisa

Bistvene informacije iz Povzetka glavnih značilnosti zdravila

Tantum Verde 1,5 mg/ml oralno pršilo, raztopina
Tantum Verde 3 mg/ml oralno pršilo, raztopina

Sestava: 1,5 mg/ml: 1 ml raztopine vsebuje 1,5 mg benzidaminijevega klorida, kar ustreza 1,34 mg benzidamina. V enem razpršku je 0,17 ml raztopine. En razpršek vsebuje 0,255 mg benzidaminijevega klorida, kar ustreza 0,2278 mg benzidamina. **Sestava 3 mg/ml:** 1 ml raztopine vsebuje 3 mg benzidaminijevega klorida, kar ustreza 2,68 mg benzidamina. V enem razpršku je 0,17 ml raztopine. En razpršek vsebuje 0,51 mg benzidaminijevega klorida, kar ustreza 0,4556 mg benzidamina. **Terapevtske indikacije:** Samozdravljenje: Lajšanje bolečine in oteklin pri vnetju v ustni votlini in žrelu, ki so lahko posledica okužb in stanj po operaciji. Po nasvetu in navodilu zdravnika: Lajšanje bolečine in oteklin v ustni votlini in žrelu, ki so posledica radiomukozitisa. **Odmerjanje in način uporabe:** Uporaba: 2- do 6-krat na dan (vsake 1,5 do 3 ure). Odmerjanje 1,5 mg/ml: Odrasli: 4 do 8 razprškov 2- do 6-krat na dan. Pediatrična populacija: Mladostniki, stari od 12 do 18 let: 4-8 razprškov 2- do 6-krat na dan. Otroci od 6 do 12 let: 4 razprški 2- do 6-krat na dan. Otroci, mlajši od 6 let: 1 razpršek na 4 kg telesne mase; do največ 4 razprške 2- do 6-krat na dan. Odmerjanje 3 mg/ml: Odrasli: 2 do 4 razprški 2- do 6-krat na dan. Pediatrična populacija: Mladostniki, stari od 12 do 18 let: 2 do 4 razprški 2- do 6-krat na dan. Otroci od 6 do 12 let: 2 razprška 2- do 6-krat na dan. Otroci, mlajši od 6 let: 1 razpršek na 8 kg telesne mase; do največ 2 razprška 2- do 6-krat na dan. Starejši bolniki, bolniki z jetrno okvaro in bolniki z ledvično okvaro: niso potrebni posebni previdnostni ukrepi. Trajanje zdravljenja ne sme biti daljše od 7 dni. Način uporabe: Za orofaringealno uporabo. Zdravilo se razprši v usta in žrelo. **Kontraindikacije:** Preobčutljivost na učinkovino ali katero koli pomožno snov. **Posebna opozorila in previdnostni ukrepi:** Pri nekaterih bolnikih lahko resne bolezni povzročijo ustne/žrelne ulceracije. Če se simptomi v treh dneh ne izboljšajo, se mora bolnik posvetovati z zdravnikom ali zobozdravnikom, kot je primerno. Uporaba benzidamina ni priporočljiva za bolnike s preobčutljivostjo na salicilno kislino ali druga nesteroidna protivnetna zdravila. Pri bolnikih, ki imajo ali so imeli bronhialno astmo, lahko pride do bronhospazma. Pri takih bolnikih je potrebna previdnost. To zdravilo vsebuje 13,6 mg alkohola (etanola) v enem razpršku (0,17 ml), kar ustreza manj kot 0,34 ml piva oziroma 0,14 ml vina. Majhna količina alkohola v zdravilu ne bo imela nobenih opaznih učinkov. To zdravilo vsebuje metilparahidroksibenzoat (E218). Lahko povzroči alergijske reakcije (lahko zapoznele). To zdravilo vsebuje manj kot 1 mmol (23 mg) natrija v enem razpršku (0,17 ml), kar v bistvu pomeni 'brez natrija'. Zdravilo vsebuje aromo poprove mete z benzilalkoholom, cinamilalkoholom, citralom, citronelolom, geraniolom, izoevgenolom, linalolom, evgenolom in D-limonen, ki lahko povzročijo alergijske reakcije. Zdravilo z jakostjo 3 mg/ml vsebuje makrogolglicerol hidroksistearat 40. Lahko povzroči želodčne težave in drisko. **Medsebojno delovanje z drugimi zdravili in druge oblike interakcij:** Študij medsebojnega delovanja niso izvedli. **Nosečnost in dojenje:** O uporabi benzidamina pri nosečnicah in doječih ženskah ni zadostnih podatkov. Uporaba zdravila med nosečnostjo in dojenjem ni priporočljiva. **Vpliv na sposobnost vožnje in upravljanja strojev:** Zdravilo v priporočenem odmerku nima vpliva na sposobnost vožnje in upravljanja strojev. **Neželeni učinki:** Neznana pogostnost (ni mogoče oceniti iz razpoložljivih podatkov): anafilaktične reakcije, preobčutljivostne reakcije, odrevenelost, laringospazem, suha usta, navzea in bruhanje, oralna hipestezija, angioedem, fotosenzitivnost, pekoč občutek v ustih. Neposredno po uporabi se lahko pojavi občutek odrevenelosti v ustih in v žrelu. Ta učinek se pojavi zaradi načina delovanja zdravila in po kratkem času izgine. **Način in režim izdaje zdravila:** BRp-Izdaja zdravila je brez recepta v lekarnah in specializiranih prodajalnah. **Imetnik dovoljenja za promet:** Aziende Chimiche Riunite Angelini Francesco – A.C.R.A.F. S.p.A., Viale Amelia 70, 00181 Rim, Italija **Datum zadnje revizije besedila:** 05. 04. 2022

Pred svetovanjem ali izdajo preberite celoten Povzetek glavnih značilnosti zdravila.

Samo za strokovno javnost.

Datum priprave informacije: julij 2024

Odgovoren za trženje: Bonifar d.o.o.

ANGELINI

IMFINZI™
durvalumab
50 mg/ml koncentrat za raztopino za infundiranje

AKTIVIRA IMUNSKI SISTEM.
PREPOZNA. **REAGIRA.**

5-LETNO CELOKUPNO PREŽIVETJE BOLNIKOV Z LOKALNO NAPREDOVALIM, NEOPERABILNIM NSCLC S PDL-1 ≥ 1%[1]

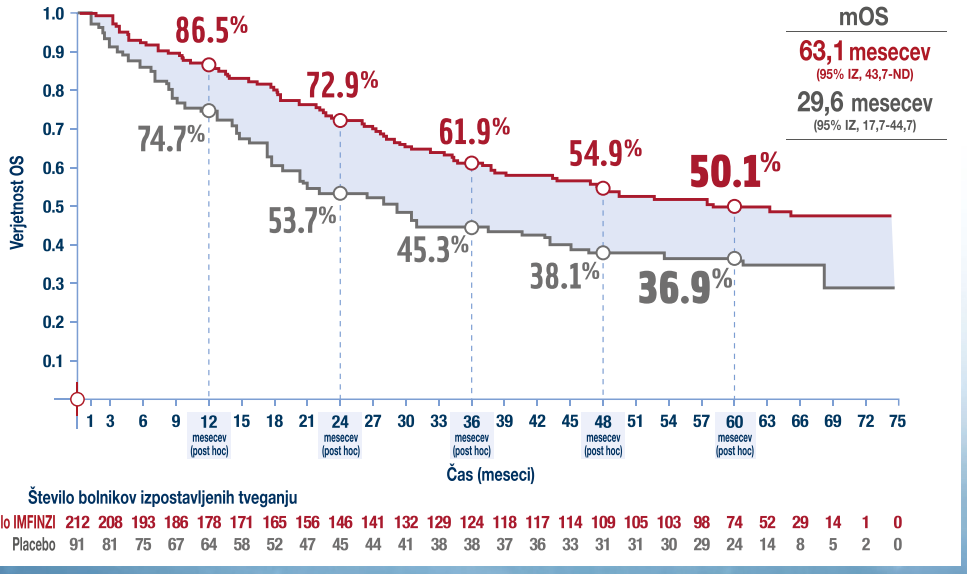

Po petih letih je bilo živih še 50% bolnikov zdravljenih z zdravilom Imfinzi po zaključeni sočasni kemoradioterapiji na osnovi platine.

NSCLC... nedrobnocelični rak pljuč (non small cell lung cancer), mOS...mediano celokupno preživetje

SKRAJŠAN POVZETEK GLAVNIH ZNAČILNOSTI ZDRAVILA

Imfinzi 50 mg/ml koncentrat za raztopino za infundiranje

SESTAVA: 1 ml koncentrata za raztopino za infundiranje vsebuje 50 mg durvalumaba. Ena viala z 2,4 ml koncentrata vsebuje 120 mg durvalumaba. Ena viala z 10 ml koncentrata vsebuje 500 mg durvalumaba. **INDIKACIJE:** *Neoperabilni nedrobnocelični rak pljuč (NSCLC).* Zdravilo IMFINZI je kot samostojno zdravljenje indicirano za zdravljenje lokalno napredovalega, neoperabilnega nedrobnoceličnega raka pljuč (NSCLC – non small cell lung cancer) pri odraslih, ki imajo tumorje z ≥ 1 % izraženostjo PD L1 na tumorskih celicah in pri katerih bolezen ni napredovala po kemoradioterapiji na osnovi platine. Zdravilo IMFINZI je v kombinaciji s tremelimumabom in kemoterapijo na osnovi platine indicirano za prvo linijo zdravljenja odraslih z metastatskim NSCLC brez senzibilizirajočih mutacij EGFR ali pozitivnih mutacij ALK. *Drobnocelični rak pljuč (SCLC).* Zdravilo IMFINZI je v kombinaciji z etopozidom in bodisi karboplatinom bodisi cisplatinom indicirano za prvo linijo zdravljenja odraslih z razsejanim drobnoceličnim rakom pljuč (ES SCLC – extensive stage small cell lung cancer). *Rak biliarnega trakta (RBT).* Zdravilo IMFINZI je v kombinaciji z gemcitabinom in cisplatinom indicirano za prvo linijo zdravljenja odraslih z neoperabilnim ali metastatskim rakom biliarnega trakta (RBT). *Hepatocelularni karcinom (HCK).* Zdravilo IMFINZI je kot samostojno zdravljenje indicirano za prvo linijo zdravljenja odraslih z napredovalim ali neoperabilnim hepatocelularnim karcinomom (HCK). Zdravilo IMFINZI je v kombinaciji s tremelimumabom indicirano za prvo linijo zdravljenja odraslih z napredovalim ali neoperabilnim karcinomom jetrnih celic (hepatocelularnim karcinomom – HCK). **ODMERJANJE IN NAČIN UPORABE:** Zdravljenje mora uvesti in nadzorovati zdravnik, ki ima izkušnje na področju zdravljenja raka. Bolnike z lokalno napredovalim nedrobnoceličnim rakom pljuč je treba za zdravljenje izbrati na podlagi izraženosti PD-L1, ugotovljene z validirano testno metodo. Odmerjanje: Priporočeni odmerek zdravila Imfinzi pri samostojnem zdravljenju pri lokalno napredovalem NSCLC je 10 mg/kg na 2 tedna ali 1500 mg na 4 tedne do napredovanja bolezni, nesprejemljivih toksičnih učinkov ali največ 12 mesecev. Pri HCK je priporočeni odmerek zdravila Imfinzi 1500 mg na 4 tedne do napredovanja bolezni ali do nesprejemljivih toksičnih učinkov. Priporočeni odmerek zdravila Imfinzi pri kombinaranem zdravljenju pri metastatskem NSCLC je med kemoterapijo s platino: 1500 mg v kombinaciji s 75 mg tremelimumaba in kemoterapijo na osnovi platine na 3 tedne (21 dni) 4 cikle (12 tednov), po kemoterapiji s platino: 1500 mg na 4 tedne kot monoterapija in vzdrževalno zdravljenje s pemetreksedom (na podlagi histologije) na 4 tedne, peti odmerek 75 mg tremelimumaba je treba dati 16. teden skupaj z zdravilom Imfinzi. Trajanje zdravljenja je do napredovanja bolezni ali nesprejemljivih toksičnih učinkov. Pri ES-SCLC je priporočeni odmerek zdravila Imfinzi 1500 mg v kombinaciji s kemoterapijo na 3 tedne (21 dni) 4 cikluse in nato 1500 mg na 4 tedne kot samostojno zdravljenje do napredovanja bolezni ali nesprejemljivih toksičnih učinkov. Pri RBT je priporočeni odmerek zdravila Imfinzi 1500 mg v kombinaciji s kemoterapijo na 3 tedne (21 dni) do 8 ciklusov, nato po 1500 mg na 4 tedne kot samostojno zdravljenje do napredovanja bolezni ali nesprejemljivih toksičnih učinkov. Pri HCK je priporočeni odmerek 1500 mg zdravila IMFINZI v kombinaciji s 300 mg tremelimumaba v enem odmerku 1. dan 1. cikla, nato zdravilo Imfinzi kot monoterapija na 4 tedne do napredovanja bolezni ali nesprejemljivih toksičnih učinkov. Povečevanje ali zmanjševanje odmerka ni priporočljivo. Glede na individualno varnost in prenašanje je lahko potrebna odložitev zdravljenja ali trajno prenehanje uporabe zdravila. V primeru domnevnih imunsko pogojenih neželenih učinkov je treba opraviti ustrezno ovrednotenje za potrditev etiologije ozioroma izključitev druge etiologije. Glede na resnost neželenega učinka je treba prenehati uporabljati zdravilo Imfinzi in/ali tremelimumab in pričeti z dajanjem kortikosteroidov. Če se stanje ne izboljša ali se poslabša, pride v poštev povečanje odmerka kortikosteroidov in/ali dodatna uporaba sistemskih imunosupresivov. Po izboljšanju na ≤ 1. stopnjo je treba začeti s postopnim zmanjševanjem kortikosteroida in ga zmanjševati v obdobju vsaj 1 meseca. Po odložitvi uporabe je mogoče zdravilo Imfinzi in/ali tremelimumab znova začeti uporabljati v času 12 tednov, če se neželeni učinki izboljšajo na ≤ 1. stopnjo in je odmerek kortikosteroida zmanjšan na ≤ 10 mg prednizona ali ekvivalenta na dan. Zdravilo Imfinzi in tremelimumab je treba dokončno ukiniti, če se imunsko pogojeni neželeni učinki 3. stopnje (močno izraženi) ponavljajo in pri katerih koli imunsko pogojenih neželenih učinkih 4. stopnje (življenjsko nevarni), razen pri endokrinopatijah, ki jih nadziramo z nadomestnimi hormoni. Način uporabe: Zdravilo Imfinzi je namenjeno za intravensko uporabo. Dati ga je treba kot raztopino za intravensko infundiranje v obdobju 1 ure. Če je zdravilo Imfinzi uporabljeno v kombinaciji s kemoterapijo, je treba dati zdravilo Imfinzi pred kemoterapijo na isti dan. Če je zdravilo Imfinzi uporabljeno v kombinaciji s tremelimumabom in kemoterapijo na osnovi platine, je treba najprej dati tremelimumab, ki mu v istem dnevu sledita zdravilo Imfinzi in nato kemoterapija na osnovi platine. Če je zdravilo Imfinzi uporabljeno v kombinaciji s petim odmerkom tremelimumaba in vzdrževalnim zdravljenjem s pemetreksedom 16. teden, je treba najprej dati tremelimumab, ki mu v istem dnevu sledita zdravilo Imfinzi in potem vzdrževalno zdravljenje s pemetreksedom. Zdravilo Imfinzi, tremelimumab in kemoterapijo na osnovi platine je treba dati v ločenih intravenskih infuzijah. Dajanje zdravila Imfinzi in tremelimumaba vsako traja po 1 uro. Če je zdravilo Imfinzi uporabljeno v kombinaciji s tremelimumabom, je treba dati tremelimumab pred zdravilom Imfinzi na isti dan. Zdravilo Imfinzi in tremelimumab je treba dati v ločenih intravenskih infuzijah. **KONTRAINDIKACIJE:** Preobčutljivost na učinkovino (učinkovine) ali katero koli pomožno snov. **OPOZORILA IN PREVIDNOSTNI UKREPI:** Za izboljšanje sledljivosti bioloških zdravil je treba jasno zabeležiti lastniško ime in številko serije uporabljenega zdravila. Imunsko pogojeni pnevmonitis: Pri bolnikih, ki so prejemali zdravilo Imfinzi ali zdravilo Imfinzi v kombinaciji s tremelimumabom, sta se pojavila imunsko pogojeni pnevmonitis ali intersticijska bolezen pljuč, opredeljeno kot potreba po uporabi sistemskih kortikosteroidov in brez jasne druge etiologije. Pnevmonitis in radiacijski pnevmonitis: Pri bolnikih, zdravljenih z radioterapijo pljuč, je pogost radiacijski pnevmonitis in klinična slika pnevmonitisa in radiacijskega pnevmonitisa je zelo podobna. V študiji PACIFIC sta se pri bolnikih, ki so opravili zdravljenje z najmanj 2 cikloma sočasne kemoradioterapije od 1 do 42 dni pred začetkom preskušanja, pnevmonitis ali radiacijski pnevmonitis pojavila pri 161 (33,9 %) bolnikih v skupini z zdravilom Imfinzi in pri 58 (24,8 %) bolnikih v skupini s placebom, vključno s 3. stopnjo (3,4 % in 3,0 %) in 5. stopnjo (1,1 % in 1,7 %). Bolnike je treba spremljati glede znakov in simptomov pnevmonitisa ali radiacijskega pnevmonitisa. Imunsko pogojeni hepatitis: Pri bolnikih, ki so prejemali zdravilo Imfinzi ali zdravilo Imfinzi v kombinaciji s tremelimumabom, se je pojavil imunsko pogojeni hepatitis, opredeljen kot potreba po sistemskih kortikosteroidih in brez jasne druge etiologije. Alanin-aminotransferazo, aspartat-aminotransferazo, celokupni bilirubin in alkalno fosfatazo kontrolirajte pred začetkom zdravljenja in pred vsako nadaljnjo infuzijo. Dodaten nadzor pride v poštev na podlagi klinične ocene. Imunsko pogojeni kolitis: Pri bolnikih, ki so prejemali zdravilo Imfinzi ali zdravilo Imfinzi v kombinaciji s tremelimumabom, sta se pojavila imunsko pogojeni kolitis ali driska, opredeljeno kot potreba po sistemskih kortikosteroidih in brez jasne druge etiologije. Pri bolnikih, ki so prejemali zdravilo Imfinzi v kombinaciji s tremelimumabom, so poročali o neželenih učinkih perforacije črevesa in perforacije debelega črevesa. Imunsko pogojene endokrinopatije: Imunsko pogojeni hipotiroidizem, hipertiroidizem in tiroiditis: Pri bolnikih, ki so prejemali zdravilo Imfinzi ali zdravilo Imfinzi v kombinaciji s tremelimumabom, so se pojavili imunsko pogojeni hipotiroidizem, hipertiroidizem in tiroiditis; hipertiroidizmu lahko sledi hipotiroidizem. Bolnike je treba spremljati glede nenormalnih izvidov delovanje ščitnice pred zdravljenjem in redno med zdravljenjem ter kot je potrebno glede na klinično oceno. Imunsko pogojena adrenalna insuficienca: Pri bolnikih, ki so prejemali zdravilo Imfinzi ali zdravilo Imfinzi v kombinaciji s tremelimumabom, se je pojavila imunsko pogojena adrenalna insuficienca. Bolnike je treba spremljati glede kliničnih znakov in simptomov adrenalne insuficience. Imunsko pogojena sladkorna bolezen tipa 1: Pri bolnikih, ki so prejemali zdravilo Imfinzi ali zdravilo Imfinzi v kombinaciji s tremelimumabom, se je pojavila imunsko pogojena sladkorna bolezen tipa 1, ki se lahko najprej kaže kot diabetična ketoacidoza, ki je lahko smrtno nevarna, če je dovolj zgodaj ne odkrijemo. Bolnike je treba spremljati glede kliničnih znakov in simptomov sladkorne bolezni tipa 1. Imunsko pogojeni hipofizitis/hipopituitarizem: Pri bolnikih, ki so prejemali zdravilo Imfinzi ali zdravilo Imfinzi v kombinaciji s tremelimumabom, sta se pojavila imunsko pogojena hipofizitis ali hipopituitarizem. Bolnike je treba spremljati glede kliničnih znakov in simptomov hipofizitisa ali hipopituitarizma. Imunsko pogojeni nefritis: Pri bolnikih, ki so prejemali zdravilo Imfinzi ali zdravilo Imfinzi v kombinaciji s tremelimumabom, se je pojavil imunsko pogojeni nefritis, opredeljen kot potreba po sistemskih kortikosteroidih in brez jasne druge etiologije. Imunsko pogojeni izpuščaj: Pri bolnikih, ki so prejemali zdravilo Imfinzi ali zdravilo Imfinzi v kombinaciji s tremelimumabom, se je pojavil imunsko pogojeni izpuščaj ali dermatitis (vključno s pemfigoidom), opredeljen kot potreba po sistemskih kortikosteroidih in brez jasne druge etiologije. Pri bolnikih, ki so bili zdravljeni z zaviralci PD-1, so poročali o pojavljanju Stevens-Johnsonovega sindroma ali toksične epidermalne nekrolize. Imunsko pogojeni miokarditis: Pri bolnikih, ki so prejemali zdravilo Imfinzi ali zdravilo Imfinzi v kombinaciji s tremelimumabom, se je pojavil imunsko pogojeni miokarditis, ki je lahko usoden. Imunsko pogojeni pankreatitis: Pri bolnikih, ki so prejemali zdravilo Imfinzi v kombinaciji s tremelimumabom in kemoterapijo, se je pojavil imunsko pogojeni pankreatitis. Drugi imunsko pogojeni neželeni učinki: Glede na mehanizem delovanja zdravila Imfinzi ali zdravila Imfinzi v kombinaciji s tremelimumabom se lahko pojavijo še drugi potencialno imunsko pogojeni učinki. Naslednji imunsko pogojeni neželeni učinki so bili opaženi pri bolnikih, ki so prejemali samostojno zdravljenje z zdravilom Imfinzi ali zdravilo Imfinzi v kombinaciji s tremelimumabom: miastenija gravis, transverzni mielitis, miozitis, polimiozitis, meningitis, encefalitis, Guillain Barréjev sindrom, imunska trombocitopenija, neinfektivni cistitis. Z infundiranjem povezane reakcije: Bolnike je treba spremljati glede znakov in simptomov z infundiranjem povezanih reakcij. Pri bolnikih, ki so prejemali zdravilo Imfinzi ali zdravilo Imfinzi v kombinaciji s tremelimumabom, so bile opisane hude z infundiranjem povezane reakcije. Za bolezen specifični previdnostni ukrepi (RBT): Holangitis in okužbe biliarnega trakta pri bolnikih z napredovalim RBT niso redke. V študiji TOPAZ-1 so o primerih holangitisa poročali v obeh terapevtskih skupinah (14,5 % v skupini z zdravilom Imfinzi + kemoterapijo, 8,2 % v skupini s placebom + kemoterapijo); ti primeri so bili večinoma povezani z biliarnimi opornicami in niso imeli imunsko posredovane etiologije. Bolnike z RBT (zlasti tiste z biliarno opornico) je treba natančno nadzorovati glede holangitisa ali okužb biliarnega trakta tako pred uvedbo zdravljenja kot redno med zdravljenjem. Metastatski NSCLC: Podatkov o starejših bolnikih (≥ 75 let), zdravljenih z zdravilom Imfinzi v kombinaciji s tremelimumabom in kemoterapijo na osnovi platine, je malo. Morebitno korist/tveganje te sheme je priporočljivo skrbno pretehtati za vsakega bolnika posebej. Bolniki, ki niso bili vključeni v klinične študije: V klinične študije niso bili vključeni bolniki z naslednjimi značilnostmi: izhodiščno oceno zmogljivosti ECOG ≥ 2; aktivno ali predhodno dokumentirano avtoimunsko boleznijo v 2 letih pred začetkom študije; anamnezo imunske pomanjkljivosti; anamnezo hudih imunsko pogojenih neželenih učinkov; boleznimi, ki so zahtevale sistemsko imunosupresijo, razen fiziološkega odmerka sistemskih kortikosteroidov (≤ 10 mg na dan prednizona ali ekvivalenta); neobvladanimi sočasnimi boleznimi; aktivno tuberkulozo ali okužbo s hepatitisom B ali C ali HIV; bolniki, ki so prejeli živo oslabljeno cepivo v 30 dneh pred začetkom zdravljenja z zdravilom Imfinzi ali v 30 dneh po začetku. Dokler takšnih podatkov ni, je treba durvalumab v teh skupinah bolnikov uporabljati previdno ter po skrbnem individualnem pretehtanju možnih koristi in tveganj za posameznega bolnika. Varnost sočasnega profilaktičnega kranialnega obsevanja obenem z zdravilom Imfinzi pri bolnikih z ES SCLC ni znana. **MEDSEBOJNO DELOVANJE Z DRUGIMI ZDRAVILI:** Razen fizioloških odmerkov sistemskih kortikosteroidov (≤ 10 mg na dan prednizona ali ekvivalenta) pred uvedbo durvalumaba ni priporočljivo uporabljati sistemskih kortikosteroidov ali imunosupresivov, ker lahko vplivajo na farmakodinamično aktivnost in učinkovitost durvalumaba. Vendar pa je mogoče kortikosteroide ali druge imunosupresive uporabiti po začetku zdravljenja z durvalumabom za zdravljenje imunsko pogojenih neželenih učinkov. Z durvalumabom niso izvedli formalnih farmakokinetičnih (PK) študij medsebojnega delovanja zdravil. Primarni poti odstranjevanja durvalumaba sta katabolizem beljakovin preko retikuloendotelijskega sistema oziroma tarčno posredovano odstranjevanje, zato ni pričakovati presnovnih medsebojnih delovanj med zdravili. Farmakokinetična medsebojna delovanja med durvalumabom in kemoterapijo so ocenjevali v študiji CASPIAN; izkazalo se je, da sočasno zdravljenje z durvalumabom ne vpliva na farmakokinetiko etopozida, karboplatina ali cisplatina. Poleg tega populacijska farmakokinetična analiza kaže, da sočasno zdravljenje s kemoterapijo ne vpliva pomembno na farmakokinetiko durvalumaba. Farmakokinetična medsebojna delovanja med durvalumabom v kombinaciji s tremelimumabom in kemoterapijo na osnovi platine so ocenili v študiji POSEIDON. Izkazalo se je, da med sočasnim zdravljenjem ni bilo klinično pomembnih farmakokinetičnih medsebojnih delovanj med tremelimumabom, durvalumabom, nab-paklitakselom, gemcitabinom, pemetreksedom, karboplatinom ali cisplatinom. **PLODNOST, NOSEČNOST IN DOJENJE:** Ženske v rodni dobi morajo med zdravljenjem z durvalumabom in vsaj še 3 mesece po zadnjem odmerku durvalumaba uporabljati učinkovito kontracepcijo. Podatkov o uporabi durvalumaba pri nosečnicah ni. Glede na mehanizem delovanja durvalumab lahko vpliva na vzdrževanje nosečnosti; v alogenskem modelu nosečnosti pri miših je bilo ugotovljeno, da moteno signaliziranje PD-L1 poveča izgubo plodov. Pri nosečnici uporabljeni durvalumab lahko škoduje plodu in ga ni priporočljivo uporabljati med nosečnostjo in pri ženskah v rodni dobi, ki ne uporabljajo učinkovite kontracepcije med zdravljenjem in vsaj še 3 mesece po zadnjem odmerku. Ni znano, ali se durvalumab pri človeku izloča v materinem mleku. Pri človeku protitelesa lahko prehajajo v materino mleko, a možnost absorpcije in škode za novorojenčka ni znana. Toda možnega tveganja za dojenega otroka ni mogoče izključiti. Odločiti se je treba, ali naj ženska prekine z dojenjem ali naj prekine zdravljenje z durvalumabom oziroma sploh ne začne zdravljenja z njim, pri čemer je treba upoštevati koristi dojenja za otroka in koristi zdravljenja za žensko. Podatkov o možnih vplivih durvalumaba na plodnost pri človeku ali živalih ni. **NEŽELENI UČINKI:** Ugotovitve o varnosti zdravila Imfinzi pri samostojnem zdravljenju temeljijo na kumulativnih podatkih 4045 bolnikov z več vrstami tumorjev. Zdravilo Imfinzi so uporabljali v odmerku 10 mg/kg na 2 tedna, 20 mg/kg na 4 tedne ali 1500 mg/kg na 4 tedne. Najpogostejši neželeni učinki (> 10 %) so bili kašelj/produktiven kašelj (18,7 %), driska (16,1 %), izpuščaj (15,5 %), artralgija (13,8 %), zvišana telesna temperatura (13,0 %), bolečine v trebuhu (13,0 %), okužbe zgornjih dihal (12,1 %), srbenje (11,4 %) in hipotiroidizem (10,9 %). Podatki o varnosti zdravila Imfinzi v kombinaciji s kemoterapijo temeljijo na kumulativnih podatkih 603 bolnikov iz 2 študij (TOPAZ-1 in CASPIAN). Najpogostejši (> 10 %) neželeni učinki so bili nevtropenija (53,1 %), anemija (43,9 %), navzea (37,5 %), utrujenost (36,8 %), trombocitopenija (28,0 %), zaprtje (25,4 %), zmanjšan apetit (22,6 %), bolečine v trebuhu (18,4 %), alopecija (18,4 %), levkopenija (17,2 %), bruhanje (16,9 %), zvišana telesna temperatura (15,1 %), izpuščaj (14,8 %), driska (13,8 %), zvišana aspartat-aminotransferaza ali zvišana alanin-aminotransferaza (10,9 %), kašelj/produktiven kašelj (10,8 %) in srbenje (10,4 %). Izsledki o varnosti zdravila Imfinzi v kombinaciji s 75 mg tremelimumaba in kemoterapijo temeljijo na podatkih 330 bolnikov z metastatskim NSCLC. Najpogostejši (> 20 %) neželeni učinki so bili anemija (49,7 %), navzea (41,5 %), nevtropenija (41,2 %), utrujenost (36,1 %), izpuščaj (25,8 %), trombocitopenija (24,5 %) in driska (21,5 %). Izsledki o varnosti zdravila Imfinzi v kombinaciji z enkratnim odmerkom 300 mg tremelimumaba temeljijo na združenih podatkih 462 bolnikov v HCK iz študije HIMALAYA in še ene študije pri bolnikih s HCK, študija 22. Najpogostejši neželeni učinki (> 10 %) so bili izpuščaj (32,5 %), srbenje (25,5 %), driska (25,3 %), bolečine v trebuhu (19,7 %), zvišana aspartat aminotransferaza/zvišana alanin aminotransferaza (18,0 %), zvišana telesna temperatura (13,9 %), hipotiroidizem (13,0 %), kašelj/produktiven kašelj (10,8 %), periferni edemi (10,4 %) in zvišana lipaza (10,0 %). **VRSTA IN VSEBINA OVOJNINE:** 2,4 ml (skupno 120 mg durvalumaba) koncentrata v stekleni viali iz stekla tipa 1 z elastomernim zamaškom in sivo snemno aluminijsko zaporo. Pakiranje vsebuje 1 vialo. 10 ml (skupno 500 mg durvalumaba) koncentrata v stekleni viali iz stekla tipa 1 z elastomernim zamaškom in belo snemno aluminijsko zaporo. Pakiranje vsebuje 1 vialo. **NAČIN IZDAJANJA ZDRAVILA:** H - Predpisovanje in izdaja zdravila je le na recept. **DATUM REVIZIJA BESEDILA:** 14.12.2023 (ŠI-3708). **IMETNIK DOVOLJENJA ZA PROMET:** AstraZeneca AB, S-151 85, Sodertalje, Švedska

Pred predpisovanjem, prosimo, preberite celoten povzetek glavnih značilnosti zdravila.
Dodatne informacije so na voljo pri družbi AstraZeneca UK Limited, Podružnica v Sloveniji, Verovškova 55, Ljubljana, telefon +386 1 51 35 600.

Samo za strokovno javnost. Informacija pripravljena januarja 2024.

Reference: 1.Spigel DR, Faivre-Finn C, Gray JE, et al. Five-year survival outcomes from the PACIFIC trial: durvalumab after chemoradiotherapy in stage III non-small-cell lung cancer. J Clin Oncol. Forthcoming 2021.

AstraZeneca

SI-3715

DOVOLI SI VERJETI

Lynparza®
olaparib
tablete 100 mg
tablete 150 mg

***Prvi in edini zaviralec PARP odobren za 4 različne lokalizacije tumorjev*[1-5]**

RAK JAJČNIKOV

Prvi zaviralec PARP odobren za vzdrževalno zdravljenje napredovalega raka jajčnikov v monoterapiji (v 1L pri bolnicah z mutacijo *gena BRCA1/2* in 2L) ali kombinaciji z bevacizumabom (pri bolnicah s HRD).[1-3, 5]

RAK DOJK

Prvi zaviralec PARP odobren za zdravljenje, pri bolnikih z zarodno mutacijo gena *BRCA1/2*, ki imajo HER2-negativni zgodnji, lokalno napredovali ali razsejan rak dojk.[1-2, 4]

RAK TREBUŠNE SLINAVKE

Edini zaviralec PARP odobren za vzdrževalno zdravljenje bolnikov z zarodno mutacijo gena *BRCA1/2*, ki imajo razsejani adenokarcinom trebušne slinavke in jim bolezen ni napredovala po najmanj 16 tednih prvega reda zdravljenja s kemoterapijo na osnovi platine.[1-4]

RAK PROSTATE

Edini zaviralec PARP odobren za zdravljenje bolnikov z razsejanim KORP v monoterapiji za bolnike z mutacijami gena *BRCA1/2*, ki jim je bolezen napredovala po zdravljenju z novim hormonskim zdravilom, in v kombinaciji z abirateronom ne glede na status mutacij.[1-4]

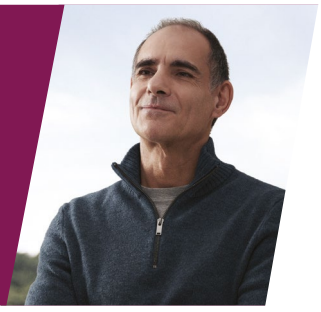

PARP – poli (ADP-riboza) polimeraza, **1L** – v prvem redu zdravljenja, **2L** – v drugem redu zdravljenja, **HRD** – pomanjkanje homologne rekombinacije, **KORP** – na kastracijo odporen rak prostate

SKRAJŠAN POVZETEK GLAVNIH ZNAČILNOSTI ZDRAVILA

LYNPARZA 100 mg filmsko obložene tablete
LYNPARZA 150 mg filmsko obložene tablete

SESTAVA: Ena filmsko obložena tableta vsebuje 100 mg olapariba ali 150 mg olapariba.
INDIKACIJE:
Rak jajčnikov: 1) *zdravilo Lynparza je indicirano kot monoterapija za*:
- vzdrževalno zdravljenje odraslih bolnic z napredovalim (stadij III in IV po FIGO) epitelijskim rakom visokega gradusa jajčnikov, jajcevodov ali primarnim peritonealnim rakom z mutacijo gena BRCA1/2 (germinalno in/ali somatsko), ki so v odzivu (popolnem ali delnem) po zaključeni prvi liniji kemoterapije na osnovi platine.
- vzdrževalno zdravljenje odraslih bolnic, pri katerih je prišlo do ponovitve epitelijskega raka visokega gradusa jajčnikov, jajcevodov ali primarnega peritonealnega raka, občutljivega na platino, ki so v popolnem ali delnem odzivu na kemoterapijo na osnovi platine.

2) *zdravilo Lynparza je v kombinaciji z bevacizumabom indicirano za*:
- vzdrževalno zdravljenje odraslih bolnic z napredovalim (stadij III in IV po FIGO) epitelijskim rakom visokega gradusa jajčnikov, jajcevodov ali primarnim peritonealnim rakom, ki so v popolnem ali delnem odzivu po zaključeni prvi liniji kemoterapije na osnovi platine v kombinaciji z bevacizumabom, pri katerih je rak povezan s pozitivnim stanjem pomanjkanja homologne rekombinacije (HRD – homologous recombination deficiency), opredeljenim z mutacijo gena *BRCA1/2* in/ali genomsko nestabilnostjo.

Rak dojk: *zdravilo Lynparza je indicirano kot*:
- monoterapija ali v kombinaciji z endokrinim zdravljenjem za adjuvantno zdravljenje odraslih bolnikov z germinalnimi mutacijami gena *BRCA1/2*, ki imajo HER2-negativnega zgodnjega raka dojk z velikim tveganjem in so bili predhodno zdravljeni z neoadjuvantno ali adjuvantno kemoterapijo.
- monoterapija za zdravljenje odraslih bolnikov z germinalno mutacijo gena *BRCA1/2*, ki imajo HER2-negativnega lokalno napredovalega ali metastatskega raka dojk. Bolniki morajo biti predhodno zdravljeni z antraciklinom in taksanom v okviru (neo)adjuvantnega zdravljenja ali zdravljenja metastatske bolezni, razen če za ti zdravljenji niso primerni. Pri bolnikih, ki imajo raka dojk s pozitivnimi hormonskimi receptorji (HR), je morala bolezen prav tako napredovati med predhodnim hormonskim zdravljenjem ali po njem, ali morajo bolniki veljati za neprimerne za hormonsko zdravljenje.

Adenokarcinom trebušne slinavke: zdravilo Lynparza je kot monoterapija indicirano za vzdrževalno zdravljenje odraslih bolnikov z germinalno mutacijo gena BRCA1/2, ki imajo metastatski adenokarcinom trebušne slinavke in njihova bolezen ni napredovala po najmanj 16 tednih zdravljenja s platino v shemi prve linije kemoterapije.
Rak prostate: *zdravilo Lynparza je indicirano:*
- kot monoterapija za zdravljenje odraslih bolnikov z metastatskim, na kastracijo odpornim rakom prostate (mKORP) in mutacijami gena *BRCA1/2* (germinalnimi in/ali somatskimi), pri katerih je bolezen napredovala po predhodni terapiji, ki je vsebovala novo hormonsko zdravilo.
- v kombinaciji z abirateronom in prednizonom ali prednizolonom za zdravljenje odraslih bolnikov z mKORP, pri katerih kemoterapija ni klinično indicirana

ODMERJANJE IN NAČIN UPORABE: Priporočeni odmerek zdravila Lynparza pri monoterapiji ali v kombinaciji z bevacizumabom pri raku jajčnikov ali v kombinaciji z abirateronom in prednizonom ali prednizolonom pri raku prostate ali z endokrinim zdravljenjem je 300 mg dvakrat na dan (to ustreza celotnemu dnevnemu odmerku 600 mg). 100-mg tablete so na voljo za zmanjšanje odmerka. Bolnice s ponovitvijo raka jajčnikov morajo začeti zdravljenje z zdravilom Lynparza najpozneje v 8 tednih po zadnjem odmerku sheme zdravljenja na osnovi platine. Če je zdravilo Lynparza uporabljeno v kombinaciji z bevacizumabom za prvo linijo vzdrževalnega zdravljenja po dokončanju prve linije zdravljenja na osnovi platine in z bevacizumabom, je odmerek bevacizumaba 15 mg/kg enkrat na 3 tedne. Glejte celotne informacije o zdravilu za bevacizumab. Za priporočeno odmerjanje partnerskega zdravila/partnerskih zdravil (zaviralec aromataze/antiestrogen in/ali LHRH) v kombinaciji endokrinega zdravljenja glejte celotne informacije o zadevnem zdravilu. Če je zdravilo Lynparza uporabljeno v kombinaciji z abirateronom za zdravljenje bolnikov z mKORP, je odmerek abiraterona 1000 mg peroralno enkrat na dan. Abirateron je treba dajati s 5 mg prednizona ali prednizolona peroralno dvakrat na dan. Glejte celotne informacije o zdravilu za abirateron. Prvo linijo vzdrževalnega zdravljenja napredovalega raka jajčnikov z mutacijo gena BRCA in prvo linijo vzdrževalnega zdravljenja HRD-pozitivnega napredovalega raka jajčnikov v kombinaciji z bevacizumabom je priporočljivo nadaljevati do radiološkega napredovanja bolezni ali nesprejemljive toksičnosti ali do največ 2 leti, če po 2 letih ni radioloških znakov bolezni. V primeru znakov bolezni po 2 letih, se lahko zdravljenje nadaljuje, če bi le to po mnenju zdravnika bilo koristno za bolnico. Glejte informacije o zdravilu bevacizumab za priporočeno celotno trajanje zdravljenja največ 15 mesecev, vključno z obdobji v kombinaciji s kemoterapijo in kot vzdrževalno zdravljenje. Pri adjuvantnem zdravljenju zgodnjega raka dojk je prporočljivo, da bolniki prejemajo zdravljenje do 1 leto ali do ponovitve bolezni ali do nesprejemljive toksičnosti, kar od tega se zgodi najprej. Zdravljenje ponovitve raka jajčnikov, raka dojk, adenokarcinoma trebušne slinavke in raka prostate je priporočljivo nadaljevati do napredovanja osnovne bolezni ali nesprejemljive toksičnosti. Učinkovitost in varnost ponovnega vzdrževalnega zdravljenja z zdravilom Lynparza po prvi ali poznejši ponovitvi bolezni pri bolnicah z rakom jajčnikov nista bili dokazani. Podatkov o učinkovitosti in varnosti ponovnega zdravljenja pri bolnicah z rakom dojk ni. Pri raku prostate je treba pri bolnikih, ki niso bili kirurško kastrirani, nadaljevati z medicinsko kastracijo z analogom luteinizirajočega hormona sproščajočega hormona. Če je zdravilo Lynparza uporabljeno v kombinaciji z abirateronom in prednizonom ali prednizolonom, je zdravljenje priporočljivo nadaljevati do napredovanja osnovne bolezni ali do nesprejemljivih toksičnih učinkov. Pri vseh bolnikih je treba med zdravljenjem še naprej uporabljati analoge GnRH (gonadotropin sproščajočega hormona) ali pa morajo bolniki pred tem opraviti obojestransko orhidektomijo. Glejte informacije o zdravilu za abirateron. Podatkov o učinkovitosti ali varnosti ponovnega zdravljenja z zdravilom Lynparza pri bolnikih z rakom prostate ni. V primeru potrebe po zmanjšanju odmerka zaradi neželenih učinkov je priporočeno zmanjšanje odmerka na 250 mg dvakrat na dan (to ustreza celotnemu dnevnemu odmerku 500 mg). Če je potrebno še dodatno zmanjšanje odmerka, je priporočljivo zmanjšanje odmerka na 200 mg dvakrat na dan (to ustreza celotnemu dnevnemu odmerku 400 mg). Zdravljenje z zdravilom Lynparza mora uvesti in nadzorovati zdravnik, ki ima izkušnje z uporabo zdravil proti raku. Mutacijsko stanje *BRCA* in/ali genomsko nestabilnost morajo imeti bolniki potrjeno z validiranim testom. Pred uporabo zdravila Lynparza v kombinaciji z abirateronom in prednizonom ali prednizolonom za zdravljenje bolnikov z mKORP genomsko testiranje ni potrebno. Genetsko svetovanje bolnikom z mutacijami *BRCA* je treba opraviti v skladu z lokalnimi predpisi. Zdravilo Lynparza se lahko pri bolnikih z blago okvaro ledvic (očistek kreatinina 51 do 80 ml/min) uporablja brez prilagoditve odmerka. Pri bolnikih z zmerno okvaro ledvic (očistek kreatinina 31 do 50 ml/min) je priporočen odmerek 200 mg dvakrat na dan. Uporaba zdravila se pri bolnikih s hudo okvaro ali končno odpovedjo ledvic (očistek kreatinina ≤ 30 ml/min) ne priporoča, ker varnost in farmakokinetika pri tej skupini bolnikov nista bili raziskani. Zdravilo Lynparza se lahko daje bolnikom z blago ali zmerno okvaro jeter (klasifikacija Child-Pugh A ali B) brez prilagoditve odmerka. Uporabe zdravila Lynparza se ne priporoča pri bolnikih s hudo okvaro jeter (klasifikacija Child-Pugh C), ker varnost in farmakokinetika pri tej skupini bolnikov nista bili raziskani. Zdravilo Lynparza je za peroralno uporabo. Tablete zdravila Lynparza je treba pogoltniti cele in se jih ne sme gristi, drobiti, raztapljati ali lomiti. Lahko se jih jemlje ne glede na obroke. **KONTRAINDIKACIJE:** Preobčutljivost na učinkovino ali katero koli pomožno snov. Dojenje med zdravljenjem in en mesec po zadnjem odmerku. **POSEBNA OPOZORILA IN PREVIDNOSTNI UKREPI:** *Hematološki toksični učinki:* Pri bolnikih, zdravljenih z zdravilom Lynparza, so bili opisani hematološki toksični učinki, vključno s klinično diagnozo in/ali laboratorijskimi izsledki, na splošno blage ali zmerne (stopnja 1 ali 2 po CTCAE) anemije, nevtropenije, trombocitopenije in limfopenije. Bolniki ne smejo začeti zdravljenja z zdravilom Lynparza, dokler ne okrevajo po hematoloških toksičnih učinkih predhodnega zdravljenja proti raku. Preiskava celotne krvne slike je priporočljiva na začetku zdravljenja, potem vsak mesec prvih 12 mesecev zdravljenja in pozneje redno. Če se pri bolniku pojavijo hudi hematološki toksični učinki ali je odvisen od transfuzij krvi, je treba zdravljenje z zdravilom Lynparza prekiniti in uvesti ustrezno hematološko testiranje. Če krvne vrednosti ostanejo klinično nenormalne še 4 tedne po prekinitvi uporabe zdravila Lynparza, je priporočljivo opraviti preiskavo kostnega mozga in/ali krvno citogenetsko analizo. *Mielodisplastični sindrom/akutna mieloična levkemija (MDS/AML):* Celokupna pojavnost MDS/AML je bila pri bolnikih, ki so v kliničnih preizkušanjih prejemali monoterapijo z zdravilom Lynparza, vključno v obdobju dolgoročnega spremljanja preživetja, < 1,5 %, z večjo pojavnostjo pri bolnicah z *BRCA*m, pri katerih je prišlo do ponovitve na platino občutljivega raka jajčnikov, ki so predhodno prejele vsaj dve liniji kemoterapije s platino in so jih spremljali 5 let. Večina teh primerov je bila s smrtnim izidom. Če obstaja sum na MDS/AML, je potrebno bolnico napotiti na nadaljnje preiskave k hematologu, vključno z analizo kostnega mozga in odvzemom krvi za citogenetiko. Če se po preiskavi dolgotrajne hematološke toksičnosti potrdi MDS/AML, je treba uporabo zdravila Lynparza prekiniti in bolnico ustrezno zdraviti. *Venski trombembolični dogodki:* Med zdravljenjem z zdravilom Lynparza so poročali o venskih trombemboličnih dogodkih, predvsem o pljučni emboliji, vendar ti dogodki niso imeli kakšnega doslednega kliničnega vzorca. V primerjavi z drugimi odobrenimi indikacijami so opažali večjo pojavnost pri bolnikih z metastatskim, na kastracijo odpornim rakom prostate, ki so prejemali tudi androgeno deprivacijsko zdravljenje. Bolnike spremljajte glede kliničnih znakov in simptomov venske tromboze in pljučne embolije, ter jih zdravite kot je medicinsko ustrezno. Bolniki z anamnezo VTE imajo morda večje tveganje za njeno ponovitev in jih je treba ustrezno spremljati. *Pnevmonitis:* V kliničnih študijah je bil pnevmonitis, vključno s smrtnim izidom, opisan pri < 1,0 % bolnikov, ki so prejemali zdravilo Lynparza, spremljali pa so jih številni predispozicijski dejavniki. Če se pri bolniku pojavijo novi ali poslabšajo obstoječi dihalni simptomi, npr. dispneja, kašelj in zvišana telesna temperatura, ali je ugotovljen nenormalen radiološki izvid prsnih organov, je treba zdravljenje z zdravilom Lynparza prekiniti in takoj opraviti preiskave. Če je pnevmonitis potrjen, je treba zdravljenje z zdravilom Lynparza prekiniti in bolnika ustrezno zdraviti. *Hepatotoksičnost:* Če se pojavijo klinični simptomi ali znaki, ki kažejo na razvoj hepatotoksičnosti, je treba takoj izvesti klinično oceno bolnika in preiskave delovanja jeter. V primeru suma na z zdravilom povzročeno okvaro jeter (DILI - drug-induced liver injury) je treba zdravljenje prekiniti. V primeru hude DILI je treba razmisliti o ukinitvi zdravljenja, kot je klinično primerno. **MEDSEBOJNO DELOVANJE Z DRUGIMI ZDRAVILI IN DRUGE OBLIKE INTERAKCIJ:** Zdravilo Lynparza se uporablja kot monoterapija in ni primerno za uporabo v kombinaciji z mielosupresivnimi zdravili proti raku, vključno z zdravili, ki poškodujejo DNA. Sočasna uporaba olapariba s cepivi ali imunosupresivnimi zdravili ni raziskana. Za presnovni očistek olapariba so pretežno odgovorni izoencimi CYP3A4/5. Sočasna uporaba zdravila Lynparza z znanimi močnimi ali zmernimi zaviralci tega izoencima ni priporočljiva. Če je treba sočasno uporabiti močne ali zmerne zaviralce CYP3A, je treba odmerek zdravila Lynparza zmanjšati. Prav tako med zdravljenjem z zdravilom Lynparza ni priporočljivo pitje grenivkinega soka. Prav tako olapariba ni priporočljivo uporabljati z znanimi močnimi ali zmernimi do močnimi induktorji tega izoencima, ker obstaja možnost, da se učinkovitost zdravila Lynparza bistveno zmanjša. Olaparib *in vitro* zavira CYP3A4 ter *in vivo* predvidoma blago zavira CYP3A. Zato je potrebna previdnost pri sočasni uporabi olapariba z občutljivimi substrati CYP3A4 ali substrati, ki imajo ozko terapevtsko okno. Bolnike, ki sočasno z olaparibom prejemajo substrate CYP3A z ozkim terapevtskim oknom, je priporočljivo ustrezno klinično spremljati. *In vitro* so ugotovili indukcijo CYP1A2, 2B6 in 3A4, prav tako ni mogoče izključiti možnosti, da olaparib inducira CYP2C9, CYP2C19 in P-gp, zato lahko olaparib po sočasni uporabi zmanjša izpostavljenost substratom teh presnovnih encimov in prenašalne beljakovine. Učinkovitost nekaterih hormonskih kontraceptivov se lahko zmanjša, če so uporabljeni sočasno z olaparibom. *In vitro* olaparib zavira efluksni prenašaleca P-gp, zato je potrebno bolnike, ki sočasno prejemajo substrate P-gp, ustrezno klinično spremljati. *In vitro* olaparib zavira BCRP, OATP1B1, OCT1, OCT2, OAT3, MATE1 in MATE2K. Ni mogoče izključiti možnosti, da olaparib poveča izpostavljenost BCRP, OATP1B1, OCT1, OCT2, OAT3, MATE1 in MATE2K. Še zlasti je previdnost potrebna, če se olaparib uporablja v kombinaciji s katerim koli statinom. Izvedli so klinično študijo za oceno kombinacije olapariba z anastrozolom, letrozolom in tamoksifenom, vendar klinično pomembnih medsebojnih delovanj niso opazili. **NEŽELENI UČINKI:** Zdravilo Lynparza je bilo povezano z neželenimi učinki, ki so bili na splošno blage ali zmerne resnosti (stopnja po CTCAE 1 ali 2) in na splošno niso zahtevali prekinitve zdravljenja. Če je zdravilo Lynparza uporabljeno v kombinaciji z bevacizumabom pri raku jajčnikov ali v kombinaciji z abirateronom in prednizonom ali prednizolonom pri raku prostate, se varnostni profil na splošno sklada z varnostnim profilom vsakega posameznega zdravila. Varnostni profil temelji na kumulativnih podatkih 4499 bolnikov s solidnimi tumorji, ki so bili v kliničnih preskušanjih zdravljeni z monoterapijo z zdravilom Lynparza v priporočenem odmerku. *Zelo pogosti neželeni učinki:* anemija, nevtropenija, levkopenija, zmanjšanje apetita, omotica, glavobol, spremenjen okus, kašelj, dispneja, bruhanje, driska, navzea, dispepsija in utrujenost (vključno z astenijo). *Pogosti neželeni učinki:* limfopenija, trombocitopenija, zvišanje transaminaz, stomatitis, bolečine v zgornjem delu trebuha, izpuščaj, zvišanje kreatinina v krvi in venska trombembolija. **PLODNOST, NOSEČNOST IN DOJENJE:** Ženske v rodni dobi ne smejo biti noseče na začetku zdravljenja z zdravilom Lynparza in ne smejo zanositi med zdravljenjem in še 6 mesecev po prejetju zadnjega odmerka. Pri vseh ženskah v rodni dobi je potrebno pred zdravljenjem opraviti test nosečnosti in ga redno izvajati med celotnim zdravljenjem. Priporočljivi sta dve visoko učinkoviti in komplementarni obliki kontracepcije. Zaradi možnega medsebojnega delovanja olapariba s hormonsko kontracepcijo je treba razmisliti o dodatni nehormonski kontracepciji. Pri ženskah s hormonsko odvisnim rakom je treba razmisliti o dveh nehormonskih načinih kontracepcije. Zdravilo Lynparza je kontraindicirano med obdobjem dojenja in še en mesec po prejetju zadnjega odmerka. Moški bolniki morajo med zdravljenjem in še 3 mesece po prejetju zadnjega odmerka zdravila Lynparza med spolnimi odnosi z nosečo žensko ali žensko v rodni dobi uporabljati kondom. Tudi partnerke moških bolnikov morajo uporabljati visoko učinkovito kontracepcijo, če so v rodni dobi. Moški bolniki med zdravljenjem z zdravilom Lynparza in še 3 mesece po zadnjem odmerku tega zdravila ne smejo darovati sperme. **REŽIM PREDPISOVANJA IN IZDAJE ZDRAVILA:** Rp/Spec. **DATUM ZADNJE REVIZIJE BESEDILA:** 5. 10. 2023 (SI-3466). **IMETNIK DOVOLJENJA ZA PROMET**: AstraZeneca AB, SE-151 85 Södertälje , Švedska. Dodatne informacije so na voljo pri podjetju AstraZeneca UK Limited, Podružnica v Sloveniji, Verovškova 55, 1000 Ljubljana, telefon: 01/51 35 600. **Pred predpisovanjem, prosimo, preberite celoten povzetek glavnih značilnosti zdravila.**

Literatura: 1. Povzetek glavnih značilnosti zdravila Lynparza, 5.10.2023, **2.** https://www.ema.europa.eu/en/medicines/human/EPAR/rubraca, dostopano 31.1.2024, **3.** https://www.ema.europa.eu/en/medicines/human/EPAR/zejula, dostopano 31.1.2024, **4.** https://www.ema.europa.eu/en/medicines/human/EPAR/talzenna, dostopano 31.1.2024, **5.** https://www.ema.europa.eu/en/news/lynparza-recommended-approval-ovarian-cancer, dostopano 31.1.2024

AstraZeneca
AstraZeneca UK Limited, Podružnica v Sloveniji,
Verovškova 55, 1000 Ljubljana, tel: 01/51 35 600

Samo za strokovno javnost. Datum priprave gradiva: februar 2024. SI-3729

KEYTRUDA® je odobrena za zdravljenje več kot 25 indikacij rakavih obolenj[1]

Referenca: 1. Keytruda EU SmPC

SKRAJŠAN POVZETEK GLAVNIH ZNAČILNOSTI ZDRAVILA • Pred predpisovanjem, prosimo, preberite celoten Povzetek glavnih značilnosti zdravila! • Ime zdravila: KEYTRUDA 25 mg/ml koncentrat za raztopino za infundiranje vsebuje pembrolizumab. • **Terapevtske indikacije:** Zdravilo KEYTRUDA je kot samostojno zdravljenje indicirano za zdravljenje: odraslih in mladostnikov, starih 12 let ali več, z napredovalim (neoperabilnim ali metastatskim) melanomom; za adjuvantno zdravljenje odraslih in mladostnikov, starih 12 let ali več, z melanomom v stadiju IIB, IIC ali III, in sicer po popolni kirurški odstranitvi; za adjuvantno zdravljenje odraslih z nedrobnoceličnim pljučnim rakom, ki imajo visoko tveganje za ponovitev bolezni po popolni kirurški odstranitvi in kemoterapiji na osnovi platine; metastatskega nedrobnoceličnega pljučnega raka (NSCLC) v prvi liniji zdravljenja pri odraslih, ki imajo tumorje z ≥ 50 % izraženostjo PD-L1 (TPS) in brez pozitivnih tumorskih mutacij EGFR ali ALK; lokalno napredovalega ali metastatskega NSCLC pri odraslih, ki imajo tumorje z ≥ 1 % izraženostjo PD-L1 (TPS) in so bili predhodno zdravljeni z vsaj eno shemo kemoterapije, bolniki s pozitivnimi tumorskimi mutacijami EGFR ali ALK so pred prejemom zdravila KEYTRUDA morali prejeti tudi tarčno zdravljenje; odraslih in pediatričnih bolnikov, starih 3 leta ali več, s ponovljenim ali neodzivnim klasičnim Hodgkinovim limfomom (cHL), pri katerih avtologna presaditev matičnih celic (ASCT) ni bila uspešna, ali po najmanj dveh predhodnih zdravljenjih kadar ASCT ne pride v poštev kot možnost zdravljenja; lokalno napredovalega ali metastatskega urotelijskega raka pri odraslih, predhodno zdravljenih s kemoterapijo, ki je vključevala platino; lokalno napredovalega ali metastatskega urotelijskega raka pri odraslih, ki niso primerni za zdravljenje s kemoterapijo, ki vsebuje cisplatin in imajo tumorje z izraženostjo PD-L1 ≥ 10, ocenjeno s kombinirano pozitivno oceno (CPS); ponovljenega ali metastatskega ploščatoceličnega raka glave in vratu (HNSCC) pri odraslih, ki imajo tumorje z ≥ 50 % izraženostjo PD-L1 (TPS), in pri katerih je bolezen napredovala med zdravljenjem ali po zdravljenju s kemoterapijo, ki je vključevala platino; za adjuvantno zdravljenje odraslih z rakom ledvičnih celic s povišanim tveganjem za ponovitev bolezni po nefrektomiji, ali po nefrektomiji in kirurški odstranitvi metastatskih lezij, za zdravljenje odraslih z MSI-H (microsatellite instability-high) ali dMMR (mismatch repair deficient) kolorektalnim rakom v naslednjih terapevtskih okoliščinah: prva linija zdravljenja metastatskega kolorektalnega raka; zdravljenje neoperabilnega ali metastatskega kolorektalnega raka po predhodnem kombiniranem zdravljenju, ki je temeljilo na fluoropirimidinu; in za zdravljenje MSI-H ali dMMR tumorjev pri odraslih z: napredovalim ali ponovljenim rakom endometrija, pri katerih je bolezen napredovala med ali po predhodnem zdravljenju, ki je vključevalo platino, v katerih koli terapevtskih okoliščinah, in ki niso kandidati za kurativno operacijo ali obsevanje; neoperabilnim ali metastatskim rakom želodca, tankega črevesa ali biliarnega trakta, pri katerih je bolezen napredovala med ali po vsaj enem predhodnem zdravljenju. Zdravilo KEYTRUDA je kot samostojno zdravljenje ali v kombinaciji s kemoterapijo s platino in 5-fluorouracilom (5-FU) indicirano za prvo linijo zdravljenja metastatskega ali neoperabilnega ponovljenega ploščatoceličnega raka glave in vratu pri odraslih, ki imajo tumorje z izraženostjo PD-L1 s CPS ≥ 1. Zdravilo KEYTRUDA je v kombinaciji s kemoterapijo, ki vključuje platino, indicirano za neoadjuvantno zdravljenje, in v nadaljevanju kot samostojno zdravljenje za adjuvantno zdravljenje odraslih z operabilnih nedrobnoceličnim pljučnim rakom, ki imajo visoko tveganje za ponovitev bolezni; v kombinaciji s pemetreksedom in kemoterapijo na osnovi platine je indicirano za prvo linijo zdravljenja metastatskega neploščatoceličnega NSCLC pri odraslih, pri katerih tumorji nimajo pozitivnih mutacij EGFR ali ALK; v kombinaciji s karboplatinom in bodisi paklitakselom bodisi nab-paklitakselom je indicirano za prvo linijo zdravljenja metastatskega ploščatoceličnega NSCLC pri odraslih; v kombinaciji z aksitinibom ali v kombinaciji z lenvatinibom je indicirano za prvo linijo zdravljenja napredovalega raka ledvičnih celic (RCC) pri odraslih; v kombinaciji s kemoterapijo s platino in fluoropirimidinom je indicirano za prvo linijo zdravljenja lokalno napredovalega neoperabilnega ali metastatskega raka požiralnika pri odraslih, ki imajo tumorje z izraženostjo PD-L1 s CPS ≥ 10; v kombinaciji s kemoterapijo za neoadjuvantno zdravljenje, in v nadaljevanju kot samostojno adjuvantno zdravljenje po kirurškem posegu, je indicirano za zdravljenje odraslih z lokalno napredovalim trojno negativnim rakom dojk ali trojno negativnim rakom dojk v zgodnjem stadiju z visokim tveganjem za ponovitev bolezni; v kombinaciji s kemoterapijo je indicirano za zdravljenje lokalno ponovljenega neoperabilnega ali metastatskega trojno negativnega raka dojk pri odraslih, ki imajo tumorje z izraženostjo PD-L1 s CPS ≥ 10 in predhodno niso prejeli kemoterapije za metastatsko bolezen; v kombinaciji z lenvatinibom je indicirano za zdravljenje napredovalega ali ponovljenega raka endometrija (EC) pri odraslih z napredovalo boleznijo med ali po predhodnem zdravljenju s kemoterapijo, ki je vključevala platino, v katerih koli terapevtskih okoliščinah, in ki niso kandidati za kurativno operacijo ali obsevanje; v kombinaciji s kemoterapijo, z bevacizumabom ali brez njega, je indicirano za zdravljenje persistentnega, ponovljenega ali metastatskega raka maternične vratu pri odraslih bolnicah, ki imajo tumorje z izraženostjo PD-L1 s CPS ≥ 1; v kombinaciji s trastuzumabom, fluoropirimidinom in kemoterapijo, ki vključuje platino, je indicirano za prvo linijo zdravljenja lokalno napredovalega neoperabilnega ali metastatskega HER2-pozitivnega adenokarcinoma želodca ali gastroezofagealnega prehoda pri odraslih, ki imajo tumorje z izraženostjo PD-L1 s CPS ≥ 1; v kombinaciji s fluoropirimidinom in kemoterapijo, ki vključuje platino, je indicirano za prvo linijo zdravljenja lokalno napredovalega neoperabilnega ali metastatskega HER2-negativnega adenokarcinoma želodca ali gastroezofagealnega prehoda pri odraslih, ki imajo tumorje z izraženostjo PD-L1 s CPS ≥ 1; v kombinaciji z gemcitabinom in cisplatinom je indicirano za prvo linijo zdravljenja lokalno napredovalega neoperabilnega ali metastatskega raka biliarnega trakta pri odraslih. • **Odmerjanje in način uporabe:** Testiranje PD-L1: Če je navedeno v indikaciji, je treba izbiro bolnika za zdravljenje z zdravilom KEYTRUDA na podlagi izraženosti PD-L1 tumorja potrditi z validirano preiskavo. Testiranje MSI/MMR: Če je navedeno v indikaciji, je treba izbiro bolnika za zdravljenje z zdravilom KEYTRUDA na podlagi MSI-H/dMMR statusa tumorja potrditi z validirano preiskavo. Odmerjanje: Priporočeni odmerek zdravila KEYTRUDA pri odraslih je bodisi 200 mg na 3 tedne ali 400 mg na 6 tednov, apliciran z intravensko infuzijo v 30 minutah. Priporočeni odmerek zdravila KEYTRUDA za samostojno zdravljenje pri pediatričnih bolnikih s cHL, starih 3 leta ali več, ali bolnikih z melanomom, starih 12 let ali več, je 2 mg/kg telesne mase (do največ 200 mg) na 3 tedne, apliciran z intravensko infuzijo v 30 minutah. Za uporabo v kombinaciji glejte povzetke glavnih značilnosti zdravil sočasno uporabljenih zdravil. Če se uporablja kot del kombiniranega zdravljenja skupaj z intravensko kemoterapijo, je treba zdravilo KEYTRUDA aplicirati prvo. Bolnike je treba zdraviti do napredovanja bolezni ali nesprejemljivih toksičnih učinkov (in do maksimalnega trajanja zdravljenja, če je le to določeno za indikacijo). Pri adjuvantnem zdravljenju melanoma, NSCLC ali RCC je treba zdravilo uporabljati do ponovitve bolezni, pojava nesprejemljivih toksičnih učinkov oziroma mora zdravljenje trajati do enega leta. Za neoadjuvantno in adjuvantno zdravljenje operabilnega NSCLC morajo bolniki neoadjuvantno prejeti zdravilo KEYTRUDA v kombinaciji s kemoterapijo, in sicer 4 odmerke po 200 mg na 3 tedne ali 2 odmerka po 400 mg na 6 tednov ali do napredovanja bolezni, ki izključuje definitivni kirurški poseg, ali do pojava nesprejemljivih toksičnih učinkov, čemur sledi adjuvantno zdravljenje z zdravilom KEYTRUDA kot samostojnim zdravljenjem, in sicer 13 odmerkov po 200 mg na 3 tedne ali 7 odmerkov po 400 mg na 6 tednov ali do ponovitve bolezni ali do pojava nesprejemljivih toksičnih učinkov. Bolniki, pri katerih pride do napredovanja bolezni, ki izključuje definitivni kirurški poseg, ali do nesprejemljivih toksičnih učinkov, povezanih z zdravilom KEYTRUDA kot neoadjuvantnim zdravljenjem v kombinaciji s kemoterapijo, ne smejo prejeti zdravila KEYTRUDA kot samostojnega zdravljenja za adjuvantno zdravljenje. Za neoadjuvantno in adjuvantno zdravljenje TNBC morajo bolniki neoadjuvantno prejeti zdravilo KEYTRUDA v kombinaciji s kemoterapijo, in sicer 8 odmerkov po 200 mg na 3 tedne ali 4 odmerke po 400 mg na 6 tednov, ali do napredovanja bolezni, ki izključuje definitivni kirurški poseg, ali do pojava nesprejemljivih toksičnih učinkov, čemur sledi adjuvantno zdravljenje z zdravilom KEYTRUDA kot samostojnim zdravljenjem, in sicer 9 odmerkov po 200 mg na 3 tedne ali 5 odmerkov po 400 mg na 6 tednov ali do ponovitve bolezni ali pojava nesprejemljivih toksičnih učinkov. Bolniki, pri katerih pride do napredovanja bolezni, ki izključuje definitivni kirurški poseg, ali do nesprejemljivih toksičnih učinkov povezanih z zdravilom KEYTRUDA kot neoadjuvantnim zdravljenjem v kombinaciji s kemoterapijo, ne smejo prejeti zdravila KEYTRUDA kot samostojnega zdravljenja za adjuvantno zdravljenje. Če je aksitinib uporabljen v kombinaciji s pembrolizumabom, se lahko razmisli o povečanju odmerka aksitiniba nad začetnih 5 mg v presledkih šest tednov ali več. V primeru uporabe v kombinaciji z lenvatinibom je treba zdravljenje z enim ali obema zdraviloma prekiniti, kot je primerno. Uporabo lenvatiniba je treba zadržati, odmerek zmanjšati ali prenehati z uporabo, v skladu z navodili v povzetku glavnih značilnosti zdravila za lenvatinib, in sicer za kombinacijo s pembrolizumabom. Pri bolnikih starih ≥ 65 let, bolnikih z blago do zmerno okvaro ledvic, bolnikih z blago ali zmerno okvaro jeter prilagoditev odmerka ni potrebna. Odložitev odmerka ali ukinitev zdravljenja: Zmanjšanje odmerka zdravila KEYTRUDA ni priporočljivo. Za obvladovanje neželenih učinkov je treba uporabo zdravila KEYTRUDA zadržati ali ukiniti, prosimo, glejte celoten Povzetek glavnih značilnosti zdravila. • **Kontraindikacije:** Preobčutljivost na učinkovino ali katero koli pomožno snov. • **Povzetek posebnih opozoril, previdnostnih ukrepov, interakcij in neželenih učinkov:** Imunsko pogojeni neželeni učinki (pnevmonitis, kolitis, hepatitis, nefritis, endokrinopatije, neželeni učinki na kožo in drugi): Pri bolnikih, ki so prejemali pembrolizumab, so se pojavili imunsko pogojeni neželeni učinki, vključno s hudimi in smrtnimi primeri. Večina imunsko pogojenih neželenih učinkov, ki so se pojavili med zdravljenjem s pembrolizumabom, je bila reverzibilnih in so jih obvladali s prekinitvami uporabe pembrolizumaba, uporabo kortikosteroidov in/ali podporno oskrbo. Pojavijo se lahko tudi po zadnjem odmerku pembrolizumaba in hkrati prizadanejo več organskih sistemov. V primeru suma na imunsko pogojene neželene učinke je treba poskrbeti za ustrezno oceno za potrditev etiologije oziroma izključitev drugih vzrokov. Glede na izrazitost neželenega učinka je treba zadržati uporabo pembrolizumaba in uporabiti kortikosteroide – za natančna navodila, prosimo, glejte Povzetek glavnih značilnosti zdravila Keytruda. Zdravljenje s pembrolizumabom lahko poveča tveganje za zavrnitev pri prejemnikih presadkov čvrstih organov. Pri bolnikih, ki so prejemali pembrolizumab, so poročali o hudih z infuzijo povezanih reakcijah, vključno s preobčutljivostjo in anafilaksijo. Pembrolizumab se iz obtoka odstrani s katabolizmom, zato presnovnih medsebojnih delovanj zdravil ni pričakovati. Uporabi sistemskih kortikosteroidov ali imunosupresivov pred uvedbo pembrolizumaba se je treba izogibati, ker lahko vplivajo na farmakodinamično aktivnost in učinkovitost pembrolizumaba. Vendar pa je kortikosteroide ali druge imunosupresive mogoče uporabiti za zdravljenje imunsko pogojenih neželenih učinkov. Kortikosteroide je mogoče uporabiti tudi kot premedikacijo, če je pembrolizumab uporabljen v kombinaciji s kemoterapijo, kot antiemetično profilakso in/ali za ublažitev neželenih učinkov, povezanih s kemoterapijo. Ženske v rodni dobi morajo med zdravljenjem s pembrolizumabom in vsaj še 4 mesece po zadnjem odmerku pembrolizumaba uporabljati učinkovito kontracepcijo, med nosečnostjo in dojenjem se ga ne sme uporabljati. Varnost pembrolizumaba pri samostojnem zdravljenju so v kliničnih študijah ocenili pri 7631 bolnikih, ki so imeli različne vrste raka, s štirimi odmerki (2 mg/kg telesne mase na 3 tedne, 200 mg na 3 tedne in 10 mg/kg telesne mase na 2 ali 3 tedne). V tej populaciji bolnikov je mediani čas opazovanja znašal 8,5 meseca (v razponu od 1 dneva do 39 mesecev), najpogostejši neželeni učinki zdravljenja s pembrolizumabom pa so bili utrujenost (31 %), diareja (22 %) in navzea (20 %). Večina poročanih neželenih učinkov pri samostojnem zdravljenju je bila po izrazitosti 1. ali 2. stopnje. Najresnejši neželeni učinki so bili imunsko pogojeni neželeni učinki in hude z infuzijo povezane reakcije. Pojavnost imunsko pogojenih neželenih učinkov pri uporabi pembrolizumaba samega za adjuvantno zdravljenje je znašala 37 % za vse stopnje in 9 % od 3. do 5. stopnje, pri metastatski bolezni pa 25 % za vse stopnje in 6 % od 3. do 5. stopnje. Pri adjuvantnem zdravljenju niso zaznali nobenih novih imunsko pogojenih neželenih učinkov. Varnost pembrolizumaba pri kombiniranem zdravljenju s kemoterapijo so ocenili pri 5183 bolnikih z različnimi vrstami raka, ki so v kliničnih študijah prejemali pembrolizumab v odmerkih 200 mg, 2 mg/kg telesne mase ali 10 mg/kg telesne mase na vsake 3 tedne. V tej populaciji bolnikov so bili najpogostejši neželeni učinki naslednji: anemija (52 %), navzea (52 %), utrujenost (35 %), diareja (33 %), zaprtost (32 %), bruhanje (28 %), zmanjšanje apetita (28 %), zmanjšano število nevtrofilcev (27 %) in nevtropenija (25 %). Pojavnost neželenih učinkov 3. do 5. stopnje je pri bolnikih z NSCLC pri kombiniranem zdravljenju s pembrolizumabom znašala 69 % in pri zdravljenju samo s kemoterapijo 61 %, pri bolnikih s HNSCC pri kombiniranem zdravljenju s pembrolizumabom 85 % in pri zdravljenju s kemoterapijo v kombinaciji s cetuksimabom 84 %, pri bolnikih z rakom požiralnika pri kombiniranem zdravljenju s pembrolizumabom 86 % in pri zdravljenju samo s kemoterapijo 83 %, pri bolnikih s TNBC pri kombiniranem zdravljenju s pembrolizumabom 80 % in pri zdravljenju samo s kemoterapijo 77 %, pri bolnicah z rakom materničnega vratu pri kombiniranem zdravljenju s pembrolizumabom 82 % in pri zdravljenju s kemoterapijo z ali brez bevacizumaba 75 %, pri bolnikih z rakom želodca pri kombiniranem zdravljenju s pembrolizumabom (kemoterapija z ali brez trastuzumaba) 74 % in pri kemoterapiji v kombinaciji z ali brez trastuzumaba 68 %, in pri bolnikih z rakom biliarnega trakta pri kombiniranem zdravljenju s pembrolizumabom 85 % in pri samostojni kemoterapiji 84 %. Varnost pembrolizumaba v kombinaciji z aksitinibom ali lenvatinibom pri napredovalem RCC in v kombinaciji z lenvatinibom pri napredovalem EC so ocenili pri skupno 1456 bolnikih z napredovalim RCC ali napredovalim EC, ki so v kliničnih študijah prejemali 200 mg pembrolizumaba na 3 tedne skupaj s 5 mg aksitiniba dvakrat na dan ali z 20 mg lenvatiniba enkrat na dan, kot je bilo ustrezno. V teh populacijah bolnikov so bili najpogostejši neželeni učinki diareja (58 %), hipertenzija (54 %), hipotiroidizem (46 %), utrujenost (41 %), zmanjšan apetit (40 %), navzea (40 %), artralgija (30 %), bruhanje (28 %), zmanjšanje telesne mase (28 %), disfonija (28 %), bolečine v trebuhu (28 %), proteinurija (27 %), sindrom palmarno-plantarne eritrodizestezije (26 %), izpuščaj (26 %), stomatitis (25 %), zaprtost (25 %), mišično-skeletna bolečina (23 %), glavobol (23 %) in kašelj (21 %). Neželenih učinkov od 3. do 5. stopnje je bilo pri bolnikih z RCC med uporabo pembrolizumaba v kombinaciji z aksitinibom ali lenvatinibom 80 % in med uporabo sunitiniba samega 71 %. Pri bolnicah z EC je bilo neželenih učinkov od 3. do 5. stopnje med uporabo pembrolizumaba v kombinaciji z lenvatinibom 89 % in med uporabo kemoterapije same 73 %. Za celoten seznam neželenih učinkov, prosimo, glejte celoten Povzetek glavnih značilnosti zdravila. Za dodatne informacije o varnosti v primeru uporabe pembrolizumaba v kombinaciji glejte povzetke glavnih značilnosti zdravila za posamezne komponente kombiniranega zdravljenja. • **Način in režim izdaje zdravila:** H – Predpisovanje in izdaja zdravila je le na recept, zdravilo se uporablja samo v bolnišnicah. • **Imetnik dovoljenja za promet z zdravilom:** Merck Sharp & Dohme B.V. , Waarderweg 39, 2031 BN Haarlem, Nizozemska.

Merck Sharp & Dohme inovativna zdravila d.o.o.
Ameriška ulica 2, 1000 Ljubljana; tel: +386 1/ 520 42 01, fax: +386 1/ 520 43 50

Samo za strokovno javnost. | H - Predpisovanje in izdaja zdravila je le na recept, zdravilo pa se uporablja samo v bolnišnicah. Pred predpisovanjem, prosimo, preberite celoten Povzetek glavnih značilnosti zdravila Keytruda, ki je na voljo pri naših strokovnih sodelavcih ali na lokalnem sedežu družbe.

Zdravilo ALECENSA je v monoterapiji indicirano za:

Adjuvantno zdravljenje nedrobnoceličnega raka pljuč (NDRP) po resekciji:
- dopolnilno zdravljenje po popolni resekciji tumorja pri odraslih bolnikih z ALK-pozitivnim (ALK – anaplastična limfomska kinaza) NDRP z velikim tveganjem za ponovitev.

Zdravljenje napredovalega NDRP:
- zdravljenje 1. reda odraslih bolnikov z ALK-pozitivnim napredovalim NDRP,
- zdravljenje odraslih bolnikov z ALK-pozitivnim napredovalim NDRP, ki so se predhodno zdravili s krizotinibom.

ALECENSA®
alektinib 150 mg kapsule

Vir: 1. Povzetek glavnih značilnosti zdravila ALECENSA. Dostopano avgust 2024 na https://www.ema.europa.eu/sl/documents/product-information/alecensa-epar-product-information_sl.pdf

Ime zdravila: Alecensa 150 mg trde kapsule
Kakovostna in količinska sestava: Ena trda kapsula vsebuje 150 mg alektiniba v obliki alektinibijevega klorida. Pomožni snovi z znanim učinkom: Ena trda kapsula vsebuje 33,7 mg laktoze in 6 mg natrija. **Terapevtske indikacije:** Adjuvantno zdravljenje nedrobnoceličnega raka pljuč (NDRP) po resekciji: zdravilo Alecensa je kot monoterapija indicirano za adjuvantno zdravljenje po popolni resekciji tumorja pri odraslih bolnikih z ALK-pozitivnim (ALK – anaplastična limfomska kinaza) NDRP z velikim tveganjem za ponovitev. Zdravljenje napredovalega NDRP: zdravilo Alecensa je kot monoterapija indicirano v prvi liniji zdravljenja odraslih bolnikov z ALKpozitivnim napredovalim NDRP. Zdravilo Alecensa je kot monoterapija indicirano za zdravljenje odraslih bolnikov z ALK-pozitivnim napredovalim NDRP, ki so se predhodno zdravili s krizotinibom. **Odmerjanje in način uporabe:** Za izbiro bolnikov, ki imajo ALK-pozitivnega NDRP, je treba opraviti validiran preizkus za ALK. Ali je bolnikov NDRP ALK-pozitiven, je treba ugotoviti pred začetkom zdravljenja z zdravilom Alecensa. Odmerjanje: Priporočeni odmerek zdravila Alecensa je 600 mg dvakrat na dan s hrano. Bolniki z obstoječo hudo okvaro jeter naj prejmejo začetni odmerek 450 mg dvakrat na dan s hrano. *Trajanje zdravljenja: Adjuvantno zdravljenje NDRP po resekciji:* Zdravljenje z zdravilom Alecensa je treba nadaljevati do ponovitve bolezni, nesprejemljivih toksičnih učinkov ali 2 leti. *Zdravljenje napredovalega NDRP:* Zdravljenje z zdravilom Alecensa je treba nadaljevati do napredovanja bolezni ali nesprejemljivih toksičnih učinkov. *Prilagoditve odmerka:* Obvladovanje neželenih učinkov lahko obsega zmanjšanje odmerka, začasno prekinitev uporabe ali ukinitev zdravljenja z zdravilom Alecensa. Odmerek zdravila Alecensa je treba zmanjševati v korakih po 150 mg dvakrat na dan, upoštevaje prenašanje. Zdravljenje z zdravilom Alecensa je treba ukiniti, če bolnik ne prenese odmerka 300 mg dvakrat na dan. Smernice za prilagoditev odmerka so opisane v povzetku glavnih značilnosti zdravila. Način uporabe: zdravilo Alecensa je namenjeno peroralni uporabi. Trde kapsule mora bolnik pogoltniti cele in jih ne sme odpirati ali raztapljati. Vzeti jih mora s hrano. **Kontraindikacije:** preobčutljivost za alektinib ali katero koli pomožno snov. **Posebna opozorila in previdnostni ukrepi:** Intersticijska bolezen pljuč (IBP)/pnevmonitis: Bolnike je treba kontrolirati glede pljučnih simptomov, ki kažejo na pnevmonitis. Bolnikom, pri katerih je diagnosticirana IBP/pnevmonitis, je treba zdravljenje z zdravilom Alecensa nemudoma prekiniti; če ni mogoče ugotoviti drugih možnih vzrokov za IBP/pnevmonitis, je treba zdravljenje ukiniti. Hepatotoksičnost: Delovanje jeter, vključno z ALT, AST in celokupnim bilirubinom, je treba kontrolirati izhodiščno in nato na 2 tedna prve 3 mesece zdravljenja. Kasneje je treba spremljanje izvajati periodično, ker se dogodki lahko pojavijo po več kot 3 mesecih; pri bolnikih, ki se jim pojavi zvišanje aminotransferaz in bilirubina, morajo biti kontrole pogostejše. Glede na izrazitost neželenega učinka je treba uporabo zdravila Alecensa začasno prekiniti in zdravilo znova uvesti v manjšem odmerku, ali pa ga je treba ukiniti. Huda mialgija in zvišanja kreatin-fosfokinaze (CPK): Bolnikom je treba naročiti, naj poročajo o vseh nepojasnjenih mišičnih bolečinah, občutljivosti ali šibkosti. Koncentracije CPK je treba določiti vsaka dva tedna v prvem mesecu zdravljenja, pri bolnikih, ki poročajo o simptomih, pa kot je klinično indicirano. Glede na izrazitost zvišanja CPK je treba uporabo zdravila Alecensa začasno prekiniti in zdravilo znova uvesti v manjšem odmerku. Bradikardija: Srčno frekvenco in krvni tlak je treba kontrolirati, kot je klinično indicirano. Če se bolniku pojavijo simptomatska bradikardija ali življenjsko ogrožujoči dogodki, je treba oceniti sočasna zdravila, za katera je znano, da povzročajo bradikardijo, in antihipertenzivna zdravila, odmerjanje zdravila Alecensa pa je treba prilagoditi. Hemolitična anemija: Če je koncentracija hemoglobina manjša od 10 g/dl in obstaja sum na hemolitično anemijo, prekinite uporabo zdravila Alecensa in uvedite ustrezne laboratorijske preiskave. V primeru potrjene hemolitične anemije zdravljenje z zdravilom Alecensa po izboljšanju znova začnite z manjšim odmerkom, kot je opisano v SmPC. Perforacija prebavil: Pri bolnikih s povečanim tveganjem, ki se zdravijo z zdravilom Alecensa, so poročali o primerih perforacije prebavil. Če se pri bolnikih razvije perforacija prebavil, je treba razmisliti o ukinitvi zdravila. Bolnike je treba obvestiti o znakih in simptomih perforacije prebavil in jim svetovati, da se v primeru pojava takoj posvetujejo z zdravnikom. Fotosenzibilnost: Bolnikom je treba naročiti, naj se med jemanjem zdravila Alecensa in vsaj še 7 dni po koncu zdravljenja izogibajo dolgotrajnejšemu izpostavljanju soncu. Prav tako jim je treba naročiti, najza preprečitev sončnih opeklin uporabljajo širokospektralno sredstvo za sončenje in mazilo za ustnice, ki ščitita pred ultravijoličnimi žarki A in B. Ženske v rodni dobi: zdravilo Alecensa lahko škoduje plodu, če je uporabljeno med nosečnostjo. Bolnice v rodni dobi morajo med zdravljenjem in še vsaj 3 mesece po zadnjem odmerku zdravila Alecensa uporabljati visoko učinkovito kontracepcijsko zaščito. **Medsebojno delovanje z drugimi zdravili in druge oblike interakcij:** Vplivi drugih zdravil na alektinib: *Induktorji CYP3A4:* Glede na učinke na skupno izpostavljenost alektinibu in M4 med sočasno uporabo zdravila Alecensa in induktorjev CYP3A odmerka ni treba prilagoditi. Priporočljivo je ustrezno spremljanje bolnikov, ki sočasno jemljejo močne induktorje CYP3A. *Zaviralci CYP3A4:* Glede na učinke na skupno izpostavljenost alektinibu in M4 med sočasno uporabo zdravila Alecensa in zaviralcev CYP3A odmerka ni treba prilagoditi. Priporočljivo je ustrezno spremljanje bolnikov, ki sočasno jemljejo močne zaviralce CYP3A. *Zdravila, ki zvišujejo pH v želodcu:* večkratni odmerki esomeprazola, zaviralca protonske črpalke, 40 mg enkrat na dan, niso imeli klinično pomembnega vpliva na skupno izpostavljenost alektinibu in M4. Vpliv prenašalcev na odstranjevanje alektiniba: M4 je substrat P-glikoproteina. Ker alektinib zavira P-gp, ni pričakovati, da bi sočasna uporaba z zaviralci P-gp pomembno vplivala na izpostavljenost M4. Učinki alektiniba na druga zdravila: *Substrati CYP:* Alektinib in M4 *in vitro* kažeta šibko časovno odvisno zavrtje CYP3A4; alektinib je v kliničnih koncentracijah pokazal šibek indukcijski potencial na CYP3A4 in CYP2B6. Tveganja za indukcijo encimov CYP2B6 in drugih encimov, reguliranih s PXR, razen encima CYP3A4, ni mogoče povsem izključiti. Učinkovitost sočasno uporabljenih peroralnih kontraceptivov se lahko zmanjša. *Substrati P-gp:* Če zdravilo Alecensa uporabljamo sočasno s substrati P-gp, je priporočljiv ustrezen nadzor. *Substrati BCRP:* Če zdravilo Alecensa uporabljamo sočasno s substrati BCRP, je priporočljiv ustrezen nadzor. **Neželeni učinki:** Najpogostejši neželeni učinki so bili zaprtost, mialgija, edemi, anemija, izpuščaj, zvišan bilirubin, zvišana ALT in zvišana AST. Poročanje o domnevnih neželenih učinkih: Poročanje o domnevnih neželenih učinkih zdravila po izdaji dovoljenja za promet je pomembno. Omogoča namreč stalno spremljanje razmerja med koristmi in tveganji zdravila. Od zdravstvenih delavcev se zahteva, da poročajo o katerem koli domnevnem neželenem učinku zdravila na: Javna agencija Republike Slovenije za zdravila in medicinske pripomočke, Sektor za farmakovigilanco, Nacionalni center za farmakovigilanco, Slovenčeva ulica 22, SI-1000 Ljubljana, Tel: +386(0)8 2000 500, Faks: +386 (0)8 2000 510, e-pošta: h-farmakovigilanca@jazmp.si , spletna stran: www.jazmp.si. **Režim izdaje zdravila:** Rp/Spec. **Imetnik dovoljenja za promet:** Roche Registration GmbH, Emil-Barell-Strasse 1, 79639 Grenzach-Wyhlen, Nemčija. **Verzija:** 1.0/24
Informacija pripravljena: avgust 2024

DODATNE INFORMACIJE SO NA VOLJO PRI:
Roche farmacevtska družba d.o.o., Stegne 13G, 1000 Ljubljana

Samo za strokovno javnost
M-SI-00001033(v2.0)

ODOBREN V PRVI LINIJI ZDRAVLJENJA mPaCa

ONIVYDE®
pegylated liposomal
V REŽIMU NALIRIFOX

UTIRA NOVO POT NA PODLAGI TRDNIH DOKAZOV

Z zdravilom ONIVYDE v režimu NALIRIFOX lahko bolnikom z mPaCa ponudite učinkovito zdravljenje z obvladljivim varnostnim profilom in omogočite, da se njihova kakovost življenja ohrani.[1, 2]

Zdravilo ONIVYDE pegylated liposomal je indicirano:
- v kombinaciji z oksaliplatinom, 5-fluorouracilom (5-FU) in levkovorinom (LV) za prvo izbiro zdravljenja metastatskega adenokarcinoma trebušne slinavke pri odraslih bolnikih,
- v kombinaciji s 5-FU in LV za zdravljenje metastatskega adenokarcinoma trebušne slinavke pri odraslih bolnikih, pri katerih je bolezen po zdravljenju na osnovi gemcitabina napredovala.

Zdravilo ni bilo preizkušano pri otrocih, mlajših od 18 let, in je indicirano le za odrasle.[1]

onivyde®
pegylated liposomal irinotecan

SKRAJŠAN POVZETEK GLAVNIH ZNAČILNOSTI ZDRAVILA Onivyde pegylated liposomal 4,3 mg/ml
SESTAVA*: Onivyde pegylated liposomal 4,3 mg/ml koncentrat za disperzijo za infundiranje: ena viala z 10 ml koncentrata vsebuje 43 mg brezvodnega irinotekana (v obliki irinotekanijeve soli saharoznega oktasulfata v pegilirani liposomski formulaciji). **TERAPEVTSKE INDIKACIJE*:** Zdravilo Onivyde pegylated liposomal je v kombinaciji z oksaliplatinom, 5-fluorouracilom (5-FU) in levkovorinom (LV) indicirano za prvo izbiro zdravljenja metastatskega adenokarcinoma trebušne slinavke pri odraslih bolniki in v kombinaciji s 5-FU in LV za zdravljenje metastatskega adenokarcinoma trebušne slinavke pri odraslih bolnikih, pri katerih je bolezen po zdravljenju na osnovi gemcitabina napredovala. **ODMERJANJE IN NAČIN UPORABE*:** Onivyde pegylated liposomal smejo bolnikom predpisati in dajati samo zdravstveni delavci, ki imajo izkušnje pri uporabi zdravil za zdravljenje raka. Zdravilo Onivyde pegylated liposomal ni enakovredno drugim neliposomskim formulacijam irinotekana, zato jih ne smemo zamenjevati. Zdravilo Onivyde pegylated liposomal se ne daje kot samostojno zdravilo. Z zdravljenjem je treba nadaljevati, dokler bolezen ne napreduje ali bolnik zdravljenja z zdravilom ne prenaša več. Priporočeni odmerek zdravila Onivyde pegylated liposomal v kombinaciji z oksaliplatinom, LV in 5-FU je 50 mg/m^2 v obliki 90-minutne intravenske infuzije, ki ji sledi 120-minutna intravenska infuzija oksaliplatina v odmerku 60 mg/m^2, nato 30-minutna intravenska infuzija LV v odmerku 400 mg/m^2 in zatem 46-urna intravenska infuzija 5-FU v odmerku 2400 mg/m^2, vsaka 2 tedna. Priporočeni začetni odmerek zdravila Onivyde pegylated liposomal pri bolnikih z znano homozigotnostjo za alel UGT1A1*28 je nespremenjen. Priporočeni odmerek in režim odmerjanja zdravila Onivyde pegylated liposomal v kombinaciji s 5-FU in LV je 70 mg/m^2 intravensko 90 minut, čemur sledi LV 400 mg/m^2 intravensko 30 minut in nato 5 FU 2400 mg/m^2 intravensko 46 ur, vsaka 2 tedna. Pri bolnikih z znano homozigotnostjo za alel UGT1A1*28 je treba razmisliti o manjšem začetnem odmerku zdravila Onivyde pegylated liposomal 50 mg/m^2. Če zdravilo bolniki dobro prenašajo, lahko v naslednjih ciklih razmislimo o odmerku zdravila Onivyde pegylated liposomal 70 mg/m^2. Prilagajanje odmerka se priporoča za obvladovanje toksičnosti, povezane z zdravilom Onivyde pegylated liposomal. **KONTRAINDIKACIJE*:** Anamneza hude preobčutljivosti na irinotekan ali katero koli pomožno snov. Dojenje. **OPOZORILA*:** *Mielosupresija/nevtropenija:* Med zdravljenjem z zdravilom Onivyde pegylated liposomal se priporoča nadziranje celotne krvne slike. Bolniki se morajo zavedati tveganja za nevtropenijo in pomena povišane telesne temperature. Febrilno nevtropenijo je treba nujno zdraviti v bolnišnici s širokospektralnimi intravenskimi antibiotiki. Pri bolnikih, ki doživijo hude hematološke neželene učinke, se priporoča zmanjšanje odmerka ali prekinitev zdravljenja. Bolnikov s hudo odpovedjo kostnega mozga ne smemo zdraviti z zdravilom Onivyde pegylated liposomal. Anamneza predhodnega obsevanja trebuha poveča tveganje za hudo nevtropenijo in febrilno nevtropenijo po zdravljenju z zdravilom Onivyde pegylated liposomal. Pri bolnikih, ki hkrati prejemajo zdravilo Onivyde pegylated liposomal in so obsevani, je potrebna previdnost. Bolniki s pomanjkljivo glukuronidacijo bilirubina, kot so bolniki z Gilbertovim sindromom, imajo med zdravljenjem z zdravilom Onivyde pegylated liposomal lahko večje tveganje za mielosupresijo. *Imunosupresivni učinki in cepiva:* Dajanje živih ali atenuiranih cepiv bolnikom z oslabljenim imunskim sistemom lahko povzroči resne ali smrtne okužbe. *Interakcije z močnimi induktorji encima CYP3A4, močnimi zaviralci encima CYP3A4 in močnimi zaviralci encima UGT1A1:* Zdravila Onivyde pegylated liposomal ne smemo dajati skupaj z močnimi induktorji encima CYP3A4, močnimi zaviralci encima CYP3A4 ali z močnimi zaviralci encima UGT1A1, razen če ni drugih terapevtskih možnosti. Zdravljenje z močnimi zaviralci encima CYP3A4 moramo prekiniti vsaj 1 teden pred začetkom zdravljenja z zdravilom Onivyde pegylated liposomal. *Driska:* Zdravilo Onivyde pegylated liposomal lahko povzroči hudo in smrtno nevarno drisko. Zdravila Onivyde pegylated liposomal se ne sme dajati bolnikom s črevesno obstrukcijo in kronično vnetno črevesno boleznijo.Pri bolnikih, ki doživijo zgodnji pojav driske (v ≤ 24 urah po začetku zdravljenja z zdravilom Onivyde pegylated liposomal) ali holinergične simptome, je treba razmisliti o terapevtskem in profilaktičnem zdravljenju z atropinom, razen če je kontraindicirano. Bolnike je treba opozoriti na tveganje za zapoznelo drisko (> 24 ur), ki je izčrpavajoča in v redkih primerih tudi življenjsko nevarna. Loperamid je treba uvesti ob prvem pojavu neoblikovanega ali mehkega blata ali takoj, ko odvajanje blata postane pogostejše kot običajno. Loperamid je treba dajati, dokler bolnik ni brez driske vsaj 12 ur. Da bi se izognili hudi driski, opustite vse izdelke, ki vsebujejo laktozo, ohranjajte hidracijo in uživajte dieto z nizko vsebnostjo maščob. Če driska traja tudi, ko bolnik prejema loperamid več kot 24 ur, je treba razmisliti o dodatni peroralni antibiotični podpori. Loperamida zaradi tveganja za paralitični ileus ne smemo uporabljati več kot 48 ur zaporedoma. Nov cikel zdravljenja se ne sme pričeti, dokler se driska ne umiri do ≤ 1. stopnje (2–3 odvajanja/dan več kot pred zdravljenjem). *Holinergične reakcije:* Zgodnjo drisko lahko spremljajo rinitis, povečano slinjenje, zardevanje, diaforeza, bradikardija, mioza in hiperperistaltika. Pri bolnikih s holinergičnimi simptomi moramo uporabiti atropin. *Preobčutljivostne reakcije, vključno z akutnimi infuzijskimi reakcijami:* V primeru hudih preobčutljivostnih reakcij je treba zdravljenje z zdravilom Onivyde pegylated liposomal prekiniti. *Predhodna Whipplova operacija:* Večje tveganje za resne okužbe. Bolnike je treba spremljati glede znakov okužbe. *Žilne bolezni:* Zdravilo Onivyde pegylated liposomal je bilo povezano s trombemboličnimi dogodki, kot so pljučna embolija, venska tromboza in arterijska trombembolija. Treba je pridobiti podrobno zdravstveno anamnezo, da bi prepoznali bolnike z več dejavniki tveganja poleg osnovne neoplazme. Bolnike je treba obvestiti o znakih in simptomih trombembolije in jim svetovati, da se v primeru katerega od teh znakov ali simptomov takoj obrnejo na svojega zdravnika ali medicinsko sestro. *Pljučna toksičnost:* Pri bolnikih, ki so prejemali neliposomski irinotekan, so se pojavili dogodki, podobni intersticijski pljučni bolezni (IPB), ki so vodili do smrtnih primerov. Pri bolnikih z dejavniki tveganja (obstoječo pljučno boleznijo, uporabo pnevmotoksičnih zdravil, kolonije stimulirajočimi dejavniki ali predhodnim zdravljenjem z obsevanjem) je treba pred zdravljenjem z zdravilom Onivyde pegylated liposomal in po njem skrbno nadzirati respiratorne simptome. Dokler ni opravljena diagnostična ocena, je treba ob pojavu nove ali napredovale dispneje, kašlja in povišane telesne temperature zdravljenje z zdravilom Onivyde pegylated liposomal začasno prekiniti. Pri bolnikih s potrjeno diagnozo IPB moramo zdravljenje z zdravilom Onivyde pegylated liposomal dokončno prekiniti. *Jetrna okvara:* Bolniki s hiperbilirubinemijo so imeli povišane koncentracije skupnega SN-38, zato je tveganje za nevtropenijo povečano. Pri bolnikih z vrednostjo skupnega bilirubina 1,0–2,0 mg/dl je treba redno nadzirati celotno krvno sliko. Previdnost je potrebna pri bolnikih z jetrno okvaro (bilirubin > 2-kratna zgornja meja normalnih vrednosti [ULN]; aminotransferaze > 5-kratna ULN). Previdnost je potrebna, če zdravilo Onivyde pegylated liposomal dajemo v kombinaciji z drugimi hepatotoksičnimi zdravili. *Bolniki s premajhno telesno maso (indeks telesne mase < 18,5 kg/m^2):* Potrebna je previdnost. *Pomožne snovi:* To zdravilo vsebuje 33,1 mg natrija na vialo, kar je enako 1,65 % največjega dnevnega vnosa natrija za odrasle osebe, ki ga priporoča SZO in znaša 2 g. En mililiter zdravila Onivyde pegylated liposomal vsebuje 0,144 mmol (3,31 mg) natrija. **INTERAKCIJE*:** *Previdnostni ukrepi:* Sočasno dajanje z induktorji encima CYP3A4 (npr. antikonvulzivi, rifampicin, rifabutin in šentjanževka) lahko zmanjša sistemsko izpostavljenost zdravilu Onivyde pegylated liposomal. Sočasno dajanje z zaviralci encima CYP3A4 (npr. grenivkinim sokom, klaritromicinom, indinavirjem, itrakonazolom, lopinavirjem, nefazodonom, nelfinavirjem, ritonavirjem, sakvinavirjem, telaprevirjem, vorikonazolom) ali encima UGT1A1 (npr. atazanavirja, gemfibrozila, indinavirja, regorafeniba) lahko poveča sistemsko izpostavljenost zdravilu Onivyde pegylated liposomal. Sočasna uporaba z zdravili z delovanjem na novotvorbe (flucitozinom) lahko poslabša neželene učinke zdravila Onivyde pegylated liposomal. **PLODNOST*:** Pred začetkom zdravljenja z zdravilom Onivyde pegylated liposomal premislite o svetovanju bolnikom glede shranjevanja spolnih celic. **NOSEČNOST*:** Uporaba ni priporočljiva. **DOJENJE*:** Zdravilo je kontraindicirano. **KONTRACEPCIJA*:** Ženske v rodni dobi morajo med zdravljenjem in še 7 mesecev po zdravljenju z zdravilom Onivyde pegylated liposomal uporabljati učinkovito kontracepcijo. Moški morajo med zdravljenjem z zdravilom Onivyde pegylated liposomal in 4 mesece po zdravljenju uporabljati kondome. **VPLIV NA SPOSOBNOST VOŽNJE IN UPRAVLJANJA STROJEV*:** Bolniki morajo biti med zdravljenjem pri vožnji in upravljanju strojev previdni. **NEŽELENI UČINKI*:** Zdravilo Onivyde pegylated liposomal v kombinaciji z oksaliplatinom, 5-fluorouracilom in levkovorinom: *Zelo pogosti:* anemija, nevtropenija, trombocitopenija, hipokaliemija, zmanjšan apetit, periferna nevropatija, disgevzija, parestezija, driska, navzea, bruhanje, bolečine/nelagodje v trebuhu, stomatitis, alopecija, astenija, vnetje sluznic, zmanjšana telesna masa. *Pogosti:* sepsa, infekcija urinarnega trakta, okužba s kandido, nazofaringitis, febrilna nevtropenija, levkopenija, limfopenija, dehidracija, hiponatriemija, hipofosfatemija, hipomagneziemija, hipoalbuminemija, hipokalciemija, tremor, nevrotoksičnost, disestezija, holinergični sindrom, glavobol, omotica, zamegljen vid, tahikardija, hipotenzija, trombembolični dogodki, pljučna embolija, kolcanje, dispneja, epistaksa, kolitis, enterokolitis, zaprtje, suha usta, napenjanje, napihnjenost trebuha, dispepsija, gastroezofagealna refluksna bolezen, hemoroidi, disfagija, hiperbilirubinemija, suha koža, sindrom palmarno-plantarne eritrodizestezije, izpuščaj, hiperpigmentacija kože, mišična šibkost, mialgija, mišični krči, akutna poškodba ledvic, pireksija, edem, mrzlica, zvišana raven transaminaz (ALT in AST), zvišana raven alkalne fosfataze v krvi, zvišana raven gama-glutamil transferaze, zvišana raven kreatinina v krvi, z infuzijo povezana reakcija. *Občasni:* divertikulitis, pljučnica, analni absces, febrilna okužba, gastroenteritis, okužba sluznice, oralna glivična okužba, okužba s Clostridium difficile, konjuktivitis, furunkel, herpes simpleks, laringitis, parodontitis, pustulozni izpuščaj, sinusitis, okužba zob, vulvovaginalna glivična okužba, peritumoralni edem, pancitopenija, hemolitična anemija, elektrolitsko neravnovesje, hiperkalciemija, celična smrt, hipokloremija, protin, hiperglikemija, hiperkaliemija, pomanjkanje železa, podhranjenost, nespečnost, zmedenost, depresija, nevroza, napadi, možganska krvavitev, možganska ishemija, ishemična možganska kap, anozmija, agevzija, motnje ravnotežja, hipersomnija, hipestezija, motnje v duševnem razvoju, letargija, motnje spomina, presinkopa, sinkopa, prehodni ishemični napad, draženje oči, zmanjšana ostrina vida, vrtoglavica, angina pektoris, akutni miokardni infarkt, palpitacije, hipertenzija, periferna hladnost, hematom, flebitis, orofaringealna bolečina, kašelj, hiperoksija, vnetje nosu, atelektaza, disfonija, pnevmonitis, gastrointestinalna toksičnost, obstrukcija dvanajstnika, analna inkontinenca, afta, oralna disestezija, bolečina v ustni votlini, motnje jezika, analna razpoka, angularni heilitis, dishezija, oralna parestezija, zobni karies, eruktacija, želodčne motnje, gastritis, motnje dlesni, boleče dlesni, hematohezija, hiperestezija zob, paralitični ileus, otekanje ustnic, razjede v ustih, spazem požiralnika, parodontalna bolezen, rektalna krvavitev, holangitis, toksični hepatitis, holestaza, hepatična citoliza, pruritus, hiperhidroza, bulozni dermatitis, generalizirani eksfoliativni dermatitis, eritem, toksičnost za nohte, papule, petehije, luskavica, občutljiva koža, luščenje kože, kožna lezija, teleangiektazija, urtikarija, artralgija, bolečine v hrbtu, bolečine v kosteh, bolečine v okončinah, poliartritis, okvara ledvic, odpoved ledvic, disurija, proteinurija, vulvovaginalna suhost, slabo počutje, splošno poslabšanje telesnega zdravja, vnetje, sindrom večorganske disfunkcije, gripi podobna bolezen, nesrčna bolečina v prsnem košu, aksilarna bolečina, bolečina v prsnem košu, hipotermija, bolečina, otekel obraz, temperaturna intoleranca, kseroza, zvišano mednarodno umerjeno razmerje, znižana raven celokupnih beljakovin, zmanjšan ledvični očistek kreatinina, podaljšan QT interval na elektrokardiogramu, povečano število monocitov, zvišana raven troponina I. Zdravilo Onivyde pegylated liposomal v kombinaciji s 5-fluorouracilom v kombinaciji z 5-fluorouracilom in levkovorinom: *Zelo pogosti:* nevtropenija, levkopenija, anemija, trombocitopenija, hipokaliemija, hipomagneziemija, dehidracija, zmanjšan apetit, omotica, driska, bruhanje, navzea, bolečine v trebuhu, stomatitis, alopecija, pireksija, periferni edem, vnetje sluznic, utrujenost, astenija, zmanjšana telesna masa. *Pogosti:* septični šok, sepsa, pljučnica, febrilna nevtropenija, gastroenteritis, oralna kandidoza, limfopenija, hipoglikemija, hiponatriemija, hipofosfatemija, nespečnost, holinergični sindrom, dizgevzija, hipotenzija, pljučna embolija, trombembolični dogodki, dispneja, disfonija, kolitis, hemoroidi, hipoalbuminemija, pruritus, akutna ledvična odpoved, z infuzijo povezana reakcija, edem, zvišana raven bilirubina, zvišana raven transaminaz (ALT in AST), zvišano mednarodno umerjeno razmerje. *Občasni:* biliarna sepsa, preobčutljivost, hipoksija, ezofagitis, proktitis, urtikarija, izpuščaj, obarvanje nohtov. *Neznana pogostnost:* anafilaktična/anafilaktoidna reakcija, angioedem, eritem. **PREVELIKO ODMERJANJE*:** Za preveliko odmerjanje zdravila ni znanega antidota. Treba je uvesti maksimalno podporno nego, s katero preprečimo dehidracijo zaradi driske in zdravimo zaplete zaradi okužb. **FARMAKODINAMIČNE LASTNOSTI*:** Irinotekan (zaviralec topoizomeraze I), inkapsuliran v vezikel z lipidnim dvoslojem oziroma liposom. Irinotekan je derivat kamptotecina. Kamptotecini delujejo kot specifični zaviralci encima DNA-topoizomeraza I. Irinotekan in njegov aktivni presnovek SN-38 se reverzibilno veženta na kompleks topoizomeraze I in DNA ter sprožita poškodbe v enoverižni DNA, kar zaustavi replikacijske vilice pri podvajanju DNA in povzroča citotoksičnost. Irinotekan se presnavlja s karboksilesterazo do SN-38. SN-38 je približno 1.000-krat močnejši kot irinotekan kot zaviralec topoizomeraze I, očiščene iz tumorskih celičnih linij človeka in glodavcev. **PAKIRANJE*:** Pakiranje vsebuje eno vialo z 10 ml koncentrata. **NAČIN PREDPISOVANJA IN IZDAJE ZDRAVILA: H - Predpisovanje in izdaja zdravila je le na recept, zdravilo pa se uporablja samo v bolnišnicah. DATUM ZADNJE REVIZIJE BESEDILA: 04. 2024. Imetnik dovoljenja za promet:** Les Laboratoires Servier, 50, rue Carnot, 92284 Suresnes cedex, Francija. ***Pred predpisovanjem preberite celoten povzetek glavnih značilnosti zdravila. Celoten povzetek glavnih značilnosti zdravila in podrobnejše informacije so na voljo pri: Servier Pharma d. o. o., Podmilščakova ulica 24, 1000 Ljubljana, www.servier.si.**

Zdravilo je na slovenskem trgu na voljo v tuji ovojnini. Za uporabnika so informacije v slovenskem jeziku dostopne na uradni spletni strani www.cbz.si. Navodila za uporabo v slovenskem jeziku so na voljo tudi na https://servier-pro.si/.

Kratice in literatura:
NALIRIFOX: liposomski irinotekan v kombinaciji z oksaliplatinom, 5-fluorouracilom in levkovorinom; mPaCa: metastatski rak trebušne slinavke; mOS: mediana celokupnega preživetja; mPFS: mediana preživetja brez napredovanja bolezni; ORR: skupna stopnja odziva.

1. Povzetek glavnih značilnosti zdravila ONIVYDE pegylated liposomal, april 2024.
2. Melisi D et al. Annals of Oncology. 2023;34:S896-S897.

SERVIER
moved by you

ONI-AD1 C1 2024-25. Samo za strokovno javnost. Datum priprave informacije: avgust 2024.

PRVO IN EDINO ODOBRENO PRI BOLNIKIH S CCA tarčno zdravljenje za mIDH1

CCA

IDH1

IDH2
FGFR2
HER2/neu
PIK3CA
NTRK
BRAF

▼TIBSOVO® 250 mg filmsko obložene tablete: PERSONALIZIRANO ZDRAVLJENJE ZA VEČJO KORIST

Pri predhodno zdravljenih bolnikih s holangiokarcinomom (CCA) in prisotno mutacijo IDH1 R132 Tibsovo (ivosidenib) omogoča:

- podaljšanje mPFS v primerjavi s placebom in 63-% zmanjšanje tveganja za napredovanje bolezni ali smrt (p<0,0001)[1]
- dvakrat daljši mOS v primerjavi s placebom in 51-% zmanjšanje tveganja za smrt (p<0,001; RPSFT-prilagojeni)[2]
- obvladljiv profil varnosti.[1-3]

Omogočite svojim bolnikom s CCA in prisotno mutacijo IDH1 R132 TARČNO ZDRAVLJENJE z zdravilom TIBSOVO®

▼Za to zdravilo se izvaja dodatno spremljanje varnosti. Tako bodo hitreje na voljo nove informacije o njegovi varnosti. Zdravstvene delavce naprošamo, da poročajo o katerem koli domnevnem neželenem učinku zdravila.

1. Abou-Alfa GK et al. Lancet Oncol. 2020;21:796-807. 2. Zhu AX et al. JAMA Oncol. 2021;7:1669-1677. 3. Povzetek glavnih značilnosti zdravila Tibsovo 250 mg filmsko obložene tablete, december 2023.

SKRAJŠAN POVZETEK GLAVNIH ZNAČILNOSTI ZDRAVILA Tibsovo 250 mg filmsko obložene tablete

▼Za to zdravilo se izvaja dodatno spremljanje varnosti. Tako bodo hitreje na voljo nove informacije o njegovi varnosti. Zdravstvene delavce naprošamo, da poročajo o katerem koli domnevnem neželenem učinku zdravila. **SESTAVA***: Ena filmsko obložena tableta vsebuje 250 mg ivosideniba. **TERAPEVTSKE INDIKACIJE***: V kombinaciji z azacitidinom za zdravljenje odraslih bolnikov z novoodkrito akutno mieloično levkemijo (AML) s prisotno mutacijo izocitrat dehidrogenaze-1 (IDH1) R132, ki niso primerni za standardno indukcijsko kemoterapijo. V monoterapiji za zdravljenje odraslih bolnikov z lokalno napredovalim ali metastatskim holangiokarcinomom (CCA) s prisotno mutacijo IDH1 R132, ki so bili predhodno zdravljeni z vsaj eno predhodno linijo sistemske terapije. **ODMERJANJE IN NAČIN UPORABE***: Zdravljenje je treba začeti pod nadzorom zdravnika, ki ima izkušnje z uporabo zdravil za zdravljenje raka. Bolniki morajo imeti pred začetkom jemanja zdravila Tibsovo z ustreznim diagnostičnim testom potrjeno mutacijo IDH1 R132. Pred uvedbo zdravljenja in med zdravljenjem je treba posneti EKG in oceniti celotno krvno sliko in biokemijske izvide krvi. Interval QT, popravljen glede na srčni utrip (QTc), mora biti pred uvedbo zdravljenja manj kot 450 ms. Priporočeni odmerek pri AML: 500 mg ivosideniba (2 x 250-mg tableta) peroralno enkrat na dan. Ivosidenib je treba začeti na 1. dan 1. cikla zdravljenja v kombinaciji z azacitidinom v odmerku 75 mg/m² telesne površine, intravensko ali subkutano, enkrat dnevno na 1. do 7. dan vsakega 28-dnevnega cikla. Priporočljivo je, da bolniki prejmejo vsaj 6 ciklov zdravljenja. Priporočeni odmerek pri holangiokarcinomu: 500 mg ivosideniba (2 x 250-mg tableta) peroralno enkrat na dan. Bolniki 2 uri pred in še 1 uro po jemanju tablet ne smejo uživati hrane. Priporočene so prilagoditve odmerka pri sočasni uporabi z zmernimi ali močnimi zaviralci CYP3A4 in za obvladovanje diferenciacijskega sindroma, levkocitoze, podaljšanja intervala QTc ter neželenih učinkov 3. ali višje stopnje. **KONTRAINDIKACIJE***: Preobčutljivost na učinkovino ali katero koli pomožno snov, sočasna uporaba z močnimi induktorji CYP3A4 ali dagibatranom (glejte Interakcije), prirojeni sindrom podaljšanega intervala QT, nenadna smrt ali polimorfna ventrikularna aritmija v družinski anamnezi, interval QT/QTc > 500 ms ne glede na metodo popravka. **OPOZORILA***: Sindrom diferenciacije pri bolnikih z AML: Brez zdravljenja je sindrom diferenciacije lahko življenje ogrožajoč ali smrten. Bolniki morajo biti obveščeni o znakih in simptomih sindroma diferenciacije. Treba jim je svetovati, naj se ob pojavu le-teh takoj posvetujejo z zdravnikom ter naj imajo vedno pri sebi opozorilno kartico za bolnika. Prekinite zdravljenje z zdravilom Tibsovo, če hudi znaki/simptomi vztrajajo več kot 48 ur po uvedbi sistemskih kortikosteroidov. Podaljšanje intervala QTc: Nepravilnosti je treba obravnavati takoj. V primeru značilne simptomatike je treba posneti EKG, kot je to klinično indicirano. V primeru hudega bruhanja in/ali driske je treba oceniti nepravilnosti serumskih elektrolitov. Bolnike je treba obvestiti o tveganju za podaljšanje intervala QT, njegovih znakih in simptomih (palpitacije, omotica, sinkopa ali celo srčni zastoj) in jim svetovati da takoj obvestijo zdravnika, če se ti pojavijo. Pri zdravljenju bolnikov je potrebna previdnost in pozorno spremljanje glede podaljšanja intervala QTc, če ni mogoča uporaba drugega ustreznega zdravljenja namesto zdravil, za katera je znano, da podaljšajo interval QTc, ali zmernih oz. močnih zaviralcev CYP3A4. Pozorno je treba spremljati bolnike s kongestivnim srčnim popuščanjem, elektrolitskimi motnjami oz. če je za obvladovanje znakov/simptomov sindroma diferenciacije klinično indicirano dajanje furosemida. Zdravljenje je treba dokončno ukiniti, če bolniki razvijejo podaljšanje intervala QTc z znaki ali simptomi življenje ogrožajoče aritmije. Ivosidenib je treba pri bolnikih, ki imajo znižane vrednosti albumina oz. imajo majhno telesno maso, uporabljati s previdnostjo. Huda ledvična okvara: previdnost pri uporabi in skrbno spremljanje. Jetrna okvara: zdravilo je treba uporabljati previdno pri bolnikih z zmerno in s hudo jetrno okvaro (Child-Pugh razreda B in C) in to skupino bolnikov je treba skrbno spremljati. Zdravilo Tibsovo je treba pri bolnikih z blago jetrno okvaro uporabljati previdno (Child-Pugh razred A). Pomožne snovi: vsebuje laktozo in natrij (v bistvu ‚brez natrija'). **INTERAKCIJE***: Kontraindicirano: močni induktorji encima CYP3A4; dabigatran. Ni priporočljivo: zmerni ali močni zaviralci CYP3A4; zdravila, za katera je znano, da podaljšujejo interval QTc; substrati OAT3 ali OATP1B1/1B3; substrati CYP3A4, CYP2B6, CYP2C8 ali CYP2C9 z ozkim terapevtskim indeksom, ali substrati CYP2C19; itrakonazol ali ketokonazol; substrati UGT. Previdnostni ukrepi: hormonski kontraceptivi. **PLODNOST*. NOSEČNOST***: Uporaba ni priporočljiva. **DOJENJE***: Med zdravljenjem in še vsaj 1 mesec po zadnjem odmerku je treba prenehati z dojenjem. **KONTRACEPCIJA***: Ženske v rodni dobi morajo pred začetkom zdravljenja z zdravilom Tibsovo opraviti test nosečnosti ter se morajo med zdravljenjem izogibati zanositvi. Med zdravljenjem in še vsaj 1 mesec po zadnjem odmerku je treba uporabljati učinkovito kontracepcijo. **VPLIV NA SPOSOBNOST VOŽNJE IN UPRAVLJANJA STROJEV***: Blag vpliv. Utrujenost in omotico je treba upoštevati pri oceni bolnikove sposobnosti vožnje in upravljanja strojev. **NEŽELENI UČINKI*: Pri AML**: Zelo pogosti: sindrom diferenciacije, levkocitoza, trombocitopenija, nevtropenija, nespečnost, glavobol, omotica, bruhanje, bolečina v okončinah, artralgija, bolečina v hrbtu, podaljšanje intervala QT. Pogosti: levkopenija, periferna nevropatija, orofaringealna bolečina. **Pri CCA**: Zelo pogosti: anemija, zmanjšan apetit, periferna nevropatija, glavobol, ascites, diareja, bruhanje, navzea, bolečina v trebuhu, izpuščaj, utrujenost, zvišanje aspartat aminotransferaze, zvišanje bilirubina. Pogosti: holestatična zlatenica, hiperbilirubinemija, padec, podaljšanje intervala QT, zvišanje alanin aminotransferaze, zmanjšanje števila belih krvnih celic, zmanjšanje števila trombocitov. **PREVELIKO ODMERJANJE***: Ni na voljo specifičnega antidota. Bolnike je treba skrbno spremljati in jim zagotoviti ustrezno podporno nego. **FARMAKODINAMIČNE LASTNOSTI***: Ivosidenib je zaviralec mutiranega encima IDH1. Mutirana oblika IDH1 pretvarja alfa-ketoglutarat (α-KG) v 2-hidroksiglutarat (2-HG), ki blokira celično diferenciacijo in spodbuja tumorigenezo tako pri hematoloških kot pri nehematoloških malignih boleznih. Mehanizem delovanja ivosideniba pri posameznih indikacijah še ni povsem pojasnjen, razen sposobnosti zaviranja 2-HG in obnavljanja celične diferenciacije. **PAKIRANJE***: Pakiranje vsebuje 60 filmsko obloženih tablet. **NAČIN PREDPISOVANJA IN IZDAJE ZDRAVILA: Rp/Spec - Predpisovanje in izdaja zdravila je le na recept zdravnika specialista ustreznega področja medicine ali od njega pooblaščenega zdravnika. DATUM ZADNJE REVIZIJE BESEDILA: december 2023. Imetnik dovoljenja za promet:** Les Laboratoires Servier, 50, rue Carnot, 92284 Suresnes cedex, Francija. ***Pred predpisovanjem preberite celoten povzetek glavnih značilnosti zdravila. Celoten povzetek glavnih značilnosti zdravila in podrobnejše informacije so na voljo pri: Servier Pharma d.o.o., Podmilščakova ulica 24, 1000 Ljubljana, www.servier.si.**

Zdravilo je na slovenskem trgu na voljo v tuji ovojnini. Navodilo za uporabo v slovenskem jeziku je priloženo ovojnini skupaj z opozorilno kartico za bolnika. Opozorilna kartica je namenjena bolnikom z AML, ki jim je bilo predpisano zdravilo Tibsovo, da zagotovi dodatne informacije glede pomembnega ugotovljenega tveganja sindroma diferenciacije (objavljena je tudi na spletni strani JAZMP: http://www.jazmp.si/dokumenti/). Informacije o zdravilu v slovenskem jeziku so dostopne na uradni spletni strani http://www.cbz.si"www.cbz.si. Na voljo so tudi na https://servier-pro.si/.

▼TIBSOVO®
250 mg filmsko obložene tablete
(ivosidenib)

SERVIER
moved by you

TIB AD1 C2 2023-24. Samo za strokovno javnost.
Datum priprave informacije: maj 2024.

Instructions for authors

The editorial policy

Radiology and Oncology is a multidisciplinary journal devoted to the publishing original and high-quality scientific papers and review articles, pertinent to oncologic imaging, interventional radiology, nuclear medicine, radiotherapy, clinical and experimental oncology, radiobiology, medical physics, and radiation protection. Papers on more general aspects of interest to the radiologists and oncologists are also published (no case reports).

The Editorial Board requires that the paper has not been published or submitted for publication elsewhere; the authors are responsible for all statements in their papers. Accepted cannot be published elsewhere without the written permission of the editors.

Submission of the manuscript

The manuscript written in English should be submitted to the journal via online submission system Editorial Manager available for this journal at: www.radioloncol.com.

In case of problems, please contact Sašo Trupej at saso.trupej@computing.si or the Editor of this journal at gsersa@onko-i.si

All articles are subjected to the editorial review and when the articles are appropriated they are reviewed by independent referees. In the cover letter, which must accompany the article, the authors are requested to suggest 3-4 researchers, competent to review their manuscript. However, please note that this will be treated only as a suggestion; the final selection of reviewers is exclusively the Editor's decision. The authors' names are revealed to the referees, but not vice versa.

Manuscripts which do not comply with the technical requirements stated herein will be returned to the authors for the correction before peer-review. The editorial board reserves the right to ask authors to make appropriate changes of the contents as well as grammatical and stylistic corrections when necessary. Page charges will be charged for manuscripts exceeding the recommended length, as well as additional editorial work and requests for printed reprints.

Articles are published printed and on-line as the open access:

(https://content.sciendo.com/raon).

All articles are subject to 1500 EUR + VAT publication fee. Exceptionally, waiver of payment may be negotiated with editorial office, at the time of article submission.

Manuscripts submitted under multiple authorship are reviewed on the assumption that all listed authors concur in the submission and are responsible for its content; they must have agreed to its publication and have given the corresponding author the authority to act on their behalf in all matters pertaining to publication. The corresponding author is responsible for informing the co-authors of the manuscript status throughout the submission, review, and production process.

Preparation of manuscripts

Radiology and Oncology will consider manuscripts prepared according to the Uniform Requirements for Manuscripts Submitted to Biomedical Journals by International Committee of Medical Journal Editors (www.icmje.org). The manuscript should be written in grammatically and stylistically correct language. Abbreviations should be avoided. If their use is necessary, they should be explained at the first time mentioned. The technical data should conform to the SI system. The manuscript, excluding the references, tables, figures and figure legends, must not exceed 5000 words, and the number of figures and tables is limited to 8. Organize the text so that it includes: Introduction, Materials and methods, Results and Discussion. Exceptionally, the results and discussion can be combined in a single section. Start each section on a new page, and number each page consecutively with Arabic numerals. For ease of review, manuscripts should be submitted as a single column, double-spaced text. The template for preparation of the manuscript is available in the editorial manager.

The Title page should include a concise and informative title, followed by the full name(s) of the author(s); the institutional affiliation of each author; the name and address of the corresponding author (including telephone, fax and E-mail), and an abbreviated title (not exceeding 60 characters). This should be followed by the abstract page, summarizing in less than 250 words the reasons for the study, experimental approach, the major findings (with specific data if possible), and the principal conclusions, and providing 3-6 key words for indexing purposes. Structured abstracts are required. Slovene authors are requested to provide title and the abstract in Slovene language in a separate file. The text of the research article should then proceed as follows:

Introduction should summarize the rationale for the study or observation, citing only the essential references and stating the aim of the study.

Materials and methods should provide enough information to enable experiments to be repeated. New methods should be described in details.

Results should be presented clearly and concisely without repeating the data in the figures and tables. Emphasis should be on clear and precise presentation of results and their significance in relation to the aim of the investigation.

Discussion should explain the results rather than simply repeating them and interpret their significance and draw conclusions. It should discuss the results of the study in the light of previously published work.

Charts, Illustrations, Images and Tables

Charts, Illustrations, Images and Tables must be numbered and referred to in the text, with the appropriate location indicated. Charts, Illustrations and Images, provided electronically, should be of appropriate quality for good reproduction. Illustrations and charts must be vector image, created in CMYK color space, preferred font "Century Gothic", and saved as .AI, .EPS or .PDF format. Color charts, illustrations and Images are encouraged, and are published without additional charge. Image size must be 2.000 pixels on the longer side and saved as .JPG (maximum quality) format. In Images, mask the identities of the patients. Tables should be typed double-spaced, with a descriptive title and, if appropriate, units of numerical measurements included in the column heading. The files with the figures and tables can be uploaded as separate files.

References

References must be numbered in the order in which they appear in the text and their corresponding numbers quoted in the text. Authors are responsible for the accuracy of their references. References to the Abstracts and Letters to the Editor must be identified as such. Citation of papers in preparation or submitted for publication, unpublished observations, and personal communications should not be included in the reference list. If essential, such material may be incorporated in the appropriate place in the text. References follow the style of Index Medicus, DOI number (if exists) should be included.

All authors should be listed when their number does not exceed six; when there are seven or more authors, the first six listed are followed by "et al.". The following are some examples of references from articles, books and book chapters:

Dent RAG, Cole P. In vitro maturation of monocytes in squamous carcinoma of the lung. *Br J Cancer* 1981; **43:** 486-95. doi: 10.1038/bjc.1981.71

Chapman S, Nakielny R. *A guide to radiological procedures*. London: Bailliere Tindall; 1986.

Evans R, Alexander P. Mechanisms of extracellular killing of nucleated mammalian cells by macrophages. In: Nelson DS, editor. *Immunobiology of macrophage.* New York: Academic Press; 1976. p. 45-74.

Authorization for the use of human subjects or experimental animals

When reporting experiments on human subjects, authors should state whether the procedures followed the Helsinki Declaration. Patients have the right to privacy; therefore, the identifying information (patient's names, hospital unit numbers) should not be published unless it is essential. In such cases the patient's informed consent for publication is needed, and should appear as an appropriate statement in the article. Institutional approval and Clinical Trial registration number is required. Retrospective clinical studies must be approved by the accredited Institutional Review Board/Committee for Medical Ethics or other equivalent body. These statements should appear in the Materials and methods section.

The research using animal subjects should be conducted according to the EU Directive 2010/63/EU and following the Guidelines for the welfare and use of animals in cancer research (Br J Cancer 2010; 102: 1555 – 77). Authors must state the committee approving the experiments, and must confirm that all experiments were performed in accordance with relevant regulations.

These statements should appear in the Materials and methods section (or for contributions without this section, within the main text or in the captions of relevant figures or tables).

Transfer of copyright agreement

For the publication of accepted articles, authors are required to send the License to Publish to the publisher on the address of the editorial office. A properly completed License to Publish, signed by the Corresponding Author on behalf of all the authors, must be provided for each submitted manuscript.

Conflict of interest

When the manuscript is submitted for publication, the authors are expected to disclose any relationship that might pose real, apparent or potential conflict of interest with respect to the results reported in that manuscript. Potential conflicts of interest include not only financial relationships but also other, non-financial relationships. In the Acknowledgement section the source of funding support should be mentioned. The Editors will make effort to ensure that conflicts of interest will not compromise the evaluation process of the submitted manuscripts; potential editors and reviewers will exempt themselves from review process when such conflict of interest exists. The statement of disclosure must be in the Cover letter accompanying the manuscript or submitted on the form available on www.icmje.org/coi_disclosure.pdf

The use and explanation of AI and AI-assisted technologies in scientific writing

When authors use artificial intelligence (AI) and AI-assisted technologies in the writing process, they should consider that:

- These technologies should only be used to improve readability and language and to assist in the investigation of data. They should not replace researchers' primary tasks of explaining, the interpretation of data and drawing valid scientific conclusions.
- Apply the technology under human supervision and control, and carefully review and edit the result, because AI can produce authoritative-sounding results that may be incorrect, incomplete, or biased.
- Do not list AI or AI-assisted technologies as authors or co-authors, and do not cite AI as an author. Authorship carries with it responsibilities and tasks that only humans can perform.
- Disclose in your manuscript the use of AI and AI-enabled technologies in the writing process by following the instructions below. An appropriate statement should appear in the published paper. Please note that authors are ultimately responsible and accountable for the content of the paper.

Disclosure notes

Authors must disclose the use of AI and AI-assisted technologies in the writing process by adding a statement at the end of their manuscript in the main manuscript file before the bibliography, at the time of manuscript submission. The statement should be included in a new section titled 'Statement on the Use of AI and AI-Assisted Technologies in the Writing Process'.

Statement: during the preparation of this paper, the author(s) used [NAME TOOL / SERVICE] to create [REASON]. After using this tool/service, the author(s) have reviewed and edited the content as required and take full responsibility for the content of the publication.

This statement does not apply to the use of basic tools to check grammar, spelling, references, etc. If there is nothing to disclose, it is not necessary to add a statement.

Page proofs

Page proofs will be sent by E-mail to the corresponding author. It is their responsibility to check the proofs carefully and return a list of essential corrections to the editorial office within three days of receipt. Only grammatical corrections are acceptable at that time.

Open access

Papers are published electronically as open access on https://content.sciendo.com/raon, also papers accepted for publication as E-ahead of print.

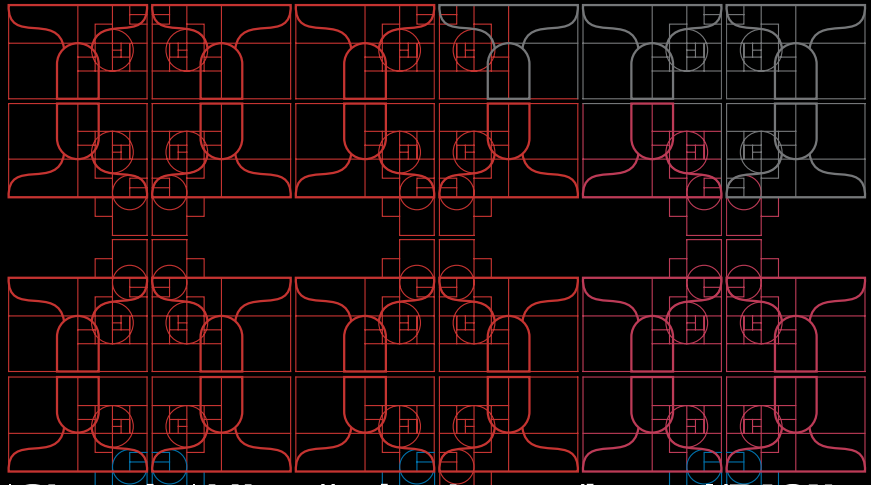

Radiology and Oncology | Ljubljana | Slovenia | https://sciendo.com/journal/RAON

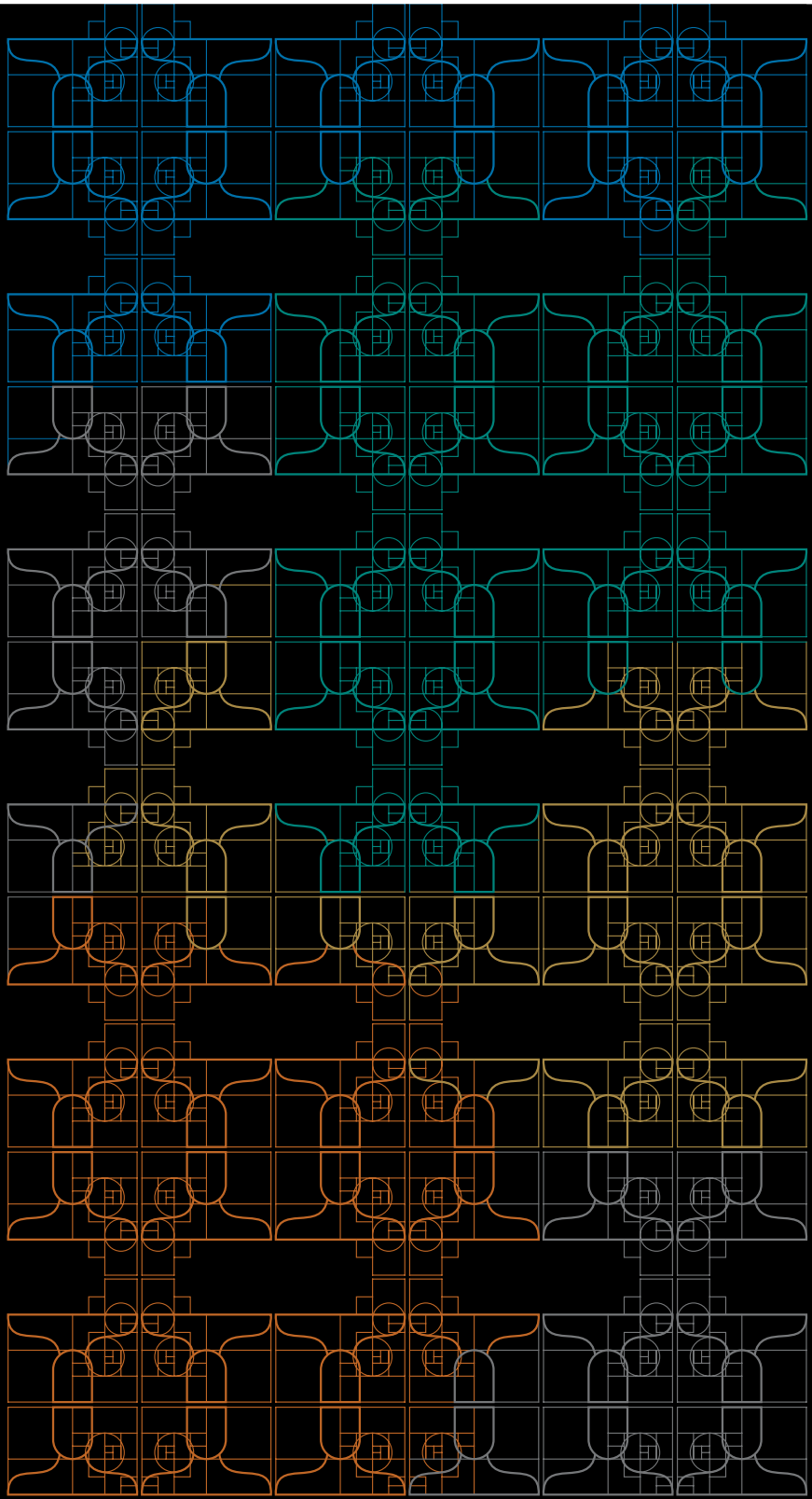

ISSN 1318 - 2099